

# **Stony Brook University**



OFFICIAL COPY

**The official electronic file of this thesis or dissertation is maintained by the University Libraries on behalf of The Graduate School at Stony Brook University.**

**© All Rights Reserved by Author.**

**Design, synthesis, and biological evaluation of novel taxoid-based small-molecule  
theranostic PET/SPECT imaging agents and nano-scale asymmetric bow-tie dendrimer  
drug conjugates towards tumor-targeted chemotherapy**

A Dissertation Presented

by

**Tao Wang**

to

The Graduate School

in Partial Fulfillment of the

Requirements

for the Degree of

**Doctor of Philosophy**

in

**Chemistry**

Stony Brook University

**August 2015**

**Stony Brook University**

The Graduate School

**Tao Wang**

We, the dissertation committee for the above candidate for the  
Doctor of Philosophy degree, hereby recommend  
acceptance of this dissertation.

**Iwao Ojima**  
**Dissertation Advisor**  
**Distinguished Professor, Department of Chemistry**

**Nancy Goroff**  
**Chairperson of Defense**  
**Professor, Department of Chemistry**

**Elizabeth Boon**  
**Third Member of Dissertation Committee**  
**Associate Professor, Department of Chemistry**

**Balaji Sitharaman**  
**Outside Committee Member**  
**Associate Professor, Department of Biomedical Engineering**  
**Stony Brook University**

This dissertation is accepted by the Graduate School

Charles Taber  
Dean of the Graduate School

Abstract of the Dissertation

**Design, synthesis, and biological evaluation of novel taxoid-based small-molecule  
theranostic PET/SPECT imaging agents and nano-scale asymmetric bow-tie dendrimer  
drug conjugates towards tumor-targeted chemotherapy**

by

**Tao Wang**

**Doctor of Philosophy**

in

**Chemistry**

Stony Brook University

**2015**

Cancer remains the second leading cause of death in the United States. Traditional chemotherapy relies on highly potent cytotoxic agents, such as paclitaxel and docetaxel, to kill rapidly dividing cancer cells. But these drugs usually cause undesired side-effects due to lack of tumor-selectivity, and decreased efficacy against MDR cancer cell lines. Accordingly, newer generation taxoids were designed and evaluated showing several orders of magnitude greater potency than paclitaxel and docetaxel.

Over the past decade, significant advancement has been made on the development of newer generation taxoids based on SAR study. As a selected example of second generation taxoid, SB-T-1214 was synthesized via  $\beta$ -Lactam Synthon Method in good overall yield and enantiomeric purity, and used as cytotoxic agent for taxoid-based drug conjugate synthesis. To elucidate the biodistribution profiles of SB-T-1214, a rapid methylation Pd-catalyzed Stille coupling reaction condition was developed toward C-11 radiolabelling SB-T-1214 as PET agent., several unexpected taxoid-based derivatives were found during the cold synthesis, indicating a complicated mechanism for the Pd-Cu co-catalyzed Stille coupling reaction. The LC/UV/MS-TOF methods were fully established to analyze the outcome of Stille coupling reaction confirm the predicted structures by mass analysis. Three new taxoid were synthesized with full characterization.

Various taxoid-based tumor-targeted drug delivery systems (TTDDSs) have been developed to efficiently and selectively deliver newer generation taxoid to the tumor microenvironment. Biotin has been utilized as tumor-targeting module (TTM) due to its receptor overexpressed on the surfaces of various cancer cells. Two biotin-linker-taxoid drug conjugates BLS and BLT-S were designed and synthesized, consisting of a biotin as tumor targeting module, a second generation taxoid SB-T-1214 as the warhead, connected with a self-immolative disulfide linker, and/or a polyethylene glycol oligomer for improving solubility and bioavailability. Biological evaluation *in vitro* and *in vivo* including internalization study using confocal microscopy and flow cytometry, and cell viability assays against various cell lines exhibited excellent target-specificity of these drug conjugates. To investigate the biodistribution of biotin-bearing conjugates *in vivo*, a key precursor toward [<sup>18</sup>F]-labeled biotin diagnostic tracer has been made readily for radio-synthesis. Furthermore, a versatile TTDDS consisting of 1,3,5-triazine as a tripod splitter module, biotin moiety, linker-drug moiety, and a chelating arm for capturing radioisotopes <sup>64</sup>Cu/<sup>99m</sup>Tc for PET/SPECT imaging, has been designed to synthesize theranostic drug conjugates. “Cold” synthesis conditions using <sup>65</sup>Cu/<sup>185</sup>Re as surrogates have been optimized to 10 minutes, and separation methods have been well established within 30 minutes.

PAMAM (poly(amidoamine)) dendrimer has highly symmetric and well-defined structure. A type of PAMAM dendrimer with cleavable cystamine core was selected to construct a novel and versatile asymmetric bow-tie dendrimer-based (ABTD) platform that was used to synthesize a series of ABTD conjugates via click chemistry. Internalization study demonstrated the multi-binding effect for enhanced cell uptake through receptor-mediated endocytosis (RME). The cell viability assays have shown that this ABTD platform is highly efficient for selectively delivering anticancer drugs to biotin-receptor overexpressing tumor cells and the platform itself is biocompatible. Purification and analysis methods have been well established to isolate nanoscale intermediates as single component in extremely good purity with full characterization.

## Table of Contents

List of Figures.....	xi
List of Schemes.....	xvi
List of Tables.....	xix
List of Abbreviations.....	xx
Acknowledgements.....	xxiv
Vita.....	xxv

## General Introduction

§0.1 Cancer.....	2
§0.2 The Hallmarks of Cancer.....	2
§0.3 Current Strategies for Cancer Treatment.....	3
§0.4 Issues in the Current Chemotherapy.....	4
§0.5 Tumor-Targeted Chemotherapy.....	5
§0.6 Outline of Chapters.....	9
§0.7 References.....	12

## Chapter 1

### Synthesis of New-Generation Taxoid SB-T-1214 via $\beta$ -Lactam Synthon Method

§1.1 Paclitaxel and Next-Generation Taxoids.....	16
§1.1.1 Paclitaxel and Taxanes.....	16
§1.1.2 Semi-synthesis of Taxanes via $\beta$ -Lactam Synthon Method ( $\beta$ -LSM).....	16
§1.1.3 Mechanism of Action and Clinical Development of Paclitaxel (Taxol®).....	19
§1.1.4 Multidrug Resistance (MDR).....	21
§1.1.5 Structure-Activity Relationship (SAR) Study of Taxanes.....	22
§1.2 Synthesis of SB-T-1214 via $\beta$ -Lactam Synthon Method.....	24
§1.2.1 Synthesis of Enantiomerically-Enriched $\beta$ -Lactam.....	24
§1.2.2 Synthesis of Second-Generation Taxoid SB-T-1214.....	26
§1.3 Summary.....	28
§1.4 Experimental Section.....	28
§1.4.1 Caution.....	28
§1.4.2 General Information.....	28
§1.4.3 Materials.....	28
§1.4.4 Experimental Procedure.....	29

§1.5 References.....	33
----------------------	----

## Chapter 2

### New-Generation Taxoid SB-T-1214 Derivatives as Imaging Agents

§2.1 Introduction .....	38
§2.2 Fluorescein-Labeled Taxoid .....	38
§2.2.1 Fluorescent Tags.....	39
§2.2.2 Synthesis of SB-T-1214-C7-Fluorescent Probe .....	40
§2.3 Development of <sup>11</sup> C-Labeled SB-T-1214 Radiotracer for PET Imaging Study.....	42
§2.3.1 Carbon-11 Radiolabeled Taxanes .....	42
§2.3.2 Establishment of LC/UV/MS-TOF Analysis Condition .....	43
§2.3.3 Analysis and Determination of the Stille Coupling Outcomes.....	47
§2.3.4 Synthesis of Taxoid Derivatives from Stille Coupling.....	53
§2.4 Summary.....	58
§2.5 Experimental Section.....	58
§2.5.1 Caution.....	58
§2.5.2 General Information.....	58
§2.5.3 Materials.....	59
§2.5.4 Experimental Procedure.....	59
§2.6 References.....	66

## Chapter 3

### Taxoid-based Vitamin-Linker-Drug Conjugates for Tumor-targeted Drug Delivery

§3.1 Tumor-Targeted Chemotherapy .....	70
§3.1.1 Biotin as Tumor-Targeting Module .....	70
§3.1.2 Mechanism-Based Self-Immolative Disulfide Linker .....	71
§3.1.3 Development on Biotin-Linker-Taxoid Construct Model .....	74
§3.2 Synthesis and Biological evaluation of Biotin-Linker-Taxoid Conjugates .....	76
§3.2.1 Synthesis of Self-immolative Disulfide Linker .....	76
§3.2.2 Synthesis of Coupling-Ready Activated Drug-Linker Constructs .....	78
§3.2.3 Synthesis of Biotin-Linker-Taxoid Conjugate BLT .....	80
§3.2.4 Synthesis of Biotin-PEG-Linker-Taxoid Conjugate BLT-S .....	81
§3.2.5 Biological Evaluation of Biotin-Linker-Taxoid Conjugates <i>in Vitro</i> Studies .....	82
§3.2.6 Biological Evaluation of BLT <i>in Vivo</i> Study .....	84
§3.3 Synthesis and Biological Evaluation of Biotin-Fluorescein Probes .....	84
§3.3.1 Synthesis of Biotin-Fluorescent Probes (Biotin-PEG-FITC and Biotin-PEG-Fluorescein).....	87
§3.3.2 Biological Evaluation of Biotin-Fluorescein Probes <i>in Vitro</i> Studies .....	88
§3.4 Synthesis towards [ <sup>18</sup> F]-Labeled Biotin-PEG-F Radiotracer for PET Imaging Study.....	89

§3.4.1 Cold Synthesis toward Biotin-PEG-F .....	89
§3.5 Summary.....	90
§3.6 Experimental Section.....	91
§3.6.1 Caution.....	91
§3.6.2 General Information.....	91
§3.6.3 Materials.....	93
§3.6.4 Experimental Procedure.....	94
§3.7 References.....	104

## Chapter 4

### Novel Taxoid-based Tumor-targeting Diagnostic/Theranostic PET/SPECT Imaging Agents

§4.1 Introduction .....	108
§4.1.1 Positron Emission Tomography (PET) .....	108
§4.1.2 Single-photon Emission Computed Tomography (SPECT) .....	109
§4.1.3 PET versus SPECT: Strengths and Limitations .....	110
§4.2 Selective Examples of Radionuclides for PET/SPECT in Pharmaceutical Development	111
§4.2.1 Carbon-11.....	111
§4.2.2 Fluorine-18.....	111
§4.2.3 Copper-64.....	112
§4.2.4 Technetium-99m.....	113
§4.3 Novel Triazine-based Tumor-targeting Diagnostic/Theranostic PET/SPECT Platform...	114
§4.3.1 Radiolabeled Vitamin-based Conjugates as Radiotracers .....	114
§4.3.2 Triazine-based Tripod Platform for Theranostics.....	115
§4.3.3 Synthesis of Biotin-Triazine-Linker-Drug-Azide Coupling-Ready Platform	116
§4.4 Diagnostic/Theranostic $^{185}\text{Re}$ (Cold)/ $^{99\text{m}}\text{Tc}$ (Hot) SPECT Imaging Agents.....	118
§4.4.1 Synthesis of Cyclooctyne-DPA( $sp^2\text{N}$ ) Trident Ligand .....	118
§4.4.2 Cold Synthesis of Biotin-Triazine-Linker-Drug-DPA( $sp^2\text{N}$ )- $^{185}\text{Re}(\text{CO})_3$ Conjugate and Ligand Disassociation <i>via</i> Re-promoted Methanolysis .....	119
§4.4.3 Synthesis of Cyclooctyne-DPA( $sp^3\text{N}$ ) Trident Ligand .....	121
§4.4.4 Cold Synthesis of Biotin-Triazine-Linker-Drug-DPA( $sp^3\text{N}$ )- $^{185}\text{Re}(\text{CO})_3$ and Biotin- DPA( $sp^3\text{N}$ )- $^{185}\text{Re}(\text{CO})_3$ Conjugates.....	121
§4.5 Diagnostic/Theranostic $^{65}\text{Cu}$ (Cold)/ $^{64}\text{Cu}$ (Hot) PET Imaging Agents.....	124
§4.5.1 Synthesis of Cyclooctyne-NOTA Hexadent Ligand.....	124
§4.5.2 Cold Synthesis of Biotin-Triazine-Linker-Drug-NOTA- $^{65}\text{Cu}$ and Biotin-NOTA- $^{65}\text{Cu}$ Conjugates.....	124
§4.6 Summary.....	126
§4.7 Experimental Section.....	126
§4.7.1 Caution.....	126
§4.7.2 General Information.....	126
§4.7.3 Materials.....	127
§4.7.4 Experimental Procedure.....	127
§4.8 References.....	138



## Chapter 5

### Novel Asymmetric Bow-Tie Dendrimer-based Drug Delivery System

§5.1 Nanomedicine .....	143
§5.1.1 Introduction: Dendritic Polymer (Dendrimer).....	144
§5.1.2 Preparation .....	149
§5.1.3 Active and Passive Targeting Strategies .....	150
§5.2 Original Design of Asymmetric Bow-Tie Dendrimer (ABTD) Drug Delivery System...	152
§5.2.1 Rational Design .....	155
§5.2.2 Proof of Concept .....	156
§5.2.3 First Attempt towards ABTD Conjugate .....	160
§5.3 Modified Design of a Novel Versatile ABTD Drug Delivery System.....	162
§5.3.1 Solubility Improvement with PEG Oligomer Spacer.....	164
§5.3.2 Biotinylated PEGylated G3 PAMAM Dendrimer .....	165
§5.3.3 Click-ready PEGylated G1 PAMAM Dendrimer.....	167
§5.3.4 Bis(maleicimido) PEGylated Linker .....	169
§5.3.5 Synthesis of Click-ready Intermediates.....	170
§5.3.6 Synthesis of ABTD Conjugates.....	171
§5.3.7 Internalization Study via RME and Multi-binding Effect .....	173
§5.3.8 Cytotoxicity Measurements.....	174
§5.4 Tribrached Dendrimer Incorporating Imaging Agents.....	176
§5.4.1 Design and Synthesis Fluorescent Tribranched Linker.....	176
§5.5 Extended Multi-binding Effect Study .....	180
§5.6 Second Generation Versatile ABTD Drug Delivery System Design .....	183
§5.7 Summary.....	188
§5.8 Experimental Section.....	188
§5.8.1 Caution.....	188
§5.8.2 General Information.....	189
§5.8.3 Materials.....	190
§5.8.4 Experimental Procedure.....	191
§5.9 References.....	206

## Chapter 6

### Hyaluronic Acid-Linker-Taxoid (HALT) Conjugate for Targeting Cancer Stem Cell

§6.1 Introduction-Cancer Stem Cell and Hyaluronic Acid .....	211
§6.2 Synthesis and Biological Evaluations.....	212
§6.2.1 Synthesis of Hyaluronic Acid-Linker-Taxoid (HALT) Conjugate .....	212
§6.2.2 Expression of Biotin Receptor and HA Receptor on CSC Surface .....	213
§6.2.3 Cytotoxicity Assay of Biotin-Linker-Taxoid against CSC .....	215
§6.3 Summary.....	217
§6.4 Experimental Section.....	217
§6.4.1 Caution.....	217

§6.4.2 General Information.....	217
§6.4.3 Materials.....	219
§6.4.4 Experimental Procedure.....	219
§6.5 References.....	220

### **Perspective**

Future directions of the ongoing projects.....	222
References.....	224

### **Appendices**

Appendix Chapter 1 NMR Spectra .....	A244-257
Appendix Chapter 2 NMR Spectra .....	A258-284
Appendix Chapter 3 NMR Spectra .....	A285-330
Appendix Chapter 4 NMR Spectra .....	A331-369
Appendix Chapter 5 NMR Spectra .....	A384-454
Appendix Chapter 6 NMR Spectra .....	A455-459

## List of Figures

### General Introduction

Figure 0.1. Estimated new cancer cases in the US in 2015 .....	17
Figure 0.2. The hallmarks of cancer .....	18
Figure 0.3. Selected examples of chemotherapeutic agents.....	19
Figure 0.4. Chemical structures of Gleevec and Tarceva for targeted therapy.....	19
Figure 0.5. Key features of a tumor-targeted drug conjugate .....	17
Figure 0.6. Receptor-mediated endocytosis of TTM-linker-drug conjugate .....	18
Figure 0.7. Selected examples of tumor-targeting moieties.....	19
Figure 0.8. Various types of linkers commonly used for tumor-targeting drug conjugate.....	19
Figure 0.9. Two models of incorporation of imaging moiety to drug conjugate .....	17
Figure 0.10. Selected examples of nano-sized carriers .....	18

### Chapter 1

Figure 1.1. Chemical structures of taxane anticancer agents: paclitaxel, docetaxel, and cabazitaxel .....	16
Figure 1.2. Pathways for the formation of cis- and trans- $\beta$ -lactams.....	19
Figure 1.3. Three types of antimetabolic drugs (vinblastine, colchicine and taxol) interact with microtubules at diverse sites.....	20
Figure 1.4. Microtubule formation in taxol and taxol-free cells.....	20
Figure 1.5. Conformational changes of ATP-binding cassette (ABC) exporters.....	22
Figure 1.6. Overview of previously conducted SAR studies on paclitaxel .....	23
Figure 1.7. Chemical structure of SB-T-1214.....	23

### Chapter 2

Figure 2.1. Chemical structures of fluorescein-labelled and radiolabeled taxanes/toxoids .....	38
Figure 2.2. Selected examples of fluorescent dyes.....	39
Figure 2.3. Three existing forms of fluorescein.....	39
Figure 2.4. Fluorescein spirolactam formation.....	39
Figure 2.5. Chemical structures of radiolabelled taxanes.....	43
Figure 2.6. Chemical structures and molecular weights of three taxoid authentic samples.....	44
Figure 2.7. LC/UV/MS trace (positive mode) of three authentic samples (1:1:1).....	45
Figure 2.8. Mass analysis results (positive mode) of three authentic samples .....	45
Figure 2.9. LC/UV/MS trace (negative mode) of three authentic samples (1:1:1) mixture.....	46
Figure 2.10. Mass analysis results (negative mode) of three authentic samples.....	46
Figure 2.11. LC/UV/MS trace of Stille coupling.....	47
Figure 2.12. Predicted chemical structures of unknown compounds with corresponding retention times .....	48
Figure 2.13. Mass analysis results of peak C and two potential taxoid compounds .....	49

Figure 2.14. Target screening result of Tc-taxoid ( <b>2-11</b> ).....	49
Figure 2.15. Mass analysis results of peak D and chemical structure of predicted compound <b>2-12</b> .....	50
Figure 2.16. Mass analysis results of peak E and chemical structure of predicted compound <b>2-13</b> .....	50
Figure 2.17. Mass analysis results of peak B .....	51
Figure 2.18. Target screen result of allene-taxoid ( <b>2-14</b> ).....	52
Figure 2.19. Two pathways of beta-hydride elimination to generate allene-taxoid ( <b>2-14</b> ) and alkyne-taxoid ( <b>2-15</b> ).....	52
Figure 2.20. Proposed mechanism for Stille coupling reaction .....	53
Figure 2.21. LC/UV/MS trace of Tc-taxoid ( <b>2-11</b> ) formation without Pd catalyst .....	54
Figure 2.22. LC/UV/MS purity check and retention time determination of isolated two products <b>2-11</b> and <b>2-14</b> (or <b>2-15</b> ).....	54
Figure 2.23. LC/UV/MS trace of Ph-taxoid ( <b>2-12</b> ) formation without Cu catalyst .....	55
Figure 2.24. Target screening result of Ph-taxoid ( <b>2-12</b> ).....	56
Figure 2.25. Mass analysis results of peaks relating to Ph-taxoid ( <b>2-12</b> ) isomers .....	56
Figure 2.26. LC/UV/MS trace and mass analysis results of Hydride-taxoid ( <b>2-26</b> ) isomers .....	57
Figure 2.27. LC/UV/MS trace and mass analysis results of taxoid dimer ( <b>2-13</b> ) isomers .....	57

### Chapter 3

Figure 3.1. Chemical Structure of D-(+)-biotin .....	71
Figure 3.2. Disulfide cleavage during glutathione-triggered cascade drug release.....	72
Figure 3.3. A time-resolved <sup>19</sup> F NMR study for linker cleavage .....	72
Figure 3.4. A time-resolved <sup>19</sup> F NMR study using BLT-F <sub>2</sub> .....	73
Figure 3.5. A time-resolved <sup>19</sup> F NMR study for the drug release of BLT-S-F <sub>6</sub> .....	74
Figure 3.6. A time-resolved <sup>19</sup> F NMR study using BLT-S-F <sub>6</sub> .....	74
Figure 3.7. Chemical structure of first generation biotin-linker-taxoid conjugate and proposed decomposition via retro-Michael reaction .....	75
Figure 3.8. Chemical structure of second generation biotin-linker-taxoid conjugates with variable substituted methyl groups .....	76
Figure 3.9. Chemical structure of biotin-PEG-linker-taxoid (BLT-S).....	76
Figure 3.10. Chemical structure of biotin-linker-taxoid (BLT).....	80
Figure 3.11. Average tumor volumes for 5 surviving SCID female Swiss Webster athymic nude mice bearing MX-1 tumor xenograft with the following dose regimen: SB-T-1214: 20 mg/kg, q7d x 3 + 40 mg/kg x 4; BLT: (a) 20 mg/kg, q7d x 4 (3 studies), (b) 40 mg/kg, q7d x 2 (2 studies) .....	84
Figure 3.12. Chemical structures of fluorescent and fluorogenic probes to validate RME of biotin conjugates .....	85
Figure 3.13. CFM images and flow cytometry analysis of L1210FR cells after 3 h incubation with the 100 nM biotin-NHNH-FITC probe under different conditions: (A) 37 °C; (B) 47 °C; (C) 37 °C, added 0.05 % NaN <sub>3</sub> ; (D) 37 °C, pretreated with excess biotin (2 mM).....	85
Figure 3.14. Glutathione-triggered linker cleavage to release coumarin and CFM images of L1210FR cells after treatment with biotin-linker-coumarin (A) Epifluorescence image with added GSH-OEt for linker cleavage to release coumarin with fluorescence	

(B) Epifluorescence image only with incubated the biotin-linker-coumarin probe (nonfluorescent form).....	86
Figure 3.15. CFM images of released fluorescent taxoid from biotin-linker-SB-T-1214-C7-fluorescein probe and its binding to the target microtubules in L1210FR cells.....	86
Figure 3.16. Chemical structure of biotin-PEG-FITC .....	87
Figure 3.17. Internalization of biotin-PEG-FITC into various cell lines at different periods of incubation time at 37 °C .....	87
Figure 3.18. Overlapped Flow cytometry analysis resulting from the extent of the internalization of 10 µM biotin-PEG-Fluorescein probe ( <b>3-25</b> ) against ID8 (top) and MX1 (bottom) for 0, 1, 2, 4, 6 and 16 h periods at 37 °C .....	88
Figure 3.19. Overlapped Flow cytometry analysis resulting from the extent of the internalization of 10 µM biotin-PEG-Fluorescein probe ( <b>3-25</b> ) against ID8 (top) and MX1 (bottom) for 0, 1, 2, 4, 6 and 16 h periods at 37 °C .....	89
Figure 3.20. Chemical Structure of [ <sup>18</sup> F]biotin-PEG-F .....	89

## Chapter 4

Figure 4.1. Schematic representation of the principle of PET imaging demonstrating positron decay and annihilation generating two 511 keV γ-rays .....	108
Figure 4.2. Chemical pathway to important carbon-11 reagents .....	111
Figure 4.3. [ <sup>18</sup> F]FDG-based PET images showing patterns of metabolic activity of patients with Alzheimer’s disease (middle), Pick’s disease (right) and elderly individuals with no dementia (left) (high FDG uptake in red, low FDG uptake in blue) .....	112
Figure 4.4. Chemical structures of acyclic and macrocyclic chelators.....	113
Figure 4.5. Chemical structure and X-ray crystal structure of Cu(II)-NOTA complexes. Common elements are color coded as follows: C (gray), N (blue), and O (red) .....	113
Figure 4.6. Stereochemistry of Tc-tricarbonyl metal fragment and replacement of liable water molecules by chelating ligands.....	114
Figure 4.7. Chemical structures of vitamin-based radiolabeled PET/SPECT imaging agents ...	115
Figure 4.8. Chemical diagram of triazine-based tripod platform .....	115
Figure 4.9. Model structures of theranostic PET/SPECT agents .....	116

## Chapter 5

Figure 5.1. Mechanism of action of nanocarrier-drug with improved features .....	143
Figure 5.2. A whole range of nanocarriers for targeting cancer .....	144
Figure 5.3. The 3D projection of dendrimer core-shell architecture .....	145
Figure 5.4. The dendritic structure .....	145
Figure 5.5. Structures of biocompatible dendrimers that have been tested for drug delivery applications.....	146
Figure 5.6. Generation 0 of ethylenediamine (EDA) cored PAMAM dendrimer.....	147
Figure 5.7. Generation 1 diaminobutane core PAMAM dendrimer (DNT-102).....	147
Figure 5.8. Instantaneous snapshots of G1-G8 EDA core PAMAM dendrimers after long MD simulations at T = 300 K. ....	148
Figure 5.9. Dendrimer conformation based on different solvents.....	148
Figure 5.10. PAMAM dendrimer’s conformation under different pH condition.....	149

Figure 5.11. Angiogenesis .....	151
Figure 5.12. Active and passive targeting approaches of nanocarriers in tumor-targeted drug delivery .....	152
Figure 5.13. Structure of multi-functional generation 5 PAMAM dendrimer conjugate bearing different functional molecules (Ac, FITC, FA, OH, and MTX) with approximate average number.....	153
Figure 5.14. Example of defect dendrimer formation and further functionalization .....	154
Figure 5.15 Theoretical distribution of dendrimer species with a mean of 4 folic acid and 5 methotrexate molecules per dendrimer.....	154
Figure 5.16. Chemical structure of PAMAM dendrimer architecture bearing cleavable core...	155
Figure 5.17. Strategy of construction of asymmetric bow-tie dendrimer scaffold using fully functionalized half dendrons .....	155
Figure 5.18. A robust and versatile bioactive dendrimer diblock platform.....	156
Figure 5.19. A robust and versatile bioactive dendrimer diblock platform .....	157
Figure 5.20. MALDI-TOF of symmetric G1 PAMAM dendrimer with bis(maleimido) octane linker ( <b>5-4</b> ).....	158
Figure 5.21. Chemical structures and molecular weights of two fully biotinylated dendrimers <b>5-5</b> and <b>5-6</b> .....	159
Figure 5.22. MALDI-TOF of fully biotinylated G1 dendrimer <b>5-5</b> .....	160
Figure 5.23. MALDI-TOF of fully biotinylated G3 dendrimer <b>5-6</b> .....	160
Figure 5.24. Structural information of asymmetric PAMAM dendrimer conjugate <b>5-12</b> .....	162
Figure 5.25. Chemical structure of modified ABTD versatile platform .....	163
Figure 5.26. Model structure of Asymmetric Bow-Tie Dendrimer-based (ABTD) conjugates	164
Figure 5.27. MALDI-TOF result of purified fully functionalized generation 3 PAMAM dendrimer.....	166
Figure 5.28. MALDI-TOF result of purified fully functionalized generation 1 PAMAM dendrimer.....	168
Figure 5.29. LC-UV-TOF results for purified fully functionalized generation 1 PAMAM dendrimer.....	168
Figure 5.30. LC-UV-TOF mass analysis results for purified fully functionalized generation 1 PAMAM dendrimer .....	169
Figure 5.31. LC-UV-TOF mass deconvolution results for purified fully functionalized generation 1 PAMAM dendrimer.....	169
Figure 5.32. CFM images and flow cytometry analysis of different types of cells after incubation with the <b>ABTD-3</b> at the final concentration of 20 $\mu$ M at 37 $^{\circ}$ C for different periods: (A) flow cytometry analysis of <b>ABTD-3</b> in ID-8 at 0 h (red, control), 1 h (green), and 3 h (blue); (B,C) CFM images and flow cytometry analysis in ID8 at 1 and 3 h, respectively; (D) flow cytometry analysis of <b>ABTD-3</b> in MX-1 at 0 h (red, control), 1 h (green), and 3 h (blue); (E,F) CFM images and flow cytometry analysis in MX-1 at 1 and 3 h, respectively.....	173
Figure 5.33. Time dependent RME rate comparison between a small fluorescent probe Biotin-PEG-Fluorescein ( <b>3-25</b> ) (in red) and <b>ABTD-3</b> (in blue).....	174
Figure 5.34. Design of dendrimer-based theranostic tribranched conjugates .....	176
Figure 5.35 Tribranched dendrimer-based theranostic conjugates bearing a fluorescent probe	176
Figure 5.36. Structure of modified PEGylated tri-branched core.....	177

Figure 5.37. Purity check of <b>5-59</b> by LC/UV/MS-TOF .....	179
Figure 5.38. MALDI-TOF analysis of <b>5-59</b> .....	180
Figure 5.39. 2 <sup>nd</sup> generation di-branched dendrimer-based drug delivery system .....	180
Figure 5.40. MALDI result for G3-PEG-biotin half dendron with click-ready alkyne moiety... 181	
Figure 5.41. MALDI result for <b>5-62</b> .....	183
Figure 5.42. Example of 1 <sup>st</sup> generation di-branched dendrimer-based drug delivery system (ABTD-2) .....	183
Figure 5.43. 2 <sup>nd</sup> generation di-branched dendrimer-based drug delivery system .....	184
Figure 5.44. Structure of 2 <sup>nd</sup> generation dendrimer-based drug delivery system versatile platform .....	185
Figure 5.45. LC-MS-TOF trace of crude <b>5-64</b> under neutral condition .....	186
Figure 5.46. Mass analysis result of LC-MS-TOF trace .....	186
Figure 5.47. Deconvolution mass analysis result of LC-MS-TOF trace .....	187
Figure 5.48. Structures and molecular weights of desired product and defect impurity.....	187
Figure 5.49. LC-MS-TOF trace of crude <b>5-64</b> under acidic condition .....	188

## Chapter 6

Figure 6.1. Structures of two fluorescent probes .....	213
Figure 6.2. Flow cytometry analysis of different receptors in prostate (PPT2) CSCs and colon (HCT116) spheroids Structures of two fluorescent probes .....	214
Figure 6.3. Colocalization of receptors depicted by confocal microscopy.....	215
Figure 6.4. Biotin-Linker-Taxoid (BLT-S) pro-drug conjugate, containing the biotin moiety as the tumor-targeting module, the polyethylene glycol (PEG) <sub>3</sub> spacer the self-immolative disulfide linker, and the cytotoxic agent SB-T-1214.....	216

## List of Schemes

### Chapter 1

Scheme 1.1. First semi-synthetic methodology for paclitaxel.....	17
Scheme 1.2. The semi-synthesis of paclitaxel and docetaxel by the Ojima-Holton coupling protocol.....	18
Scheme 1.3. Synthesis of imine by condensation reaction.....	24
Scheme 1.4. Staudinger [2+2] ketene-imine cycloaddition reaction.....	25
Scheme 1.5. Optical enzymatic resolution of isolating enantiopure (+) <b>1-2</b> .....	25
Scheme 1.6. Hydrolysis and TIPS protection of (+) <b>1-3</b> .....	25
Scheme 1.7. CAN-deprotection and <i>t</i> -Boc protection reaction .....	26
Scheme 1.8. Mono TES protection on C7 of 10-DAB III .....	26
Scheme 1.9. Acylation of C10 position.....	27
Scheme 1.10. Ojima-Holton coupling reaction .....	27
Scheme 1.11. Deprotection of silyl groups to form final product SB-T-1214.....	27

### Chapter 2

Scheme 2.1. Reduction of terminal acid group.....	40
Scheme 2.2. Esterification on C2' and modification on C3 of fluorescein .....	41
Scheme 2.3. Possible TFA deprotection .....	41
Scheme 2.4. Synthesis of SB-T-1214-C7-fluorescein <b>2-8</b> .....	42
Scheme 2.5. Key synthetic steps towards SB-T-1214 <i>via</i> Stille coupling .....	43
Scheme 2.6. Cold synthesis of SB-T-1214 <i>via</i> Stille coupling .....	47
Scheme 2.7. Synthesis of Tc-taxoid ( <b>2-11</b> ) in the absence of Pd catalyst .....	53
Scheme 2.8. Synthesis of Ph-taxoid ( <b>2-12</b> ) in the absence of Cu catalyst .....	55
Scheme 2.9. Synthesis of alkyne-taxoid ( <b>2-15</b> ).....	58

### Chapter 3

Scheme 3.1. Synthesis of (2-mercapto-phenyl) acetic acid <b>3-2</b> .....	77
Scheme 3.2. Synthesis of 1,2-di(pyridine-2-yl)disulfane.....	77
Scheme 3.3. Synthesis of isothiuronium bromide salt and SH-alkyl linker .....	77
Scheme 3.4. First and second disulfide exchange reaction and TIPS protection.....	78
Scheme 3.5. Synthesis towards coupling-ready drug-linker-OSu activated ester <b>3-11</b> .....	79
Scheme 3.6. Synthesis towards coupling-ready drug-linker-C-fluorescein-OSu activated ester <b>3-14</b> .....	79
Scheme 3.7. Formation of biotin hydrazide <b>3-16</b> .....	80
Scheme 3.8. Formation of biotin-linker-taxoid (BLT) conjugate .....	80
Scheme 3.9. Modification of tetra ethylene glycol .....	81
Scheme 3.10. Synthesis of biotin-PEG-amine ( <b>3-22</b> ).....	81
Scheme 3.11. Synthesis of the biotin-PEG-linker-taxoid (BLT-S) conjugate .....	82
Scheme 3.12. Synthesis of the biotin-PEG-FITC probe ( <b>3-24</b> ).....	88
Scheme 3.13. Synthesis of the biotin-PEG-Fluorescein probe ( <b>3-25</b> ).....	88
Scheme 3.14. Synthesis of the 11-azido-3,6,9-trioxaundecanyl-1-methylsulfonate ( <b>3-27</b> )...90	



Scheme 3.15. Synthesis of the biotin-PEG-OMs (3-29).....	90
--	----

## Chapter 4

Scheme 4.1. Mono-Boc protection of 1,2-diamine .....	117
Scheme 4.2. Temperature-related tri-substitution.....	117
Scheme 4.3. Synthesis of biotin-triazine-linker-drug-azide intermediate (4-5).....	118
Scheme 4.4. Synthesis of cyclooctyne moiety and cyclooctyne-DPA( <i>sp</i> <sup>2</sup> N) trident chelating ligand 4-9.....	118
Scheme 4.5. Synthesis of rhenium tricarbonyl species .....	119
Scheme 4.6. SPAAC reaction .....	119
Scheme 4.7. Rhenium tricarbonyl chelation and Re-promoted methanolysis .....	120
Scheme 4.8. Synthesis of two click-ready cyclooctyne-DPA( <i>sp</i> <sup>3</sup> N) trident ligand .....	121
Scheme 4.9. SPAAC of cyclooctyne-DPA( <i>sp</i> <sup>3</sup> N) trident ligand .....	122
Scheme 4.10. Cold Synthesis of Biotin-Triazine-Linker-Drug-DPA( <i>sp</i> <sup>3</sup> N)- <sup>185</sup> Re(CO) <sub>3</sub> .....	123
Scheme 4.11. Synthesis of Biotin-DPA-Re(CO) <sub>3</sub> conjugate 4-21.....	123
Scheme 4.12. Synthesis of cyclooctyne-p-SCN-Bn-NOTA 4-24.....	124
Scheme 4.13. Synthesis of Biotin-Triazine-Linker-Drug-NOTA-Cu conjugate 4-26.....	125
Scheme 4.14. Synthesis of Biotin-NOTA-Cu conjugate 4-28.....	126

## Chapter 5

Scheme 5.1. Schematic of divergent synthesis of dendrimers.....	149
Scheme 5.2. PAMAM dendrimer growth from core to high generation .....	150
Scheme 5.3. Schematic of convergent synthesis of dendrimers.....	150
Scheme 5.4. Synthesis of bis(maleimido) butane and octane linkers.....	156
Scheme 5.5. Acylation of G1 dendrimer .....	158
Scheme 5.6. Synthesis of acetylated G1 PAMAM dendrimer with bis(maleimido) octane linker (5-4) .....	158
Scheme 5.7. Synthesis of two fully biotinylated dendrimers .....	159
Scheme 5.8. Formation of fully biotinylated half dendrons with linker mono adduct intermediate.....	161
Scheme 5.9. Synthesis of fluorescein functionalized G1 dendrimer 5-9.....	161
Scheme 5.10. Synthesis of fluorescein functionalized half dendron .....	161
Scheme 5.11. Attempts towards asymmetric PAMAM dendrimer conjugates.....	162
Scheme 5.12. Modification of PEG oligomer spacer.....	165
Scheme 5.13. Fully functionalization with PEGylated biotin on generation 3 PAMAMA dendrimer.....	166
Scheme 5.14. Fully functionalization with click-ready PEGylated terminal alkyne on generation 1 PAMAMA dendrimer.....	167
Scheme 5.15. Synthesis of Bis(maleimido) PEGylated Linker .....	170
Scheme 5.16. Synthesis of three click-ready intermediates .....	170
Scheme 5.17. Synthesis of asymmetric bow-tie dendrimer click-ready scaffold.....	171
Scheme 5.18. Synthesis Diagram of Asymmetric Bow-tie Dendrimer-based (ABTD) Conjugates.....	172
Scheme 5.19. Synthesis of intermediate 5-53.....	177

Scheme 5.20. Synthesis of intermediate <b>3-53</b> .....	177
Scheme 5.21. Third arm installation on intermediate <b>5-55</b> .....	177
Scheme 5.22. Synthesis of click-ready intermediate <b>5-57</b> .....	178
Scheme 5.23. One pot reaction of synthesis of intermediate <b>5-58</b> .....	178
Scheme 5.24. Double click reaction towards the final compound <b>5-59</b> .....	179
Scheme 5.25. Synthesis of G3-PEG-biotin half dendron with click-ready alkyne moiety .....	180
Scheme 5.26. Synthesis of click-ready azido-PEG <sub>3</sub> -FITC <b>5-61</b> .....	182
Scheme 5.27. Synthesis of G3-PEG-biotin half dendron-FITC construct via click reaction	182
Scheme 5.28. NHS activation of 4-pentynoic acid .....	185
Scheme 5.29. Fully functionalization on G3 dendrimer .....	185

## Chapter 6

Scheme 6.1. Synthesis of HA-alkyne intermediate.....	212
Scheme 6.2. Synthesis of HALT through click chemistry.....	212

## List of Tables

### Chapter 1

Table 1.1. Structure and Cytotoxicity ( $IC_{50}$ , nM) of Selected Second Generation Taxoids against various Cancer Cell Lines.....	24
--	----

### Chapter 2

Table 2.1. Spirolactams Formation of Fluorescein Methyl Ester with Amines.....	40
--	----

### Chapter 3

Table 3.1. Discrepancy of vitamin receptor overexpressed on the surface of various tumor cell lines.....	70
Table 3.2. Cytotoxicity Measurement ( $IC_{50}$ , nM) of Paclitaxel, SB-T-1214, BLT (3-17) and BLT-S (3-23) against BR+ and BR- cell lines.....	82
Table 3.3 Cytotoxicity Measurement ( $IC_{50}$ , nM) of Paclitaxel, SB-T-1214, and BLT-S (3-23) in the presence of GSH-OEt after internalization .....	83

### Chapter 4

Table 4.1. The most commonly used positron-emitting radionuclides in PET .....	109
Table 4.2. The most commonly used single-photon emitting radionuclides in SPECT .....	110

### Chapter 5

Table 5.1. Cytotoxicity ( $IC_{50}$ , nM) of paclitaxel, SB-T-1214, SB-T-1214-fluorescein, BLT-S and ABTD conjugates.....	174
---	-----

### Chapter 6

Table 6.1. Summary of biotin and hyaluronic acid binding to TTM receptors, CD133, and CD44 receptors in PPT2 and HCT116, as shown by flow cytometry .....	214
Table 6.2. Cytotoxicities ( $IC_{50}$ , nM) of paclitaxel, SB-T-1214, and BLT-S against various cell lines (WI38 lung fibroblast are negative for biotin).....	216

## List of Abbreviations

$\beta$ -LSM	$\beta$ -Lactam Synthase Method
$\delta$	chemical shift
$\Delta$	difference
$\lambda$	wavelength
ABC	ATP-binding cassette
ABTD	asymmetric bow-tie dendrimer
Ac	acetyl
ADC	antibody-drug conjugate
ATP	adenosine triphosphate
BLT	biotin-linker-taxoid
BMS	Bristol-Myers Squibb
Bn	benzyl
Boc	butoxycarbonyl
BR	biotin receptor
Bu	butyl
C	centigrade; carbon
CAN	cerium(IV) ammonium nitrate
CIC	cancer initiate cell
CD	cluster of differentiation
CFM	confocal fluorescence microscopy
CFPAC-1	human pancreatic carcinoma cell line
CML	chronic myelogenous leukemia
CSC	cancer stem cell
CuAAC	copper(I)-catalyzed azide-alkyne cycloaddition
CX-1	human colon adenocarcinoma cell line
d	doublet
DAB	deacetylcholine
DCM	dichloromethane
dd	doublet of doublets
DIC	<i>N,N'</i> -diisopropylcarbodiimide
DIPEA	<i>N,N</i> -diisopropylethylamine
DLAR	Division of Laboratory Animal Resources at Stony Brook University
DLD-1	human colon carcinoma cell line
DMAP	4-(dimethylamino)pyridine
DMF	<i>N,N</i> -dimethylformamide
DMSO	dimethyl sulfoxide
DNA	deoxyribonucleic acid
DNT	Dendritic Nanotechnologies, Inc <sup>®</sup>
DPA	di-picolylamine
DPC	di-2-pyridyl carbonate
dt	doublet of triplets
DVT	deep vein thrombosis
EC	Endocyte; electron capture (PET)
EDA	ethylenediamine

EDC	1-ethyl-3-(3-dimethylaminopropyl)carbodiimide
ee	enantiomeric excess
EGFR	epidermal growth factor receptor
EPR	enhanced permeability and retention time
ESI	electrospray ionization
Et	ethyl
eV	electronvolt
FA	folic acid
FDA	U.S. Food and Drug Administration
FDG	2-[ <sup>18</sup> F]fluoro-2-deoxy-D-glucose
FITC	fluorescein isothiocyanate
FR	folate-receptor
g	gram
G	generation
GSH	glutathione reduced form
GTP	guanoside-5'-triphosphate
h	hour
HA	hyaluronic acid
HALT	Hyaluronic Acid-Linker-Taxoid
HF	hydrogen fluoride
HPLC	high-performance liquid chromatography
HRMS	high-resolution mass spectrometry
HSA	human serum albumin
HT-29	human colon cancer cell line
Hz	hertz
IC <sub>50</sub>	half-maximum inhibitory concentration
ID8	murine ovarian cancer cell line
IDN	Investigational New Drug
IT	isomeric transition
<i>J</i>	coupling constant
k	kilo- (scale)
L	liter
L1210FR	murine leukemia cell line
L1210	murine leukemia cell line
LC	liquid chromatography
LDA	lithium diisopropylamide
LHMDS	lithium bis(trimethylsilyl)amide
m	milli- (scale); multiplet (NMR)
M	mega- (scale); molar
μ	micro- (scale)
m/z	mass-to-charge ratio
mAb	monoclonal antibody
MALDI	Matrix-assisted laser desorption/ionization
MAP	microtubule-associated protein
MCF-7	human breast carcinoma cell line
MCF-7R	(see NCI/ADR-RES)

MDR	multidrug resistant
Me	methyl
Mg	magnesium
min	minute
mol	mole
MP	melting point
MRI	magnetic resonance imaging
Ms	mesyl (4-methanesulfonyl)
MS	mass spectrometry
MTT	3-(4,5-dimethylthiazol-2-yl)-2,5-diphenyltetrazolium bromide
MTX	methotrexate
MX-1	human breast carcinoma cell line
n	nano- (scale)
NBD	nucleotide-binding domain
NCI	National Cancer Institute
NCI/ADR-RES	platinum-resistant metastatic ovarian cancer cell line
NHS	<i>N</i> -hydroxysuccinimide
NM	nuclear medicine
NMR	nuclear magnetic resonance
NOTA	1,4,7-triazacyclononane- <i>N,N',N''</i> -triacetic acid
NP	nanoparticle
NSCLC	non-small cell lung cancer
HYNIC	Hydrazinonicotinic acid
<i>p</i>	<i>para</i>
PAMAM	poly (amidoamine)
PAMAMOS	poly (amidoamine-organosilicon)
PBS	phosphate buffered saline
PEG	polyethylene glycol
PET	positron emission tomography
Pgp	P-glycoprotein
Ph	phenyl
PMP	para-methoxyphenyl
PPI	poly (propylene imine)
ppm	parts per million
PTX	paclitaxel (Taxol®)
PUFA	polyunsaturated fatty acid
py	pyridine
q	quartet
Rf	retention factor
RME	receptor-mediated endocytosis
RNA	ribonucleic acid
RPMI	Roswell Park Memorial Institute medium
s	singlet
S	aqueous solubility promoted
SAR	structure-activity relationship
SB-T	Stony Brook taxoid

SCID	severe combined immunodeficient
SET	single-electron transfer
SPAAC	Strain-Promoted Alkyne-Azide Cycloaddition
SPECT	single-photon emission computed tomography
SS	disulfide bond
Su	succinimide
t	time; triplet (NMR)
<i>t</i>	<i>tert</i>
TACN	triazacyclononane
TBDMS/TBS	tert-butyldimethylsilyl
Tc	thiophene-2-carboxylate; technetium (SPECT)
TCEP	Tris-(2-Carboxyethyl)phosphine
TEA	triethylamine
TES	triethylsilyl
TFA	trifluoroacetic acid
TIPS	triisopropylsilyl
THF	tetrahydrofuran
TLC	thin-layer chromatography
TMS	trimethylsilyl
TOF	time-of-flight
TPPO	Triphenylphosphine oxide
$t_R$	retention time
Ts	tosyl (4-toluenesulfonyl)
TTDDS	tumor-targeted drug delivery system
TTM	tumor-targeting module
US	ultrasound
UV	ultraviolet
WI38	normal human lung fibroblast

## Acknowledgments

I would like to thank my dissertation advisor, Distinguished Professor Iwao Ojima, with my sincerest gratitude. I am so fortunate to have received my multidisciplinary training in your laboratory, including synthetic organic chemistry, medicinal chemistry, polymer science, cell biology, and pharmaceutical sciences for six years. With your guidance and mentorship, I gradually grew up to an independent, productive, and responsible scientist. I appreciate every challenge you gave to me which made my brain not dead, I appreciate every critical comment you had on me which kept me away from nonsense, and I appreciate every moment you support me which allow me to stand on your shoulder and see farther. I also would like to thank you and your wife Mrs. Yoko Ojima for every party you prepared at your home which embraced and cheered my wandering soul and homesick heart.

I also would like to thank my dissertation committee members, Professor Nancy Goroff and Professor Elizabeth Boon for their scientific insights and advice for my Ph.D. program. And I would like to extend my utmost appreciation to Professor Balaji Sitharaman for his willingness to serve as an outside member for my defense.

In addition, I want to thank Dr. Galina Botchkina for her mentorship on cell biology, and Dr. Anne Savitt for responding my cell request in a timely manner. I also want to thank Dr. Jonathan Rudick for his helpful advice and insights for my project. And I want to also thank Dr. Guo-Wei Tian (Central Microscopy Imaging Center), Research Flow Cytometry Core Facility Staff for their contribution to cell based experiments. Besides, I really want to thank Dr. Błażej Ruzsicska a lot for his mentorship and contribution on mass spectrometry and I hope everything will be getting better for him. And I would like to thank Dr. Jim Marecek and Dr. Francis Picart for their diligent work and help for NMR spectrometry.

I learned my chemistry courses from Professor Iwao Ojima, Nancy Goroff, Kathlyn Parker, Daniel Raleigh, Robert Rizzo and I appreciate their input for my research knowledge. I also want to thank Professor Frank Fowler, Joseph Lauher, Dr. Zackary Katsamanis, Dr. Rong Chen and Mrs. Kuan for their support and guidance for my TA assistant in organic lecture and laboratory courses. I also would like to thank Mrs. Roxanne Brockner from ICBDD for her assistant in lab chemical ordering, and all the staff working in the Stony Brook Chemistry Department.

I want to thank Mrs. Patricia Marinaccio for being a big Mom for the Ojima lab including me. She is always supportive and reliable without hesitations. I had an unforgettable experience with all previous and current postdoc, graduate, undergraduate and high school students who I met in the lab. Also I want to thank all of the chemistry students in this building, especially the 7<sup>th</sup> floor chemistry students for allowing me to borrow chemicals and solvents.

Most importantly, I would like to thank my friends and family for their continuous love and support. I cannot be here and be what I am without my parents for their years support. I met my wife Yuchen Liu here in Stony Brook and she dedicated so much for helping me go through the most difficult time. And I spent a really good time with my friends whom I met in Stony Brook. I also want to thank my landlord who accepted and took care of me and my wife like their family members. And I would like to thank everyone who helped me but not be mentioned above.



## Vita

### Education

State University of New York at Stony Brook, Stony Brook, NY  
Doctor of Philosophy Candidate in Chemistry, 2015

Nankai University, Tianjin, China  
Bachelor of Science in Chemistry, 2008

### Peer-reviewed Publications and Patents

Iwao Ojima, **Tao Wang**, and Yu-Han Gary Teng. Synthesis of novel asymmetric bow-tie pamam dendrimer-based conjugates for tumor-targeting drug delivery. *PCT Int. Appl.* **2015**, WO 2015038493.

Iwao Ojima, Jacob G. Vineberg, and **Tao Wang**. “Triazine-Based Tripod Linker System for Drug Delivery and Diagnosis”, US Provisional Patent Appl. 61/954,908 (filed on 3/18/2014); Iwao Ojima, Jacob G. Vineberg and **Tao Wang**. “Therapeutic Agent for Treating Tumors”, International Patent Application, PCT/US 2015/038493 (filed on 3/18/2015).

Jacob G. Vineberg, **Tao Wang**, Edison S. Zuniga, and Iwao Ojima. Design, Synthesis, and Biological Evaluation of Theranostic Vitamin-Linker-Taxoid Conjugates. *J. Med. Chem.* **2015**, 58 (5), pp 2406–2416. DOI: 10.1021/jm5019115.

**Tao Wang**, Yu-Han Gary Teng, Longfei Wei, Wei Li, Bela Ruzsicska, and Iwao Ojima. Design, Synthesis, and Biological Evaluations of Novel Asymmetric Bow-Tie PAMAM Dendrimer-based Conjugates for Tumor-Targeted Drug Delivery. *J. Am. Chem. Soc.* (to be submitted shortly).

**Tao Wang**, Longfei Wei, and Iwao Ojima. Design and Synthesis of Tumor-Targeting Drug Conjugates for PET/SPECT/MRI Imaging Study. *J. Org. Chem.* (to be submitted shortly).

Joshua D. Seitz, **Tao Wang**, Jacob G. Vineberg, and Iwao Ojima, “Synthesis of a Next-Generation Taxoid by Rapid Methylation Amenable for [11C]-Labeling”. *J. Org. Chem.* (to be submitted shortly)

### Selected Presentations

Longfei Wei, **Tao Wang**, Yu-Han Gary Teng, and Iwao Ojima. “Design and synthesis of a novel tri-branched asymmetric bowtie PAMAM dendrimer-based drug conjugate as a cancer theranostic agent”. Poster Presentation, 249<sup>th</sup> ACS Meeting, Denver, CO, 2015.

**Tao Wang**, Yu-Han Gary Teng, Longfei Wei, Wei Li, Bela Ruzsicska, and Iwao Ojima. “Design, Synthesis, and Development of a Novel PAMAM-Based Asymmetric Bow-Tie Dendrimer (ABTD) Platform for Tumor-Targeted Drug Delivery.” Poster Presentation, 248<sup>th</sup> ACS Meeting, San Francisco, CA, 2014.

Jacob Vineberg, **Tao Wang**, Joshua Seitz, Joanna S. Fowler, and Iwao Ojima. “Development of robust tumor-targeted drug delivery system (TTDDS) platform and its applications to novel taxane-based drug conjugates with biotin as the tumor-targeting module.” **Oral Presentation**, 247<sup>th</sup> ACS Meeting, Dallas, TX, 2014.

**Tao Wang**, Gary Yu-Han Teng, Longfei Wei, Wei Li, and Iwao Ojima. “Synthesis and biological evaluation of novel asymmetric bow-tie PAMAM dendrimer-based tumor-targeting drug conjugates.” **Oral Presentation**, 246<sup>th</sup> ACS Meeting, Indianapolis, IN, 2013.

### **Certification Programs**

Fundamentals of the Bioscience Industry Program, Center for Biotechnology, Stony Brook University, 2015

### **Honors and Awards**

Chemistry Department Award for Outstanding Doctoral Student, Stony Brook University, 2015

Sigma Xi Travel Award, 2015

Ajinomoto Travel Award, 2014

### **Memberships**

American Chemical Society, 2012-present

New York Academy of Sciences, 2012-present

Fundamentals of Biosciences Industry Alumni Network Executive Committee Member, May 2015-present

## **General Introduction**

§0.1 Cancer.....	2
§0.2 The Hallmarks of Cancer.....	2
§0.3 Current Strategies for Cancer Treatment.....	3
§0.4 Issues in the Current Chemotherapy.....	4
§0.5 Tumor-Targeted Chemotherapy.....	5
§0.6 Outline of Chapters.....	9
§0.7 References .....	12

## General Introduction

### §0.1 Cancer

Cancer is a collection of diseases characterized by the rapid proliferation and uncontrolled growth of abnormal cells. These abnormal cells lose the sensitivity to anti-grow signals, develop sustained angiogenesis, divide with limitless potential, evade apoptosis and have the tendency to spread and invade surrounding tissue or implant into distant tissues through the blood stream circulation, resulting in metastasis. The cause of cancer can be divided into internal factor such as inherited genetic mutation and malfunction, and external factors including smoking tobacco, sunlight exposure, chemical or radiation exposure, unhealthy diet, physical inactivity, obesity and infectious organism.

Cancer remains the major public health problem that leads to numerous deaths throughout the world. In a recent study, cancer ranked 2<sup>nd</sup> among the leading causes to death by age and sex in US, only exceeded by heart disease, accounting nearly a quarter of all deaths. In addition, the number of reported cancer cases is still increasing. It has been estimated that about 1,658,370 new cancer cases are expected to be diagnosed in the US (**Figure 0.1**)<sup>1</sup>, and around 589,430 Americans are expected to die of cancer, approximately 1,620 people per day in 2015.<sup>2</sup> Furthermore, it has been estimated that the global burden is expected to grow to 21.7 million new cancer cases and 13 million cancer deaths simply due to the growth and aging of the population by 2030.<sup>3</sup> To develop effective treatment for cancer, it requires understanding the nature of cancer and how it grows and spreads in the human body.

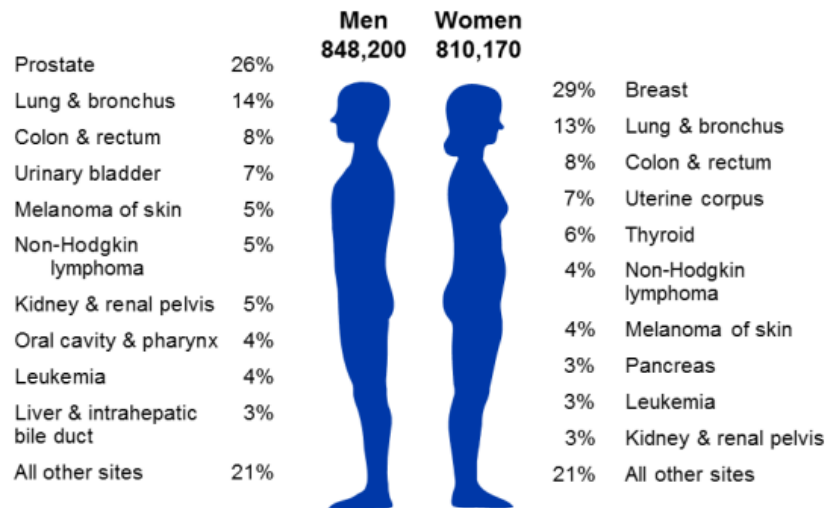


**Figure 0.1** Estimated new cancer cases in the US in 2015 (reprinted from reference 1)<sup>1</sup>

### §0.2 The Hallmarks of Cancer

Several lines of evidence indicate that tumor genesis in humans is a multistep process and that these steps reflect genetic alterations that drive the progressive transformation of normal human cells into highly malignant derivatives. The tumor genesis might be triggered by carcinogens, such as chemicals, radiations, or infectious agents. Typically, they increase the risk of cancer by altering cellular metabolism or damaging DNA directly in cells. The damaged cells

will not undergo the programmed cell death, resulting in loss of respect for normal tissue boundaries. The abnormal cells will gain the ability to become more established in diverse tissue environments, and accumulate to form malignant tumor.

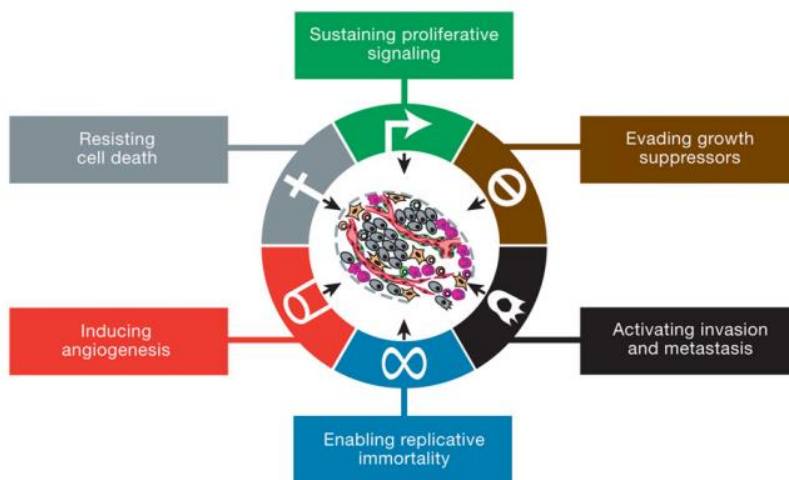


**Figure 0.2** The hallmarks of cancer (reprinted from reference 4)<sup>4</sup>

Tumor are more than insular masses of rapid proliferating cancer cells. The biology of tumors can no longer solely based on the understanding of cancer cell traits. Consequently, over the past decade, six hallmarks of cancer have been proposed to provide a useful conceptual framework for solid foundation and understanding of complex biology and chemical mechanism of cancer.<sup>4,5</sup> Various therapeutic approaches hold promise as cancer therapeutics by targeting the hallmarks of cancer. Novel medicines were developed for interfering with each of the acquired capabilities necessary for tumor growth and progression had been developed and are in clinical trials or in some cases approved for clinical use in treating certain forms of human cancer.<sup>4</sup>

### §0.3 Current Strategies for Cancer Treatment

Although extensive efforts have been made, currently there is no well-established cure-all treatment for cancer. Primary cancer treatment options include surgery, chemotherapy, radiation, immunotherapy, hormonal suppression, gene therapy, and targeted therapy. Usually depending on the stage and progression of the disease as well as tumor accessibility, a single method or a combination of different treatment options is employed. Whereas surgery and radiation are both localized treatments, chemotherapy is an invasive systemic therapy capable of treating even micrometastases that would otherwise escape detection. Chemotherapy relies on the use of chemical and biochemical agents as anti-cancer drugs to kill the cancerous cells and prevent them from growing and spreading in the body. Many classes of chemotherapeutic agents have been discovered for different cancer treatment approaches, including microtubule stabilizing agents (paclitaxel), topoisomerase inhibitors (topotecan), thymidylate synthase inhibitors (5-fluorouracil), DNA alkylating agents (cisplatin), and protein kinase inhibitors (Gleevec®). To achieve the maximum therapeutic results, two or more drugs are used in combination (combination chemotherapy) to block different processes of cell division based on non-overlapping mechanisms of action.

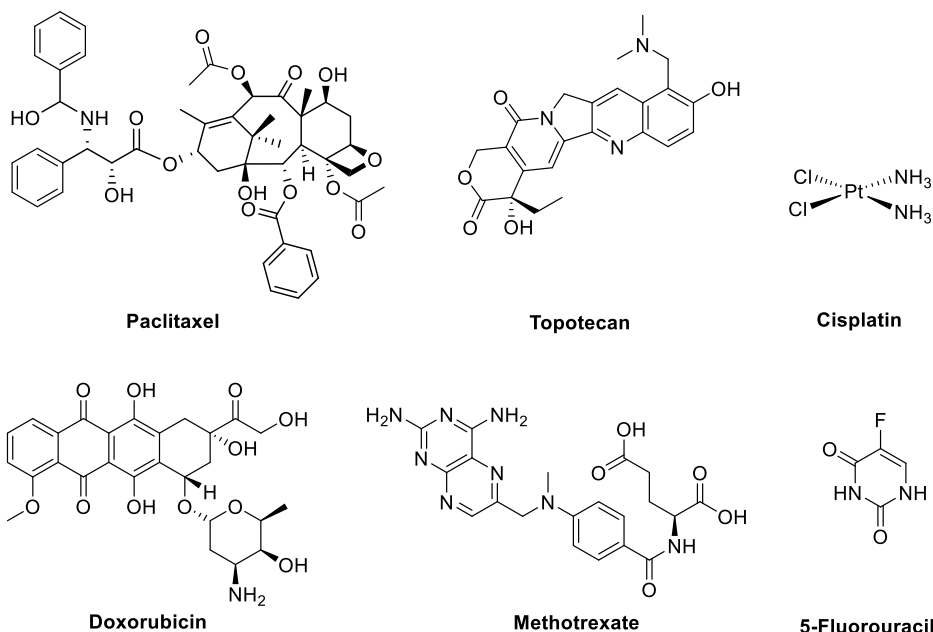


**Figure 0.3** Selected examples of chemotherapeutic agents

#### §0.4 Issues in the Current Chemotherapy

Multidrug resistance (MDR) is one of the major obstacles of current chemotherapy. It is the principal mechanism in which cancer cells develop resistance to chemotherapeutic agents.<sup>6</sup> During chemotherapeutic treatment, drugs only kill drug-sensitive cells but have limited effectiveness against drug-resistant cells. These remaining drug-resistant tumor cells can survive and result in the continuous growth of tumor. Many factors may increase the MDR including decreased cell wall permeability of chemotherapeutic agents, altered drug-target sites induced by gene-mutation, increased cell gene mutation rates caused by continuous drug treatment, or cell efflux process of hydrophobic drugs. Therefore, new drugs need to be developed with increased efficacy against MDR cancers.

Another important reason that may lead to the failure of current chemotherapy is lack of tumor specificity. Traditional chemotherapy relies on the premise that the rapidly proliferating tumor cells are more likely to be killed by cytotoxic agents than normal cells. However, these highly potent drugs have limited specificity and selectivity towards cancer cells which often cause undesired severe side effects, such as damage to kidney and bone marrow, hair loss, a compromised immune system, bleeding, and fatigue.

The developments of imatinib mesylate (Gleevec®) and erlotinib hydrochloride (Tarceva®) (Figure 0.4) were remarkable for the treatment of certain cancers, such as chronic myelogenous leukemia (CML), non-small cell lung cancer (NSCLC) and pancreatic cancer. As FDA approved in 2001, Gleevec specifically targets Abl tyrosine kinase which is overexpressed in CML cells.<sup>7</sup> And Tarceva specifically targets the epidermal growth factor receptor that is mutated in different types of cancers. However, due to the complicated cancer mechanism,<sup>5</sup> the use of these targeted-therapies is only limited to specific cancer types.

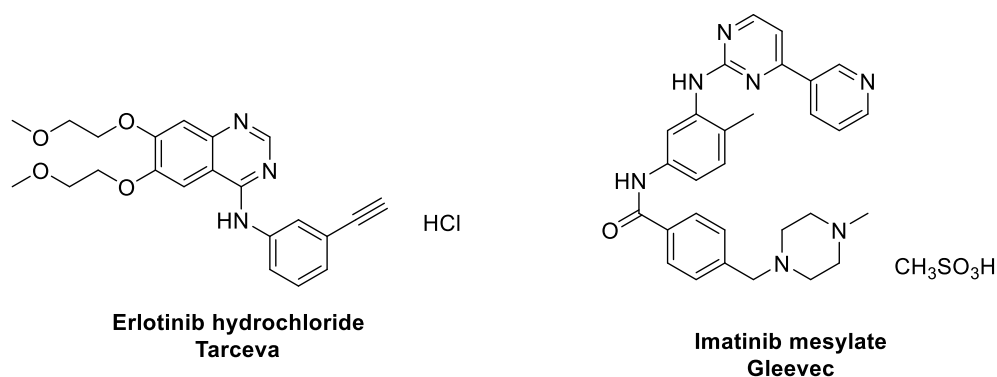


**Figure 0.4** Chemical structures of Gleevec and Tarceva for targeted therapy

Accordingly, cancer-specific/cancer-targeting anti-cancer agents require to be designed. If the modified anti-cancer agent can have specificity towards the cancer cells, it is very likely that patients can take lower doses of the drug to maintain the drug's effect without causing systemic toxicity. Thus, extensive efforts have been made for developing tumor-specific delivery systems to overcome the shortcomings of conventional chemotherapy in the last few decades.<sup>8-9</sup>

### §0.5 Tumor-Targeted Chemotherapy

In general, a tumor-targeted drug conjugate is designed for built-up of a tumor recognition moiety and a cytotoxic agent connected directly or through a suitable linker. **(Figure 0.5)** A tumor-targeted drug conjugate relies on the tumor-targeting module to guide the drug by specifically targeting cancer cells and assist the drug conjugate internalization via receptor-mediated endocytosis. Direct linkage by a covalent bond may result in reduction of the activity and toxicity. The cytotoxic agent may not be efficiently cleaved or not released in its original form. Therefore, a suitable linker or vehicle is designed to connect the tumor-targeting moiety with drug, and control the release of the drug at the tumor site. The linker should be stable during blood circulation to keep the pro-drug inactive, and readily be cleaved to release the drug in its active form and restore its biological activity.<sup>10</sup> **(Figure 0.6)**

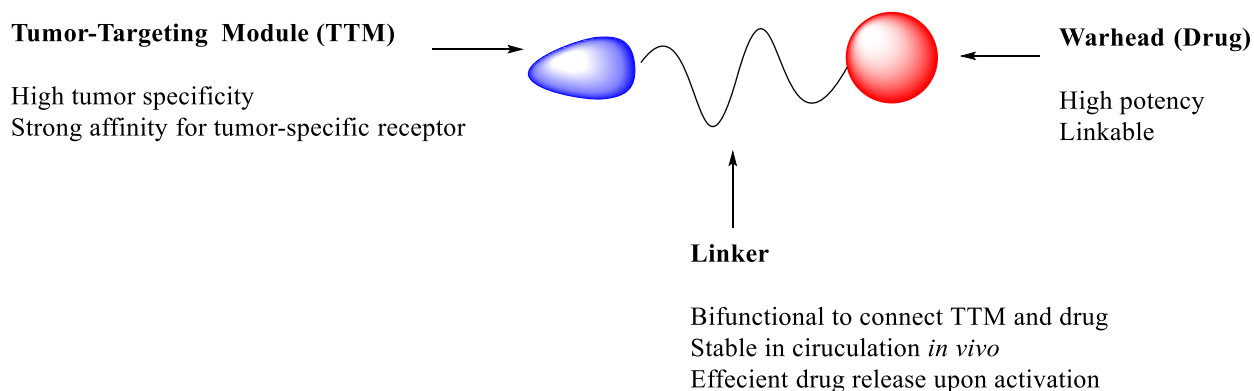


**Figure 0.5** Key features of a tumor-targeted drug conjugate

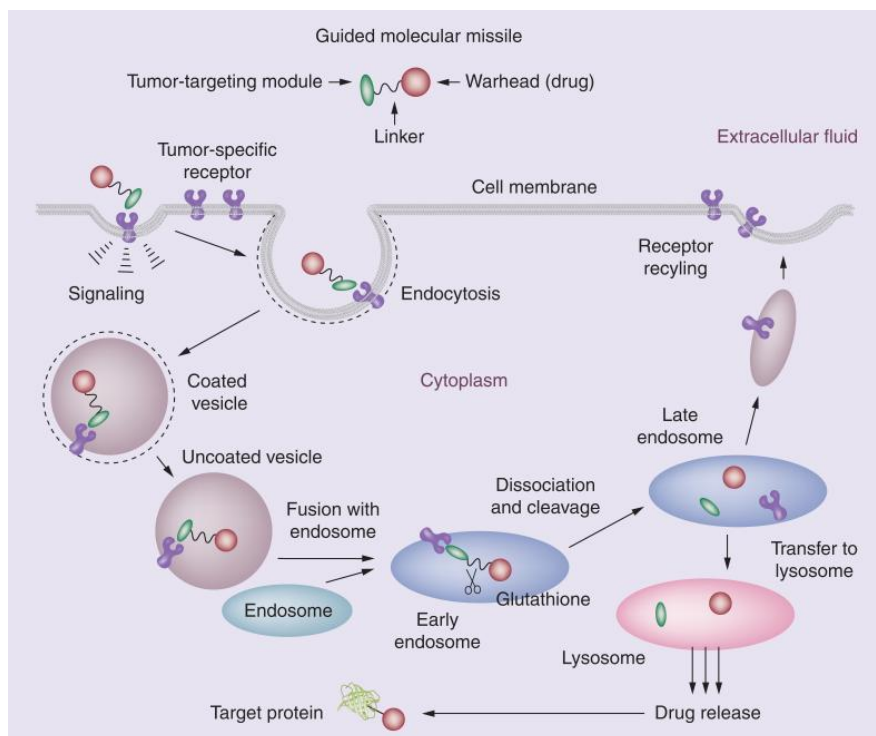


**Figure 0.6** Receptor-mediated endocytosis of TTM-linker-drug conjugate (reprinted from reference 11)<sup>11</sup>

Rapidly growing cancer cells require various nutrients and vitamins so that certain cancer-specific receptors are overexpressed to enhance the uptake. These receptors can be used as targets to deliver the cytotoxic drugs specifically to the cancer cells via receptor-mediated endocytosis (RME). Various ligands including monoclonal antibodies (mAbs),<sup>12-16</sup> polyunsaturated fatty acids (PUFAs),<sup>17-18</sup> biotin<sup>19-20</sup>, folic acid,<sup>21-22</sup> transferrin,<sup>23</sup> oligopeptides,<sup>24</sup> aptamers<sup>25</sup> and hyaluronic acid<sup>26</sup> (**Figure 0.7**) have been studied as tumor-targeting moieties (TTMs) to construct the tumor-targeted drug conjugates.

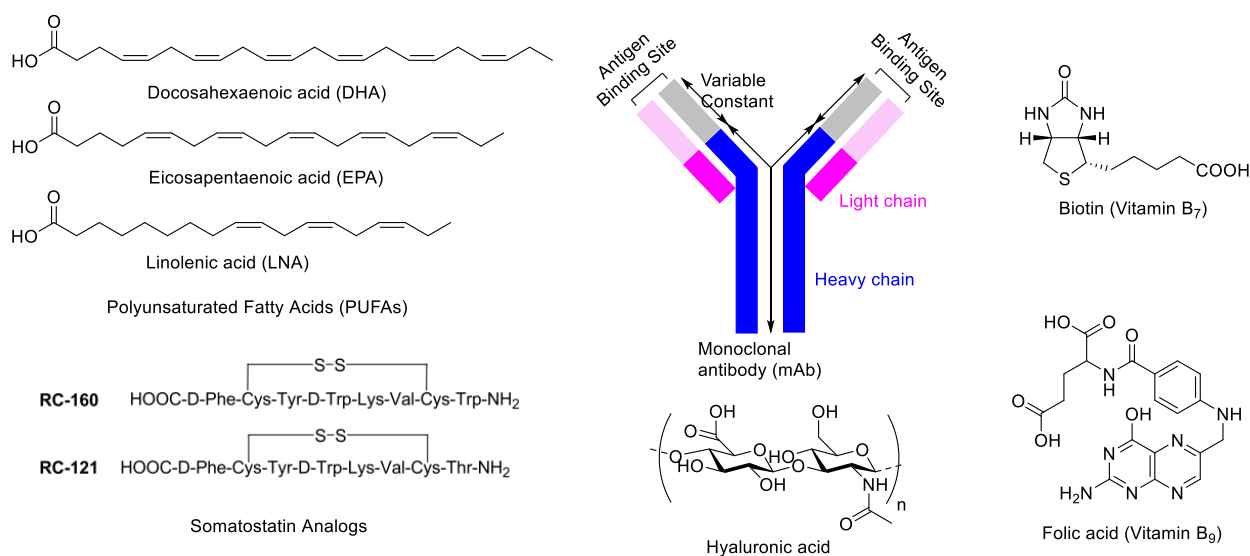


**Figure 0.7** Selected examples of tumor-targeting moieties (adapted from reference 27)<sup>27</sup>



To connect drug to tumor-targeting module effectively and under mild chemistry conditions, commonly used linkers can be categorized into four classes on the basis of their cleavage modes: acid labile linker, proteolytic linker, disulfide linker and hydrolytic linker. Examples of several types of cleavable linkers are shown in **Figure 0.8**.<sup>28</sup>

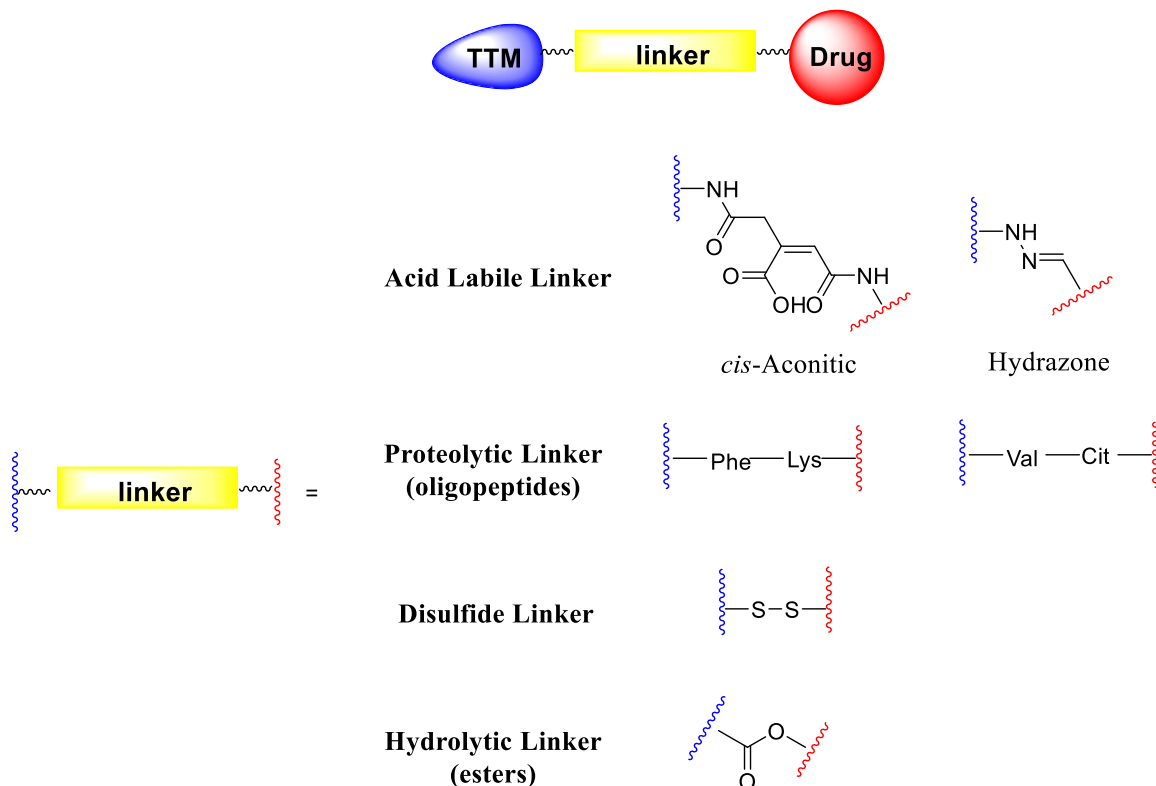


**Figure 0.8** Various types of linkers commonly used for tumor-targeting drug conjugate (adapted from reference 28)<sup>28</sup>

An imaging agent can simply be attached to the drug moiety to construct theranostic tumor-targeted drug conjugates for *in vitro/in vivo* biological evaluations. However, this model has to chemically modify the drug structure which will result in the loss of potency without release in its original form. Instead, the linker can be modified to afford an additional branch to attach the imaging agent, for example, a fluorescent probe, a radionuclide for PET (Positron Emission Tomography)/SPECT (Single-photon Emission Computed Tomography) imaging study, or a MRI (Magnetic resonance imaging) contrast agent.

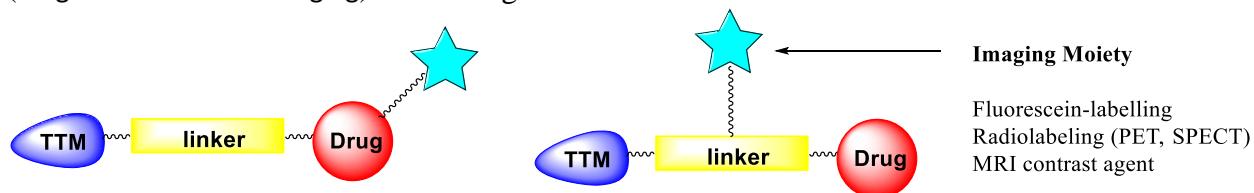


**Figure 0.9** Two models of incorporation of imaging moiety to drug conjugate

Macromolecular tumor-targeted drug conjugates can also be obtained by application of suitable nano-sized vehicles or carriers. (**Figure 0.10**) Compared to small molecule drug

conjugates, enhanced accumulation of nano-sized drug conjugates within tumor tissues have been found due to EPR (enhanced permeability and retention) effect which will be discussed in Chapter 5. In addition, nano-sized carriers with highly symmetric structures or repeating units possess multiple functional groups which can largely increase the payload of tumor-targeted module for enhanced receptor-mediated endocytosis, chemotherapeutic agents for enhanced efficacy, and imaging agent for increased imaging signal strength. These nano-sized tumor-targeted drug conjugates may overpass the efflux mechanism resulting in the increased concentration of released chemotherapeutic agents inside the cancer cells. Therefore these macromolecular drug conjugates are also referred to “Trojan horse” prodrugs.

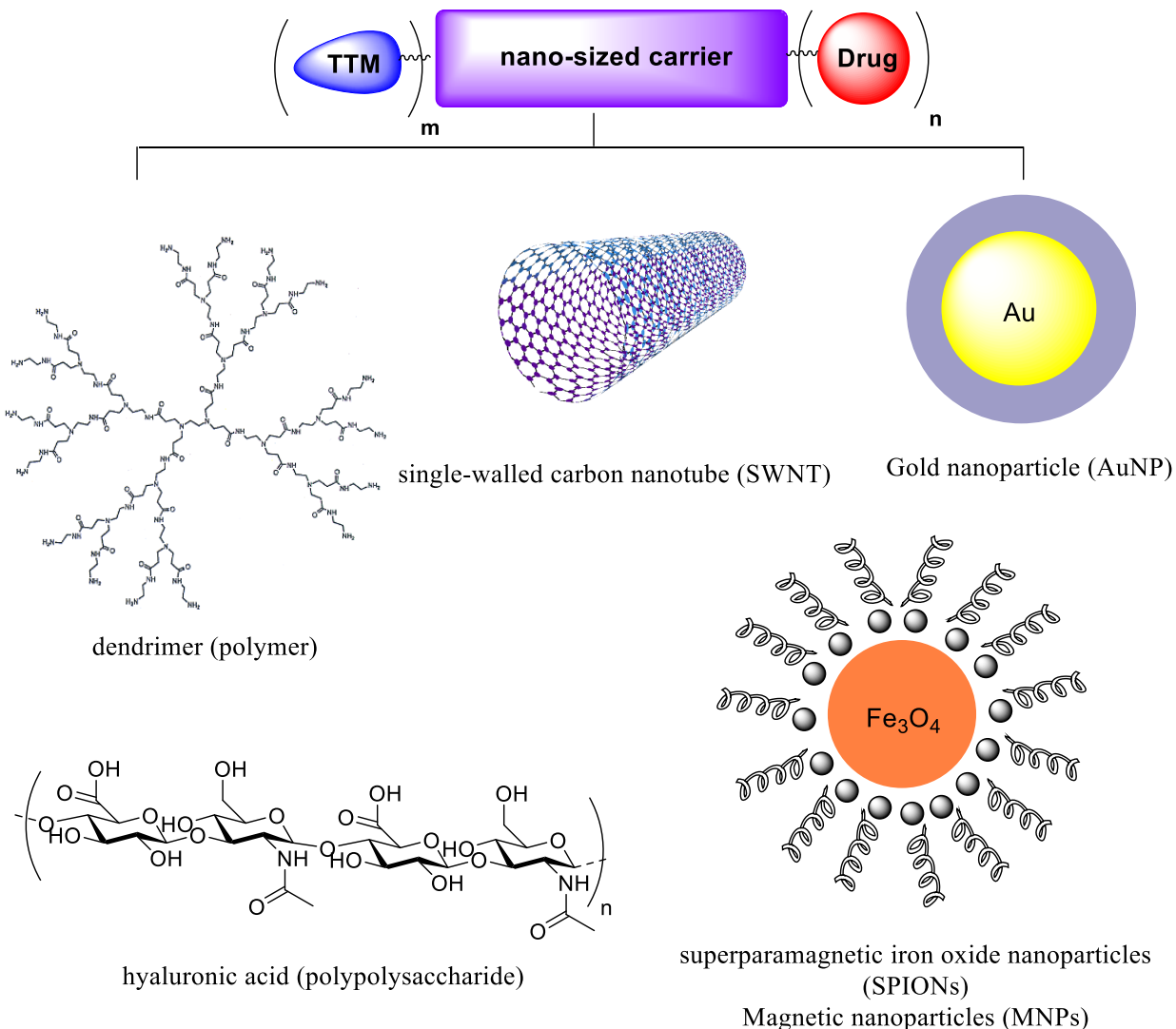


**Figure 0.10** Selected examples of nano-sized carriers

## §0.6 Outline of the Thesis

This section is used to clarify the previous research work related to the contents including reaction schemes and compounds presented in this thesis, as well as the new and unpublished research results by chapters.

In Chapter 1, the (3*R*,4*S*)-1-(*tert*-butoxycarbonyl)-3-triisopropylsiloxy-4-(2-methylpropen-2-yl)azetidin-2-one ((+) **1-6**) was synthesized based on the published synthetic protocol. The enantiopure (+) **1-6** was obtained in good overall yield and used as the side chain toward the semi-synthesis of second generation taxoid **SB-T-1214**. The SAR study to identify second generation taxoid **SB-T-1214** as drug candidate was previously done in Ojima lab. The **SB-T-1214 (1-10)** was resynthesized following the published synthetic protocol from modification of 10-DAB III in overall good yield.

In Chapter 2, application of taxoid as fluorescein-labelled and radio-labeled imaging agents was developed. To obtain fluorescein derivatives towards synthesis of new taxoid-fluorescent probe **SB-T-1214-C7-fluorescein (2-8)**, biotin-fluorescent probes (**3-25**), dendrimer-fluorescent probes (**6-11, 6-12, and ABTD-3**), and tribranched fluorescent core (**5-59**), two new fluorescein compounds **2-4 A** and **2-4 B** were synthesized following the published protocol, but with different protecting groups on C2' position (isopropyl and isobutyl groups, respectively). The rapid methylation *via* Stille coupling reaction toward <sup>11</sup>C-labeled **SB-T-1214** radiotracer for PET imaging study was also demonstrated in Chapter 2. The cold synthesis in the presence of Pd and Cu co-catalysts was run based on the previous established reaction condition developed by Dr. Joshua Seitz. The starting material stannylvinyl-taxoid (**2-9**) was also prepared by Dr. Joshua Seitz. Previous LC/UV/MS-TOF analytic method development for the cold synthesis was done by Dr. Jacob Vineberg and Dr. Bora Park, but only under positive mode. Several new but unknown taxoid-based derivatives were only detected from the LC/UV/MS-TOF without defined structures and isolated form. In this thesis, the LC/UV/MS-TOF analysis methods were well established using negative mode to observe parent ions and their acetate and trifluoroacetate adduct ions. In addition, the target screening function of LC/UV/MS-TOF was utilized to confirm seven predicted structures (**Figure 2.12**) by target compound mass value input and screening. The program successfully identified peaks matching the interested mass values with discrete retention times. Accordingly, three new taxoid-based derivatives Tc-taxoid (**2-11**), Ph-taxoid (**2-12**), and alkyne-taxoid (**2-15**) were synthesized and isolated by preparative HPLC. These compounds retention times were identified using pure samples which were all in consistent with the corresponding peaks from the cold synthesis reaction mixture LC trace. One of the key findings was identification of Tc-taxoid (**2-11**) by high-resolution mass spectrum. Its corresponding peak in the reaction mixture was thought to be iodo-taxoid (**2-10**) intermediate with only 0.0799 mass value difference. High-resolution mass spectrum clearly differentiated these two compounds, and retention times of these two compounds were also measured with around 2 minute's difference (21.25 min for Tc-taxoid and 19.44 min for iodo-taxoid, respectively). Another key finding was detection of allene-taxoid (**2-14**) and alkyne-taxoid (**2-15**) with identical mass values but different retention times, which were possibly generated during beta-hydride elimination (**Figure 2.19**). On the basis of new important findings, a comprehensive and more complicated mechanism for Stille coupling reaction was proposed to explain the formation of each identified taxoid-based derivatives as **Figure 2.20**.

In Chapter 3, three biotin-disulfide linker-taxoid conjugates (**Figure 3.7, 3.8 and 3.9**) were designed by Dr. Manisha Das, Dr. Joshua Seitz, and Dr. Jacob Vineberg, and synthesized/currently

being synthesized. The recent time-resolved  $^{19}\text{F}$  NMR (**Figure 3.4, 3.5 and 3.6**) was done by Dr. Joshua Seitz, Dr. Jacob Vineberg, Longfei Wei and other group members to validate the glutathione triggered self-immolative disulfide linker cleavage for tumor-targeted drug delivery. The disulfide linker component **3-8** was resynthesized following the published protocol, and was used to resynthesize BLT (**3-17**) and BLT-S (**3-23**) described in this thesis. These two biotin-linker-taxoid drug conjugates have been previously obtained in our lab, but the cytotoxicity measurement against different cell lines (BR+ and BR-) with paclitaxel and SB-T-1214 as controls were first measured in this thesis (**Table 3.2**). Moreover, the cytotoxicity measurement in the presence of glutathione ethyl ester addition against two biotin-receptor overexpressing cancer cell lines (MX1 and ID8) to fully release drug moiety from the internalized drug conjugates were demonstrated in this chapter (**Table 3.3**). The *in vivo* biological evaluation on SCID mice bearing MX-1 tumor xenograft using BLT was previously done by Jean Rooney and Dr. Thomas Zimmerman at the Division of Laboratory Animal Resources (DLAR) at Stony Brook University. The tested compound BLT was prepared by Dr. Joshua Seitz. For visualizing the internalization of biotin-bearing conjugates, three biotin-bearing fluorescent or fluorogenic probes were designed, prepared and analyzed by Dr. Shuyi Chen (**Figure 3.12**). A solubility improved fluorescent probe biotin-PEG-FITC (**3-23**) was designed by Dr. Jacob Vineberg for examination of biotin receptor expression level against several cell lines (**Figure 3.17**). So biotin-PEG-FITC (**3-24**) was resynthesized in gram scale, and another new fluorescent probe biotin-PEG-fluorescein (**3-25**) was synthesized to investigate the internalization rate and saturation vs recycle of biotin receptor on the surface of cancer cells (**Figure 3.18 and 3.19**).

In Chapter 3, a biotin-PEG-F probe towards fluorine-18 radiolabeled PET tracer (**Figure 3.20**) was previously designed and synthesized by Dr. Jacob Vineberg. The radiosynthesis and semi-preparative HPLC purification method for cold synthesis has been developed in our lab and hot synthesis and separation was done in collaboration with Dr. Joanna S. Fowler in Brookhaven National Laboratory (BNL). To apply this PET tracer for *in vivo* biological assay, the key precursor biotin-PEG-OMs (**3-29**) was resynthesized following the protocol provided by Dr. Jacob Vineberg and obtained in overall good yield. This intermediate was kept in  $-20\text{ }^{\circ}\text{C}$  freezer ready for radiosynthesis.

Extended imaging studies were discussed in Chapter 4. A robust and versatile 1,3,5-triazine-based tripod platform (**Figure 4.8**) was designed by Dr. Jacob Vineberg for constructing theranostic PET tracer bearing triazine core (tripod splitter), biotin (tumor-targeting module), SB-T-1214 (cytotoxic agent) and fluorine-18 (radisotope for PET imaging) moieties. Cold synthesis has been done and the resulting final conjugate has been used for cytotoxicity measurement results. HPLC analysis condition for radiosynthesis has also been done with optimized separation condition previously. In this thesis, this tripod platform was modified to incorporate longer half-life radioisotopes copper-64 and technetium-99m for PET and SPECT imaging, respectively (**Figure 4.9**). For cold synthesis,  $^{65}\text{Cu}$  and  $^{185}\text{Re}$  were used as surrogates to establish the separation HPLC methods of final conjugates. Two chelating arms bearing a 1,4,7-triazacyclononane-*N,N',N''*-triacetic acid (NOTA) moiety and a di-picolylamine (DPA) moiety for capturing  $^{65}\text{Cu}$  and  $^{185}\text{Re}$ , respectively. Since the previous design for incorporation of third arm with imaging moiety *via* CuAAC (Copper-Catalyzed Alkyne-Azide Cycloaddition) click reaction was not applicable in the presence of the chelating arms, the most important modification of the platform shown in this thesis was establishment of SPAAC (Strain-Promoted Alkyne-Azide Cycloaddition)

as copper-free click method to install the chelating arm on the tripod platform. Accordingly, a cold theranostic probe biotin-triazine-linker-drug-NOTA-<sup>65</sup>Cu conjugate (**4-26**) and a cold diagnostic probe biotin-triazine-NOTA-<sup>65</sup>Cu (**4-28**) towards PET imaging study were synthesized and purified by preparative HPLC in good isolated yields. The final chelation reaction condition was optimized to room temperature in aqueous solution for 10 minutes. Purification and isolation by preparative HPLC using C18 column was done within 30 minutes. During built-up of cold theranostic probe biotin-triazine-linker-drug-DPA(*sp*<sup>2</sup>N)-<sup>185</sup>Re(CO)<sub>3</sub> (**4-12**) as SPECT imaging tracer, a Re-promoted methanolysis (**Scheme 4.7**) was observed using a cyclooctyne-DPA(*sp*<sup>2</sup>N) trident ligand bearing a *sp*<sup>2</sup> nitrogen atom for coordination, and resulted in amide bond cleavage and ligand disassociation confirmed by HPLC. Therefore, an alternative cyclooctyne-DPA(*sp*<sup>3</sup>N) trident chelating ligand (**4-17**) was synthesized in methanol under microwave condition in 100 °C for 10 minutes, and a cold diagnostic probe biotin-triazine-DPA(*sp*<sup>3</sup>N)-<sup>185</sup>Re(CO)<sub>3</sub> (**4-21**) was generated in good isolated yield. Purification of these two conjugates were done within 30 minutes.

In Chapter 5, nano-sized macromolecular polymer-based tumor-targeting drug conjugates were designed, synthesized and used for biological evaluations. The novel design was originally proposed by Dr. Gary Teng in his PhD research proposal in 2010. PAMAM (poly (amidoamine)) dendrimer with cleavable cystamine core was selected as macromolecular vehicles. Upon fully functionalization of different functionalities on different generation dendrimers followed by the cleavage of the fully functionalized dendrimer, the two half dendrons could be re-coupled through a linker to construct an asymmetric bow-tie dendrimer (ABTD)-based drug conjugates (**Figure 4.8**). This macromolecular dendrimer-based drug conjugate can utilize two prodrug delivery strategies including active targeting by functionalization with tumor-targeting module on the surface for receptor-mediated endocytosis (RME), and passive targeting by selectively accumulation in tumor tissues resulting from enhanced permeability and retention (EPR) effect. This advanced design also overcome the drawbacks of the most common and feasible strategy for dendrimer-based drug delivery system (DDS) which uses dendrimer as multivalent platform to carry multiple components. However, currently traditional strategy leads to dendrimer-based products represented by the average number of each type of functional molecules regardless of their distribution on the surface, and often results in dendrimer-based drug conjugates with inconsistent number of each functionalities and low quality/purity which largely affects the reproductivity of the biological assay. In this thesis, this issue was taken into account and single component dendrimer intermediates were synthesized and purified to solve this problem. Moreover, the ABTD platform was modified by insertion of a short PEG oligomer to increase the solubility, and the original design of ABTD platform was further optimized to a versatile platform. Instead of fully functionalizing the G1 dendrimer with functional molecules in early assembly stage, a PEGylated terminal alkyne moiety was left on each arm of G1 dendrimer, allowing for the coupling of drug or imaging agent *via* click chemistry in the final step. (**Figure 5.25 and 5.26**) Different functionalities can be orthogonally and efficiently installed to the ABTD drug delivery system. Accordingly, three ABTD conjugates (**ABTD-1**, **ABTD-2**, and **ABTD-3**) were synthesized. Internalization study by flow cytometry and confocal microscopy (CFM) showed selective internalization of ABTD conjugates to biotin receptor overexpressing cancer cell lines through RME. Multi-binding effect resulting from the multiple targeting moiety on each dendrimer-based drug conjugate was also observed compared to a small biotinylated single fluorescent probe (**3-24**). The IC<sub>50</sub> values observed for **ABTD-1** clearly showed the high efficiency

of this dendrimer-based drug delivery system compared to paclitaxel or SB-T-1214 and a small drug conjugate BLT-S (**3-23**). And the IC<sub>50</sub> values observed for **ABTD-3** indicated the non-toxicity and biocompatibility of this ABTD platform. Purification methods and characterization methods for dendrimer-based intermediates were fully established.

Furthermore, two tribranched dendrimer-based theranostic model structures were proposed with modification of bismaleimido linker. A triazine core was used to afford the third arm for incorporation of an imaging group (e.g. fluorescent probe, PET/SPECT tracer, or MRI contrast agent) without interfering the potency by chemically modified the taxoid structure. (**Figure 5.34**) A tribranched linker bearing a fluorescent probe **5-59** was designed and synthesized *via* a double click reaction. To investigate the multi-binding effect and estimate the optimized ratio of TTM per nanocarrier, different generations of half dendrons fully functionalized with biotin (TTM) were designed to attach only one fluorescent probe (imaging agent) *via* click reaction. (**Figure 5.39**) In addition, 2<sup>nd</sup> generation dendrimer-based DDS was proposed in Chapter 5 as shown in **Figure 5.43 and 5.44**. This platform allows a controlled catalyst-based regioselectivity when different functionalities are conjugated to it, and a series of library of drug conjugates will be easily built up. In addition, a good amount of this platform should be easily prepared and accumulated in large scale.

In Chapter 6, a hyaluronic acid-linker-taxoid (HALT) conjugate was designed for targeting cancer stem cells (CSCs) based on the strong affinity of hyaluronic acid (HA) with CD44 biomarker overexpressing on the CSCs. In addition, HA can also serve as a macromolecular platform which can be used to afford multiple anti-cancer drugs, such as highly potent newer generation taxoid. This hyaluronic acid-linker-taxoid (HALT) conjugate can be described as a “Trojan horse” type drug conjugate. Synthesis towards HALT followed the original design and procedure provided by Dr. Jacob Vineberg. In this thesis, quantitative analysis by flow cytometry (**Figure 6.2 and Table 6.1**) and qualitative analysis by CFM (**Figure 6.3**) using a biotin fluorescent probe and a commercially available HA fluorescent probe (**Figure 6.1**) were performed to identify the overexpression level of biotin receptor, HA receptor, CD44 and CD133, as well as their coexpression level against PPT2 (prostate CSC) and HTC116 (colon cancer spheroids), which was comparable to the previous results against PPT2 and XCR4 (colon CSC) using the same two fluorescent probes performed by Dr. Jacob Vineberg. Previously, cytotoxicity measurements were only done against L1210 and L1210FR (leukemia cell line), as well as WI38 (normal lung fibroblast cell line) using BLT-S. In this thesis, to validate the biotin-receptor mediated endocytosis for CSC-targeted drug delivery, BLT-S was used to treat PPT2 and HCT116 with paclitaxel and SB-T-1214 as control. (**Table 6.2**) The biological evaluation result presented BLT-S for consideration as a highly effective and potent as a new generation CSC-targeted drug delivery system.

## §0.7 References

- (1) American Cancer Society, Inc. Cancer Statistics 2015: A Presentation from the American Cancer Society. **2015**.
- (2) American Cancer Society, Atlanta, Georgia. Cancer Facts & Figures. **2015**.
- (3) Atlanta: American Cancer Society. Global Cancer Facts & Figures 3rd Edition. **2015**.

- (4) Hanahan, D.; Weinberg, Robert A. Hallmarks of Cancer: The Next Generation. *Cell* **2011**, *144*, 646-674.
- (5) Hanahan, D.; Weinberg, R. A. The Hallmarks of Cancer. *Cell* **2000**, *100*, 57-70.
- (6) Gottesman, M. M.; Pastan, I. Biochemistry of Multidrug Resistance Mediated by the Multidrug Transporter. *Annu. Rev. Biochem.* **1993**, *62*, 385-427.
- (7) Druker, B. J.; Lydon, N. B. Lessons learned from the development of an Abl tyrosine kinase inhibitor for chronic myelogenous leukemia. *J. Clin. Invest.* **2000**, *105*, 3-7.
- (8) Jaracz, S.; Chen, J.; Kuznetsova, L. V.; Ojima, I. Recent advances in tumor-targeting anticancer drug conjugates. *Bioorg. Med. Chem.* **2005**, *13*, 5043-5054.
- (9) Ducry, L.; Stump, B. Antibody–Drug Conjugates: Linking Cytotoxic Payloads to Monoclonal Antibodies. *Bioconj. Chem.* **2009**, *21*, 5-13.
- (10) Ojima, I.; Zuniga, E. S.; Berger, W. T.; Seitz, J. D. Tumor-targeting drug delivery of new-generation taxoids. *Future Med. Chem.* **2012**, *4*, 33-50.
- (11) Ojima, I.; Zuniga, E. S.; Berger, W. T.; Seitz, J. D. Tumor-targeting drug delivery of new-generation taxoids. *Future Med Chem.* **2012**, *4*, 33-50.
- (12) Chen, J.; Jaracz, S.; Zhao, X.; Chen, S.; Ojima, I. Antibody–cytotoxic agent conjugates for cancer therapy. *Expert Opinion on Drug Delivery* **2005**, *2*, 873-890.
- (13) Wu, X.; Ojima, I. Tumor Specific Novel Taxoid-Monoclonal Antibody Conjugates. *Curr. Med. Chem.* **2004**, *11*, 429-438.
- (14) Ojima, I.; Geng, X.; Wu, X.; Qu, C.; Borella, C. P.; Xie, H.; Wilhelm, S. D.; Leece, B. A.; Bartle, L. M.; Goldmacher, V. S.; Chari, R. V. J. Tumor-Specific Novel Taxoid–Monoclonal Antibody Conjugates. *J. Med. Chem.* **2002**, *45*, 5620-5623.
- (15) Hamann, P. R.; Hinman, L. M.; Hollander, I.; Beyer, C. F.; Lindh, D.; Holcomb, R.; Hallett, W.; Tsou, H.-R.; Upeslakis, J.; Shochat, D.; Mountain, A.; Flowers, D. A.; Bernstein, I. Gemtuzumab Ozogamicin, A Potent and Selective Anti-CD33 Antibody–Calicheamicin Conjugate for Treatment of Acute Myeloid Leukemia. *Bioconj. Chem.* **2001**, *13*, 47-58.
- (16) Chari, R. V. J. Targeted delivery of chemotherapeutics: tumor-activated prodrug therapy. *Adv. Drug Del. Rev.* **1998**, *31*, 89-104.
- (17) Bradley, M. O.; Webb, N. L.; Anthony, F. H.; Devanesan, P.; Witman, P. A.; Hemamalini, S.; Chander, M. C.; Baker, S. D.; He, L.; Horwitz, S. B.; Swindell, C. S. Tumor Targeting by Covalent Conjugation of a Natural Fatty Acid to Paclitaxel. *Clin. Cancer. Res.* **2001**, *7*, 3229-3238.
- (18) Kuznetsova, L.; Chen, J.; Sun, L.; Wu, X.; Pepe, A.; Veith, J. M.; Pera, P.; Bernacki, R. J.; Ojima, I. Syntheses and evaluation of novel fatty acid-second-generation taxoid conjugates as promising anticancer agents. *Bioorg. Med. Chem. Lett.* **2006**, *16*, 974-977.
- (19) Chen, J.; Chen, S.; Zhao, X.; Kuznetsova, L. V.; Wong, S. S.; Ojima, I. Functionalized Single-Walled Carbon Nanotubes as Rationally Designed Vehicles for Tumor-Targeted Drug Delivery. *J. Am. Chem. Soc.* **2008**, *130*, 16778-16785.
- (20) Chen, S.; Zhao, X.; Chen, J.; Chen, J.; Kuznetsova, L.; Wong, S. S.; Ojima, I. Mechanism-Based Tumor-Targeting Drug Delivery System. Validation of Efficient Vitamin Receptor-Mediated Endocytosis and Drug Release. *Bioconjugate Chem.* **2010**, *21*, 979-987.
- (21) Leamon, C. P.; Reddy, J. A. Folate-targeted chemotherapy. *Adv. Drug Del. Rev.* **2004**, *56*, 1127-1141.
- (22) Lu, Y.; Low, P. S. Folate-mediated delivery of macromolecular anticancer therapeutic agents. *Adv. Drug Del. Rev.* **2002**, *54*, 675-693.
- (23) Wagner, E.; Curiel, D.; Cotten, M. Delivery of drugs, proteins and genes into cells using

- transferrin as a ligand for receptor-mediated endocytosis. *Adv. Drug Del. Rev.* **1994**, *14*, 113-135.
- (24) Nagy, A.; Schally, A. V.; Halmos, G.; Armatis, P.; Cai, R.-Z.; Csernus, V.; Kovács, M.; Koppán, M.; Szepesházi, K.; Kahán, Z. Synthesis and biological evaluation of cytotoxic analogs of somatostatin containing doxorubicin or its intensely potent derivative, 2-pyrrolinodoxorubicin. *Proc. Natl. Acad. Sci. U. S. A.* **1998**, *95*, 1794-1799.
- (25) Chu, T. C.; Marks, J. W.; Lavery, L. A.; Faulkner, S.; Rosenblum, M. G.; Ellington, A. D.; Levy, M. Aptamer:Toxin Conjugates that Specifically Target Prostate Tumor Cells. *Cancer Res.* **2006**, *66*, 5989-5992.
- (26) Luo, Y.; Bernshaw, N.; Lu, Z.-R.; Kopecek, J.; Prestwich, G. Targeted Delivery of Doxorubicin by HPMA Copolymer-Hyaluronan Bioconjugates. *Pharm. Res.* **2002**, *19*, 396-402.
- (27) Jaracz, S.; Chen, J.; Kuznetsova, L. V.; Ojima, I. Recent advances in tumor-targeting anticancer drug conjugates. *Bioorg. Med. Chem.* **2005**, *13*, 5043-5054.
- (28) Chen, J.; Jaracz, S.; Zhao, X.; Chen, S.; Ojima, I. Antibody–cytotoxic agent conjugates for cancer therapy. *Expert Opin. Drug Deliv.* **2005**, *2*, 873-890.

## Chapter 1



## **Synthesis of New-Generation Taxoid SB-T-1214 via $\beta$ -Lactam Synthon Method**

§1.1 Paclitaxel and Next-Generation Taxoids.....	16
§1.1.1 Paclitaxel and Taxanes.....	16
§1.1.2 Semi-synthesis of Taxanes via $\beta$ -Lactam Synthon Method ( $\beta$ -LSM).....	16
§1.1.3 Mechanism of Action and Clinical Development of Paclitaxel (Taxol®).....	19
§1.1.4 Multidrug Resistance (MDR).....	21
§1.1.5 Structure-Activity Relationship (SAR) Study of Taxanes.....	22
§1.2 Synthesis of SB-T-1214 via $\beta$ -Lactam Synthon Method.....	24
§1.2.1 Synthesis of Enantiomerically-Enriched $\beta$ -Lactam.....	24
§1.2.2 Synthesis of Second-Generation Taxoid SB-T-1214.....	26
§1.3 Summary.....	28
§1.4 Experimental Section.....	28
§1.4.1 Caution.....	28
§1.4.2 General Information.....	28
§1.4.3 Materials.....	28
§1.4.4 Experimental Procedure.....	29
§1.5 References.....	33

### **§1.1 Paclitaxel and Next-Generation Taxoids**

### §1.1.1 Paclitaxel and Taxanes

Paclitaxel is one of the most widely used chemotherapeutic agents today. In 1966, Wall and Wani first found that extracts of bark from the Pacific Yew, *Taxus brevifolia*, showed significant cytotoxicity towards leukemic cells.<sup>1</sup> Later the chemically active compound for the cytotoxicity was discovered to be the natural diterpenoid paclitaxel, and its structure was reported in 1971.<sup>1</sup> The structure of paclitaxel is composed of a tetracyclic baccatin III skeleton with four fused rings including a cyclohexene (A ring), cyclooctane (B ring), cyclohexane (C ring), a highly rigid oxetane (D-ring), and an N-benzoyl-phenylisoserine side chain at the C-13 position of the A ring (**Figure 1.1**).

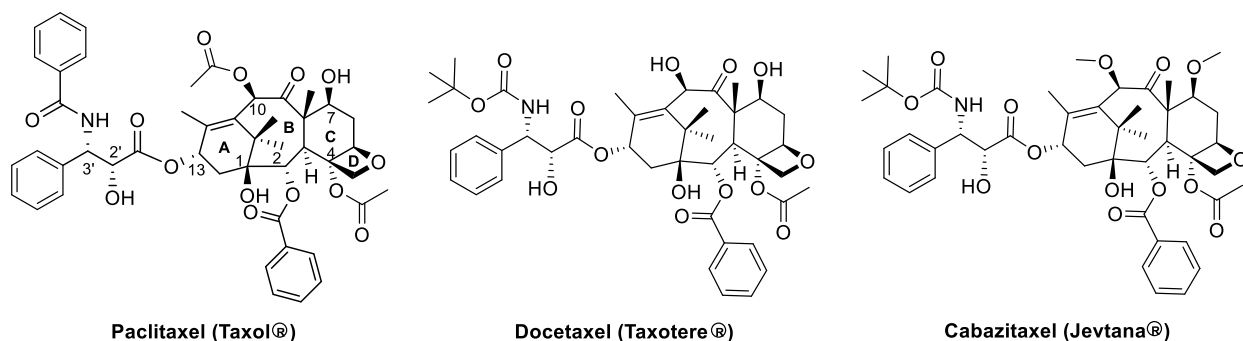


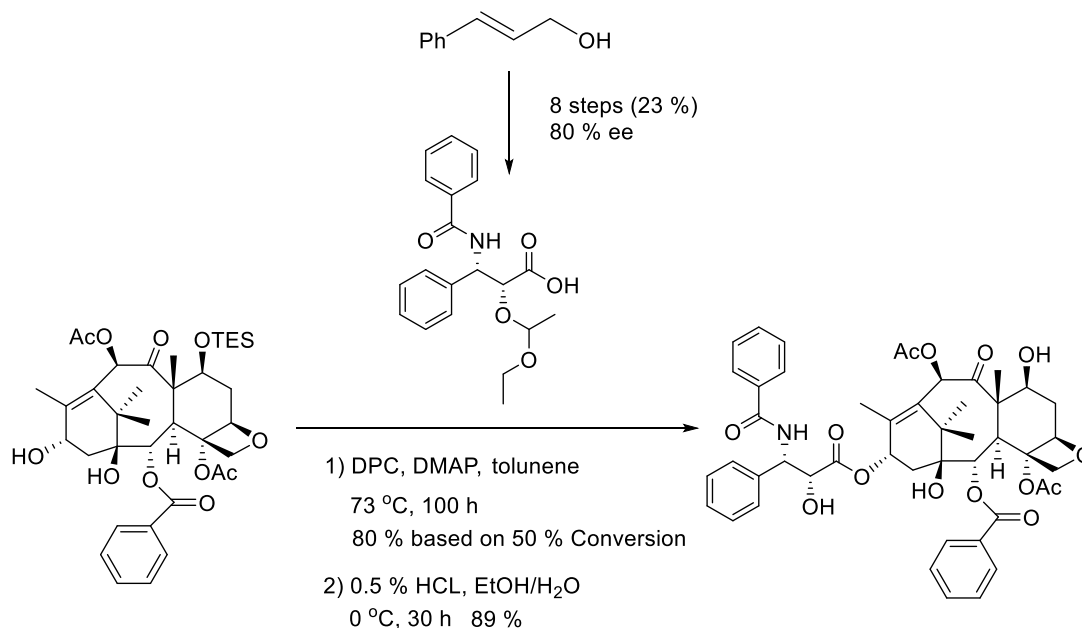
**Figure 1.1** Chemical structures of taxane anticancer agents: paclitaxel, docetaxel, and cabazitaxel

Two other synthetic taxane derivatives, docetaxel and cabazitaxel (**Figure 1.1**) are also FDA-approved chemotherapeutics.<sup>2</sup> As a semi-synthetic analogue of paclitaxel, docetaxel (Taxotere®) showed twice activity than paclitaxel, therefore was approved by FDA for treatment of advance breast cancer in 1996 and non-small cell lung cancer in 1999.<sup>3</sup> Another semi-synthetic taxane cabazitaxel (Jevtana®) recently got approved by FDA for hormone-refractory metastatic prostate cancer in 2009,<sup>4</sup> and currently in Phase III clinical trials for breast cancer.<sup>5</sup>

### §1.1.2 Semi-synthesis of Taxanes via $\beta$ -Lactam Synthone Method ( $\beta$ -LSM)

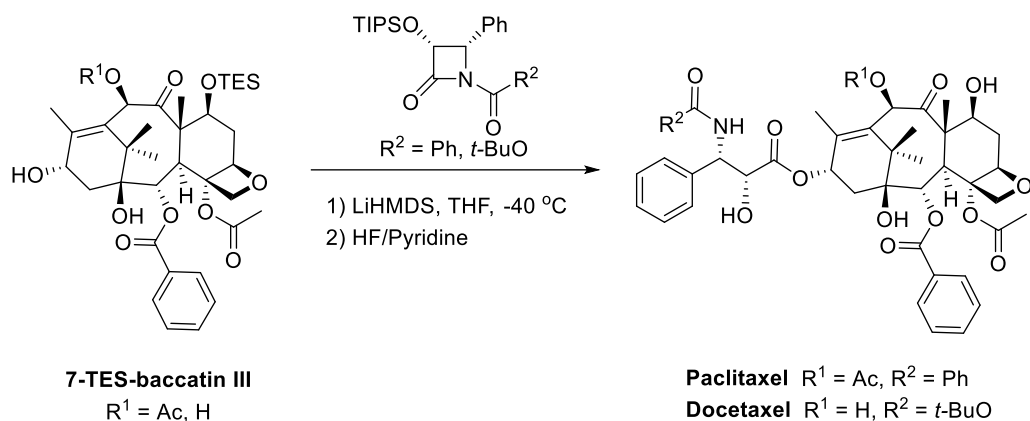
As paclitaxel has shown great anticancer activity, increasing demand of paclitaxel outweighs its supply. Unfortunately, isolation of paclitaxel requires harvesting of the bark of *T. brevifolia* resulting in death of several trees, but extraction process has very low yield as 10,000 kg of bark only can produce only 1 kg of paclitaxel. This problem challenged synthetic chemists to find alternative way to synthesize. Since 1994, several research groups have attempted and successfully established the total synthesis of paclitaxel, such as Holton (1994),<sup>6-7</sup> Nicolaou (1995),<sup>8-11</sup> Danishefsky (1996),<sup>12</sup> Wender (1997),<sup>13</sup> Kuwajima (1998),<sup>14</sup> Mukaiyama (1999),<sup>15</sup> and Takahashi (2006).<sup>16</sup> Although each synthetic approach requires several steps and in low overall yield, it is worthy of attention that a baccatin III derivative is involved. Discovery of 10-deacetyl baccatin III (10-DAB III) as a key intermediate extracted from the regenerative leaves of *Taxus Baccata* in yields of (1g / 1kg)<sup>17-19</sup> provided motivation for semi-synthetic methodology.

The first semi-synthetic methodology for paclitaxel was developed by Greene and Potier.<sup>20</sup> A protocol was derived coupling a modified 10-DAB III core to a  $\beta$ -phenylisoserine moiety in the presence of di-2-pyridyl carbonate (DPC) and 4-(dimethylamino)-pyridine (DMAP), resulting in the synthesis of paclitaxel in 80 % yield based on 50% conversion (**Scheme 1.1**). However, 8 steps were required to synthesize the optically pure isoserine acid with an overall yield of 23% and 80% enantiomeric excess (ee) selectivity.



**Scheme 1.1** First semi-synthetic methodology for paclitaxel

In the early 1980s, Ojima and co-workers discovered that enantiopure  $\beta$ -lactams could be used in the semi-synthesis of paclitaxel, which is also termed as “ $\beta$ -Lactam Synthons Method”.<sup>21</sup> Furthermore, this coupling method can be used to synthesize new generation taxoids. First 7-TES-baccatin III could be synthesized from DAB III, followed by 10-position modification. To give enantiomerically and diastereomerically pure taxenes, enantiopure  $\beta$ -lactams were required to be synthesized to couple with the former intermediates. The Staudinger [2+2] ketene-imine cycloaddition process followed by kinetic enzymatic resolution were applied to generate 3-hydroxy-4-aryl- $\beta$ -lactams with excellent enantiomeric purity, which was readily applied for the asymmetric synthesis of optically pure paclitaxel and docetaxel.<sup>22</sup> The two chiral centers on the lactam branch of the final product could be enantiopurely determined which was related with the bioactivity of the drug. And this process of C13 side-chains modification towards the synthesis of paclitaxel and docetaxel through  $\beta$ -Lactam Synthons Method ( $\beta$ -LSM) became known as the Ojima-Holton coupling protocol (**Scheme 1.2**).<sup>21,23-24</sup> The Ojima-Holton coupling protocol not only provided the chemists an efficient method for the semi-synthesis of paclitaxel and docetaxel, as well as next generation taxoids with better bioavailability and higher potency, but also supported the understanding of the structure-activity relationship (SAR) for the taxane class.<sup>25</sup>



**Scheme 1.2** The semi-synthesis of paclitaxel and docetaxel by the Ojima-Holton coupling protocol

Various synthetic methods have been reported towards the synthesis of enantiomerically pure  $\beta$ -lactams.<sup>26</sup> One of the most common approaches is the ketene-imine Staudinger [2+2] cycloaddition<sup>27</sup> followed by the chemoenzymatic resolution to yield the desired  $\beta$ -lactams in high enantiomeric excess, and the other approach is lithium chiral ester enolate-imine cyclocondensation.<sup>28</sup>

To obtain the enantiopure  $\beta$ -lactams, the four-membered heterocyclic ring core needed to be synthesized via a thermal [2+2] cycloaddition of a Schiff base (imine) generated from aniline and benzaldehyde with ketene formed *in situ*. This reaction route to yield the first synthesized  $\beta$ -lactam (1,3,3,4-tetraphenylazetid-2-one) also was known as Staudinger reaction which was developed by Herman Staudinger in 1907.<sup>27</sup> This reaction is regarded as one of the most reliable methods to synthesize  $\beta$ -lactams, as its simplicity in experimental procedure, as well as the broad scope in the substrate structures, including alkyl-, amino-, halo-, alkoxy- and siloxy-ketenes.<sup>26</sup> Although this synthetic method has been commonly applied in the past, explanations on the mechanism details have been discussed and not reach the agreement. The widely accepted mechanism takes place in a stepwise process, which involves the nucleophilic attack of the imine nitrogen on the ketene carbon to form a zwitterionic intermediate, followed by an electrocyclic conrotatory ring closure to yield the four member ring system with two additional stereocenters at the C3 and C4 positions of the lactam.<sup>29</sup> Since the ketene is formed by acid chloride and a base *in situ*, the stereochemical outcome is influenced by various experimental factors including solvent, base, temperature, additives, order of reagents, and other chiral pendant groups.<sup>30</sup> According to the proposed mechanism, the zwitterionic intermediate bearing the (E)-imine moiety will generate *cis*- $\beta$ -lactam, however, the isomerization may take place at this zwitterionic intermediate to afford the (Z)-imine moiety, which will lead to the formation of *trans*- $\beta$ -lactam.<sup>26</sup> Thus the relative ratio of *cis*- and *trans*- product are determined by direct ring closure and isomerization.<sup>30</sup> (**Figure 1.2**) Then the obtained racemic mixtures can be applied to kinetic enzymatic resolution with suitable lipase to yield enantiopure  $\beta$ -lactams.<sup>31</sup>

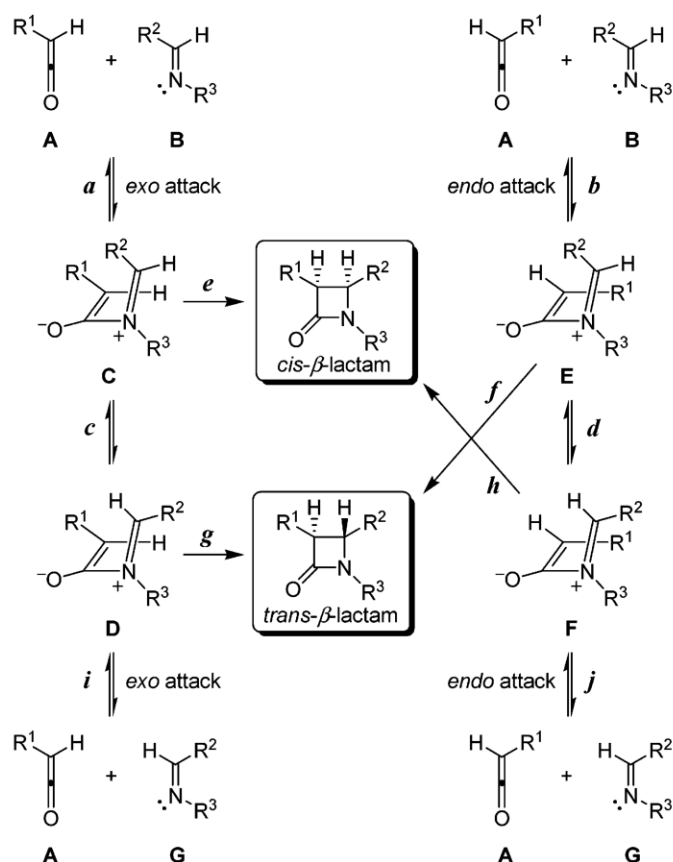


**Figure 1.2** Pathways for the formation of cis- and trans- $\beta$ -lactams (reprinted from reference 30)<sup>30</sup>

### §1.1.3 Mechanism of Action and Clinical Development of Paclitaxel (Taxol®)

Despite its complex structure, low availability from natural source, and poor water solubility, subsequent development with NCI revealed excellent antitumor activity against human solid tumor xenografts, including CX-1 colon, LX1 lung and MX-1 breast tumor xenografts, leading to preclinical formulation and eventual clinical development.<sup>32</sup> In 1979, the unique mechanism of action of paclitaxel was discovered as a microtubule assembly promoter by Dr. Susan Horwitz et al.<sup>33-34</sup> Unlike other tubulin polymerization inhibitors, such as vinblastine and colchicine which inhibit the polymerization of spindle microtubules or depolymerize existing spindle microtubules, paclitaxel stimulates microtubule polymerization by stabilizing the microtubules through directly binding to tubulin along the length of the microtubule and preventing depolymerization.<sup>35</sup> (**Figure 1.3**) Microtubules play critical role in cell reproduction and division. Polymerization of microtubules takes place by a nucleation-elongation mode during the formation of a short microtubule “nucleus”, followed by the elongation of the microtubule at the ends by addition of tubulin dimers. Two polypeptide subunits,  $\alpha$ - and  $\beta$ -tubulin heterodimers, polymerize in the presence of guanoside-5'-triphosphate (GTP), magnesium ions ( $Mg^{2+}$ ), and microtubule-associated proteins (MAPs). The resulting protofilaments comprise the microtubule skeleton and each microtubule consists of 13 protofilaments with an average 23 nm diameter (**Figure 1.4**).<sup>36-37</sup> However, there is a taxol-binding site on each molecule of tubulin in microtubules. Taxol has nearly stoichiometric binding to tubulin heterodimers to irreversibly stabilize the formed microtubules. The resulting microtubule contains 12 protofilaments with an

average 22 nm diameter and is stabilized against depolymerization conditions (**Figure 1.4**),<sup>36</sup> which lead to inhibition of cell cycle progression at the G2/M phase of mitosis, eventually inducing apoptosis.<sup>38</sup>

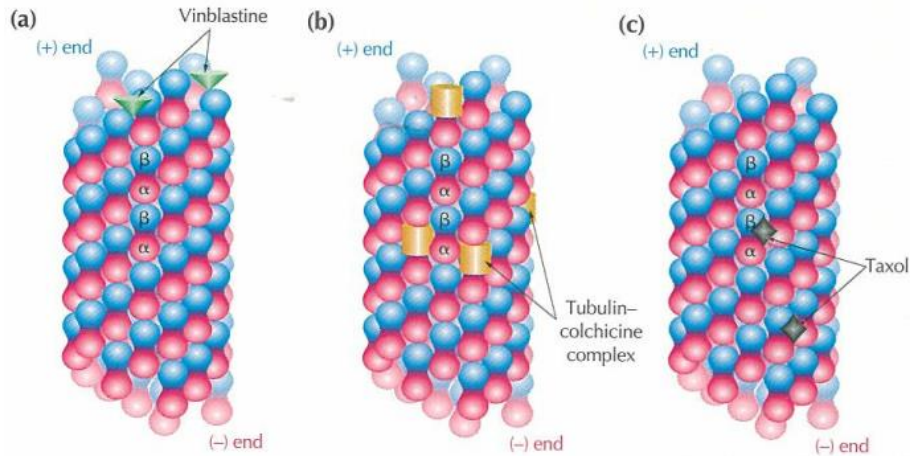


**Figure 1.3** Three types of antimitotic drugs (vinblastine, colchicine and taxol) interact with microtubules at diverse sites (reprinted from reference 35)<sup>35</sup>

In 1984, taxol began Phase I clinical trials formulated with Cremophor EL (a mixture of 50% alcohol and polyethoxylated castor oil). However, severe hypersensitivity reactions, including hypotension and death, were observed, resulting in cessation of many Phase I clinical trials.<sup>39</sup> The reason was thought to be consistent with toxic effects from the diluent Cremophor EL, thus to overcome this issue, National Cancer Institute (NCI) suggested that taxol Phase I and II clinical trials should adjust the infusion period to 24-hour, and an antiallergic premedication regimen was also reinforced.<sup>40</sup> Phase II studies were performed under the recommended dose of taxol around 250 mg/m<sup>2</sup> by 24-hour infusion repeated every 21 days,<sup>39</sup> and showed appreciable efficacy against lung, ovarian and breast cancers.<sup>41</sup> Taxol became one of the most successful FDA-approved chemotherapeutic agents, and currently taxol is being tested in Phase II and III clinical trials.

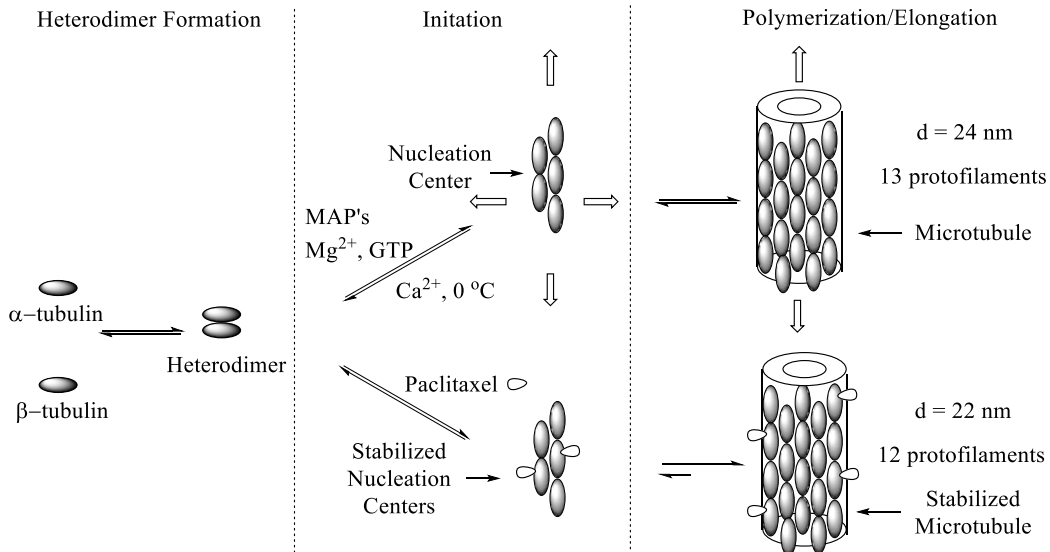


**Figure 1.4** Microtubule formation in taxol and taxol-free cells (adapted from reference 36)<sup>36</sup>

### §1.1.4 Multidrug Resistance (MDR)

Although taxenes have been widely used in current clinical trials, however, it has been reported that a broad-spectrum drug resistance was found in paclitaxel-based chemotherapy,<sup>42</sup> and many paclitaxel-resistant multidrug resistance (MDR) cell lines have been identified.<sup>43</sup> MDR can be associated with overexpression of ATP-binding cassettes (ABC) transporter. Several transmembrane transporter proteins have been reported to be involved in tumor resistance to chemotherapeutic agents. P-glycoprotein (Pgp) is well characterized for drug resistance.<sup>44</sup> P-gp was discovered 20 years ago as a ubiquitous marker of multidrug resistance. As gene product encoded and expressed from multidrug resistance MDR1 gene, P-gp is a high molecular weight (170KDa) integral plasma membrane glycoprotein. It has 12 transmembrane domains and two ATP-binding sites, which confers multidrug resistance to mammalian cells by acting as an ATP-dependent drug efflux pump that exports hydrophobic compounds (i.e. vinblastine, vincristine, doxorubicin, daunorubicin, etoposide, and paclitaxel) from the intracellular compartment.<sup>45-47</sup> P-gp has a very broad poly-specificity, enabling it to recognize hundreds of compounds as small as 330 daltons up to 4000 daltons, pull substrates from the membrane and expel them to promote MDR.<sup>48</sup>

The first crystal structure of a mammalian P-glycoprotein was reported using mouse P-gp (ABCB1), which has 87 % sequence identity to human P-gp in a drug binding competent state.<sup>48</sup> It represents a nucleotide-free inward-facing conformation arranged as two “halves” with pseudo two-fold molecular symmetry spanning around 136 angstroms perpendicular to and around 70 angstroms in the plane of the bilayer. The nucleotide-binding domains (NBDs) are separated by around 30 angstroms. The inward-facing conformation provides a large internal cavity open to both the cytoplasm and the inner leaflet. Two portals allow access for entry of hydrophobic compounds directly from the membrane.<sup>48</sup> In a typical drug efflux cycle, the drug binds first to the TMDs. This binding triggers a conformational change by which each NBD comes closer to the other, generating the ATP binding sites. The binding of two ATPs blocks the protein in a close state that leads it to undergo a second large conformational change from the inward-facing to the outward-facing conformation. (**Figure 1.5**)<sup>47</sup> Both NBDs remain bound together with their ATP while the outer leaflet part of each TMD becomes distant, open to the extracellular face of the drug-binding sites. Drugs are released by changes in the affinity of the sites. Finally, the protein comes back to the initial inward-facing conformation by hydrolyzing ATP, which gives the energy to the protein to allow separation of each moiety.<sup>47</sup>

Since paclitaxel and docetaxel were both found ineffective against certain cells lines with high expression levels of MDR1 gene such as colon and renal carcinoma,<sup>49-50</sup> hundreds of new taxoids have been synthesized with highly potency against MDR cancer cells and tumor. To logically determine the modification position and substitutions at each position on taxane skeleton to improve the potency and susceptibility to drug resistance of newer generation taxoid, comprehensive and detailed structure-activity relationship study will be necessary.

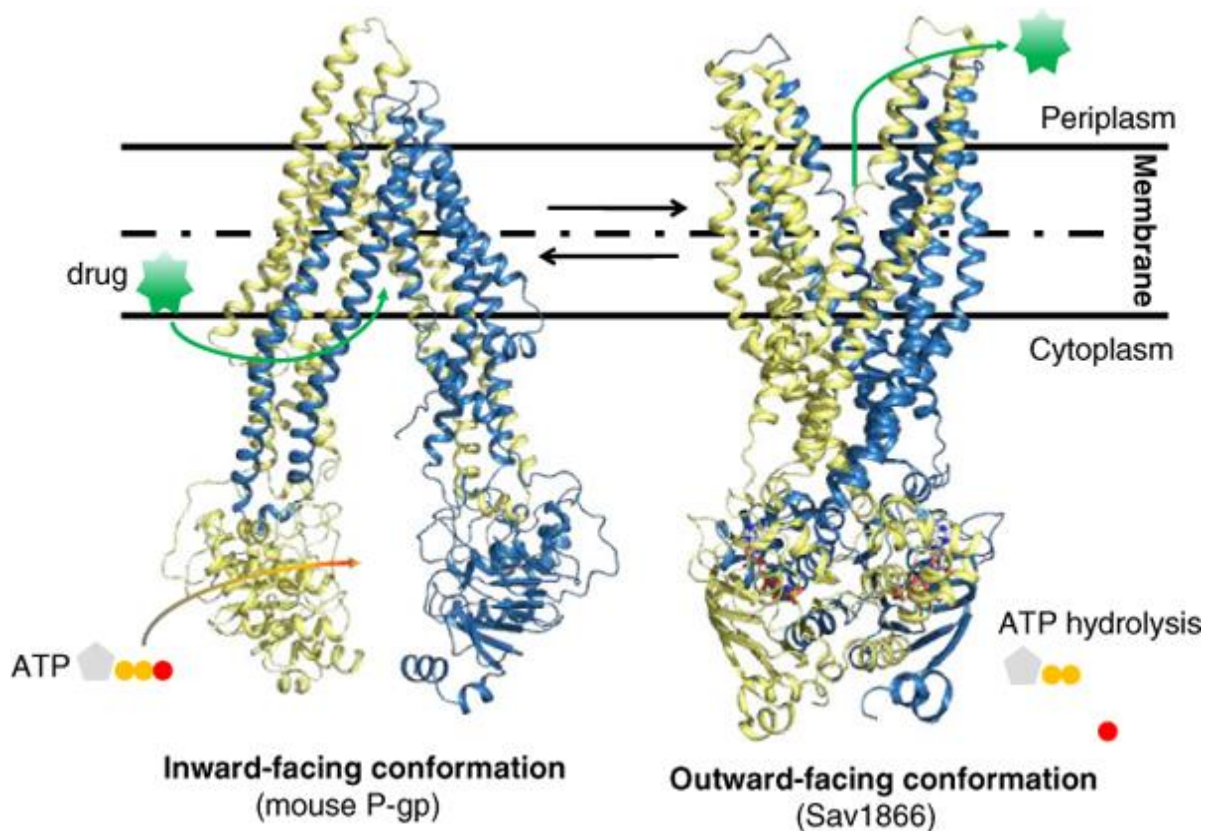


**Figure 1.5** Conformational changes of ATP-binding cassette (ABC) exporters (reprinted from reference 47)<sup>47</sup>

### §1.1.5 Structure-Activity Relationship (SAR) Study of Taxanes

Extensive structure activity relationship (SAR) studies of paclitaxel and docetaxel have been conducted. (Figure 1.6)<sup>51</sup> The main structure of taxol includes four fused ring (A-D ring). (Figure 1.1) The baccatin scaffold itself is not necessarily responsible for the stabilization of microtubules and resulting cytotoxicity. To maintain the binding affinity and drug activity, it is very crucial to maintain the 2'R and 3'S configuration on the C13 position of the A ring, but the substituent group on C3' position is tolerated for replacement with alkyl or alkenyl group, and C3'N-phenyl group is allowed to be changed to *t*-Boc group with higher potency.<sup>19</sup> (For the carbon atom number, refer to Figure 1.1) In addition, the free hydroxyl group at C2' is critical for biological activity, and potential for the connection of linker by forming hydrolysable ester bond. On the B ring, modification of the C2 and C10 positions virtually overcome the MDR effect in several cancer cell lines. It is found that *meta* substitution of the C2-benzoyl functionality can increase the biological activity. The acetate group on C10 could be removed or replaced by various alkyl substitution through an ester linkage. The C7 position can epimerize with little effect on potency. Modification on C7 position, such as attachment of fluorescent probe for imaging study, is permitted, but 1 to 2 orders of magnitude reduced potency was observed.<sup>52</sup> The D-ring (Oxetane Ring) cannot be replaced or removed, since it is a hydrogen-bond acceptor and also serves as a rigid "lock" on the taxoid skeleton.



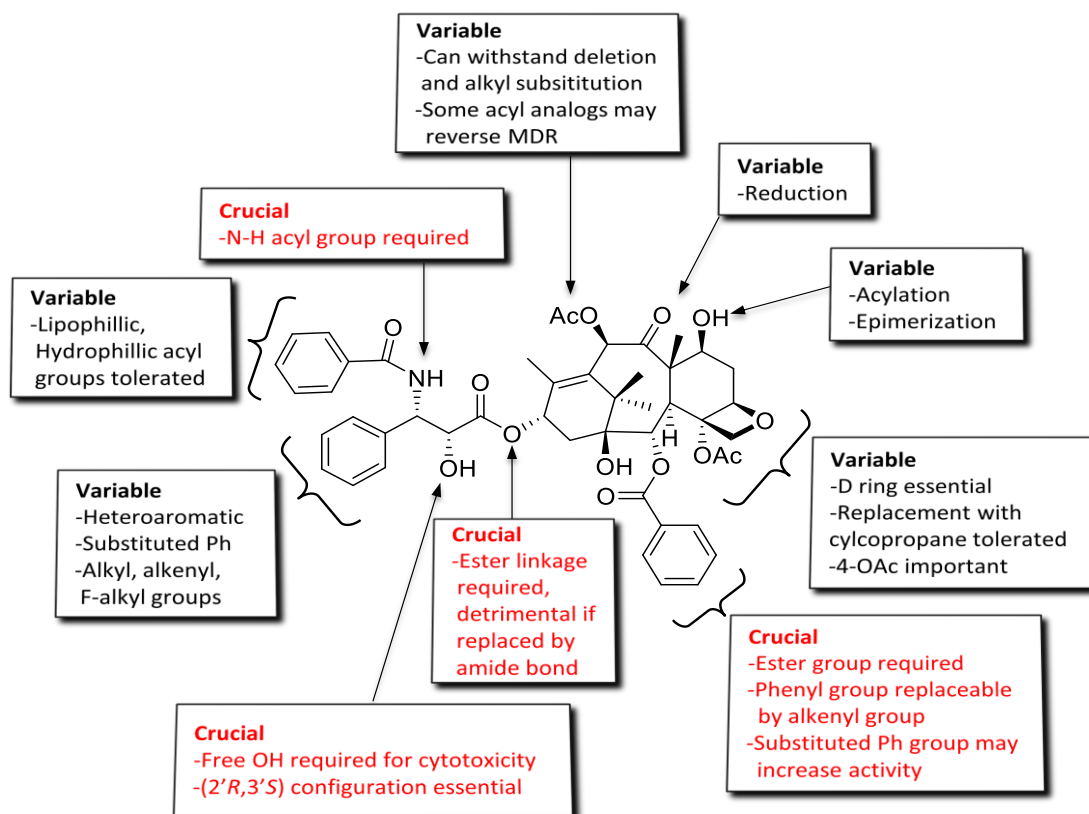


**Figure 1.6** Overview of previously conducted SAR studies on paclitaxel

In the SAR study of paclitaxel and docetaxel analogs, the 3'-phenyl group was found not an essential component for the potent cytotoxicity and antitumor activity. A series of analogs with 3'-phenyl group replaced by either a 3'-alkenyl or 3'-alkyl moiety, showed substantially higher potency than paclitaxel and docetaxel, especially against a drug-resistant human breast cancer cell line.<sup>53-54</sup> Moreover, analogs with acetyl group modified at C10 position exhibited 2 to 3 order of magnitude better cytotoxicity than 10-unmodified analogs against the doxorubicin-resistant human breast cancer cell line MCF-7R which is defined as one of the MDR cancer cell lines. Overall, modifications at C3' and C10 positions have been instrumental in the discovery of more potent second generation taxoids. One of the second generation taxoids, SB-T-1214, (**Figure 1.7**) has been shown to possess two fold improvement in multidrug resistant (MDR) cancer lines compared to paclitaxel and docetaxel, as shown in **Table 1.1**.<sup>33,53</sup>

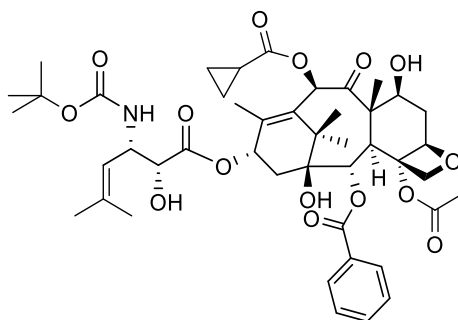
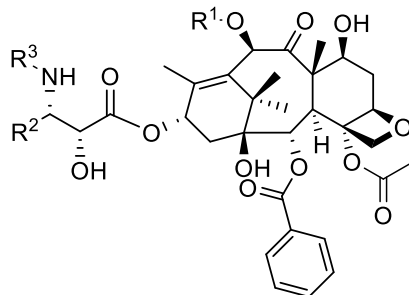


**Figure 1.7** Chemical structure of SB-T-1214

**Table 1.1 Structure and Cytotoxicity (IC<sub>50</sub>, nM) of Selected Second Generation Taxoids against various Cancer Cell Lines (adapted from reference 33)<sup>33</sup>**



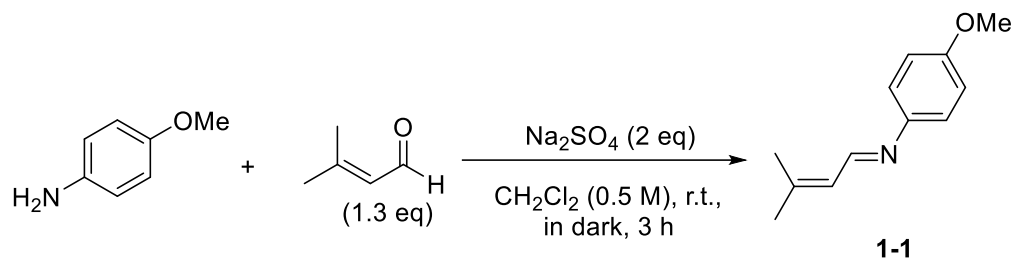
Taxane	R <sup>1</sup>	R <sup>2</sup>	R <sup>3</sup>	MCF7 <sup>a</sup>	NCI/A-DR <sup>b</sup>	LCC6-MDR <sup>c</sup>	CFPAC-1 <sup>d</sup>	HT-29 <sup>e</sup>	DLD-1 <sup>f</sup>
Paclitaxel	Ac	Ph	PhCO	1.7	550	346	68	12	300
Docetaxel	H	Ph	<i>t</i> -Boc	1.0	723	120	-	-	-
SB-T-1213	EtCO	<i>t</i> -butenyl	<i>t</i> -Boc	0.18	4.0	-	4.6	0.37	3.9
SB-T-1214	<i>c</i> -PrCO	<i>t</i> -butenyl	<i>t</i> -Boc	0.20	3.9	-	0.38	0.73	3.8
SB-T-1216	Me <sub>2</sub> NCO	<i>t</i> -butenyl	<i>t</i> -Boc	0.13	7.4	-	0.66	0.052	5.4

<sup>a</sup>Human mammary cancer cell line (Pgp-); <sup>b</sup>Human ovarian cancer cell line (Pgp+); <sup>c</sup>mdr1 transduced human breast cancer cell line (Pgp+); <sup>d</sup>Human pancreatic cancer cell line; <sup>e</sup>Human colon cancer cell line (Pgp-); <sup>f</sup>Human colon cancer cell line (Pgp+); <sup>g</sup>Cells were incubated with a taxane for 72 h at 37 °C with a 5% CO<sub>2</sub> atmosphere.

## §1.2 Synthesis of SB-T-1214 via β-Lactam Synthone Method

### §1.2.1 Synthesis of Enantiomerically-Enriched β-Lactam

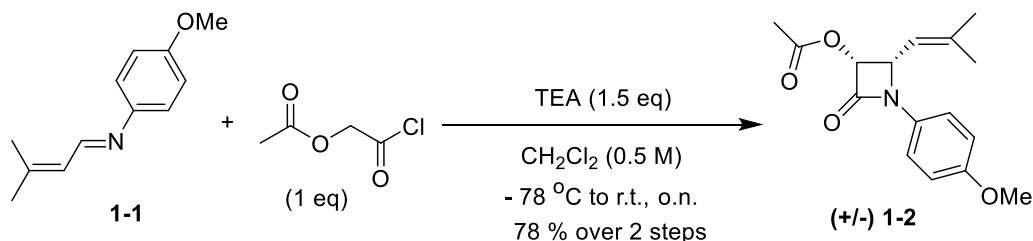
The synthesis of enantiopure β-lactams began with the formation of four-membered heterocyclic ring core between an imine and a ketene via the Staudinger [2+2] cycloaddition. In the presence of sodium sulfate as a drying reagent, imine **1-1** was obtained in the condensation reaction of 3-methyl-2-butenal and *p*-anisidine (Scheme 1.3). Since the imine **1-I** was sensitive to light, the reaction was done in dark to avoid the decomposition or isomerization of the imine.



**Scheme 1.3** Synthesis of imine by condensation reaction

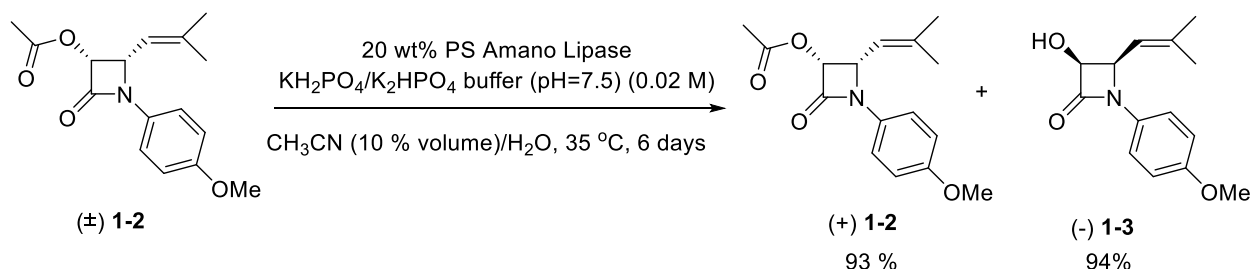
Upon the completion of the reaction, the reaction mixture was filtered, the solvent then was evaporated under vacuum pressure and the resulting imine **1-I** was used immediately without further purification. The [2+2] cycloaddition between the imine **1-1** and acetoxyacetyl chloride generated a racemic mixture of (±)**1-2** (Scheme 1.4). The cold -78 °C temperature must be

maintained to prevent *trans*-isomer formation of the  $\beta$ -lactam. The acetoxyacetyl chloride was slowly added against the inside glass wall to prevent forming the thermodynamic *trans*- product. In addition, the dilution of acetoxyacetyl chloride was also helpful to avoid the *trans*- form product because it decreased the local heat release when it was added to the reaction system. Recrystallization in hexanes was used to generate racemic *cis*- $\beta$ -lactam ( $\pm$ )**1-2** in good yield (78 % over 2 steps) in an exclusively *cis*-stereochemical outcome.



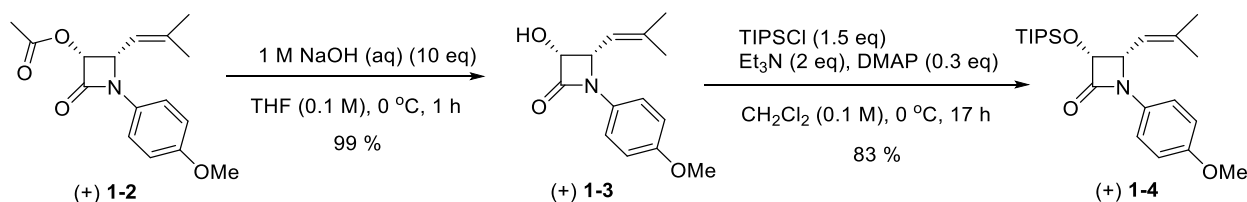
**Scheme 1.4** Staudinger [2+2] ketene-imine cycloaddition reaction

The two enantiomers of *cis*- $\beta$ -lactam ( $\pm$ )**1-2** were resolved by enzymatic resolution by using “PS-Amano” lipase which was derived from the bacteria *Burkholderia cepacia*. The lipase preferentially cleaved the acetate group of the (-) enantiomer (-)**1-2** and left the (+) enantiomer (+)**1-2** intact, allowing for the selective preservation of (+)**1-2** in excellent enantiopurity (>99% ee). (**Scheme 1.5**) Acetonitrile and phosphate buffer solution were mixed to accommodate the solubility of substrate *cis*- $\beta$ -lactam ( $\pm$ )**1-2**, and provide physiological condition of the PS-Amano” lipase for optimal enzymatic activity. The enzymatic resolution was monitored by NMR, and a 50% conversion of the acetate moiety to the hydroxyl moiety was carefully monitored to quench the reaction and ensure high enantioselectivity.



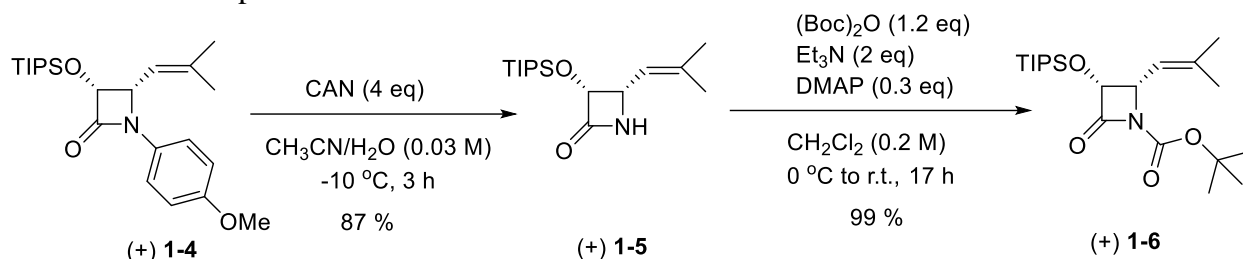
**Scheme 1.5** Optical enzymatic resolution of isolating enantiopure (+) **1-2**

The desired (+) **1-2** was converted to (+) **1-3** via basic hydrolysis, followed by subsequent TIPS protection to give (+) **1-4** in good yield. (**Scheme 1.6**) Excess TIPSCl was used and triisopropyldisiloxane was formed. Recrystallization with hexanes could get pure (+) **1-4** as white crystal.



**Scheme 1.6** Hydrolysis and TIPS protection of (+) **1-3**

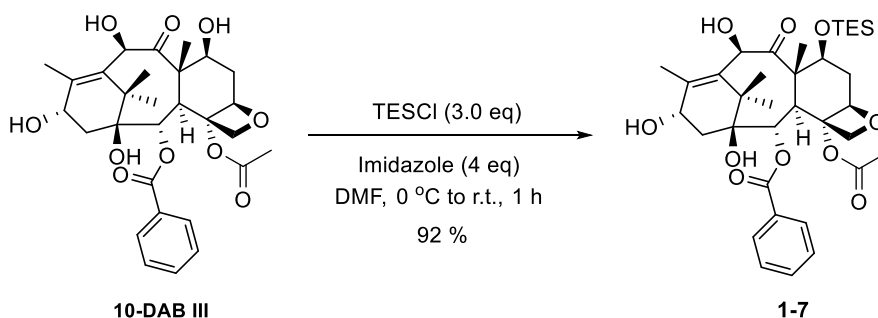
Further modification of (+) **1-4** entails the deprotection of the *p*-methoxyphenyl (PMP) moiety in the presence of ceric ammonium nitrate (CAN) to give (+) **1-5** in modest yield. This oxidative cleavage step involved two single electron transfers (SET). First SET step generated a radical cation at the para position on the PMP group, allowing the nucleophilic attack by water and loss of methanol. The second SET took place and lead to the C-N bond break to afford (+) **1-5** and loss of a quinone. After deprotection, the (+) **1-5** was treated with di-*tert*-butyl dicarbonate to generate the desired enantiopure (+) **1-6** in excellent yield. (**Scheme 1.7**) This enantiopure (+) **1-6** was used as the side chain in the semi-synthesis of second generation taxoid SB-T-1214 and its derivatives in Chapter 2.



**Scheme 1.7** CAN-deprotection and *t*-Boc protection reaction

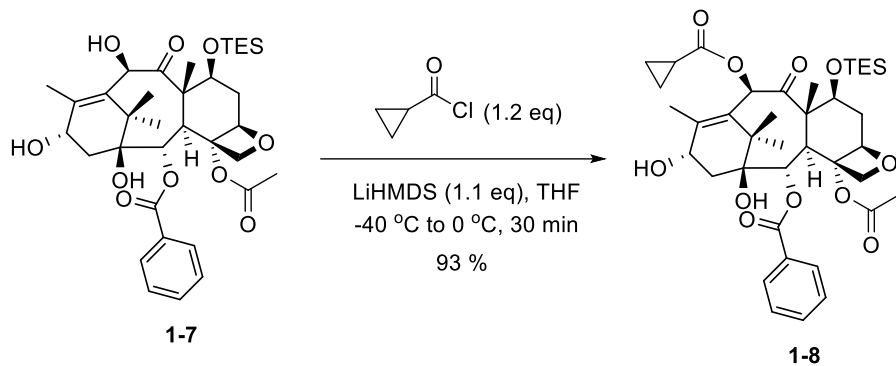
### §1.2.2 Synthesis of Second-Generation Taxoid SB-T-1214

The synthesis of second generation taxoid SB-T-1214 began with the silyl protection of the C7 hydroxyl group of 10-deacetylbaccatin III (10-DAB III) in the presence of chlorotriethylsilane and imidazole to give **1-7** in excellent yield. (**Scheme 1.8**) This protection was done at 0 °C and monitored closely to assure that multiple protections did not occur. With increased reaction time, it is possible to protect C10 and C13 hydroxyl groups, which will form the intermediate to make third generation taxoid before modification on C2 benzoyl group.



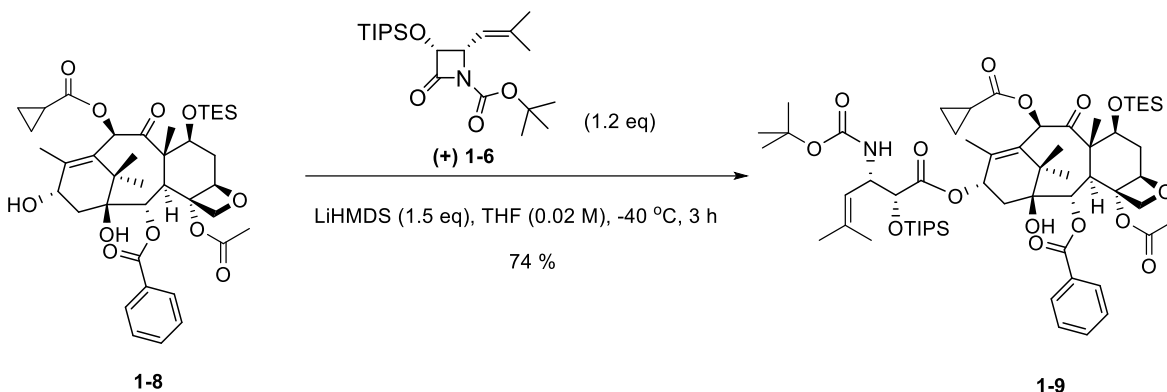
**Scheme 1.8** Mono TES protection on C7 of 10-DAB III

Modification of the C10 hydroxyl group to a cyclopropanecarbonyl moiety was carried out in the presence of Lithium bis(trimethylsilyl)amide (LiHMDS) to give **1-8** in good yield. (**Scheme 1.9**) Reaction need to be carefully monitored by TLC as C13 position can also to be substituted by excess cyclopropanecarbonyl chloride.



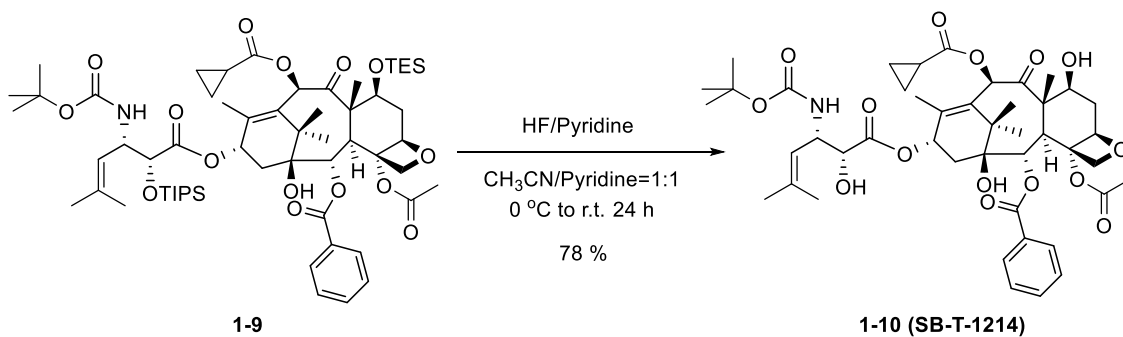
**Scheme 1.9** Acylation of C10 position

The C13 isoserine side chain was installed via  $\beta$ -lactam synthon method. The enantiopure  $\beta$ -lactam (+) **1-6** was coupling to the C-13 position of 7-TES-10-acyl-baccatins **1-8** in the presence of LiHMDS by the Ojima-Holton coupling reaction. (**Scheme 1.10**) As a result, the ring was opened and stereochemistry was maintained.



**Scheme 1.10** Ojima-Holton coupling reaction

Final step towards second generation taxoid SB-T-1214 was done by the silyl deprotection in the presence of HF-pyridine complex solution to remove the TIPS group at the C2' position and the TES group on the C7 position (**Scheme 1.11**). Recrystallization in ethyl acetate of SB-T-1214 afford this taxoid in crystal solid form in over 99% purity determined by reverse-phase HPLC analysis. The biological evaluation of SB-T-1214 in comparison with paclitaxel and other SB-T-1214-based drug conjugates will be discussed in Chapter 3, 4 and 5.



## **Scheme 1.11** Deprotection of silyl groups to form final product SB-T-1214

### **§1.3 Summary**

Paclitaxel is one of the most widely used drugs in diverse types of cancer treatment. As microtubule-stabilizing chemotherapeutic agent, paclitaxel shows great antitumor activity. But it has been reported largely decreased efficacy against MDR cancer cell lines. Accordingly, newer generation taxoids were designed and evaluated showing several orders of magnitude greater potency than paclitaxel. As a selected example of second generation taxoid, SB-T-1214 was synthesized via  $\beta$ -Lactam Synthon Method ( $\beta$ -LSM) in good overall yield and enantiomeric purity. High enantiomeric excess was achieved via an enzymatic kinetic resolution of  $\beta$ -lactam obtained by Staudinger [2+2] ketene-imine cycloaddition. The synthesized SB-T-1214 will be used as cytotoxic agent for various taxoid-based drug conjugate synthesis.

### **§1.4 Experimental Sections**

#### **§1.4.1 Caution**

Taxoids have been classified as potent cytotoxic agents. Thus, all drugs and structurally related compounds and derivatives must be considered as mutagens and potential reproductive hazards for both males and females. Some of the chemicals and solvents have been used and designated as hazardous materials such as explosives, gases, flammable liquid and combustible liquid, flammable solid or dangerous when wet, oxidizer or organic peroxide, poison inhalation hazard, irritant or corrosive. Hydrofluoric acid (HF) can penetrate the skin, causing destruction of deep tissue layers, including bone. Appropriate precautions (i.e. use of gloves, goggles, lab coat and fume hood) must be taken while handling these compounds.

#### **§1.4.2 General Methods**

$^1\text{H}$  and  $^{13}\text{C}$  NMR were measured on 300, 400 MHz Varian spectrometer or 400, 500 MHz Bruker NMR spectrometer. The melting points were measured on a "Uni-melt" capillary melting point apparatus from Arthur H. Thomas Company, Inc and are uncorrected. TLC analyses were performed on Sorbent Technologies aluminum-backed Silica G TLC plates (Sorbent Technologies, 200  $\mu\text{m}$ , 20 x 20 cm) and were visualized with UV light and stained with sulfuric acid-EtOH, 10 % PMA-EtOH or 10 % Vanillin-EtOH with 1% sulfuric acid. Column chromatography was carried out on silica gel 60 (Merck, 230-400 mesh ASTM). Chemical purity was determined with a Shimadzu L-2010A HPLC HT series HPLC assembly, using a Phenomenex Curosil-B column, employing  $\text{CH}_3\text{CN}$ /water as the solvent system with a flow rate of 1 mL/min. Chiral HPLC analysis for the determination of enantiomeric excess was carried out with a Shimadzu L-2010A HPLC HT series HPLC assembly, using a DAICEL-CHIRACEL OD chiral column (250 mm x 4.6 mm), employing hexane/isopropanol as the solvent system with a flow rate of 0.6 mL/min.

#### **§1.4.3 Materials**

The chemicals were purchased from Sigma-Aldrich, Fischer Scientific or VWR International, and used as received or purified before use by standard methods. Dichloromethane

was dried before use by distillation over calcium hydride under nitrogen. Tetrahydrofuran was dried before use by distillation over sodium and benzophenone, and kept under nitrogen. Dry DMF was purchased from EMD chemical company, and used without further purification. Reaction flasks were dried in a 100 °C oven and allowed to cool to room temperature in a desiccator over “Drierite” (calcium sulfate) and assembled under an inert nitrogen gas atmosphere.

#### §1.4.4 Experimental Procedure

##### 4-Methoxy-*N*-(3-methyl-2-buten-1-ylidene)-benzenamine (**1-1**)<sup>55</sup>

To a solution of *p*-anisidine (recrystallized from hexanes) (3.98 g, 32 mmol) and 2 eq of anhydrous Na<sub>2</sub>SO<sub>4</sub> (9.09 g, 64 mmol) in 0.5 M CH<sub>2</sub>Cl<sub>2</sub> (64 mL) under inert conditions. The container was covered by foil to avoid the light. To the solution was added 1.3 eq 3-methylbut-2-enal (4 mL, 3.51g, 42 mmol) dropwise, and the mixture was allowed to stir at room temperature for at least 3 hours and monitored *via* TLC. Upon completion, the reaction mixture was filtered to remove the Na<sub>2</sub>SO<sub>4</sub> and the solvent was evaporated without heat. The crude product was concentrated *in vacuo* to remove excess 3-methylbut-2-enal monitored by NMR. Crude **1-1** was obtained as a dark red liquid which should be used immediately in the subsequent step without further purification. <sup>1</sup>H NMR (300 MHz, CDCl<sub>3</sub>) δ 1.93 (s, 3 H), 1.99 (s, 3 H), 3.78 (s, 3 H), 6.21 (d, *J* = 9.6 Hz, 1 H), 6.86 (d, *J* = 6.6 Hz, 2 H), 7.09 (d, *J* = 6.9 Hz, 2 H), 8.35 (d, *J* = 9.3 Hz, 1 H). All data are in agreement with literature values.<sup>55</sup>

##### (+/-)-*cis*-1-(4-Methoxyphenyl)-3-acetoxyl-4-(2-methylprop-1-enyl)azetid-2-one ((+/-) **1-2**)<sup>56</sup>

To a solution of crude **1-1** in 0.5 M CH<sub>2</sub>Cl<sub>2</sub> (107 mL) at -78 °C maintained for at least 30 min under inert conditions, 1.5 eq triethylamine (6.68 mL, 48 mmol, 4.86 g) was added to the cooled solution, followed by the slow and dropwise addition of 1 eq acetoxyacetyl chloride (3.44 mL, 32 mmol, 4.37 g) by a jacketed addition funnel. The -78 °C temperature of the mixture was maintained for at least 2 h. Then the mixture was stirred and allowed to warm slowly to room temperature overnight. The reaction was monitored *via* TLC. Upon completion, the reaction was quenched with saturated NH<sub>4</sub>Cl (100 mL). Then the solution was extracted with CH<sub>2</sub>Cl<sub>2</sub> (100 mL x 3). The organic layer was washed with brine (50 mL x 3), dried over anhydrous MgSO<sub>4</sub>, and concentrated *in vacuo*. Purification was done *via* column chromatography on silica gel with increasing amounts of eluent (hexanes:ethyl acetate) to yield crude racemic (+/-) **1-2** (7.22 g, 25 mmol, 78 % over 2 steps). <sup>1</sup>H NMR (300 MHz, CDCl<sub>3</sub>) δ 1.79 (s, 3 H), 1.82 (s, 3 H), 2.11 (s, 3 H), 3.78 (s, 3 H), 4.97 (dd, *J* = 9.6 Hz, 4.8 Hz, 1 H), 5.14 (d, *J* = 9.6 Hz, 1 H), 5.80 (d, *J* = 4.8 Hz, 1 H), 6.87 (d, *J* = 9.0 Hz, 2 H), 7.33 (d, *J* = 9.3 Hz, 2 H). All data are in agreement with literature values.<sup>56</sup>

##### (3*S*,4*R*)-1-(4-Methoxyphenyl)-3-acetoxyl-4-(2-methylprop-1-enyl)azetid-2-one ((+) **1-2**)<sup>57</sup>

A solution of racemic (+/-) **1-2** (2.349 g, 8.12 mmol) dissolved in 0.02 M potassium phosphate buffer (pH 7.5) (406 mL) with 10 volume % acetonitrile (41 mL) was heated to 35 °C. To the solution was added 20 % wt PS-Amano Lipase (0.47 g). After addition, the mixture was stirred vigorously with a mechanical stirrer. The reaction was monitored *via* TLC and <sup>1</sup>H-NMR until 50% conversion of the acetate moiety to the hydroxyl moiety was observed. Upon completion, the remaining Lipase was filtered off *via* vacuum filtration and was washed with CH<sub>2</sub>Cl<sub>2</sub> (100 mL x

3). The organic layer was collected, washed with brine (20 mL x 3), dried over anhydrous MgSO<sub>4</sub>, and concentrated *in vacuo*. Purification was done *via* column chromatography on silica gel with increasing amounts of eluent (hexanes:ethyl acetate) to yield enantiopure (+) **1-2** (0.933 g, 3.23 mmol, 93 % yield) and the resulting alcohol (-) **1-3** (1.074 g, 4.35 mmol, 94 %). <sup>1</sup>NMR (300 MHz, CDCl<sub>3</sub>) δ 1.78 (s, 3 H), 1.81 (s, 3 H), 2.11 (s, 3 H), 3.77 (s, 3 H), 4.97 (dd, *J* = 9.6 Hz, 4.5 Hz, 1 H), 5.14 (d, *J* = 9.6 Hz, 1 H), 5.80 (d, *J* = 4.8 Hz, 1 H), 6.86 (d, *J* = 9.0, 2 H), 7.29 (d, *J* = 11.1 Hz, 2 H). M.P. 86~88 °C. The enantiometric excess was monitored *via* Normal Phase HPLC by using OD-H chiral column. t<sub>R</sub> = 15.91 min, >98 % ee. All data are in agreement with literature values.<sup>57</sup>

**(3R,4S)-1-(4-Methoxyphenyl)-3-hydroxy-4-(2-methylprop-1-enyl)azetidin-2-one ((+) 1-3)<sup>56</sup>**

The enantiomerically pure (+) **1-2** (0.794 g, 2.85 mmol) was dissolved in 0.1 M THF (27.5 mL) and cooled to 0 °C. To this mixture was added 1 M chilled NaOH (27.5 mL) in an equal amount of THF (27.5 mL). The reaction was stirred for 1 h. Upon completion the reaction was quenched with saturated NH<sub>4</sub>Cl (30 mL) and extracted with CH<sub>2</sub>Cl<sub>2</sub> (30 mL x 3). The organic layer was collected, washed with brine (15 mL x 3), dried over anhydrous MgSO<sub>4</sub>, and concentrated *in vacuo* to yield (+) **1-3** (0.672 g, 2.72 mmol, 99 %) as a white solid. <sup>1</sup>H NMR (300 MHz, CDCl<sub>3</sub>) δ 1.84 (s, 6 H), 3.74 (s, 3 H), 4.89 (dd, *J* = 9.0 Hz, 5.1 Hz, 1 H), 5.02 (d, *J* = 5.4 Hz, 1 H), 5.28 (d, *J* = 9.0 Hz, 1 H), 6.81 (d, *J* = 8.7, 2 H), 7.26 (d, *J* = 8.7 Hz, 2 H). M.P. 158-160 °C. All data are in agreement with literature values.<sup>56</sup>

**(3R,4S)-1-(4-Methoxyphenyl)-3-triisopropylsiloxy-4-(2-methylpropen-2-yl)azetidin-2-one ((+) 1-4)<sup>56</sup>**

An aliquot of (+) **1-3** (0.5 g, 2 mmol) and 0.3 eq DMAP (0.073 g, 0.6 mmol) were dissolved in 0.1 M CH<sub>2</sub>Cl<sub>2</sub> (20 mL). The solution was cooled to 0 °C under inert conditions. Then 2 eq triethylamine (0.56 mL, 0.405 g, 4 mmol) was added to the solution followed by the dropwise addition of 1.5 eq TIPSCl (0.65 mL, 0.585 g, 3 mmol). Then the ice-water bath was removed and the reaction was allowed to stir for 17 h at room temperature. Upon completion the reaction was quenched with saturated NH<sub>4</sub>Cl (10 mL) and extracted with CH<sub>2</sub>Cl<sub>2</sub> (15 mL x 3). The organic layer was collected, washed with brine (15 mL x 3), dried over anhydrous MgSO<sub>4</sub>, concentrated *in vacuo* and recrystallized to yield (+) **1-4** (0.675 g, 1.67 mmol, 83 %) as a white crystalline. <sup>1</sup>H NMR (500 MHz, CDCl<sub>3</sub>) δ 1.05 (m, 21 H), 1.79 (s, 3 H), 1.84 (s, 3 H), 3.77 (s, 3 H), 4.79 (dd, *J* = 9.0 Hz, 5.1 Hz, 1 H), 5.05 (d, *J* = 5.4 Hz, 1 H), 5.31 (d, *J* = 9.0 Hz, 1 H), 6.82 (d, *J* = 9.0, 2 H), 7.31 (d, *J* = 9.3 Hz, 2 H). <sup>13</sup>C NMR (125 MHz, CDCl<sub>3</sub>) δ 11.9, 17.6, 18.3, 26.1, 55.4, 57.5, 114.2, 118.3, 120.1, 131.5, 139.1, 165.6. M.P. 94-95 °C. All data are in agreement with literature values.<sup>56</sup>

**(3R,4S)-3-Triisopropylsilyloxy-4-(2-methylpropen-2-yl)azetidin-2-one ((+) 1-5)<sup>55</sup>**

An aliquot of (+) **1-4** (1 g, 2.48 mmol) was dissolved in acetonitrile/water (~0.03 M) (80 mL) and cooled to -10 °C by using dry ice. To this solution was added 4 eq CAN (5.4 g, 9.9 mmol) dissolved in H<sub>2</sub>O (80 mL) dropwise *via* an addition funnel. The ratio of acetonitrile to H<sub>2</sub>O was 1:1. The reaction temperature of -10 °C should be maintained throughout the reaction by keeping adding dry ice. The reaction was allowed to stir for 3 h. Upon completion, the mixture was quenched with saturated aqueous Na<sub>2</sub>SO<sub>3</sub> (50 mL). The aqueous layer was extracted by using ethyl acetate (75 mL x 3), and the combined organic layers were washed with brine (50 mL x 3). The residue was



dried over MgSO<sub>4</sub> and concentrated *in vacuo*. Purification was done *via* column chromatography on silica gel with increasing amounts of eluent (hexanes:ethyl acetate) to yield (+) **1-5** (641 mg, 2.16 mmol, white solid) in 87 % yield. <sup>1</sup>H NMR (500 MHz, CDCl<sub>3</sub>) δ 1.03 (m, 21 H), 1.68 (s, 3 H), 1.76 (s, 3 H), 4.42 (dd, *J* = 9.0 Hz, 5.1 Hz, 1 H), 4.98 (d, *J* = 4.8 Hz, 1 H), 5.30 (d, *J* = 9.6 Hz, 1 H), 5.96 (s, 1 H). <sup>13</sup>C NMR (125 MHz, CDCl<sub>3</sub>) δ 11.8, 17.6, 18.2, 26.0, 53.4, 79.3, 121.4, 138.0, 169.9. M.P. 83-85 °C. All data are in agreement with literature values.<sup>55</sup>

**(3*R*,4*S*)-1-(*tert*-Butoxycarbonyl)-3-triisopropylsiloxy-4-(2-methylpropen-2-yl)azetidin-2-one ((+) **1-6**)<sup>55</sup>**

An aliquot of (+) **1-5** (180 mg, 0.6 mmol), 0.3 eq DMAP (22 mg, 0.18 mmol) and 2 eq triethylamine (1.21 g, 1.2 mmol, 0.16 mL) were dissolved in CH<sub>2</sub>Cl<sub>2</sub> (~0.2 M) (3 mL) under inert conditions. To the mixture was added 1.1 eq di-*tert*-butyl dicarbonate (0.14 g, 0.66 mmol). The reaction was stirred at room temperature for 17 h. Upon completion the reaction was quenched with saturated NH<sub>4</sub>Cl (3 mL) and extracted with CH<sub>2</sub>Cl<sub>2</sub> (10 mL x 3). The organic layer was collected, washed with brine (10 mL x 3), dried over anhydrous MgSO<sub>4</sub>, and concentrated *in vacuo*. Purification was done *via* column chromatography on silica gel with increasing amounts of eluent (hexanes:ethyl acetate) to yield (+) **1-6** (242 mg, 0.6 mmol, 99 %). <sup>1</sup>H NMR (500 MHz, CDCl<sub>3</sub>) δ 1.07 (m, 21 H), 1.48 (s, 9 H), 1.76 (s, 3 H), 1.78 (s, 3 H), 4.73 (dd, *J* = 9.6 Hz, 5.8 Hz, 1 H), 4.95 (d, *J* = 5.6 Hz, 1 H), 5.26 (d, 1 H). <sup>13</sup>C NMR (125 MHz, CDCl<sub>3</sub>) δ 11.7, 17.5, 18.2, 26.0, 28.0, 56.8, 82.9, 118.4, 139.6, 148.1, 166.3. All data are in agreement with literature values.<sup>55</sup>

**10-Deacetyl-7-triethylsilylbaccatin III (**1-7**)<sup>2</sup>**

An aliquot of 10-deacetyl baccatin III (500 mg, 0.917 mmol) and 4 eq imidazole (272 mg, 4 mmol) were dissolved in 0.1 M DMF (10 mL) and cooled to 0 °C under inert condition. To the mixture was added 3 eq TESCO (0.5 mL, 452 mg, 3 mmol) dropwise. The mixture was stirred, allowed to warm to room temperature for 1 hour. Upon completion the reaction was quenched with saturated NH<sub>4</sub>Cl (15 mL) and extracted with ethyl acetate (10 mL x 3). The organic layer was collected, washed with brine (10 mL x 3), dried over anhydrous MgSO<sub>4</sub>, and concentrated *in vacuo*. Purification was done *via* column chromatography on silica gel with increasing amounts of eluent (hexanes:ethyl acetate) to yield **1-7** as white solid (558 mg, 0.846 mmol, 92 %). <sup>1</sup>H NMR (500 MHz, CDCl<sub>3</sub>) δ 0.55 (m, 6 H), 0.93 (t, *J* = 7.5 Hz, 9 H), 1.07 (s, 6 H), 1.58 (s, 3 H), 1.73 (s, 3 H), 2.04 (d, *J* = 4.5 Hz, 1 H), 2.08 (s, 3 H), 2.24 (s, 1 H), 2.28 (s, 3 H), 3.96 (d, *J* = 6.9 Hz, 1 H), 4.17 (d, *J* = 9.0 Hz, 1 H), 4.26 (d, *J* = 2.4 Hz, 1 H), 4.32 (d, *J* = 8.1 Hz, 1 H), 4.41 (dd, *J* = 6.6 Hz, 4.2 Hz, 1 H), 4.87 (q, 1H), 4.96 (d, *J* = 8.1 Hz, 1 H), 5.17 (s, 1 H), 5.60 (d, *J* = 6.6 Hz, 1 H), 7.47 (t, *J* = 7.2 Hz, 2 H), 7.60 (t, *J* = 7.5 Hz, 1 H), 8.09 (d, *J* = 6.9, 2 H). All data are in agreement with literature values.<sup>2</sup>

**10-Cyclopropanecarbonyl-10-deacetyl-7-triethylsilylbaccatin III (**1-8**)<sup>53</sup>**

An aliquot of **1-7** (300 mg, 0.455 mmol) was dissolved in 0.05 M THF (9 mL) and cooled to -40 °C under inert conditions. To the mixture was added 1.2 eq cyclopropanecarboxylic acid chloride (0.05 mL, 57.5 mg, 0.55 mmol) dropwise, followed by the addition of 1.1 eq LiHMDS in 1.0 M THF (0.5 mL, 84 mg, 0.5 mmol) dropwise. The mixture was stirred, allowed to warm to 0 °C for 30 minutes. Upon completion the reaction was quenched with saturated NH<sub>4</sub>Cl (10 mL) and

extracted with ethyl acetate (10 mL x 3). The organic layer was collected, washed with brine (10 mL x 3), dried over anhydrous MgSO<sub>4</sub>, and concentrated *in vacuo*. Purification was done *via* column chromatography on silica gel with increasing amounts of eluent (hexanes:ethyl acetate) to afford **1-8** (308 mg, 0.424 mmol, 93 %) as a white solid. <sup>1</sup>H NMR (500 MHz, CDCl<sub>3</sub>) δ 0.57 (m, 6 H), 0.91 (t, *J* = 8.1 Hz, 9 H), 1.04 (s, 3 H), 1.20 (s, 3 H), 1.59 (s, 3 H), 1.67 (s, 3 H), 1.76 (m, 1 H), 1.87 (m, 1 H), 2.04 (s, 1 H), 2.19 (s, 3 H), 2.28 (s, 3 H), 2.52 (m, 1 H), 3.88 (d, *J* = 8.7 Hz, 1 H), 4.14 (d, *J* = 8.4 Hz, 1 H), 4.29 (s, 1 H), 4.32 (d, *J* = 8.4 Hz, 1 H), 4.48 (dd, *J* = 6.6 Hz, 10.2 Hz, 1 H), 4.83 (m, 1 H), 4.96 (d, *J* = 7.8 Hz, 1 H), 5.63 (d, *J* = 6.9 Hz, 1 H), 6.46 (s, 1 H), 7.47 (t, *J* = 7.8 Hz, 2 H), 7.60 (t, *J* = 7.2 Hz, 1 H), 8.11 (d, *J* = 6.9, 2 H). <sup>13</sup>C NMR (125 MHz, CDCl<sub>3</sub>) δ 5.2, 6.8, 8.6, 8.7, 9.9, 13.0, 14.2, 14.9, 20.1, 21.0, 22.7, 26.8, 37.2, 38.2, 42.7, 47.2, 58.6, 60.4, 68.0, 72.3, 74.7, 75.5, 78.8, 80.9, 84.2, 128.6, 129.4, 130.1, 132.8, 133.6, 143.9, 167.1, 170.7, 171.2, 173.2, 202.3. M.P. 196-197 °C. All data are in agreement with literature values.<sup>53</sup>

### **10-Cyclopropanecarbonyl-3'-dephenyl-3'-(2-methyl-2-propenyl)-7-triethylsilyl-2'-triisopropylsilyldocetaxel (1-9)<sup>53</sup>**

An aliquot of **1-8** (912 mg, 1.25 mmol), and 1.2 eq β-lactam (+) **1-6** (596 mg, 1.5 mmol) were dissolved in 0.02 M THF (60 mL) and cooled to -40 °C under inert conditions for at least 30 minutes. To the mixture was added 1.5 eq LiHMDS in 1.06 M THF (1.77 mL, 1.88 mmol) dropwise. The mixture was stirred at -40 °C for 3 hours. Upon completion the reaction was quenched with saturated NH<sub>4</sub>Cl (40 mL) and extracted with ethyl acetate (40 mL x 3). The organic layer was collected, washed with brine (40 mL x 3), dried over anhydrous MgSO<sub>4</sub>, and concentrated *in vacuo*. Purification was done *via* column chromatography on silica gel with increasing amounts of eluent (hexanes:ethyl acetate) to give **1-9** (1.04 g, 0.93 mmol, 74 %) as a white solid. <sup>1</sup>H NMR (500 MHz, CDCl<sub>3</sub>) δ 0.56 (m, 6 H), 0.90 (t, *J* = 8.0 Hz, 9 H), 1.10 (s, 18 H), 1.74 (s, 3 H), 1.90 (dt, 1 H), 2.00 (d, *J* = 5.0 Hz, 1 H), 2.04 (s, 3 H), 2.35 (s, 3 H), 3.95 (d, *J* = 7.0 Hz, 1 H), 4.16 (d, *J* = 9.0 Hz, 1 H), 4.25 (s, 1 H), 4.31 (d, *J* = 8.5 Hz, 1 H), 4.41 (dd, *J* = 7.0 Hz, 11.0 Hz, 1 H), 4.88 (q, 1H), 4.95 (d, *J* = 9.0 Hz, 1 H), 5.17 (s, 1 H), 5.60 (d, *J* = 7.0 Hz, 1 H), 7.47 (t, *J* = 7.5 Hz, 2 H), 7.60 (t, *J* = 8.0 Hz, 1 H), 8.10 (d, *J* = 7.5, 2 H). <sup>13</sup>C NMR (125 MHz, CDCl<sub>3</sub>) δ 5.3, 6.7, 8.6, 8.7, 10.1, 12.5, 12.9, 14.2, 14.3, 17.9, 18.0, 18.5, 21.3, 22.5, 25.7, 26.3, 28.2, 35.5, 37.1, 43.2, 46.7, 52.0, 58.3, 60.4, 71.9, 72.2, 74.8, 75.0, 75.2, 78.8, 79.4, 81.0, 84.3, 122.1, 128.5, 129.4, 130.1, 133.3, 133.5, 140.9, 155.2, 16.8, 169.8, 171.2, 171.9, 173.1, 202.1. All data are in agreement with literature values.<sup>53</sup>

### **10-Cyclopropanecarbonyl-3'-dephenyl-3'-(2-methyl-2-propenyl)docetaxel (SB-T-1214) (1-10)<sup>53</sup>**

An aliquot of **1-9** (996 mg, 0.886 mmol) was dissolved in a 1:1 mixture of 0.02 M acetonitrile:pyridine (44 mL) and cooled to 0 °C under inert conditions. To the mixture was added 10 mL HF/pyridine dropwise (0.01 mL per every 1 mg was added). The reaction was stirred at room temperature for 24 h. Upon completion the reaction was quenched with 0.2 M citric acid in H<sub>2</sub>O (3.8 %) (10 mL) and extracted with ethyl acetate (20 mL x 3). The organic layer was collected, washed with CuSO<sub>4</sub>, washed with diluted water until the organic layer became clear, then washed with brine (20 mL x 3), dried over anhydrous MgSO<sub>4</sub>, and concentrated *in vacuo*. Purification was done *via* column chromatography on silica gel with increasing amounts of eluent (hexanes:ethyl acetate) to yield crude **1-10** (SB-T-1214) followed by recrystallization using ethyl acetate to afford

pure **1-10** (SB-T-1214) (587 mg, 0.69 mmol, 78 %) as white solid, HPLC purity > 99 %. <sup>1</sup>H NMR (300 MHz, CDCl<sub>3</sub>) δ 0.98 (m, 2 H), 1.26 (m, 2 H), 1.35 (s, 9 H), 1.66 (s, 3 H), 1.76 (m, 6 H), 1.89 (s, 3 H), 2.04 (s, 2 H), 2.35 (s, 4 H), 2.61 (d, *J* = 3.9, 1 H), 3.44 (d, *J* = 6.6 Hz, 1 H), 3.81 (d, *J* = 6.9 Hz, 1 H), 4.21 (m, 2 H), 4.29 (d, *J* = 8.4 Hz, 1 H), 4.40 (m, 1 H), 4.76 (t, *J* = 8.4 Hz, 1 H), 4.83 (d, *J* = 8.7 Hz, 1 H), 4.95 (d, *J* = 7.8 Hz), 5.30 (d, *J* = 9.6 Hz, 1 H), 5.67 (d, *J* = 6.9 Hz, 1 H), 6.17 (t, *J* = 8.1 Hz, 1 H), 6.30 (s, 1 H), 7.46 (t, *J* = 7.8 Hz, 2 H), 7.60 (t, *J* = 7.2 Hz, 1 H), 8.09 (d, *J* = 6.8, 2 H). <sup>13</sup>C NMR (150 MHz, CDCl<sub>3</sub>) δ 9.1, 9.4, 9.5, 13.0, 14.9, 18.5, 21.9, 22.4, 25.7, 26.7, 28.2, 35.5, 35.6, 43.2, 45.6, 51.6, 58.6, 72.2, 72.3, 73.7, 75.0, 75.4, 76.5, 77.0, 77.5, 79.2, 80.0, 81.1, 84.4, 120.7, 128.6, 129.2, 130.1, 133.0, 133.6, 137.9, 142.6, 155.4, 166.9, 170.1, 175.1, 203.9. All data are in agreement with literature values.<sup>53</sup>

## §1.5 Reference

- (1) Wani, M. C.; Taylor, H. L.; Wall, M. E.; Coggon, P.; McPhail, A. T. Plant antitumor agents. VI. Isolation and structure of taxol, a novel antileukemic and antitumor agent from *Taxus brevifolia*. *J. Am. Chem. Soc.* **1971**, *93*, 2325-2327.
- (2) Rowinsky, M., Eric K. The development and clinical utility of the taxane class of antimicrotubule chemotherapy agents. *Annu. Rev. Med.* **1997**, *48*, 353-374.
- (3) Bissery, M.-C.; Nohynek, G.; Sanderink, G.-J.; Lavelie, F. Docetaxel (Taxotere(R)) a review of preclinical and clinical experience. Part I: preclinical experience. *Anti-Cancer Drug.* **1995**, *6*, 339-355.
- (4) Galsky, M. D.; Dritselis, A.; Kirkpatrick, P.; Oh, W. K. Cabazitaxel. *Nat Rev Drug Discov* **2010**, *9*, 677-678.
- (5) Pivot, X.; Koralewski, P.; Hidalgo, J. L.; Chan, A.; Gonçalves, A.; Schwartzmann, G.; Assadourian, S.; Lotz, J. P. A multicenter phase II study of XRP6258 administered as a 1-h i.v. infusion every 3 weeks in taxane-resistant metastatic breast cancer patients. *Ann. Oncol.* **2008**, *19*, 1547-1552.
- (6) Holton, R. A.; Somoza, C.; Kim, H. B.; Liang, F.; Biediger, R. J.; Boatman, P. D.; Shindo, M.; Smith, C. C.; Kim, S. First total synthesis of taxol. 1. Functionalization of the B ring. *J. Am. Chem. Soc.* **1994**, *116*, 1597-1598.
- (7) Holton, R. A.; Kim, H. B.; Somoza, C.; Liang, F.; Biediger, R. J.; Boatman, P. D.; Shindo, M.; Smith, C. C.; Kim, S. First total synthesis of taxol. 2. Completion of the C and D rings. *J. Am. Chem. Soc.* **1994**, *116*, 1599-1600.
- (8) Nicolaou, K. C.; Nantermet, P. G.; Ueno, H.; Guy, R. K.; Couladouros, E. A.; Sorensen, E. J. Total Synthesis of Taxol. 1. Retrosynthesis, Degradation, and Reconstitution. *J. Am. Chem. Soc.* **1995**, *117*, 624-633.
- (9) Nicolaou, K. C.; Liu, J. J.; Yang, Z.; Ueno, H.; Sorensen, E. J.; Claiborne, C. F.; Guy, R. K.; Hwang, C. K.; Nakada, M.; Nantermet, P. G. Total Synthesis of taxol. 2. Construction of A and C ring intermediates and initial attempts to construct the ABC ring system. *J. Am. Chem. Soc.* **1995**, *117*, 634-644.
- (10) Nicolaou, K. C.; Yang, Z.; Liu, J. J.; Nantermet, P. G.; Claiborne, C. F.; Renaud, J.; Guy, R. K.; Shibayama, K. Total Synthesis of Taxol. 3. Formation of Taxol's ABC Ring Skeleton. *J. Am. Chem. Soc.* **1995**, *117*, 645-652.
- (11) Nicolaou, K. C.; Ueno, H.; Liu, J. J.; Nantermet, P. G.; Yang, Z.; Renaud, J.; Paulvannan, K.; Chadha, R. Total Synthesis of Taxol. 4. The Final Stages and Completion of the Synthesis. *J. Am. Chem. Soc.* **1995**, *117*, 653-659.

- (12) Danishefsky, S. J.; Masters, J. J.; Young, W. B.; Link, J. T.; Snyder, L. B.; Magee, T. V.; Jung, D. K.; Isaacs, R. C. A.; Bornmann, W. G.; Alaimo, C. A.; Coburn, C. A.; Di Grandi, M. J. Total Synthesis of Baccatin III and Taxol. *J. Am. Chem. Soc.* **1996**, *118*, 2843-2859.
- (13) Wender, P. A.; Badham, N. F.; Conway, S. P.; Floreancig, P. E.; Glass, T. E.; Gränicher, C.; Houze, J. B.; Jänichen, J.; Lee, D.; Marquess, D. G.; McGrane, P. L.; Meng, W.; Mucciario, T. P.; Mühlebach, M.; Natchus, M. G.; Paulsen, H.; Rawlins, D. B.; Satkofsky, J.; Shuker, A. J.; Sutton, J. C.; Taylor, R. E.; Tomooka, K. The Pinene Path to Taxanes. 5. Stereocontrolled Synthesis of a Versatile Taxane Precursor. *J. Am. Chem. Soc.* **1997**, *119*, 2755-2756.
- (14) Morihira, K.; Hara, R.; Kawahara, S.; Nishimori, T.; Nakamura, N.; Kusama, H.; Kuwajima, I. Enantioselective Total Synthesis of Taxol. *J. Am. Chem. Soc.* **1998**, *120*, 12980-12981.
- (15) Mukaiyama, T.; Shiina, I.; Iwadare, H.; Saitoh, M.; Nishimura, T.; Ohkawa, N.; Sakoh, H.; Nishimura, K.; Tani, Y.-i.; Hasegawa, M.; Yamada, K.; Saitoh, K. Asymmetric Total Synthesis of Taxol. *Chem.-Eur. J.* **1999**, *5*, 121-161.
- (16) Doi, T.; Fuse, S.; Miyamoto, S.; Nakai, K.; Sasuga, D.; Takahashi, T. A Formal Total Synthesis of Taxol Aided by an Automated Synthesizer. *Chem Asian J.* **2006**, *1*, 370-383.
- (17) Chauvière, G. G., D.; Picot, F.; Sénilh, V.; Potier, P. Structural Analysis and Biochemical Study of Isolated Products of the Yew: *Taxus Baccata* L. (Taxaceae). *C. R. Seances Acad. Sci., Ser 2* **1981**, *293*, 501-503.
- (18) American Cancer Society, Atlanta, Georgia. Cancer Facts & Figures. **2015**.
- (19) Guenard, D.; Gueritte-Voegelein, F.; Potier, P. Taxol and taxotere: discovery, chemistry, and structure-activity relationships. *Acc. Chem. Res.* **1993**, *26*, 160-167.
- (20) Denis, J. N.; Greene, A. E.; Guenard, D.; Gueritte-Voegelein, F.; Mangatal, L.; Potier, P. Highly efficient, practical approach to natural taxol. *J. Am. Chem. Soc.* **1988**, *110*, 5917-5919.
- (21) Ojima, I.; Habus, I.; Zhao, M.; Georg, G. I.; Jayasinghe, L. R. Efficient and practical asymmetric synthesis of the taxol C-13 side chain, N-benzoyl-(2R,3S)-3-phenylisoserine, and its analogs via chiral 3-hydroxy-4-aryl- $\beta$ -lactams through chiral ester enolate-imine cyclocondensation. *J. Org. Chem.* **1991**, *56*, 1681-1683.
- (22) Ojima, I.; Habus, I.; Zhao, M.; Zucco, M.; Park, Y. H.; Sun, C. M.; Brigaud, T. New and efficient approaches to the semisynthesis of taxol and its C-13 side chain analogs by means of  $\beta$ -lactam synthon method. *Tetrahedron* **1992**, *48*, 6985-7012.
- (23) Ojima, I.; Kuduk, S. D.; Pera, P.; Veith, J. M.; Bernacki, R. J. Synthesis and Structure-Activity Relationships of Nonaromatic Taxoids: Effects of Alkyl and Alkenyl Ester Groups on Cytotoxicity. *J. Med. Chem.* **1997**, *40*, 279-285.
- (24) Ojima, I.; Slater, J. C.; Kuduk, S. D.; Takeuchi, C. S.; Gimi, R. H.; Sun, C.-M.; Park, Y. H.; Pera, P.; Veith, J. M.; Bernacki, R. J. Syntheses and Structure-Activity Relationships of Taxoids Derived from 14 $\beta$ -Hydroxy-10-deacetylbaccatin III. *J. Med. Chem.* **1997**, *40*, 267-278.
- (25) Ojima, I.; Slater, J. C.; Michaud, E.; Kuduk, S. D.; Bounaud, P.-Y.; Vrignaud, P.; Bissery, M.-C.; Veith, J. M.; Pera, P.; Bernacki, R. J. Syntheses and Structure-Activity Relationships of the Second-Generation Antitumor Taxoids: Exceptional Activity against Drug-Resistant Cancer Cells. *J. Med. Chem.* **1996**, *39*, 3889-3896.
- (26) Kamath, A.; Ojima, I. Advances in the chemistry of  $\beta$ -lactam and its medicinal applications. *Tetrahedron* **2012**, *68*, 10640-10664.
- (27) Staudinger, H. Zur Kenntniss der Ketene. Diphenylketen. *Justus Liebigs Ann. Chem.* **1907**, *356*, 51-123.
- (28) Ojima, I.; Habus, I. Asymmetric synthesis of  $\beta$ -lactams by chiral ester enolate - imine

- condensation. *Tetrahedron Lett.* **1990**, *31*, 4289-4292.
- (29) Lopez, R.; Sordo, T. L.; Sordo, J. A.; Gonzalez, J. Torquoelectronic effect in the control of the stereoselectivity of ketene-imine cycloaddition reactions. *J. Org. Chem.* **1993**, *58*, 7036-7037.
- (30) Jiao, L.; Liang, Y.; Xu, J. Origin of the Relative Stereoselectivity of the  $\beta$ -Lactam Formation in the Staudinger Reaction. *J. Am. Chem. Soc.* **2006**, *128*, 6060-6069.
- (31) Brieva, R.; Crich, J. Z.; Sih, C. J. Chemoenzymic synthesis of the C-13 side chain of taxol: optically active 3-hydroxy-4-phenyl .beta.-lactam derivatives. *J. Org. Chem.* **1993**, *58*, 1068-1075.
- (32) Cragg, G. M., Kingston, D. G. I., Newman, D. J. Anticancer agents from natural products. CRC Press. **2011**.
- (33) Ojima, I.; Zuniga, E. S.; Berger, W. T.; Seitz, J. D. Tumor-targeting drug delivery of new-generation taxoids. *Future Med Chem.* **2012**, *4*, 33-50.
- (34) Al-Hajj, M.; Wicha, M. S.; Benito-Hernandez, A.; Morrison, S. J.; Clarke, M. F. Prospective identification of tumorigenic breast cancer cells. *Proc. Natl. Acad. Sci. U. S. A.* **2003**, *100*, 3983-3988.
- (35) Wilson, L.; Jordan, M. A. Microtubule dynamics: taking aim at a moving target. *Chem. Biol.* **1995**, *2*, 569-573.
- (36) Zhao, X. R. Design, synthesis and biological evaluation of novel taxane-based anticancer agents and their applications to tumor-targeting drug delivery systems (Doctoral Dissertation). *State University of New York at Stony Brook* **2009**.
- (37) Jordan, M. A.; Wilson, L. Microtubules as a target for anticancer drugs. *Nat Rev Cancer* **2004**, *4*, 253-265.
- (38) Schiff, P. B.; Fant, J.; Horwitz, S. B. Promotion of microtubule assembly in vitro by taxol. *Nature* **1979**, *277*, 665-667.
- (39) Holmes, F. A.; Walters, R. S.; Theriault, R. L.; Buzdar, A. U.; Frye, D. K.; Hortobagyi, G. N.; Forman, A. D.; Newton, L. K.; Raber, M. N. Phase II Trial of Taxol, an Active Drug in the Treatment of Metastatic Breast Cancer. *J. Natl. Cancer Inst.* **1991**, *83*, 1797-1805.
- (40) Weiss, R. B.; Donehower, R. C.; Wiernik, P. H.; Ohnuma, T.; Gralla, R. J.; Trump, D. L.; Baker, J. R.; Van Echo, D. A.; Von Hoff, D. D.; Leyland-Jones, B. Hypersensitivity reactions from taxol. *J Clin. Oncol.* **1990**, *8*, 1263-1268.
- (41) Rowinsky, E. K.; Donehower, R. C. Paclitaxel (Taxol). *N. Engl. J. Med.* **1995**, *332*, 1004-1014.
- (42) Gottesman, M. M.; Pastan, I. Biochemistry of Multidrug Resistance Mediated by the Multidrug Transporter. *Annu. Rev. Biochem.* **1993**, *62*, 385-427.
- (43) Szakacs, G.; Paterson, J. K.; Ludwig, J. A.; Booth-Genthe, C.; Gottesman, M. M. Targeting multidrug resistance in cancer. *Nat Rev Drug Discov* **2006**, *5*, 219-234.
- (44) Germann, U. A. P-glycoprotein—A mediator of multidrug resistance in tumour cells. *Eur. J. Cancer* **1996**, *32*, 927-944.
- (45) Ducry, L.; Stump, B. Antibody–Drug Conjugates: Linking Cytotoxic Payloads to Monoclonal Antibodies. *Bioconjugate Chem.* **2009**, *21*, 5-13.
- (46) Penson, R. T.; Oliva, E.; Skates, S. J.; Glyptis, T.; Fuller Jr, A. F.; Goodman, A.; Seiden, M. V. Expression of multidrug resistance-1 protein inversely correlates with paclitaxel response and survival in ovarian cancer patients: a study in serial samples. *Gynecol. Oncol.* **2004**, *93*, 98-106.
- (47) Martinez, L.; Falson, P. Multidrug resistance ATP-binding cassette membrane transporters as targets for improving oropharyngeal candidiasis treatment. *Advances in Cellular and Molecular Otolaryngology* **2014**, *2*, 23955.

- (48) Aller, S. G.; Yu, J.; Ward, A.; Weng, Y.; Chittaboina, S.; Zhuo, R.; Harrell, P. M.; Trinh, Y. T.; Zhang, Q.; Urbatsch, I. L.; Chang, G. Structure of P-Glycoprotein Reveals a Molecular Basis for Poly-Specific Drug Binding. *Science* **2009**, *323*, 1718-1722.
- (49) Lage, H.; Dietel, M. Multiple mechanisms confer different drug-resistant phenotypes in pancreatic carcinoma cells. *J. Cancer Res. Clin. Oncol.* **2002**, *128*, 349-357.
- (50) O'Driscoll, L.; Walsh, N.; Larkin, A.; Ballot, J.; Ooi, W. S.; Gullo, G.; O'Connor, R.; Clynes, M.; Crown, J.; Kennedy, S. MDR1/P-glycoprotein and MRP-1 Drug Efflux Pumps in Pancreatic Carcinoma. *Anticancer Res.* **2007**, *27*, 2115-2120.
- (51) Donnenberg, V. S.; Donnenberg, A. D. Multiple Drug Resistance in Cancer Revisited: The Cancer Stem Cell Hypothesis. *J Clin Pharmacol.* **2005**, *45*, 872-877.
- (52) Borcard, F.; Godinat, A.; Staedler, D.; Comas Blanco, H.; Dumont, A.-L.; Chapuis-Bernasconi, C.; Scaletta, C.; Applegate, L. A.; Krauss Juillerat, F.; Gonzenbach, U. T.; Gerber-Lemaire, S.; Juillerat-Jeanneret, L. Covalent Cell Surface Functionalization of Human Fetal Osteoblasts for Tissue Engineering. *Bioconjugate Chem.* **2011**, *22*, 1422-1432.
- (53) American Cancer Society, Inc. Cancer Statistics 2015: A Presentation from the American Cancer Society. **2015**.
- (54) Ojima, I.; Duclos, O.; Kuduk, S. D.; Sun, C.-M.; Slater, J. C.; Lavelle, F.; Veith, J. M.; Bernacki, R. J. Synthesis and biological activity of 3'-alkyl- and 3'-alkenyl-3'-dephenyldocetaxels. *Bioorg. Med. Chem. Lett.* **1994**, *4*, 2631-2634.
- (55) Ojima, I.; Fumero-Oderda, C. L.; Kuduk, S. D.; Ma, Z.; Kirikae, F.; Kirikae, T. Structure-activity relationship study of taxoids for their ability to activate murine macrophages as well as inhibit the growth of macrophage-like cells. *Bioorg. Med. Chem.* **2003**, *11*, 2867-2888.
- (56) Kuznetsova, L. V.; Pepe, A.; Ungureanu, I. M.; Pera, P.; Bernacki, R. J.; Ojima, I. Syntheses and Structure-Activity Relationships of Novel 3'-Difluoromethyl and 3'-Trifluoromethyl-Taxoids. *J. Fluorine Chem.* **2008**, *129*, 817-828.
- (57) Kuznetsova, L.; Ungureanu, I. M.; Pepe, A.; Zanardi, I.; Wu, X.; Ojima, I. Trifluoromethyl- and difluoromethyl- $\beta$ -lactams as useful building blocks for the synthesis of fluorinated amino acids, dipeptides, and fluoro-taxoids. *J. Fluorine Chem.* **2004**, *125*, 487-500.

## Chapter 2

### New-Generation Taxoid SB-T-1214 Derivatives as Imaging Agents

§2.1 Introduction .....	38
§2.2 Fluorescein-Labeled Taxoid .....	38
§2.2.1 Fluorescent Tags.....	39
§2.2.2 Synthesis of SB-T-1214-C7-Fluorescent Probe .....	40
§2.3 Development of <sup>11</sup> C-Labeled SB-T-1214 Radiotracer for PET Imaging Study.....	42
§2.3.1 Carbon-11 Radiolabeled Taxanes .....	42
§2.3.2 Establishment of LC/UV/MS-TOF Analysis Condition .....	43
§2.3.3 Analysis and Determination of the Stille Coupling Outcomes.....	47
§2.3.4 Synthesis of Taxoid Derivatives from Stille Coupling.....	53
§2.4 Summary.....	58
§2.5 Experimental Section.....	58
§2.5.1 Caution.....	58
§2.5.2 General Information.....	58
§2.5.3 Materials.....	59
§2.5.4 Experimental Procedure.....	59
§2.6 References.....	66

## §2.1 Introduction

To study and visualize the interaction of taxane and tubulin/microtubule system, taxane-based fluorescent probes can provide a useful method to explore the microtubule dynamics in the presence of taxane using fluorescence spectroscopy.<sup>1</sup> Moreover, taxanes have been radiolabeled with various positron-emitting radionuclides including <sup>11</sup>C, <sup>18</sup>F, <sup>76</sup>Br, and <sup>124</sup>I for PET imaging study. For instance, modification at para position of the C3'-N-phenyl group on paclitaxel gave several paclitaxel-based PET tracers to elucidate its biodistribution profiles. Examples of fluorescein-labelled and radiolabeled taxenes/taxoids<sup>2-4</sup> are shown in **Figure 2.1**.

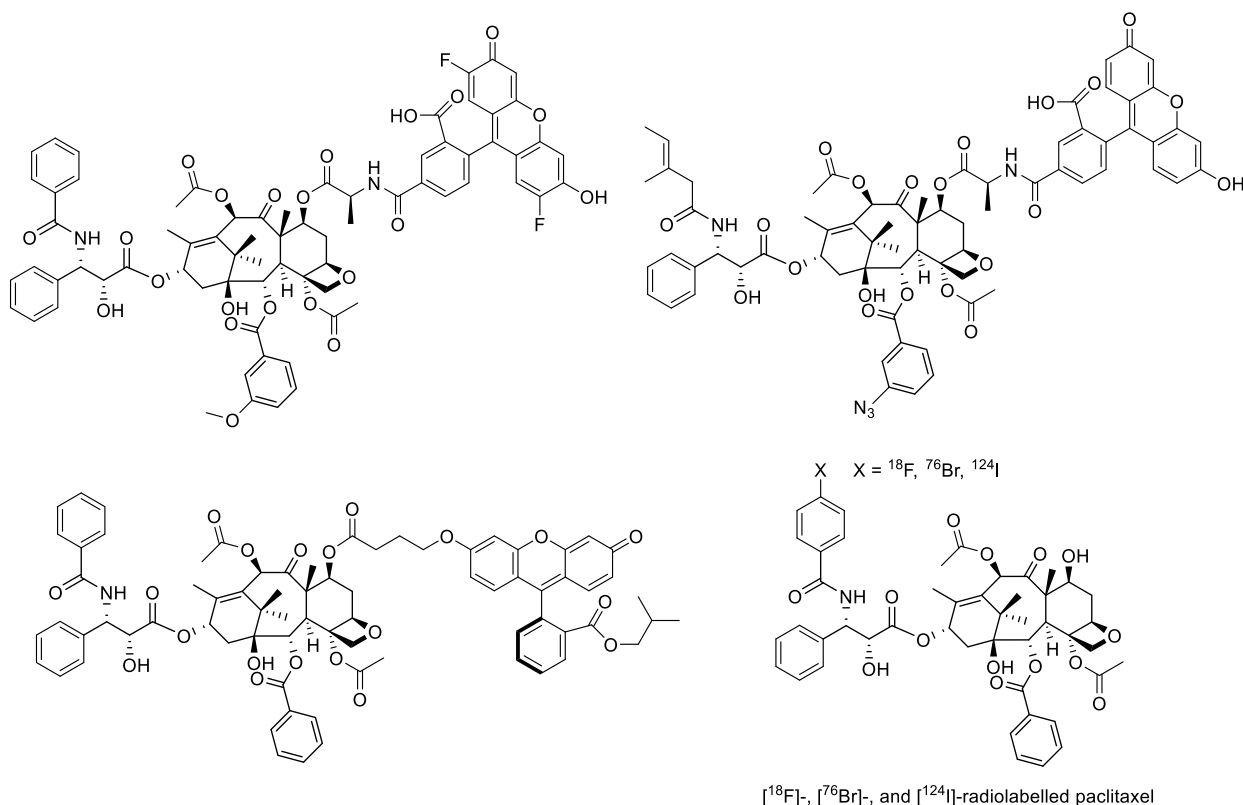


**Figure 2.1** Chemical structures of fluorescein-labelled and radiolabeled taxanes/toxoids (adapted from references 2-4)<sup>2-4</sup>

## §2.2 Fluorescein-Labeled Taxoid

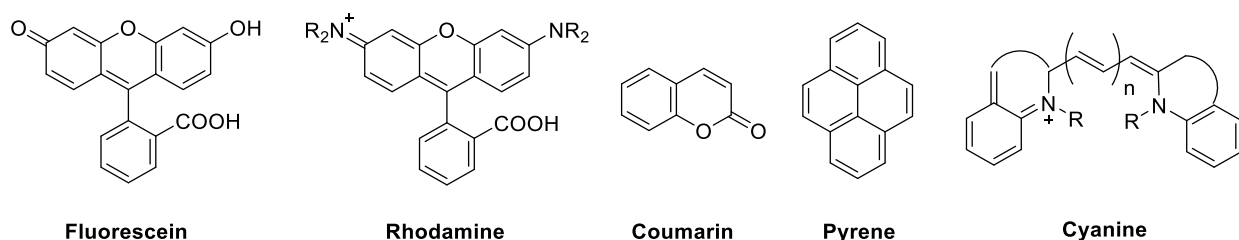
As availability of modification on the taxane scaffold without affecting the binding affinity and biological activity, most taxane-based fluorescent probes were prepared by introduction of a fluorophore at C7 position through a proper linkage. In this way the interference of fluorescent groups with tubulin can be minimized the most, while it is still possible to determine the thermodynamic and kinetic parameters for the taxane-tubulin binding process.<sup>1</sup> Moreover, taxane-fluorescent probe can be linked with a tumor-targeting moiety (vitamin, monoclonal antibody, peptide, etc.) through mechanism-based cleavable linker to form tumor-targeted drug conjugates. Fluorescence spectroscopy can provide information and help understand the enhanced cell uptake



of drug through receptor-mediated endocytosis in the presence of tumor-targeting module, as well as the mechanism of linker cleavage to release the drug in its bioactive form.<sup>5</sup>

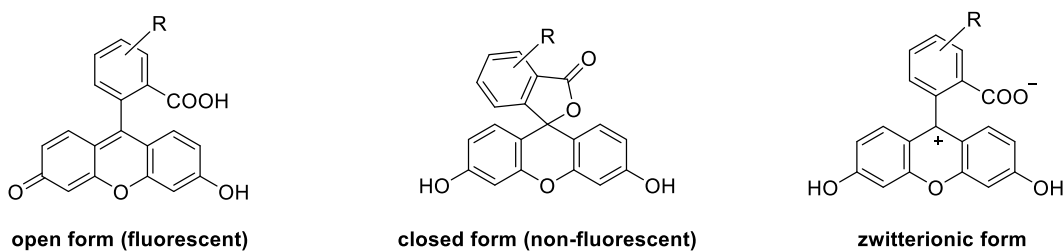
### §2.2.1 Fluorescent Tags

Previously, various fluorescent dyes have been synthesized and utilized as fluorescent probes to provide higher sensitivity for visualizing biomolecules such as proteins and DNA in biological application.<sup>6</sup> These fluorescent dyes can be classified according to their structures, such as fluorescein, rhodamines, coumarins, pyrenes, cyanines, etc. (**Figure 2.2**)



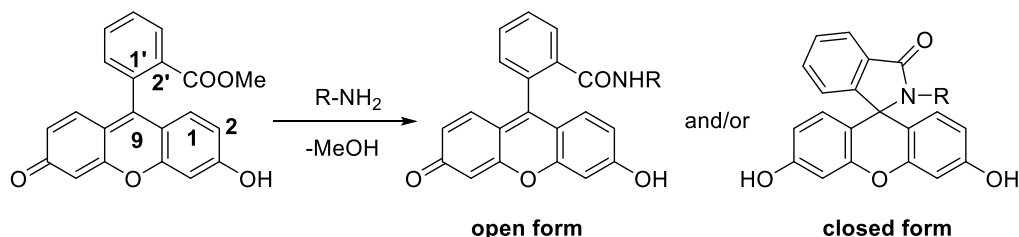
**Figure 2.2** Selected examples of fluorescent dyes

Fluoresceins are commonly used because of their solubility in aqueous buffers, as well as high fluorescence quantum yield at physiological pH.<sup>6</sup> They have been viewed to exist in three forms: a highly fluorescent quinone form (open form), a non-fluorescent spirolactone form (closed form), and a zwitterion structure (zwitterionic form) in aqueous environment. (**Figure 2.3**)<sup>7</sup>



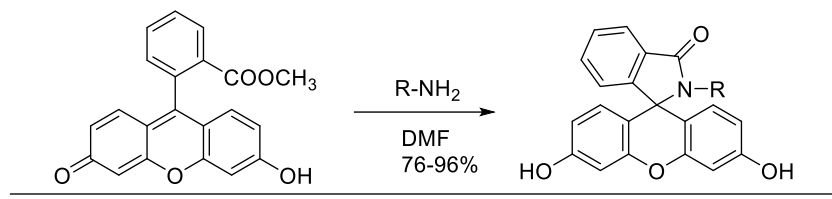
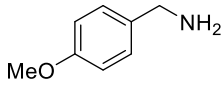
**Figure 2.3** Three existing forms of fluorescein (adapted from reference7)<sup>7</sup>

The most convenient way to keep the fluorescence is to protect the C2' carboxyl acid group with alkyl substituent to avoid the ring close and spirolactone formation. A methyl ester on C2' position certainly can solve the issue since it represented a known open form of fluorescein, however, the fluorescein methyl ester can also rapidly react with a variety of primary amines, resulting in a nearly colorless non-fluorescent spirolactam.<sup>7</sup> (**Figure 2.4**) These off-white spirolactam products have been purified by preparative reversed-phase HPLC (**Table 2.1**) and confirmed by NMR.<sup>5,7</sup> Accordingly, considering the existence of primary amine in the physiological system, a bulk alkyl group will need to take place of methyl group on C2' position.



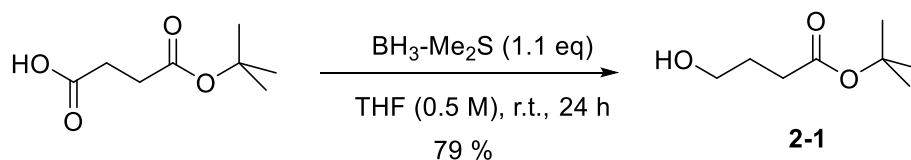
**Figure 2.4** Fluorescein spirolactam formation (adapted from reference 7)<sup>7</sup>

**Table 2.1** Spirolactams Formation of Fluorescein Methyl Ester with Amines (adapted from reference 5)<sup>5</sup>

			
Amine	Yield %	Amine	Yield %
	77	H <sub>2</sub> N-NH <sub>2</sub>	96
MeOOC-CH <sub>2</sub> -NH <sub>3</sub> Cl	83	BnO-NH <sub>3</sub> Cl	83
(HOOC-CH <sub>2</sub> -CNH <sub>2</sub> ) <sub>2</sub> HCl	95	BOC-NH-NH <sub>2</sub>	90
HO-CH <sub>2</sub> -CH <sub>2</sub> -CH <sub>2</sub> -NH <sub>2</sub>	78	H <sub>2</sub> N-CH <sub>2</sub> -CH <sub>2</sub> -NH <sub>2</sub>	84
HO-NH <sub>3</sub> Cl	76	H <sub>2</sub> N-CH <sub>2</sub> -CH <sub>2</sub> -CH <sub>2</sub> -NH <sub>2</sub>	92

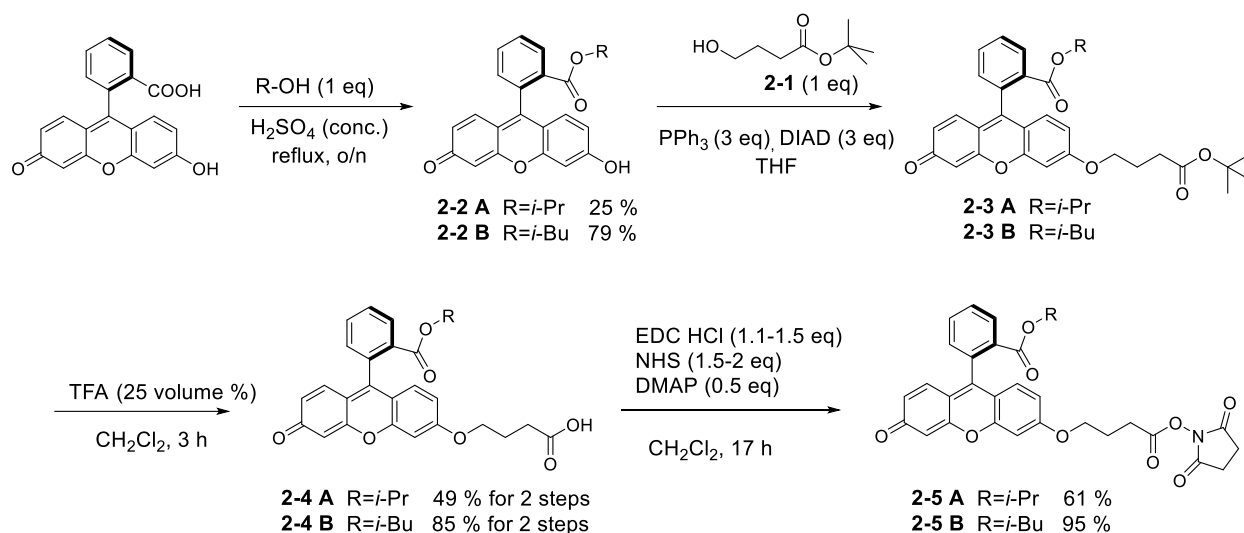
### §2.2.2 Synthesis of SB-T-1214-C7-Fluorescent Probe

To give fluorescein more space to couple to other moiety, succinic acid mono-*tert*-butyl ester was reduced to *tert*-butyl 4-hydroxybutanoate (**2-1**) in good yield (79 %). (**Scheme 2.1**)



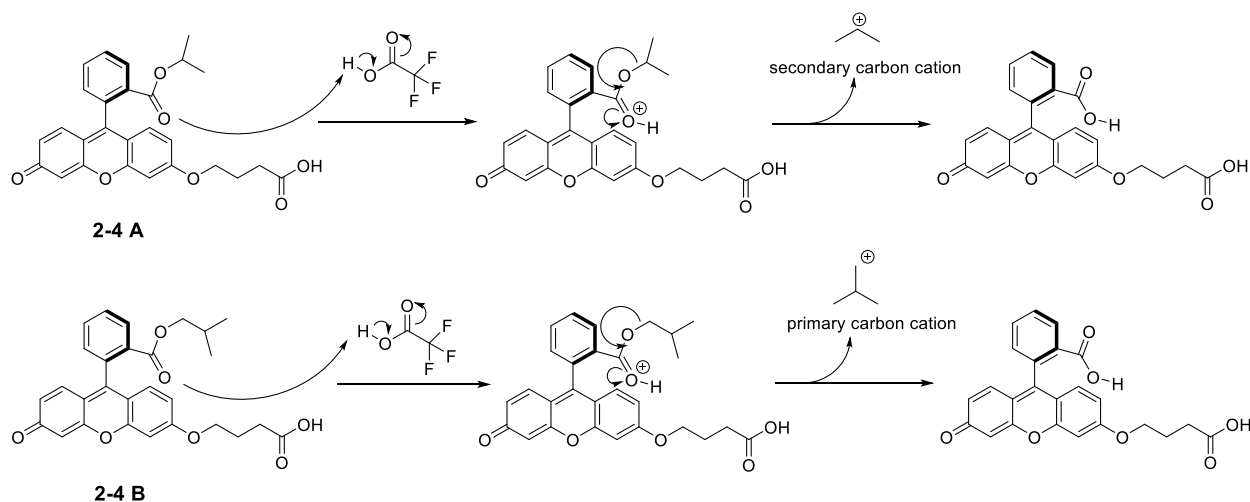
**Scheme 2.1** Reduction of terminal acid group

The C2' carboxylic acid group of fluorescein was protected by esterification with isopropanol to give **2-2 A** followed by the reported literature procedure,<sup>8-9</sup> then Mitsunobu reaction was applied for modification on C3 position to generate **2-3 A**. TPPO (triphenylphosphine oxide) was generated and hard to be removed due to its close R<sub>f</sub> value with the desired product **2-3 A**. So the crude was directly taken for next step to give **2-4 A** by removal of *t*-Boc group in the presence of trifluoroacetic acid, and the product **2-4 A** can be easily separated from TPPO. Then EDC coupling was performed to give **2-5 A** activated ester which is ready for later use. (**Scheme 2.2**)



**Scheme 2.2** Esterification on C2' and modification on C3 of fluorescein

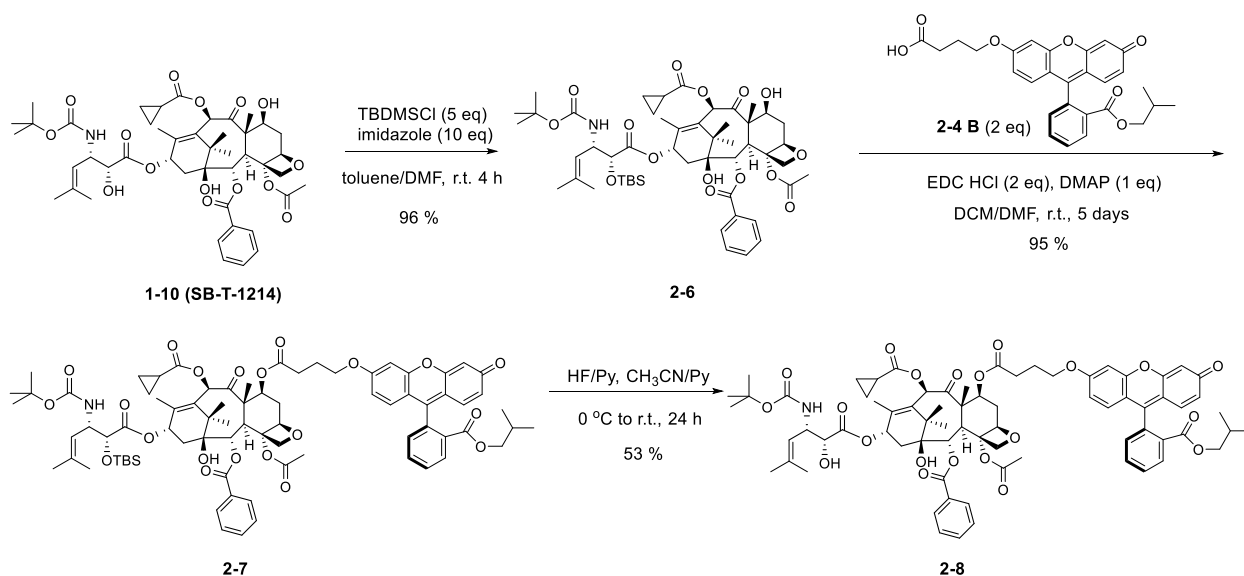
However, the overall yield of **2-5 A** synthesis with isopropyl group on C2' position was very low, especially *t*-Boc deprotection step. A plausible explanation was that the isopropyl protecting group was removed by TFA, most likely a *t*-Boc deprotection process, resulting in the protected ester group cleavage. (**Scheme 2.3**) Therefore, isobutyl protecting group was used solve this problem. With one more carbon atom, the intermediate **2-3 B** was found more stable in the presence of TFA due to the unlikely formation of less stable carbon cation according to the TFA deprotection mechanism. (**Scheme 2.3**) Consequently, **2-4 B** was obtained followed the same process in good overall yield for later use as fluorescent probe. (**Scheme 2.2**)



**Scheme 2.3** Possible TFA deprotection

To introduce fluorescent tag **2-4 B** on the C7 position of previously made second generation taxoid SB-T-1214, C2' hydroxyl group was first protected as *tert*-butyldimethylsilyl (TBS) ether to give **2-6** in good yield. By EDC coupling, **2-7** was generated in 92 % yield over 7 days, followed by HF-pyridine deprotection to remove the silyl protecting group to give **2-12** in

quantitative yield. (**Scheme 2.4**) The synthesis using **2-5 B** and **2-8** as fluorescent probes to construct various conjugates, and biological evaluation in comparison with paclitaxel, SB-T-1214 and SB-T-1214-based drug conjugates will be discussed in Chapter 3 and 5.



**Scheme 2.4** Synthesis of SB-T-1214-C7-fluorescein **2-8**

### §2.3 Development of $^{11}\text{C}$ -Labeled SB-T-1214 Radiotracer for PET Imaging Study

Positron emission tomography (PET) is a non-invasive molecular imaging technology. By detection of positron emitting radiopharmaceuticals, PET provides a useful tool to visualize the physiological interactions between the targets and ligands in living biological systems.<sup>10-11</sup> As one of the commonly used radionuclides for PET study, carbon-11 has short half-life (20.3 min), thus it is a well suited for radiolabelling molecules with short biological half-lives. In addition, carbon-11 radiolabelled pharmaceuticals has advantage over the other commonly used radionuclide fluorine-18 because carbon is present in framework of all natural products and drug compounds. Radiolabelling bioactive compounds with carbon-11 does not introduce any exogenous atom, therefore the original chemical and biological properties of testing compounds remain the same.<sup>10</sup> Detailed discussion on PET and carbon-11 radiolabelling will be discussed in Chapter 4.

#### §2.3.1 Carbon-11 Radiolabeled Taxanes

Several taxanes have been successfully radiolabelled with carbon-11 for PET imaging, including paclitaxel, docetaxel, and ortataxel. (**Figure 2.5**)<sup>12-14</sup> [ $^{11}\text{C}$ ]Paclitaxel was synthesized by reacting [ $\alpha$ - $^{11}\text{C}$ ]benzoyl chloride with the primary amine precursor of paclitaxel in 7 % average decay corrected radiochemical yield and over 99 % radiochemical purity.<sup>12</sup> [ $^{11}\text{C}$ ]Docetaxel was prepared *via* [ $^{11}\text{C}$ ]tert-butoxycarbonylation of the free amine precursor of docetaxel in a satisfactory decay corrected yield of 10 $\pm$ 1 % determined by consumption of [ $^{11}\text{C}$ ]CO<sub>2</sub>.<sup>13</sup> [ $^{11}\text{C}$ ]Ortataxel (IDN-5109, BAY 59-8862) was synthesized by reacting [1- $^{11}\text{C}$ ] acetyl chloride with the lithium salt of the free secondary hydroxyl precursor of ortataxel followed by silyl deprotection. The decay corrected radiochemical yield achieved 12-23 % related to [ $^{11}\text{C}$ ]CO<sub>2</sub>.<sup>14</sup>

All of these compounds were radio-synthesized *via* nucleophilic substitution or acylation reactions with relatively low radiochemical yield.

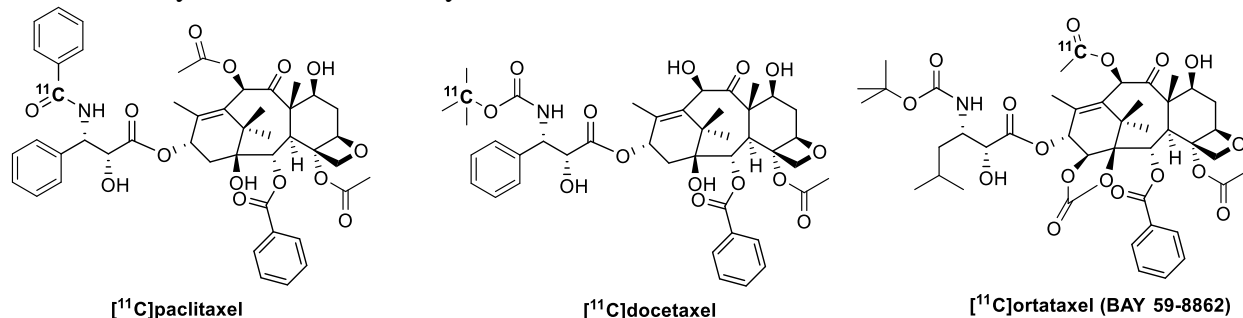
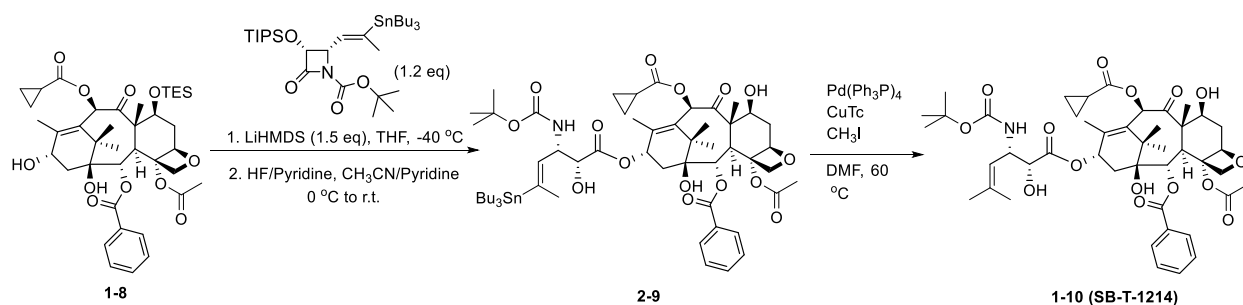


**Figure 2.5** Chemical structures of radiolabeled taxanes

Most recently, palladium-catalyzed  $^{11}\text{C}$ -C bond formation *via* Stille, Suzuki, or Sonogashira cross-coupling reactions are providing a new perspective for preparation of carbon-11 radiolabelling pharmaceuticals.<sup>10</sup> Several examples have applied palladium (0)-mediated Stille-type coupling for the introduction of  $[^{11}\text{C}]$  methyl group into organic molecules for carbon-11 radiolabelling. Stille coupling involves stannanes intermediates which usually possess good functional group tolerances and low polarity. Rapid separation and purification of the radiolabelled product from excess stannane starting material can be easily accomplished by chromatography.<sup>10</sup> Accordingly, a novel synthetic route towards rapid  $[^{11}\text{C}]$ methylation to give carbon-11 labelled second generation taxoid SB-T-1214 was developed by Dr. Joshua D. Seitz in our group.<sup>15-16</sup> The reaction condition was optimized to give the cold product SB-T-1214 in the presence of  $\text{CH}_3\text{I}$ , tetrakis(triphenylphosphine)palladium(0)  $[\text{Pd}(\text{Ph}_3\text{P})_4]$ , and copper(I)-thiophene-2-carboxylate (CuTc). The key synthetic steps are illustrated in **Scheme 2.5**. However, in the final step we found several taxoid structure-based unknown compounds formed along with the desired methylated product SB-T-1214. These compounds will be identified in section 2.4.2 by LC/UV/MS-TOF and facilitate better understanding of the methylation mechanism in the presence of Pd and Cu catalytic system, as well as establish the protocol for further carbon-11 labelling application for PET.



**Scheme 2.5** Key synthetic steps towards SB-T-1214 *via* Stille coupling

### §2.3.2 Establishment of LC/UV/MS-TOF Analysis Condition

Previously the “cold” rapid methylation step *via* Stille coupling towards SB-T-1214 formation was only briefly measured and analyzed by LC/UV/MS-TOF under positive mode without further method development by Dr. Joshua Seitz and Dr. Jacob Vineberg. Although the methylation product SB-T-1214 was confirmed with identified retention time compared to an

authentic SB-T-1214 sample as external standard, at least five major peaks showed existence of taxoid structure-based derivatives indicating a more complicated Stille coupling mechanism than expected. Those unidentified peaks were analyzed by ESI in positive mode, however, this analysis method did not provide sufficient information for predicting the chemical structures on the basis of mass values. This is mainly due to easy fragmentation of taxoid-derivatives under positive mode ESI acquisition. The side chain was removed through C-O bond break on C13 position, resulting in an allylic secondary carbon cation which can be delocalized and stabilized by the adjacent C=C bond. Thus mass analysis of interested peaks under positive mode all gave  $[M+H]^+$   $m/z$  595.25 as the major detected peak relating to the C13 side chain-removed baccatin core.

To overcome this problem, negative mode has been recently developed to analyze the outcomes of Stille coupling reaction. In addition, the target screening function of LC-TOF was exploited to facilitate the structure determination. Three authentic samples (**Figure 2.6**) were used to compare the positive/negative mode results, as well as to obtain their retention times under current analysis method (Kinetex F5 column, 2.1 mm x 150 mm, 2.6  $\mu$ m, 100 angstroms, solvents solvent A-H<sub>2</sub>O+10mM AmAc/solvent B-MeOH, flow rate 0.375 mL/min, temperature 30 °C, UV detector 275 and 230 nm, gradient 60-95% MeOH increasing over 35 min). Compound **2-10** (iodo-taxoid) was thought as the key intermediate generated and consumed *in situ* during the Stille coupling reaction, thus the authentic sample was prepared by Dr. Joshua D. Seitz and the determination of retention time was included to investigate the Stille coupling mechanism.

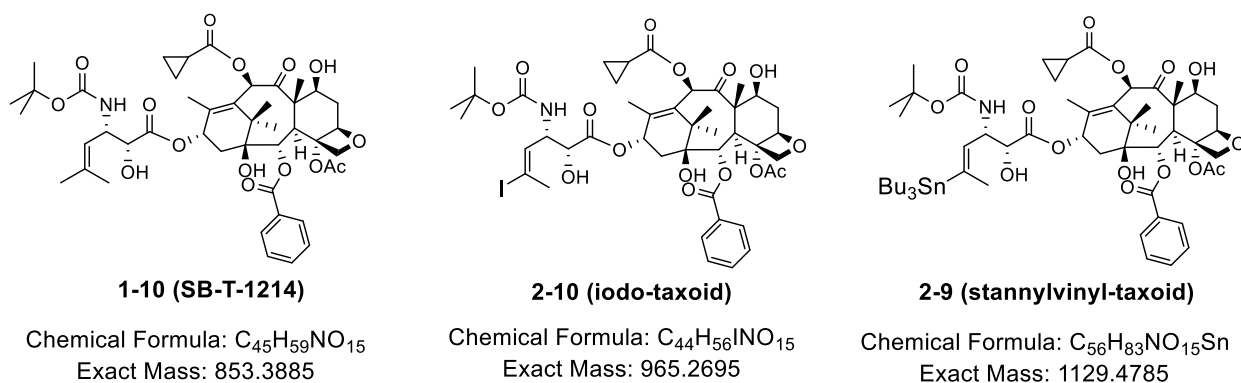


**Figure 2.6** Chemical structures and molecular weights of three taxoid authentic samples

**Figure 2.7** showed the LC/UV/MS trace of a mixture of **1-10/2-9/2-10** in 1:1:1 ratio by weight with UV detector of 220 nm and 254 nm under positive ESI mode. Stannylvinyl-taxoid (**2-9**) as starting material of Stille coupling reaction showed up at 35.94 min due to its non-polarity. The methylation product SB-T-1214 (**1-10**) gave peak with retention time of 17.09 min. And iodo-taxoid (**2-10**) had retention time of 19.44 min. Although mass analysis results showed parent ion of each sample, it is worthy noticing that these samples have been purified, and C13 side chain removed baccatin fragment with  $m/z$  595.25 has higher signal intensity. (**Figure 2.8**)

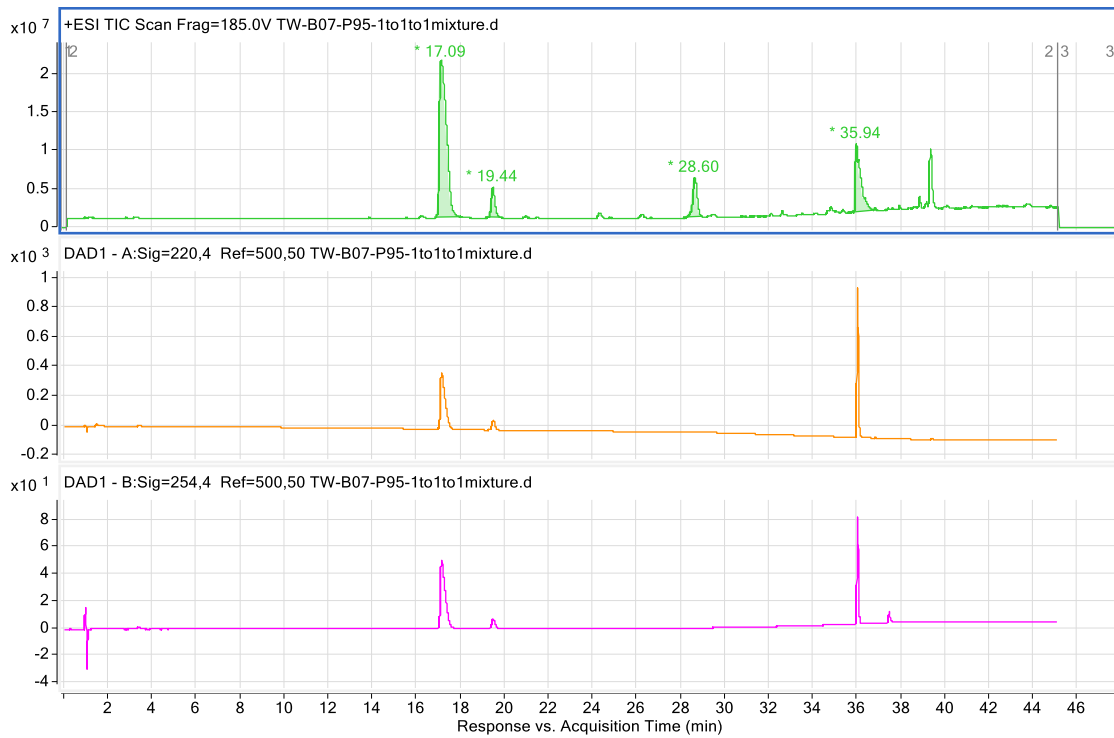


**Figure 2.7** LC/UV/MS trace (positive mode) of three authentic samples (1:1:1)

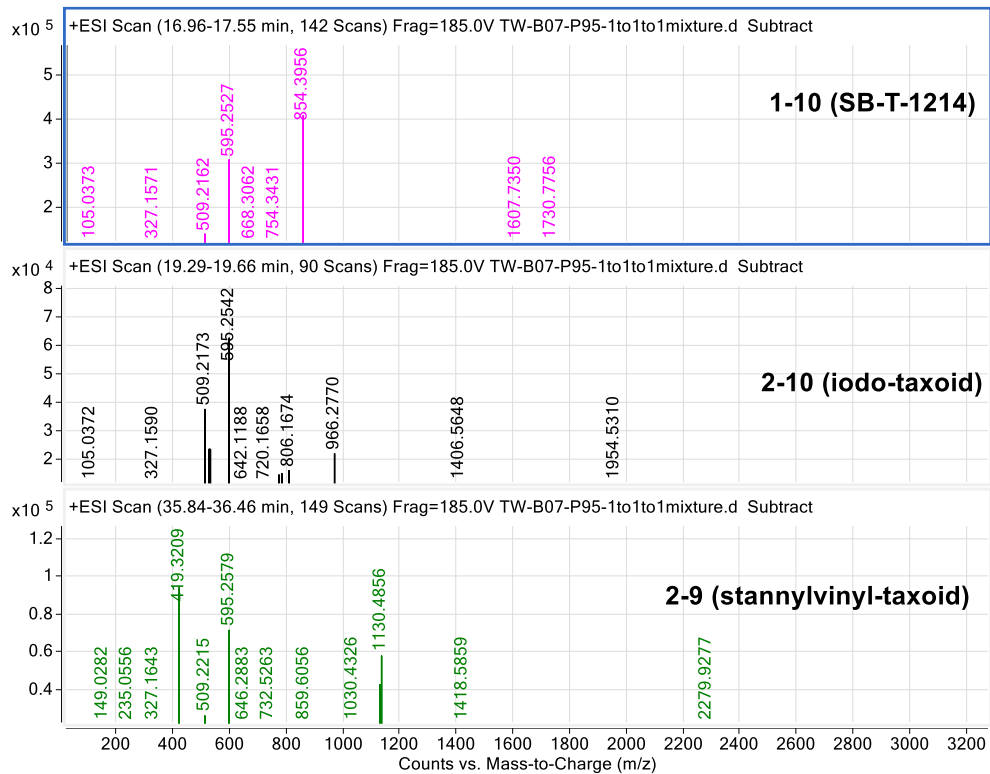


**Figure 2.8** Mass analysis results (positive mode) of three authentic samples

In contrast, LC/UV/MS trace of the mixture under negative mode gave a much cleaner TIC trace with same retention times (**Figure 2.9**), and more importantly, the mass analysis result detected the acetate adduct as the strongest signal which has great value for structure determination. (**Figure 2.10**) Therefore, the negative mode was selected for further LC/UV/MS analysis.

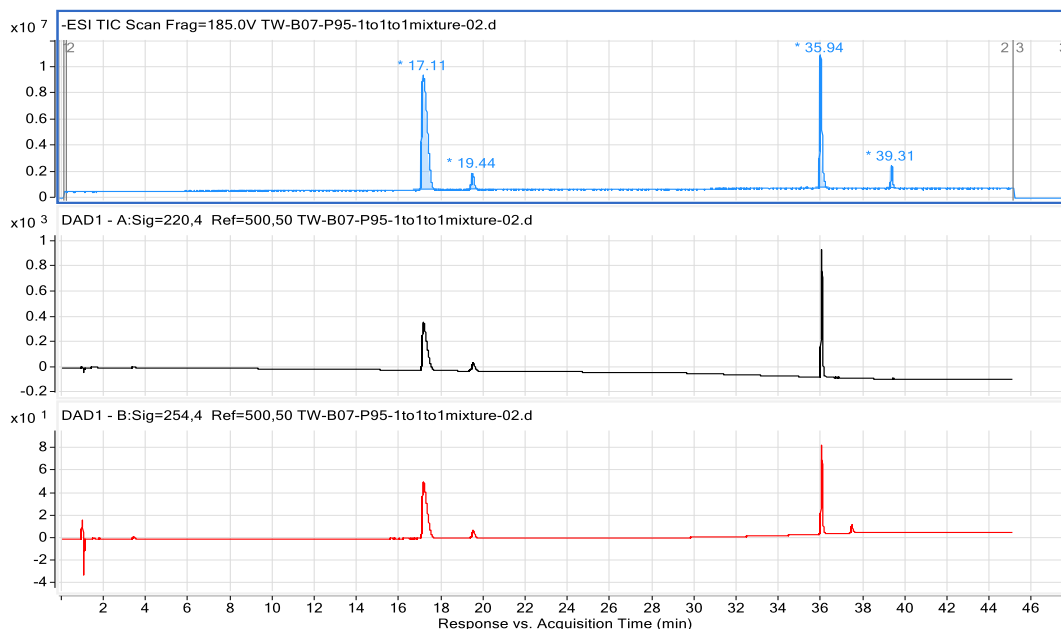


**Figure 2.9** LC/UV/MS trace (negative mode) of three authentic samples (1:1:1) mixture

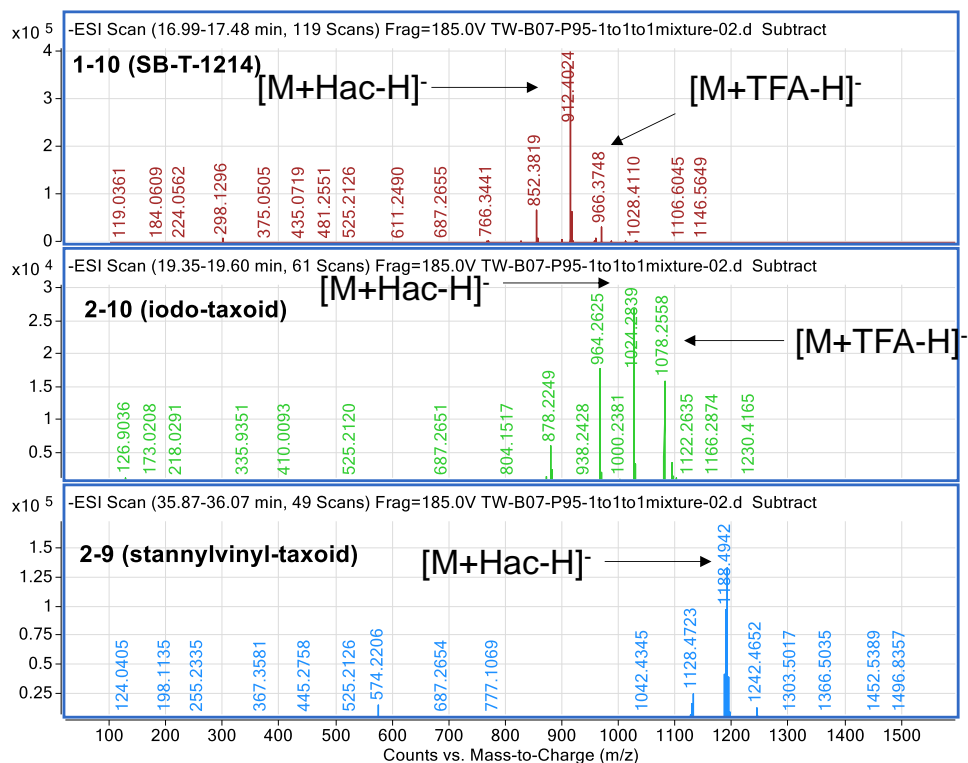
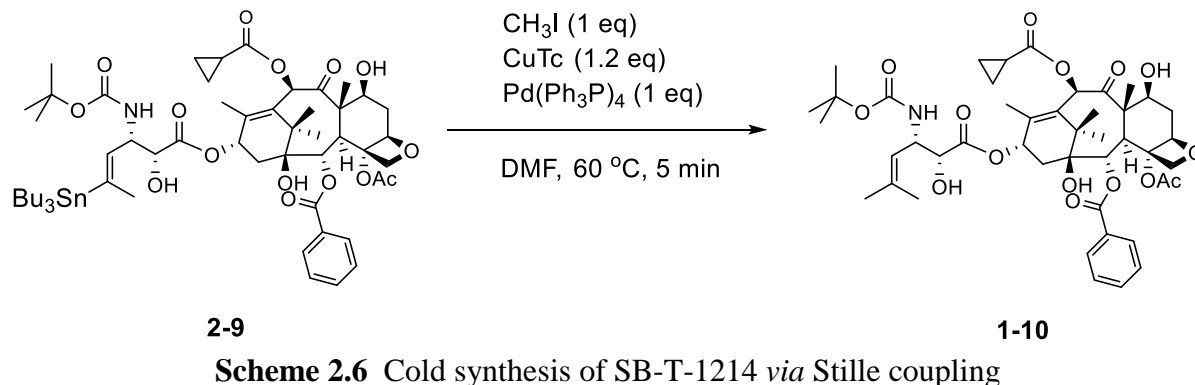


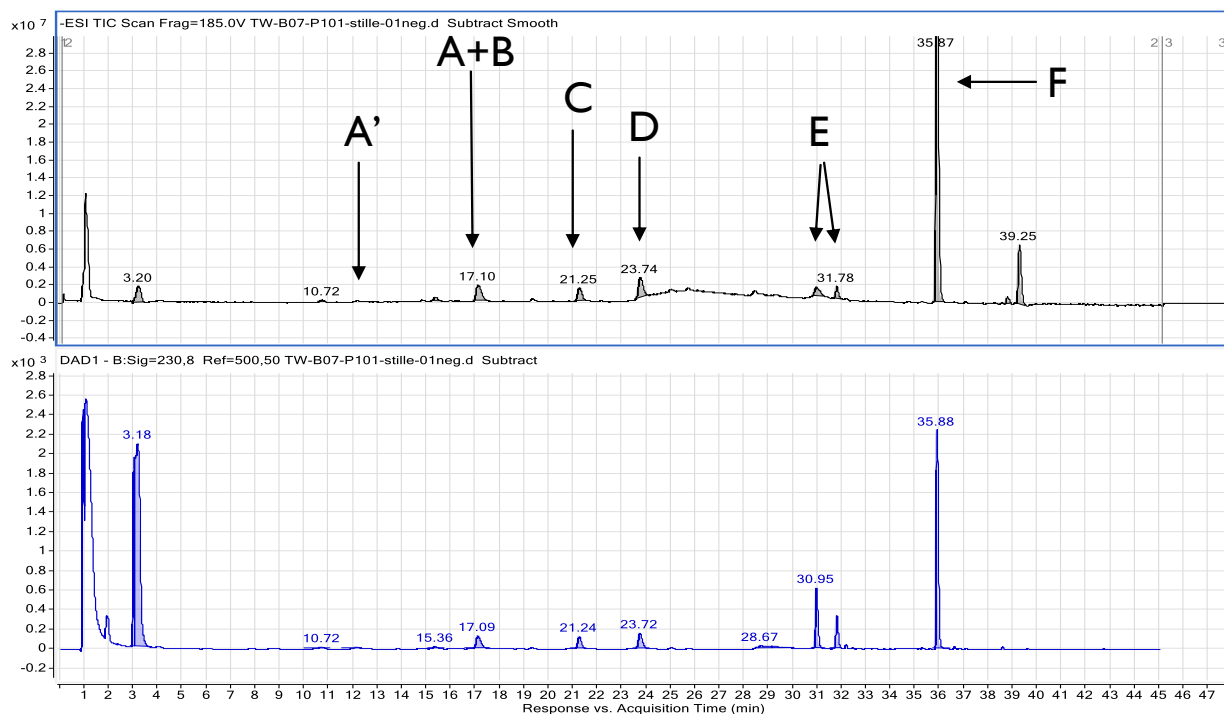
**Figure 2.10** Mass analysis results (negative mode) of three authentic samples



### §2.3.3 Analysis and Determination of the Stille Coupling Outcomes



The Stille coupling was then performed in the presence of 1 eq CH<sub>3</sub>I, 0.5 eq tetrakis(triphenylphosphine)palladium(0) [Pd(Ph<sub>3</sub>P)<sub>4</sub>], and 1.2 eq copper(I)-thiophene-2-carboxylate (CuTC) in DMF as solvent. (**Scheme 2.6**) The reaction was in only 2 mg scale for LC analysis. The reaction was allowed to stir for 5 min under 60 °C, then equal amount methanol to DMF was added, followed by direct injection for LC/UV/MS analysis. Seven major compounds including starting material and product were identified as major peaks under 230 nm UV channel. (**Figure 2.11**)



Based on the calculation and mass analysis result of each peak, structures A to F were predicted in **Figure 2.12**. Interestingly, the peak C was previously observed and was assigned as iodo-taxoid (**2-14**) at the time. However, in this systemic study, it is clear that the peak C in **Figure 2.11** stands for another compound with different retention time at 21.25 min (**2-10**,  $t_R=19.44$  min,

in **Figure 2.9**) but very close molecular weight (**Figure 2.12**). According, Tc-taxoid (**2-11**) was proposed as the resulting compound for peak C generated by incorporation of Tc anion from CuTC, and compound **2-11** will be separately synthesized to confirm our hypothesis. High-resolution mass (HRMS) analysis supported this hypothesis. The calculated HRMS  $[M-H]^-$   $m/z$  for iodo-taxoid (**2-10**) is 964.2622 ( $C_{44}H_{55}INO_{15}^-$ ), which is in consist with the observed result 964.2625 in **Figure 2.10**. The mass result for peak C was observed as 964.3424, thus it clearly showed the peak C was different from the mass value of **2-10**, and it should be assigned to Tc-taxoid (**2-11**) which has calculated HRMS  $[M-H]^-$   $m/z$  964.3431 ( $C_{49}H_{58}NO_{17}S^-$ ).

It is worthy noticing that the target screening function of LC/UV/MS-TOF was exploited to help the compound identification and structure determination. Take **2-11** (Tc-taxoid) as an example, this target screening function allows to screen entire TIC trace to find any peak matching the predicted structure. With calculated mass values of Tc-taxoid acetate adduct and trifluoroacetate adduct, the program found the peak at 21.26 min matches the two calculated numbers, indicating the selected peak in TIC include the predicted compound. (**Figure 2.14**)

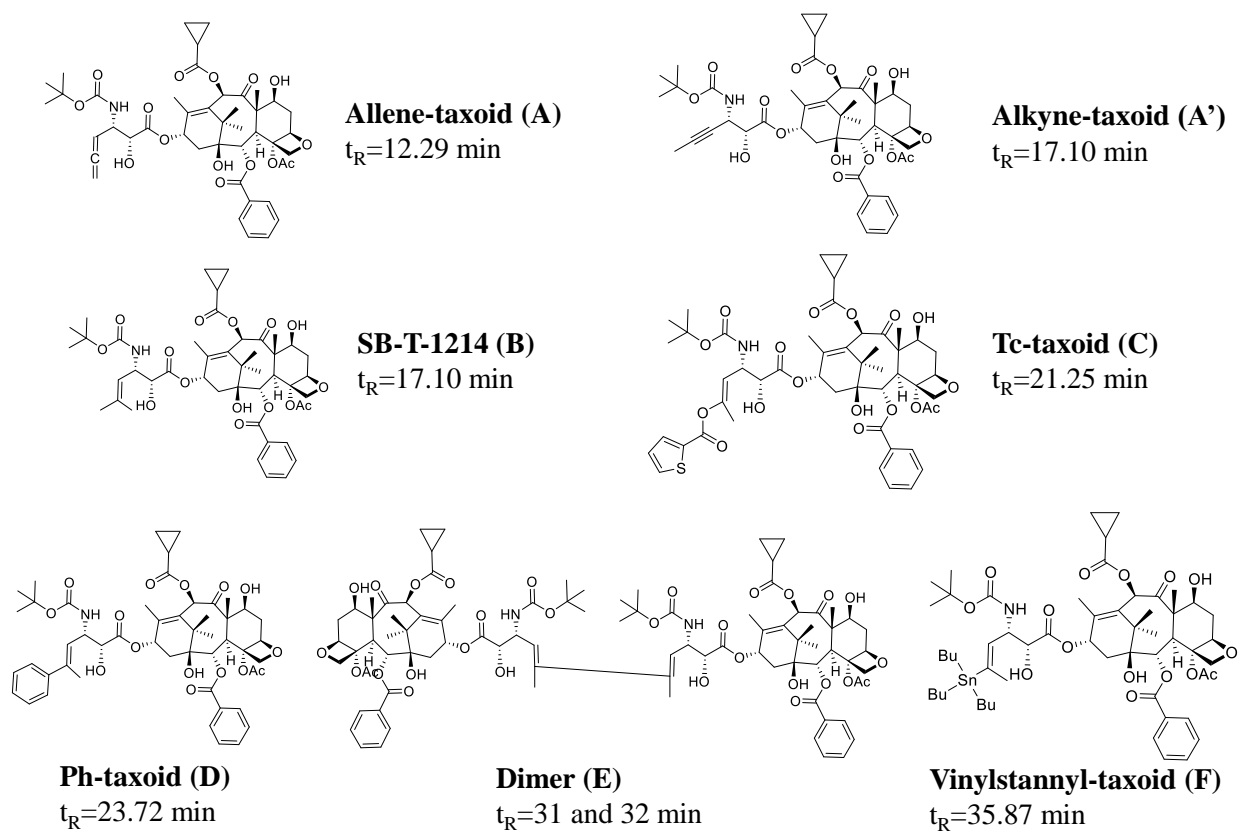


**Figure 2.12** Predicted chemical structures of unknown compounds with corresponding retention times

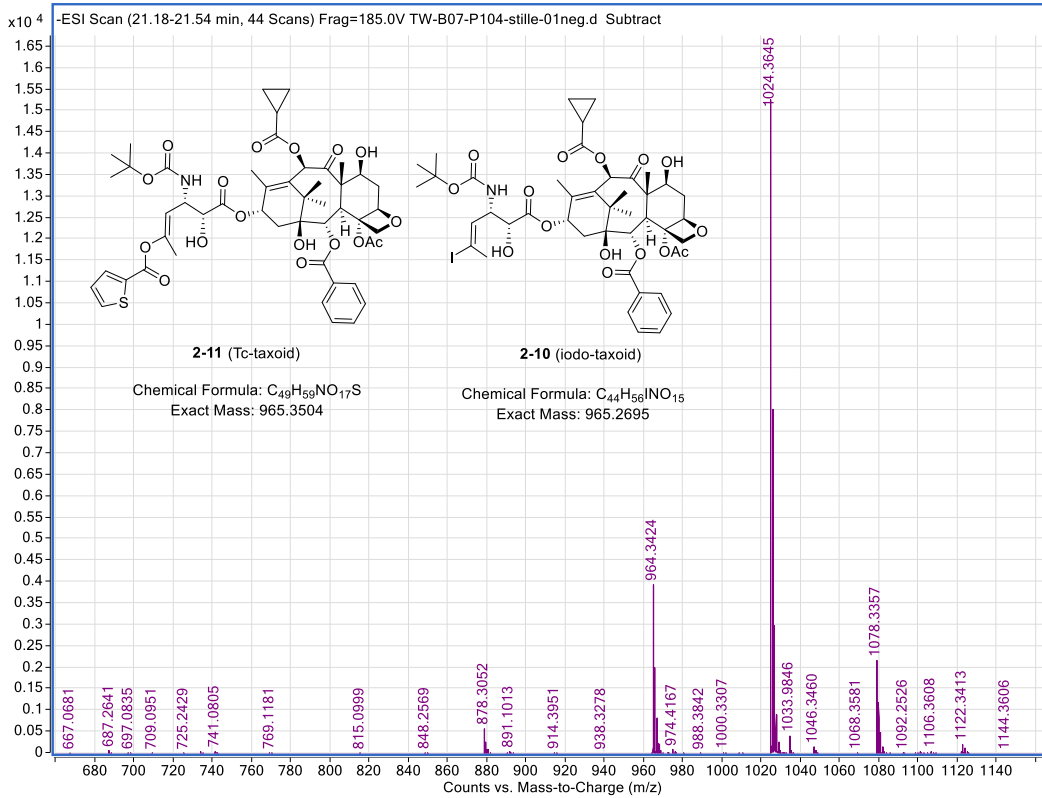


Figure 2.13 Mass analysis results of peak C and two potential taxoid compounds

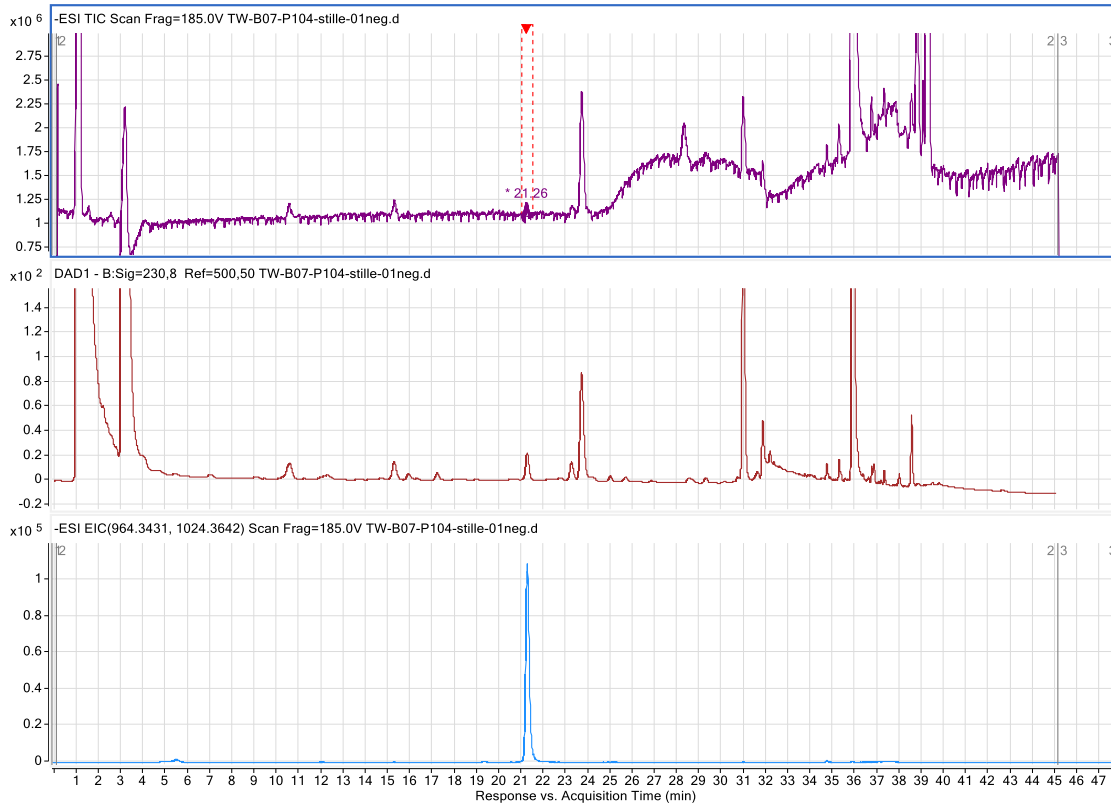
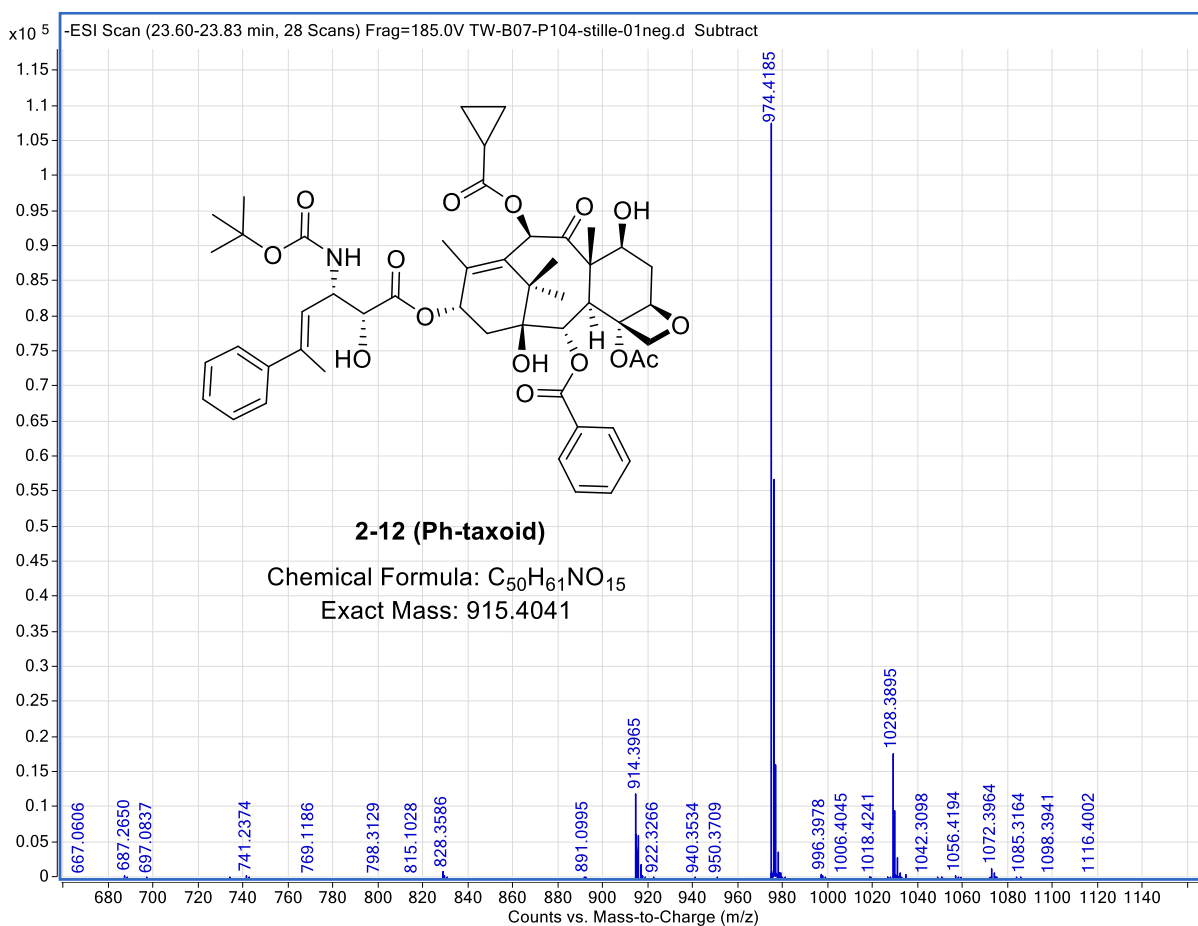
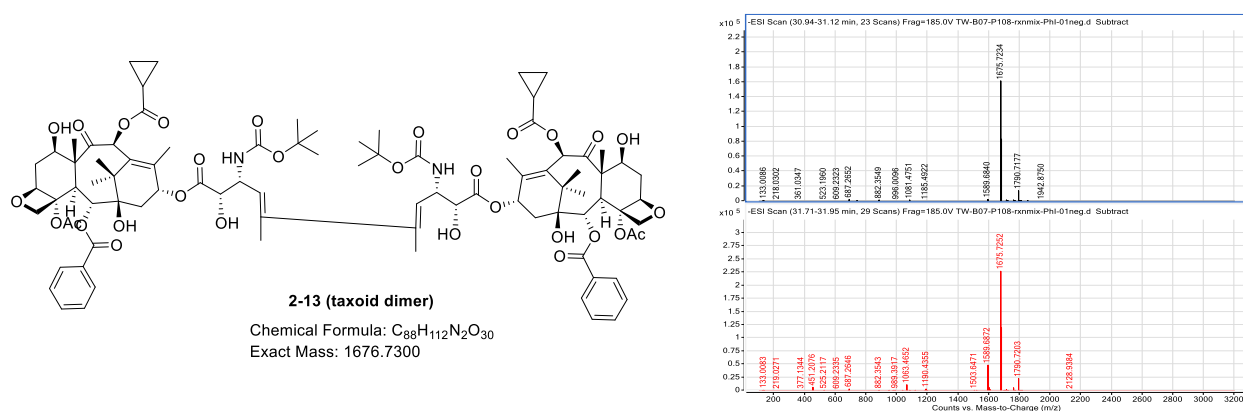


Figure 2.14 Target screening result of Tc-taxoid (2-11)



**Figure 2.15** Mass analysis results of peak D and chemical structure of predicted compound **2-12**



**Figure 2.16** Mass analysis results of peak E and chemical structure of predicted compound **2-13**

Taking advantage of this technique, compound D and E (**Figure 2.12**) were identified as Ph-taxoid (**2-12**) and a taxoid dimer (**2-13**) based on the mass analysis results for peak D (**Figure 2.15**) and peak E (**Figure 2.16**), respectively. The compound **2-12** may result from the ligand dissociation from the Pd catalyst, and a similar reaction system with phenyl iodide to replace methyl iodide will be investigate whether **2-12** (Ph-taxoid) can be exclusively obtained. The formation of taxoid dimer may indicate the radical mechanism for the Stille coupling.

Another interesting finding was related to the analysis of peak A and peak A' in **Figure 2.11**. When peak B as corresponding peak of **1-10** (SB-T-1214) was analyzed, besides the characteristic pattern of SB-T-1214 with its acetate adduct, another pattern was found and assigned to the allene-taxoid (**2-14**). (**Figure 2.17**) Then when the TIC trace was screened based on the allene-taxoid (**2-14**), it showed at least three peaks (12.29-17.21 min) (**Figure 2.18**) include the compounds with same molecular weight as allene-taxoid (**2-14**). Accordingly, a new taxoid derivative alkyne-taxoid (**2-15**) was proposed to explain the existence of extra peak, and as constitution isomers, allyene-taxoid (**2-14**) and alkyne-taxoid (**2-15**) can be generated simultaneously during the  $\beta$ -hydride elimination. (**Figure 2.19**) To distinguish these two isomers, alkyne-taxoid (**2-15**) is readily to be synthesized *via* Ojima-Holton coupling, and its retention time will be measured for structure determination of peak A and A'.

On the basis of all predicted and identified structures, a comprehensive mechanism was illustrated as **Figure 2.20**. During the Stille coupling, the starting material stannylvinyl-taxoid (**2-9**) can have the transmetalation with copper catalyst (CuTc) to form the vinylcuprate intermediate and a SnTc intermediate. The vinylcuprate intermediate may react with another equivalent CuTc, and another equivalent stannylvinyl-taxoid (**2-9**) may react with the resulting SnTc intermediate, and both will give the Tc-taxoid (**2-11**) via radical reaction. Meanwhile, the active vinylcuprate intermediate can then undergo a second transmetalation step from the copper to the Pd(II) complex resulting in the formation of vinyl-palladium species, which can then undergo reductive elimination to afford **1-10** (SB-T-1214). However, starting from the vinyl-palladium species, it also may undergo two pathways of  $\beta$ -hydride elimination to give allene-taxoid (**2-11**) and alkyne-taxoid (**2-12**). In addition, the vinyl-palladium species may also undergo an isomerization followed by the ligand dissociation to end up with Ph-taxoid (**2-12**).

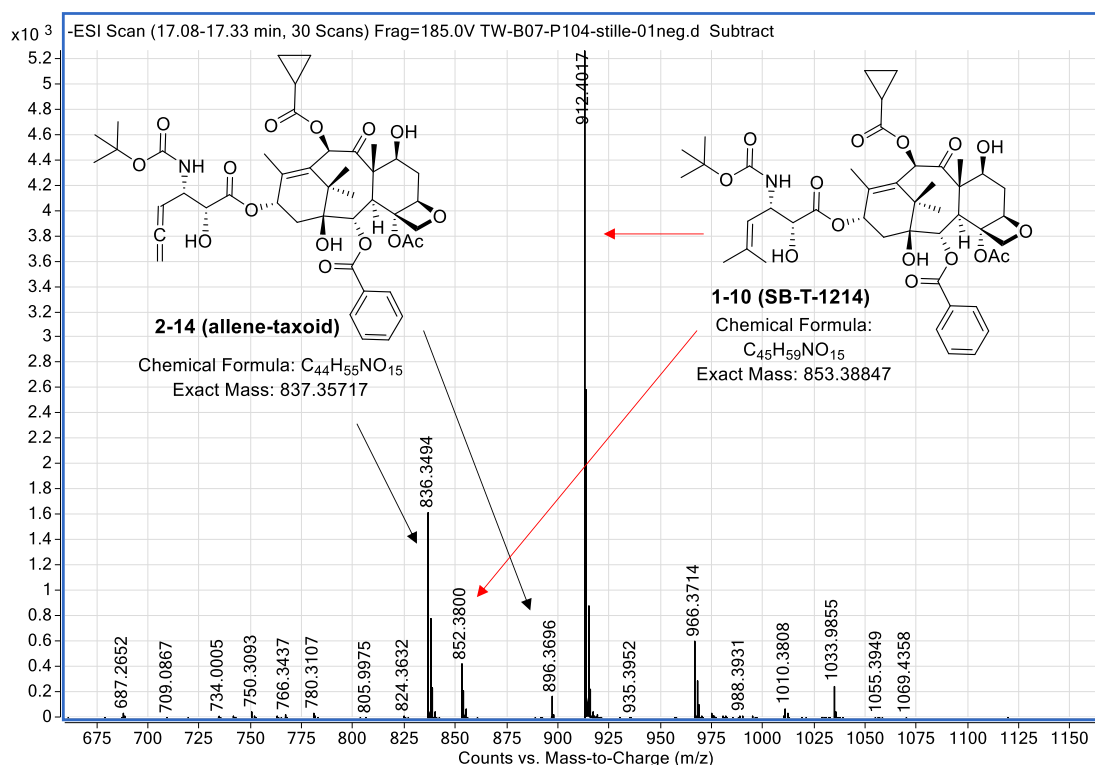


**Figure 2.17** Mass analysis results of peak B

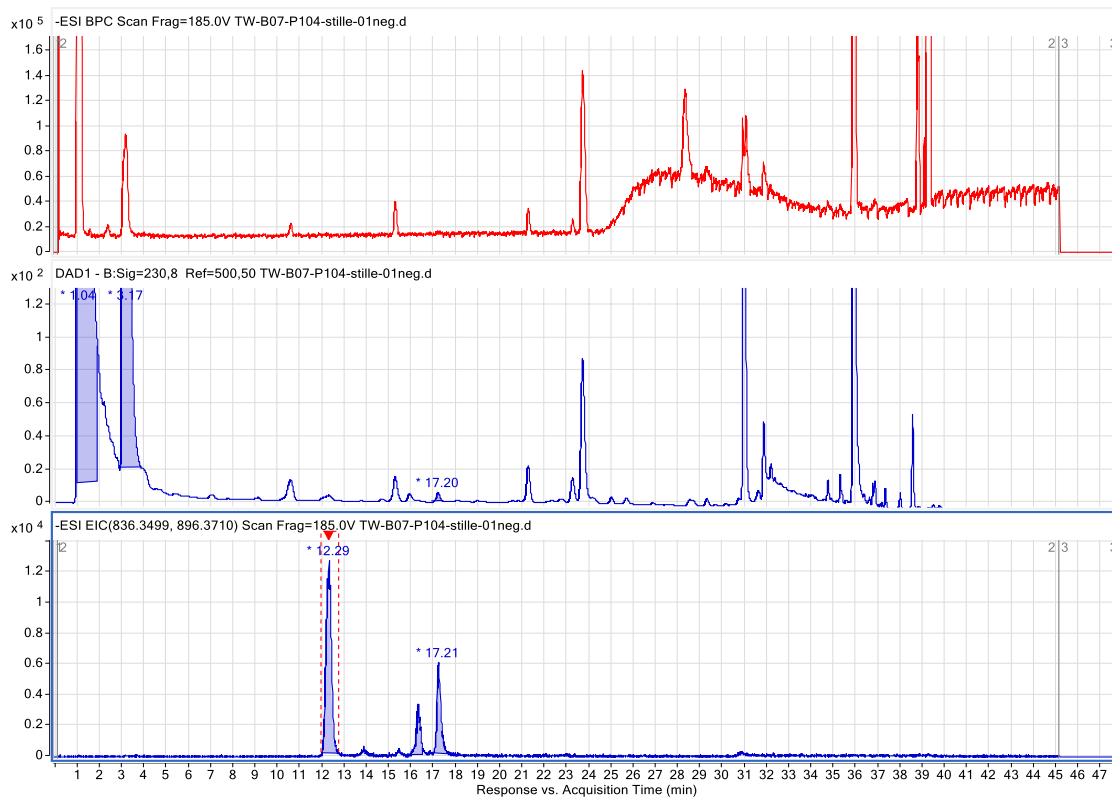


**Figure 2.18** Target screen result of allene-taxoid (2-14)

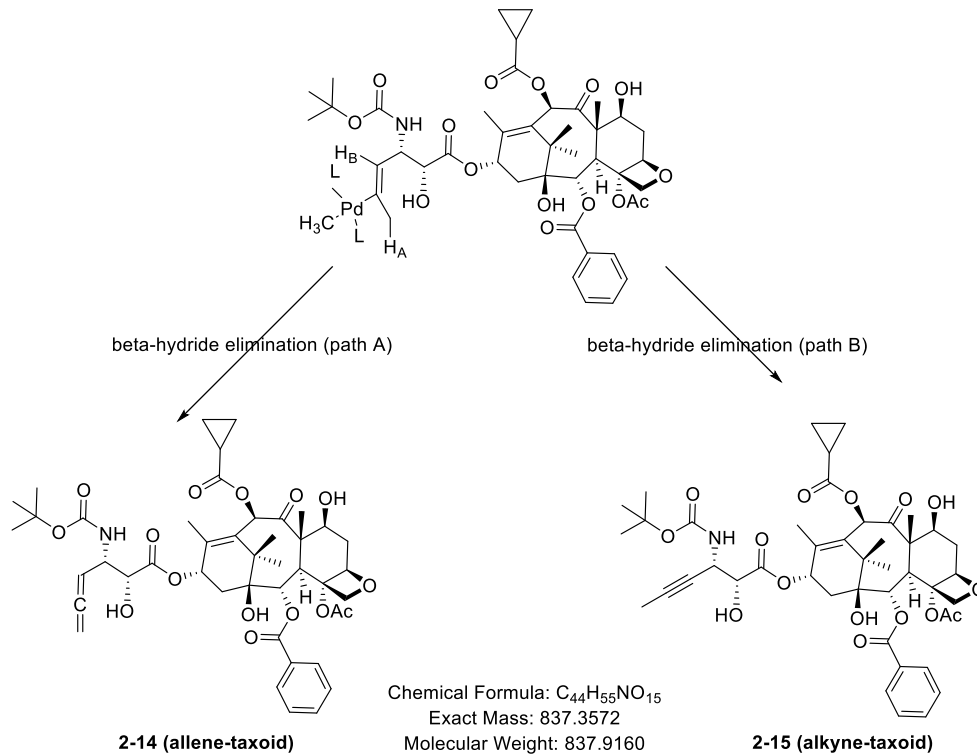


**Figure 2.19** Two pathways of beta-hydride elimination to generate allene-taxoid (2-14) and alkyne-taxoid (2-15)

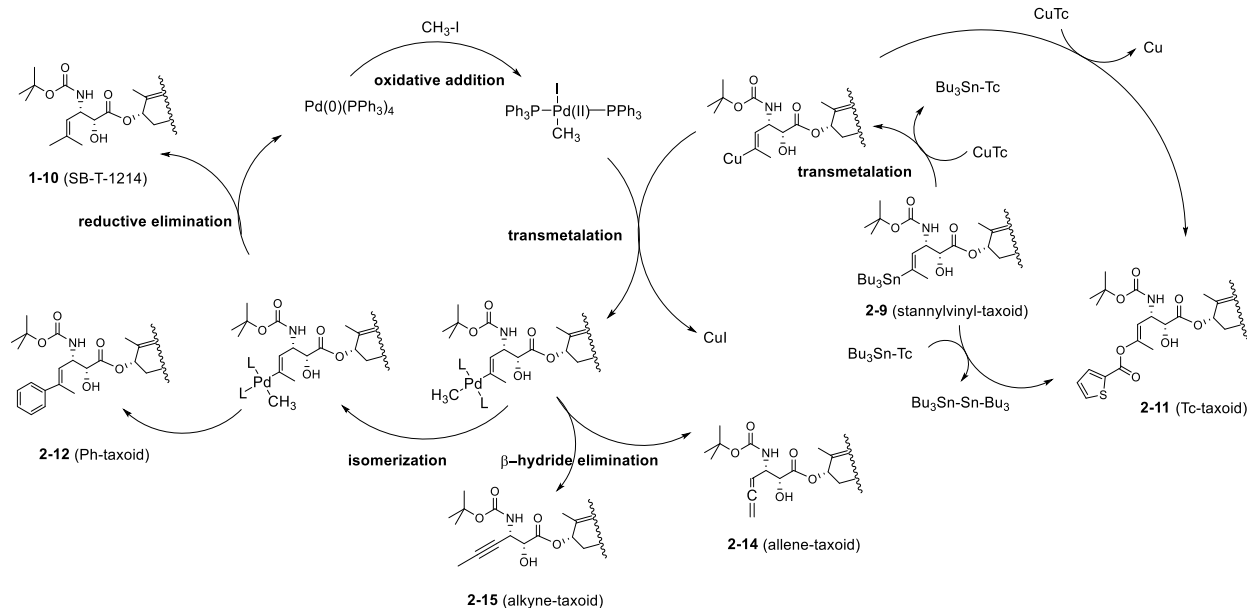
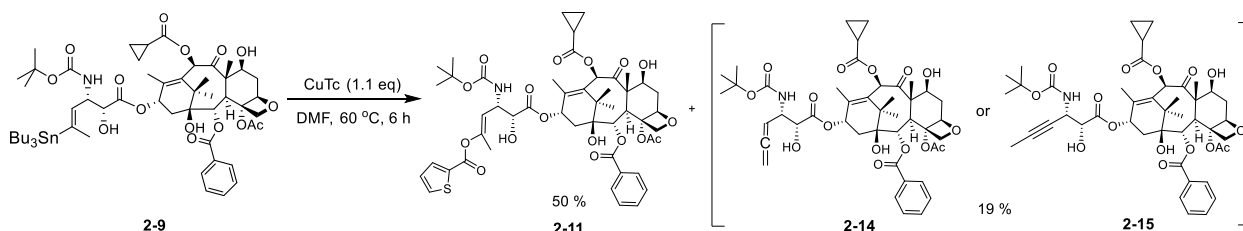


**Figure 2.20** Proposed mechanism for Stille coupling reaction

### §2.3.4 Synthesis of Taxoid Derivatives from Stille Coupling

To confirm the peak C in **Figure 2.11** is the Tc-taxoid (**2-11**) instead of iodo-taxoid (**2-10**), **2-9** was selectively reacted with 1.1 eq CuTc in the absence of Pd catalyst. (**Scheme 2.7**) Due to the limited amount of **2-9** in stock, the reaction was set up in 8 mg scale to get sufficient amount product for full characterization.



**Scheme 2.7** Synthesis of Tc-taxoid (**2-11**) in the absence of Pd catalyst

Without addition of Pd catalyst and  $\text{CH}_3\text{I}$ , Tc-taxoid (**2-11**) was formed as anticipated with retention time 21.61 min. The reaction did not go completion, around 1 mg of **2-9** was recovered. In addition, 1 mg of **2-14** or **2-15** was also isolated by preparative HPLC in 19 % yield with retention time around 17.35 min. (**Figure 2.21**) The isolated **2-11** and **2-14** (or **2-15**) were re-subjected for LC/UV/MS-TOF and their purity and retention times were also checked. (**Figure 2.22**).

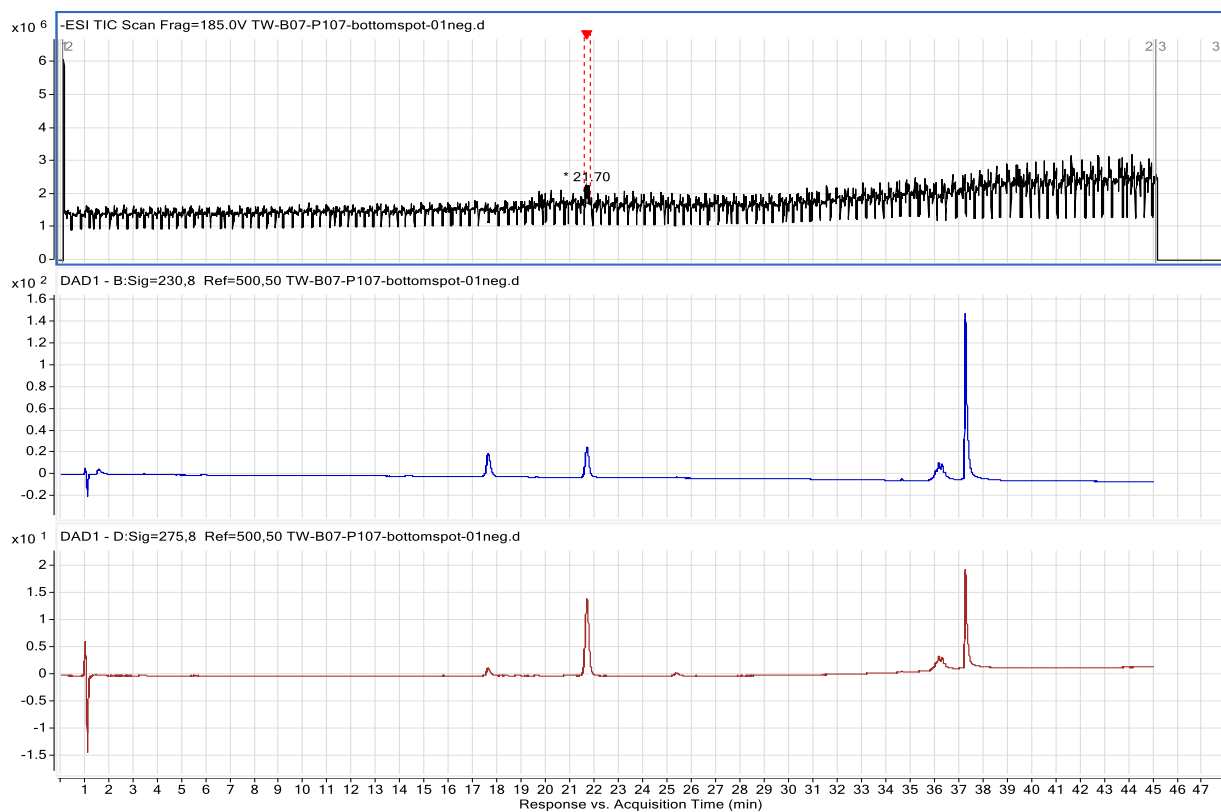


**Figure 2.21** LC/UV/MS trace of Tc-taxoid (**2-11**) formation without Pd catalyst

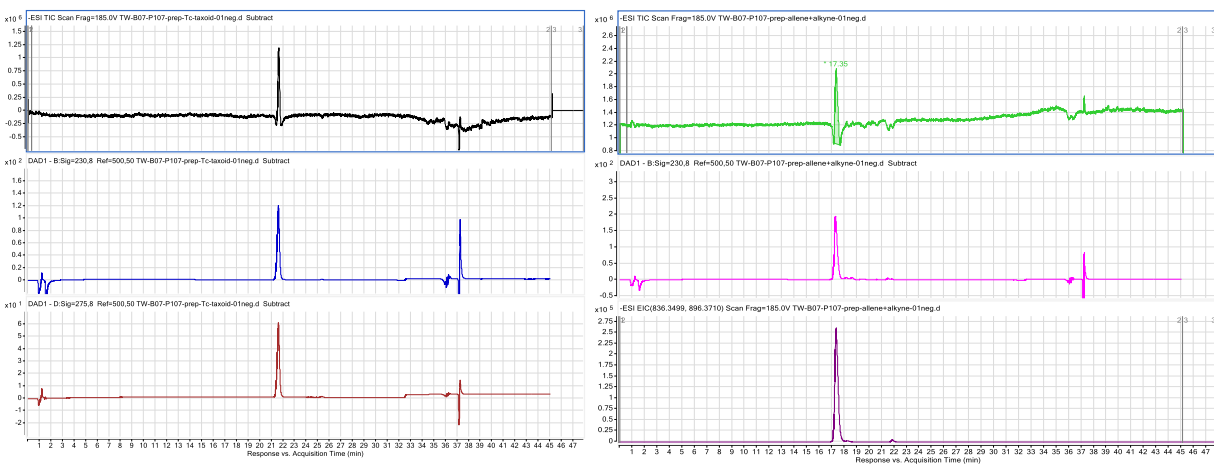
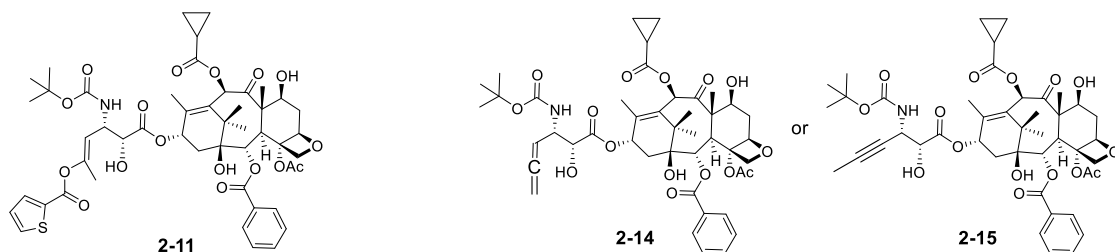
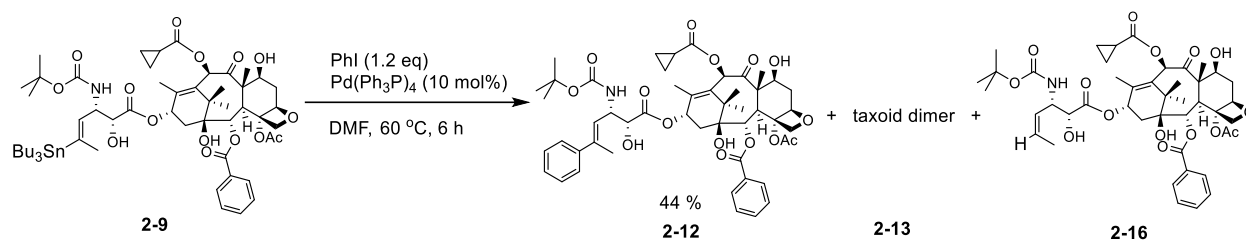


**Figure 2.22** LC/UV/MS purity check and retention time determination of isolated two products **2-11** and **2-14** (or **2-15**)





**Scheme 2.8** Synthesis of Ph-taxoid (**2-12**) in the absence of Cu catalyst

To selectively obtain **2-12** (Ph-taxoid), **2-9** was treated with 1.2 eq PhI and 10 mol% Pd catalyst in the absence of CuTC. (**Scheme 2.8**) However, in this reaction system, two close peaks around 24 min were observed (**Figure 2.23**) and later confirmed by target screening and mass analysis that both peaks were relating to the Ph-taxoid (**2-12**). (**Figure 2.24 and 2.25**) These two peaks may be assigned to E/Z isomers of **2-12**, and taking account into the hindrance and energy, the former peak at 23.25-23.45 min is (Z)-isomer of **2-12** and the latter one at 23.56-24.10 min is (E)-isomer of **2-12**.

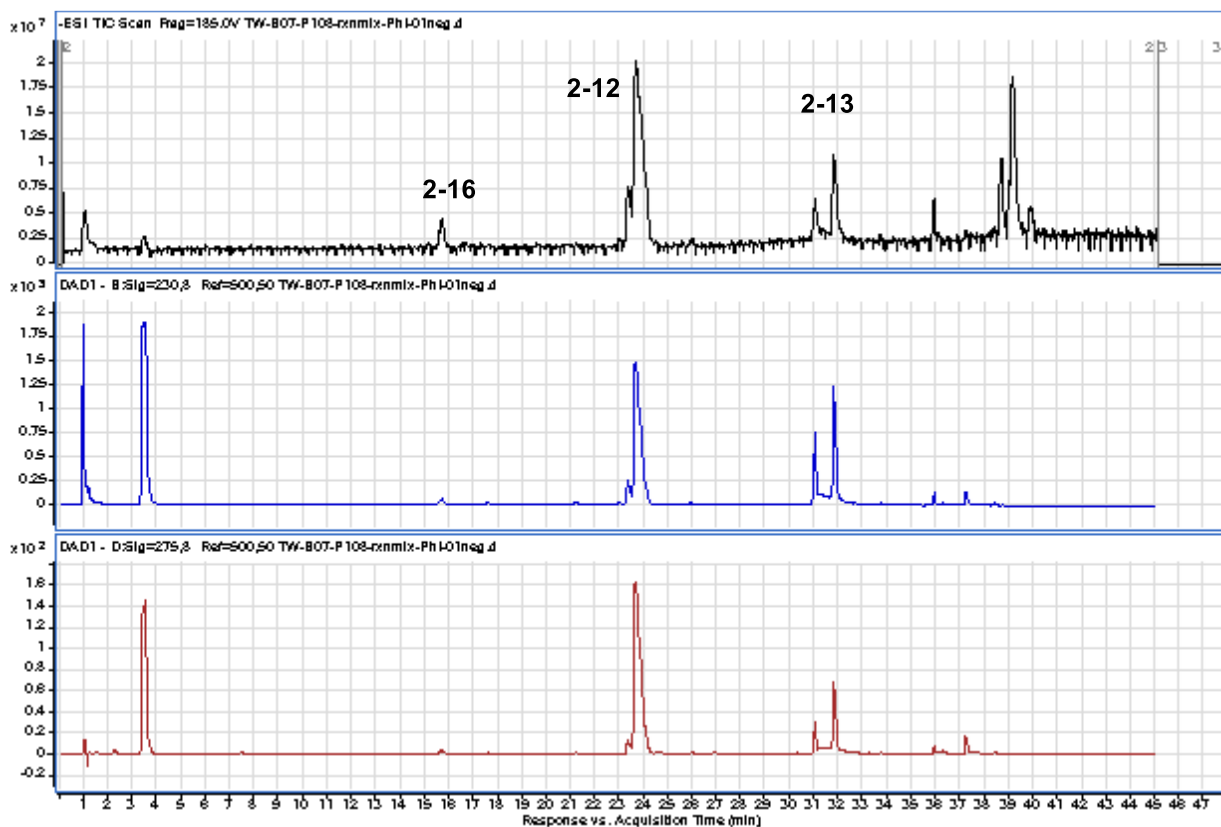


**Figure 2.23** LC/UV/MS trace of Ph-taxoid (**2-12**) formation without Cu catalyst

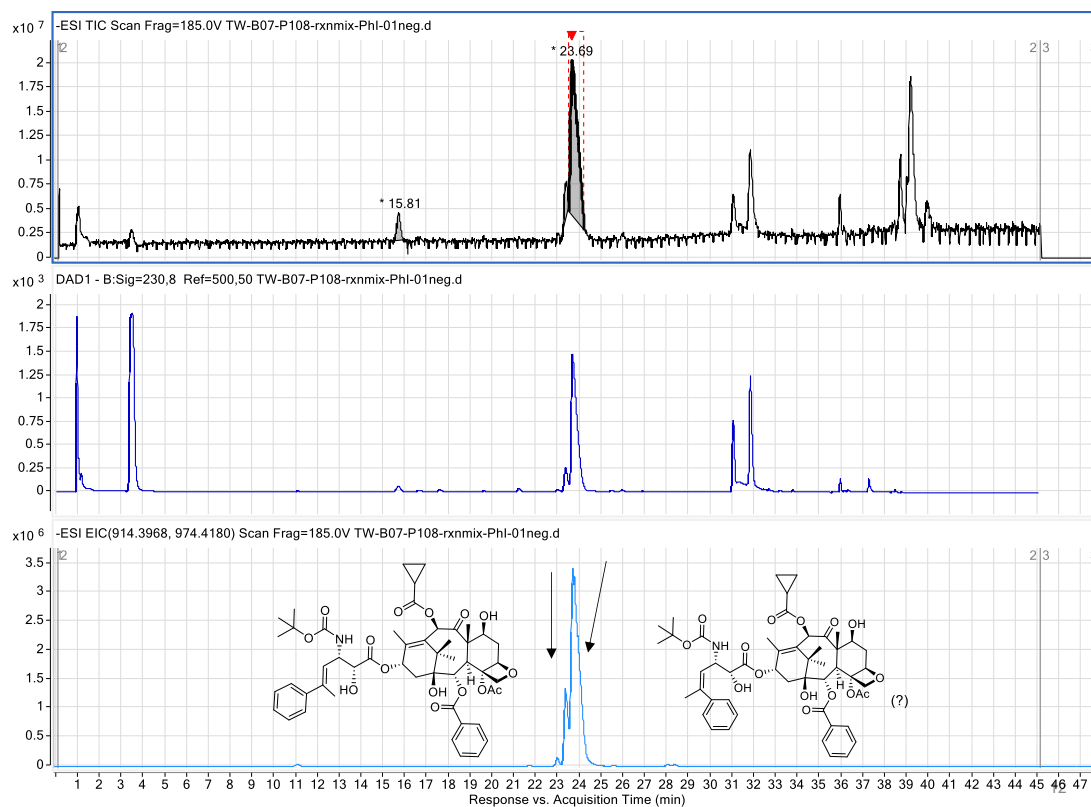


Figure 2.24 Target screening result of Ph-taxoid (2-12)

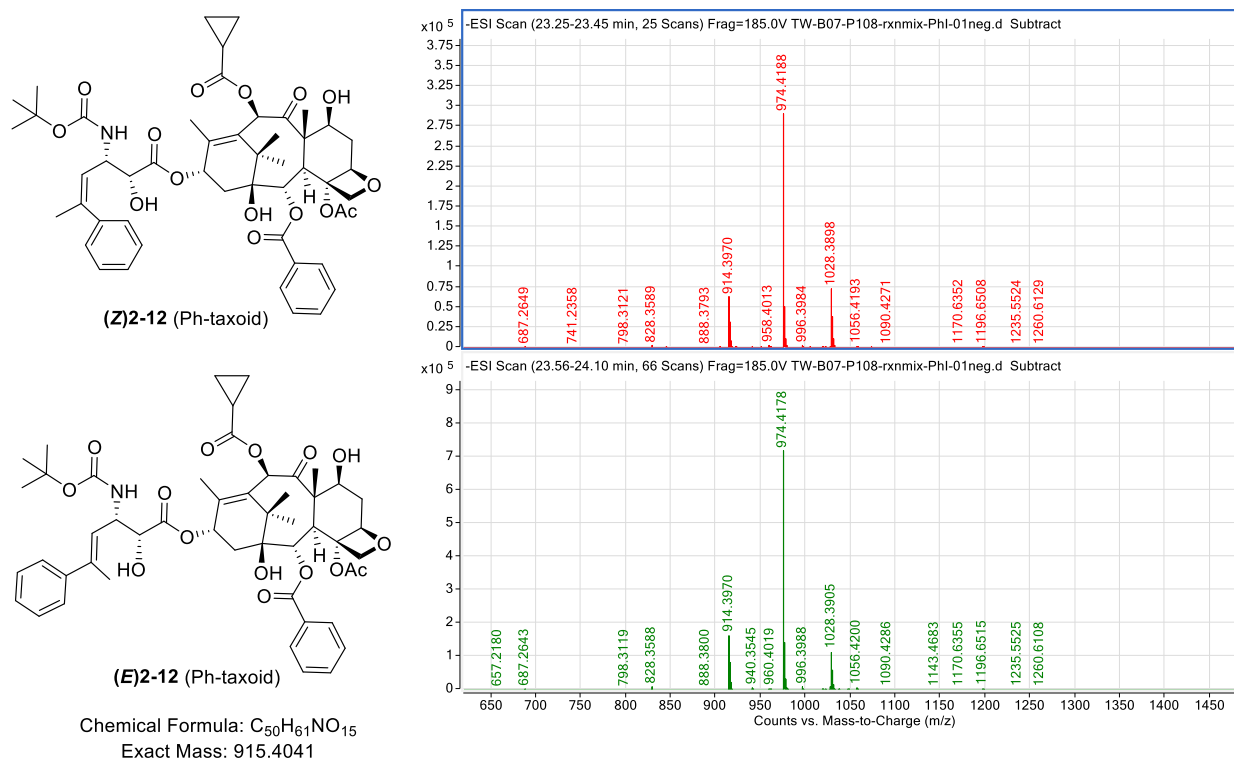
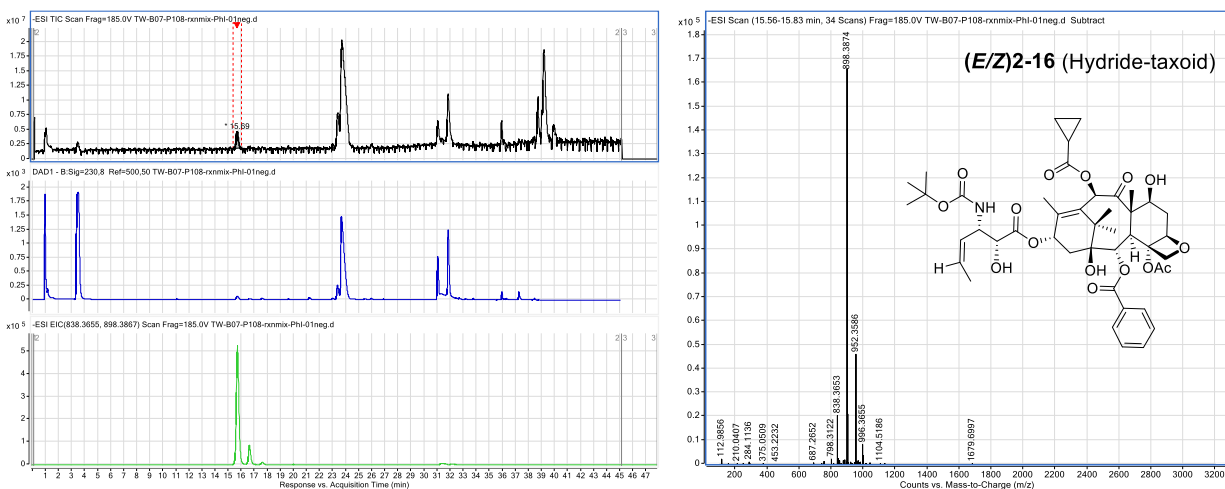
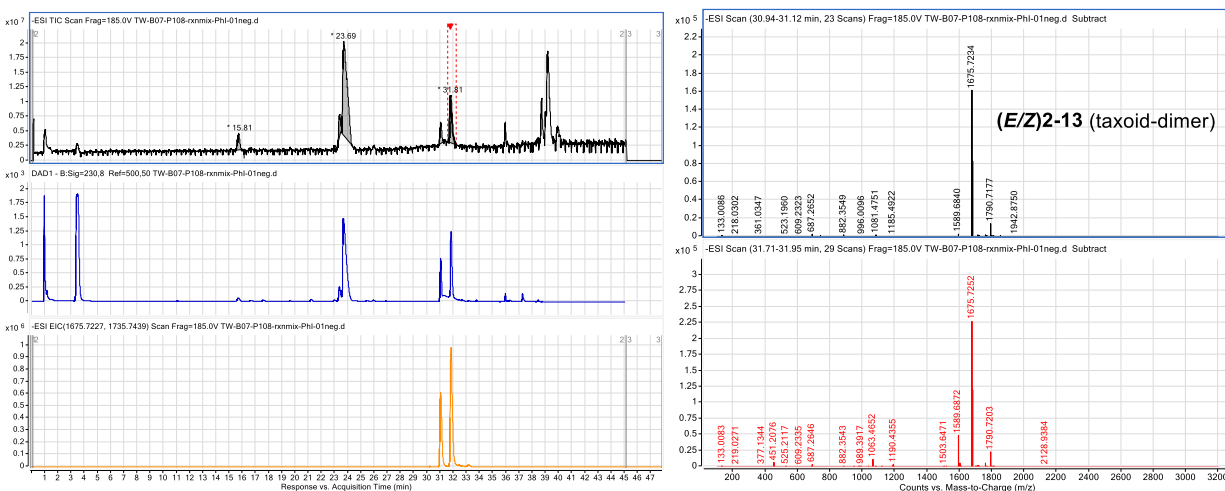
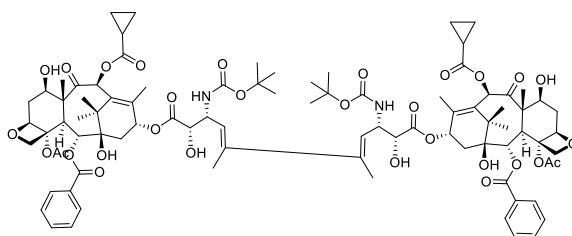


Figure 2.25 Mass analysis results of peaks relating to Ph-taxoid (2-12) isomers

The isomer patterns were also observed for the peaks at 15.69 min and 16.5 min (**2-16**, Hydride-taxoid) (**Figure 2.26**) and the peaks at 31-32 min (**2-13**, taxoid dimer) (**Figure 2.27**). Compared to the outcomes of Tc-taxoid synthesis which the stereochemistry was preserved, the Ph-taxoid reaction gave isomers for each taxoid derivative maybe resulting from the isomerization of vinyl-palladium species.



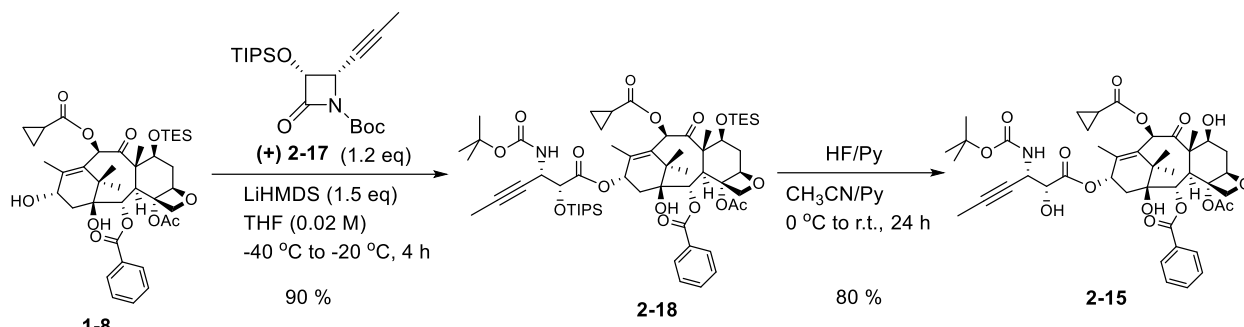
**Figure 2.26** LC/UV/MS trace and mass analysis results of Hydride-taxoid (**2-16**) isomers



**Figure 2.27** LC/UV/MS trace and mass analysis results of taxoid dimer (**2-13**) isomers

Another taxoid derivative alkyne-taxoid (**2-15**) was synthesized in relatively larger scale via Ojima-Holton coupling with a modified baccatin intermediate **1-8** and an enantiopure alkyne

$\beta$ -lactam ((+) **2-17**)<sup>15,17</sup> prepared by Dr. Joshua D. Seitz. Synthesis of **2-15** can help to determine that the byproduct in **Scheme 2.7** is **2-14** (allene-taxoid) or **2-15** (alkyne-taxoid). Compound **2-18** was prepared in excellent yield (90 %), followed by the silyl deprotection using HF-pyridine complex to give **2-15** in good yield (80 %). (**Scheme 2.9**)



**Scheme 2.9** Synthesis of alkyne-taxoid (**2-15**)

## §2.4 Summary

To visualize the drug release and cell internalization by confocal fluorescence microscopy, SB-T-1214-C7-fluorescein as a taxoid-based fluorescent probe was designed, synthesized and fully characterized. In addition, for elucidating the biodistribution profiles of SB-T-1214, a rapid methylation Pd-catalyzed Stille coupling reaction condition was developed toward C-11 radiolabelling SB-T-1214 as PET agent. During the cold synthesis, several taxoid-based derivatives were found unexpectedly, indicating a more complicated mechanism for the Pd-Cu co-catalyzed Stille coupling reaction. The LC/UV/MS-TOF methods were fully established to analyze the outcome of Stille coupling reaction and confirm the predicted structures by mass analysis. Three new taxoid were synthesized with full characterization.

## §2.5 Experimental Sections

### §2.5.1 Caution

Taxoids have been classified as potent cytotoxic agents. Thus, all drugs and structurally related compounds and derivatives must be considered as mutagens and potential reproductive hazards for both males and females. Hydrofluoric acid (HF) can penetrate the skin, causing destruction of deep tissue layers, including bone. Appropriate precautions (i.e. use of gloves, goggles, lab coat and fume hood) must be taken while handling these compounds.

### §2.5.2 General Methods

<sup>1</sup>H and <sup>13</sup>C NMR were measured on 300, 400 MHz Varian spectrometer or 400, 500, 700 MHz Bruker NMR spectrometer. The melting points were measured on a “Uni-melt” capillary melting point apparatus from Arthur H. Thomas Company, Inc and are uncorrected. TLC analyses were performed on Sorbent Technologies aluminum-backed Silica G TLC plates (Sorbent Technologies, 200  $\mu$ m, 20 x 20 cm) and were visualized with UV light and stained with sulfuric acid-EtOH, 10 % PMA-EtOH or 10 % Vanillin-EtOH with 1% sulfuric acid. Column

chromatography was carried out on silica gel 60 (Merck, 230-400 mesh ASTM). Preparative HPLC purification was carried out using a Jupiter C18 preparative HPLC column (5  $\mu\text{m}$ , 300 A, 250  $\times$  21.2 mm) on a Shimadzu CBM-10AW VP communications bus module, Shimadzu SPD-10A VP UV-Vis detector, and Shimadzu LC-6AD liquid chromatography assembly, employing methanol/water as the gradient solvent system, a flow rate of 10 mL/min under room temperature and with the UV detector set at 275 and 230 nm. The gradient was run from 20% to 95% methanol in water over a 30 minute period. Chemical purity was determined with a Shimadzu L-2010A HPLC HT series HPLC assembly, using a Kinetex PFP column (4.6 mm  $\times$  100 mm, 2.6  $\mu\text{m}$ ), employing CH<sub>3</sub>CN/water as the gradient solvent system with a flow rate of 1 mL/min. LC-UV-MS analysis was performed on an Agilent LC-UV-TOF mass spectrometer at the Institute of Chemical Biology and Drug Discovery, using a Kinetex F5 column (2.1 mm  $\times$  150 mm, 2.6  $\mu\text{m}$ , 100 angstroms), employing methanol/water with 10mM AmAc as the gradient solvent system, a flow rate of 0.375 mL/min under 30 °C, and with the UV detector set at 275 and 230 nm. The gradient was run from 60% to 95% methanol in water over a 45 minute period. Low resolution mass spectrometry was performed on an Agilent LC-MSD mass spectrometer at the Institute of Chemical Biology and Drug Discovery, Stony Brook, NY. High resolution mass spectrometry analysis was carried out on an Agilent LC-UV-TOF mass spectrometer at the Institute of Chemical Biology Drug Discovery, Stony Brook, NY or at the Mass Spectrometry Laboratory, University of Illinois at Urbana-Champaign, Urbana, IL

### §2.5.3 Materials

The chemicals were purchased from Sigma-Aldrich, Fischer Scientific or VWR International, and used as received or purified before use by standard methods. Dichloromethane was dried before use by distillation over calcium hydride under nitrogen. Tetrahydrofuran was dried before use by distillation over sodium-benzophenone kept under nitrogen. Dry DMF was purchased from EMD chemical company, and used without further purification. 10-Deacetylbaicatin III was obtained from Indena, SpA, Italy. Reaction flasks were dried in a 100 °C oven and allowed to cool to room temperature in a desiccator over “*Drierite*” (calcium sulfate) and assembled under an inert nitrogen gas atmosphere.

### §2.5.4 Experimental Procedure

#### *tert*-Butyl 4-hydroxybutanoate (2-1)<sup>18</sup>

To a round bottomed flask was added 4-*tert*-butoxy-4-oxobutanoic acid (1.4 g, 8 mmol) dissolved in 0.5 M THF (16 mL) under 0 °C stirring for 15 minutes. Then slowly add 2 M borane-methyl sulfide complex in THF (8.8 mmol, 4.4 mL) and the resulting solution was allowed to warm to room temperature for 24 hours. The reaction was monitored by TLC and stained in vanillin. Then the resulting solution was quenched with sodium bicarbonate (10 mL  $\times$  3) and extracted with DCM (10 mL  $\times$  3). Then the collected organic layer was dried with magnesium sulfate and concentrated *in vacuo*. Purification was done *via* column chromatography on silica gel with increasing amounts of eluent (hexanes:ethyl acetate) to yield **2-1** (1.0 g, 6.3 mmol, 79 %) as colorless oil. <sup>1</sup>H NMR (500 MHz, CDCl<sub>3</sub>)  $\delta$  1.40 (s, 9 H), 1.79 (quint, *J* = 6 Hz, 2 H), 2.29 (d, *J* = 7.2 Hz, 2 H), 2.64 (bs, 1 H), 3.61 (t, *J* = 6.3 Hz, 2 H). <sup>13</sup>C NMR (125 MHz, CDCl<sub>3</sub>)  $\delta$  27.8, 28.1, 32.5, 62.3, 80.5, 173.4. All data are in agreement with literature values.<sup>18</sup>

### Isopropyl 2-(6-hydroxy-3-oxo-3*H*-xanthen-9-yl)benzoate (2-2 A)

To a 10 mL round bottomed flask were added fluorescein (664 mg, 2 mmol) and 1 eq 2-propanol (120 mg, 2 mmol), followed by addition of concentrated sulfuric acid (0.05 mL, 1 mmol) dropwise. Then the resulting solution was heated to 100 °C to reflux overnight. The reaction was monitored by TLC. Upon completion, add 15 mL distilled water to dilute solution and use ethyl acetate to extract, then used brine, dry with magnesium sulfate and concentrate *in vacuo*. Purification was done *via* column chromatography on silica gel with increasing amounts of eluent (hexanes:ethyl acetate) to yield crude **2-2 A**. Further purification was done *via* column chromatography on silica gel with pure ethyl acetate to flush and collect to afford **2-2 A** in red solid (192 mg, 0.5 mmol, 25 %). <sup>1</sup>H NMR (300 MHz, CD<sub>3</sub>OD) δ 0.80 (d, *J* = 6.3 Hz, 6 H), 4.07 (m, 1 H), 6.68 (d, *J* = 9.3 Hz, 2 H), 6.75 (s, 2 H), 7.00 (d, *J* = 9.3 Hz, 2 H), 7.41 (dd, *J* = 7.2 Hz, 1.2 Hz, 1 H), 7.74 (m, 2 H), 8.23 (dd, *J* = 7.8 Hz, 1.5 Hz, 1 H). HRMS (TOF) [M + H]<sup>+</sup> *m/z* calcd for C<sub>23</sub>H<sub>19</sub>O<sub>5</sub><sup>+</sup>: 375.1227, found 375.1225. (Δ = -0.5 ppm).

### Isobutyl 2-(6-hydroxy-3-oxo-3*H*-xanthen-9-yl)benzoate (2-2 B)<sup>19</sup>

To a round bottom flask fluorescein (1g, 3 mmol) was added, and 10 mL 2-methyl-1-propanol (excess) was added as well as solvent, followed by addition of concentrated sulfuric acid (0.75 mL) dropwise. Then the resulting solution was heated to 120 °C to reflux overnight. The reaction was monitored by TLC. Upon completion, the resulting solution was allowed to cool to room temperature and diluted by using ethyl acetate (10 mL). The organic layer was separated and washed with (sat. aq) NaHCO<sub>3</sub> (10 mL x 3). Then organic layer was washed with brine (20 mL x 3), dry with magnesium sulfate and concentrate *in vacuo*. Purification was done *via* column chromatography on silica gel with increasing amounts of eluent (dichloromethane:methanol) to yield **2-2 B** as a red solid (924 mg, 2.4 mmol) in 79 % yield; m.p. 91-92 °C. <sup>1</sup>H NMR (500 MHz, CDCl<sub>3</sub>) δ 0.65 (s, 3 H), 0.67 (s, 3 H), 1.53 (sept, *J* = 6.6 Hz, 1 H), 3.73 (d, *J* = 6.6 Hz, 2 H), 6.78 (d, *J* = 2.15 Hz, 1 H), 6.80 (d, *J* = 2.15 Hz, 1 H), 6.87 (d, *J* = 2.1 Hz, 2 H), 6.97 (s, 1 H), 6.99 (s, 1 H), 7.29 (dd, *J<sub>a</sub>* = 0.95 Hz, *J<sub>b</sub>* = 7.4 Hz, 1 H), 7.66 (dt, *J<sub>a</sub>* = 1.35 Hz, *J<sub>b</sub>* = 7.6 Hz, 1 H), 7.71 (dt, *J<sub>a</sub>* = 1.5 Hz, *J<sub>b</sub>* = 7.5 Hz, 1 H), 8.26 (dd, *J<sub>a</sub>* = 1.25 Hz, *J<sub>b</sub>* = 7.85 Hz, 1 H). <sup>13</sup>C NMR (500 MHz, CDCl<sub>3</sub>) δ 18.8, 27.4, 71.9, 103.7, 114.8, 122.2, 129.8, 130.3, 130.6, 130.6, 131.3, 132.5, 134.1, 155.8, 157.8, 165.4, 175.6. HRMS (TOF) [M + H]<sup>+</sup> *m/z* calcd for C<sub>24</sub>H<sub>21</sub>O<sub>5</sub><sup>+</sup>: 389.1384, found 389.1400. (Δ = 4.1 ppm). All data are in agreement with literature values.<sup>19</sup>

### Isopropyl 2-(6-(4-(*tert*-butoxy)-4-oxobutoxy)-3-oxo-3*H*-xanthen-9-yl)benzoate (2-3 A)

To a small round bottomed flask were added **2-2 A** (174 mg, 0.47 mmol), 3 eq triphenylphosphine (PPh<sub>3</sub>) (370 mg, 1.4 mmol) and diisopropyl azodicarboxylate (DIAD) (285 mg, 0.28 mL, 1.4 mmol) dissolved in 4 mL THF under room temperature, then **2-1** (75 mg, 0.47 mmol) dissolved in 4 mL THF was slowly added. The resulting solution was allowed to stir for overnight. Upon completion, 10 mL distilled water was added to dilute solution and 20 mL ethyl acetate was used to extract product. Then the solution was dried with magnesium sulfate and concentrated *in vacuo*. Purification was done *via* column chromatography on silica gel with increasing amounts of eluent (hexanes:ethyl acetate) and further the crude product was precipitated out by using 20% ethyl

acetate in hexane to remove triphenylphosphine oxide (TPPO) to yield crude **2-3 A** (400 mg) with TPPO.

#### **Isobutyl 2-(6-(4-(*tert*-butoxy)-4-oxobutoxy)-3-oxo-3*H*-xanthen-9-yl)benzoate (2-3 B)**

To a solution of **2-2 B** (300 mg, 0.77 mmol), 3 eq triphenylphosphine (PPh<sub>3</sub>) (606 mg, 2.31 mmol) and 3 eq diisopropyl azodicarboxylate (DIAD) (467 mg, 0.46 mL, 2.31 mmol) dissolved in 5 mL THF was slowly added a solution of **2-1** (124 mg, 0.77 mmol) dissolved in 5 mL THF. The resulting solution was allowed to stir for 4 hours under room temperature. Upon completion, 10 mL distilled water was added to dilute solution and 20 mL ethyl acetate was used to extract product. Then the solution was dried with magnesium sulfate and concentrated *in vacuo*. Purification was done *via* column chromatography on silica gel with increasing amounts of eluent (hexanes:ethyl acetate) to yield crude **2-3 B** (343 mg) with by-product TPPO (triphenylphosphine oxide) which had very close R<sub>f</sub> value. HRMS (TOF) [M + H]<sup>+</sup> m/z calcd for C<sub>32</sub>H<sub>35</sub>O<sub>7</sub><sup>+</sup>: 531.2377, found 531.2374. (Δ = -0.5 ppm).

#### **4-((9-(2-(Isopropoxycarbonyl)phenyl)-3-oxo-3*H*-xanthen-6-yl)oxy)butanoic acid (2-4 A)**

To a round bottomed flask was added crude **2-3 A** (400 mg) with TPPO dissolved in 0.05 M CH<sub>2</sub>Cl<sub>2</sub> (10 mL). Then TFA solution (25 volume %) was slowly added and reaction was allowed to stir for 3 hours. Purification was done *via* column chromatography on silica gel with 10 % methanol in DCM to afford **2-4 A** (105 mg, 0.23 mmol, 49 % over 2 steps). <sup>1</sup>H NMR (300 MHz, CDCl<sub>3</sub>) δ 0.57 (t, *J* = 7.5 Hz, 3 H), 0.84 (d, *J* = 6 Hz, 3 H), 0.90 (m, 2 H), 2.19 (t, 2 H), 2.62 (t, 2 H), 4.26 (m, 1 H), 4.81 (m, 1 H), 6.90 (m, 2 H), 7.10 (m, 2 H), 7.30 (d, 1 H), 7.73 (m, 2 H), 8.27 (d, 1 H). HRMS (TOF) [M + H]<sup>+</sup> m/z calcd for C<sub>27</sub>H<sub>25</sub>O<sub>7</sub><sup>+</sup>: 461.1595, found 461.1592. (Δ = -0.6 ppm).

#### **4-((9-(2-(Isobutoxycarbonyl)phenyl)-3-oxo-3*H*-xanthen-6-yl)oxy)butanoic acid (2-4 B)<sup>19</sup>**

To a solution of crude **2-3 B** (300 mg) with TPPO dissolved in 0.2 M CH<sub>2</sub>Cl<sub>2</sub> (2.5 mL) was added TFA (25 volume %) and reaction was allowed to stir for 3 hours under room temperature. Purification was done *via* column chromatography on silica gel with increasing amounts of eluent (dichloromethane:methanol) up to 5 % methanol to yield **2-4 B** as an orange solid (313 mg, 0.66 mmol) in 86 % yield for successive 2 steps; m.p. 213-214 °C. <sup>1</sup>H NMR (500 MHz, DMSO-*d*<sup>6</sup>) δ 0.69 (s, 3 H), 0.70 (s, 3 H), 0.71 (enantiomer, s, 3 H), 0.72 (enantiomer, s, 3 H), 1.56 (sept, *J* = 6.65 Hz, 2 H), 2.13 (quint, *J* = 6.95 Hz, 2 H), 2.52 (t, *J* = 7.2 Hz, 2 H), 3.73 (dd, *J*<sub>a</sub> = 6.45 Hz, *J*<sub>b</sub> = 10.75 Hz, 1 H), 3.79 (dd, *J*<sub>a</sub> = 6.55 Hz, *J*<sub>b</sub> = 10.75 Hz, 1 H), 4.25 (t, *J* = 6.3 Hz, 2 H), 6.53 (d, *J* = 2 Hz, 1 H), 6.60 (dd, *J*<sub>a</sub> = 2 Hz, *J*<sub>b</sub> = 9.6 Hz, 1 H), 6.97 (dd, *J*<sub>a</sub> = 2.35 Hz, *J*<sub>b</sub> = 9 Hz, 1 H), 7.08 (d, *J* = 3.3 Hz, 1 H), 7.10 (d, *J* = 2.7 Hz, 1 H), 7.28 (d, *J* = 2.4 Hz, 1 H), 7.45 (dt, *J*<sub>a</sub> = 0.95 Hz, *J*<sub>b</sub> = 7.5 Hz, 1 H), 7.80 (dt, *J*<sub>a</sub> = 1.3 Hz, *J*<sub>b</sub> = 7.65 Hz, 1 H), 7.86 (dt, *J*<sub>a</sub> = 1.35 Hz, *J*<sub>b</sub> = 7.5 Hz, 1 H), 8.32 (dd, *J*<sub>a</sub> = 1.1 Hz, *J*<sub>b</sub> = 7.85 Hz, 1 H). <sup>13</sup>C NMR (125 MHz, DMSO-*d*<sup>6</sup>) δ 17.7, 17.8, 24.1, 27.4, 29.8, 60.8, 68.0, 71.4, 100.6, 104.0, 114.6, 114.8, 116.7, 127.9, 129.5, 160.1, 164.9, 165.5, 175.4, 185.8. HRMS (TOF) [M + H]<sup>+</sup> m/z calcd for C<sub>28</sub>H<sub>28</sub>O<sub>7</sub><sup>+</sup>: 475.1751, found 475.1751. (Δ = 0 ppm). All data are in agreement with literature values.<sup>19</sup>

**Isopropyl 2-(6-(4-((2,5-dioxopyrrolidin-1-yl)oxy)-4-oxobutoxy)-3-oxo-3H-xanthen-9-yl)benzoate (2-5 A)**

To a two neck round bottomed flask were added **2-4 A** (61 mg, 0.13 mmol), 2 eq *N*-hydroxysuccinimide (30 mg, 0.26 mmol), 0.5 eq 4-dimethylaminopyridine (DMAP) (7.3 mg, 0.06 mmol) and 1-ethyl-3-(3-dimethyl amino-propyl) carbodiimide hydrochloride (EDC HCl) (30 mg, 0.16 mmol) dissolved in 0.1 M DCM (1.3 mL). The resulting solution was allowed to stir 17 hours under room temperature. Upon completion, the solution was concentrated and purification was done *via* column chromatography on silica gel with increasing amounts of eluent (hexanes:ethyl acetate) to yield **2-5 A** (44 mg, 0.08 mmol) in 61% yield. <sup>1</sup>H NMR (300 MHz, CDCl<sub>3</sub>) δ 0.80 (d, 6 H), 1.21 (m, 2 H), 2.23 (m, 2 H), 2.84 (s, 4 H), 4.16 (t, *J* = 5.7 Hz, 2 H), 4.81 (m, 1 H), 6.53 (m, 2 H), 6.76 (d, 2 H), 6.87 (m, 3 H), 6.97 (d, 1 H), 7.27 (d, 1 H), 7.63 (m, 2 H), 8.21 (d, *J* = 7.5 Hz, 1 H). HRMS (TOF) [M + H]<sup>+</sup> m/z calcd for C<sub>31</sub>H<sub>28</sub>NO<sub>9</sub><sup>+</sup>: 558.1759, found 558.1760. (Δ = 0.2 ppm).

**Isobutyl 2-(6-(4-((2,5-dioxopyrrolidin-1-yl)oxy)-4-oxobutoxy)-3-oxo-3H-xanthen-9-yl)benzoate (2-5 B)**

To a round bottom flask were added **2-4 B** (100 mg, 0.21 mmol), 1.5 eq NHS (36.8 mg, 0.32 mmol), 0.5 eq DMAP (12.8 mg, 0.11 mmol) and 1.5 eq EDC HCl salt (61.3 mg, 0.32 mmol) and were dissolved in 0.02 M DCM (10 mL). The solution turned to dark orange. The resulting solution was allowed to stir under room temperature for 17 hours and monitored by TLC. Upon completion, the solvent was removed by rotary evaporation and the crude reaction mixture was directly purified *via* column chromatography on silica gel with increasing amounts of eluent (dichloromethane: methanol) to yield fluorescein-OSu ester **2-5 B** as an orange solid (114 mg, 0.2 mmol) in 95 % yield. <sup>1</sup>H NMR (700 MHz, CDCl<sub>3</sub>) δ 0.68 (t, *J* = 8.6 Hz, 6 H), 0.84 (m, 1 H), 1.25 (m, 2 H), 1.59 (sept, *J* = 6.6 Hz, 1 H), 2.26 (quint, *J* = 6.3 Hz, 2 H), 2.84 (s, 4 H), 3.69-3.81 (m, 2 H), 4.16 (t, *J* = 5.7 Hz, 2 H), 6.43 (s, 1 H), 6.52 (d, *J* = 9.7 Hz, 1 H), 6.74 (d, *J* = 8.9 Hz, 1 H), 6.86 (dd, *J<sub>a</sub>* = 9.7 Hz, *J<sub>b</sub>* = 15.3 Hz, 2 H), 6.95 (s, 1 H), 7.28 (d, *J* = 7.3 Hz, 1 H), 7.65 (t, *J* = 7.5 Hz, 1 H), 7.7 (t, *J* = 7.5 Hz, 1 H), 8.24 (d, *J* = 7.7 Hz, 1 H). <sup>13</sup>C NMR (176 MHz, CD<sub>3</sub>OD) δ 18.9, 19.0, 24.2, 25.6, 27.5, 27.7, 66.8, 71.9, 100.9, 105.8, 113.7, 115.1, 117.8, 129.1, 129.7, 130.0, 130.3, 130.6, 130.8, 131.3, 132.6, 134.2, 150.2, 154.3, 159.0, 163.0, 165.6, 168.1, 169.1, 185.8. HRMS (TOF) [M + H]<sup>+</sup> calcd. for C<sub>32</sub>H<sub>30</sub>NO<sub>9</sub><sup>+</sup> 572.1915, found 572.2016. (Δ = 17 ppm).

**2'-tert-Butyl-di-methylsilyl-3'-dephenyl-10-(cyclopropylcarbonyl)-3'-(2-methyl-2-propenyl) docetaxel (SB-T-1214) (2-6)<sup>18</sup>**

An aliquot of **1-10** (SB-T-1214) (230 mg, 0.27 mmol) and 10 eq imidazole (184 mg, 2.7 mmol) were dissolved in DMF (0.5 mL) under inert condition. To the mixture was added 5 eq TBDMSCl dissolved in 50 % toluene (0.35 mL, 404 mg, 1.35 mmol) dropwise. The mixture was stirred under room temperature for 4 hours and monitored *via* TLC. Upon completion the reaction was diluted with water (10 mL) and extracted with ethyl acetate (10 mL x 3). The organic layer was collected, washed with brine (10 mL x 3), dried over anhydrous MgSO<sub>4</sub>, and concentrated *in vacuo*. Purification was done *via* column chromatography on silica gel with increasing amounts of eluent (hexanes:ethyl acetate) to yield **2-6** as a white solid (249 mg, 0.257 mmol, 96 % yield). <sup>1</sup>H NMR (500 MHz, CDCl<sub>3</sub>) δ 0.08 (s, 3 H), 0.11 (s, 3 H), 0.93 (s, 9 H), 1.34 (s, 9 H), 1.66 (s, 3 H), 1.74-



1.78 (d, 6 H), 1.87 (s, 3 H), 2.06 (s, 1 H), 2.23 (m, 1 H), 2.41 (s, 3 H), 2.56 (m, 2 H), 3.81 (d,  $J = 7.1$  Hz, 1 H), 4.18 (d,  $J = 8.45$  Hz, 1 H), 4.23 (d,  $J = 3.5$  Hz, 1 H), 4.29 (d,  $J = 8.45$  Hz, 1 H), 4.40 (q,  $J = 3.5$  Hz, 1 H), 4.74 (broad, 1 H), 4.80 (d,  $J = 9.35$  Hz, 1 H), 4.96 (d,  $J = 8$  Hz, 1 H), 5.22 (d,  $J = 8.5$  Hz, 1 H), 5.65 (d,  $J = 7.1$  Hz, 1 H), 6.16 (t,  $J = 8.7$  Hz, 1 H), 6.28 (s, 1 H), 7.45 (t,  $J = 7.7$  Hz, 2 H), 7.59 (t,  $J = 7.4$  Hz, 1 H), 8.09 (d,  $J = 7.45$ , 2 H).  $^{13}\text{C}$  NMR (500 MHz,  $\text{CDCl}_3$ )  $\delta$  9.2, 9.4, 9.5, 13.0, 14.8, 14.9, 18.4, 18.6, 20.3, 22.2, 22.6, 25.7, 25.8, 26.6, 28.2, 31.6, 34.6, 35.4, 35.6, 58.5, 71.3, 72.2, 75.2, 75.3, 75.4, 79.3, 80.9, 84.5, 121.8, 128.6, 129.2, 130.1, 132.5, 133.6, 143.2, 155.0, 166.9, 170.1, 171.7, 174.8, 175.2, 204.0. All data are in agreement with literature values.<sup>18</sup>

### 7-Fluorescein-SB-T-1214-OTBS (2-7)

To a round bottom flask were added **2-6** (184 mg, 0.19 mmol), 1 eq DMAP (23 mg, 0.19 mmol) and 2 eq **2-4 B** (180 mg, 0.38 mmol) and 2 eq EDC HCl salt (72.8 mg, 0.38 mmol) and were dissolved in DCM (10 mL) and DMF (1mL) at room temperature with stirring. The mixture was stirred for 5 days at room temperature monitored by TLC. The crude product was purified on a silica gel column with increasing eluent (dichloromethane:methanol) to yield **2-7** as an orange solid (260 mg, 0.18 mmol) in 95 % yield.  $^1\text{H}$  NMR (500 MHz,  $\text{CDCl}_3$ )  $\delta$  0.07 (s, 3 H), 0.10 (s, 3 H), 0.67-0.70 (dt,  $J = 1.25$  Hz, 6 H), 0.93 (s, 14 H), 1.16 (s, 3 H), 1.23 (s, 3 H), 1.34 (s, 9 H), 1.59 (m, 1 H), 1.67 (m, 1 H), 1.74 (s, 3 H), 1.77 (d, 6 H), 1.93 (s, 3 H), 2.03 (d,  $J = 4.8$  Hz, 2 H), 2.09 (m, 2 H), 2.29 (m, 1 H), 2.40 (s, 3 H), 2.87 (s, 3 H), 2.94 (s, 3 H), 3.71-3.80 (m, 2 H), 3.96 (d,  $J = 6.95$  Hz, 1 H), 4.05-4.11 (m, 2 H), 4.17 (d,  $J = 8.4$  Hz, 1 H), 4.23 (d,  $J = 3.35$  Hz, 1 H), 4.30 (d,  $J = 8.45$  Hz, 1 H), 4.75 (broad, 1 H), 4.82 (d,  $J = 9.7$  Hz, 1 H), 4.94 (d,  $J = 9.2$  Hz, 1 H), 5.22 (d,  $J = 8.55$  Hz, 1 H), 5.59 (q,  $J = 7.25$  Hz, 1 H), 5.66 (d,  $J = 7$  Hz, 1 H), 6.12 (t,  $J = 8.75$  Hz, 1 H), 6.29 (s, 1 H), 6.46 (s, 1 H), 6.54 (d, 1 H), 6.71 (d, 1 H), 6.86 (t,  $J = 9.55$  Hz, 2 H), 6.95 (t, 1 H), 7.27 (d,  $J = 7.4$  Hz, 1 H), 7.45 (t,  $J = 7.7$  Hz, 2 H), 7.59 (t,  $J = 7.4$  Hz, 1 H), 7.64 (t,  $J = 7.6$  Hz, 1 H), 7.70 (t,  $J = 7.35$  Hz, 1 H), 8.00 (s, 1 H), 8.08 (d,  $J = 7.4$  Hz, 2 H), 8.24 (d,  $J = 7.75$  Hz, 1 H).  $^{13}\text{C}$  NMR (125 MHz,  $\text{CDCl}_3$ )  $\delta$  8.8, 8.8, 10.9, 12.8, 13.7, 14.2, 14.5, 18.4, 18.6, 18.8, 18.9, 20.7, 21.4, 22.5, 23.7, 26.1, 27.5, 28.2, 30.4, 31.6, 33.3, 35.4, 36.5, 43.2, 46.8, 56.0, 60.4, 64.4, 67.9, 71.2, 71.4, 71.9, 74.6, 74.9, 75.0, 78.8, 80.7, 84.0, 100.7, 105.7, 113.9, 114.7, 117.5, 121.8, 128.6, 128.9, 129.2, 129.6, 129.8, 130.1, 130.3, 130.5, 130.8, 131.3, 132.3, 132.5, 133.7, 134.2, 136.5, 141.6, 150.6, 154.4, 155.1, 159.0, 162.6, 163.6, 165.5, 166.8, 169.9, 171.7, 171.9, 172.9, 173.8, 185.7, 202.4. HRMS (TOF)  $[\text{M} + \text{H}]^+$  calcd. for  $\text{C}_{79}\text{H}_{98}\text{NO}_{21}\text{Si}^+$  1424.6395, found 1424.6398. ( $\Delta = 0.2$  ppm).

### 7-Fluorescein-SB-T-1214 (2-8)

To a cooled solution of **2-7** (243 mg, 0.17 mmol) dissolved in a 1:1 mixture of 0.02 M acetonitrile:pyridine (9 mL) was slowly added 2.4 mL HF/pyridine (0.01 mL per every 1 mg) under inert conditions. The reaction was stirred at room temperature for 24 hours. Upon completion the reaction was quenched with 0.2 M citric acid in  $\text{H}_2\text{O}$  (3.8 %) (5 mL) and extracted with ethyl acetate (30 mL x 3). The organic layer was collected, washed with  $\text{CuSO}_4$ , washed with diluted water until the organic layer became clear, then washed with brine (30 mL x 3), dried over anhydrous  $\text{MgSO}_4$ , and concentrated *in vacuo*. Purification was done *via* column chromatography on silica gel with increasing amounts of eluent (dichloromethane:methanol) to yield **2-8** as an orange solid (115 mg, 0.09 mmol) in 53 % yield.  $^1\text{H}$  NMR (500 MHz,  $\text{CDCl}_3$ )  $\delta$  0.67 (t,  $J = 6.95$  Hz, 6 H), 0.85-0.92 (m, 6 H), 1.18 (s, 3 H), 1.23 (s, 3 H), 1.35 (s, 9 H), 1.59 (m, 1 H), 1.68 (m, 2

H), 1.76 (s, 3 H), 1.80 (s, 6 H), 2.01 (s, 3 H), 2.08 (m, 2 H), 2.37 (s, 3 H), 2.56 (m, 1 H), 3.73-3.78 (m, 2 H), 3.96 (d,  $J = 6.65$  Hz, 1 H), 4.13 (m, 2 H), 4.17 (d,  $J = 8.4$  Hz, 1 H), 4.26 (s, 1 H), 4.31 (d,  $J = 8.5$  Hz, 1 H), 4.75 (t,  $J = 8.15$  Hz, 1 H), 4.95 (m, 2 H), 5.35 (d,  $J = 7.8$  Hz, 1 H), 5.65 (t,  $J = 10.95$  Hz, 2 H), 6.11 (t,  $J = 8.75$  Hz, 1 H), 6.31 (s, 1 H), 6.43 (s, 1 H), 6.53 (d, 1 H), 6.72 (d,  $J = 8.95$  Hz, 1 H), 6.86 (t,  $J = 9.2$  Hz, 2 H), 7.11 (s, 1 H), 7.28 (d,  $J = 4.1$  Hz, 1 H), 7.46 (t,  $J = 7.55$  Hz, 2 H), 7.59 (t,  $J = 7.55$  Hz, 1 H), 7.65 (t,  $J = 7.55$  Hz, 1 H), 7.70 (t,  $J = 7.4$  Hz, 1 H), 8.09 (d,  $J = 7.85$  Hz, 2 H), 8.24 (d,  $J = 7.75$  Hz, 1 H).  $^{13}\text{C}$  NMR (125 MHz,  $\text{CDCl}_3$ )  $\delta$  8.8, 8.9, 10.8, 12.9, 14.1, 14.7, 18.6, 18.8, 18.9, 21.1, 22.3, 22.6, 23.4, 25.7, 26.2, 27.5, 28.1, 28.2, 30.0, 30.1, 31.6, 33.4, 34.6, 35.5, 43.2, 47.0, 51.5, 56.1, 56.1, 67.9, 71.5, 71.9, 72.0, 73.6, 74.4, 75.1, 78.6, 79.7, 80.8, 83.9, 100.8, 105.7, 114.3, 114.7, 117.4, 120.9, 128.7, 128.8, 128.9, 129.1, 129.6, 129.8, 130.1, 130.3, 130.5, 130.8, 130.9, 131.3, 132.5, 133.8, 134.2, 137.5, 141.2, 150.8, 154.5, 155.4, 159.1, 163.7, 165.5, 166.8, 170.1, 172.1, 172.1, 172.9, 173.1, 185.7, 202.4. M.P. 170-172 °C. HRMS (TOF)  $[\text{M} + \text{H}]^+$  calcd. for  $\text{C}_{73}\text{H}_{84}\text{NO}_{21}^+$  1310.5530, found 1310.5540. ( $\Delta = 0.7$  ppm).

### SB-T-1214 (1-10) via Stille Coupling Methylation (Cold Synthesis)

To a solution of tetrakis(triphenylphosphine)palladium(0) (2.0 mg, 1.77  $\mu\text{mol}$ ) in DMF (100  $\mu\text{L}$ ) was added a solution of methyl iodide (25  $\mu\text{g}$ , 0.177  $\mu\text{mol}$ ) in DMF (100  $\mu\text{L}$ ), and the solution was added to a suspension of copper(I)-thiophene-2-carboxylate (0.4 mg, 1.77  $\mu\text{mol}$ ) and 10-cyclopropanecarbonyl-3'-dephenyl-3'-(2-methyl-2-tributylstannyl)docetaxel (**2-9**) (2 mg, 1.77  $\mu\text{mol}$ ) in DMF (100  $\mu\text{L}$ ). The reaction mixture was heated to 60 °C and allowed to react for 5 min with stirring. The reaction was quenched with methanol (300  $\mu\text{L}$ ), and the reaction mixture was passed through a solid-phase extraction filter. The filtrate was analyzed by LC/UV/MS-TOF with a Kinetex F5 column (2.1 mm x 150 mm, 2.6  $\mu\text{m}$ , 100 angstroms) employing methanol/water with 10mM AmAc as the gradient solvent system, a flow rate of 0.375 mL/min under 30 °C, and with the UV detector set at 275 and 230 nm. The gradient was run from 60% to 95% methanol in water over a 45 minute period. HRMS  $[\text{M}-\text{H}]^-$  for  $\text{C}_{45}\text{H}_{58}\text{NO}_{15}^-$  calcd. 852.3812, found 852.3800. ( $\Delta = -1.4$  ppm). SB-T-1214 (**1-10**):  $t_{\text{R}} = 17.1$  min.

### 10-Cyclopropanecarbonyl-3'-dephenyl-3'-(2-methyl-2-(thiophene-2-carboxylate))docetaxel (Tc-taxoid 2-11)

To an empty vial were added copper(I)-thiophene-2-carboxylate (1.62 mg, 8.5  $\mu\text{mol}$ ) and 10-cyclopropanecarbonyl-3'-dephenyl-3'-(2-methyl-2-tributylstannyl)docetaxel (**2-9**) (8 mg, 7.1  $\mu\text{mol}$ ) suspended in DMF (400  $\mu\text{L}$ ) The reaction mixture was heated to 60 °C and allowed to react for 6 hours with stirring. The reaction was quenched with methanol (400  $\mu\text{L}$ ). The reaction mixture was lyophilized to remove DMF, and the crude product was purified by column chromatography on silica gel with increasing amounts of eluent (hexanes:ethyl acetate) to give crude **2-11**. A portion of starting material **2-9** (1 mg, 0.9  $\mu\text{mol}$ ) was recovered. Further purification was carried out by preparative HPLC using a Jupiter C18 preparative HPLC column (5  $\mu\text{m}$ , 300 A, 250 x 21.2 mm) on a Shimadzu CBM-10AW VP communications bus module, Shimadzu SPD-10A VP UV-Vis detector, and Shimadzu LC-6AD liquid chromatography assembly, employing methanol/water as the gradient solvent system, a flow rate of 10 mL/min under room temperature and with the UV detector set at 275 and 230 nm. The gradient was run from 20% to 95% methanol in water over a 30 minute period. The fractions containing **2-11** were combined and lyophilized to give **2-11** (3 mg, 3.1  $\mu\text{mol}$ , 50 %) as white solid. The purified **2-11** was analyzed by LC/UV/MS-TOF with a

Kinetex F5 column (2.1 mm x 150 mm, 2.6  $\mu\text{m}$ , 100 angstroms) employing methanol/water with 10mM AmAc as the gradient solvent system, a flow rate of 0.375 mL/min under 30  $^{\circ}\text{C}$ , and with the UV detector set at 275 and 230 nm. The gradient was run from 60% to 95% methanol in water over a 45 minute period.  $^1\text{H}$  NMR (500 MHz,  $\text{CDCl}_3$ )  $\delta$  1.01 (m, 1 H), 1.16 (m, 1 H), 1.19 (s, 2 H), 1.40 (s, 6 H), 1.61 (s, 9 H), 1.71 (s, 2 H), 1.80 (m, 1 H), 1.88 (m, 1 H), 1.94 (s, 2 H), 2.16 (s, 2 H), 2.43 (s, 3 H), 2.55 (m, 1 H), 3.50 (s, 1 H), 3.85 (d,  $J = 7$  Hz, 1 H), 4.20 (d,  $J = 8.45$  Hz, 1 H), 4.33 (m, 2 H), 4.44 (m, 1 H), 4.86 (t, 1 H), 4.99 (d,  $J = 11.1$  Hz, 2 H), 5.54 (d,  $J = 8.75$  Hz, 1 H), 5.69 (d,  $J = 6.9$  Hz, 1 H), 6.21 (t,  $J = 8.55$  Hz, 1 H), 6.34 (s, 1 H), 7.15 (t,  $J = 4.65$  Hz, 1 H), 7.49 (d,  $J = 7.6$  Hz, 1 H), 7.62 (m, 1 H), 7.88 (d,  $J = 2.8$  Hz, 1 H), 8.13 (d,  $J = 7.6$  Hz, 1 H).  $^{13}\text{C}$  NMR (125 MHz,  $\text{CDCl}_3$ )  $\delta$  9.2, 9.4, 9.5, 13.0, 15.1, 16.3, 21.8, 22.4, 26.7, 28.2, 35.5, 43.2, 45.7, 50.8, 58.6, 72.2, 72.4, 73.2, 75.0, 75.4, 7.1, 80.3, 81.1, 84.4, 114.8, 128.0, 128.6, 129.2, 130.1, 132.7, 133.1, 133.4, 133.7, 134.5, 142.4, 150.2, 155.2, 160.4, 167.0, 170.2, 172.5, 175.1, 203.9. HRMS  $[\text{M}-\text{H}]^-$   $\text{C}_{49}\text{H}_{58}\text{NO}_{17}\text{S}^-$  calcd. 964.3431, found 964.3427. ( $\Delta = -0.4$  ppm). Tc-taxoid (**2-11**):  $t_{\text{R}} = 21.6$  min.

### 10-Cyclopropanecarbonyl-3'-Diphenyl-3'-(2-methyl-2-(thiophene-2-phenyl)docetaxel (Ph-taxoid **2-12**)

To a solution of 10 mol% tetrakis(triphenylphosphine)palladium(0) (0.82 mg, 0.71  $\mu\text{mol}$ ) in DMF (1 mL) was added a solution of 1.2 eq phenyl iodide (8.5  $\mu\text{g}$ , 1.73  $\mu\text{mol}$ ) in DMF (1 mL), and the solution was added to 10-cyclopropanecarbonyl-3'-diphenyl-3'-(2-methyl-2-tributylstannyl)docetaxel (**2-9**) (8.0mg, 7.1  $\mu\text{mol}$ ) in DMF (400  $\mu\text{L}$ ). The reaction mixture was heated to 60  $^{\circ}\text{C}$  and allowed to react for 6 hours with stirring. The reaction was quenched with methanol (400  $\mu\text{L}$ ). The reaction mixture was lyophilized to remove DMF, and the crude product was purified by column chromatography on silica gel with increasing amounts of eluent (hexanes:ethyl acetate) to give crude **2-12**. Further purification was carried out by preparative HPLC using a Jupiter C18 preparative HPLC column (5  $\mu\text{m}$ , 300 A, 250  $\times$  21.2 mm) on a Shimadzu CBM-10AW VP communications bus module, Shimadzu SPD-10A VP UV-Vis detector, and Shimadzu LC-6AD liquid chromatography assembly, employing methanol/water as the gradient solvent system, a flow rate of 10 mL/min under room temperature and with the UV detector set at 275 and 230 nm. The gradient was run from 20% to 95% methanol in water over a 30 minute period. The fractions containing **2-12** were combined and lyophilized to give **2-12** (3 mg, 3.1  $\mu\text{mol}$ , 44 %) as white solid. The purified **2-12** was analyzed by LC/UV/MS-TOF with a Kinetex F5 column (2.1 mm x 150 mm, 2.6  $\mu\text{m}$ , 100 angstroms) employing methanol/water with 10mM AmAc as the gradient solvent system, a flow rate of 0.375 mL/min under 30  $^{\circ}\text{C}$ , and with the UV detector set at 275 and 230 nm. The gradient was run from 60% to 95% methanol in water over a 45 minute period.  $^1\text{H}$  NMR (500 MHz,  $\text{CDCl}_3$ )  $\delta$  1.19 (s, 2 H), 1.26 (m, 3 H), 1.40 (s, 9 H), 1.70 (s, 2 H), 1.93 (s, 2 H), 2.20 (s, 3 H), 2.41 (s, 3 H), 3.46 (s, 3 H), 3.84 (d,  $J = 6.95$  Hz, 2 H), 4.21 (d,  $J = 8.4$  Hz, 2 H), 4.33 (m, 2 H), 4.44 (m, 2H), 4.91 (d,  $J = 8.9$  Hz, 2 H), 4.99 (m, 2 H), 5.70 (d,  $J = 7.05$  Hz, 2 H), 5.95 (d,  $J = 8.1$  Hz, 2 H), 6.21 (t,  $J = 8.85$  Hz, 2 H), 6.33 (s, 1 H), 7.31 (t,  $J = 7.25$  Hz, 2 H), 7.35 (t,  $J = 7.75$  Hz, 2 H), 7.43 (d,  $J = 7.25$  Hz, 2 H), 7.50 (t,  $J = 7.7$  Hz, 2 H), 7.63 (t,  $J = 7.2$  Hz, 1 H), 8.14 (d,  $J = 7.5$  Hz, 2 H).  $^{13}\text{C}$  NMR (125 MHz,  $\text{CDCl}_3$ )  $\delta$  9.22, 9.53, 13.0, 15.0, 16.7, 21.9, 22.4, 26.7, 28.2, 29.7, 35.6, 43.2, 45.6, 51.8, 58.6, 72.2, 72.6, 73.6, 75.0, 75.4, 79.1, 80.2, 81.1, 84.4, 123.1, 125.9, 127.8, 128.4, 128.6, 129.2, 130.1, 133.7, 142.2, 166.9, 170.1, 175.1, 203.9. HRMS  $[\text{M}-\text{H}]^-$   $\text{C}_{50}\text{H}_{60}\text{NO}_{15}^-$  calcd. 914.3968, found 964.3970. ( $\Delta = 0.2$  ppm). (*E/Z*)Ph-taxoid (**2-12**):  $t_{\text{R}} = 23.3$  min and 23.6 min.

### 10-Cyclopropanecarbonyl-3'-dephenyl-3'-(2-methyl-2-(prop-1-yn-1-yl))-7-triethylsilyl-2'-triisopropylsilyldocetaxel (2-18)

An aliquot of **1-8** (41 mg, 0.056 mmol), and 1.2 eq  $\beta$ -lactam (+) **2-17** (27 mg, 0.067 mmol) were dissolved in 0.02 M THF (6 mL) and cooled to  $-40\text{ }^{\circ}\text{C}$  under inert conditions for at least 30 minutes. To the mixture was added 1.5 eq LiHMDS in 1.06 M THF (0.07 mL, 0.08 mmol) dropwise. The mixture was stirred and allowed to slightly warm up to  $-20\text{ }^{\circ}\text{C}$  for 4 hours. Upon completion the reaction was quenched with saturated  $\text{NH}_4\text{Cl}$  (20 mL) and extracted with ethyl acetate (20 mL x 3). The organic layer was collected, washed with brine (20 mL x 3), dried over anhydrous  $\text{MgSO}_4$ , and concentrated *in vacuo*. Purification was done *via* column chromatography on silica gel with increasing amounts of eluent (hexanes:ethyl acetate) to give **2-18** (56 mg, 0.051 mmol, 90 %) as a white solid.  $^1\text{H}$  NMR (500 MHz,  $\text{CDCl}_3$ )  $\delta$  0.57 (m, 6 H), 0.92 (m, 12 H), 1.15 (m, 21 H), 1.21 (m, 4 H), 1.25 (m, 4 H), 1.35 (s, 6 H), 1.46 (s, 2 H), 1.71 (s, 3 H), 1.83 (m, 2 H), 2.00 (s, 3 H), 2.20 (m, 1 H), 2.34 (m, 1 H), 2.45 (s, 2 H), 3.85 (d,  $J = 7\text{ Hz}$ , 1 H), 4.19 (d,  $J = 8.25\text{ Hz}$ , 1 H), 4.31 (d,  $J = 8.35\text{ Hz}$ , 1 H), 4.46 (t,  $J = 6.65\text{ Hz}$ , 1 H), 4.61 (d,  $J = 2.45\text{ Hz}$ , 1 H), 5.04 (d,  $J = 9.3\text{ Hz}$ , 1 H), 5.70 (d,  $J = 7\text{ Hz}$ , 1 H), 6.17 (t,  $J = 8.75\text{ Hz}$ , 1 H), 6.49 (s, 1 H), 7.50 (t,  $J = 7.55\text{ Hz}$ , 2 H), 7.61 (t,  $J = 7.45\text{ Hz}$ , 1 H), 8.13 (d,  $J = 7.2\text{ Hz}$ , 2 H). HRMS  $[\text{M}+\text{H}]^+$   $\text{C}_{59}\text{H}_{90}\text{NO}_{15}\text{Si}_2^+$  calcd. 1108.5844, found 1108.5839. ( $\Delta = -0.4\text{ ppm}$ ); fragmentation of side chain cleaved on C13 position  $[\text{M}'+\text{H}]^+$   $\text{C}_{39}\text{H}_{53}\text{O}_{10}\text{Si}^+$  calcd. 709.3403, found 709.3401. ( $\Delta = -0.3\text{ ppm}$ )

### 10-Cyclopropanecarbonyl-3'-dephenyl-3'-(2-methyl-2-(thiophene-2--(prop-1-yn-1-yl))docetaxel (alkyne-taxoid 2-15)

An aliquot of **2-18** (56 g, 0.051 mmol) was dissolved in a 1:1 mixture of 0.02 M acetonitrile:pyridine (3 mL) and cooled to  $0\text{ }^{\circ}\text{C}$  under inert conditions. To the mixture was added 0.56 mL HF/pyridine dropwise (0.01 mL per every 1 mg was added). The reaction was stirred at room temperature for 24 h. Upon completion the reaction was quenched with 0.2 M citric acid in  $\text{H}_2\text{O}$  (3.8 %) (10 mL) and extracted with ethyl acetate (10 mL x 3). The organic layer was collected, washed with  $\text{CuSO}_4$ , washed with diluted water until the organic layer became clear, then washed with brine (10 mL x 3), dried over anhydrous  $\text{MgSO}_4$ , and concentrated *in vacuo*. Purification was done *via* column chromatography on silica gel with increasing amounts of eluent (hexanes:ethyl acetate) to give **2-15** (34 mg, 0.041 mmol, 80 %), followed by recrystallization using ethyl acetate to afford pure **2-15** as white solid, HPLC purity > 99 %.  $^1\text{H}$  NMR (500 MHz, MeOD)  $\delta$  1.00 (m, 2 H), 1.06 (m, 1 H), 1.13 (m, 1 H), 1.21 (m, 6 H), 1.44 (s, 9 H), 1.70 (s, 3 H), 1.78 (m, 2 H), 1.84 (m, 1 H), 1.86 (d,  $J = 2.35\text{ Hz}$ , 2 H), 2.00 (d,  $J = 1\text{ Hz}$ , 3 H), 2.28 (m, 1 H), 2.43 (m, 1 H), 2.47 (s, 3 H), 2.51 (m, 1 H), 3.90 (d,  $J = 7.05\text{ Hz}$ , 1 H), 4.21 (q,  $J = 8.45\text{ Hz}$ , 2 H), 4.35 (m, 2 H), 4.76 (s, 1 H), 5.03 (d,  $J = 9.6\text{ Hz}$ , 1 H), 5.70 (d,  $J = 7.1\text{ Hz}$ , 1 H), 6.21 (t,  $J = 8.8\text{ Hz}$ , 1 H), 6.51 (s, 1 H), 7.53 (t,  $J = 7.55\text{ Hz}$ , 2 H), 7.65 (t,  $J = 7.45\text{ Hz}$ , 1 H), 8.14 (d,  $J = 7.2\text{ Hz}$ , 2 H).  $^{13}\text{C}$  NMR (125 MHz, MeOD)  $\delta$  1.9, 7.7, 7.8, 9.0, 12.3, 13.5, 20.8, 21.6, 25.5, 27.3, 35.4, 36.1, 43.2, 46.7, 57.9, 70.8, 70.9, 73.5, 74.8, 75.0, 75.3, 76.1, 77.6, 79.4, 80.1, 80.9, 84.5, 128.3, 129.7, 129.9, 133.2, 133.5, 140.8, 156.0, 166.2, 170.6, 171.8, 173.7, 203.7. HRMS  $[\text{M}-\text{H}]^-$   $\text{C}_{50}\text{H}_{60}\text{NO}_{15}^-$  calcd. 836.3499, found 836.3494. ( $\Delta = -0.6\text{ ppm}$ ).

## §2.6 References

- (1) Li, X.; Barasoain, I.; Matesanz, R.; Fernando Díaz, J.; Fang, W.-S. Synthesis and biological activities of high affinity taxane-based fluorescent probes. *Bioorg. Med. Chem. Lett.* **2009**, *19*, 751-754.
- (2) Li, X.; Barasoain, I.; Matesanz, R.; Fernando Díaz, J.; Fang, W.-S. Synthesis and biological activities of high affinity taxane-based fluorescent probes. *Bioorg. Med. Chem. Lett.* **2009**, *19*, 751-754.
- (3) Vineberg, J. G.; Wang, T.; Zuniga, E. S.; Ojima, I. Design, Synthesis, and Biological Evaluation of Theranostic Vitamin–Linker–Taxoid Conjugates. *J. Med. Chem.* **2015**, *58*, 2406-2416.
- (4) Kiesewetter, D. O.; Jagoda, E. M.; Kao, C.-H. K.; Ma, Y.; Ravasi, L.; Shimoji, K.; Szajek, L. P.; Eckelman, W. C. Fluoro-, bromo-, and iodopaclitaxel derivatives: synthesis and biological evaluation. *Nucl. Med. Biol.* **2003**, *30*, 11-24.
- (5) Adamczyk, M.; Grote, J. Efficient fluorescein spirolactam and bis-spirolactam synthesis. *Synth. Commun.* **2001**, *31*, 2681-2690.
- (6) Mason, W. T., Ed. Fluorescent and Luminescent Probes for Biological Activity. *Wiley Interscience: New York*, **1983**, Chapter 2.
- (7) Adamczyk, M.; Grote, J. Synthesis of novel spirolactams by reaction of fluorescein methyl ester with amines. *Tetrahedron Lett.* **2000**, *41*, 807-809.
- (8) Brown, L.; Halling, P. J.; Johnston, G. A.; Suckling, C. J.; Valivety, R. H. The synthesis of some water insoluble dyes for the measurement of pH in water immiscible solvents. *J. Chem. Soc., Perkin Trans. 1* **1990**, 3349-3353.
- (9) Brown, L.; Halling, P. J.; Johnston, G. A.; Suckling, C. J.; Valivety, R. H. Water insoluble indicators for the measurement of pH in water immiscible solvents. *Tetrahedron Lett.* **1990**, *31*, 5799-5802.
- (10) Miller, P. W.; Long, N. J.; Vilar, R.; Gee, A. D. Synthesis of <sup>11</sup>C, <sup>18</sup>F, <sup>15</sup>O, and <sup>13</sup>N Radiolabels for Positron Emission Tomography. *Angew. Chem. Int. Ed.* **2008**, *47*, 8998-9033.
- (11) Ametamey, S. M.; Honer, M.; Schubiger, P. A. Molecular Imaging with PET. *Chem. Rev.* **2008**, *108*, 1501-1516.
- (12) Ravert, H. T.; Klecker, R. W.; Collins, J. M.; Mathews, W. B.; Pomper, M. G.; Wahl, R. L.; Dannals, R. F. Radiosynthesis of [<sup>11</sup>C]paclitaxel. *J. Labelled Comp Radiopharm.* **2002**, *45*, 471-477.
- (13) van Tilburg, E. W.; Franssen, E. J. F.; van der Hoeven, J. J. M.; van der Meij, M.; Elshove, D.; Lammertsma, A. A.; Windhorst, A. D. Radiosynthesis of [<sup>11</sup>C]docetaxel. *J. Labelled Comp Radiopharm.* **2004**, *47*, 763-777.
- (14) Mäding, P.; Zessin, J.; Pleiß, U.; Füchtner, F.; Wüst, F. Synthesis of a <sup>11</sup>C-labelled taxane derivative by [1-<sup>11</sup>C]acetylation. *J. Labelled Compd. Radiopharmaceut.* **2006**, *49*, 357-365.
- (15) Seitz, J. D. The design, synthesis and biological evaluation of novel taxoid anticancer agents and their tumor-targeted drug conjugates. Doctoral Dissertation. Stony Brook University. **2013**.
- (16) Joshua D. Seitz, T. W., Jacob G. Vineberg and Iwao Ojima Synthesis of a next-generation taxoid by rapid methylation amenable for [<sup>11</sup>C]-labeling. *To be submitted shortly*
- (17) Seitz, J. D.; Vineberg, J. G.; Wei, L.; Khan, J. F.; Lichtenthal, B.; Lin, C.-F.; Ojima, I. Design, synthesis and application of fluorine-labeled taxoids as <sup>19</sup>F NMR probes for the metabolic stability assessment of tumor-targeted drug delivery systems. *J. Fluorine Chem.* **2015**, *171*, 148-161.
- (18) Borcard, F.; Godinat, A.; Staedler, D.; Comas Blanco, H.; Dumont, A.-L.; Chapuis-Bernasconi, C.; Scaletta, C.; Applegate, L. A.; Krauss Juillerat, F.; Gonzenbach, U. T.; Gerber-

Lemaire, S.; Juillerat-Jeanneret, L. Covalent Cell Surface Functionalization of Human Fetal Osteoblasts for Tissue Engineering. *Bioconj. Chem.* **2011**, *22*, 1422-1432.

(19) Vineberg, J. G.; Wang, T.; Zuniga, E. S.; Ojima, I. Design, Synthesis, and Biological Evaluation of Theranostic Vitamin–Linker–Taxoid Conjugates. *J. Med. Chem.* **2015**, *58*, 2406-2416.

## Chapter 3

### Taxoid-based Vitamin-Linker-Drug Conjugates for Tumor-targeted Drug Delivery

§3.1 Tumor-Targeted Chemotherapy .....	70
§3.1.1 Biotin as Tumor-Targeting Module .....	70
§3.1.2 Mechanism-Based Self-Immolative Disulfide Linker .....	71
§3.1.3 Development on Biotin-Linker-Taxoid Construct Model .....	74
§3.2 Synthesis and Biological evaluation of Biotin-Linker-Taxoid Conjugates .....	76
§3.2.1 Synthesis of Self-immolative Disulfide Linker .....	76
§3.2.2 Synthesis of Coupling-Ready Activated Drug-Linker Constructs .....	78
§3.2.3 Synthesis of Biotin-Linker-Taxoid Conjugate BLT .....	80
§3.2.4 Synthesis of Biotin-PEG-Linker-Taxoid Conjugate BLT-S .....	81
§3.2.5 Biological Evaluation of Biotin-Linker-Taxoid Conjugates <i>in Vitro</i> Studies .....	82
§3.2.6 Biological Evaluation of BLT <i>in Vivo</i> Study .....	84
§3.3 Synthesis and Biological Evaluation of Biotin-Fluorescein Probes .....	84
§3.3.1 Synthesis of Biotin-Fluorescent Probes (Biotin-PEG-FITC and Biotin-PEG-Fluorescein).....	87
§3.3.2 Biological Evaluation of Biotin-Fluorescein Probes <i>in Vitro</i> Studies .....	88
§3.4 Synthesis towards [18F]-Labeled Biotin-PEG-F Radiotracer for PET Imaging Study.....	89
§3.4.1 Cold Synthesis toward Biotin-PEG-F .....	89
§3.5 Summary.....	90
§3.6 Experimental Section.....	91
§3.6.1 Caution.....	91
§3.6.2 General Information.....	91
§3.6.3 Materials.....	93
§3.6.4 Experimental Procedure.....	94
§3.7 References.....	104

### §3.1 Tumor-Targeted Chemotherapy

To specifically deliver anticancer drug to cancer cells, tumor-targeted drug conjugates are designed for built-up of a tumor recognition moiety and a cytotoxic agent connected directly or through a suitable linker. Receptors for certain biomarkers have been found overexpressed on the cell surfaces of cancer cells to maintain sufficient uptake. The increased expression level of these cell surface receptors has emerged as a tumor-specific biomarker for tumor-targeted drug delivery. In addition, the linker should be bifunctional so that the cytotoxic agent and the tumor-targeting moiety can be connected to the each end of the linker. The tumor-targeted drug conjugate should be systemically nontoxic which means the linker must be stable during the blood circulation but readily cleaved to release the cytotoxic agent efficiently upon internalization into the tumor cells.

#### §3.1.1 Biotin as Tumor-Targeting Module

Vitamins family include many essential nutrients, such as riboflavin, folic acid, and biotin, which act as cofactors for numerous cell division processes relating to beta-oxidation of fatty acids and proteins and nucleic acids synthesis.<sup>1</sup> All living cells depend on vitamins for survival, however, rapidly dividing cancer cells highly require the certain vitamins for proliferation more than healthy cells, resulting in the overexpression of the vitamin receptors on the surface of cancer cells.<sup>2-3</sup> In 2004, Russell-Jones and co-workers used rhodamine-labeled polymers to examine the vitamin-targeting accumulation of various tumors and found that many types of cancer cells overexpressed receptors for folate, cobalamin and biotin to facilitate the enhanced uptake.<sup>4</sup>

**Table 3.1 Discrepancy of vitamin receptor overexpressed on the surface of various tumor cell lines (adapted from reference 4)<sup>4</sup>**

Tumor	Mouse	Type	Folate	Cbl	Biotin
O157	Balb/C	Bcell lymph	+/-	+/-	+/-
BW5147	AKR/J	Lymphoma	+/-	+/-	+/-
B16	C57/B1	Melanoma	-	-	-
LL-2	C57/B1	Lung	-	-	-
HCT-116	Balb/C-Nu	Colon	-	-	-
L1210	DBA/2	Leukemia	+/-	+/-	-
L1210FR	DBA/2	Leukemia	++	+	+++
Ov 2008	Balb/C-Nu	Ovarian	+++	-	++
ID8	C57/B1	Ovarian	+++	-	++
Ovcar-3		Ovarian	+++	-	+++
Colo-26	Balb/C	Colon	+/-	++	+++
P815	DBA/2	Mastocytoma	+/-	++	+++
M109	Balb/C	Lung	+	+++	+++



RENCA	Balb/C	Renal cell	+	+++	+++
RD995	C3H/HeJ	Renal cell	+	++	+++
4T1	Balb/C	Breast	+	++	+++
JC	Balb/C	Breast	+	++	+++
MMT060562	Balb/C	Breast	+	++	+++

Biotin (**Figure 3.1**), as well known as vitamin H or B<sub>7</sub>, is an essential enzyme for the division of cell growth. Considerable evidence has shown that rapidly dividing cells associated with cancers overexpress biotin receptors more than most normal cells.<sup>4</sup> Furthermore, on the surface of certain cancer cells, such as L1210FR, Colo-26, P815, RD995, 4TI, JC, and MMT060562, biotin receptors were more overexpressed than folate and cobalamin receptors. (**Table 3.1**) In our recent work, we used a biotin-PEG-FITC probe for confocal microscopy and flow cytometry experiments to assess the biotin receptor overexpression on several selected cell lines, including MX-1 (breast), MCF-7 (breast), ID8 (ovary), L1210 (murine leukemia), L1210FR (murine leukemia) and WI38 (lung fibroblast, normal) cell lines, and demonstrated the highly expression of biotin receptor (BR) level in MCF-7 (BR<sup>+++</sup>) and ID8 (BR<sup>+++</sup>), a little lower expression level in L1210FR (BR<sup>++</sup>) and MX-1(BR<sup>++</sup>), and negligible expression level in WI38 and L1210 (BR-).<sup>5</sup> Furthermore, several cancer cell lines were also examined and identified their BR overexpression level, including BT-20 (BR<sup>++</sup>), LCC6-WT (BR<sup>++</sup>), LCC6-MDR (BR<sup>+</sup>), MDA-MB 231 (BR<sup>++</sup>), and SkBr3 (BR<sup>++</sup>).<sup>5</sup> Accordingly, biotin receptor may serve as useful targets for tumor-targeted drug delivery, therefore we employed biotin as the primary tumor-targeting moiety to construct our drug conjugate with cytotoxic agents.

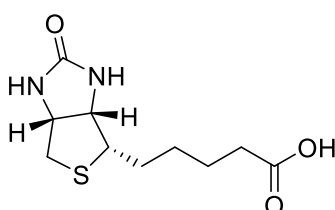


**Figure 3.1** Chemical Structure of D-(+)-biotin

### §3.1.2 Mechanism-Based Self-Immolative Disulfide Linker

A tumor-targeted drug conjugate relies on the tumor-targeting module to guide the drug by specifically targeting cancer cells and assist the drug conjugate internalization via receptor-mediated endocytosis. Direct linkage by a covalent bond may result in reduction of the activity and toxicity. The cytotoxic agent may not be efficiently cleaved or not released in its original form. Therefore, a suitable linker is designed to connect the tumor-targeting moiety with drug, and control the release of the drug at the tumor site. The linker should be stable during blood circulation to keep the pro-drug inactive, and readily be cleaved to release the drug in its active form and restore its biological activity.<sup>6</sup>

As one class of linker, disulfide linkers take advantage of three important factors<sup>7</sup>: (1) their stability at physiological pH; (2) the concentration of glutathione (GSH) which can cause

scission of the disulfide bond and release of drug was reported to be in 2-8 nM range in cancer cells; and (3) the low levels of glutathione in blood plasma (1-2  $\mu\text{M}$  range).<sup>8-9</sup> Thus the cytotoxicity of the drug will be masked when attached to the linker until the drug conjugate becomes internalized in the tumor cells where glutathione exists at higher concentrations (up to 1000-fold higher). Glutathione-triggered disulfide bond exchange takes place to give a ring-closed thiolactone, and irreversibly release the drug. The mechanism of cleavage of linker is shown.<sup>6</sup> (**Figure 3.2**)

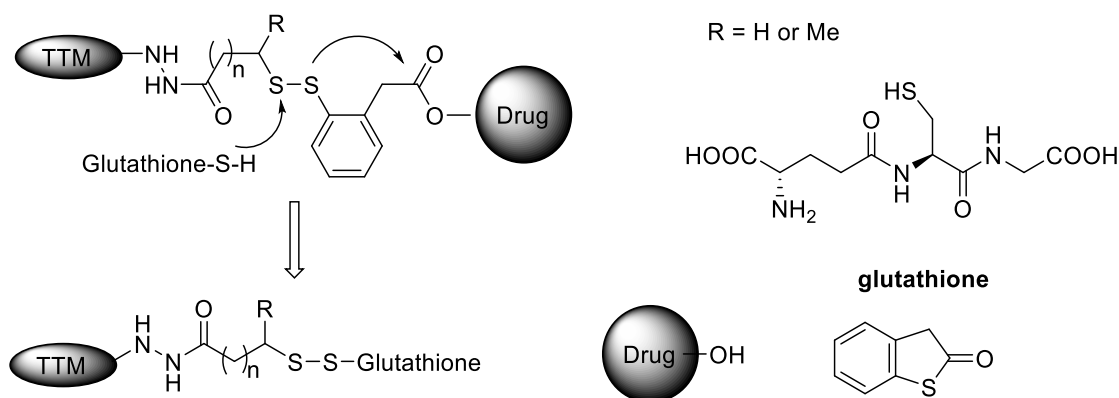


**Figure 3.2** Disulfide cleavage during glutathione-triggered cascade drug release

This drug-release mechanism was validated by a time dependent  $^{19}\text{F}$  NMR experiment of a model disulfide linked compound which bears two distinct fluorine moieties. The experiment showed the formation of thiolactone after the addition of cysteine.<sup>10-11</sup> (**Figure 3.3**)

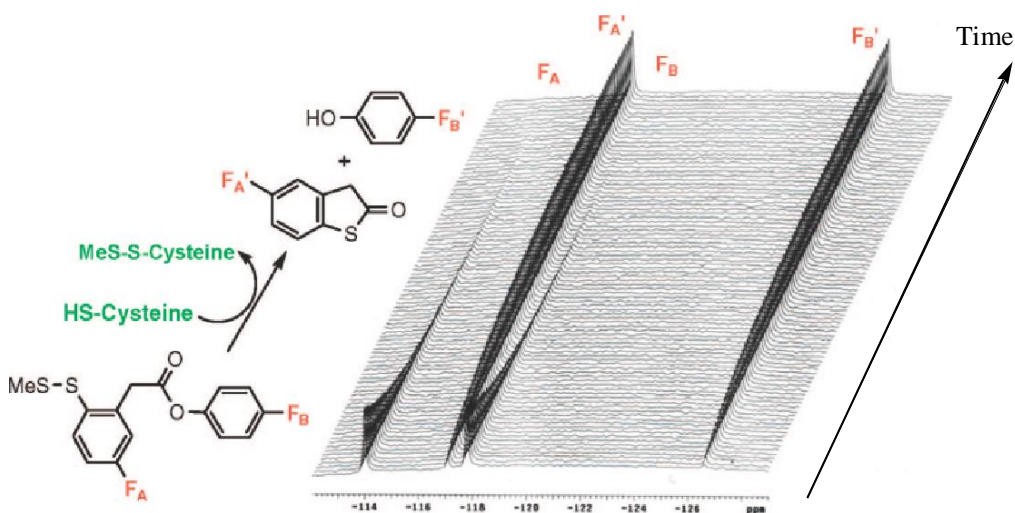


**Figure 3.3** A time-resolved  $^{19}\text{F}$  NMR study for linker cleavage (reprinted from reference 10 and 11)

In a recent published paper,<sup>12</sup> a through  $^{19}\text{F}$  NMR study using BLT (biotin-linker-taxoid) conjugates was reported to elucidate the linker cleavage and drug release. Previously, a BLT- $\text{F}_2$  compound (compound **1** in **Figure 3.4**) as  $^{19}\text{F}$  NMR probe was used for the metabolic stability measurement to tumor-targeted drug delivery system. One fluorine was on the meta-position of C2 benzoate moiety of the fluorotaxoid SB-T-12145, and another fluorine was introduced to the

4-position of the self-immolative disulfide linker ring. The time-resolved  $^{19}\text{F}$  NMR spectra showed a stepwise mechanism of drug release triggered by the glutathione (GSH), generating the **3A** which was detectable, as well as the desired ring-closed thiolactone **9** and the resulting free drug **3**.

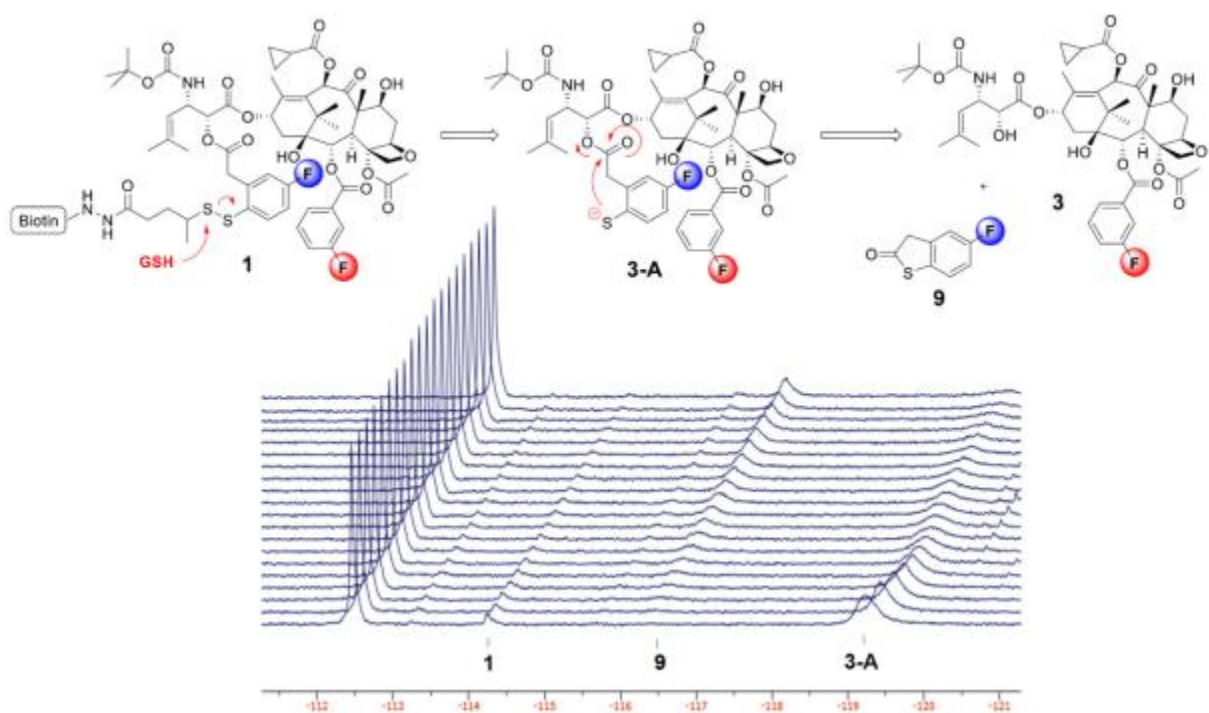


**Figure 3.4** A time-resolved  $^{19}\text{F}$  NMR study using BLT-F<sub>2</sub> (reprinted from reference 12)<sup>12</sup>

But due to the poor solubility in cell culture medium or blood plasma of BLT-F<sub>2</sub>, another probe, BLT-S-F<sub>6</sub>, with a polyethylene glycol spacer for enhancement of solubility, was designed for  $^{19}\text{F}$  NMR study. (**Figure 3.5**) In this case, instead of introducing fluorine in the linker, a meta- $-\text{OCF}_3$  group on the C2 position of fluorotaxoid SB-T-12822-5 (compound **4** in **Figure 3.5**) was used as internal reference for  $^{19}\text{F}$  NMR study, where another  $-\text{CF}_3$  moiety on C3' position on the side chain can shift to generate distinguishable fluorine signals. The linker system was shown to be quite stable in blood plasma with less than 10% cleavage and drug release after two days.

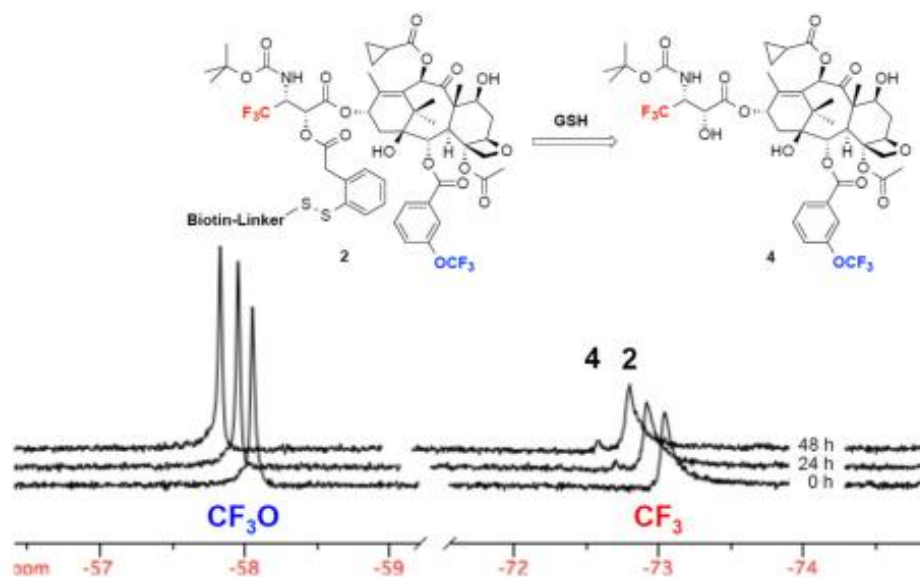


**Figure 3.5** A time-resolved  $^{19}\text{F}$  NMR study for the drug release of BLT-S-F<sub>6</sub> (reprinted from reference 12)<sup>12</sup>

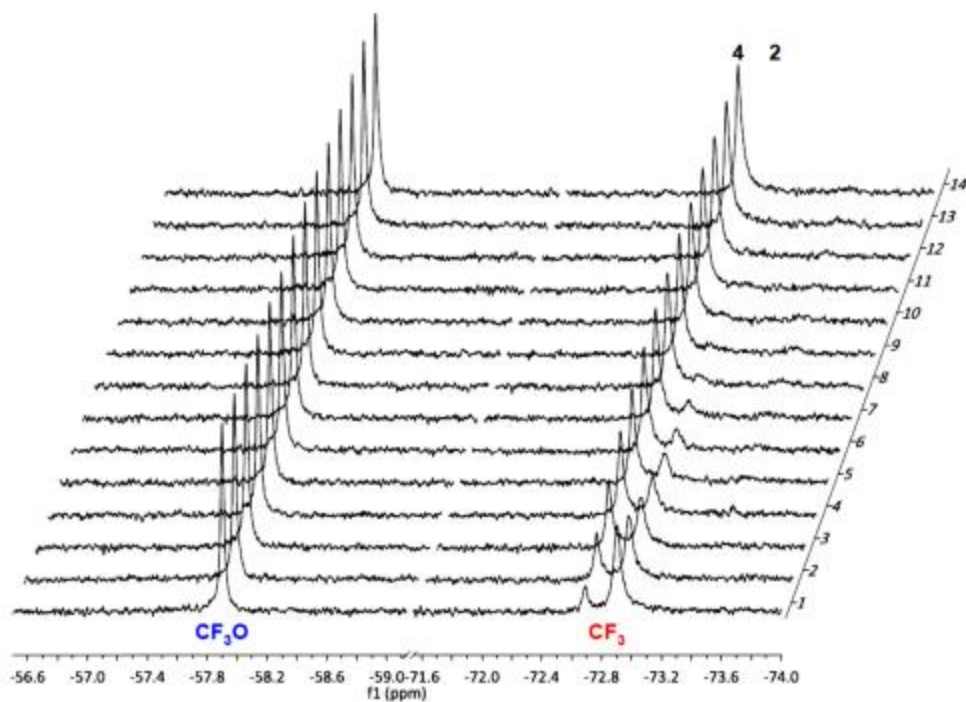


**Figure 3.6** A time-resolved  $^{19}\text{F}$  NMR study using BLT-S-F<sub>6</sub> (reprinted from reference 12)<sup>12</sup>

### §3.1.3 Development on Biotin-Linker-Taxoid Construct Model

In our lab, we have been developed several biotin-linker-taxoid conjugates in order to improve the stability in aqueous media, efficiency of linker cleavage for drug release, and solubility of the drug conjugate towards formulation. The first generation of biotin-linker-taxoid conjugate which consists of biotin as tumor-targeting module connected to a second generation

taxoid SB-T-1214 as cytotoxic agent through a 3-carbon self-immolative disulfide linker and a hydrazide spacer<sup>13</sup>, is shown in **Figure 3.7**. This drug conjugate have been evaluated its target-specificity against three cell lines L1210FR (murine leukemia cell line, BR+), L1210 (parent murine leukemia cell line, BR-) and WI-38 (normal human lung fibroblast cell line, BR-), and exhibited high potency ( $IC_{50}$  8.8 nM) against the biotin receptor overexpressing cell lines (L1210FR), but the values against the cell lines which do not overexpress biotin receptor, such as L1210 and WI38 cell lines, were 59 times (522 nM) and 65 times (570 nM) larger (less potent), respectively.<sup>13</sup> In comparison, SB-T-1214 was also evaluated against these cell lines as control, but did not show selectivity with similar  $IC_{50}$  values.<sup>13</sup>

However, the first generation BLT conjugate bearing a 3-carbon disulfide linker was found instable in aqueous media and slowly decompose to an  $\alpha,\beta$ -unsaturated ketone and the free disulfide via retro-Michael reaction. This is due to the elimination reaction of the 3-carbon disulfide linker under the basic condition. (**Figure 3.7**)

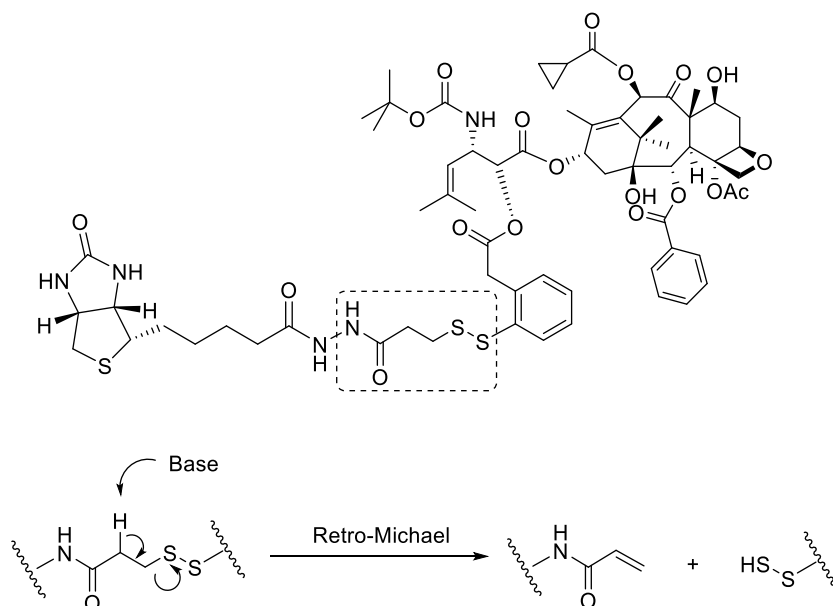


**Figure 3.7** Chemical structure of first generation biotin-linker-taxoid conjugate and proposed decomposition via retro-Michael reaction

To solve the problem, the second-generation biotin-linker-taxoid design exploited a 4-carbon disulfide linker can prevent the decomposition. On the  $\alpha$  position carbon adjacent to the disulfide bond, one or two methyl substituted groups may contribute to the kinetics of the glutathione-induced disulfide exchange by increasing the steric bulk, resulting in the enhanced stability and rate change for the ring close and drug release. These three second-generation biotin-linker-taxoid drug conjugates bearing different number of substituted methyl groups (**Figure 3.8**) have been synthesized for further biological evaluations.<sup>14-16</sup>

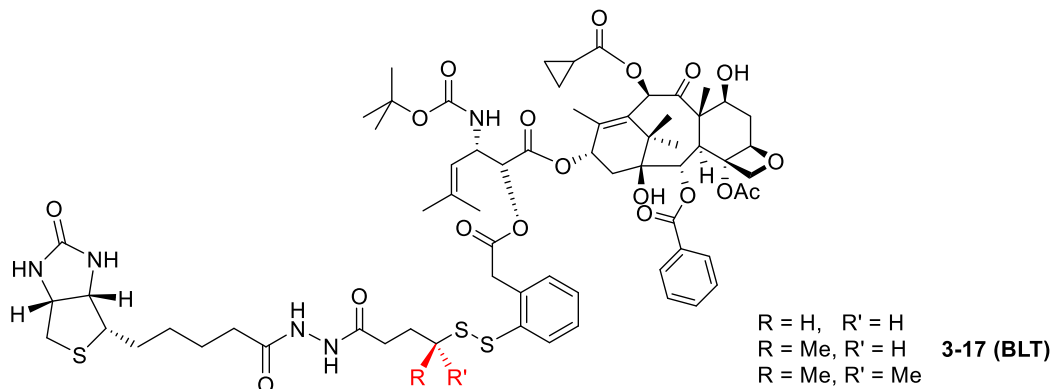


**Figure 3.8** Chemical structure of second generation biotin-linker-taxoid conjugates with variable substituted methyl groups

To increase the solubility and better formulate the biotin-linker-taxoid drug conjugate, a polyethylene glycol (PEG) short oligomer was inserted between the biotin and linker. These PEG short oligomer should be able to wrap the most hydrophobic portions of the molecule to largely improve the solubility and prevent the aggregation that leads to precipitation from the solution. One of the second-generation biotin-linker-taxoid drug conjugate bearing a methyl-branched disulfide linker (BLT) was selected, and its derivatives biotin-PEG-linker-taxoid with a PEG oligomer (BLT-S) was also made. (**Figure 3.9**) Synthesis of these two biotin-linker-taxoid drug conjugates will be described in sections 3.2.3 and 3.2.4, respectively.

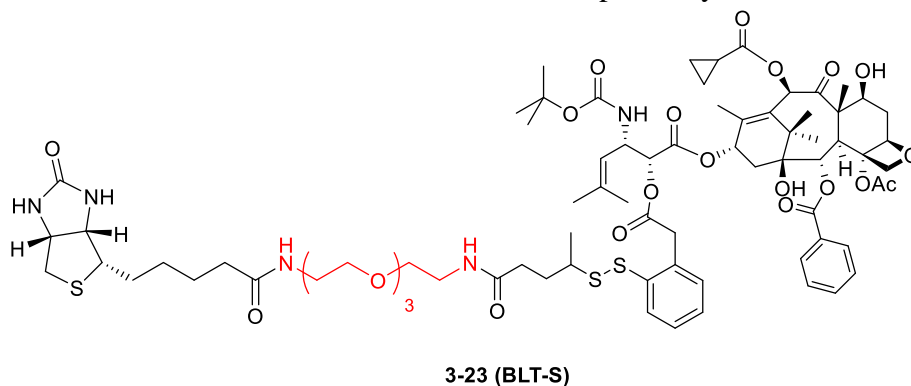
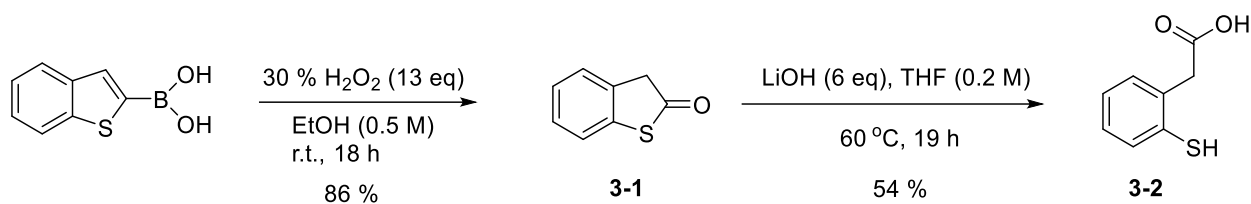


**Figure 3.9** Chemical structure of biotin-PEG-linker-taxoid (BLT-S)

## §3.2 Synthesis and Biological evaluation of Biotin-Linker-Taxoid Conjugates

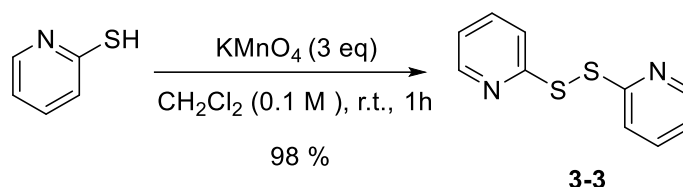
### §3.2.1 Synthesis of Self-Immolative Disulfide Linker

The self-immolative disulfide linker was synthesized by two fragments. The upper aromatic moiety began with oxidation of benzo-thiophen-2-ylboronic acid to form the corresponding thiolactone (**3-1**) (**Scheme 3.1**). Then the thiolactone was subsequently hydrolyzed with LiOH to form the carboxylic acid/thiol product (**3-2**).



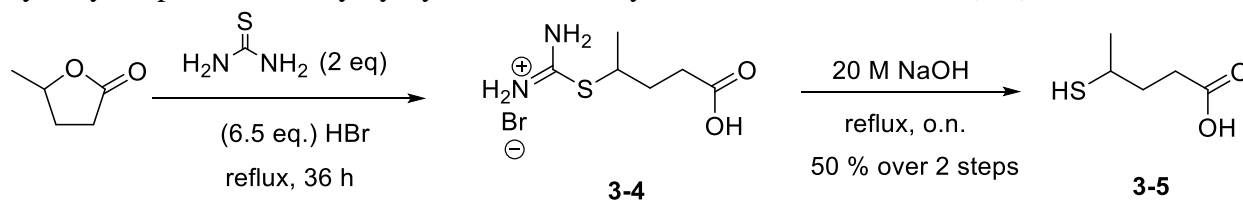
**Scheme 3.1** Synthesis of (2-mercapto-phenyl) acetic acid **3-2**

Before synthesis of the lower linear chain, 1,2-di(pyridine-2-yl)disulfane (**2-3**) (**Scheme 3.2**) was obtained by treatment of pyridine-2(1H)-thione with a large excess of potassium permanganate in DCM.



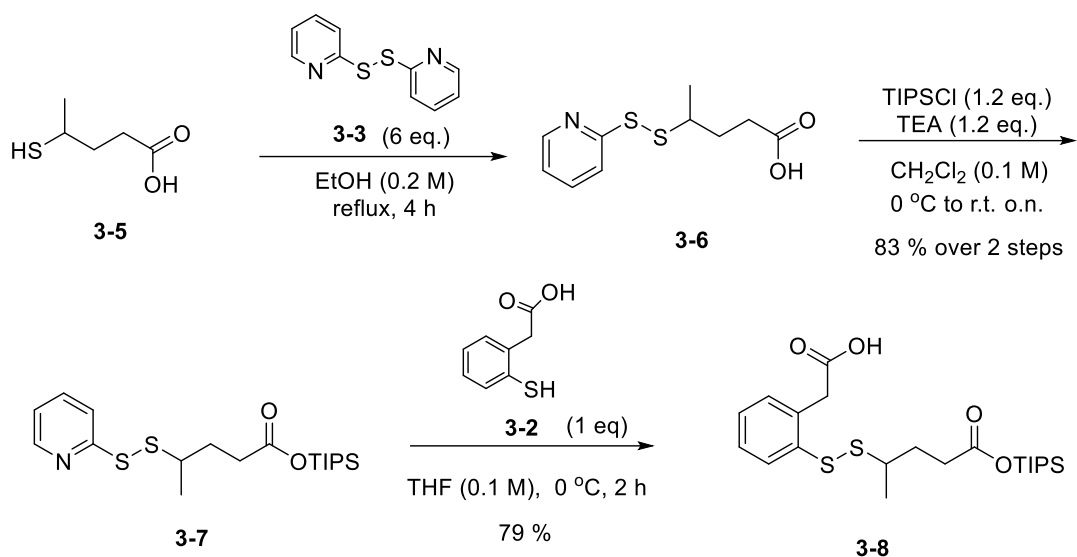
**Scheme 3.2** Synthesis of 1,2-di(pyridine-2-yl)disulfane

Then the synthesis of the lower linear chain moiety started with a substitution reaction of gamma-valerolactone. Thiourea as a nucleophile was used to form the thiuronium bromide salt (**3-4**). (**Scheme 3.3**) This salt was then subsequently treated with aqueous NaOH to afford the hydrolyzed product 4-sulphydrylbutanoic/methyl branched butanoic acid (**3-5**).



**Scheme 3.3** Synthesis of isothiuronium bromide salt and SH-alkyl linker

After methyl branched butanoic acid (**3-5**) was obtained, the first of two disulfide exchanges was performed with 1, 2-di(pyridine-2-yl)disulfane (**3-3**) to form **3-6** which was then subsequently protected with TIPS to form **3-7**. The second disulfide exchange was performed coupling the upper linker moiety **3-2** with the lower linker moiety **3-7** to form the final linker **3-8**. (**Scheme 3.4**) Due to the instability of the TIPS group, the final linker component would be used immediately to couple with the drug by DIC coupling reaction.

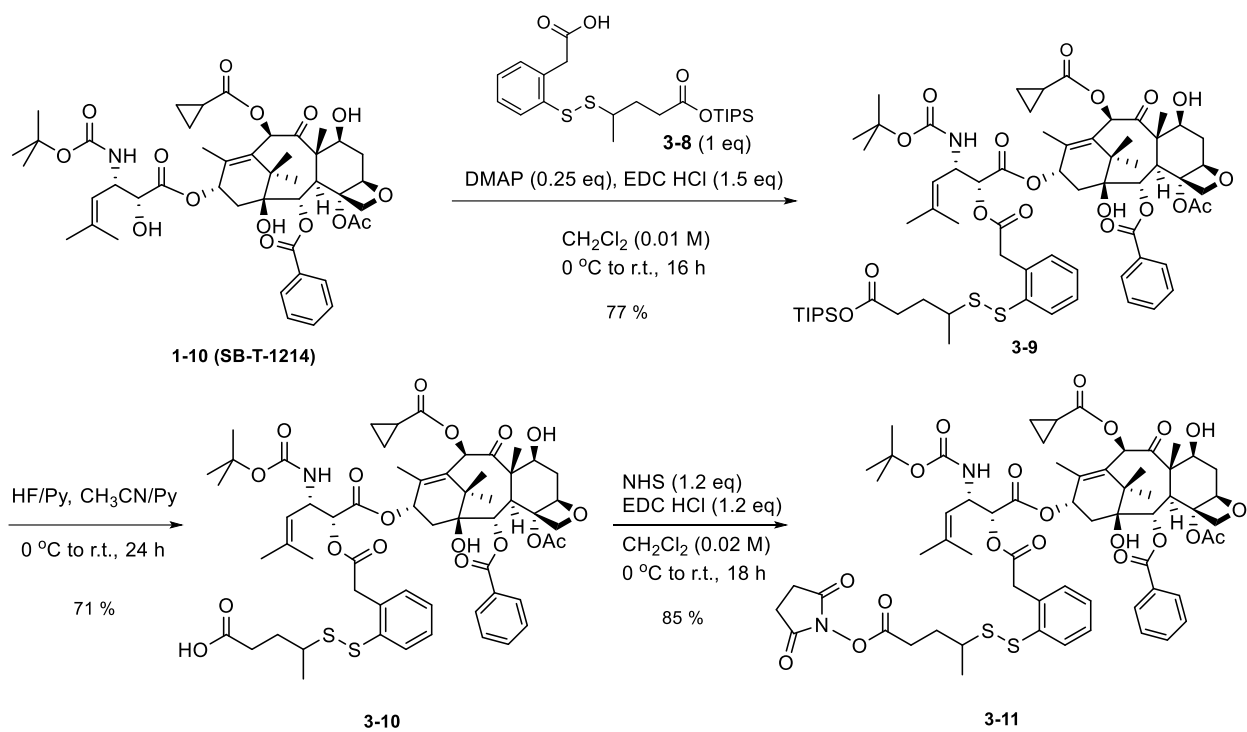


**Scheme 3.4** First and second disulfide exchange reaction and TIPS protection

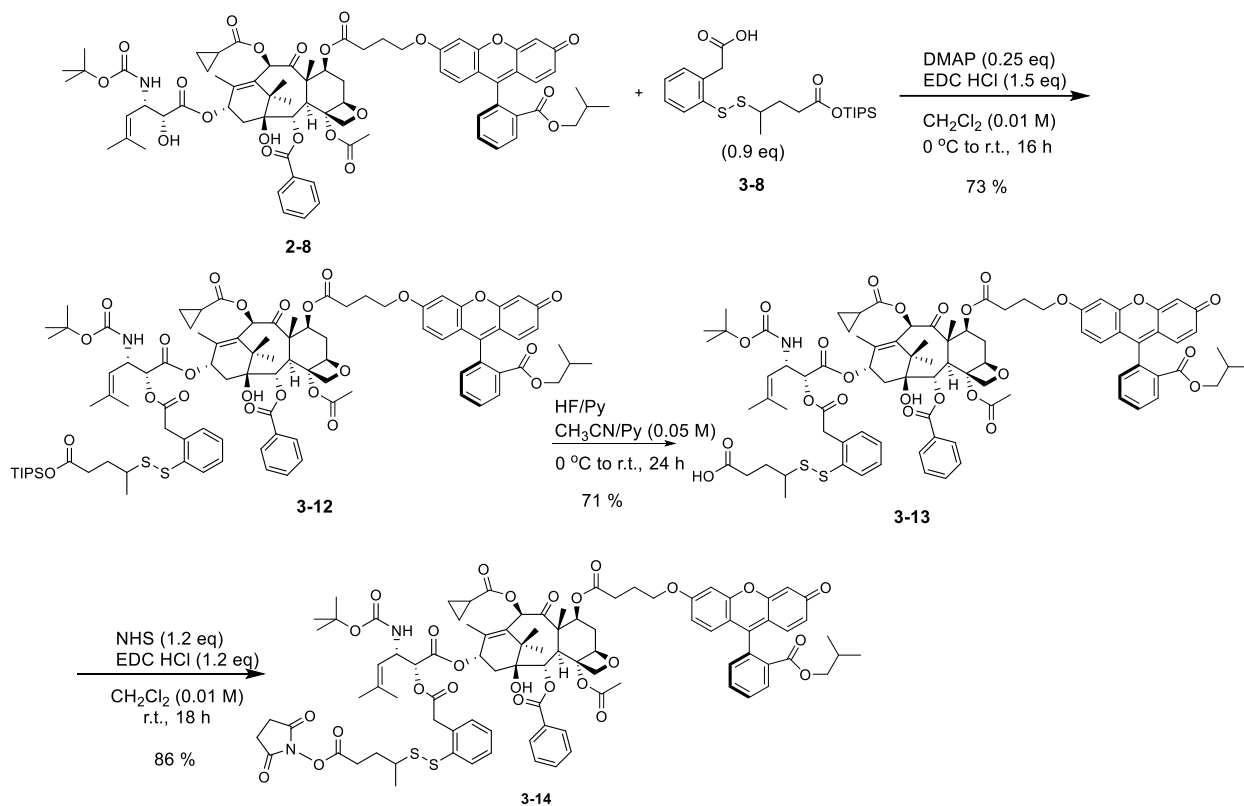
### §3.2.2 Synthesis of Coupling-Ready Activated Drug-Linker Constructs

Synthesis of coupling-ready warhead-linker construct **3-11** began with the coupling of the carboxyl acid group of the methyl-branched disulfide linker **3-8** to the C2' hydroxyl group of **1-10** (SB-T-1214) in the presence of EDC HCl and DMAP. Reaction progress was closely monitored by TLC to minimize di-substitution at the C7 hydroxyl group. Deprotection of the silyl group of **3-9** in the presence of HF-pyridine gave **3-10** in excellent yield (91%), and the free carboxylic acid of **3-10** was activated with *N*-hydroxysuccinimide in the presence of EDC HCl to afford **3-11** in good yield (70%). Purification by column chromatography gave the activated drug-linker in sufficient purity for subsequent reactions. (**Scheme 3.5**) Following the same process, another coupling-ready activated drug-linker construct bearing a fluorescent tag on C7 position was also obtained in good overall yield. (**Scheme 3.6**)





**Scheme 3.5** Synthesis towards coupling-ready drug-linker-OSu activated ester **3-11**



**Scheme 3.6** Synthesis towards coupling-ready drug-linker-C-fluorescein-OSu activated ester **3-14**

### §3.2.3 Synthesis of Biotin-Linker-Taxoid Conjugate BLT

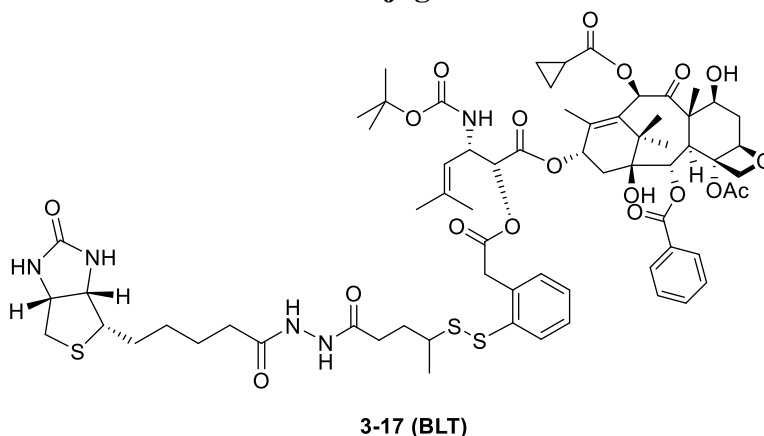
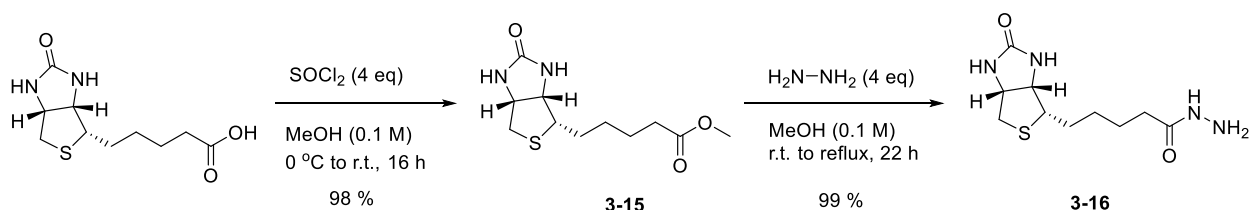
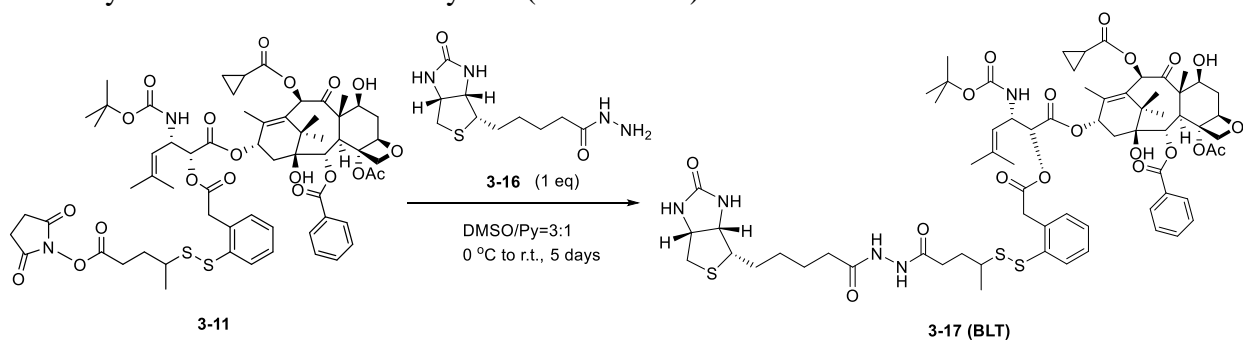


**Figure 3.10** Chemical structure of biotin-linker-taxoid (BLT)

Second-generation biotin-linker-taxoid drug conjugate **3-17** (BLT) consists of biotin as the tumor-targeting module connected to SB-T-1214 through a methyl-branched self-immolative disulfide linker and a hydrazine spacer. (**Figure 3.10**)



After acid chloride activation using thionyl chloride, biotin was converted to its methyl ester **3-15** in the presence of methanol, followed by treating with using excess hydrazine to afford biotin hydrazide **3-16** in excellent yield. (**Scheme 3.7**)

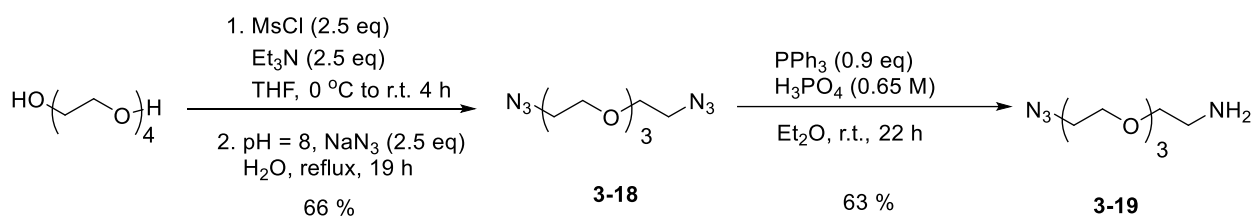


Then the reaction of coupling biotin hydrazide **3-16** to coupling-ready warhead-linker construct **3-11** to afford final biotin-methyl branched disulfide linker-SB-T-1214 **3-17** (BLT) conjugate proceeded slowly at room temperature, and finished in 5 days. (**Scheme 3.8**) After purification, the purity of **3-17** exceeded 99 % determined by HPLC, and the biological evaluations

*in vitro* against BR+ cancer cell lines and *in vivo* in a SCID mice bearing MX-1 tumor xenograft will be discussed in section 3.2.5 and 3.2.6.

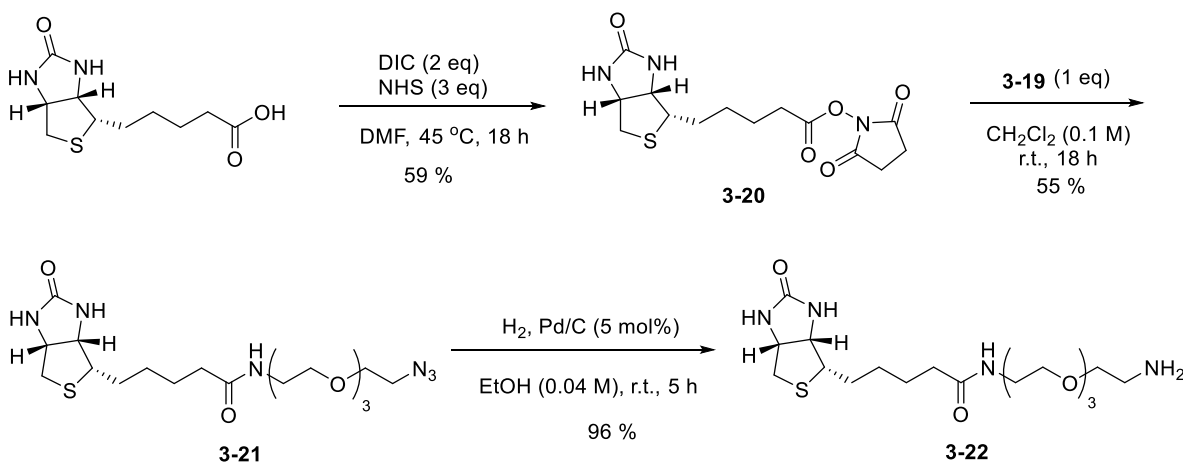
### §3.2.4 Synthesis of Biotin-PEG-Linker-Taxoid Conjugate BLT-S

Despite of the validated *in vitro* biological evaluation studies of the second-generation biotin-linker-taxoid drug conjugate BLT, this conjugate was found limited aqueous solubility during the preliminary *in vivo* study and NMR stability tests. It was necessary to add a substantial amount of surfactant to wrap the most hydrophobic portions of the conjugate to prevent the aggregation which resulted in the precipitation from the solution. Thus, incorporation of an intramolecular hydrophilic moiety will be helpful to increase the solubility and pharmacokinetics, and achieve the maximized therapeutic efficacy. The applicable strategy is to insert a short polyethylene glycol (PEG) oligomer between tumor-targeting module and linker (**Figure 3.10**), which can act as an intramolecular surfactant without interfere the potency of the released drug. In fact, PEG unit is a water soluble, nontoxic, non-immunogenic and biocompatible polymer, commonly used to increase the solubility, stability, safety and bioavailability of various biomedical conjugates.<sup>8</sup>



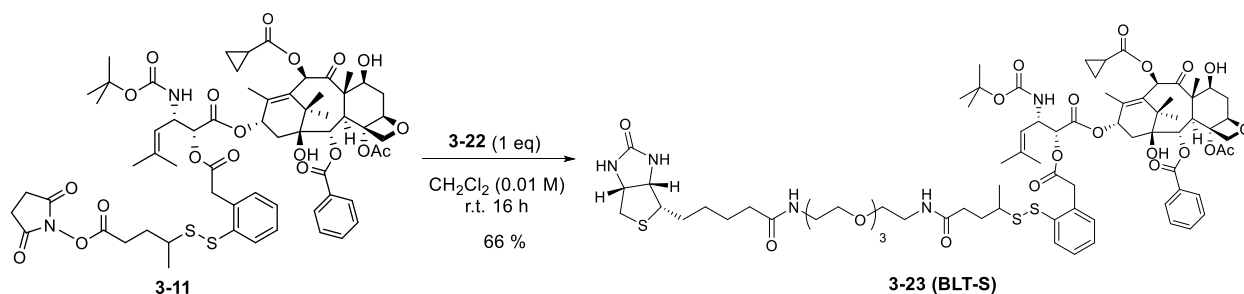
**Scheme 3.9** Modification of tetra ethylene glycol

Tetraethylene glycol was selected for the short PEG oligomer. It was reacted with methanesulfonyl chloride in the presence of triethylamine to give dimesylate intermediate, which further was converted to PEG-diazide intermediate **3-18** by treating with sodium azide under reflux condition, then followed by a subsequent 2-phase selective mono-reduction in the presence of  $\text{PPh}_3/\text{H}_3\text{PO}_4$  to afford amino-PEG-azide **3-19**. (**Scheme 3.9**)



**Scheme 3.10** Synthesis of biotin-PEG-amine (**3-22**)

Biotin was activated by NHS under DIC coupling condition, then the activated ester **3-20** was treated with **3-19** to afford **3-21** in good yield, followed by the hydrogenation to reduce the azido group to amino group to afford **3-22**. (**Scheme 3.10**) The solubility of **3-22** has been found largely increased. Most organic solvents, even chloroform, can dissolve this PEGylated biotin intermediate.



**Scheme 3.11** Synthesis of the biotin-PEG-linker-taxoid (BLT-S) conjugate

Biotin-PEG-amine **3-22** was directly used for the final conjugation with linker-drug-OSu activated ester **3-11** in dichloromethane as solvent to form BLT-S **3-23**. (**Scheme 3.11**) Compared to the reaction to form BLT (**Scheme 3.8**), this step finish within 24 hours. Biological evaluation and comparison of the two biotin-bearing drug conjugated will be discussed in section 3.2.5 and Chapter 5.

### §3.2.5 Biological Evaluation of Biotin-Linker-Taxoid Conjugates *in Vitro* Studies

The potency of two biotin-linker-taxoid drug conjugates BLT (**3-17**) and BLT-S (**3-23**) were examined against various BR<sup>+</sup> and BR<sup>-</sup> cell lines, including MX-1(BR<sup>++</sup>), ID8 (BR<sup>+++</sup>), MCF7 (BR<sup>+++</sup>), NCI/ADR (also known as MCF-7R, BR<sup>+</sup>), HCT116 (BR<sup>-</sup>), and WI38 (BR<sup>-</sup>). Paclitaxel and SB-T-1214 were also evaluated as control for comparison. All cytotoxicity measurements were based on MTT assay method, and experiments were performed for 72 h of drug exposure at 37 °C with 5 % CO<sub>2</sub> without supplemental GSH-OEt. Each average IC<sub>50</sub> was calculated based on 3 or 4 times repeated experiments. The results are shown in **Table 3.2**.

**Table 3.2** Cytotoxicity Measurement (IC<sub>50</sub>, nM) of Paclitaxel, SB-T-1214, BLT (**3-17**) and BLT-S (**3-23**) against BR<sup>+</sup> and BR<sup>-</sup> cell lines

Compound	MX1 <sup>a</sup>	ID8 <sup>b</sup>	MCF7 <sup>c</sup>	NCI/ADR <sup>d</sup>	HCT116 <sup>e</sup>	WI38 <sup>f</sup>
Paclitaxel	3.83 ± 0.59	35.3 ± 8.30	35.8 ± 1.76	1220 ± 430	7.34 ± 4.06	175 ± 51.6
SB-T-1214	2.90 ± 0.47	1.40 ± 0.46	30.8 ± 4.52	11.5 ± 1.97	7.38 ± 2.31	4.14 ± 0.82
BLT ( <b>3-17</b> )	-	15.1 ± 5.10	11.3 ± 1.08	13.1 ± 1.33	5.85 ± 1.34	-
BLT-S ( <b>3-23</b> )	26.7 ± 3.44	8.85 ± 2.68	8.22 ± 0.41	12.1 ± 3.53	6.15 ± 1.98	519 ± 90.3

<sup>a</sup>Human breast carcinoma cell line (BR<sup>+</sup>, Pgp<sup>-</sup>); <sup>b</sup>murine ovarian carcinoma cell (BR<sup>+</sup>); <sup>c</sup>Human breast carcinoma cell line (BR<sup>+</sup>, Pgp<sup>-</sup>); <sup>d</sup>Multidrug resistant human ovarian carcinoma cell line (BR<sup>+</sup>, Pgp<sup>+</sup>); <sup>e</sup>Colorectal CSC-enriched (CD133<sup>++</sup>) cancer cell (BR<sup>-</sup>); <sup>f</sup>Human lung fibroblast cell line (BR<sup>-</sup>); <sup>g</sup>Concentration of compound that inhibits 50% (IC<sub>50</sub>, nM) of the growth of human cell line after 72 h of drug or drug conjugate exposure at 37 °C with 5 % CO<sub>2</sub>. Each average IC<sub>50</sub> was calculated based on 3 or 4 times experiments.

As anticipated, the results in Table 3.2 showed that IC<sub>50</sub> values of paclitaxel against MX1, ID8 and MCF7 three cancer cell lines ranged from 3.83-35.8 nM, while the IC<sub>50</sub> value against WI38 healthy cell line was 175 nM, exhibiting slightly selectivity difference between cancer cells and normal cells. The IC<sub>50</sub> values of SB-T-1214 against three cancer cell lines ranged from 1.40-30.8 nM, and 4.14 nM against health cell line suggesting SB-T-1214 does not distinguish targeted cancer cells from normal cells, as anticipated. For HCT116 cell line which is defined as drug-sensitive cancer cell line, the IC<sub>50</sub> values of paclitaxel and SB-T-1214 were similar due to its high sensitivity to cytotoxic agent. For NCI/ADR cancer cell line which is defined as MDR cancer cell line with overexpression of Pgp, SB-T-1214 exhibited more than 100 times higher potency than paclitaxel. Therefore, as second generation taxoid, SB-T-1214 has possessed one to two orders of magnitude greater potency and better activity toward MDR cell line than paclitaxel.

Two biotin-linker-taxoid drug conjugates BLT and BLT-S demonstrated excellent target specificity against biotin cell lines with IC<sub>50</sub> values in a range of 11.3-15.1 nM and 8.22-26.7 nM, respectively. BLT-S possessed one to two orders of magnitude greater potency against BR+ cancer cell lines than BR- normal cell line. However, in the absence of supplemented GSH-OEt, the potency of BLT and BLT-S remained slightly below that of paclitaxel and SB-T-1214 by ½ to 1½ orders of magnitude. This may due to the endogenous glutathione level (and possibly some other thiols) was not sufficient to cleave all the internalized drug conjugate to release the cytotoxic agent in 72 hours incubation. Thus to evaluate the complete potency of BLT-S **3-23**, additional experiment were performed to introduce supplemental GSH-OEt to fully release the drug of internalized drug conjugate (**Table 3.3**). Accordingly, after 24 hours incubation with BLT-S, the cultured cells was thoroughly washed with DPBS buffer, and the drug media was replaced by fresh media with added glutathione ethyl ester (GSH-OEt), followed by additional 48 h incubation. It should be noted that the resulting cancer cells only contained BLT-S internalized in the first 24 h period. Under these conditions, BLT-S demonstrated an approximate two-fold increase in potency compared to its 72 h incubation without supplemental GSH-OEt against MX1, whereas only a slight increase in potency against ID8 was observed. This may disclose that the endogenous glutathione level vary in different types of cancer cells, and internalized drug conjugates may not be able to fully release the cytotoxic agents depending on which kind of cancer was treated.

**Table 3.3 Cytotoxicity Measurement (IC<sub>50</sub>, nM) of Paclitaxel, SB-T-1214, and BLT-S (3-23) in the presence of GSH-OEt after internalization**

Compound	MX1 <sup>a</sup>	ID8 <sup>b</sup>
Paclitaxel <sup>c</sup>	3.83 ± 0.59	21.2 ± 4.30
SB-T-1214 <sup>c</sup>	2.90 ± 0.47	1.89 ± 0.30
BLT-S ( <b>3-23</b> ) <sup>c</sup>	26.7 ± 3.44	7.84 ± 1.85
BLT-S ( <b>3-23</b> ) + GSH-OEt <sup>d</sup>	1.52 ± 0.34	5.91 ± 0.32

<sup>a</sup>Human breast carcinoma cell line (BR+, Pgp-); <sup>b</sup>murine ovarian carcinoma cell (BR+); <sup>c</sup>Cells were incubated with 72 hours of drug exposure at 37 °C under 5 % CO<sub>2</sub>; <sup>d</sup>Cells were incubated with 24 hours of drug conjugate exposure, followed by thorough washing of drug media with DPBS, then addition of 6 equivalents of glutathione-ethyl ester (GSH-OEt) for linker cleavage and drug release, and additional 48 hours incubation at 37 °C under 5 % CO<sub>2</sub>. Total drug or drug conjugate incubation was 72 hours for all experiments.

### §3.2.6 Biological Evaluation of BLT *in Vivo* Study

The efficacy of BLT was investigated *in vivo* using several combined immunodeficient (SCID) female Swiss Webster athymic nude mice bearing human MX-1 tumor xenografts intravenously with BLT and SB-T-1214 as comparison. Dosage for BLT was administered to three mice at 20 mg/kg per week x 4, and to two mice at 40 mg/kg per week x 2; SB-T-1214 was administered to five mice at 20 mg/kg per week x 3, followed by 40 mg/kg x 4 (**Figure 3.11**). The total dose administered to all five mice remained constant at 80 mg/kg for BLT; whereas the dose regimen for SB-T-1214 was escalated from 20 mg/kg to 40 mg/kg over time. These animal studies were conducted by Jean Rooney and Dr. Thomas Zimmerman at the Division of Laboratory Animal Resources (DLAR) at Stony Brook University and testing drug and drug conjugate were prepared by Dr. Joshua D. Seitz.

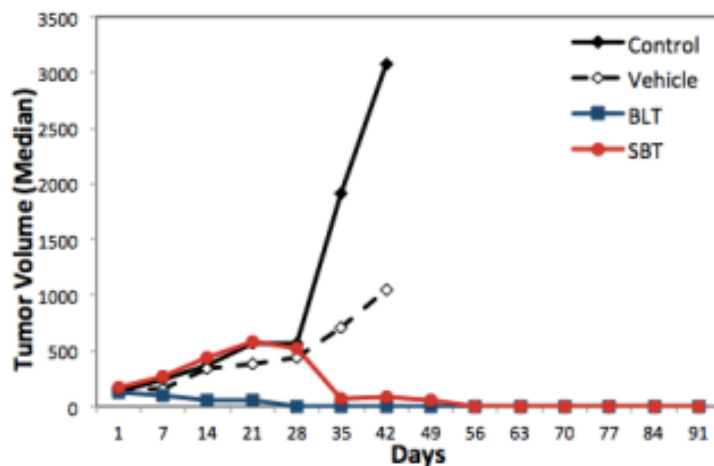


**Figure 3.11** Average tumor volumes for 5 surviving SCID female Swiss Webster athymic nude mice bearing MX-1 tumor xenograft with the following dose regimen: SB-T-1214: 20 mg/kg, q7d x 3 + 40 mg/kg x 4; BLT: (a) 20 mg/kg, q7d x 4 (3 studies), (b) 40 mg/kg, q7d x 2 (2 studies) (adapted from reference 17)<sup>17</sup>

Complete tumor regressions were obtained in three of five mice treated with SB-T-1214, whereas all mice receiving treatment with the biotin conjugate BLT achieved full regression. Only moderate weight loss of treated mice were observed, indicating a significant reduction in toxicity to normal cells. Response to treatment with the biotin conjugate BLT appeared to be substantially faster and more consistent than SB-T-1214, which validated the *in vivo* application of biotin-mediated tumor-targeting. However, it must be noticed that this study was not performed using an optimized formulation or dosing regimen, and the erratic tumor growth rates complicate the analysis of the data. Future studies will focus on improving the formulation and dosing regimens, and new generation BLT with modification are currently under development.

### §3.3 Synthesis and Biological Evaluation of Biotin-Fluorescein Probes

Previously three fluorescent or fluorogenic probes (**Figure 3.12**) were designed, prepared and analyzed by Dr. Shuyi Chen to identify the biotin receptor for tumor-targeting drug delivery and quantify the cellular uptake of the biotin conjugate *via* receptor-mediated endocytosis (RME).<sup>13</sup>

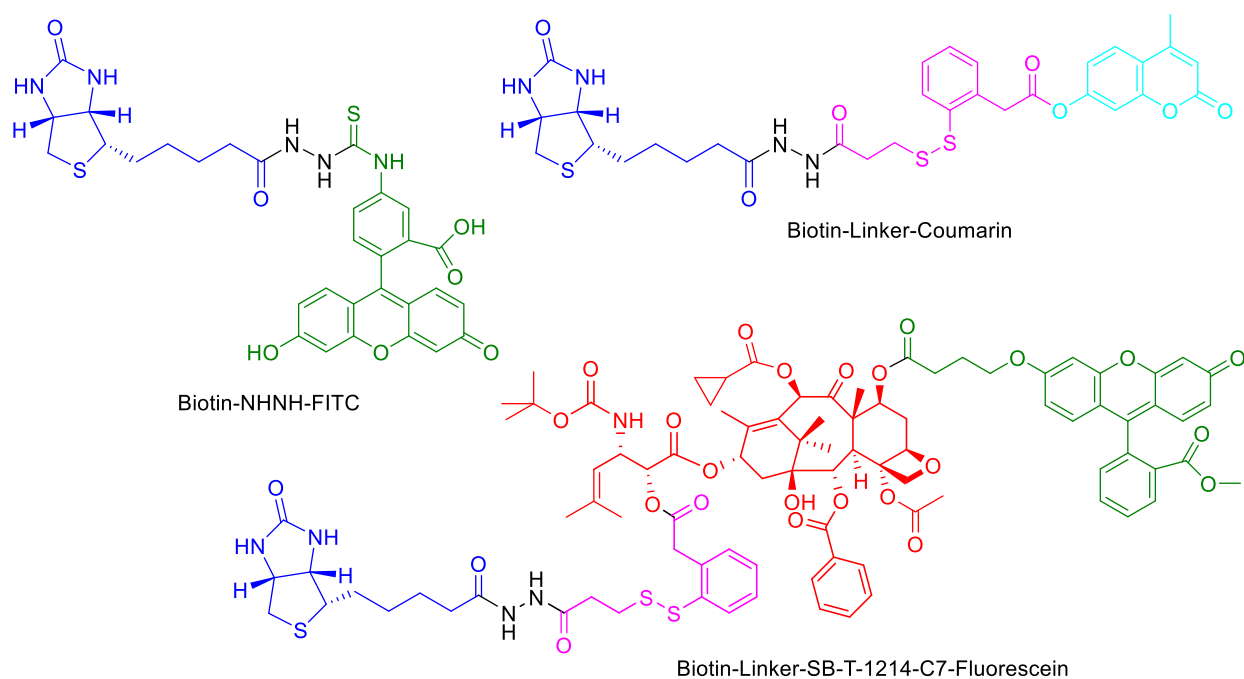


**Figure 3.12** Chemical structures of fluorescent and fluorogenic probes to validate RME of biotin conjugates (adapted from reference 13)<sup>13</sup>

Biotin moiety was directly connected to a fluorescent probe FITC through a hydrazine spacer to afford a biotin-NHNH-FITC probe. This probe was designed for validating biotin receptor-mediated endocytosis through energy-dependent, metabolic inhibition, and receptor saturation experiments.<sup>13</sup> (**Figure 3.13**)

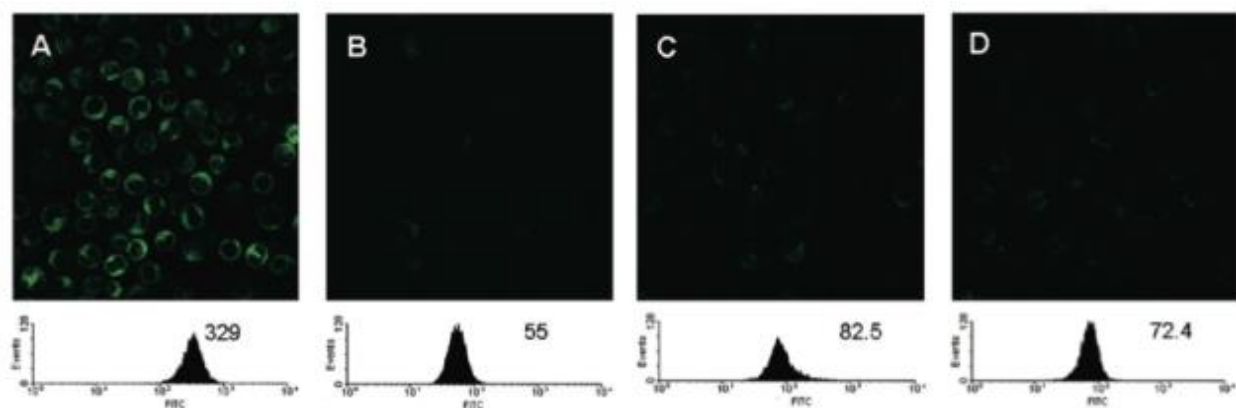


**Figure 3.13** CFM images and flow cytometry analysis of L1210FR cells after 3 h incubation with the 100 nM biotin-NHNH-FITC probe under different conditions: (A) 37 °C; (B) 4 °C; (C) 37 °C, added 0.05 % NaN<sub>3</sub>; (D) 37 °C, pretreated with excess biotin (2 mM) (reprinted from reference 13)<sup>13</sup>

The second probe biotin-linker-coumarin was designed to confirm the internalization of the biotin conjugate via RME and observe glutathioine-triggered linker cleavage upon release of fluorogenic coumarin, which only becomes fluorescent as a free molecule. The result clearly

demonstrated that the intracellular release of coumarin via glutathione-triggered disulfide linkage cleavage and the subsequent thiolactonization.<sup>13</sup> (**Figure 3.14**)

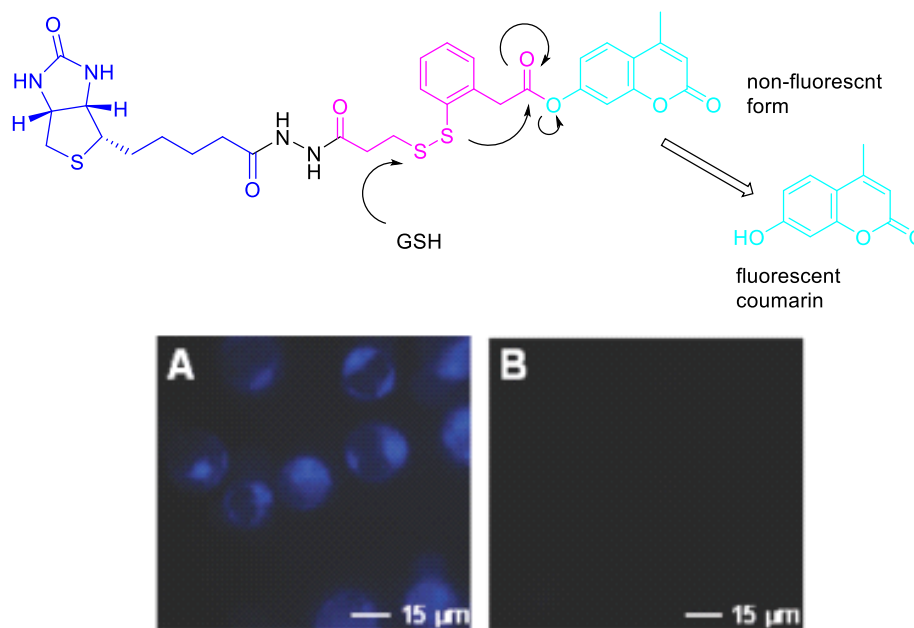


**Figure 3.14** Glutathione-triggered linker cleavage to release coumarin and CFM images of L1210FR cells after treatment with biotin-linker-coumarin (A) Epifluorescence image with added GSH-OEt for linker cleavage to release coumarin with fluorescence (B) Epifluorescence image only with incubated the biotin-linker-coumarin probe (nonfluorescent form) (reprinted from adapted from reference 13)<sup>13</sup>

The biotin-linker-SB-T-1214-C7-fluorescein probe was designed to monitor released fluorescent taxoid binding to the target protein, microtubules and visualize the fluorescent microtubule network in the cancer cells.<sup>13</sup> (**Figure 3.15**) This probe also exhibited tumor-targeting specificity to BR+ cell line (L1210FR), compared to BR- cell lines (L1210 and WI38).<sup>13</sup>

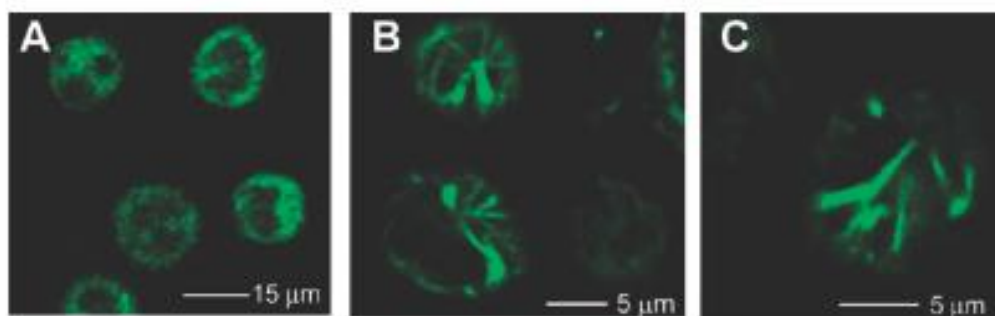
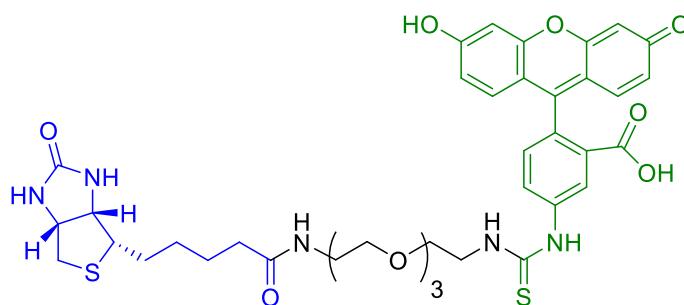


**Figure 3.15** CFM images of released fluorescent taxoid from biotin-linker-SB-T-1214-C7-fluorescein probe and its binding to the target microtubules in L1210FR cells (reprinted from adapted from reference 13)<sup>13</sup>

Another biotin-PEG-FITC probe was designed and synthesized by Dr. Jacob Vineberg for assessment of BR expression levels in several human cancer cell lines.<sup>5</sup> This probe has increased solubility by incorporation of a PEG spacer. (**Figure 3.16**)





Biotin-PEG-FITC (**3-24**)

**Figure 3.16** Chemical structure of biotin-PEG-FITC

This biotin-PEG-FITC probe was used to examine the biotin receptor expression level against MX-1 and MCF-7 (human breast carcinoma), ID8 (murine ovarian carcinoma), L1210FR and L1210 (murine leukemia cell lines), and WI38 (normal lung fibroblast) by means of confocal fluorescence microscopy and flow cytometry, and MX-1 (BR<sup>++</sup>) and MCF-7 (BR<sup>+++</sup>) were newly identified as cell lines that overexpress the biotin receptor.<sup>5</sup> (**Figure 3.17**)

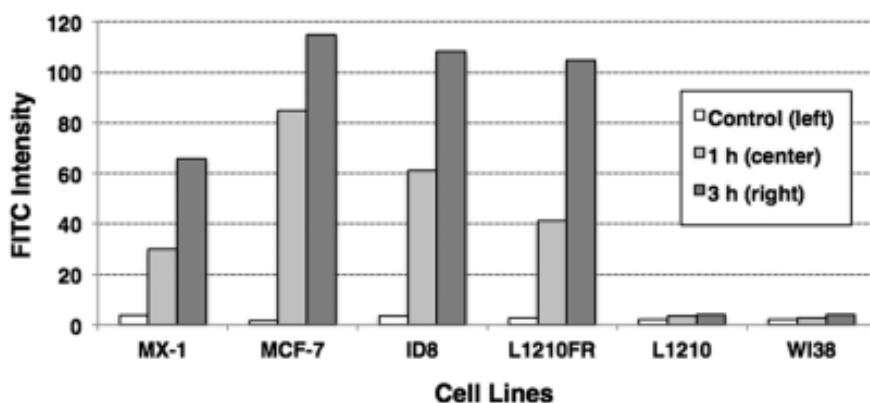
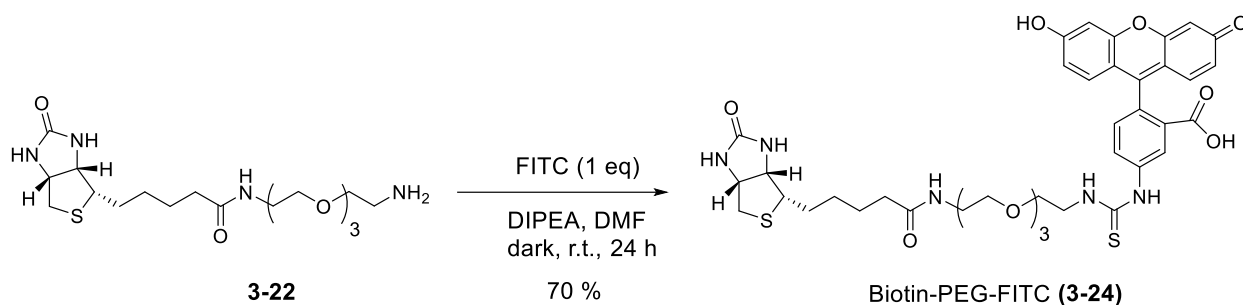


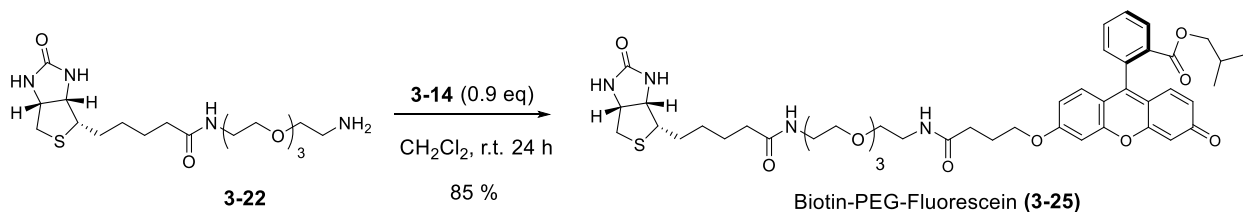
**Figure 3.17** Internalization of biotin-PEG-FITC into various cell lines at different periods of incubation time at 37 °C (reprinted from adapted from reference 5)<sup>5</sup>

### §3.3.1 Synthesis of Biotin-Fluorescent Probes (Biotin-PEG-FITC and Biotin-PEG-Fluorescein)

Two biotin-fluorescent probes were synthesized as described in **Scheme 3.12** and **Scheme 3.13**. Fluorescein isothiocyanate (FITC) was directly reacted with biotin-PEG-amine **3-22** in the presence of DIPEA to give biotin-PEG-FITC fluorescent probe **3-24** in good yield (70 %), shown in **Scheme 3.12**. The other biotin-PEG-fluorescein probe **3-25** was obtained by treating **3-22** with fluorescein activated OSu ester **3-14**, shown in **Scheme 3.13**.



**Scheme 3.12** Synthesis of the biotin-PEG-FITC probe (**3-24**)



**Scheme 3.13** Synthesis of the biotin-PEG-Fluorescein probe (**3-25**)

### §3.3.2 Biological Evaluation of Biotin-Fluorescein Probes *in Vitro* Studies

Since biotin-PEG-FITC has been used for short internalization period (3 h) study, biotin-PEG-fluorescein probe was used in longer incubation periods against ID8 and MX1 cell lines to investigate the internalization rate and saturation vs recycle of biotin receptor on the surface of cancer cells. (**Figure 3.18**) Based on the FACS result of each sampling time, the internalization curves were drawn in **Figure 3.19**.

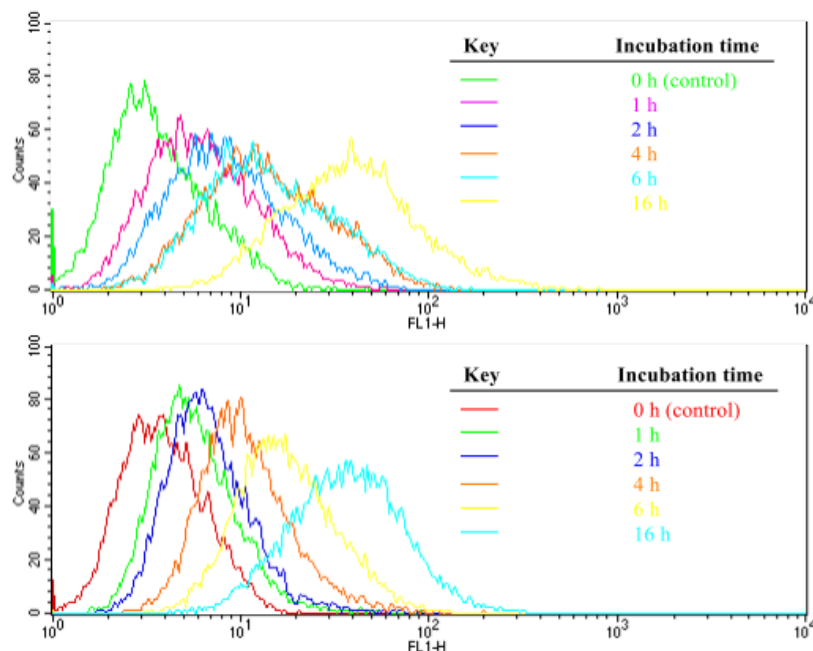


**Figure 3.18** Overlapped Flow cytometry analysis resulting from the extent of the internalization of 10  $\mu$ M biotin-PEG-Fluorescein probe (**3-25**) against ID8 (top) and MX1 (bottom) for 0, 1, 2, 4, 6 and 16 h periods at 37 °C

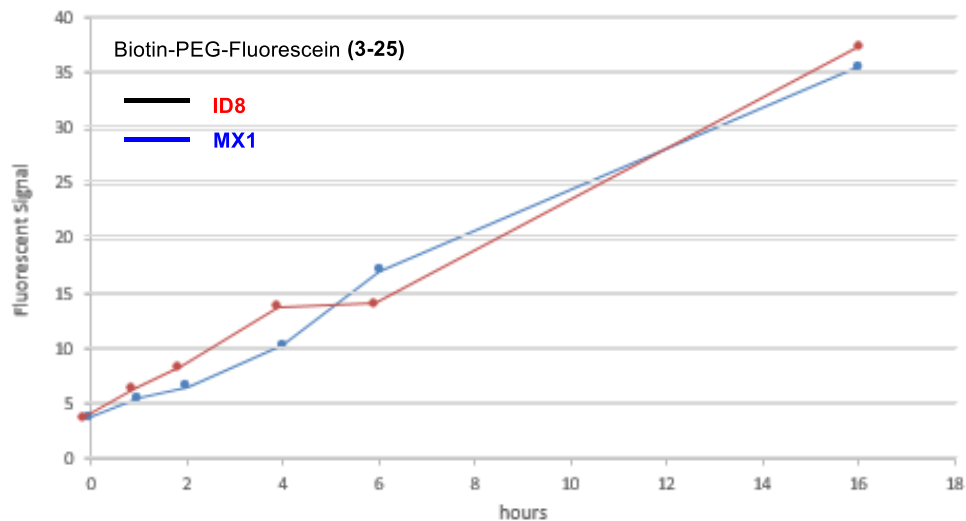


**Figure 3.19** Overlapped Flow cytometry analysis resulting from the extent of the internalization of 10  $\mu$ M biotin-PEG-Fluorescein probe (3-25) against ID8 (top) and MX1 (bottom) for 0, 1, 2, 4, 6 and 16 h periods at 37 °C

The biotin-PEG-fluorescein probe will be used as a small molecule fluorescent probe to compare with a nanosized drug conjugate fluorescent probe to investigate the multibinding effect which will be discussed in Chapter 5. In addition, the biotin-PEG-FITC will be used as small molecule fluorescent probe for investigation on the biotin receptor on cancer stem cells which will be discussed in Chapter 6.

### §3.4 Synthesis towards [ $^{18}$ F]-Labeled Biotin-PEG-F Radiotracer for PET Imaging Study

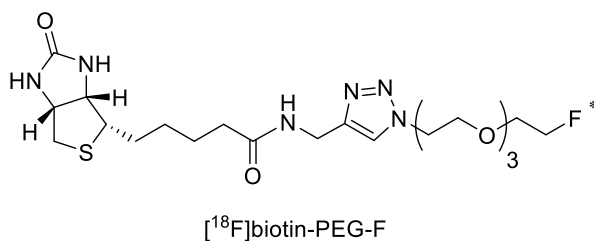
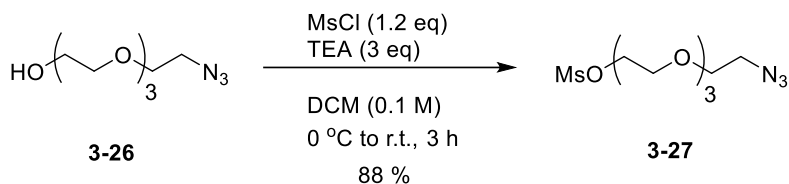


**Figure 3.20** Chemical Structure of [ $^{18}$ F]biotin-PEG-F

Biotin as a tumor-targeting module, its mechanism has not been well understood and established. To evaluate the biodistribution and localization of biotin-guided conjugate *in vivo*, we developed the method to synthesize a fluorine-18 radio-labeled biotin-PEG-F tracer (**Figure 3.20**) for positron emission tomography (PET) imaging study. This PET tracer has been reported recently by Claesener and co-workers for a qualitative biotin-avidin binding study to reveal its high affinity and site-specificity. Biodistribution studies showed that biotin-PEG-F was cleared quickly and efficiently from the body by hepatobiliary and renal elimination.<sup>18</sup>

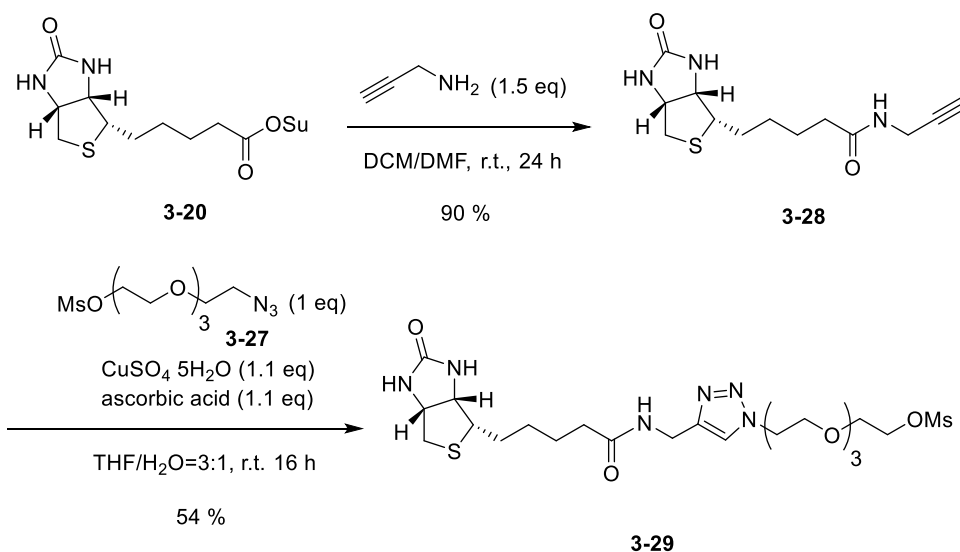
#### §3.4.1 Cold Synthesis toward Biotin-PEG-F

To efficiently synthesize a [ $^{18}\text{F}$ ]-labeled radiotracer, a biotin-PEG-OMs intermediate (**3-29**) was designed and synthesized. After coupling of biotin moiety and a PEG oligomer spacer through click chemistry, a terminal mesylate intermediate (**3-29**) could be used to quickly converted into [ $^{18}\text{F}$ ]biotin-PEG-F for PET study. The radiosynthesis and semi-preparative HPLC purification method has been recently developed in our lab and collaboration with Dr. Joanna S. Fowler in Brookhaven National Laboratory (BNL).<sup>16</sup>



**Scheme 3.14** Synthesis of the 11-azido-3,6,9-trioxaundecanyl-1-methylsulfonate (**3-27**)

The intermediate **3-26** was obtained from Dr Jacob Vineberg. Conversion the hydroxyl group of **3-26** to corresponding mesylated **3-27** was done in the presence of methanesulfonyl chloride and triethylamine in excellent yield (88 %). (**Scheme 3.14**)



**Scheme 3.15** Synthesis of the biotin-PEG-OMs (**3-29**)

To introduce an alkyne moiety to biotin for click reaction, propargylamine was coupled to biotin OSu ester **3-20** to give **3-28** in excellent yield (90 %). Then in the presence of copper sulfate and ascorbic acid, the click reaction gave **3-29** in modest yield (54 %). This intermediate was kept in  $-20\text{ }^\circ\text{C}$  freezer and waiting for further radio-labeling study in collaboration with German research group.

### §3.5 Summary

Rapidly proliferating cancer cells have been found overexpressing biotin receptors on the surface which makes biotin as a good tumor-targeting biomarker for tumor-targeted drug delivery. Two biotin-linker-taxoid drug conjugates BLS and BLT-S were synthesized. BLT is consisted of

a biotin as tumor targeting module, a second generation taxoid SB-T-1214 as the warhead, and connected with a self-immolative disulfide linker. To increase the solubility and bioavailability, a polyethylene glycol oligomer was inserted between the biotin moiety and linker-drug. Both of the two biotin-linker-taxoid drug conjugates have been evaluated *in vitro* against various BR+ and BR- cell lines with paclitaxel and SB-T-1214 as control, and these biotin-linker-taxoid drug conjugates demonstrated excellent target specificity and high potency. BLT was tested against MX-1 xenografts in SCID mice, demonstrating biotin-mediated tumor targeted drug delivery *in vivo*. To validate the biotin-receptor mediated endocytosis (RME), two biotin fluorescent probes, biotin-PEG-FITC and biotin-PEG-fluorescein, were designed and synthesized. Confocal microscopy and flow cytometry results elucidated enhanced uptake of biotin-PEG-fluorescein *via* RME. In addition, to investigate the biodistribution and localization of biotin *in vivo*, a key intermediate biotin-PEG-OMs was synthesized for radiolabeling process toward [<sup>18</sup>F]biotin-PEG-F for PET imaging study.

### §3.6 Experimental Sections

#### §3.6.1 Caution

Taxoids have been classified as potent cytotoxic agents. Thus, all drugs and structurally related compounds and derivatives must be considered as mutagens and potential reproductive hazards for both males and females. Hydrofluoric acid (HF) can penetrate the skin, causing destruction of deep tissue layers, including bone. Appropriate precautions (i.e. use of gloves, goggles, lab coat and fume hood) must be taken while handling these compounds.

#### §3.6.2 General Methods

<sup>1</sup>H and <sup>13</sup>C NMR were measured on 300, 400 MHz Varian spectrometer or 400, 500, 700 MHz Bruker NMR spectrometer. The melting points were measured on a “Uni-melt” capillary melting point apparatus from Arthur H. Thomas Company, Inc and are uncorrected. TLC analyses were performed on Sorbent Technologies aluminum-backed Silica G TLC plates (Sorbent Technologies, 200 μm, 20 x 20 cm) and were visualized with UV light and stained with sulfuric acid-EtOH, 10 % PMA-EtOH or 10 % Vanillin-EtOH with 1% sulfuric acid. Column chromatography was carried out on silica gel 60 (Merck, 230-400 mesh ASTM). Chemical purity was determined with a Shimadzu L-2010A HPLC HT series HPLC assembly, using a Kinetex PFP column (4.6 mm x 100 mm, 2.6 μm), employing CH<sub>3</sub>CN/water as the gradient solvent system with a flow rate of 1 mL/min. LC-UV-MS analysis was performed on an Agilent LC-UV-TOF mass spectrometer at the Institute of Chemical Biology and Drug Discovery, using a Kinetex F5 column (2.1 mm x 150 mm, 2.6 μm, 100 angstroms), employing methanol/water with 10mM AmAc as the gradient solvent system, a flow rate of 0.375 mL/min under 30 °C, and with the UV detector set at 275 and 230 nm. The gradient was run from 60% to 95% methanol in water over a 45 minute period. Low resolution mass spectrometry was performed on an Agilent LC-MSD mass spectrometer at the Institute of Chemical Biology and Drug Discovery, Stony Brook, NY. High resolution mass spectrometry analysis was carried out on an Agilent LC-UV-TOF mass spectrometer at the Institute of Chemical Biology Drug Discovery, Stony Brook, NY or at the Mass Spectrometry Laboratory, University of Illinois at Urbana-Champaign, Urbana, IL.

## Cell Culture

All cell lines were obtained from ATCC and maintained at SBU Cell Culture/Hybridoma Facility. Cells were cultured in RPMI-1640 cell culture medium (Gibco), supplemented with 10% (v/v) heat-inactivated fetal bovine serum (FBS, Thermo Scientific, HyClone, SH3007003), and 1% (v/v) penicillin and streptomycin (PenStrep) at 37 °C in a humidified atmosphere with 5% CO<sub>2</sub>. Human breast carcinoma (MX1 and MCF7), and murine ovarian carcinoma (ID8), human ovarian carcinoma (NCI/ADR), human colon carcinoma (HCT116), and normal human lung fibroblast (WI-38) were cultured as monolayers on 100 mm tissue culture dishes in a supplemented RPMI-1640 cell culture medium. Cells were harvested, collected by centrifugation at 950 rpm for 5 min, and resuspended in fresh culture medium. Cell cultures were routinely divided by treatment with trypsin (TrypLE, Gibco) as needed every 2-4 days and collected by centrifugation at 950 rpm for 5 min, and resuspended in fresh cell culture medium, containing varying cell densities for subsequent biological experiments and analysis.

### Incubation of Cells with Biotin-PEG-Fluorescein (3-25)

Cell suspensions (3 mL) of MX-1 and ID8 at  $5 \times 10^5$  cells/mL were added to each individual well of 6-well plates, and the plates were subsequently incubated overnight in the appropriate cell culture media. The fluorescent probe **3-25** in DMSO was diluted in RPMI-1640 cell culture medium (3 mL) at final concentration of 10  $\mu$ M for internalization through RME study, and was used to replace the medium in each well followed by incubated at 37 °C for different periods (16 h, 6 h, 4 h, 2 h, 1 h). One well with cells was incubated without addition of fluorescent probe **3-25** as control for 16 h. Following incubation, the medium was aspirated and the cells were removed by treatment with trypsin as needed, washed twice with phosphate buffered solution (DPBS), collected by centrifugation, and resuspended in DPBS (300  $\mu$ L) for subsequent confocal fluorescence microscopy imaging or flow cytometry analysis.

### Confocal Fluorescence Microscopy (CFM) Imaging of the Treated Cells

Cells treated as described above were resuspended in 300  $\mu$ L of PBS after each experiment, and dropped onto an uncoated microslide with coverslip (MatTek Corp). CFM experiments were performed using a Zeiss LSM 510 META NLO two-photon laser scanning confocal microscope system, operating at a 488 nm excitation wavelength and at  $527 \pm 23$  nm detecting emission wavelength using a 505-550 nm bandpass filter. Images were captured using a C-Apochromat 63x/1.2 water (corr.) objective. Acquired data were analyzed using LSM 510 Meta software.

### Flow Cytometry Fluorescent Measurements of the Cells

Flow cytometry analysis of the cells treated with probes **3-25** was performed with a flow cytometer, FACSCalibur, operating at a 488 nm excitation wavelength and detecting 530 nm emission wavelengths with a 30 nm bandpass filter (515-545 nm range). Cells treated as described above were resuspended in 0.5 mL of PBS. Approximately 10,000 cells were counted for each experiment using CellQuest 3.3 software (Becton Dickinson), and the distribution of FITC fluorescence was analyzed using WinMDI 2.8 freeware (Joseph Trotter, Scripps Research

Institute). Propidium iodide staining was used in all experiments to rule out dead cell count in the analysis.

### ***In Vitro* Cytotoxicity Assays**

The cytotoxicities ( $IC_{50}$ , nM) of paclitaxel, SB-T-1214, BLT (**3-17**) and BLT-S (**3-23**) were evaluated against various BR+ and BR- cell lines, including MX-1 (human breast carcinoma cell line, BR<sup>+</sup>), ID8 (murine ovarian carcinoma cell, BR<sup>+++</sup>), MCF7 (human breast carcinoma cell line, BR<sup>+++</sup>), NCI/ADR (also known as MCF-7R, multidrug resistant human ovarian carcinoma cell line, BR<sup>+</sup>), HCT116 (colorectal CSC-enriched (CD133<sup>++</sup>) cancer cell, BR<sup>-</sup>), and WI38 (human lung fibroblast cell line, BR<sup>-</sup>) by means of the standard quantitative colorimetric assay using a tetrazolium salt-based analysis (“MTT assay”<sup>19</sup>; MTT = 3-(4,5-dimethylthiazol-2-yl)-2,5-diphenyltetrazolium bromide; Sigma Chemical Co.). The inhibitory activity of each compound is represented by the  $IC_{50}$  value, which is defined as the concentration required for inhibiting 50% of the cell growth. Cells were harvested, collected, and resuspended in 200  $\mu$ L cell culture medium RPMI-1640 at a concentration of  $0.5\sim 1.5 \times 10^4$  per well over a 96-well plate. Cells were allowed to descend to the bottom of the plates overnight and fresh medium was added to each well upon removal of the old medium. For the MTT assay of paclitaxel, SB-T-1214, BLT (**3-17**) and BLT-S (**3-23**), cells were resuspended in 200  $\mu$ L medium with 8,000 to 10,000 cells per well of a 96-well plate and incubated at 37  $^{\circ}$ C for 24 h before drug treatment. In DMSO stock solutions, each drug or conjugate was diluted to a series of concentrations in cell culture medium to prepare test solutions. These test solutions at different concentrations ranging from 500 pM to 5  $\mu$ M (100  $\mu$ L each) were added to the wells in the 96-well plate and cells were subsequently cultured for 72 h. For the GSH-OET addition experiments, cells were incubated with BLT-S (**3-23**) at 37  $^{\circ}$ C for 24 h and the drug medium was removed. Then, treated cells were washed with PBS, and GSH-OEt (6 equivalents) in cell culture medium (200  $\mu$ L) was added to the wells. These cells were incubated at 37  $^{\circ}$ C for an additional 48 h, the total incubation time was 72 h. For all experiments, after removing the test medium by aspiration, 50  $\mu$ L DPBS buffer containing MTT (0.5 mg/mL) was added to each well and incubated at 37  $^{\circ}$ C for 3 h. The resulting DPBS buffer was then removed and as-produced insoluble violet formazan crystals were dissolved into 50  $\mu$ L 0.1 N HCl in isopropanol to give a violet solution. The plate was allowed to shake for 8 minutes to fully dissolve the violet formazan crystal, then the spectrophotometric absorbance measurement of each well in the 96-well plate was run at 568 nm using a Labsystems Multiskan Ascent microplate reader. The  $IC_{50}$  values and their standard errors were calculated from the viability-concentration curve using the Four Parameter Logistic Model of Sigmaplot. The concentration of DMSO per well was  $\leq 1\%$  in all cases.

### **§3.6.3 Materials**

The chemicals were purchased from Sigma-Aldrich, Fischer Scientific or VWR International, and used as received or purified before use by standard methods. Dichloromethane was dried before use by distillation over calcium hydride under nitrogen. Tetrahydrofuran was dried before use by distillation over sodium-benzophenone kept under nitrogen. Dry DMF was purchased from EMD chemical company, and used without further purification. Reaction flasks were dried in a 100  $^{\circ}$ C oven and allowed to cool to room temperature in a desiccator over “Drierite” (calcium sulfate) and assembled under an inert nitrogen gas atmosphere. Biological materials

including RPMI-1640 cell culture media, DPBS buffer, fetal bovine serum, PenStrep, and TrypLE were obtained from Gibco and VWR International, and used as received for cell-based assays.

### §3.6.4 Experimental Procedure

#### Benzothiophen-2-one (3-1)<sup>20</sup>

Preparation of **3-1** was accomplished by the addition of 13 eq 30 % H<sub>2</sub>O<sub>2</sub> (13 mL, 4.4 g, 1.3 mol) added dropwise to a solution of thianaphthene-2-boronic acid (2 g, 0.1 mol) in 0.5 M EtOH (22.5 mL). The mixture should be stirred at room temperature for 18 hours and open to the atmosphere. After completion, the mixture was diluted with water (20 mL) and extracted with aliquots of CH<sub>2</sub>Cl<sub>2</sub> (20 mL x 3). The resulting organic layer was dried over anhydrous MgSO<sub>4</sub>, and concentrated *in vacuo*. Purification was performed using column chromatography with hexanes and ethyl acetate to obtain **3-1** (1.29 g, 8.6 mmol, 86 % yield) as light yellow solid. <sup>1</sup>H NMR (500 MHz, CDCl<sub>3</sub>) δ 3.97 (s, 2 H), 7.19-7.23 (dt, *Ja* = 1.3 Hz, *Jb* = 6.95, 1 H), 7.27-7.35 (m, 3 H). <sup>13</sup>C NMR (125 MHz, CDCl<sub>3</sub>) δ 47.3, 123.0, 124.8, 126.1, 128.3, 132.2, 137.1, 203.1. All data are in agreement with literature values.<sup>5,20</sup>

#### (2-Mercapto-phenyl)acetic acid (3-2)<sup>13</sup>

A solution of **3-1** (1.28 g, 8.5 mmol) in 0.2 M THF (42 mL) was refluxed at 60 °C. A 6 eq volume LiOH monohydrate (2.1 g, 51 mmol) in 1.2 M distilled water (42 mL) previously degassed was then added dropwise. The reaction was stirred overnight at 60 °C for 19 hours. After completion the resulting solution was cooled to room temperature and diluted with a solution of water (40 mL) and diethyl ether (20 mL). The solution was placed in an ice bath and the pH of the mixture was then subsequently adjusted to 2 using 1 M HCl. The resulting organic layer was extracted with CH<sub>2</sub>Cl<sub>2</sub> (20 mL x 3) and washed with brine (15 mL x 3), dried over Mg<sub>2</sub>SO<sub>4</sub>, and concentrated *in vacuo*. Purification was performed using column chromatography with hexanes and ethyl acetate to obtain light yellow oil **3-2** (772 mg, 4.6 mmol) in 54 % yield. <sup>1</sup>H NMR (500 MHz, CDCl<sub>3</sub>) δ 3.49 (s, 1 H), 3.81 (s, 2 H), 7.17-7.20 (m, 2 H), 7.23-7.24 (m, 1 H), 7.39-7.41 (m, 1 H). <sup>13</sup>C NMR (125 MHz, CDCl<sub>3</sub>) δ 39.9, 126.9, 128.2, 129.1, 130.7, 131.0, 132.4, 133.3, 176.2. All data are in agreement with literature values.<sup>5,13</sup>

#### 1,2-Di(pyridine-2-yl)disulfane (3-3)<sup>21</sup>

Pyridine-2(1H)-thione (11.1 g, 0.1 mol) was dissolved in 0.1M CH<sub>2</sub>Cl<sub>2</sub> (110 mL). Then 3 eq KMnO<sub>4</sub> (47g, 0.3 mol) was slowly added and the reaction was stirred vigorously. Subsequently, the resulting solution was filtered over celite and concentrated *in vacuo* to get white crystal **3-3** (10.83 g, 0.049 mol, 98 % yield). m.p. 58-59 °C <sup>1</sup>H NMR (300 MHz, CDCl<sub>3</sub>) δ 7.11 (dd, *J* = 7.5 Hz, 2 H), 7.63 (m, 4 H), 8.46 (d, *J* = 6.5 Hz, 1 H). All data are in agreement with literature values.<sup>21</sup>

#### 2-(5-Methoxy-5-oxopentan-2-yl)isothiuronium bromide (3-4)

To gamma-valerolactone (5.25 g, 0.05 mol), 5.0 eq thiourea (19.03 g, 0.25 mol) and 6.5 eq 47-49 % HBr (aq) (38.3 mL) was added dropwise. The solution was refluxed for 36 hours. After that, the



resulting solution was extracted with CH<sub>2</sub>Cl<sub>2</sub> (20 mL x 3). The resulting aqueous solution containing crude **3-4** in its bromide salt form was taken to the next step.

#### **4-Sulfhydrylpentanoic acid (3-5)<sup>22</sup>**

To **3-4** in 20 M NaOH (20 mL) was added slowly to adjust pH to 10 and then refluxed overnight. After completion the resulting aqueous solution was allowed to cool to room temperature and then washed with CH<sub>2</sub>Cl<sub>2</sub> (15 mL x 3). Then the pH of the aqueous solution was adjusted to 2 with 1 M HCl and extracted with CH<sub>2</sub>Cl<sub>2</sub> (15 mL x 3). The combined organic layers was subsequently washed with brine and H<sub>2</sub>O (15 mL x 3 each), then dried with MgSO<sub>4</sub> and concentrated *in vacuo* to yield **3-5** (26 mmol, 3.44 g, 50 % yield over 2 steps). <sup>1</sup>H NMR (300 MHz, CDCl<sub>3</sub>) δ 1.38-1.40 (d, 3 H), 1.48-1.51 (d, 1 H), 1.77-1.82 (m, 1 H), 1.98-2.01 (m, 1 H), 2.52-2.59 (q, 2 H), 2.96-3.00 (m, 1 H), 11.88 (s, 1 H). All data are in agreement with literature values.<sup>22</sup>

#### **4-(Pyridin-2-yl-disulfanyl) pentanoic acid (3-6)**

To a solution of 1,2-di(pyridine-2-yl)disulfane (**3-3**) (5.92 g, 27 mmol) in 0.2 M EtOH (134.5 mL), 0.17 eq **3-5** (0.6 g, 4.5 mmol) in 0.2 M EtOH (23 mL) was added dropwise. The reaction was then refluxed for 4 hours. After completion, the resulting solution was evaporated and the crude product **3-6** was used then taken to the next step.

#### **Triisopropylsilyl 4-(pyridine-2-yl-disulfanyl) pentanoate (3-7)<sup>23</sup>**

4-(Pyridin-2-yl)disulfanyl) pentanoic acid **3-6** was dissolved in 0.1 M CH<sub>2</sub>Cl<sub>2</sub> (44.8 mL) respectively and 1.2 eq TEA (1.25 mL, 0.906 g, 8.96 mmol) was added. The solution was then cooled to 0 °C. 1.2 eq chlorotriisopropylsilane (1.15 mL, 1.037 g, 5.38 mmol) was then added dropwise. The mixture was stirred and allowed to warm to room temperature overnight. After completion, the resulting solution was quenched with saturated ammonium chloride (30 mL). The aqueous layer was extracted with CH<sub>2</sub>Cl<sub>2</sub> (20 mL x 3) and the combined organic layers were combined and washed with brine (20 mL x 3). The organic layer was dried over MgSO<sub>4</sub>, and concentrated *in vacuo*, and the resulting crude product was purified *via* column chromatography on silica gel with increasing amounts of eluent (hexanes: ethyl acetate) to give **2-7** (1.483 g, 3.72 mmol, 83 % yield over 2 steps), and was kept under nitrogen in the freezer. <sup>1</sup>H NMR (500 MHz, CDCl<sub>3</sub>) δ 1.03 (m, 34 H), 1.23 (m, 3 H), 1.32 (d, 3 H), 1.85 (m, 1 H), 1.94 (m, 1 H), 2.49 (m, 2 H), 2.99 (m, 1 H), 7.04 (m, 1 H), 7.59 (m, 1 H), 7.70 (m, 1 H), 8.42 (m, 1 H). <sup>13</sup>C NMR (125 MHz, CDCl<sub>3</sub>) δ 11.8, 112.2, 17.7, 20.5, 31.1, 33.2, 46.2, 119.7, 120.5, 136.9, 149.4, 160.8, 173.0. All data are in agreement with literature values.<sup>23</sup>

#### **2-(2-5-Oxo-5-(triisopropylsilyloxy)-4-methyl butan-2-yl)disulfanylphenyl) acetic acid (3-8)<sup>23</sup>**

An aliquot of **3-7** (479 mg, 1.2 mmol) was dissolved in 0.1 M THF (12 mL) and cooled to 0 °C under inert conditions. To this mixture was added 1 eq **3-2** (202 mg, 1.2 mmol) dissolved in 0.1 M THF (12 mL) previously cooled to 0 °C. The mixture was stirred at 0 °C for 2 hours and allowed to warm to room temperature. The reaction was monitored *via* TLC. Upon completion, the solvent was evaporated and the residual was purified *via* column chromatography on silica gel with increasing amounts of eluent (hexanes: ethyl acetate) to give to give **3-8** (434 mmol, 0.95 mg, 79

% yield). <sup>1</sup>H NMR (300 MHz, CDCl<sub>3</sub>) δ 1.04 (d, 18 H), 1.25 (m, 3 H), 1.77-1.87 (m, 1 H), 1.91-1.98 (m, 1 H), 2.38-2.43 (m, 2 H), 2.89 (m, 1 H), 3.89 (s, 2 H), 7.19-7.20 (m, 2 H), 7.28 (m, 1 H), 7.80 (d, 2 H). All data are in agreement with literature values.<sup>23</sup>

### Drug-Linker-TIPS (3-9)<sup>5</sup>

To a round bottom flask were added **1-10** (430 mg, 0.94 mmol), 1.5 eq of EDC HCl salt (270 mg, 1.4 mmol), 0.25 eq DMAP (28.7 mg, 0.23 mmol) and 1.1 eq **3-8** (883 mg, 1.0 mmol) dissolved in CH<sub>2</sub>Cl<sub>2</sub> (0.02 M) (19 mL) under 0 °C. The resulting solution was allowed to warm to room temperature and stir for 16 hours. Upon completion, the solvent was evaporated and the residual was purified *via* column chromatography on silica gel with increasing amounts of eluent (hexanes: ethyl acetate) to yield **3-9** (929 mg, 0.72 mmol, 77 % yield). <sup>1</sup>H NMR (500 MHz, CDCl<sub>3</sub>) δ 1.04 (d, *J*= 7.45 Hz, 18 H), 1.14 (s, 3 H), 1.25 (s, 3 H), 1.29 (d, *J*= 6.8 Hz, 4 H), 1.58 (s, 3 H), 1.65 (s, 3 H), 1.69 – 1.72 (m, 6 H), 1.77 (m, 1 H), 1.90 (s, 6 H), 2.35 (s, 3 H), 2.41-2.43 (m, 2 H), 2.49-2.55 (m, 1 H), 2.59 (d, *J*= 3.6 Hz, 1 H), 2.92-2.96 (m, 1 H), 3.79 (d, *J*= 7 Hz, 1 H), 3.92 (dd, *J*<sub>a</sub>= 7.35 Hz, *J*<sub>b</sub>= 16.25 Hz, 1 H), 4.07 (dd, *J*<sub>a</sub>= 6.15 Hz, *J*<sub>b</sub>= 16.3 Hz, 1 H), 4.16 (d, *J*= 8.4 Hz, 1 H), 4.29 (d, *J*= 8.4 Hz, 1 H), 4.42 (m, 1 H), 4.79 (d, 2 H), 4.91 (m, 3 H), 5.06 (d, *J*= 8.55 Hz, 1 H), 5.65 (d, *J*= 7.05 Hz, 1 H), 6.18 (t, *J*= 9 Hz, 1 H), 6.27 (s, 1 H), 7.21 – 7.31 (m, 2 H), 7.47 (t, *J*= 7.8 Hz, 2 H), 7.59 (t, *J*= 7.4 Hz, 1 H), 7.79 (d, *J*= 7.8 Hz, 1 H), 8.10 (d, *J*= 7.3 Hz, 2 H). <sup>13</sup>C NMR (500 MHz, CDCl<sub>3</sub>) δ 9.1, 9.4, 9.5, 11.8, 13.0, 14.1, 14.8, 17.8, 18.5, 20.5, 20.5, 20.7, 22.2, 22.4, 22.6, 25.3, 25.7, 26.7, 28.2, 30.9, 30.9, 32.9, 33.0, 34.6, 35.4, 35.5, 38.8, 43.1, 45.5, 46.0, 46.0, 58.4, 71.8, 72.2, 74.9, 75.2, 75.4, 79.3, 80.9, 84.5, 127.7, 128.3, 128.6, 129.2, 130.1, 130.2, 130.8, 132.3, 133.1, 133.6, 137.4, 137.6, 154.9, 167.0, 168.0, 169.6, 170.1, 173.0, 175.1, 204.1. All data are in agreement with literature values.<sup>5</sup>

### Drug-Linker-Carboxylic Acid Compound (3-10)<sup>5</sup>

An aliquot of the Drug-Linker-TIPS compound **3-9** (450 mg, 0.35 mmol) was dissolved in a 1:1 mixture of acetonitrile:pyridine (~0.05 M) (14 mL) and cooled to 0 °C under inert conditions. To the mixture was added HF/pyridine (9.3 mL) dropwise (0.01 mL per every 1 mg will be added). The reaction was stirred at room temperature for 24 hours. Upon completion the reaction was quenched with 0.2 M citric acid in H<sub>2</sub>O (3.8 %) (30 mL) and extracted with ethyl acetate (30 mL x 3). The organic layer was collected, washed with CuSO<sub>4</sub>, washed with diluted water until the organic layer became clear, then washed with brine (30 mL x 3), dried over anhydrous MgSO<sub>4</sub>, and concentrated *in vacuo*. Purification was done *via* column chromatography on silica gel with increasing amounts of eluent (hexanes:ethyl acetate) to give **3-10** (326 mg, 0.3 mmol, 71 % yield). <sup>1</sup>H NMR (500 MHz, CDCl<sub>3</sub>) δ 1.34 (s, 9 H), 1.65 (s, 3 H), 1.70 (m, 6 H), 1.77 (m, 1 H), 1.90 (s, 3 H), 2.04 (s, 2 H), 2.36 (m, 6 H), 2.52 (m, 1 H), 3.78 (d, *J*= 6.45 Hz, 1 H), 3.93 (m, 1 H), 4.04-4.12 (m, 2 H), 4.16 (d, *J*= 8.2 Hz, 1 H), 4.29 (d, *J*= 8.4 Hz, 1 H), 4.41 (t, *J*= 7.45 Hz, 1 H), 4.95 (d, 3 H), 5.10 (d, 1 H), 5.65 (d, *J*= 6.85 Hz, 1 H), 6.19 (m, *J*= 7.6 Hz, 1 H), 6.28 (s, 1 H), 7.24 – 7.30 (m, 2 H), 7.46 (t, *J*= 7.35 Hz, 2 H), 7.59 (t, *J*= 7.25 Hz, 1 H), 7.79 (d, *J*= 7.45 Hz, 1 H), 8.08 (d, *J*= 7.4 Hz, 2 H). <sup>13</sup>C NMR (125 MHz, CDCl<sub>3</sub>) δ 9.2, 9.3, 9.5, 13.0, 13.7, 14.1, 14.2, 14.8, 18.5, 19.1, 20.2, 20.4, 22.1, 22.2, 22.4, 22.6, 25.7, 26.6, 28.2, 30.4, 30.6, 30.8, 31.6, 34.6, 35.4, 43.1, 45.7, 45.7, 48.9, 58.4, 60.4, 64.4, 71.7, 72.1, 72.1, 74.9, 75.2, 75.4, 75.5, 76.3, 79.2, 81.0, 81.0, 84.4, 127.7, 127.8, 128.3, 128.4, 128.6, 129.2, 130.1, 130.9, 132.4, 133.1, 133.2, 133.6, 143.4, 166.9, 168.2, 170.2, 175.1, 175.1, 177.0, 177.1. All data are in agreement with literature values.<sup>5</sup>

### Coupling-Ready Drug-Linker-OSu Construct (3-11)<sup>5</sup>

An aliquot of the deprotected drug-linker compound **3-10** (326 mg, 0.3 mmol), 1.2 eq EDC HCl salt (67 mg, 0.35 mmol) and 1.2 eq *N*-hydroxy succinimide (40 mg, 0.35 mmol) were dissolved in CH<sub>2</sub>Cl<sub>2</sub> (~0.02 M) (15 mL) and cooled to 0 °C. The reaction was stirred for 18 hours at room temperature and monitored *via* TLC. Upon completion, the solvent was evaporated and the residual was purified *via* column chromatography on silica gel with increasing amounts of eluent (hexanes:ethyl acetate) to give the desired activated Drug-Linker-OSu compound **3-11** (315 mg, 0.25 mmol, 85 % yield). <sup>1</sup>H NMR (500 MHz, CDCl<sub>3</sub>) δ 1.12 (s, 3 H), 1.23 (s, 6 H), 1.32 (s, 9 H), 1.63 (s, 3 H), 1.69 (m, 6 H), 1.75 (m, 1 H), 1.88 (s, 3 H), 1.93 (m, 1 H), 2.03 (m, 1 H), 2.33 (s, 6 H), 2.50 (m, 1 H), 2.64 (t, *J* = 7.5 Hz, 2 H), 2.79 (broad, 4 H), 2.95 (m, 1 H), 3.77 (d, *J* = 7 Hz, 1 H), 3.94 (dd, 1 H), 4.06-4.10 (dd, 1 H), 4.14 (d, *J* = 8.45 Hz, 1 H), 4.27 (d, *J* = 8.45 Hz, 1 H), 4.38 (q, *J* = 6.75 Hz, 1 H), 4.82 (dd, 1 H), 4.90-4.95 (m, 3 H), 5.07 (d, 1 H), 5.63 (d, *J* = 7.1 Hz, 1 H), 6.16 (t, *J* = 8.8 Hz, 1 H), 6.26 (s, 1 H), 7.22 – 7.33 (m, 2 H), 7.44 (t, *J* = 7.7 Hz, 2 H), 7.57 (t, *J* = 7.45 Hz, 1 H), 7.77 (d, *J* = 7.75 Hz, 1 H), 8.07 (d, *J* = 7.4 Hz, 2 H). <sup>13</sup>C NMR (125 MHz, CDCl<sub>3</sub>) δ 9.1, 9.3, 9.5, 13.0, 14.1, 14.8, 18.5, 20.3, 20.4, 22.2, 22.4, 22.6, 25.2, 25.5, 25.7, 26.6, 28.2, 28.2, 30.2, 30.2, 31.6, 34.6, 35.4, 35.5, 38.7, 38.7, 43.1, 45.5, 45.6, 45.6, 48.9, 58.4, 71.8, 72.1, 75.0, 75.2, 75.4, 76.3, 79.2, 79.8, 80.9, 84.5, 119.9, 128.0, 128.4, 128.6, 129.3, 130.1, 130.6, 130.6, 130.9, 132.4, 133.4, 133.4, 133.6, 137.1, 137.7, 143.4, 154.9, 166.9, 168.1, 168.1, 169.1, 169.6, 170.2, 170.2, 175.0, 204.1. HRMS (TOF) [M + H]<sup>+</sup> calcd. for C<sub>62</sub>H<sub>77</sub>N<sub>2</sub>O<sub>20</sub>S<sub>2</sub><sup>+</sup> 1233.4506, found 1233.4491. (Δ = -1.2 ppm). All data are in agreement with literature values.<sup>5</sup>

### SB-T-1214-fluorescein-methyl branched triisopropyl disulfide linker (3-12)

To an empty round bottomed flask were added **3-8** (38 mg, 0.084 mmol), 0.25 eq of DMAP (2.6 mg, 0.02 mmol), 1.5 eq of EDC HCl salt (24 mg, 0.126 mmol) and 1.1 eq of SB-T-1214-C7-fluorescein **2-8** (115 mg, 0.09 mmol) was dissolved in CH<sub>2</sub>Cl<sub>2</sub> (0.01 M) (9 mL). The reaction should be maintained under 0 °C at least 10 minutes, and then allowed to warm to room temperature. Then the reaction was allowed to stir for 16 hours. Upon completion, the solvent was evaporated and the residual was purified *via* column chromatography on silica gel with increasing amounts of eluent (dichloromethane: methanol) to give **3-12** (101 mg, 0.06 mmol, 73 % yield). <sup>1</sup>H NMR (500 MHz, CDCl<sub>3</sub>) δ 0.66 (t, *J* = 7.35 Hz, 6 H), 0.91-0.95 (m, 27 H), 1.36 (s, 9 H), 1.58 (m, 2 H), 1.68 (s, 3 H), 1.70 (s, 3 H), 1.78 (s, 3 H), 1.96 (s, 3 H), 2.06 (m, 2 H), 2.35 (s, 3 H), 2.61 (m, 1 H), 2.91 (m, 1 H), 3.70-3.80 (m, 2 H), 3.91-3.95 (m, 2 H), 4.06-4.11 (m, 3 H), 4.15 (d, *J* = 8.45 Hz, 1 H), 4.29 (d, *J* = 8.5 Hz, 1 H), 4.84 (m, 1 H), 4.93 (m, 3 H), 5.05 (d, *J* = 7.9 Hz, 1 H), 5.58 (t, *J* = 2.95 Hz, 1 H), 6.11 (t, *J* = 6.95 Hz, 1 H), 6.31 (t, *J* = 8.7 Hz, 1 H), 6.28 (s, 1 H), 6.43 (s, 1 H), 6.51 (d, *J* = 11.05 Hz, 1 H), 6.72 (d, *J* = 8.9 Hz, 1 H), 6.84 (m, 2 H), 6.94 (t, 1 H), 7.20 (m, 1 H), 7.27 (m, 2 H), 7.44 (t, *J* = 7.65 Hz, 2 H), 7.57 (t, *J* = 7.55 Hz, 1 H), 7.64 (t, *J* = 7.45 Hz, 1 H), 7.69 (t, *J* = 7.4 Hz, 1 H), 7.78 (t, *J* = 7.75 Hz, 1 H), 8.08 (d, *J* = 7.6 Hz, 2 H), 8.24 (d, *J* = 7.7 Hz, 1 H). <sup>13</sup>C NMR (125 MHz, CDCl<sub>3</sub>) δ 8.7, 8.8, 10.8, 11.4, 11.8, 12.8, 14.1, 14.5, 17.8, 18.5, 18.8, 18.9, 20.5, 20.5, 20.7, 21.4, 22.3, 22.6, 22.6, 23.7, 25.2, 25.7, 26.2, 27.5, 28.1, 28.2, 29.0, 29.7, 30.3, 30.3, 30.9, 30.9, 31.6, 32.9, 33.0, 33.3, 34.5, 34.6, 35.3, 36.0, 38.7, 43.2, 45.9, 46.0, 46.8, 56.0, 68.0, 71.5, 71.7, 71.8, 74.6, 74.8, 75.0, 78.7, 79.7, 80.6, 83.9, 100.7, 105.7, 113.9, 114.7, 117.5, 119.9, 127.7, 128.3, 128.6, 128.9, 129.2, 129.6, 129.8, 130.0, 130.1, 130.2, 130.5, 130.8, 130.8, 130.9, 131.3, 132.1, 132.5, 133.1, 133.6, 134.2, 137.3, 137.7, 150.4, 154.3, 155.0, 159.0, 163.6, 165.5, 166.9, 168.1, 169.5, 169.6, 169.9, 171.7, 172.8, 173.0,

185.6. HRMS (TOF)  $[M + H]^+$  calcd. for  $C_{95}H_{118}NO_{24}S_2Si^+$  1749.7283, found 1749.7279. ( $\Delta = -0.2$  ppm).

### SB-T-1214-fluorescein-methyl branched disulfide linker (3-13)

An aliquot of **3-12** (120 mg, 0.07 mmol) was dissolved in a 1:1 mixture of acetonitrile:pyridine (0.05 M) (1.4 mL) and cooled to 0 °C under inert conditions. To the mixture was added HF/pyridine (1.2 mL) dropwise (0.01 mL per every 1 mg was added). The reaction was allowed to warm to room temperature and stir for 24 hours. Upon completion the reaction was quenched with 0.2 M citric acid in H<sub>2</sub>O (3.8 %) (10 mL) and extracted with ethyl acetate (10 mL x 3). The organic layer was collected, washed with CuSO<sub>4</sub>, washed with diluted water until the organic layer became clear, then washed with brine (10 mL x 3), dried over anhydrous MgSO<sub>4</sub>, and concentrated *in vacuo*. Purification was done *via* column chromatography on silica gel with increasing amounts of eluent (dichloromethane: methanol) to yield **3-13** (79 mg, 0.05 mmol, 71 % yield). <sup>1</sup>H NMR (500 MHz, CDCl<sub>3</sub>)  $\delta$  0.66-0.70 (m, 6 H), 0.88 (m, 3 H), 1.16 (s, 3 H), 1.22 (s, 3 H), 1.24 (s, 3 H), 1.26 (d, 3 H), 1.34 (s, 9 H), 1.58 (m, 2 H), 1.64 (m, 1 H), 1.70 (s, 3 H), 1.78 (s, 3 H), 1.96 (s, 3 H), 2.03 (m, 3 H), 2.37 (m, 3 H), 2.60 (m, 1 H), 2.95 (m, 1 H), 3.70-3.79 (m, 2 H), 3.92-3.95 (m, 3 H), 4.07-4.10 (t, 2 H), 4.30 (d,  $J = 8.45$  Hz, 1 H), 4.94 (t,  $J = 8.2$  Hz, 3 H), 5.57 (t,  $J = 7.7$  Hz, 1 H), 5.66 (d,  $J = 6.9$  Hz, 1 H), 6.15 (q,  $J = 7.5$  Hz, 1 H), 6.28 (s, 1 H), 6.56 (s, 1 H), 6.59 (d,  $J = 9.7$  Hz, 1 H), 6.74 (d,  $J = 8.95$  Hz, 1 H), 6.88 (t,  $J = 10$  Hz, 2 H), 6.99 (s, 1 H), 7.21-7.28 (m, 4 H), 7.45 (t,  $J = 7.65$  Hz, 2 H), 7.58 (t,  $J = 7.5$  Hz, 1 H), 7.65 (t,  $J = 7.2$  Hz, 1 H), 7.70 (t,  $J = 7.45$  Hz, 1 H), 7.78 (d,  $J = 7.8$  Hz, 1 H), 8.08 (d,  $J = 8.15$  Hz, 2 H), 8.25 (d,  $J = 7.75$  Hz, 1 H). <sup>13</sup>C NMR (125 MHz, CDCl<sub>3</sub>)  $\delta$  8.7, 10.8, 12.8, 14.1, 14.6, 18.5, 18.8, 18.9, 20.3, 20.4, 21.3, 22.3, 22.7, 22.9, 23.6, 23.7, 25.2, 25.7, 27.5, 28.1, 28.2, 29.3, 29.7, 30.1, 30.4, 30.7, 30.7, 31.1, 31.9, 33.3, 35.3, 38.7, 43.2, 45.7, 46.0, 46.9, 49.0, 55.9, 68.0, 71.5, 71.8, 74.6, 74.8, 75.0, 76.3, 78.7, 79.8, 80.7, 83.9, 100.6, 105.4, 114.6, 114.7, 117.3, 119.9, 127.7, 128.3, 128.6, 129.0, 129.1, 129.5, 129.7, 130.1, 130.5, 130.7, 130.7, 131.0, 131.3, 132.1, 132.5, 133.2, 133.7, 134.1, 141.9, 151.8, 154.6, 159.3, 164.0, 165.4, 166.9, 168.3, 170.1, 171.8, 172.8, 175.7, 185.7, 202.5. HRMS (TOF)  $[M + H]^+$  calcd. for  $C_{86}H_{98}NO_{24}S_2^+$  1592.5915, found 1592.5934. ( $\Delta = 1.2$  ppm).

### SB-T-1214-fluorescein-methyl branched disulfide linker OSu activated ester (3-14)

An aliquot of **3-13** (79 mg, 0.05 mmol), 1.2 eq of *N*-hydroxy succinimide (6.3 mg, 0.055 mmol) and 1.2 eq of EDC HCl salt (10.5 mg, 0.055 mmol) were dissolved in CH<sub>2</sub>Cl<sub>2</sub> (~0.01 M) (5 mL) at room temperature. The reaction was stirred for 18 hours. Upon completion, the solvent was evaporated and the residual was purified *via* column chromatography on silica gel with increasing amounts of eluent (dichloromethane: methanol) to give the product **3-14** (73 mg, 0.043 mmol, 86 %) as yellow solid. <sup>1</sup>H NMR (500 MHz, CDCl<sub>3</sub>)  $\delta$  0.66-0.69 (m, 6 H), 0.86-0.91 (m, 3 H), 0.98 (m, 1 H), 1.04 (m, 1 H), 1.15 (s, 3 H), 1.21 (s, 3 H), 1.24 (s, 3 H), 1.28 (m, 3 H), 1.33 (s, 9 H), 1.57 (m, 2 H), 1.68 (d,  $J = 9.3$  Hz, 6 H), 1.77 (s, 3 H), 1.83 (m, 1 H), 1.94 (s, 3 H), 2.02 (s, 1 H), 2.05-2.12 (m, 3 H), 2.35 (s, 3 H), 2.44 (m, 2 H), 2.55 (m, 1 H), 2.63 (m, 2 H), 2.80 (broad, 4 H), 2.95 (m, 1 H), 3.69-3.79 (m, 2 H), 3.92-3.96 (m, 2 H), 4.06-4.10 (m, 3 H), 4.14 (d,  $J = 8.45$  Hz, 1 H), 4.29 (d,  $J = 8.45$  Hz, 1 H), 4.83 (d, 1 H), 4.93 (s, 3 H), 5.07 (m, 1 H), 5.56 (q,  $J = 7.45$  Hz, 1 H), 5.66 (d,  $J = 6.9$  Hz, 1 H), 6.12 (t,  $J = 8.7$  Hz, 1 H), 6.27 (s, 1 H), 6.43 (s, 1 H), 6.51 (d,  $J = 9.7$  Hz, 1 H), 6.71 (d,  $J = 8.95$  Hz, 1 H), 6.84-6.88 (m, 2 H), 6.94 (t,  $J = 2.4$  Hz, 1 H), 7.21-7.31 (m, 3 H), 7.44 (t,  $J = 7.7$  Hz, 2 H), 7.57 (t,  $J = 7.45$  Hz, 1 H), 7.64 (t,  $J = 7.55$  Hz, 1 H), 7.69 (t,  $J$

= 7.35 Hz, 1 H), 7.76 (d,  $J = 7.75$  Hz, 1 H), 8.08 (d,  $J = 7.45$  Hz, 2 H), 8.23 (d,  $J = 7.75$  Hz, 1 H).  $^{13}\text{C}$  NMR (125 MHz,  $\text{CDCl}_3$ )  $\delta$  8.7, 8.8, 10.8, 12.8, 14.1, 14.2, 14.5, 18.5, 18.8, 18.9, 20.3, 20.4, 21.0, 21.4, 22.3, 23.7, 25.5, 25.7, 26.2, 27.5, 28.2, 29.7, 30.2, 30.3, 30.3, 30.3, 31.5, 33.3, 35.3, 38.7, 38.7, 43.2, 45.5, 45.6, 46.8, 49.0, 56.0, 60.4, 68.0, 71.5, 71.7, 71.8, 74.6, 74.8, 75.0, 76.3, 78.7, 79.8, 80.6, 83.9, 100.7, 105.7, 113.9, 114.7, 117.4, 119.9, 127.9, 128.4, 128.6, 128.9, 129.2, 129.6, 129.8, 130.1, 130.3, 130.5, 130.5, 130.8, 130.9, 131.0, 131.3, 132.1, 132.5, 133.3, 133.4, 133.6, 134.2, 137.1, 137.1, 137.8, 141.9, 150.5, 154.3, 155.0, 159.0, 163.6, 165.5, 166.8, 168.1, 169.1, 169.5, 170.0, 171.1, 171.7, 172.8, 185.6, 202.5. HRMS (TOF)  $[\text{M} + \text{H}]^+$  calcd. for  $\text{C}_{90}\text{H}_{101}\text{N}_2\text{O}_{26}\text{S}_2^+$  1689.6078, found 1689.6060. ( $\Delta = -1$  ppm).

### **Methyl 5-((3aS,4S,6aR)-2-oxohexahydro-1H-thieno[3,4-d]imidazol-4-yl)pentanoate (3-15)<sup>24</sup>**

To a 25 mL round bottomed flask was added D-(+)-biotin (400 mg, 1.64 mmol) dissolved in 0.1 M methanol (16 mL) and cool to 0 °C. To this suspension was added 4 eq thionyl chloride (779 mg, 6.55 mmol, 0.5 mL) slowly and turned to clear solution. The resulting solution was allowed to warm to room temperature and stirred for 16 hours. The reaction was monitored by TLC. Upon completion, the solvent was removed by rotary evaporation and get the yellowish crude solid. The residue was purified *via* column chromatography on silica gel with increasing amounts of eluent (dichloromethane:methanol) to yield the off-white solid **3-15** (417 mg, 1.61 mmol, 98 % yield).  $^1\text{H}$  NMR (300 MHz,  $\text{CDCl}_3$ )  $\delta$  1.41 (m, 2 H), 1.67 (m, 2 H), 2.34 (t,  $J = 7.2$  Hz, 2 H), 2.71 (d,  $J = 12.6$  Hz, 1 H), 2.91 (dd,  $J_a = 12.9$  Hz,  $J_b = 4.8$  Hz, 1 H), 3.15 (m, 1 H), 3.67 (s, 3 H), 4.32 (m, 1 H), 4.51 (m, 1 H), 4.883 (s, 1 H), 5.20 (s, 1 H). All data are in agreement with literature values.<sup>24</sup>

### **5-((3aS,4S,6aR)-2-Oxohexahydro-1H-thieno[3,4-d]imidazol-4-yl)pentanehydrazide (3-16)<sup>24</sup>**

To a 25 mL round bottomed flask was added **3-15** (300 mg, 1.16 mmol) dissolved in methanol (10 mL) under room temperature. To this solution was added 4 eq hydrazine monohydrate (233 mg, 4.65 mmol, 0.23 mL) slowly and suspension generated. Then the suspension was allowed to heat to reflux for 22 hours. Upon completion, the precipitate was isolate by filtration and washed with methanol. The combined white solid was dried with lyophilization to yield white solid **3-16** (295 mg, 1.14 mmol, 99 % yield).  $^1\text{H}$  NMR (300 MHz,  $\text{CDCl}_3$ )  $\delta$  1.21 (m, 2 H), 1.43 (m, 4 H), 2.06 (t,  $J = 7.2$  Hz, 2 H), 2.59 (d,  $J = 13.2$  Hz, 1 H), 2.81 (dd,  $J_a = 12.9$  Hz,  $J_b = 4.8$  Hz, 1 H), 3.16 (m, 1 H), 4.24 (m, 1 H), 4.42 (m, 1 H). All data are in agreement with literature values.<sup>24</sup>

### **Biotin-methyl branched disulfide linker-SB-T-1214 (BLT) (3-17)**

To a 25 mL round bottomed flask was added **3-11** (697 mg, 0.56 mmol) and 1 eq **3-16** (144 mg, 0.56 mmol) dissolved in DMSO/pyridine=3:1 (7.2 mL/2.4 mL) under 0 °C. Then the solution was allowed to warm to room temperature and allowed to stir for 5 days. Upon completion, the solvent was removed by rotary evaporation and the residue was purified *via* column chromatography on silica gel with increasing amounts of eluent (dichloromethane:methanol) to white solid **3-17** (608 mg, 0.44 mmol, 79 % yield).  $^1\text{H}$  NMR (500 MHz,  $\text{CDCl}_3$ )  $\delta$  0.97 (t,  $J = 8.25$  Hz, 2 H), 1.11 (t,  $J = 4.3$  Hz, 2 H), 1.16 (s, 3 H), 1.22 (s, 3 H), 1.28 (d,  $J = 6.7$  Hz, 2 H), 1.36 (s, 6 H), 1.66 (s, 3 H), 1.71 (s, 6 H), 1.72 (s, 6 H), 1.91 (s, 2 H), 2.20 (m, 3 H), 2.35 (d,  $J = 6.4$  Hz, 3 H), 2.50 (quint,  $J = 6.8$  Hz, 1 H), 2.61 (s, 1 H), 2.70 (d,  $J = 13.05$  Hz, 1 H), 2.86-2.93 (m, 2 H), 3.08 (q,  $J = 6.6$  Hz, 1 H), 3.47 (m, 1 H), 3.79 (d,  $J = 7$  Hz, 1 H), 3.97 (d,  $J = 16.8$  Hz, 1 H), 4.06 (dd,  $J_a = 16.45$  Hz,  $J_b =$

4.45 Hz, 1 H), 4.15 (d,  $J = 8.5$  Hz, 1 H), 4.28 (m, 2 H), 4.39 (m, 1 H), 4.46 (m, 1 H), 4.96 (m, 3 H), 5.11 (m, 1 H), 5.66 (d,  $J = 6.95$  Hz, 1 H), 5.84 (d,  $J = 7.4$  Hz, 1 H), 6.16 (m, 1 H), 6.32 (d,  $J = 2.1$  Hz, 1 H), 6.84 (s, 1 H), 7.23 (m, 1 H), 7.30 (m, 1 H), 7.46 (t,  $J = 7.75$  Hz, 2 H), 7.59 (t,  $J = 7.45$  Hz, 1 H), 7.77 (d,  $J = 7.95$  Hz, 1 H), 8.09 (d,  $J = 7.95$  Hz, 2 H), 8.55 (broad, 1 H), 9.44 (broad, 1 H).  $^{13}\text{C}$  NMR (125 MHz,  $\text{CDCl}_3$ )  $\delta$  9.2, 9.3, 10.5, 13.9, 15.1, 18.7, 20.9, 22.5, 23.3, 26.2, 26.4, 27.1, 28.9, 29.4, 29.6, 32.1, 32.4, 34.4, 37.6, 40.5, 41.1, 44.7, 47.3, 48.2, 57.0, 59.4, 61.7, 63.3, 72.4, 76.4, 76.6, 76.8, 77.5, 79.2, 82.4, 86.0, 121.3, 129.0, 129.5, 129.8, 131.2, 131.5, 131.6, 132.5, 134.7, 134.9, 135.0, 138.8, 138.9, 138.9, 142.7, 157.6, 166.2, 167.7, 170.4, 171.6, 172.4, 174.2, 174.9, 175.2, 205.2. HR-MS  $[\text{M}+\text{H}]^+$  calcd. 1376.5387, found: 1376.5378. ( $\Delta = -0.6$  ppm).

### 1-Azido-2-(2-(2-(2-azidoethoxy)ethoxy)ethoxy)ethane (3-18)<sup>25</sup>

To a 100 mL round bottomed flask was added an aliquot of tetra ethylene glycol (10 g, 50 mmol) dissolved in 1 M THF (50 mL) in an ice-bath. The resulting solution was allowed to stir under 0 °C for 10 minutes, then 2.5 eq methanesulfonyl chloride (14.7 g, 120 mmol, 9.9 mL) was slowly added, followed by addition of 2.5 eq triethylamine (12 g, 120 mmol, 16.7 mL) dropwise. White precipitate was formed while TEA was adding. Then the ice-bath was removed and the suspension solution was stirred for 4 hours. Then the organic solvent was removed by rotary evaporation and the yellow residue was dissolved in distilled water (50 mL). The aqueous solution was allowed to stir in a chilled ice-bath and sodium bicarbonate (solid) was used to adjust the pH to 8. Then 2.5 eq sodium azide (7.8 g, 120 mmol) was added slowly and the suspension solution was allowed to reflux for 19 hours. Upon completion, the product was extract with ether (150 mL), then washed with brine (50 mLx3), dried over anhydrous  $\text{MgSO}_4$  and concentrated *in vacuo*. Purification was done *via* column chromatography on silica gel with increasing amounts of eluent (hexane:ethyl acetate) to yield **3-18** (8.1 g, 33 mmol, 66 % yield) in light yellow oil.  $^1\text{H}$  NMR (500 MHz,  $\text{CDCl}_3$ )  $\delta$  3.36 (t,  $J = 4.8$  Hz, 4 H), 3.66 (m, 12 H).  $^{13}\text{C}$  NMR (125 MHz,  $\text{CDCl}_3$ )  $\delta$  50.6, 70.0, 70.7. HRMS  $[\text{M}+\text{Na}]^+$   $\text{C}_8\text{H}_{16}\text{N}_6\text{NaO}_3^+$  calcd. 267.1176, found: 267.1181. ( $\Delta = 1.8$  ppm). All data are in agreement with literature values.<sup>25</sup>

### 2-(2-(2-(2-Azidoethoxy)ethoxy)ethoxy)ethanamine (3-19)<sup>25</sup>

To a 250 mL round bottomed flask was added **3-18** (7.3 g, 30 mmol) dissolved in 0.65 M  $\text{H}_3\text{PO}_4$  (aq) (80 mL) which previously prepared by dilution using distilled water under room temperature. To this solution was slowly added 0.9 eq triphenyl phosphine (7 g, 27 mmol) in ether (60 mL) and the resulting solution was allowed to stir for 22 hours. The reaction mixture was separated to two layers. To the bottom aqueous layer was added 6 g potassium hydroxide pellets and stored in the freezer under 0 °C for overnight. Then the product was extract with dichloromethane (250 mL), then washed with brine (100 mLx3), dried over anhydrous  $\text{MgSO}_4$  and concentrated *in vacuo*. Purification was done *via* column chromatography on alumina gel with increasing amounts of eluent (dichloromethane:methanol) to give **3-19** (4.1 g, 19 mmol, 63 %) as light yellow oil.  $^1\text{H}$  NMR (500 MHz,  $\text{CDCl}_3$ )  $\delta$  2.91 (t,  $J = 5.1$  Hz, 2 H), 3.38 (t,  $J = 4.8$  Hz, 2 H), 3.54 (t,  $J = 5.1$  Hz, 2 H), 3.62-3.67 (m, 10 H).  $^{13}\text{C}$  NMR (125 MHz,  $\text{CDCl}_3$ )  $\delta$  41.3, 50.7, 70.0, 70.2, 70.5, 70.6, 71.9. HRMS  $[\text{M}+\text{H}]^+$   $\text{C}_8\text{H}_{19}\text{N}_4\text{O}_3^+$  calcd. 219.1452, found: 219.1457. ( $\Delta = 2.3$  ppm). All data are in agreement with literature values.<sup>25</sup>

### 1H-Thieno[3,4-d]imidazole-4-pentanoic acid (Biotin-OSu activated ester) (3-20)

To a 25 mL round bottomed flask was added D (+)-biotin (366 mg, 1.5 mmol) and 3 eq *N*-hydroxysuccinimide (517 mg, 4.5 mmol). Then 7.5 mL of dimethylformamide was added and the resulting solution was heated to 45 °C while stirring under inert condition. After heating, DIC (*N,N'*-diisopropylcarbodiimide) (378 mg, 0.46 mL, 3 mmol) was added dropwise and solution slowly turn to yellow. The resulting solution was allowed to stir for 18 hours and then cooled to room temperature. After the reaction, 20 mL isopropanol was added and a white precipitate crushed out and was filtered out. Then the white solid was washed by isopropanol and generate white solid which was subsequently dried *in vacuo* to give **3-20** (300 mg, 0.88 mmol) in 59 % yield. <sup>1</sup>H NMR (500 MHz, CD<sub>3</sub>OD) δ 1.51- 1.62 (m, 2 H), 1.73-1.83 (m, 4 H), 2.65 (t, 3 H), 2.82 (s, 4 H), 2.90 (d, 1 H), 2.94 (d, 1 H), 3.22 (m, 1 H), 4.30 (m, 1 H), 4.48 (m, 1 H). <sup>13</sup>C NMR (125 MHz, CD<sub>3</sub>OD) δ 22.1, 24.6, 28.0, 28.3, 28.6, 30.5, 32.4, 39.6, 41.3, 55.5, 60.2, 61.9. HRMS [M+H]<sup>+</sup> C<sub>14</sub>H<sub>20</sub>N<sub>3</sub>O<sub>5</sub>S<sup>+</sup> calcd. 342.1118, found: 342.1121. (Δ = 0.8 ppm).

***N*-(2-(2-(2-(2-Azidoethoxy)ethoxy)ethoxy)ethyl)-5-((3a*S*,4*S*,6a*R*)-2-oxohexahydro-1*H*-thieno[3,4-*d*]imidazol-4-yl)pentanamide (3-21)<sup>26</sup>**

To a 100 mL round bottomed flask was added **3-20** (489 mg, 1.43 mmol) and 1 eq **3-19** (312 mg, 1.43 mmol) dissolved in 0.1 M CH<sub>2</sub>Cl<sub>2</sub> (14 mL). The resulting solution was allowed to stir under room temperature for 18 hours. Upon completion, the solvent was removed and the crude product was purified by silica gel column chromatography eluting 0-10 % methanol in dichloromethane to yield **3-21** as a light yellow sticky solid (371 mg, 0.84 mmol, 55 %). <sup>1</sup>H NMR (500 MHz, CDCl<sub>3</sub>) δ 1.38 (quart, *J* = 7.4 Hz, 2 H), 1.60 (m, *J* = 7.85 Hz, 2 H), 1.76 (m, *J* = 7.95 Hz, 2 H), 2.19 (t, *J* = 7.55 Hz, 2 H), 2.71 (d, *J* = 12.75 Hz, 1 H), 2.86 (dd, *J*<sub>a</sub> = 4.9 Hz, *J*<sub>b</sub> = 12.8 Hz, 1 H), 3.10 (m, 1 H), 3.37 (t, *J* = 4.9 Hz, 2 H), 3.40 (m, 2 H), 3.53 (t, *J* = 5 Hz, 2 H), 3.59-3.66 (m, 10 H), 4.28 (m, 1 H), 4.47 (m, 1 H), 5.82 (s, 1 H), 6.69 (s, 1 H), 6.84 (t, *J* = 5.45 Hz, 1 H). <sup>13</sup>C NMR (125 MHz, CDCl<sub>3</sub>) δ 25.6, 28.0, 28.2, 35.9, 39.1, 40.5, 50.6, 55.7, 60.2, 61.8, 69.9, 70.0, 70.4, 70.6, 164.3, 173.5. HRMS calcd. for C<sub>18</sub>H<sub>33</sub>N<sub>6</sub>O<sub>5</sub>S<sup>+</sup> [M+H]<sup>+</sup> 445.2228, found 445.2223. (Δ = -1.1 ppm). All data are in agreement with literature values.<sup>26</sup>

***N*-(2-(2-(2-(2-Aminoethoxy)ethoxy)ethoxy)ethyl)-5-((3a*S*,4*S*,6a*R*)-2-oxohexahydro-1*H*-thieno[3,4-*d*]imidazol-4-yl)pentanamide (3-22)<sup>27</sup>**

To a 50 mL round bottomed flask was added **3-21** (331 mg, 0.75 mmol) dissolved in 0.04 M EtOH. To the resulting solution was added 5mol% Pd/C (10 %wt on carbon) powder and aspirate the inside air and refilled with hydrogen gas. The reaction was allowed to stir under room temperature for 5 hours. Upon completion, the Pd/C was removed by filtration with celite, and the solvent was evaporate and the product **3-22** was obtained as sticky solid (302 mg, 0.72 mmol) in 96 % yield. <sup>1</sup>H NMR (500 MHz, CD<sub>3</sub>OD) δ 1.40 (quart, *J* = 7.75 Hz, 2 H), 1.55-1.76 (m, 4 H), 2.19 (t, *J* = 7.45 Hz, 2 H), 2.68 (d, *J* = 12.75 Hz, 1 H), 2.80 (t, *J* = 5.3 Hz, 1 H), 2.90 (dd, *J*<sub>a</sub> = 5 Hz, *J*<sub>b</sub> = 12.75 Hz, 1 H), 3.18 (quart, *J* = 5.6 Hz, 1 H), 3.33 (t, *J* = 5.5 Hz, 2 H), 3.51 (m, 4 H), 3.60-3.65 (m, 8 H), 4.28 (dd, *J*<sub>a</sub> = 4.45 Hz, *J*<sub>b</sub> = 7.85 Hz, 1 H), 4.47 (dd, *J*<sub>a</sub> = 4.9 Hz, *J*<sub>b</sub> = 7.8 Hz, 1 H). <sup>13</sup>C NMR (125 MHz, CD<sub>3</sub>OD) δ 25.4, 28.1, 28.3, 35.3, 38.9, 39.6, 40.5, 55.6, 60.2, 61.9, 69.2, 69.8, 70.1, 71.3, 164.7, 174.7. HRMS calcd. for C<sub>18</sub>H<sub>35</sub>N<sub>4</sub>O<sub>5</sub>S<sup>+</sup> [M+H]<sup>+</sup> 419.2323, found 419.2326. (Δ = 0.7 ppm). All data are in agreement with literature values.<sup>27</sup>

### Biotin-PEG<sub>3</sub>-(CH<sub>2</sub>)<sub>2</sub>-(SS-Linker)-SB-T-1214 (BLT-S) (3-23)

To a round bottom flask were added biotin-PEG<sub>3</sub>-amine **3-22** (30 mg, 0.07 mmol) and 1 equivalent SB-T-1214-(SS-Linker)-OSu ester **3-11** (90 mg, 0.07 mmol) dissolved in 0.01 M DCM (7 mL) under room temperature. The reaction was allowed to stir for 16 hours and monitored by TLC. Upon completion, the solvent was removed and the crude was purified *via* column chromatography on silica gel with increasing amounts of eluent (dichloromethane:methanol) to give BLT-S **3-23** as an off-white solid (71 mg, 0.046 mmol) in 66 % yield. <sup>1</sup>H NMR (700 MHz, CDCl<sub>3</sub>) δ 0.94 (t, *J* = 8.2 Hz, 2 H), 1.08 (m, 3 H), 1.13 (s, 3 H), 1.22 (s, 3 H), 1.33 (s, 9 H), 1.63 (s, 3 H), 1.68 (t, *J* = 8.05 Hz, 6 H), 1.88 (s, 3 H), 2.18 (m, 3 H), 2.33 (s, 3 H), 2.63 (s, 1 H), 2.68 (m, 2 H), 2.83 (m, 2 H), 3.10 (m, 2 H), 3.34 (m, 3 H), 3.39 (m, 3 H), 3.49 (q, *J* = 3.7 Hz, 2 H), 3.52 (m, 2 H), 3.60-3.67 (m, 12 H), 3.78 (m, 2 H), 3.93 (d, *J* = 16.45 Hz, 1 H), 4.05 (d, *J* = 16.45 Hz, 1 H), 4.30 (d, *J* = 16.35 Hz, 1 H), 4.14 (d, *J* = 8.35 Hz, 1 H), 4.26 (m, 2 H), 4.37 (m, 1 H), 4.43 (m, 1 H), 4.91 (m, 3 H), 5.00 (s, 2 H), 5.63 (m, 2 H), 6.15 (m, 1 H), 6.29 (s, 1 H), 6.45 (s, 1 H), 6.56 (s, 1 H), 6.87 (s, 1 H), 7.21 (m, 2 H), 7.28 (m, 1 H), 7.43 (t, *J* = 7.65 Hz, 2 H), 7.56 (t, *J* = 7.4 Hz, 1 H), 7.75 (q, *J* = 3.85 Hz, 1 H), 8.07 (d, *J* = 7.55 Hz, 2 H). <sup>13</sup>C NMR (176 MHz, CDCl<sub>3</sub>) δ 9.1, 9.2, 9.6, 13.0, 14.7, 18.3, 18.5, 20.6, 22.1, 22.4, 25.6, 25.7, 26.6, 28.0, 28.2, 29.7, 31.3, 33.3, 33.4, 35.4, 35.7, 35.8, 35.9, 38.7, 39.1, 40.5, 42.8, 43.2, 45.8, 46.2, 46.3, 46.9, 49.0, 50.6, 53.4, 55.6, 56.6, 58.3, 60.2, 61.8, 69.8, 69.9, 70.0, 70.3, 70.4, 71.8, 75.0, 75.1, 75.4, 76.3, 79.0, 79.8, 81.0, 84.4, 119.9, 127.7, 128.3, 128.6, 129.3, 130.1, 130.3, 131.0, 132.6, 133.2, 133.6, 137.4, 137.5, 137.8, 142.9, 155.0, 164.1, 166.8, 168.2, 169.7, 170.4, 172.5, 173.5, 174.8, 204.0. HRMS (TOF) [M + H]<sup>+</sup> calcd. for C<sub>76</sub>H<sub>106</sub>N<sub>5</sub>O<sub>22</sub>S<sub>3</sub><sup>+</sup> [M + H]<sup>+</sup> 1536.6486, found 1536.6468. (Δ = -1.1 ppm).

### Biotin-PEG-FITC (3-24)

To a 10 mL round bottomed flask were added **3-22** (40 mg, 0.1 mmol) and 1 eq FITC (37 mg, 0.1 mmol) dissolved in DMF (1 mL). To this solution was added DIPEA (25 μL) and the resulting solution turned to dark red. The reaction was allowed to stir for 24 hours in dark, and the resulting crude product was concentrated and purified by prep HPLC using a Jupiter C18 preparative HPLC column (5 μm, 300 Å, 250 × 21.2 mm) on a Shimadzu CBM-10AW VP communications bus module, Shimadzu SPD-10A VP UV-Vis detector, and Shimadzu LC-6AD liquid chromatography assembly, employing methanol/water as the gradient solvent system, a flow rate of 10 mL/min under room temperature and with the UV detector set at 275 and 230 nm. The gradient was run from 20% to 95% methanol in water over a 30 minute period. The fractions containing **3-24** were combined and lyophilized to give **3-24** as orange solid (57 mg, 0.071 mmol) in 70 % yield. <sup>1</sup>H NMR (500 MHz, DMSO-*d*<sub>6</sub>) δ 1.28-1.34 (m, 2 H), 1.42-1.50 (m, 3 H), 1.58-1.64 (m, 1 H), 2.06 (t, *J* = 7.3 Hz, 2 H), 2.51 (s, 1 H), 2.57 (d, *J* = 12.4 Hz, 1 H), 2.80 (dd, *J* = 5.3 Hz, 1 H), 2.90 (dd, *J*<sub>a</sub> = 5 Hz, *J*<sub>b</sub> = 12.75 Hz, 1 H), 3.18 (quart, *J* = 5.6 Hz, 1 H), 3.33 (t, *J* = 5 Hz, 12.35 Hz, 1 H), 3.08 (m, 1 H), 3.17 (quart, *J* = 5.7 Hz, 2 H), 3.39 (t, *J* = 5.85 Hz, 3 H), 3.52-3.60 (m, 10 H), 3.67 (m, 2 H), 4.12 (m, 1 H), 4.29 (m, 1 H), 6.37 (s, 1 H), 6.44 (s, 1 H), 6.54 (d, *J* = 8.6 Hz, 2 H), 6.62 (m, 4 H), 7.15 (d, *J* = 8.25 Hz, 1 H), 7.72 (d, *J* = 6.9 Hz, 1 H), 7.84 (d, *J* = 5.4 Hz, 1 H), 8.29 (s, 1 H), 8.35 (s, 1 H), 10.3 (s, 1 H). <sup>13</sup>C NMR (500 MHz, DMSO-*d*<sub>6</sub>) δ 25.7, 28.5, 28.6, 35.5, 38.9, 44.1, 55.9, 59.6, 61.5, 68.8, 69.6, 70.0, 70.1, 70.2, 102.7, 110.7, 114.5, 117.9, 125.3, 128.7, 129.7, 141.7, 153.1, 163.2, 169.1, 172.6, 181.0. HRMS [M+H]<sup>+</sup> for C<sub>39</sub>H<sub>46</sub>N<sub>5</sub>O<sub>10</sub>S<sub>2</sub><sup>+</sup> calcd. 808.2681, found 808.2674. M.P. 135-136 °C. (Δ = -0.8 ppm).



### Biotin-PEG-Fluorescein (3-25)

To a round bottomed flask were added biotin-PEG<sub>3</sub>-amine **3-22** (27 mg, 0.064 mmol) and 0.9 eq fluorescein OSu ester **3-14** (33 mg, 0.058 mmol) dissolved in CH<sub>2</sub>Cl<sub>2</sub> under room temperature. The reaction was allowed to stir for 24 hours and monitored by TLC. Upon completion, the solvent was removed and the crude was purified *via* column chromatography on silica gel with increasing amounts of eluent (dichloromethane:methanol) to yield **3-25** as a sticky orange solid (43 mg, 0.049 mmol) in 85 % yield. <sup>1</sup>H NMR (700 MHz, CD<sub>3</sub>OD) δ 0.70 (t, *J* = 6.09 Hz, 6 H), 1.42 (quint, *J* = 6.93 Hz, 2 H), 1.59 (m, 2 H), 1.64 (m, 2 H), 1.71 (m, *J* = 6.72 Hz, 2 H), 2.15 (quint, *J* = 6.79 Hz, 2 H), 2.20 (t, *J* = 7.28 Hz, 2 H), 2.43 (t, *J* = 7.28 Hz, 2 H), 2.69 (d, *J* = 12.39 Hz, 1 H), 2.90 (dd, *J<sub>a</sub>* = 12.74 Hz, *J<sub>b</sub>* = 4.9 Hz, 2 H), 3.19 (m, 1 H), 3.32 (s, 3 H), 3.35 (q, *J* = 5.39 Hz, 2 H), 3.38 (q, *J* = 5.39 Hz, 2 H), 3.53 (q, *J* = 5.46 Hz, 2 H + 2 H), 3.61 (dd, *J<sub>a</sub>* = 14.49 Hz, *J<sub>b</sub>* = 2.31 Hz, 8 H), 3.73-3.81 (m, 2 H), 4.21 (t, *J* = 6.16 Hz, 2 H), 4.29 (m, 1 H), 4.48 (m, 1 H), 6.51 (d, *J* = 1.68 Hz, 1 H), 6.59 (dd, *J<sub>a</sub>* = 9.66 Hz, *J<sub>b</sub>* = 1.75 Hz, 1 H), 6.96 (dd, *J<sub>a</sub>* = 8.96 Hz, *J<sub>b</sub>* = 2.17 Hz, 1 H), 7.06 (m, 2 H), 7.25 (d, *J* = 2.1 Hz, 1 H), 7.44 (d, *J* = 7.42 Hz, 1 H), 7.80 (t, *J* = 7.7 Hz, 1 H), 7.85 (t, *J* = 7.7 Hz, 1 H), 8.00 (m, 1 H), 8.09 (m, 1 H), 8.31 (d, *J* = 7.91 Hz, 1 H). <sup>13</sup>C NMR (176 MHz, CD<sub>3</sub>OD) δ 17.8, 17.9, 24.8, 25.4, 27.4, 28.1, 28.3, 31.8, 31.9, 35.3, 35.4, 39.0, 39.1, 39.6, 55.5, 60.2, 61.9, 68.1, 69.2, 69.8, 70.1, 71.4, 100.6, 104.1, 114.6, 114.8, 116.7, 128.0, 129.5, 129.9, 130.3, 130.5, 130.9, 131.2, 132.6, 133.6, 154.7, 154.9, 160.0, 164.6, 164.8, 165.4, 173.8, 173.9, 174.6, 174.7, 185.7. HRMS (TOF) [M + H]<sup>+</sup> calcd. for C<sub>46</sub>H<sub>59</sub>N<sub>4</sub>O<sub>11</sub>S<sup>+</sup> [M + H]<sup>+</sup> 875.3896, found 875.3909. (Δ = 1.5 ppm). LC-UV-TOF t<sub>R</sub> = 13.19 min.

### 11-Azido-3,6,9-trioxaundecanyl-1-methylsulfonate (3-27)<sup>16,28</sup>

To a cooled solution of 11-azido-3,6,9-trioxaundecan-1-ol **3-26** (404 mg, 1.84 mmol) in dichloromethane (18 mL) at 0 °C was added 3 eq Et<sub>3</sub>N (559 mg, 5.5 mmol, 0.77 mL) and 1.2 eq methanesulfonyl chloride (252 mg, 2.2 mmol, 0.17 mL), and the mixture was allowed to stir for 3 h at 0 °C. The reaction was diluted with H<sub>2</sub>O (15 mL), and the mixture was extracted with dichloromethane (3 x 30 mL). The combined organic layers were dried over MgSO<sub>4</sub> and concentrated *in vacuo* to afford an orange oil. Purification of the crude product by column chromatography on silica gel with hexanes/ethyl acetate as eluent to yield **3-27** (481 mg, 1.62 mmol, 88 %) as a colorless oil. <sup>1</sup>H NMR (500 MHz, CDCl<sub>3</sub>) δ 3.06 (m, 3H), 3.37 (t, *J* = 4.55 Hz, 2 H), 3.64 (m, 10 H), 3.74 (m, 2 H), 4.35 (m, 2 H). <sup>13</sup>C NMR (125 MHz, CDCl<sub>3</sub>) δ 37.6, 50.6, 69.0, 69.2, 70.0, 70.6, 70.7. All data are in agreement with literature values.<sup>16,28</sup>

### N-Biotinylpropargylamine (3-28)<sup>16,29</sup>

To a solution of *N*-succinimido-D-(+)-biotin **3-20** (200 mg, 0.59 mmol) in dichloromethane (10 mL) was added 1.5 eq propargylamine (48 mg, 0.88 mmol, 60 μL), and the mixture was allowed to react for 8 h at room temperature. The reaction mixture was concentrated *in vacuo* to give a yellow oil. Purification of the crude product by column chromatography on silica gel with 15% methanol in dichloromethane as eluent yield **3-28** (149 mg, 0.53 mmol, 90 %) as a white solid. <sup>1</sup>H NMR (500 MHz, CD<sub>3</sub>OD) δ 1.43 (quint, *J* = 7.65 Hz, 2 H), 1.58 (m, 4 H), 2.22 (t, *J* = 7.55 Hz, 2 H), 2.58 (t, *J* = 2.55 Hz, 2 H), 2.72 (d, *J* = 12.75 Hz, 2 H), 2.93 (dd, *J* = 4.95 Hz, 12.75 Hz, 1 H), 3.21 (quint, *J* = 5.6 Hz, 1 H), 3.96 (d, *J* = 2.5 Hz, 2 H), 4.31 (dd, *J* = 4.5, 7.85 Hz, 1 H), 4.50 (dd, *J* = 4.5, 7.85 Hz, 1 H). <sup>13</sup>C NMR (125 MHz, CD<sub>3</sub>OD) δ 25.3, 28.0, 28.0, 28.3, 35.1, 39.6, 53.4,

55.5, 60.2, 61.9, 70.6, 79.2, 164.7, 174.2. HRMS [M+H]<sup>+</sup> for C<sub>13</sub>H<sub>20</sub>N<sub>3</sub>O<sub>2</sub>S<sup>+</sup> calcd. 282.1271, found 282.1276. (Δ = 1.7 ppm). All data are in agreement with literature values.<sup>16,29</sup>

### **Biotin-Triazole-PEG-Mesylate (3-29)<sup>16,18</sup>**

To a solution of **3-28** (88 mg, 0.3 mmol), 1 eq **3-27** (84.3 mg, 0.3 mmol), and 1.1 eq ascorbic acid (58 mg, 0.33 mmol) in THF (3 mL) was added a solution of 1.1 eq CuSO<sub>4</sub> · 5H<sub>2</sub>O (88 mg, 0.33 mmol) in H<sub>2</sub>O (0.75 mL), and the mixture was allowed to react for 16 h at room temperature with stirring. Upon completion, the solvent was removed by lyophilization and the crude product was purified column chromatography on alumina oxide gel with 10% methanol in dichloromethane as eluent to yield **3-29** (94 mg, 0.16 mmol, 54 %) as a white solid. <sup>1</sup>H NMR (500 MHz, MeOD) δ 1.42 (m, 2 H), 1.57 (m, 4 H), 2.25 (t, *J* = 7.4 Hz, 2 H), 2.72 (d, *J* = 12.65 Hz, 1 H), 2.93 (dd, *J* = 4.95, 12.75 Hz, 1 H), 3.12 (s, 3H), 3.20 (m, 1 H), 3.62 (m, 6 H), 3.66 (m, 2 H), 3.76 (m, 2 H), 3.90 (t, *J* = 5 Hz, 2 H), 4.31 (m, 1 H), 4.37 (m, 2 H), 4.46 (s, 2 H), 4.51 (m, 1 H), 4.57 (t, *J* = 5 Hz, 2 H), 7.93 (s, 1H). <sup>13</sup>C NMR (125 MHz, MeOD) δ 25.3, 28.0, 28.3, 34.2, 35.2, 36.1, 39.7, 50.0, 55.6, 60.2, 61.9, 68.7, 69.0, 69.6, 70.0, 70.1, 70.2, 123.6, 144.7, 164.6, 174.4. HRMS [M+H]<sup>+</sup> for C<sub>22</sub>H<sub>39</sub>N<sub>6</sub>O<sub>8</sub>S<sub>2</sub><sup>+</sup> calcd. 579.2265, found 579.2273. (Δ = 1.4 ppm). All data are in agreement with literature values.<sup>16,18</sup>

### **§3.7 References**

- (1) Zempleni, J.; Wijeratne, S. S. K.; Hassan, Y. I. Biotin. *BioFactors* **2009**, *35*, 36-46.
- (2) Leamon, C. P. Folate-targeted drug strategies for the treatment of cancer. *Curr Opin Investig Drugs* **2008**, *9*, 1277-1286.
- (3) Lu, Y.; Low, P. S. Folate-mediated delivery of macromolecular anticancer therapeutic agents. *Adv. Drug Delivery Rev.* **2012**, *64*, Supplement, 342-352.
- (4) Russell-Jones, G.; McTavish, K.; McEwan, J.; Rice, J.; Nowotnik, D. Vitamin-mediated targeting as a potential mechanism to increase drug uptake by tumours. *J. Inorg. Biochem.* **2004**, *98*, 1625-1633.
- (5) Vineberg, J. G.; Zuniga, E. S.; Kamath, A.; Chen, Y.-J.; Seitz, J. D.; Ojima, I. Design, Synthesis, and Biological Evaluations of Tumor-Targeting Dual-Warhead Conjugates for a Taxoid–Camptothecin Combination Chemotherapy. *J. Med. Chem.* **2014**, *57*, 5777-5791.
- (6) Ojima, I.; Zuniga, E. S.; Berger, W. T.; Seitz, J. D. Tumor-targeting drug delivery of new-generation taxoids. *Future Med Chem.* **2012**, *4*, 33-50.
- (7) Ojima, I.; Slater, J. C.; Michaud, E.; Kuduk, S. D.; Bounaud, P.-Y.; Vrignaud, P.; Bissery, M.-C.; Veith, J. M.; Pera, P.; Bernacki, R. J. Syntheses and Structure–Activity Relationships of the Second-Generation Antitumor Taxoids: Exceptional Activity against Drug-Resistant Cancer Cells. *J. Med. Chem.* **1996**, *39*, 3889-3896.
- (8) Harris, J. M.; Chess, R. B. Effect of pegylation on pharmaceuticals. *Nat Rev Drug Discov* **2003**, *2*, 214-221.
- (9) Vlashi, E.; Kelderhouse, L. E.; Sturgis, J. E.; Low, P. S. Effect of Folate-Targeted Nanoparticle Size on Their Rates of Penetration into Solid Tumors. *ACS Nano* **2013**, *7*, 8573-8582.
- (10) Ojima, I. Guided Molecular Missiles for Tumor-Targeting Chemotherapy—Case Studies Using the Second-Generation Taxoids as Warheads. *Acc. Chem. Res.* **2008**, *41*, 108-119.
- (11) Ojima, I. Use of Fluorine in the Medicinal Chemistry and Chemical Biology of Bioactive Compounds—A Case Study on Fluorinated Taxane Anticancer Agents. *ChemBioChem* **2004**, *5*,

628-635.

- (12) Seitz, J. D.; Vineberg, J. G.; Wei, L.; Khan, J. F.; Lichtenthal, B.; Lin, C.-F.; Ojima, I. Design, synthesis and application of fluorine-labeled taxoids as <sup>19</sup>F NMR probes for the metabolic stability assessment of tumor-targeted drug delivery systems. *J. Fluorine Chem.* **2015**, *171*, 148-161.
- (13) Chen, S.; Zhao, X.; Chen, J.; Chen, J.; Kuznetsova, L.; Wong, S. S.; Ojima, I. Mechanism-Based Tumor-Targeting Drug Delivery System. Validation of Efficient Vitamin Receptor-Mediated Endocytosis and Drug Release. *Bioconjugate Chem.* **2010**, *21*, 979-987.
- (14) Das, M. Design, Synthesis and Biological Evaluation of Novel Tumor-targeting Taxane-based Drug Delivery Systems. Doctoral Dissertation. Stony Brook University. **2011**.
- (15) Seitz, J. D. The design, synthesis and biological evaluation of novel taxoid anticancer agents and their tumor-targeted drug conjugates. Doctoral Dissertation. Stony Brook University. **2013**.
- (16) Vineberg, J. G. Design, synthesis, and biological evaluation of novel taxoid-based drug conjugates and theranostic imaging agents towards tumor-targeted chemotherapy. Doctoral Dissertation. Stony Brook University. **2014**.
- (17) Joshua D. Seitz, J. G. V., Tao Wang, and Iwao Ojima Synthesis of a Next-Generation Taxoid by Rapid Methylation Amenable for [<sup>11</sup>C]-Labeling. *J. Org. Chem. To be submitted shortly*
- (18) Claesener, M.; Breyholz, H.-J.; Hermann, S.; Faust, A.; Wagner, S.; Schober, O.; Schäfers, M.; Kopka, K. Efficient synthesis of a fluorine-18 labeled biotin derivative. *Nucl. Med. Biol.*, *39*, 1189-1194.
- (19) Mosmann, T. Rapid colorimetric assay for cellular growth and survival: Application to proliferation and cytotoxicity assays. *J. Inorg. Biochem.* **1983**, *65*, 55-63.
- (20) Bordwell, F. G.; Fried, H. E. Heterocyclic aromatic anions with 4n + 2 .pi.-electrons. *J. Org. Chem.* **1991**, *56*, 4218-4223.
- (21) Shaabani, A.; Tavasoli - Rad, F.; Lee, D. G. Potassium Permanganate Oxidation of Organic Compounds. *Synth. Commun.* **2005**, *35*, 571-580.
- (22) Widdison, W. C.; Wilhelm, S. D.; Cavanagh, E. E.; Whiteman, K. R.; Leece, B. A.; Kovtun, Y.; Goldmacher, V. S.; Xie, H.; Steeves, R. M.; Lutz, R. J.; Zhao, R.; Wang, L.; Blättler, W. A.; Chari, R. V. J. Semisynthetic Maytansine Analogues for the Targeted Treatment of Cancer. *J. Med. Chem.* **2006**, *49*, 4392-4408.
- (23) Banerjee, P. S.; Zuniga, E. S.; Ojima, I.; Carrico, I. S. Targeted and armed oncolytic adenovirus via chemoselective modification. *Bioorg. Med. Chem. Lett.* **2011**, *21*, 4985-4988.
- (24) Rich, D. H.; Gesellchen, P. D.; Tong, A.; Cheung, A.; Buckner, C. K. Alkylating derivatives of amino acids and peptides. Synthesis of N-maleoylamino acids, [1-(N-maleoylglycyl)cysteinyl]oxytocin, and [1-(N-maleoyl-11-aminoundecanoyl)cysteinyl]oxytocin. Effects on vasopressin-stimulated water loss from isolated toad bladder. *J. Med. Chem.* **1975**, *18*, 1004-1010.
- (25) Goswami, L. N.; Houston, Z. H.; Sarma, S. J.; Jalisatgi, S. S.; Hawthorne, M. F. Efficient synthesis of diverse heterobifunctionalized clickable oligo(ethylene glycol) linkers: potential applications in bioconjugation and targeted drug delivery. *Org. Biomol. Chem.* **2013**, *11*, 1116-1126.
- (26) Fusz, S.; Srivatsan, S. G.; Ackermann, D.; Famulok, M. Photocleavable Initiator Nucleotide Substrates for an Aldolase Ribozyme. *J. Org. Chem.* **2008**, *73*, 5069-5077.
- (27) Borcard, F.; Godinat, A.; Staedler, D.; Comas Blanco, H.; Dumont, A.-L.; Chapuis-Bernasconi, C.; Scaletta, C.; Applegate, L. A.; Krauss Juillerat, F.; Gonzenbach, U. T.; Gerber-Lemaire, S.; Juillerat-Jeanneret, L. Covalent Cell Surface Functionalization of Human Fetal

Osteoblasts for Tissue Engineering. *Bioconjugate Chem.* **2011**, *22*, 1422-1432.

(28) Luo, Z.; Ding, X.; Hu, Y.; Wu, S.; Xiang, Y.; Zeng, Y.; Zhang, B.; Yan, H.; Zhang, H.; Zhu, L.; Liu, J.; Li, J.; Cai, K.; Zhao, Y. Engineering a Hollow Nanocontainer Platform with Multifunctional Molecular Machines for Tumor-Targeted Therapy in Vitro and in Vivo. *ACS Nano* **2013**, *7*, 10271-10284.

(29) Rong, L.; Liu, L.-H.; Chen, S.; Cheng, H.; Chen, C.-S.; Li, Z.-Y.; Qin, S.-Y.; Zhang, X.-Z. A coumarin derivative as a fluorogenic glycoproteomic probe for biological imaging. *Chem. Commun.* **2014**, *50*, 667-669.

## Chapter 4

### Novel Taxoid-based Tumor-targeting Diagnostic/Theranostic PET/SPECT Imaging Agents

§4.1 Introduction .....	108
§4.1.1 Positron Emission Tomography (PET) .....	108
§4.1.2 Single-photon Emission Computed Tomography (SPECT) .....	109
§4.1.3 PET versus SPECT: Strengths and Limitations .....	110
§4.2 Selective Examples of Radionuclides for PET/SPECT in Pharmaceutical Development	111
§4.2.1 Carbon-11 .....	111
§4.2.2 Fluorine-18 .....	111
§4.2.3 Copper-64 .....	112
§4.2.4 Technetium-99m .....	113
§4.3 Novel Triazine-based Tumor-targeting Diagnostic/Theranostic PET/SPECT Platform...	114
§4.3.1 Radiolabeled Vitamin-based Conjugates as Radiotracers .....	114
§4.3.2 Triazine-based Tripod Platform for Theranostics .....	115
§4.3.3 Synthesis of Biotin-Triazine-Linker-Drug-Azide Coupling-Ready Platform	116
§4.4 Diagnostic/Theranostic $^{185}\text{Re}$ (Cold)/ $^{99\text{m}}\text{Tc}$ (Hot) SPECT Imaging Agents.....	118
§4.4.1 Synthesis of Cyclooctyne-DPA( $sp^2\text{N}$ ) Trident Ligand .....	118
§4.4.2 Cold Synthesis of Biotin-Triazine-Linker-Drug-DPA( $sp^2\text{N}$ )- $^{185}\text{Re}(\text{CO})_3$ Conjugate and Ligand Disassociation <i>via</i> Re-promoted Methanolysis .....	119
§4.4.3 Synthesis of Cyclooctyne-DPA( $sp^3\text{N}$ ) Trident Ligand .....	121
§4.4.4 Cold Synthesis of Biotin-Triazine-Linker-Drug-DPA( $sp^3\text{N}$ )- $^{185}\text{Re}(\text{CO})_3$ and Biotin- DPA( $sp^3\text{N}$ )- $^{185}\text{Re}(\text{CO})_3$ Conjugates.....	121
§4.5 Diagnostic/Theranostic $^{65}\text{Cu}$ (Cold)/ $^{64}\text{Cu}$ (Hot) PET Imaging Agents.....	124
§4.5.1 Synthesis of Cyclooctyne-NOTA Hexadent Ligand.....	124
§4.5.2 Cold Synthesis of Biotin-Triazine-Linker-Drug-NOTA- $^{65}\text{Cu}$ and Biotin-NOTA- $^{65}\text{Cu}$ Conjugates.....	124
§4.6 Summary.....	126
§4.7 Experimental Section.....	126
§4.7.1 Caution.....	126
§4.7.2 General Information.....	126
§4.7.3 Materials.....	127
§4.7.4 Experimental Procedure.....	127
§4.8 References.....	138

## §4.1 Introduction

Radiopharmaceuticals are drugs containing a radionuclide in their composition. Currently two major molecular imaging modalities in nuclear medicine as radiopharmaceuticals for diagnosis and therapy are positron emission tomography (PET) and single photon emission computed tomography (SPECT).<sup>1</sup> Different from other common imaging techniques, such as computerized tomography (CT), magnetic resonance imaging (MRI), ultrasound (US), bioluminescence and fluorescence optical imaging modalities, PET and SPECT are non-invasive functional imaging techniques. PET and SPECT utilize the emission of radio-isotopic particles (positron- and  $\gamma$ -emitting radionuclides, respectively) as they decay for diagnosis.<sup>2</sup> The most significant advantage of PET and SPECT is their high detection sensitivity which can detect radiotracer concentration in the picomolar or nanomolar range to study and visualize the physiology abnormality or disturbed biochemical process.<sup>3</sup>

At the present time, approximately 40 million radiopharmaceutical-based clinical scans are made annually worldwide.<sup>4</sup> SPECT imaging dominates 95% of scans mostly *via*  $^{99m}\text{Tc}$ , whereas PET imaging only accounts for one million scans as the result of  $^{18}\text{F}$ -FDG (fluorine 18-labeled fluorodeoxyglucose) is the only PET agent currently being widely used, but this number is predicted to quadruple over the next couple of years.<sup>4</sup> Thus the number of publications on PET has tendency to keep growing over this period, however, the publications on SPECT have remained the level at about 26% of current PET imaging papers mainly because SPECT has been seen as a mature technique lack of innovation.<sup>4</sup>

### §4.1.1 Positron Emission Tomography (PET)

Positron emission tomography (PET) relies on the decay of positron-emitting radionuclides from the radiolabeled PET imaging agents. After emission from the nucleus, the released positive particle travels a short distance, also known as the positron range, in the surrounding matter or tissue and annihilates with an electron. This collision produces two gamma-ray photons with 511 keV which are emitted in the opposite directions simultaneously. (**Figure 4.1**) Then an array of surrounding detectors can detect and accumulate a large number of coincidence events to reconstruct the sequence of annihilation events with spatial distribution of radioactivity as a function of time.<sup>5</sup>

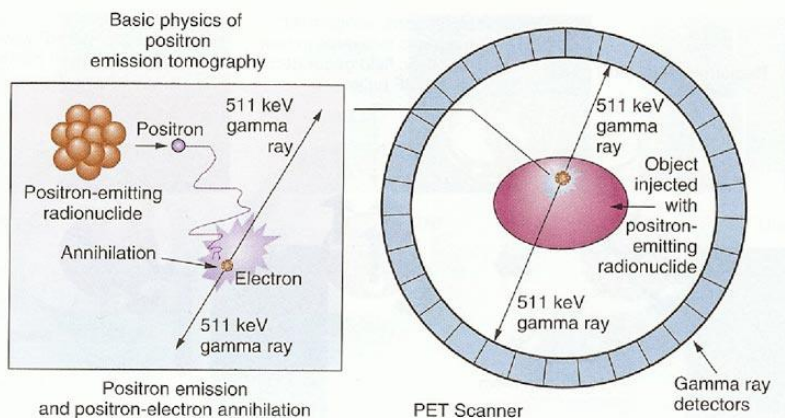


**Figure 4.1** Schematic representation of the principle of PET imaging demonstrating positron decay and annihilation generating two 511 keV  $\gamma$ -rays (reprinted from reference 6)<sup>6</sup>

PET can provide functional information on biological tissues and molecular information on biological processes by the use of radiopharmaceuticals. **Table 4.1** lists the most commonly used PET nuclides for radiolabeling biomolecules, but currently most of the PET imaging probes have been labeled with either  $^{11}\text{C}$  or  $^{18}\text{F}$ .

**Table 4.1 The most commonly used positron-emitting radionuclides in PET (adapted from reference 5)<sup>5</sup>**

Radionuclide	Half-life (min)	Maximum energy (MeV)	Mode of decay	Theoretical specific activity (GBq/ $\mu\text{mol}$ )
$^{11}\text{C}$	20.3	0.97	$\beta^+$ (99 %)	$3.4 \times 10^5$
$^{13}\text{N}$	10	1.20	$\beta^+$ (100 %)	$7.0 \times 10^5$
$^{15}\text{O}$	2	1.74	$\beta^+$ (100 %)	$3.4 \times 10^6$
$^{18}\text{F}$	110	0.64	$\beta^+$ (97 %) EC (3 %)	$6.3 \times 10^4$
$^{64}\text{Cu}$	762	0.655	$\beta^+$ (19 %) EC (41 %) $\beta^+$ (40 %)	$9.13 \times 10^3$
$^{68}\text{Ga}$	68.1	1.90	$\beta^+$ (89 %) EC (11 %)	$1.02 \times 10^5$
$^{76}\text{Br}$	972	4.0	$\beta^+$ (57 %) EC (43 %)	$7.2 \times 10^3$
$^{124}\text{I}$	60 192	2.14	$\beta^+$ (25 %) EC (75 %)	$1.15 \times 10^3$

EC: electron capture

The main challenges of PET is related to the short-lived positron-emitting isotopes. The radio-labeled probes need to be synthesized, purified, analyzed and formulated within minutes, and period of three isotope half-lives is the maximum time for the synthetic process to make sure existence of enough radiolabeled material for administration.<sup>7</sup> Before administration of PET radiotracer to patients, the radiolabeled compounds have to meet the pharmaceutical quality requirement in terms of rapid characterization and purification. All PET radiopharmaceuticals for human or animal use should show a high level (>95 %) of radiochemical purity which is most frequently achieved by high pressure liquid chromatography (HPLC) purification.<sup>5</sup> To help accelerate the radiosynthesis rate and fully convert the radionuclides to radiolabeling probes, a large excess of unlabeled precursor is often employed as  $10^3$ - $10^4$  fold. Depending on the half-life of used radioisotope, reaction time can vary from 1 to 30 min, reaction volume is typically within the range of 0.2-1 mL, and reaction temperature can rise up to 190 °C, either by conventional heating or under microwave heating condition.<sup>5</sup>

#### §4.1.2 Single Photon Emission Computed Tomography (SPECT)

Single Photon Emission Computed Tomography (SPECT) is a medical imaging modality which combines nuclear medicine (NM) imaging and computed tomography (CT) technique.<sup>8</sup> The radiation detectors in SPECT can capture the gamma photons emitted from the radiopharmaceuticals to reconstruct three-dimensional image about the presence of the internal distributed radiopharmaceuticals. Compared to PET imaging, SPECT imaging usually has a longer

time window, mainly due to the fact that gamma decay radioisotopes generally have longer half-lives and are easier to obtain. The most commonly used SPECT radionuclides are shown in **Table 4.2**. In SPECT, a chelating ligand is being introduced into an organic compound for capturing the metal radioisotopes such as  $^{99m}\text{Tc}$  and  $^{111}\text{In}$ . Many radiolabeled peptides and monoclonal antibodies have been successfully synthesized in the sequence of first conjugation only in the presence of a bifunctional chelating ligand, then bind the radio-metal to the chelating ligand to give radiolabeled conjugated molecules.

**Table 4.2 The most commonly used single-photon emitting radionuclides in SPECT (adapted from reference 3)<sup>3</sup>**

Radionuclide	Half-life	Energy	Mode of decay
Tc-99m	6.02 h	142 keV	IT (100 %)
I-131	8.03 days	364 keV	$\beta^-$ (100 %)
I-123	13.22 h	159 keV	EC (100 %)
In-111	2.80 days	171,245 keV	EC (100 %)

IT: isomeric transition,  $\beta^-$ : beta-minus, EC: electron capture

Preclinical SPECT systems have a great applications in cardiovascular research, such as myocardial functions and vascular disorder investigations.<sup>3</sup> In addition, in stem cell research, SPECT is applied to validate the efficacy and safety of stem cell-based therapies. Stem cells can be labelled with radionuclides before transplantation, their viability, function and differentiation status can be tracked and monitored to investigate the stem cell regeneration.<sup>3</sup> SPECT imaging technique also contribute in preclinical cancer research including cancer cell targets imaging to study pharmacokinetics and pharmacodynamics responses to treatments, and drug development, in particular for validation of drug targeting, safety and efficacy.<sup>3</sup>

#### §4.1.3 PET versus SPECT: Strengths and Limitations

Because of the ability to localize annihilation using two gamma photons, PET imaging enables the detection and record of a higher percentage of emitted events and generates extremely accurate images, which addresses higher sensitivity as the most important advantage of PET imaging over SPECT. In fact, PET imaging exhibits 2-3 orders of magnitude greater sensitivity than SPECT.<sup>1</sup> Besides higher sensitivity, PET also possess ease of quantification and introduction of a radiolabel (mostly *via*  $^{11}\text{C}$  or  $^{18}\text{F}$ ) with minimal structural modification.<sup>4</sup> This is particularly advantageous when labelling small molecules for targeting structurally sensitive targets such as the brain.<sup>4</sup> But SPECT can provide expended observational time window due to the longer half-life intrinsic nature of single photo emitters. This allows several hours or days after administration of labelled molecules to be observed and detected in a biological process *in vivo*.<sup>1</sup> In addition, SPECT scanners can provide a submillimeter or subhalf millimeters spatial resolution in preclinical, compared to 1-2 mm spatial resolution of PET.<sup>3</sup> Small animal imaging using PET radiopharmaceuticals exhibited better capability in tracer kinetic studies when compared to its SPECT counterparts, while SPECT has relatively lower cost and wide availability of the radioligands as well as relative ease of labeling.<sup>3</sup> Detailed comparative studies of PET and SPECT agents in the clinical have demonstrated that the actual diagnostic information obtained from the two techniques are very similar.<sup>4</sup>



## §4.2 Selective Examples of Radionuclides for PET/SPECT in Pharmaceutical Development

### §4.2.1 Carbon-11

Carbon-11 is the positron-emitting isotope of carbon with 20.3 min half-life. Radiolabelling biomolecules using carbon-11 are viewed no chemically or biologically change compared to unlabeled equivalents. Without introducing “artificial” PET tag, such as introducing a fluorine-18 atom, it is assumed that the biological properties of the radiopharmaceuticals remain the same,<sup>7</sup> resulting in more reliable imaging information. Although there are many different nuclear reactions for carbon-11 production, the most widely used method is  $^{14}\text{N}(p,\alpha)^{11}\text{C}$  cyclotron reaction using bombardment of nitrogen-14 with protons.<sup>9-10</sup>  $^{11}\text{CO}_2$  as the most versatile primary carbon-11 synthon can produce most the  $^{11}\text{C}$ -labelling precursor reagents. (Figure 4.2)  $^{11}\text{C}$ -methyl iodide can be widely used in most methylation reactions for PET radiochemistry *via* N-, O-, or S-methylations, and recently  $^{11}\text{C}$ -C coupling reactions *via* Stille, Suzuki and Sonogashira cross-coupling reactions provide a new perspective for preparation of carbon-11 radiolabelling pharmaceuticals.<sup>7</sup>

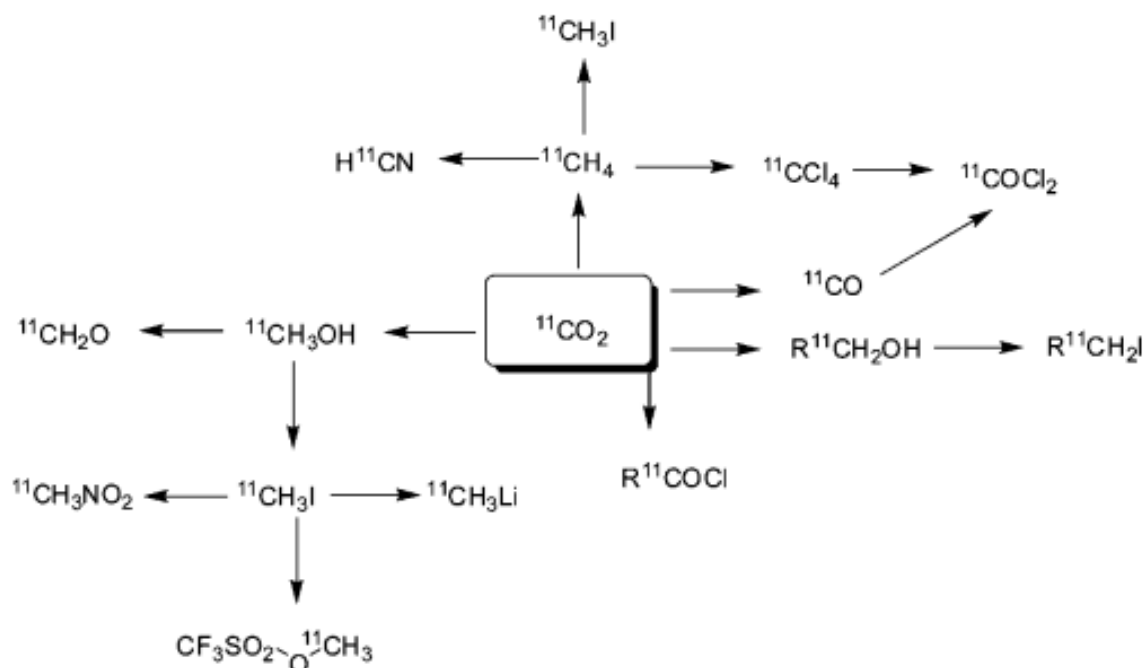
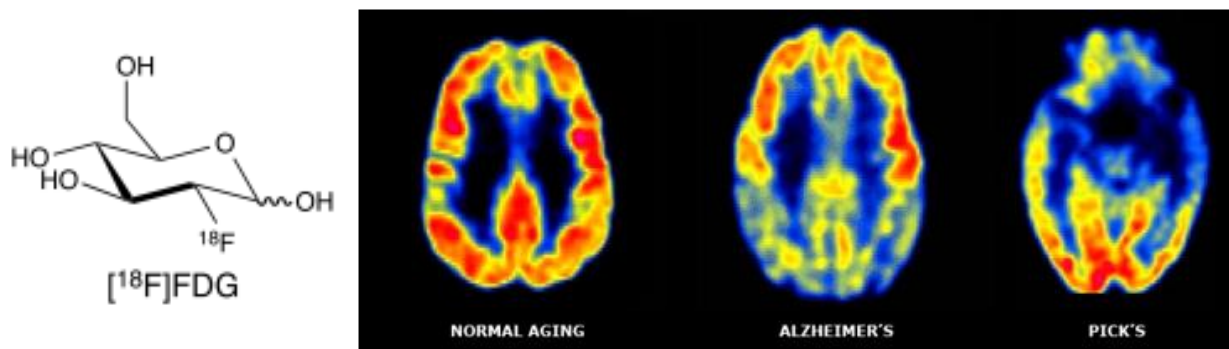


Figure 4.2 Chemical pathway to important carbon-11 reagents (reprinted from reference 5)<sup>5</sup>

### §4.2.2 Fluorine-18

Fluorine-18 is the most important positron-emitting isotope for PET imaging. Unlike carbon-11 (half-life around 20.3 min), fluorine-18 has physical half-life of 110 min which allows for multistep radiosynthesis and purification, a short positron linear range in tissue (2.3 mm) with highest resolution PET images compared to other available positron emitters, and possibility to transportation to other clinical PET institutions without radiochemistry laboratory.<sup>5,7</sup> Thus,  $^{18}\text{F}$  is often referred to as the “radionuclide of choice”.<sup>7</sup> The most commonly used radiopharmaceutical 2- $^{18}\text{F}$ fluoro-2-deoxy-d-glucose ( $^{18}\text{F}$ FDG) in PET has been widely used in cancer treatments and neurosciences research. The uptake of  $^{18}\text{F}$ FDG by tissues is a good biomarker for the tissue

uptake of glucose. Thus, by monitoring the distribution of [ $^{18}\text{F}$ ]FDG within the body, fluorine-18 radiolabeled PET study can disclose information of certain types of tissue metabolism. A good example shown in **Figure 4.3** applied [ $^{18}\text{F}$ ]FDG-PET technique to distinguish between Alzheimer's and Pick's disease (fronto-temporal dementias). The rate of glucose metabolism correlates to the metabolic rate of active neurons in brain, especially in the cortex. The regional low distribution of FDG was observed in the temporal and parietal regions of the brain which is consistent of the characteristic pattern from Alzheimer's patients, but very different from what have been seen from patients with Pick's disease.<sup>11</sup> Therefore, [ $^{18}\text{F}$ ]FDG allows the differential diagnoses of various diseases depending on the rate change of glucose uptake.



**Figure 4.3** [ $^{18}\text{F}$ ]FDG-based PET images showing patterns of metabolic activity of patients with Alzheimer's disease (middle), Pick's disease (right) and elderly individuals with no dementia (left) (high FDG uptake in red, low FDG uptake in blue) (reprinted from reference 11)<sup>11</sup>

### §4.2.3 Copper-64

The long-lived  $^{64}\text{Cu}$  isotope, although less prevalent than  $^{18}\text{F}$  and  $^{11}\text{C}$ , continues to attract interest.  $^{64}\text{Cu}$  has a half-life of 12.7 h and a  $\beta^+$  emission (18%,  $E_{\text{max}} = 0.655$  meV). It can be produced and prepared in a carrier-free state by bombarding the target of  $^{64}\text{Zn}(n,p)$   $^{64}\text{Cu}$  nuclear reaction in a reactor with fast neutrons.<sup>12</sup> Recent breakthroughs in  $^{64}\text{Cu}$  production with high specific activity does not require on-site cyclotron facilities.<sup>13</sup> This provides small institutions a great opportunity to replace  $^{18}\text{F}$  by  $^{64}\text{Cu}$  with high sensitivity, high spatial resolution but affordable cost for PET research.<sup>14</sup>

Coordination numbers of Cu(II) ranges from 4 to 6 to form square planar, square pyramidal, trigonal bipyramidal and octahedral Cu(II) complexes.<sup>12</sup> Tetradentate chelators favors a square-planar geometry, while full envelopment of Cu(II) in its maximum six-coordinate mode with hexadentate chelators has been most investigated in radiocopper chemistry. Among numerous acyclic and macrocyclic chelators (**Figure 4.4**), 1,4,7-triazacyclononane- $N,N',N''$ -triacetic acid (NOTA) as a derivative of triazacyclononane (TACN) with three carboxymethyl pendant arms can form Cu(II) complex in 6-coordination mode (**Figure 4.5**) with good affinity.<sup>12</sup>

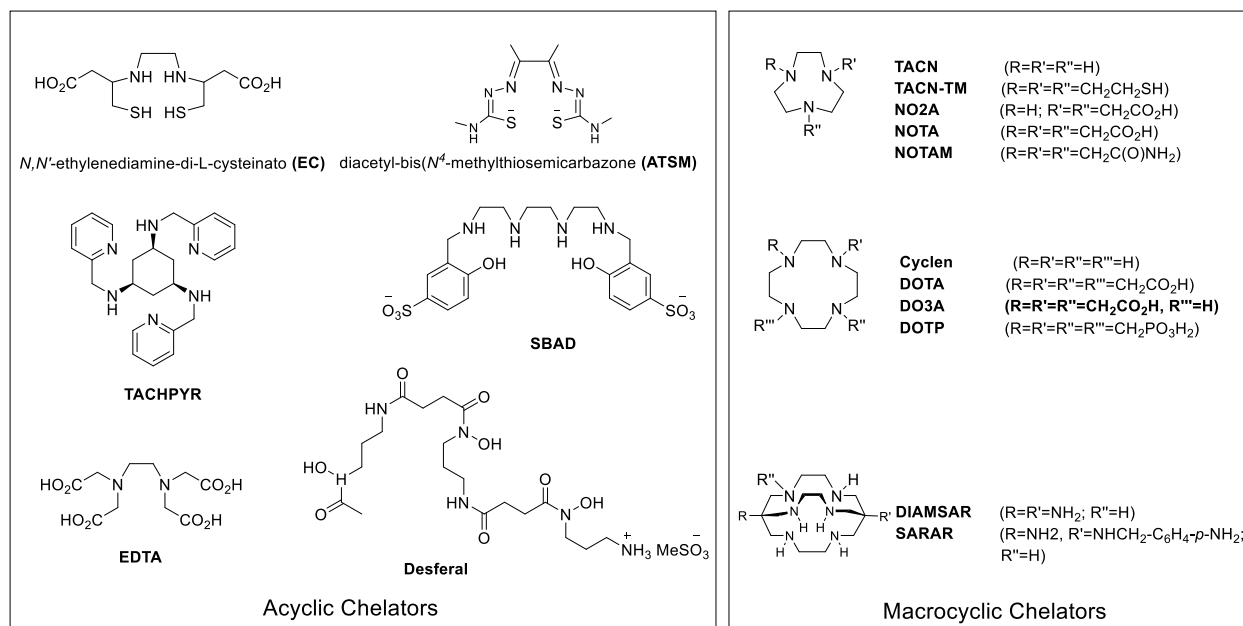


**Figure 4.4** Chemical structures of acyclic and macrocyclic chelators (adapted from reference 12)<sup>12</sup>

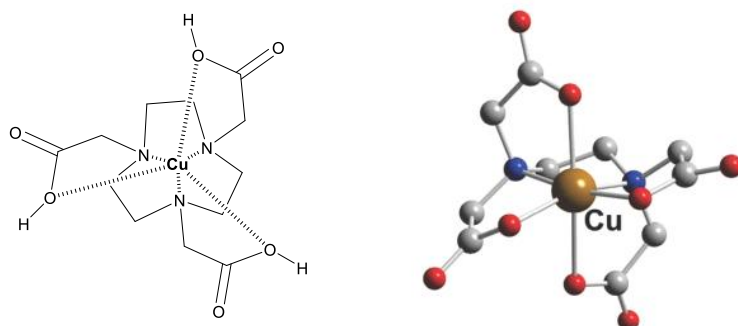


**Figure 4.5** Chemical structure and X-ray crystal structure of Cu(II)-NOTA complexes. Common elements are color coded as follows: C (gray), N (blue), and O (red) (reprinted from reference 12)<sup>12</sup>

#### §4.2.4 Technetium-99m

Technetium-99m (<sup>99m</sup>Tc) is so far the most commonly used radionuclide in SPECT imaging. <sup>99m</sup>Tc has 6 h half-life and 140 keV gamma photon emission which makes it suitable for both effective imaging and patient safety.<sup>15</sup> Therefore, more than 80 % of all commonly used radiopharmaceuticals contain <sup>99m</sup>Tc as metastable radionuclide. In 1960s, a <sup>99</sup>Mo/<sup>99m</sup>Tc generator was developed to produce <sup>99m</sup>Tc as column elutes which makes it readily available for diseases diagnosis.<sup>15</sup>

Technetium-99m has been applied to several radiolabelling monoclonal antibodies and peptides built-up, such as <sup>99m</sup>Tc-CEA-Scan complexes for detection of recurrence and metastatic carcinomas of the colon or rectum,<sup>16</sup> <sup>99m</sup>Tc-sulesomab for infection and inflammation detection,<sup>17</sup> <sup>99m</sup>Tc-annexin V for thrombi detection in vivo,<sup>18</sup> <sup>99m</sup>Tc-depreotide for SSTR-bearing pulmonary

masses detection,<sup>19</sup> and <sup>99m</sup>Tc-apticide for detection of acute deep vein thrombosis (DVT) in lower extremities.<sup>20</sup>

Extensive efforts have been done to develop a “metal-fragment strategy” involving construction of a platform comprising the metal core and a suitably tailored polydentate ligand. This platform should remain the coordinating groups but selectively be substituted by different chelating ligands in the final step to obtain desired <sup>99m</sup>Tc labeled radiopharmaceuticals. Therefore, three robust core structures have been developed as metal-fragment platforms including technetium oxo core [Tc<sup>VO</sup>]<sup>3+</sup>, technetium-hydrazino core [Tc<sup>III</sup>(HYNIC)<sub>x</sub>]<sup>n+</sup>, and most recently, the technetium tricarbonyl core [Tc(CO)<sub>3</sub>]<sup>+</sup>.<sup>21</sup> One-pot reduction of aqueous pertechnetate in the presence of boranocarbonate gives a technetium carbonyl complex [<sup>99m</sup>Tc(CO)<sub>3</sub>(H<sub>2</sub>O)<sub>3</sub>]<sup>+</sup> in excellent yield.<sup>22-23</sup> The six coordinated groups stay as an octahedral geometry, and each carbonyl groups faces a *trans*- coordinated water molecule to give a facial configuration (**Figure 4.6**), thus this metal-fragment is also presented by “*fac*-[Tc(CO)<sub>3</sub>]<sup>+</sup>”.<sup>21</sup> This water-soluble aqua ion remains intact while water molecules can be efficiently replaced by bidentate or tridentate ligands. A large number of chelates have been synthesized and this process is also termed as “[Tc(CO)<sub>3</sub>]<sup>+</sup> synthon” method.<sup>21</sup>

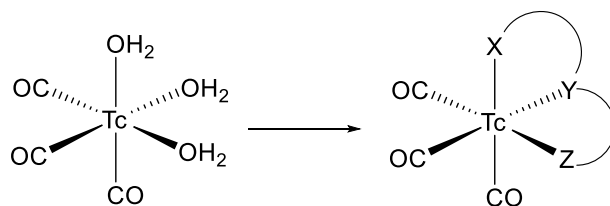


**Figure 4.6** Stereochemistry of Tc-tricarbonyl metal fragment and replacement of labile water molecules by chelating ligands (adapted from reference 21)<sup>21</sup>

### §4.3 Novel Triazine-based Tumor-targeting Diagnostic/Theranostic PET/SPECT Platform

#### §4.3.1 Radiolabeled Vitamin-based Conjugates as Radiotracers

Many radiolabeled vitamin-based (folic acid or biotin) conjugates have been reported for PET/SPECT imaging studies.<sup>21,24-29</sup> Folate is required for nucleotide biosynthesis and cell division,<sup>24</sup> and it has been found folate receptor (FR) is highly expressed in many types of human cancer, such as ovarian, cervical, endometrial, lung, kidney, and breast cancer,<sup>25</sup> making FR as a valuable target for the imaging of cancer. Several folate-based <sup>99m</sup>Tc conjugates have been developed including <sup>99m</sup>Tc-6-hydrazinonicotinamido-hydrazido (HYNIC), <sup>99m</sup>Tc-12-amino-3,3,9,9-tetramethyl-5-oxa-4,8 diaza-2,10-dodecanedioxime (OXA), <sup>99m</sup>Tc-ethylenedicycysteine, and <sup>99m</sup>Tc-DTPA-folate.<sup>26</sup> Etarfolatide (<sup>99m</sup>Tc-EC20, Endocyte Inc.) is the most advanced Technetium-99m labeled imaging agent which currently being evaluated in a Phase III study together with vintafolide in platinum-resistant ovarian cancer and in a Phase IIb study in non-small cell lung cancer.<sup>24</sup> The first reported <sup>18</sup>F-labeled folate radiotracer <sup>18</sup>F- $\alpha,\gamma$ -4-fluorobenzylamine-folate (<sup>18</sup>F- $\alpha,\gamma$ -FBA-folate) clearly visualized FR-positive tumors.<sup>27</sup> An alternative <sup>18</sup>F-labeled folate derivative 3'-aza-2'-[<sup>18</sup>F] fluorofolic acid has been synthesized with efficient and reproducible two-step radiosynthesis in increased radiochemical yield.<sup>25</sup> Another vitamin, biotin, has also been radiolabelled by fluorine-18<sup>28-29</sup> or technetium-99m<sup>21</sup> and used in (strept)avidin-biotin system to study the biodistribution of various antibodies *in vivo* and *in vitro*. Selected vitamin-based PET/SPECT radiotracers are illustrated in **Figure 4.7**.

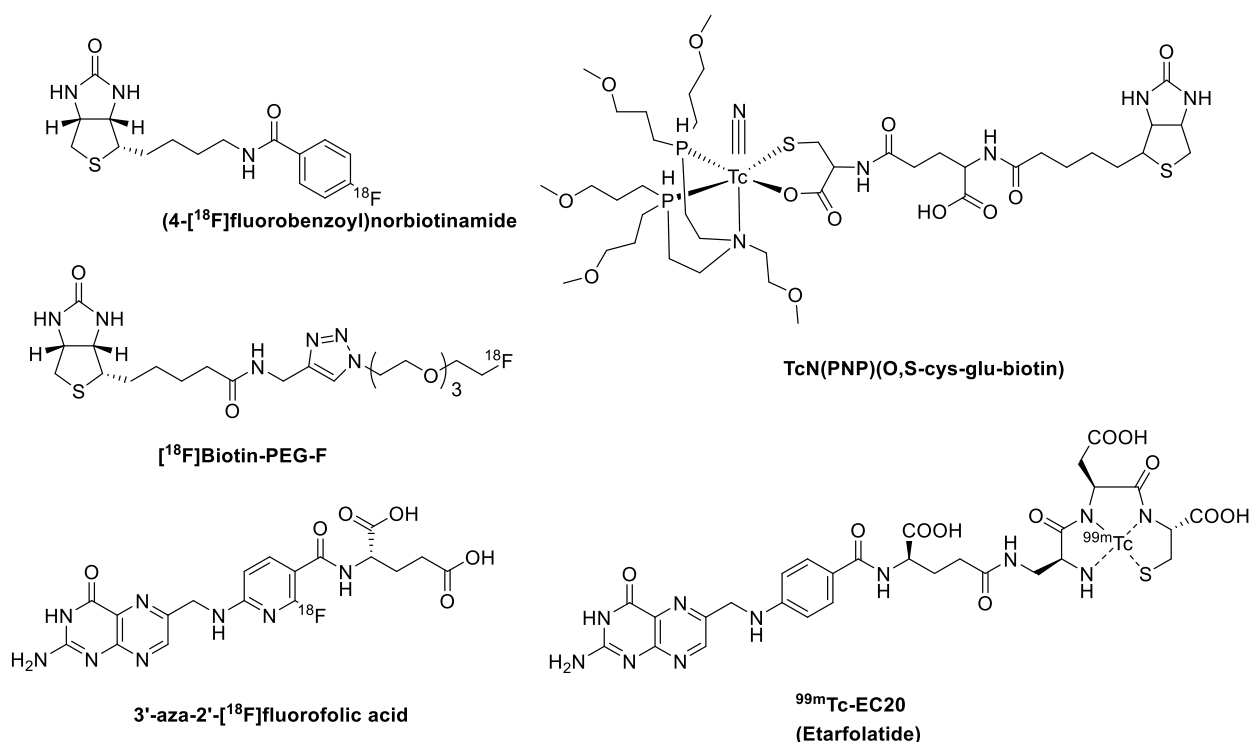


**Figure 4.7** Chemical structures of vitamin-based radiolabeled PET/SPECT imaging agents (adapted from references)<sup>21,25-26,28-29</sup>

### §4.3.2 Triazine-based Tripod Platform for Theranostics

Recently, we reported the design and synthesis of a robust and versatile 1,3,5-triazine-based tripod platform.<sup>30-31</sup> This triazine molecule serves as a key tripod splitter module to separate vitamin (tumor-targeting) module, drug and imaging (fluorescent or PET imaging) moiety in three arms (**Figure 4.8**).<sup>31</sup> A theranostic precursor towards fluorine-18 PET radiolabelling was synthesized, and its cold conjugate bearing fluorine group has been used to evaluate the cytotoxicity and establishment of the optimized radiosynthesis condition.

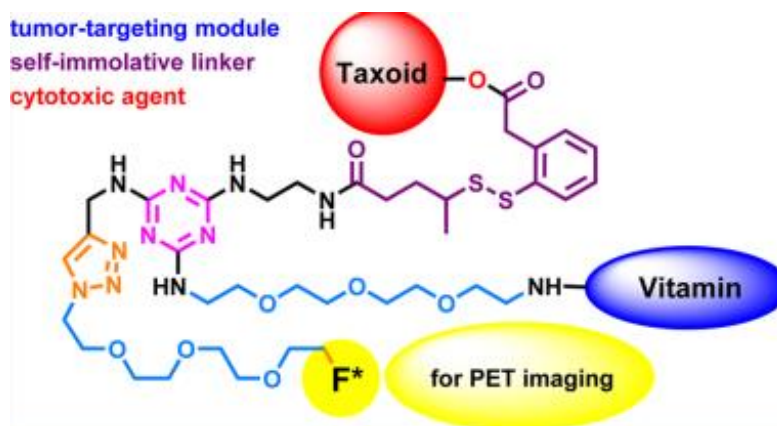


**Figure 4.8** Chemical diagram of triazine-based tripod platform (reprinted from reference 31)<sup>31</sup>

The fluorein-18 radiolabelling was designed as nucleophilic substitution of a PEGylated mesylate-azide intermediate to give a  $^{18}\text{F}$ -PEG-azide agent, which was installed to the biotin-triazine-linker-drug scaffold bearing a alkyne moiety *via* CuAAC (Copper-Catalyzed Alkyne-Azide Cycloaddition) click reaction. As discussed earlier, fluorine-18 has a short half-life which restricted the application on PET imaging studies. Thus this triazine tripod platform was modified to incorporate copper-64 and technetium-99m with longer half-lives for PET and SPECT imaging, respectively. To assembly triazine-based PET/SPECT theranostic conjugates, a cyanuric chloride as triazine splitter core remains to afford three arms for different functionalities including a biotin molecule as tumor-targeting moiety, an anti-cancer drug molecule (second generation taxoid SB-T-1214) with a self-immolative disulfide linker, and an imaging arm for chelation with radiotracer. (**Figure 4.9**) However, the chelating moiety should not be installed *via* CuAAC click reaction simply because the chelating group will easily coordinate the copper catalyst resulting in no active ligands for radiolabelling. Consequently, to overcome this problem, we applied an alternative click condition SPAAC (Strain-Promoted Alkyne-Azide Cycloaddition) to avoid the usage of copper catalyst. A cyclooctyne moiety with chelating ligand allows the click reaction to occur spontaneously without any metal catalyst. In addition, we selected  $^{64}\text{Cu}$  and  $^{99\text{m}}\text{Tc}$  as radioactive tracers for PET and SPECT imaging, therefore,  $^{65}\text{Cu}$  and  $^{185}\text{Re}$  were investigated as surrogates for establishing the “cold” synthetic routes. For the chelating arms, we designed two chelating arms bearing a 1,4,7-triazacyclononane- $N,N',N''$ -triacetic acid (NOTA) moiety and a di-picolylamine (DPA) moiety for capturing  $^{65}\text{Cu}$  and  $^{185}\text{Re}$ , respectively. The model structure of the PET/SPECT theranostic agents were illustrated in **Figure 4.9**.

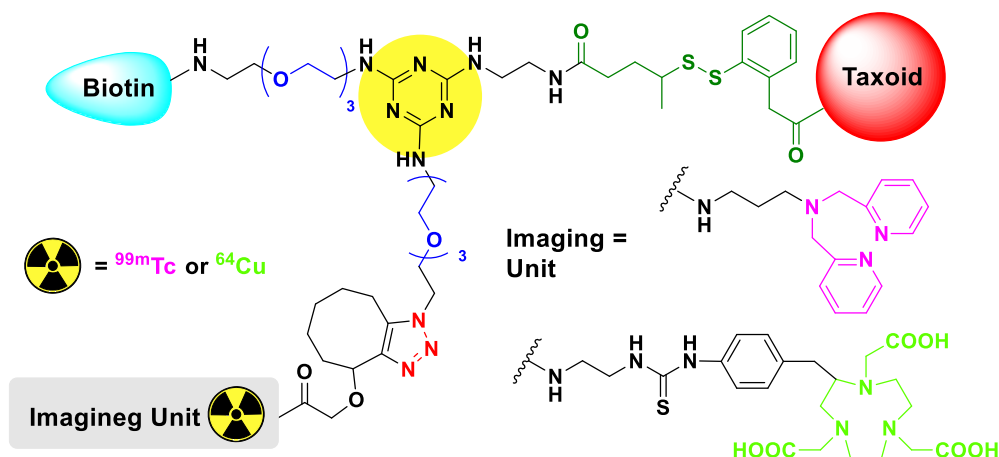
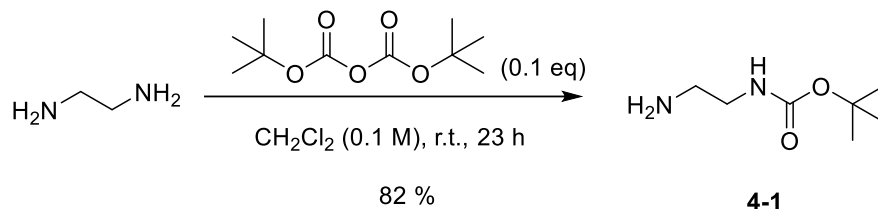


**Figure 4.9** Model structures of theranostic PET/SPECT agents

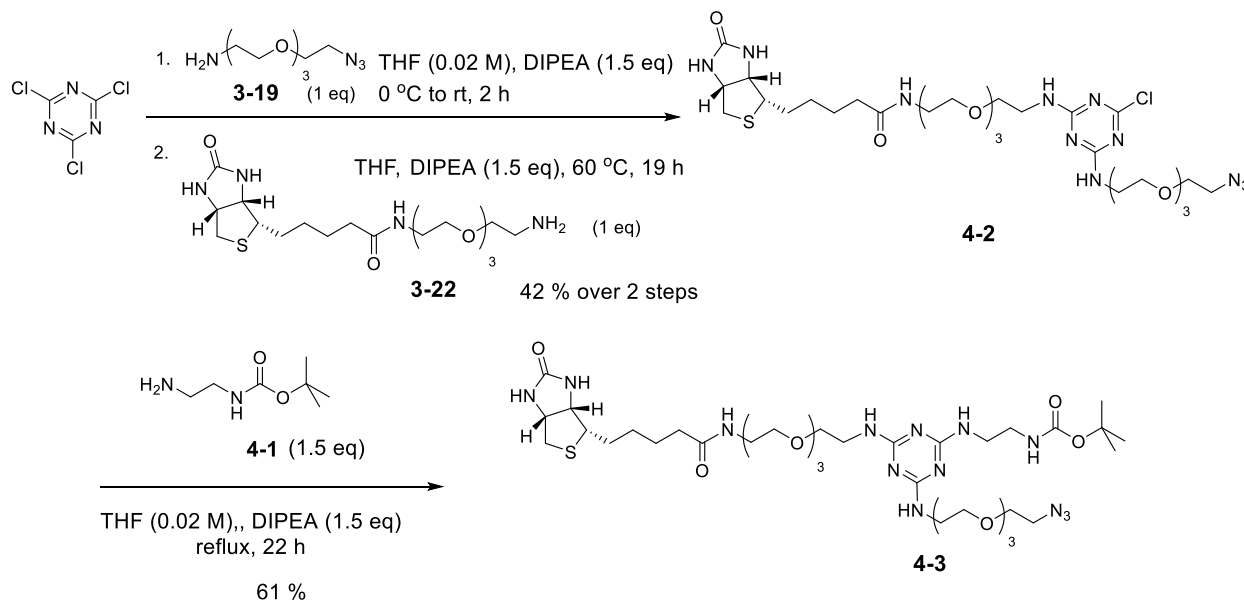
### §4.3.3 Synthesis of Biotin-Triazine-Linker-Drug-Azide Coupling-Ready Platform

Three different arms on triazine core were installed in sequence by controlling the reaction temperature based on temperature-related reactivity. A mono-Boc-protected 1,2-diamine **4-1**<sup>32-33</sup> was synthesized by treated 1,2-diamine with limiting amount of Boc anhydride to generate the desired product **4-1** in excellent yield (82 %). (**Scheme 4.1**)



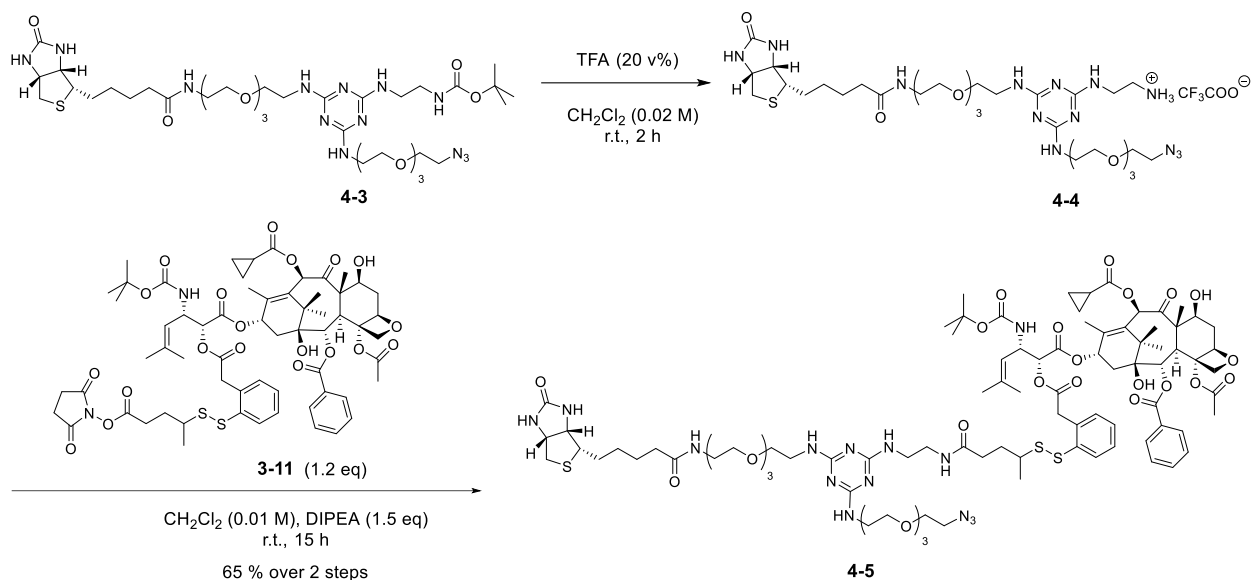
**Scheme 4.1** Mono-Boc protection of 1,2-diamine

The first arm was installed on the cyanuric chloride in the presence of DIPEA as base using 11-azido-3,6,9-trioxaundecan-1-amine **3-19**, which could be readily prepared.<sup>34-35</sup> This step was run under 0 °C for 3 hours, followed by the addition of the biotin-PEG<sub>3</sub>-(CH<sub>2</sub>)<sub>2</sub>-NH<sub>2</sub> **3-22** as the second arm under room temperature. The mono-chloro intermediate **4-2** was isolated in moderate yield. Then the third arm was installed using **4-1** under reflux condition to give intermediate **4-3**. (**Scheme 4.2**).



**Scheme 4.2** Temperature-related tri-substitution

Then the boc protecting group was removed by using trifluoroacetic acid to generate **4-4**, followed by treating with *N,N'*-diisopropylethylamine to generate primary amine *in situ*. The primary amine was used to react with SB-T-1214-methyl branched disulfide linker-activated OSu ester **3-11**<sup>30,36</sup> to form the click-ready biotin-triazine-linker-drug-azide intermediate **4-5** (**Scheme 4.3**).

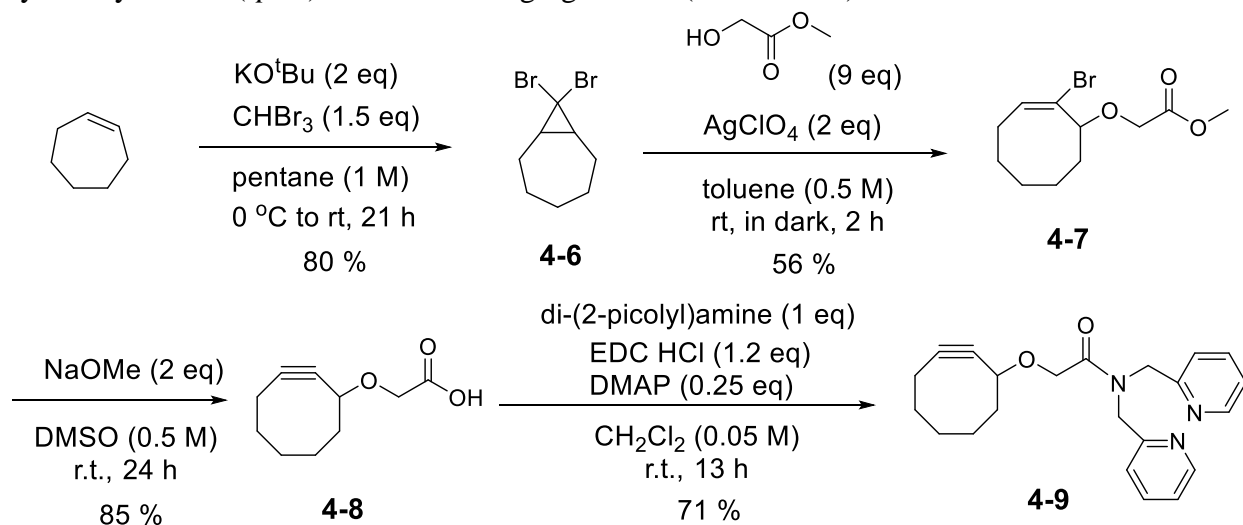


**Scheme 4.3** Synthesis of biotin-triazine-linker-drug-azide intermediate (**4-5**)

## §4.4 Diagnostic/Theranostic <sup>185</sup>Re (Cold)/<sup>99m</sup>Tc (Hot) SPECT Imaging Agents

### §4.4.1 Synthesis of Cyclooctyne-DPA(*sp*<sup>2</sup>N) Trident Ligand

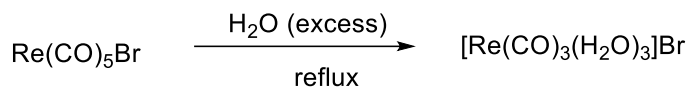
The cyclooctyne moiety was synthesized based on the reported procedures,<sup>37-39</sup> starting from the cycloheptene through a carbene reaction to obtain the dibromobicyclo intermediate **4-6**, followed by the ring expansion and formation of vinyl bromo intermediate **4-7** in the presence of silver perchlorate, and elimination to generate cyclooctyne-acid **4-8** by using sodium methoxide. Direct amidation with a commercial available di-(2-picoly)amine to generate the click-ready cyclooctyne-DPA(*sp*<sup>2</sup>N) trident chelating ligand **4-9** (**Scheme 4.4**).



**Scheme 4.4** Synthesis of cyclooctyne moiety and cyclooctyne-DPA(*sp*<sup>2</sup>N) trident chelating ligand **4-9**



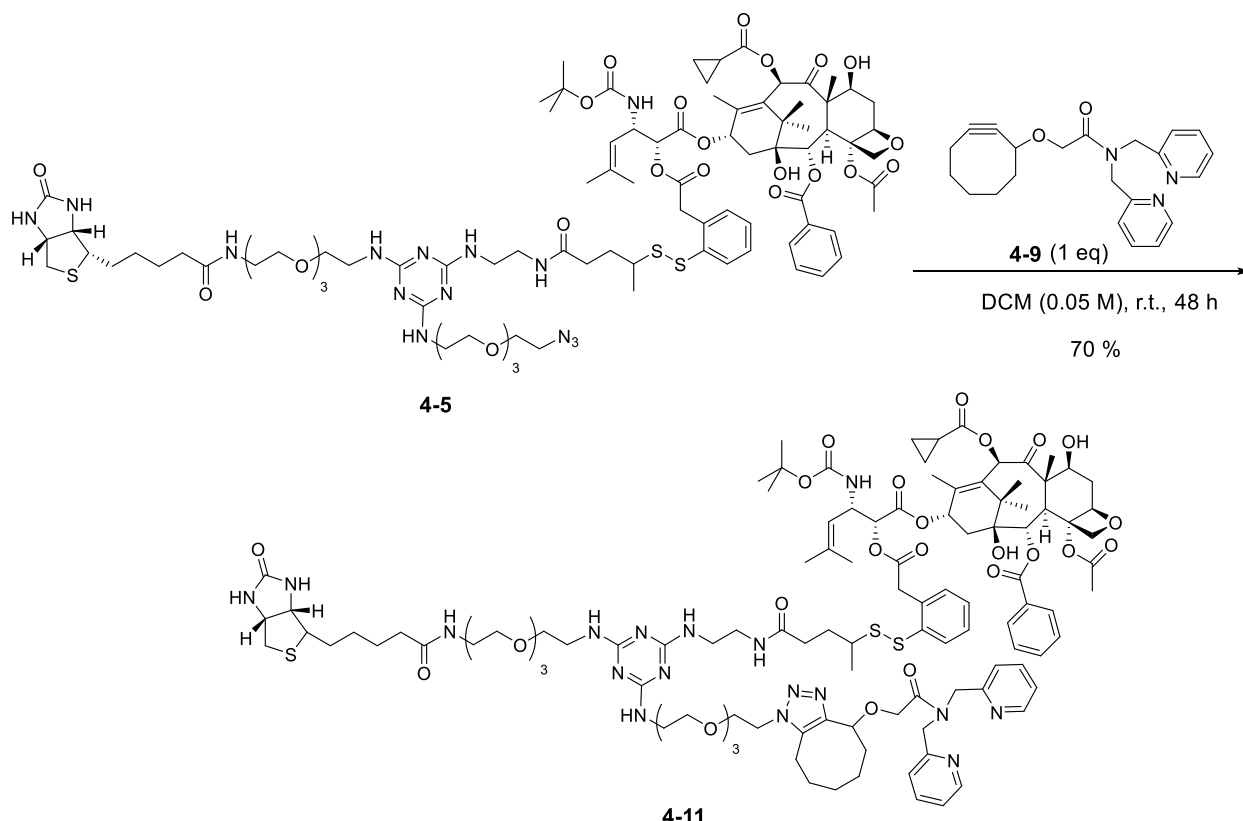
#### §4.4.2 Cold Synthesis of Biotin-Triazine-Linker-Drug-DPA(*sp*<sup>2</sup>N)-<sup>185</sup>Re(CO)<sub>3</sub> Conjugate and Ligand Disassociation *via* Re-promoted Methanolysis



**4-10**

**Scheme 4.5** Synthesis of rhenium tricarbonyl species

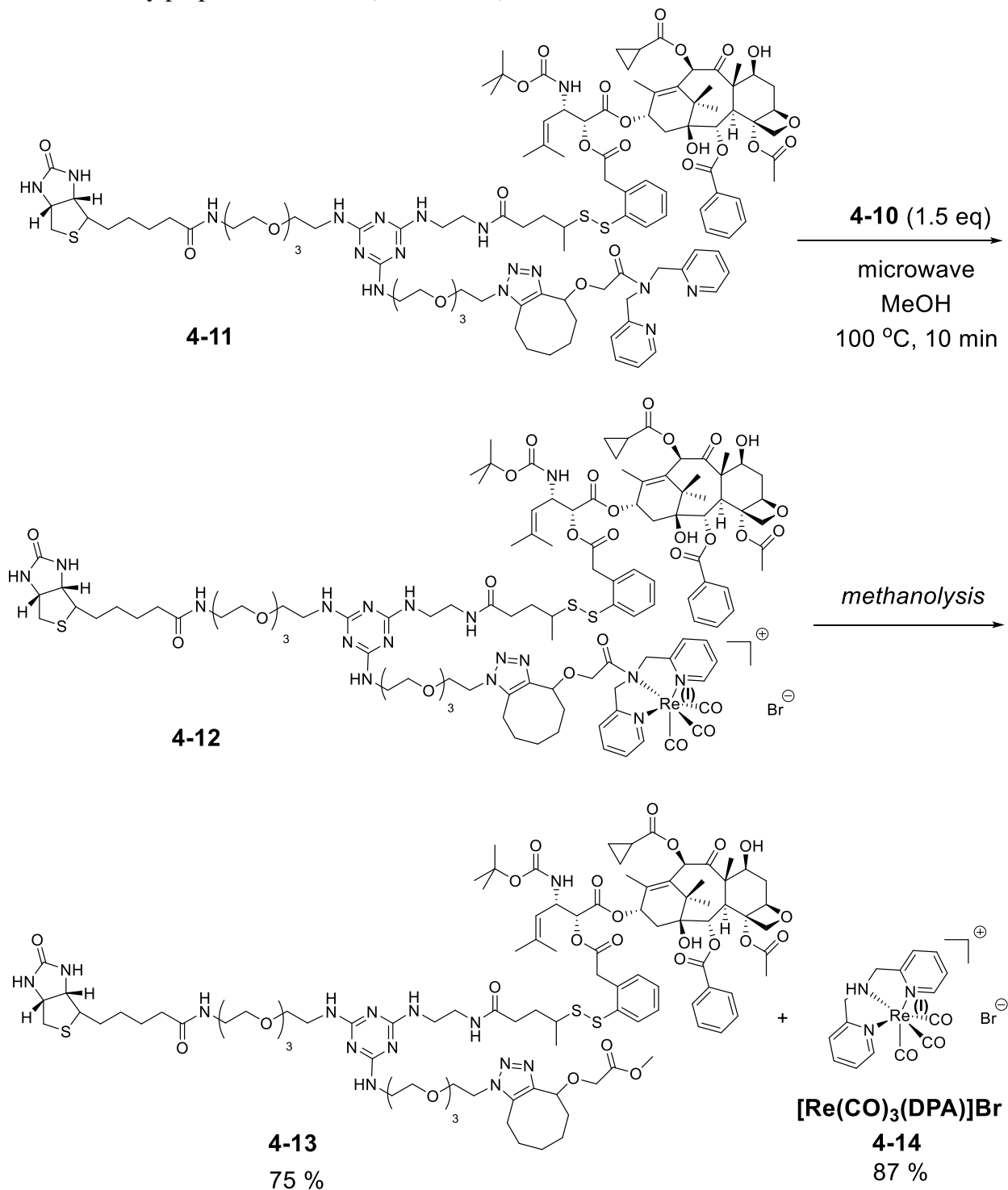
The rhenium (Re) species **4-10** was synthesized from commercial available bromopentacarbonylrhenium (I) (Re(CO)<sub>5</sub>Br) followed by the reported procedure.<sup>40</sup> (**Scheme 4.5**) Then the first attempt to synthesize the Biotin-Triazine-Linker-Drug-DPA(*sp*<sup>2</sup>N) **4-11** with amide nitrogen atom for direct coordination was done by SPAAC reaction between **4-5** and **4-9**. (**Scheme 4.6**) **4-11** could be isolated in high yield by preparative HPLC.



**Scheme 4.6** SPAAC reaction

Then we examined the feasibility of the amide N coordination of our dpa ligand with Re tricarbonyl species in the presence of methanol. The first example to support the possibility of coordination between amide N and a metal was reported in 1996.<sup>41</sup> A X-ray structure of a crystalline complex with CuCl<sub>2</sub> clearly showed the Cu-amide N coordination. However, in the presence of methanol, many cases showed the metal-amide N coordination will lead to an amide bond activation and cleavage by a metal (Cu or Re)-promoted methanolysis.<sup>42-44</sup> The Re-bpa complexes could only be obtained in dry acetonitrile, and readily undergo methanolysis once

treated with methanol.<sup>44</sup> Exceptionally there was a stable cadmium (Cd)-dpa complex can avoid the solvolysis.<sup>43</sup> So the chelation with  $[\text{Re}(\text{CO})_3(\text{H}_2\text{O})_3]^+$  was done in microwave sealed tube under 100 °C in methanol for 10 minutes. However, this chelation reaction did not give **4-12** as expected, but ended up with two products **4-13** and **4-14** which were confirmed by LC-MS-TOF and isolated by preparative HPLC. (Scheme 4.7)

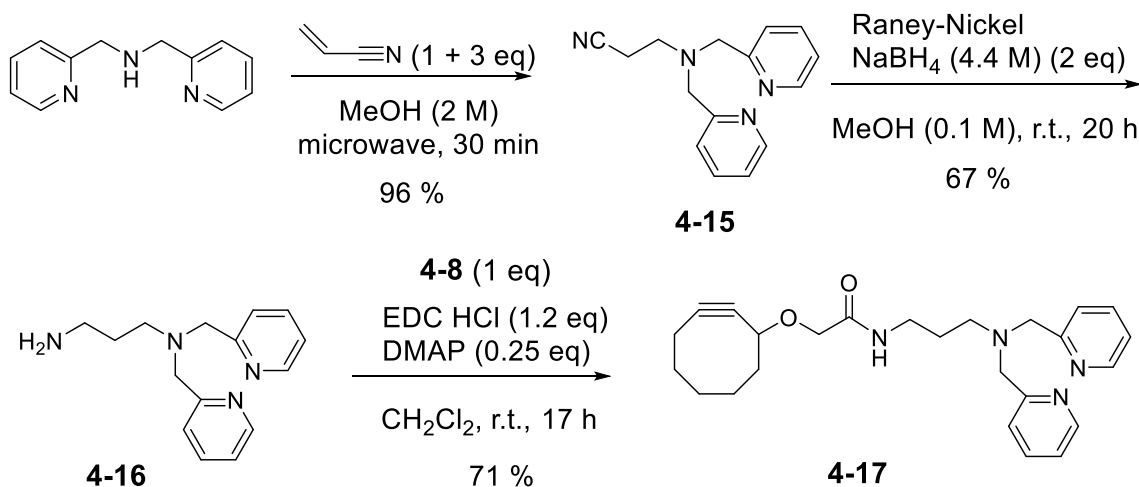


### Scheme 4.7 Rhenium tricarbonyl chelation and Re-promoted methanolysis

It turned out the Re-promoted methanolysis did occur during the chelation with metal species (rhenium tricarbonyl). Although literature supported that the  $sp^2$  nitrogen from amide bond could serve as a electron donor to coordinate with the metal, we found this chelated product was not stable in the methanol, and it favored to cleave the amide bond by replacement of methanol molecule to release a  $sp^3$  nitrogen to give a stable by-product. Also importantly, the successful isolation of **4-13** and **4-14** suggested the formation of intermediate **4-12**, indicating the addition of Re species was safe to the disulfide linker and taxoid moiety.

### §4.4.3 Synthesis of Cyclooctyne-DPA( $sp^3$ N) Trident Ligand

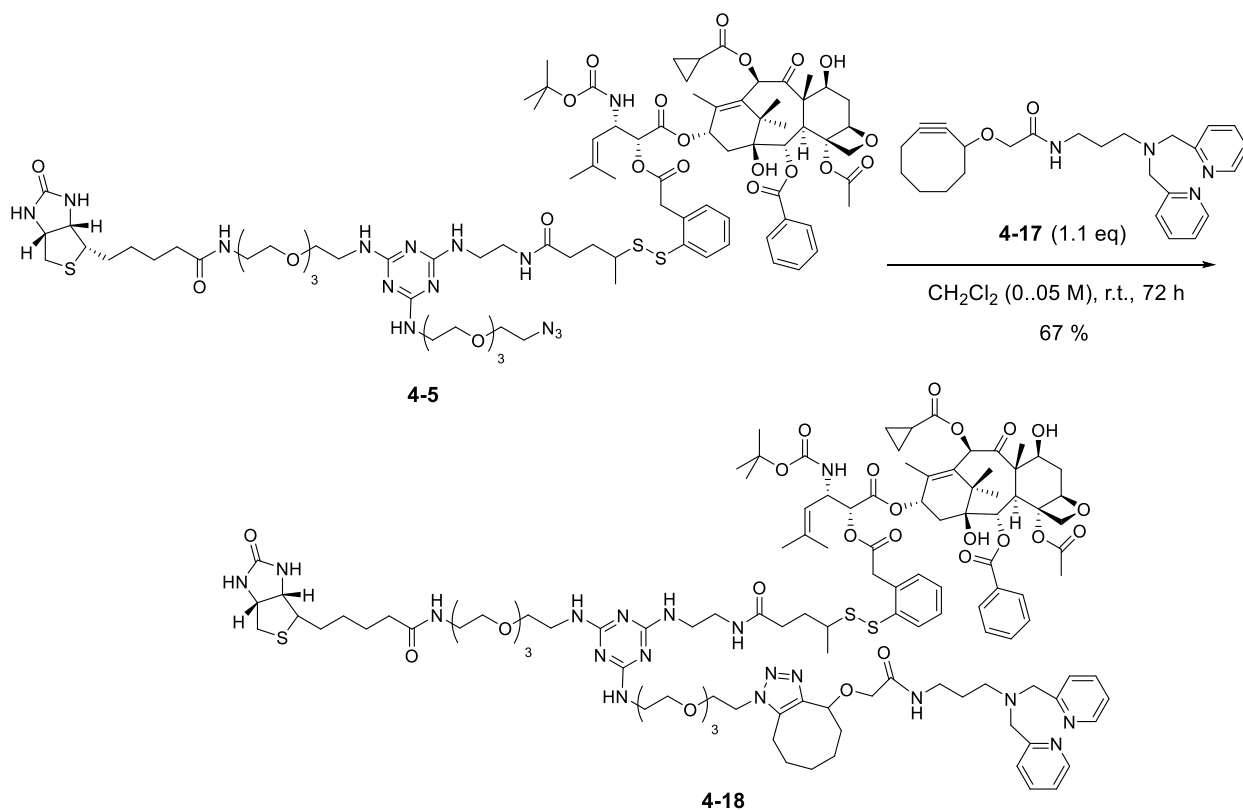
Consequently, an alternative cyclooctyne-DPA( $sp^3$ N) trident chelating ligand **4-17** was synthesized according to the reported procedures.<sup>45-46</sup> To obtain **4-17**, di-(2-picoly)amine was treated with acrylonitrile under microwave for 30 minutes, and reduced to **4-16** using Raney-Nickel solution with  $\text{NaBH}_4$ . Then **4-16** was coupled with **4-8** under EDC coupling condition to give **4-17** as modified cyclooctyne-DPA( $sp^3$ N) trident ligand for capturing rhenium (**Scheme 4.8**).



**Scheme 4.8** Synthesis of two click-ready cyclooctyne-DPA( $sp^3$ N) trident ligand

### §4.4.4 Cold Synthesis of Biotin-Triazine-Linker-Drug-DPA( $sp^3$ N)- $^{185}\text{Re}(\text{CO})_3$ and Biotin-DPA( $sp^3$ N)- $^{185}\text{Re}(\text{CO})_3$ Conjugates

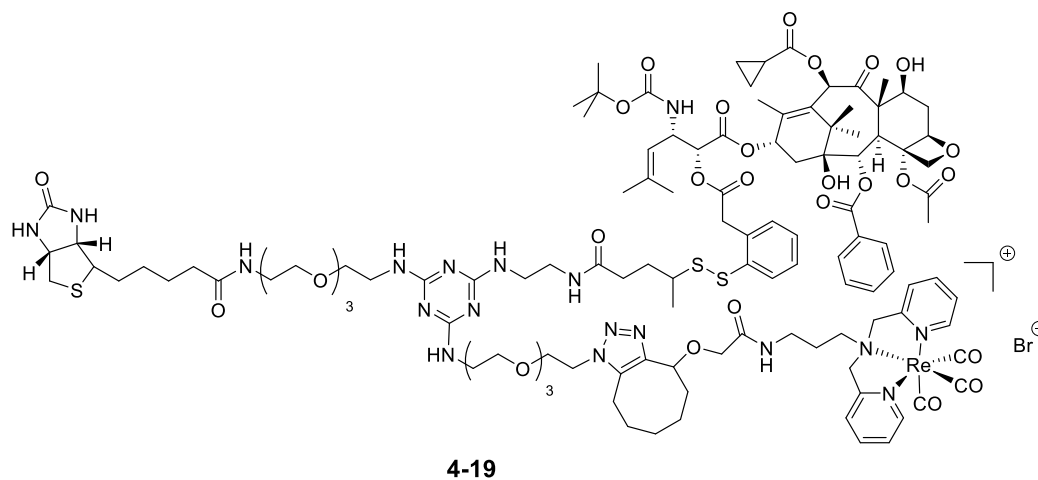
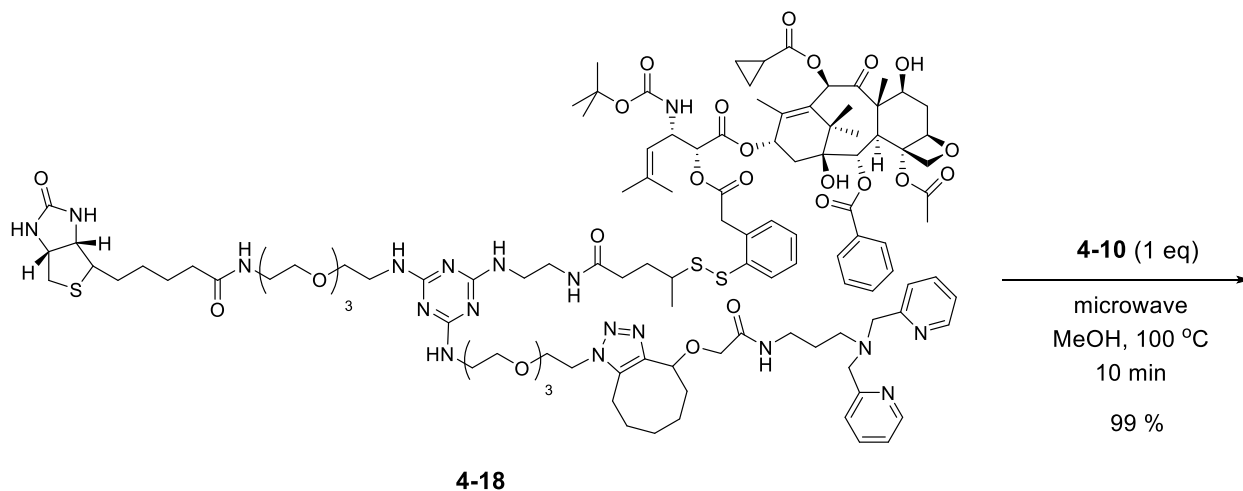
Followed the same SPAAC protocol, Intermediate **4-18** was obtained in good yield. (**Scheme 4.9**)



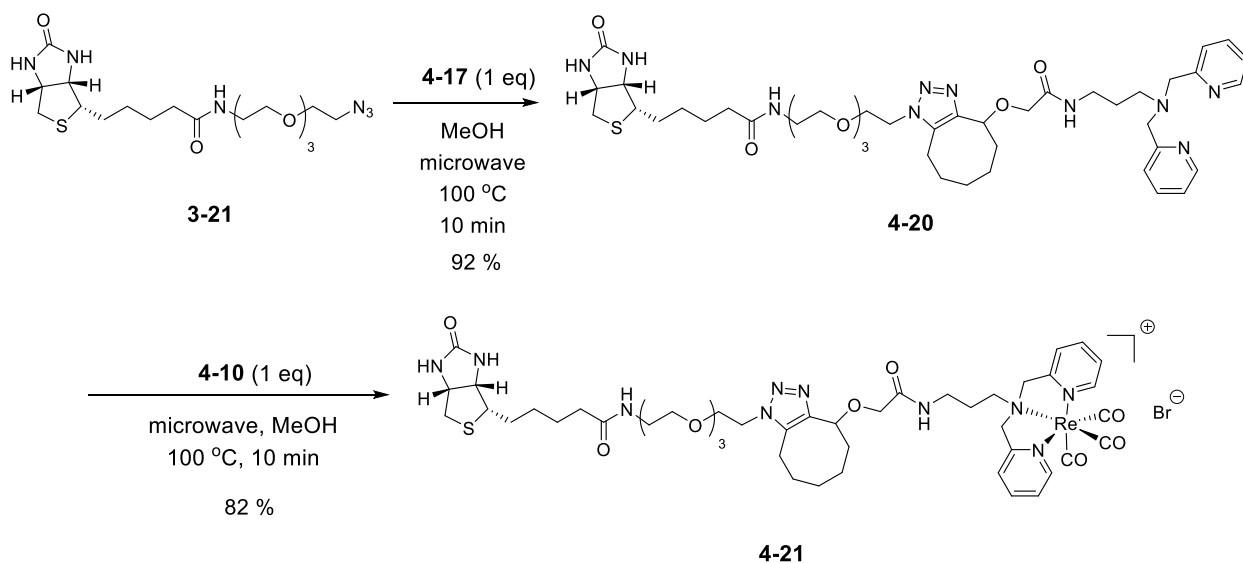
**Scheme 4.9** SPAAC of cyclooctyne-DPA( $sp^3N$ ) trident ligand

As anticipated, **4-19** was generated in the same microwave condition and stable to methanol without methanolysis (**Scheme 4.10**), which was confirmed by LC-MS-TOF. Product **4-19** was isolated by prep HPLC as a white solid. For hot synthesis with  $^{99m}\text{Tc}$  tricarbonyl species, intermediate **4-18** should be readily used for capturing  $^{99m}\text{Tc}$  by coordinate it under the same reaction condition. The reaction time has been optimized to 10 minutes and the purification has been established for *in vivo* SPECT study.

To primarily investigate the biotin distribution and localization, we also synthesized a simpler Biotin-Triazine-DPA-Re( $\text{CO}$ )<sub>3</sub> conjugate without drug-linker attached. (**Scheme 4.11**) Biotin-PEG<sub>3</sub>-(CH<sub>2</sub>)<sub>2</sub>-N<sub>3</sub> **3-21** was readily prepared from biotin and commercially available 11-azido-3,6,9 trioxaundecan-1-amine through amide coupling,<sup>47</sup> followed by the click reaction with **4-17** to give **4-20**. Then **4-21** was readily generated and isolated. This method was also ready for *in vivo* SPECT radiolabelling.



**Scheme 4.10** Cold Synthesis of Biotin-Triazine-Linker-Drug-DPA(*sp*<sup>3</sup>N)-<sup>185</sup>Re(CO)<sub>3</sub>

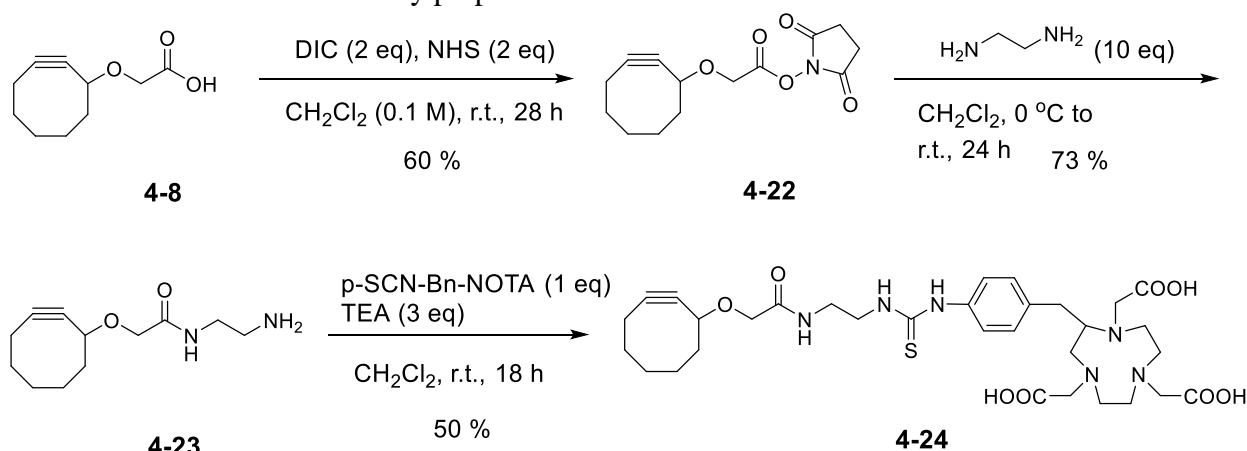


**Scheme 4.11** Synthesis of Biotin-Triazine-DPA-Re(CO)<sub>3</sub> conjugate **4-21**

## §4.5 Diagnostic/Theranostic $^{65}\text{Cu}$ (Cold)/ $^{64}\text{Cu}$ (Hot) PET Imaging Agents

### §4.5.1 Synthesis of Cyclooctyne-NOTA Hexadent Ligand

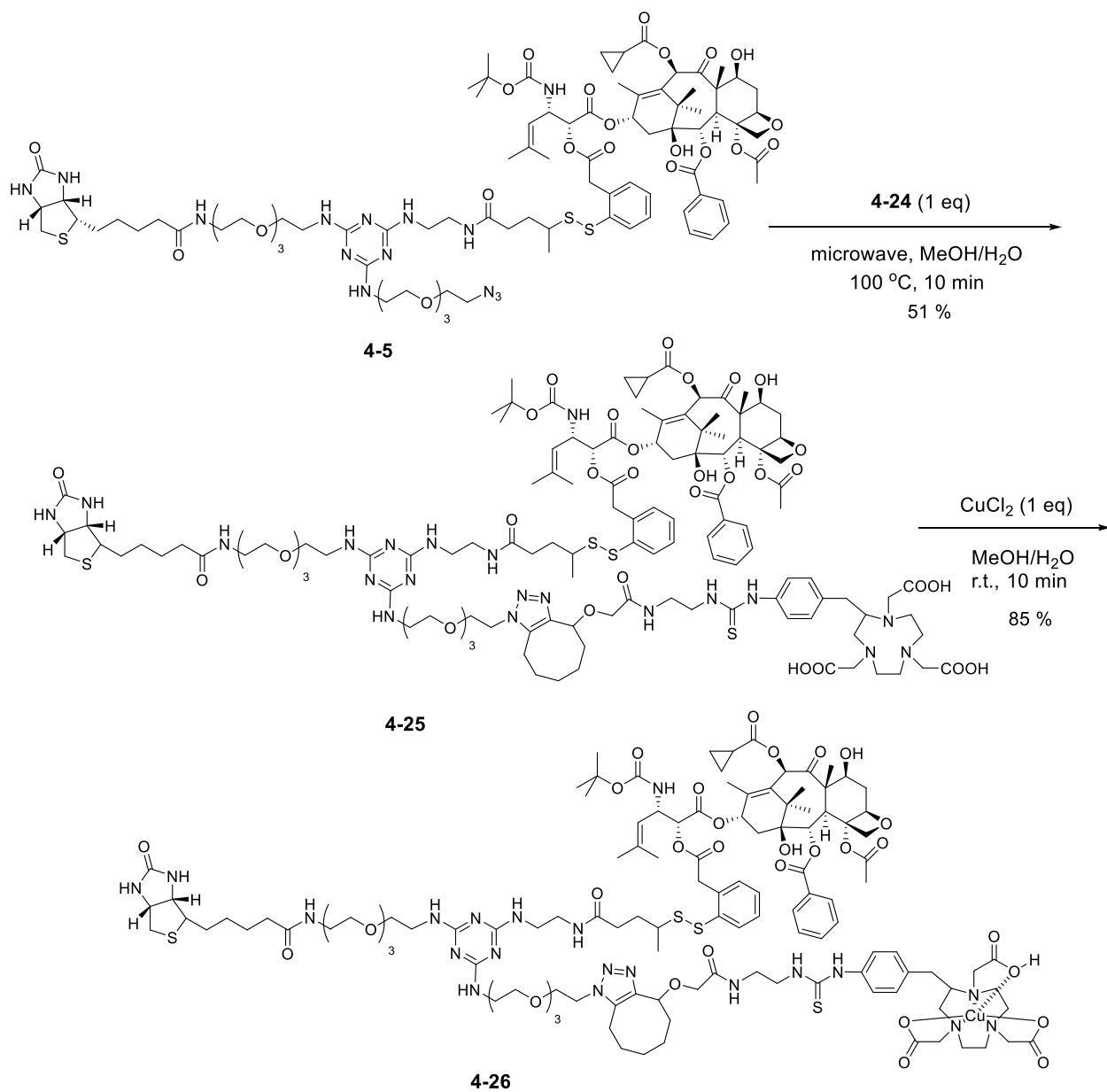
To chelate Cu species for PET study, we selected NOTA moiety which was commonly used to chelate Gallium 68 ( $^{68}\text{Ga}$ ),<sup>48-49</sup> Copper 64 ( $^{64}\text{Cu}$ )<sup>49-50</sup> or Indium 111 ( $^{111}\text{In}$ ).<sup>51</sup> To attach the copper-free click cyclooctyne with NOTA to generate compound **4-24**, extra steps were required. Because we planned to leave one amino group to react with p-SCN-Bn-NOTA (p-isothiocyanatobenzyl-1,4,7-triazacyclononane-*N,N',N''*-triacetic acid), instead of directly coupling **4-8** with ethylenediamine, we generated activated OSu ester **4-22**. Then to a solution of 10 eq excess diamine in DCM, **4-23** was dissolved previously and slowly added under 0 °C. Then commercially available p-SCN-Bn-NOTA was reacted with **4-23** to yield **4-24** (Scheme 4.12). Purification of **4-24** was done by prep HPLC.



**Scheme 4.12** Synthesis of cyclooctyne-p-SCN-Bn-NOTA **4-24**

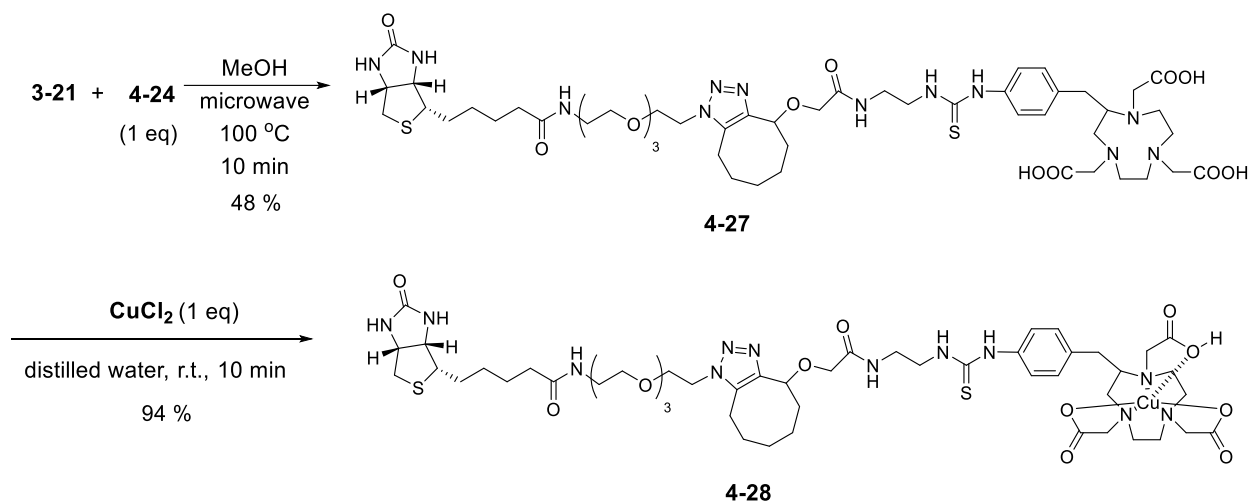
### §4.5.2 Cold Synthesis of Biotin-Triazine-Linker-Drug-NOTA- $^{65}\text{Cu}$ and Biotin-NOTA- $^{65}\text{Cu}$ Conjugates

The Biotin-Triazine-Linker-Drug-NOTA-Cu conjugate **4-26** was made by Cu-free click between intermediate **4-5** and **4-24** by microwave irradiation, followed by addition of copper (II) chloride to generate Cu-chelated **4-25** (Scheme 4.13).



**Scheme 4.13** Synthesis of Biotin-Triazine-Linker-Drug-NOTA-Cu conjugate **4-26**

A simple Cu-chelated molecule without the linker drug moiety was made in the same protocol (**Scheme 4.14**).



**Scheme 4.14** Synthesis of Biotin-Triazine-NOTA-Cu conjugate **4-28**

## §4.6 Summary

A triazine-based tripod platform has been applied to synthesize two theranostic probes bearing a DPA arm and NOTA arm for capturing Re and Cu, respectively. These two arms will be used to chelate  $^{99m}\text{Tc}$  and  $^{64}\text{Cu}$  for SPECT and PET, respectively, for *in vivo* imaging study. Two single molecule have also been constructed without warhead for biotin bearing biodistribution imaging study using SPECT/PET approaches. SPAAC as catalyst-free click reaction was applied with efficient reaction rate under microwave condition, and the resulting products were successfully purified by preparative HPLC in good purity. The chelation step condition of Re-DPA was optimized to 10 min under microwave, and Cu-NOTA chelation was optimized to 10 min under room temperature in aqueous solution. Both final chelated conjugates were isolated by preparative HPLC within 30 min. In addition, a Re-promoted methanolysis was found for DPA ligand bearing a  $\text{sp}^2$  nitrogen atom for coordination resulting in amide bond cleavage and ligand disassociation, which rarely be reported before.

## §4.7 Experimental Sections

### §4.7.1 Caution

Taxoids have been classified as potent cytotoxic agents. Thus, all drugs and structurally related compounds and derivatives must be considered as mutagens and potential reproductive hazards for both males and females. Silver perchlorate should be store away heat and direct sunlight. Appropriate precautions (i.e. use of gloves, goggles, lab coat and fume hood) must be taken while handling these compounds.

### §4.7.2 General Methods

$^1\text{H}$  and  $^{13}\text{C}$  NMR were measured on 300, 400 MHz Varian spectrometer or 400, 500, 700 MHz Bruker NMR spectrometer. The melting points were measured on a “Uni-melt” capillary melting point apparatus from Arthur H. Thomas Company, Inc and are uncorrected. TLC analyses were performed on Sorbent Technologies aluminum-backed Silica G TLC plates (Sorbent



Technologies, 200  $\mu\text{m}$ , 20 x 20 cm) and were visualized with UV light and stained with sulfuric acid-EtOH, 10 % PMA-EtOH or 10 % Vanillin-EtOH with 1% sulfuric acid. Column chromatography was carried out on silica gel 60 (Merck, 230-400 mesh ASTM). Chemical purity was determined with a Shimadzu L-2010A HPLC HT series HPLC assembly, using a Kinetex PFP column (4.6 mm x 100 mm, 2.6  $\mu\text{m}$ ), employing  $\text{CH}_3\text{CN}$ /water as the gradient solvent system with a flow rate of 1 mL/min. LC-UV-MS analysis was performed on an Agilent LC-UV-TOF mass spectrometer at the Institute of Chemical Biology and Drug Discovery, using a Kinetex C18 column (2.1 mm x 100 mm, 2.6  $\mu\text{m}$ , 100 angstroms), employing methanol/water with 10mM AmAc as the gradient solvent system, a flow rate of 0.5 mL/min under 35  $^\circ\text{C}$ , and with the UV detector set at 275 and 230 nm. The gradient was run from 60% to 95% methanol in water over a 45 minute period. Low resolution mass spectrometry was performed on an Agilent LC-MSD mass spectrometer at the Institute of Chemical Biology and Drug Discovery, Stony Brook, NY. High resolution mass spectrometry analysis was carried out on an Agilent LC-UV-TOF mass spectrometer at the Institute of Chemical Biology Drug Discovery, Stony Brook, NY or at the Mass Spectrometry Laboratory, University of Illinois at Urbana-Champaign, Urbana, IL.

### §4.7.3 Materials

The chemicals were purchased from Sigma-Aldrich, Fischer Scientific or VWR International, and used as received or purified before use by standard methods. Dichloromethane was dried before use by distillation over calcium hydride under nitrogen. Tetrahydrofuran was dried before use by distillation over sodium-benzophenone kept under nitrogen. Dry DMF was purchased from EMD chemical company, and used without further purification. Reaction flasks were dried in a 100  $^\circ\text{C}$  oven and allowed to cool to room temperature in a desiccator over “*Drierite*” (calcium sulfate) and assembled under an inert nitrogen gas atmosphere. Biological materials including RPMI-1640 cell culture media, DPBS buffer, fetal bovine serum, PenStrep, and TrypLE were obtained from Gibco and VWR International, and used as received for cell-based assays.

### §4.7.4 Experimental Procedure

#### **Tert-butyl (2-aminoethyl)carbamate (4-1)**<sup>52</sup>

To a 100 mL round-bottom flask was added ethylenediamine (10 g, 0.17 mol) dissolved in 0.1 M  $\text{CH}_2\text{Cl}_2$ . 0.1 eq Boc anhydride (3.71 g, 0.17 mol) was dissolved in 0.1 M  $\text{CH}_2\text{Cl}_2$  and was slowly added by addition funnel through 2 hours. The resulting solution was allowed to stir under room temperature for 23 hours. White solid started to form. Upon completion, the solvent was rotary evaporated and dissolved in distilled water, then the product was extracted with  $\text{CH}_2\text{Cl}_2$  and the organic layers were combined and dried with  $\text{MgSO}_4$ . Then the product was concentrated to yield light yellow oil **4-1** (2.3 g, 0.014 mol) in 82 % yield.  $^1\text{H}$  NMR (500 MHz,  $\text{CDCl}_3$ )  $\delta$  1.43 (s, 9 H), 2.79 (t,  $J$  = 5.85 Hz, 2 H), 3.16 (m, 2 H), 4.90 (broad, 1 H).  $^{13}\text{C}$  NMR (125 MHz,  $\text{CDCl}_3$ )  $\delta$  28.4, 31.2, 41.8, 43.3, 79.2, 156.2. All data are in accordance with literature values.<sup>52</sup>

#### **2-Chloro-4-(11-biotinylamino-3,6,9-trioxaundecyl)amino-6-(11-azido-3,6,9-trioxaundecyl)amino-1,3,5-triazine (4-2)**

To a 100 mL round bottom flask was added cyanuric chloride (124 mg, 0.67 mmol) dissolved in 0.02 THF (33.5 mL) under 0  $^\circ\text{C}$  in an ice-water bath. To this solution was slowly added 1 eq **3-19**

(146 mg, 0.67 mmol) dissolved in 2 mL THF, followed by addition of 1.5 eq DIPEA (86.6 mg, 0.67 mmol, 0.12 mL). The resulting solution was allowed to warm to room temperature and stirred for 2 hours. Then the reaction mixture was transferred to another round bottomed flask containing 1 eq **3-22** (280 mg, 0.67 mmol), followed by addition of 1.5 eq DIPEA (86.6 mg, 0.67 mmol, 0.12 mL). The reaction mixture was heated to 60 °C and allowed to stir for 19 hours. Upon completion, the solvent was removed and the product was purified by silica gel column chromatography eluting 0-10 % methanol in dichloromethane to yield **4-2** as a white sticky solid (210 mg, 0.28 mmol, 42 %). <sup>1</sup>H NMR (700 MHz, MeOD) δ 0.74-0.77 (m, *J* = 6.37 Hz, 1 H), 0.78 (t, *J* = 6.93 Hz, 1 H), 1.02 (d, *J* = 6.51 Hz, 1 H), 1.16-1.20 (m, 2 H), 1.32-1.35 (m, 3 H), 1.43-1.46 (m, 2 H), 1.54-1.59 (m, 3 H), 1.64-1.65 (m, 1 H), 2.10-2.14 (m, 2 H), 2.65 (d, *J* = 12.67 Hz, 1 H), 2.79 (dd, *J<sub>a</sub>* = 4.76 Hz, *J<sub>b</sub>* = 12.74 Hz, 1 H), 3.00-3.05 (m, 2 H), 3.30-3.33 (m, 3 H), 3.48-3.58 (m, 26 H), 3.58-3.68 (m, 1 H), 4.22 (m, 1 H), 4.41 (t, *J* = 5.53 Hz, 1 H), 6.14 (m, 1 H). <sup>13</sup>C NMR (125 MHz, MeOD) δ 11.3, 11.9, 14.0, 17.3, 18.5, 22.5, 23.4, 25.5, 25.6, 28.1, 28.3, 28.9, 29.5, 31.4, 34.5, 35.8, 35.9, 35.9, 39.0, 40.4, 40.5, 40.6, 40.7, 41.9, 42.8, 50.6, 53.6, 55.6, 56.6, 60.2, 61.7, 69.2, 69.9, 69.9541, 70.0, 70.3, 70.5, 70.5, 71.2, 164.3, 165.5, 165.6, 168.1, 168.9, 169.0, 173.3, 173.4. HRMS (TOF) [M+H]<sup>+</sup> *m/z* calcd. for C<sub>29</sub>H<sub>51</sub>ClN<sub>11</sub>O<sub>8</sub>S<sup>+</sup>: 748.3326, found 748.3321. (Δ = -0.6 ppm).

#### **2-(*N*-Bocaminoethyl)amino-4-(11-Biotinylamino-3,6,9-trioxaundecyl)amino-6-(11-azido-3,6,9-trioxaundecyl)amino-1,3,5-triazine (4-3)**

To a small round bottom flask **4-2** (210 mg, 0.28 mmol) was dissolved in 0.02 M THF (14 mL). To the solution was added 1.5 eq **4-1** (67.3 mg, 0.42 mmol), followed by addition of 1.5 eq DIPEA (54 mg, 0.42 mmol, 0.07 mL). The resulting solution was allowed to heat to reflux for 22 hours. The reaction was monitored by FIA. Upon completion, the solvent was removed and the product was purified by silica gel column chromatography eluting 0-15 % methanol in dichloromethane to yield **4-3** as a white sticky solid (150 mg, 0.17 mmol, 61 %). <sup>1</sup>H NMR (700 MHz, MeOD) δ 0.78 (m, 1 H), 0.79 (t, *J* = 6.8 Hz, 2 H), 1.17 (m, 2 H), 1.34 (s, 9 H), 1.54-1.57 (m, 3 H), 1.64-1.65 (m, 1 H), 2.14 (m, 2 H), 2.70 (d, *J* = 12.75 Hz, 1 H), 2.81 (dd, *J<sub>a</sub>* = 4.7 Hz, *J<sub>b</sub>* = 12.55 Hz, 1 H), 3.03-3.07 (m, 2 H), 3.20 (m, 2 H), 3.32 (m, 3 H), 3.51-3.62 (36 H), 4.27 (m, 1 H), 4.44 (m, 1 H), 6.70 (m, 1 H). <sup>13</sup>C NMR (176 MHz, MeOD) δ 11.3, 14.0, 18.7, 20.6, 22.6, 25.2, 25.6, 28.0, 28.3, 29.0, 29.6, 31.5, 34.4, 34.6, 35.6, 38.3, 39.1, 40.2, 40.3, 40.4, 40.6, 50.1, 50.6, 53.4, 55.7, 60.2, 60.3, 62.0, 69.8, 69.9, 70.0, 70.1, 70.2, 70.3, 70.5, 70.5, 79.0, 79.5, 156.2, 156.5, 164.3, 173.8. HRMS (TOF) [M+H]<sup>+</sup> *m/z* calcd. for C<sub>36</sub>H<sub>66</sub>N<sub>13</sub>O<sub>10</sub>S<sup>+</sup>: 872.4771, found 872.4766. (Δ = -0.6 ppm).

#### **2-(2-Aminoethyl)amino-4-(11-Biotinylamino-3,6,9-trioxaundecyl)amino-6-(11-azido-3,6,9-trioxaundecyl)amino-1,3,5-triazine TFA Salt (4-4)**

To a 10 mL round bottom flask was added **4-3** (150 mg, 0.17 mmol) dissolved in 0.02 M CH<sub>2</sub>Cl<sub>2</sub> (9 mL). To this solution was added 20 volume% TFA (1.8 mL) and the resulting solution was stirred for 2 hours under room temperature. The reaction was monitored by TLC. Upon completion, the solvent was removed by lyophilization to afford the formation of crude **4-3** (234 mg) which was directly taken for the next step <sup>1</sup>H NMR (700 MHz, MeOD) δ 1.16-1.18 (m, 2 H), 1.31-1.48 (m, 6 H), 1.77 (s, 2 H), 1.96 (s, 2 H), 2.44 (d, *J* = 12.74 Hz, 1 H), 2.65 (dd, *J<sub>a</sub>* = 4.83 Hz, *J<sub>b</sub>* = 12.74 Hz, 1 H), 2.94 (m, 3 H), 3.05 (s, 2 H), 3.09 (m, 3 H), 3.28 (m, 3 H), 3.38 (m, 32 H), 4.04 (m, 1 H), 4.23 (m, 1 H). <sup>13</sup>C NMR (176 MHz, MeOD) δ 25.4, 28.1, 28.3, 35.3, 37.9, 38.8, 38.9, 39.1, 39.6, 40.2, 40.3, 50.3, 55.5, 60.2, 62.0, 68.5, 69.1, 69.2, 69.6, 69.8, 69.9, 70.0, 70.1,

113.2, 114.9, 116.5, 116.7, 118.2, 155.0, 155.7, 156.3, 57.3, 159.6, 159.8, 162.7, 163.4, 164.0, 164.6, 174.7. HRMS (TOF)  $[M+H]^+$   $m/z$  calcd. for  $C_{31}H_{58}N_{13}O_8S^+$ : 772.4247, found 386.7166, 772.4257. ( $\Delta = 1.3$  ppm).

### **2-[2-(Taxoid-SS-Linker)amidoethyl]amino-4-(11-Biotinylamino-3,6,9-trioxaundecyl)amino-6-(11-azido-3,6,9-trioxaundecyl)amino-1,3,5-triazine (4-5)**

To a 25 mL round bottom flask were added crude **4-4** (234 mg) and 1.2 eq **3-11** (246 mg, 0.2 mmol). 0.01 M DCM (17 mL) was added to partially dissolve the mixture, followed by the addition of 1.5 eq DIPEA (33 mg, 0.26 mmol, 0.045 mL). The reaction mixture was allowed to stir under room temperature for 15 hours. Upon completion, the solvent was removed and the product was purified by silica gel column chromatography eluting 0-20 % methanol in dichloromethane to yield **4-5** as a white solid (209 mg, 0.11 mmol, 65 % for two steps).  $^1H$  NMR (700 MHz, MeOD)  $\delta$  0.91-0.92 (m, 3 H), 1.05 (m, 2 H), 1.10 (m, 2 H), 1.30 (s, 9 H), 1.60 (s, 2 H), 1.66 (s, 3 H), 1.67 (s, 3 H), 1.79-1.81 (m, 2 H), 1.85 (s, 3 H), 2.03 (s, 1 H), 2.13 (m, 2 H), 2.30 (s, 3 H), 2.46 (m, 1 H), 2.68 (m, 1 H), 2.82 (m, 2 H), 3.50-3.66 (m, 40 H), 3.74 (d,  $J = 6.75$  Hz, 1 H), 3.90 (d,  $J = 16.55$  Hz, 1 H), 4.02 (d,  $J = 16.4$  Hz, 1 H), 4.11 (d,  $J = 8.05$  Hz, 1 H), 4.23 (s, 2 H), 4.35 (m, 1 H), 4.43 (m, 1 H), 4.89-4.92 (m, 3 H), 5.08 (s, 1 H), 5.26 (s, 2 H), 5.61 (d,  $J = 6.6$  Hz, 1 H), 6.12 (m, 1 H), 6.26 (s, 1 H), 7.17-7.20 (m, 2 H), 7.41 (t,  $J = 7.45$  Hz, 2 H), 7.54 (t,  $J = 7.25$  Hz, 1 H), 7.73 (d,  $J = 7.6$  Hz, 1 H), 8.04 (d,  $J = 7.55$  Hz, 2 H), 10.74 (broad, 1 H).  $^{13}C$  NMR (176 MHz, MeOD) 9.1, 9.2, 9.5, 11.8, 13.0, 14.7, 17.5, 18.4, 18.7, 20.3, 20.6, 22.0, 22.4, 25.2, 25.6, 26.5, 27.8, 29.0, 29.6, 31.2, 33.3, 34.4, 34.6, 35.5, 35.6, 36.0, 38.6, 39.0, 40.1, 41.9, 43.1, 45.8, 46.1, 50.6, 53.0, 55.5, 58.3, 60.5, 62.1, 69.2, 69.9, 70.0, 70.2, 70.4, 71.7, 71.9, 75.0, 75.1, 75.4, 76.3, 79.0, 79.7, 80.8, 84.4, 113.2, 115.6, 117.9, 119.8, 120.2, 127.6, 128.3, 128.6, 129.2, 130.1, 130.9, 132.4, 133.1, 133.6, 137.4, 137.5, 137.8, 143.0, 155.0, 161.2, 161.5, 161.8, 162.1, 164.6, 166.8, 168.2, 169.7, 170.4, 173.1, 173.9, 174.8, 204.0. HRMS (TOF)  $[M+H]^+$   $m/z$  calcd. for  $C_{89}H_{129}N_{14}O_{25}S_3^+$ : 1889.8410, found 1889.8398. ( $\Delta = -0.6$  ppm).

### **8,8-Dibromobicyclo[5.0.1]octane (4-6)<sup>37-39</sup>**

To a 100 mL round bottom flask was added cycloheptene (4 g, 41.7 mmol) and dissolved in pentane (1 M) (40 mL) at 0 °C. To the solution, 2 eq potassium tert-butoxide (9.3 g, 83.4 mmol) was added and stir for 15 minutes under 0 °C. 1.5 eq bromoform (15.8 g, 5.6 mL, 62.6 mmol) was added dropwise over 20 minutes and the mixture turned pale brown. The resulting mixture was allowed to warm to room temperature and stir for 21 hours. Then water (30 mL) was added and the mixture was neutralized with HCl 1 M. The product was extracted with pentane (2 x 50 mL) and the combined organic layers were washed with water (2 x 20 mL), dried over  $MgSO_4$  and concentrated *in vacuo* to give crude material as a brown oil. The crude material was purified by silica gel chromatography, eluting with 0-2 % ethyl acetate in hexanes, to yield pure product **4-6** (9 g, 33.4 mmol, 80 %) as a colorless oil.  $^1H$  NMR (500 MHz,  $CDCl_3$ )  $\delta$  1.14-1.21 (m, 3 H), 1.32-1.37 (m, 2 H), 1.68-1.72 (m, 2 H), 1.80-1.91 (m, 3 H), 2.24-2.27 (m, 2 H).  $^{13}C$  NMR (125 MHz,  $CDCl_3$ )  $\delta$  28.0, 28.9, 32.2, 34.7, 40.7. All data are in accordance with literature values.<sup>37-39</sup>

### **Methyl 2-bromocyclooct-1-en-3-glycolate (4-7)<sup>37-39</sup>**

An aliquot of **4-5** (1.6 g, 6.2 mmol) was dissolved in 0.5 M toluene (12 mL) under room temperature. To this solution 9 eq methyl glycolate (5 g, 4.2 mL, 55.5 mmol) was added, followed by addition of 2 eq silver perchlorate (2.57 g, 12.4 mmol). The reaction mixture was protected from light by an aluminum foil and stirred at room temperature for 2 hours. Silver salts were then filtered and washed with toluene. The clear filtrate is concentrated and the color turned from colorless to purple/brown during rotary evaporation. The residue was purified straight away by column chromatography, eluting with 0-30 % ethyl acetate in hexanes to afford **4-7** as a yellow oil (966 mg, 3.5 mmol, 56 %). <sup>1</sup>H NMR (500 MHz, CDCl<sub>3</sub>) δ 0.75-0.82 (m, 1 H), 1.21-1.30 (m, 1 H), 1.42-1.50 (m, 1 H), 1.66- 1.72 (m, 1 H), 1.86-1.94 (m, 2 H), 1.98-2.09 (m, 2 H), 2.25-2.29 (m, 1 H), 2.67-2.73 (m, 1 H), 3.72 (s, 3 H), 3.94 (d, J =16.5 Hz, 1 H), 4.01 (dd, *Ja* = 5.1 Hz, *Jb* = 10.7 Hz, 1 H), 4.20 (d, J =16.5 Hz, 1 H), 6.18 (dd, *Ja* = 4.1 Hz, *Jb* = 11.7 Hz, 1 H). <sup>13</sup>C NMR (125 MHz, CDCl<sub>3</sub>) δ 26.3, 28.1, 33.4, 36.5, 39.4, 51.8, 65.5, 84.8, 131.5, 133.0, 170.7. All data are in accordance with literature values.<sup>37-39</sup>

### Cyclooct-1-yn-3-glycolic acid (**4-8**)<sup>37-39</sup>

An aliquot of **4-7** (961 mg, 3.48 mmol) was dissolved in 0.5 M anhydrous dimethylsulfoxide (DMSO) (7 mL) under room temperature. To this solution was added 2 eq NaOMe (276 mg, 6.96 mmol) and reaction turned dark yellow. The mixture was stirred at room temperature for 24 hours. Upon completion, 2 ml of water was added to the solution and the reaction was acidified with 1 M HCl to adjust pH to 2 and the product was extracted with ethyl acetate (30 mL x 3). The combined organic layers were washed with water (10 mL), dried over MgSO<sub>4</sub> and concentrated *in vacuo* to obtain crude material as a yellow oil. The crude material was purified by silica gel column chromatography eluting 0-35 % ethyl acetate in hexanes to yield **4-8** as a slight yellow oil (540 mg, 2.97 mmol, 85 %). <sup>1</sup>H NMR (700 MHz, CDCl<sub>3</sub>) δ 1.33 (m, 1 H), 1.47-1.51 (m, 1 H), 1.63-1.65 (m, 2 H), 1.76-1.82 (m, 2 H), 1.93 (m, 1 H), 2.04 (m, 1 H), 2.10-2.29 (m, 2 H), 4.07-4.12 (d, J= 17.0 Hz, 1 H), 4.22-4.26 (d, J = 17.0 Hz, 1 H), 4.37-4.40 (m, 1 H), 9.95 (broad, 1H). <sup>13</sup>C NMR (176 MHz, CDCl<sub>3</sub>) δ 20.7, 26.2, 29.6, 34.2, 42.2, 65.7, 73.1, 91.0, 102.0, 175.1. All data are in accordance with literature values.<sup>37-39</sup>

### 2-(Cyclooct-2-yn-1-yloxy)-*N,N*-bis(pyridin-2-ylmethyl)acetamide (**4-9**)

To a round bottom flask was added **4-8** (200 mg, 1.1 mmol), 0.25 eq DMAP (34 mg, 0.28 mmol), and 1.2 eq EDC HCl salt (253 mg, 1.32 mmol) dissolved in 0.05 M CH<sub>2</sub>Cl<sub>2</sub> (22 mL) under room temperature. To this solution was added 1 eq di-(2-picoly)amine (219 mg, 1.1 mmol) dissolved in 2 mL CH<sub>2</sub>Cl<sub>2</sub> dropwise. The reaction was allowed to stir under room temperature for 13 hours and monitored by TLC. Upon completion, the product was purified straight away by column chromatography, eluting with pure ethyl acetate to afford **4-9** as a yellow oil (289 mg, 0.79 mmol, 71 %). <sup>1</sup>H NMR (500 MHz, MeOD) δ 1.20-1.26 (m, 1 H), 1.32-1.43 (m, 1 H), 1.51-1.55 (m, 1 H), 1.60-1.65 (m, 2 H), 1.74-1.79 (m, 4 H), 1.82-1.96 (m, 1 H), 2.00-2.09 (m, 1 H), 2.10-2.17 (m, 1 H), 2.20-2.23 (m, 1 H), 2.61-2.67 (m, 2 H), 4.20-4.47 (m, 2 H), 4.68 (m, 4H), 7.10-7.16 (m, 6 H), 7.25-7.28 (m, 2 H), 7.55-7.60 (m, 4 H), 8.84 (d, *J* = 4.4 Hz, 2H), 8.84 (d, *J* = 4.6 Hz, 2H). <sup>13</sup>C NMR (125 MHz, MeOD) δ 20.6, 23.5, 26.2, 26.8, 29.6, 34.2, 37.3, 42.1, 51.9, 60.4, 68.4, 73.0, 91.3, 101.5, 122.0, 123.0, 123.1, 136.4, 149.0, 159.4, 169.4. HRMS (TOF) [M+H]<sup>+</sup> m/z calcd. for C<sub>22</sub>H<sub>26</sub>N<sub>3</sub>O<sub>2</sub><sup>+</sup>: 364.2020, found 364.2019. (Δ = -0.3 ppm).

### Rhenium tricarbonyl-water complex bromide salt (**4-10**)<sup>40</sup>

To a round bottomed flask was added bromopentacarbonylrhenium (I) (1 g, 2 mmol) mixed with distilled water (4 mL). The suspension was allowed to heat to reflux for 24 hours. The crude mixture was cooled to room temperature and filtered through celite to remove impurities. Then the solution was concentrated in vacuum to give **4-10** (505 mg) in 55 % as pale yellow solid.<sup>40</sup>

### Biotin-Triazine-Linker-Drug-DPA(*sp*<sup>2</sup>N) Construct (**4-11**)

To a 5 mL round-bottomed flask was added **4-5** (76 mg, 40  $\mu$ mol) dissolved in 0.05 M DCM (0.1 mL). To the solution was added 1 eq **4-9** (15 mg, 40  $\mu$ mol) dissolved in 0.1 mL DCM. The resulting solution was allowed to stir under room temperature for 48 hours and the reaction was monitored by TLC. Upon completion, the solvent was removed and the product was purified by silica gel column chromatography eluting 0-30 % methanol in dichloromethane to yield **4-11** as a white solid (62 mg, 28  $\mu$ mol, 70 %). <sup>1</sup>H NMR (500 MHz, CDCl<sub>3</sub>)  $\delta$  0.86-0.88 (m, 2 H), 0.95-0.98 (t, *J* = 6.9 Hz, 2 H), 1.10 (s, 2 H), 1.15 (s, 2 H), 1.23-1.25 (m, 15 H), 1.34 (s, 8 H), 1.65 (s, 3 H), 1.70 (s, 3 H), 1.71 (s, 3 H), 1.85-1.87 (m, 3 H), 1.90 (s, 3 H), 2.19 (m, 3 H), 2.35 (s, 3 H), 2.50 (quinine, 1 H), 2.68 (m, 1 H), 2.74-2.76 (m, 2 H), 2.84 (m, 2 H), 3.08 (m, 2 H), 3.34 (m, 4 H), 3.55-3.62 (m, 20 H), 3.79 (d, *J* = 4.8 Hz, 1 H), 3.89 (s, 1 H), 3.95 (d, *J* = 11.9, 1 H), 4.06 (d, *J* = 11.5, 1 H), 4.11 (m, 1 H), 4.16 (d, *J* = 6 Hz, 1 H), 4.24 (m, 2 H), 4.28 (d, *J* = 5.95 Hz, 2 H), 4.38-4.41 (m, 1 H), 4.44 (m, 1 H), 4.58 (m, 2 H), 4.72 (m, 1 H), 4.94 (s, 2 H), 5.07 (m, 1 H), 5.11 (m, 1 H), 5.28 (m, 2 H), 5.66 (d, *J* = 4.85 Hz, 1 H), 6.16 (t, 1 H), 6.31 (s, 1 H), 7.09 (m, 1 H), 7.15 (m, 2 H), 7.22 (m, 1 H), 7.27 (t, *J* = 6.05 Hz, 1 H), 7.45 (t, *J* = 5.4 Hz, 2 H), 7.58 (m, 2 H), 7.77 (m, 1 H), 8.09 (d, *J* = 5.35 Hz, 1 H), 8.46 (m, 1 H), 8.50 (s, 1 H). <sup>13</sup>C NMR (125 MHz, CDCl<sub>3</sub>)  $\delta$  9.1, 9.2, 9.6, 13.0, 14.1, 14.2, 14.7, 18.5, 20.5, 21.0, 21.1, 22.0, 22.3, 22.4, 22.6, 24.0, 24.7, 25.7, 26.6, 28.2, 29.7, 31.0, 31.3, 31.9, 33.4, 33.5, 33.7, 35.4, 35.6, 38.7, 39.0, 40.5, 41.7, 43.2, 45.8, 46.3, 46.4, 47.5, 48.4, 49.0, 51.1, 51.2, 52.0, 52.1, 53.4, 55.6, 55.9, 58.4, 60.2, 60.3, 61.9, 66.1, 67.4, 68.6, 69.8, 70.1, 70.3, 70.4, 71.5, 71.8, 71.9, 75.0, 75.1, 75.4, 76.4, 79.1, 79.7, 81.0, 84.4, 113.9, 115.3, 115.9, 117.6, 119.9, 121.3, 121.5, 122.5, 122.7, 127.7, 128.3, 128.6, 129.3, 130.1, 130.3, 130.9, 132.6, 133.0, 133.2, 133.6, 136.8, 137.5, 137.6, 137.8, 143.0, 143.6, 144.9, 149.1, 149.2, 149.7, 149.8, 155.0, 155.8, 156.2, 156.6, 161.9, 162.1, 166.9, 168.2, 169.6, 170.1, 170.4, 172.8, 173.5, 174.8, 204.0. HRMS (TOF) [M+H]<sup>+</sup> *m/z* calcd. for C<sub>114</sub>H<sub>154</sub>N<sub>17</sub>O<sub>27</sub>S<sub>3</sub><sup>+</sup>: 2253.0357, found 752.0170, 1127.5220, deconvolution result 2253.0295. ( $\Delta$  = -2.8 ppm).

### Biotin-Triazine-Linker-Drug-Methyl Ester (**4-13**)

To a 10 mL microwave tube was added **4-11** (47 mg, 20.9  $\mu$ mol) and 1.5 eq **4-10** (12.6 mg, 31.3  $\mu$ mol) dissolved in 2 mL MeOH. The tube was sealed and allowed to be heated by microwave under 100 °C for 10 minutes while stirring. Then the solution was cooled down to room temperature and filter out to remove undissolved solid. The filtrate was concentrated and later be purified by prep HPLC to yield construct **4-13** as white solid (33 mg, 15.8  $\mu$ mol, 75 %). <sup>1</sup>H NMR (700 MHz, MeOD)  $\delta$  0.89-0.90 (m, 12 H), 0.98-0.99 (m, 3 H), 1.14 (s, 3 H), 1.18 (s, 3 H), 1.28 (m, 19 H), 1.37 (s, 9 H), 1.69 (s, 3 H), 1.73 (s, 3 H), 1.74 (s, 3 H), 1.93 (m, 6 H), 2.06 (m, 2 H), 2.11 (m, 2 H), 2.24 (m, 2 H), 2.38 (m, 4 H), 2.54 (m, 1 H), 2.74 (m, 1 H), 2.92 (m, 2 H), 3.11 (m, 2 H), 3.41-3.76 (m, 36 H), 3.94 (m, 2 H), 4.02 (s, 1 H), 4.12 (m, 3 H), 4.20 (m, 1 H), 4.31 (m, 2 H), 4.42 (m, 2 H), 4.49 (s, 1 H), 4.62-4.68 (m, 1 H), 4.97 (m, 4 H), 5.14 (m, 2 H), 5.69 (m, 2 H), 6.20 (m, 1 H),

6.34 (s, 1 H), 7.49 (m, 2 H), 7.62 (m, 1 H), 7.80 (m, 1 H), 8.12 (m, 2 H).  $^{13}\text{C}$  NMR (176 MHz, MeOD)  $\delta$  9.1, 9.3, 9.6, 11.4, 13.0, 14.1, 14.7, 18.5, 18.7, 20.1, 20.7, 20.8, 21.0, 22.1, 22.4, 22.6, 24.1, 24.5, 25.2, 25.5, 25.7, 26.6, 26.7, 27.6, 28.0, 28.2, 29.0, 31.3, 31.6, 33.4, 33.6, 34.5, 34.6, 35.3, 35.4, 35.7, 36.0, 38.7, 39.2, 39.9, 40.4, 41.3, 43.2, 45.8, 46.5, 47.5, 48.5, 49.1, 51.7, 51.9, 58.3, 60.0, 60.4, 62.0, 64.9, 65.7, 69.9, 70.2, 70.5, 70.6, 71.8, 71.9, 74.9, 75.1, 75.4, 79.1, 79.7, 81.0, 84.5, 119.9, 127.7, 128.3, 128.6, 129.3, 130.1, 130.5, 131.0, 132.6, 133.3, 133.6, 135.3, 137.6, 137.8, 143.8, 155.0, 165.8, 166.9, 168.3, 169.7, 170.4, 170.9, 172.7, 173.2, 174.8, 204.0. HRMS (TOF)  $[\text{M}+\text{H}]^+$   $m/z$  calcd. for  $\text{C}_{100}\text{H}_{145}\text{N}_{14}\text{O}_{28}\text{S}_3^+$ : 2085.9509, found 696.3228, 1043.9800, deconvolution result 2085.9458. ( $\Delta = -2.4$  ppm). LC/UV/MS-TOF  $t_{\text{R}} = 17.87$  min.

### Rhenium tricarbonyl-DPA(*sp*<sup>2</sup>N) complex bromide salt (**4-14**)

To a 10 mL microwave tube was added **4-11** (47 mg, 20.9  $\mu\text{mol}$ ) and 1.5 eq **4-10** (12.6 mg, 31.3  $\mu\text{mol}$ ) dissolved in 2 mL MeOH. The tube was sealed and allowed to heated by microwave under 100  $^{\circ}\text{C}$  for 10 minutes while stirring. Then the solution was cooled down to room temperature and filter out to remove undissolved solid. The filtrate was concentrated and later be purified by prep HPLC to yield construct **4-14** as yellow solid (10 mg, 18  $\mu\text{mol}$ , 87 %).  $^1\text{H}$  NMR (500 MHz, MeOD)  $\delta$  5.51 (s, 4 H), 7.38 (t,  $J = 6.6$  Hz, 2 H), 7.60 (d,  $J = 7.9$  Hz, 2 H), 7.77 (s, 1 H), 7.95 (t,  $J = 6.65$  Hz, 2 H), 8.94 (d,  $J = 5.5$  Hz, 2 H).  $^{13}\text{C}$  NMR (125 MHz, MeOD)  $\delta$  53.4, 62.0, 123.0, 125.3, 140.0, 151.8, 160.8. HRMS (TOF)  $[\text{M}+\text{H}]^+$   $m/z$  calcd. for  $\text{C}_{15}\text{H}_{13}\text{N}_3\text{O}_3\text{Re}^+$ : 470.0514, found 470.0512. ( $\Delta = -0.4$  ppm). LC/UV/MS-TOF  $t_{\text{R}} = 3.69$  min.

### 3-(Bis(pyridin-2-ylmethyl)amino)propanenitrile (**4-15**)<sup>45-46</sup>

To a 10 mL microwave tube was added di-(2-picoly) amine (1 g, 5 mmol) and 1 eq acrylonitrile (265 mg, 5 mmol, 0.33 mL) dissolved in 2 M MeOH (2.5 mL). The tube was sealed and allowed to heat to 100  $^{\circ}\text{C}$  using microwave (260 W) for 30 mins. The reaction was monitored by TLC. Another 3 eq of acrylonitrile were added and the resulting solution was allowed to run under microwave condition for additional 30 mins to push reaction go completion. Upon completion, the solvent was removed and the product was purified by silica gel column chromatography eluting 0-5 % methanol in dichloromethane to yield **4-15** as a yellow oil (1.2 g, 4.8 mmol, 96 %).  $^1\text{H}$  NMR (500 MHz,  $\text{CDCl}_3$ )  $\delta$  2.51 (t,  $J = 6.85$  Hz, 2 H), 2.87 (t,  $J = 6.75$  Hz, 2 H), 3.85 (s, 4 H), 7.14 (m, 2 H), 7.53 (d,  $J = 7.85$  Hz, 2 H), 7.64 (dt,  $J_a = 1.75$  Hz,  $J_b = 7.6$  Hz, 2 H), 8.49 (d,  $J = 4.3$  Hz, 2 H).  $^{13}\text{C}$  NMR (700 MHz,  $\text{CDCl}_3$ )  $\delta$  16.4, 49.3, 59.9, 118.8, 122.3, 123.2, 136.7, 149.1, 158.4. HRMS calcd. for  $\text{C}_{15}\text{H}_{17}\text{N}_4^+$   $[\text{M}+\text{H}]^+$  253.1448, found 253.1510. ( $\Delta = 24$  ppm). All data are in accordance with literature values.<sup>45-46</sup>

### *N,N*-Bis(pyridin-2-ylmethyl)propane-1,3-diamine (**4-16**)<sup>45-46</sup>

To a 100 mL 3 neck round-bottomed flask was added **4-15** (1.2 g, 4.8 mmol) dissolved in 0.1 M MeOH (50 mL) under room temperature. To the resulting solution was slowly added Raney-Nickel 2800 in water slurry solution (5 mL) and then vigorously stirred. To this suspension, 2 eq 4.4 M  $\text{NaBH}_4$  in NaOH (aq) (9.5 mmol, 2.2 mL) was slowly added and the resulting suspension was stirred under room temperature for 20 hours. Upon completion, the Raney-Nickel catalyst was removed by filtration with celite. The solvent was removed by rotary evaporation and 10 M KOH (aq) was added to the residue, followed by extraction with dichloromethane, wash with brine and

dry with MgSO<sub>4</sub>. Purification was done by alumina oxide gel column chromatography eluting 0-10 % methanol in dichloromethane to yield **4-16** as a yellow/orange oil (819 mg, 3.2 mmol, 67 %). <sup>1</sup>H NMR (500 MHz, CDCl<sub>3</sub>) δ 1.96 (quart, *J* = 5.2 Hz, 2 H), 2.69 (t, *J* = 5.45 Hz, 2 H), 3.14 (t, *J* = 5.55 Hz, 2 H), 3.81 (s, 4 H), 7.12 (q, *J* = 5 Hz, 2 H), 7.24 (d, *J* = 7.75 Hz, 1 H), 7.58 (dt, *J<sub>a</sub>* = 1.8 Hz, *J<sub>b</sub>* = 7.7 Hz, 2 H), 8.64 (d, *J* = 4.9 Hz, 2 H). <sup>13</sup>C NMR (125 MHz, CDCl<sub>3</sub>) δ 23.8, 40.2, 53.1, 59.6, 122.5, 123.2, 137.1, 149.3, 158.0. HRMS calcd. for C<sub>15</sub>H<sub>21</sub>N<sub>4</sub><sup>+</sup> [M+H]<sup>+</sup> 257.1761, found 257.1775. (Δ = 5.4 ppm). All data are in accordance with literature values.<sup>45-46</sup>

### ***N*-(3-(Bis(pyridin-2-ylmethyl)amino)propyl)-2-(cyclooct-2-yn-1-yloxy)acetamide (4-17)**

To a 25 mL round bottom flask was added **4-16** (67 mg, 0.37 mmol), 0.25 eq DMAP (11.3 mg, 0.09 mmol), and 1.2 eq EDC HCl salt (85 mg, 0.44 mmol) dissolved in 8 mL CH<sub>2</sub>Cl<sub>2</sub> under room temperature. To this solution was added 1 eq **4-8** (95 mg, 0.37 mmol) dissolved in 2 mL CH<sub>2</sub>Cl<sub>2</sub> dropwise. The reaction was allowed to stir under room temperature for 17 hours. Upon completion, the product was purified straight away by column chromatography, eluting with 0-10 % methanol in dichloromethane to afford **4-17** as a yellow oil (110 mg, 0.26 mmol, 71 %). <sup>1</sup>H NMR (500 MHz, MeOD) δ 1.22-1.29 (m, 1 H), 1.36-1.43 (m, 1 H), 1.53-1.59 (m, 1 H), 1.58-1.64 (m, 2 H), 1.69-1.83 (m, 4 H), 1.85-1.93 (m, 1 H), 2.04-2.09 (m, 1 H), 2.15-2.20 (m, 1 H), 2.20-2.25 (m, 1 H), 2.57 (t, *J* = 6.7 Hz, 2 H), 3.27 (t, *J* = 7 Hz, 2 H), 3.79 (s, 4 H), 3.98 (d, *J* = 14.9 Hz, 1 H), 7.11 (dt, *J<sub>a</sub>* = 1.05 Hz, *J<sub>b</sub>* = 4.85 Hz, 2 H), 7.46 (d, *J* = 7.85 Hz, 2 H), 7.61 (dt, *J<sub>a</sub>* = 1.8 Hz, *J<sub>b</sub>* = 7.65 Hz, 2 H), 8.85 (dd, *J<sub>a</sub>* = 1.8 Hz, *J<sub>b</sub>* = 4.2 Hz, 2 H). <sup>13</sup>C NMR (125 MHz, MeOD) δ 20.6, 23.5, 26.2, 26.8, 29.6, 34.2, 37.3, 42.1, 51.9, 60.4, 68.4, 73.0, 91.3, 101.5, 122.0, 123.0, 123.1, 136.4, 149.0, 159.4, 169.4. HRMS (TOF) [M+H]<sup>+</sup> *m/z* calcd. for C<sub>25</sub>H<sub>33</sub>N<sub>4</sub>O<sub>2</sub><sup>+</sup>: 421.2598, found 421.2625. (Δ = 6.4 ppm).

### **Biotin-Triazine-Linker-Drug-DPA(*sp*<sup>3</sup>N) Construct (4-18)**

To a 5 mL round-bottomed flask was added **4-5** (50 mg, 26 μmol) dissolved in 0.05 M CH<sub>2</sub>Cl<sub>2</sub> (0.5 mL). To the solution was added 1.1 eq **4-17** (12 mg, 30 μmol) dissolved in 0.1 mL CH<sub>2</sub>Cl<sub>2</sub>. The resulting solution was allowed to stir under room temperature for 72 hours and the reaction was monitored by TLC. Upon completion, the solvent was removed and the product was purified by silica gel column chromatography eluting 0-30 % methanol in dichloromethane to yield **4-18** as a white solid (40 mg, 17 μmol, 67 %). <sup>1</sup>H NMR (700 MHz, MeOD) δ 0.83-0.84 (m, 2 H), 0.86-0.88 (t, *J* = 7.1 Hz, 2 H), 0.95 (d, *J* = 6.7 Hz, 1 H), 1.10 (m, 2 H), 1.14 (s, 2 H), 1.23 (s, 3 H), 1.24 (s, 3 H), 1.34 (s, 3 H), 1.40 (broad, 4 H), 1.43-1.44 (t, *J* = 7.4 Hz, 2 H), 1.55 (m, 3 H), 1.65 (s, 3 H), 1.69 (s, 3 H), 1.71 (s, 3 H), 1.89 (s, 2 H), 2.20 (m, 2 H), 2.34 (s, 2 H), 2.50 (quinine, 1 H), 2.60 (m, 1 H), 2.69 (m, 1 H), 2.74-2.76 (m, 1 H), 2.86 (m, 2 H), 3.08-3.11 (quart, *J* = 7.4 Hz, 4 H), 3.30 (s, 2 H), 3.45 (t, *J* = 4 Hz, 2 H), 3.54-3.62 (m, 16 H), 3.67 (quinine, *J* = 6.8 Hz, 2 H), 3.79 (d, *J* = 6.9 Hz, 2 H), 3.81 (s, 2 H), 3.86 (s, 1 H), 3.94 (m, 1 H), 4.06 (d, *J* = 16.7, 1 H), 4.16 (d, *J* = 8.5, 1 H), 4.28 (d, *J* = 8.5 Hz, 1 H), 4.38 (m, 1 H), 4.48 (m, 1 H), 4.67 (s, 1 H), 4.94 (m, 2 H), 5.11 (s, 1 H), 5.65 (d, *J* = 7 Hz, 1 H), 6.16 (t, 1 H), 6.30 (s, 1 H), 7.14 (s, 2 H), 7.20 (t, *J* = 7.3 Hz, 1 H), 7.27 (t, *J* = 7.6 Hz, 1 H), 7.45 (t, *J* = 7.6 Hz, 3 H), 7.58 (t, *J* = 7.4 Hz, 1 H), 7.64 (t, 2 H), 7.71 (m, 1 H), 7.77 (d, *J* = 7.3 Hz, 1 H), 8.09 (d, *J* = 7.6 Hz, 2 H), 8.15 (m, 1 H). <sup>13</sup>C NMR (176 MHz, MeOD) δ 9.1, 9.2, 9.6, 11.4, 11.8, 13.0, 14.1, 14.8, 18.5, 18.8, 20.4, 20.7, 22.1, 22.4, 22.6, 25.3, 25.7, 26.6, 28.2, 29.1, 29.7, 31.6, 33.4, 34.5, 34.7, 35.5, 36.1, 38.7, 39.0, 40.5, 41.9, 43.2, 45.8, 46.3, 47.6, 49.1, 50.7, 51.8, 58.4, 60.3, 61.9, 68.4, 69.4, 69.8, 70.1, 70.2, 70.4, 70.5, 71.8, 72.0, 75.0, 75.1, 75.5, 76.4, 79.1, 79.8, 80.1, 84.5, 115.9, 117.6, 119.9, 122.1, 123.1, 127.7, 128.3, 128.6, 129.3,

130.2, 132.6, 133.6, 134.3, 136.7, 137.6, 137.9, 143.0, 149.1, 155.0, 162.1, 166.9, 168.3, 169.7, 170.5, 172.9, 173.5, 174.9, 204.1. HRMS (TOF)  $[M+H]^+$   $m/z$  calcd. for  $C_{114}H_{161}N_{18}O_{27}S_3^+$ : 2310.0935, found 771.0345, 1156.0487, deconvolution result 2310.0829. ( $\Delta = -4.6$  ppm).

#### **Biotin-Triazine-Linker-Drug-DPA( $sp^3N$ )- $^{185}Re(CO)_3$ bromide salt (4-19)**

To a 10 mL microwave tube was added **4-18** (2.3 mg, 1  $\mu$ mol) and 1 eq **4-10** (0.4 mg, 1  $\mu$ mol) dissolved in 1 mL MeOH. The tube was sealed and allowed to be heated by microwave under 100 °C for 10 minutes while stirring. Then the solution was cooled down to room temperature and filtered out to remove undissolved solid. Then the filtrate was concentrated to form crude construct **4-19** bromide salt, and later be purified by prep HPLC as white solid (3 mg, 1  $\mu$ mol, 99 %).  $^1H$  NMR (700 MHz, MeOD)  $\delta$  0.85-0.87 (m, 2 H), 0.88-0.89 (t,  $J = 6.9$  Hz, 2 H), 0.96 (d,  $J = 6.7$  Hz, 1 H), 1.10 (m, 1 H), 1.15 (s, 2 H), 1.24 (s, 3 H), 1.25 (s, 3 H), 1.35 (s, 3 H), 1.43 (d,  $J = 6.7$  Hz, 4 H), 1.50-1.54 (m, 5 H), 1.65 (s, 3 H), 1.71 (s, 2 H), 1.76 (broad, 4 H), 1.89 (s, 2 H), 2.24 (m, 2 H), 2.35 (s, 2 H), 2.52 (m, 1 H), 2.88 (m, 1 H), 3.11-3.14 (m, 2 H), 3.35 (s, 1 H), 3.43 (broad, 2 H), 3.64 (m, 8 H), 3.70 (m, 2 H), 3.79 (d,  $J = 5.8$  Hz, 2 H), 3.97 (m, 1 H), 4.07 (m, 1 H), 4.17-4.19 (m, 2 H), 4.29 (d,  $J = 8.1$  Hz, 1 H), 4.40 (m, 1 H), 4.48 (m, 1 H), 4.95 (m, 2 H), 5.11 (s, 1 H), 5.6 (d,  $J = 6.7$  Hz, 1 H), 6.16 (m, 1 H), 6.30 (s, 1 H), 7.10 (s, 1 H), 7.41 (s, 1 H), 7.46 (t,  $J = 7.4$  Hz, 1 H), 7.59 (t,  $J = 6.9$  Hz, 1 H), 7.78 (m, 2 H), 7.84 (s, 2 H), 8.10 (d,  $J = 7.4$  Hz, 2 H), 8.65 (m, 2 H).  $^{13}C$  NMR (176 MHz, MeOD)  $\delta$  9.1, 9.6, 11.4, 11.9, 13.0, 14.1, 14.8, 17.4, 18.5, 18.6, 18.8, 20.4, 20.7, 22.1, 22.5, 22.7, 25.3, 25.7, 26.6, 28.2, 29.1, 29.4, 29.7, 31.6, 31.9, 34.5, 34.7, 35.5, 38.7, 42.1, 43.2, 53.8, 58.4, 70.1, 71.8, 75.1, 75.5, 79.2, 80.1, 84.5, 115.9, 117.5, 128.4, 128.7, 129.3, 130.2, 133.6, 140.4, 162.3, 166.9. HRMS (TOF)  $[M+H]^+$   $m/z$  calcd. for  $C_{117}H_{160}N_{18}O_{30}ReS_3^+$ : 2581.0305, found 861.0172, 1291.0206, 2581.0318. ( $\Delta = 0.5$  ppm).

#### **Biotin-DPA( $sp^3N$ ) Construct (4-20)**

To a 10 mL microwave tube was added **3-21** (226 mg, 0.51 mmol) and 1 eq **4-17** (214 mg, 0.51 mmol) dissolved in 5 mL MeOH. The tube was sealed and allowed to be heated by microwave under 100 °C for 10 minutes while stirring. Then the solution was cooled down to room temperature. The resulting solution was concentrated to form crude construct **4-20**, and later be purified by prep HPLC as white solid (405 mg, 0.46 mmol, 92 %).  $^1H$  NMR (500 MHz, MeOD)  $\delta$  1.15 (m, 1 H), 1.22 (m, 1 H), 1.38-1.41 (quint,  $J = 7.5$  Hz, 2 H), 1.55 (m, 3 H), 1.63-1.73 (m, 6 H), 1.78-1.81 (m, 1 H), 1.91 (m, 1 H), 2.06 (m, 1 H), 2.17 (m, 2 H), 2.57-2.61 (m, 2 H), 2.68-2.75 (m, 2 H), 2.83-2.86 (dd,  $J_a = 4.75$  Hz,  $J_b = 12.65$  Hz, 1 H), 2.91 (m, 1 H), 3.08 (q,  $J = 7.15$  Hz, 1 H), 3.30 (m, 2 H), 3.37 (m, 2 H), 3.50-3.53 (m, 10 H), 3.76 (s, 1 H), 3.78 (s, 2 H), 3.85 (m, 1 H), 3.89 (m, 1 H), 3.92 (m, 1 H), 4.26 (t,  $J = 4.75$  Hz, 1 H), 4.35 (t,  $J = 5.4$  Hz, 1 H), 4.43 (m, 1 H), 4.69 (m, 1 H), 5.68 (s, 1 H), 6.52 (s, 1 H), 6.82 (s, 1 H), 7.10 (t,  $J = 5.55$  Hz, 2 H), 7.47 (d,  $J = 7.75$  Hz, 2 H), 7.59 (m, 2 H), 8.45 (m, 2 H).  $^{13}C$  NMR (125 MHz, MeOD)  $\delta$  20.7, 21.8, 22.5, 24.2, 24.3, 24.8, 25.6, 26.5, 26.8, 27.8, 28.1, 28.2, 29.6, 30.7, 33.1, 35.9, 37.2, 37.3, 39.1, 40.5, 47.6, 48.6, 51.8, 53.4, 55.6, 60.1, 60.3, 61.7, 67.4, 68.4, 69.8, 69.9, 70.0, 70.1, 70.3, 70.5, 70.6, 71.9, 75.3, 122.0, 122.1, 123.0, 123.1, 133.1, 134.3, 136.5, 143.9, 144.5, 148.9, 149.0, 159.2, 159.5, 163.9, 164.0, 169.0, 169.9, 173.3, 173.4. HRMS (TOF)  $[M+H]^+$   $m/z$  calcd. for  $C_{43}H_{65}N_{10}O_7S^+$ : 865.4753, found 433.2412, 865.4768. ( $\Delta = 1.7$  ppm).

#### **Biotin-DPA( $sp^3N$ )- $^{185}Re(CO)_3$ bromide salt (4-21)**



To a microwave vial was added **4-20** (36 mg, 0.042 mmol) and 1 equivalent **4-10** (17 mg, 0.042 mmol) dissolved in 2 mL methanol. The vial was sealed and heated to 100 °C for 10 minutes by microwave. Then the solid was filtered out and the product **4-20** bromide salt was purified as white solid (42 mg, 0.035 mmol, 82 %) by prep HPLC. <sup>1</sup>H NMR (700 MHz, MeOD) δ 1.31 (m, 1 H), 1.44-1.49 (quint, *J* = 7.6 Hz, 2 H), 1.66 (m, 6 H), 1.73-1.80 (m, 3 H), 2.07 (q, *J* = 6.1 Hz, 1 H), 2.22-2.30 (m, 4 H), 2.71 (d, *J* = 12.7 Hz, 1 H), 2.88-2.90 (m, 1 H), 2.93 (dd, *J*<sub>a</sub> = 4.95 Hz, *J*<sub>b</sub> = 12.7 Hz, 1 H), 3.03 (m, 1 H), 3.22 (quint, *J* = 4.4 Hz, 1 H), 3.33-3.34 (quint, *J* = 1.6 Hz, 4 H), 3.36 (t, *J* = 5.5 Hz, 2 H), 3.44 (m, 1 H), 3.55-3.59 (m, 10 H), 3.78 (t, *J* = 5.15 Hz, 1 H), 3.84 (m, 1 H), 3.96-3.99 (m, 2 H), 4.04 (t, *J* = 5.65 Hz, 2 H), 4.32 (m, 1 H), 4.37 (t, *J* = 5.05 Hz, 1 H), 4.51 (m, 1 H), 4.92-5.00 (m, 2 H), 5.52 (s, 2 H), 7.39 (t, *J* = 7.05 Hz, 2 H), 7.59 (d, *J* = 7.85 Hz, 2 H), 7.96 (t, *J* = 7.75 Hz, 2 H), 8.88 (m, 2 H). <sup>13</sup>C NMR (176 MHz, MeOD) δ 20.4, 21.9, 24.6, 24.9, 25.4, 26.3, 28.1, 28.3, 33.5, 35.3, 35.9, 36.0, 38.9, 39.7, 53.4, 55.6, 60.2, 61.9, 67.4, 67.8, 68.2, 69.1, 69.4, 69.8, 70.1, 70.2, 75.2, 123.3, 125.5, 135.2, 140.2, 143.7, 151.7, 151.8, 160.6, 160.8, 160.9, 171.7, 174.7, 195.0, 195.8. HRMS (TOF) [M+H]<sup>+</sup> *m/z* calcd. for C<sub>46</sub>H<sub>64</sub>N<sub>10</sub>O<sub>10</sub>ReS<sup>+</sup>: 1135.4085, found 568.2074, 1135.4093. (Δ = 0.7 ppm).

### **2,5-Dioxopyrrolidin-1-yl 2-(cyclooct-2-yn-1-yloxy)acetate (4-22)**

To an empty round bottomed flask **4-8** (180 mg, 1 mmol) was dissolved in 0.1 M CH<sub>2</sub>Cl<sub>2</sub> (10 mL) under room temperature. To the resulting solution was added 2 eq NHS (228 mg, 2 mmol), followed by addition of 2 eq DIC (280 mg, 2 mmol, 0.3 mL) dropwise. The reaction was allowed to stir under room temperature for 28 hours. The white precipitate was filtered out and solvent was removed by rotary evaporation. The crude material was purified by silica gel column chromatography eluting 0-35 % ethyl acetate in hexanes to yield **4-22** as a slight yellow solid (172 mg, 0.6 mmol, 60 %). <sup>1</sup>H NMR (500 MHz, CDCl<sub>3</sub>) δ 1.43-1.50 (m, 1 H), 1.59-1.64 (m, 2 H), 1.74-1.91 (m, 3 H), 1.99-2.05 (m, 1 H), 2.09-2.18 (m, 2 H), 2.21-2.27 (m, 1 H), 2.82 (s, 4 H), 4.36-4.39 (d, *J* = 17.05 Hz, 1 H), 4.49-4.53 (d, *J* = 17.1 Hz, 1H). <sup>13</sup>C NMR (500 MHz, CDCl<sub>3</sub>) δ 20.6, 23.4, 25.5, 26.0, 29.5, 34.2, 42.1, 63.8, 73.4, 90.7, 102.3, 165.8, 168.8. HRMS (TOF) [M + H]<sup>+</sup> *m/z* calcd. for C<sub>14</sub>H<sub>18</sub>NO<sub>5</sub><sup>+</sup>: 280.1179, found 280.1167. (Δ = -4.3 ppm).

### **N-(2-Aminoethyl)-2-(cyclooct-2-yn-1-yloxy)acetamide (4-23)**

To an empty round bottomed flask **4-22** (172 mg, 0.6 mmol) was dissolved in 5 mL CH<sub>2</sub>Cl<sub>2</sub>. In another round bottom flask was dissolved 10 eq ethylenediamine (360 mg, 6 mmol) dissolved in 0.01 M CH<sub>2</sub>Cl<sub>2</sub> (60 mL) under 0 °C in an ice-water bath. To this solution was added the **4-21** in CH<sub>2</sub>Cl<sub>2</sub> dropwise. Solution turned cloudy while adding. The reaction mixture was allowed to warm to room temperature and stirred for 24 hours. Upon completion, the precipitate was filtered out. 50 ml of water was added and the product was extracted with CH<sub>2</sub>Cl<sub>2</sub> (30 mL x 3). The combined organic layers were dried over MgSO<sub>4</sub> and concentrated in vacuum to obtain **4-23** as a yellow oil (99 mg, 0.44 mmol, 73 %). <sup>1</sup>H NMR (500 MHz, CDCl<sub>3</sub>) δ 1.43-1.49 (m, 1 H), 1.61-1.68 (m, 2 H), 1.80-2.01 (m, 3 H), 2.14-2.24 (m, 2 H), 2.84 (t, *J* = 5.75 Hz, 2 H), 3.34 (m, 2 H), 3.88-3.91 (d, *J* = 15.15 Hz, 1 H), 4.04-4.07 (d, *J* = 15.15 Hz, 1 H). 4.24 (m, 1 H), 6.81 (broad, 1 H). <sup>13</sup>C NMR (125 MHz, CDCl<sub>3</sub>) δ 20.6, 26.3, 29.6, 29.7, 34.2, 41.5, 41.7, 42.2, 68.4, 73.3, 91.2, 101.8, 170.0. HRMS (TOF) [M + H]<sup>+</sup> *m/z* calcd. for C<sub>12</sub>H<sub>21</sub>N<sub>2</sub>O<sub>2</sub><sup>+</sup>: 225.1598, found 225.1597. (Δ = -0.4 ppm).

### **2,2',2''-(2-(4-(3-(2-(2-(Cyclooct-2-yn-1-yloxy)acetamido)ethyl)thioureido)benzyl)-1,4,7-triazonane-1,4,7-triyl)triacetic acid (4-24)**

To a round bottom flask was added **4-23** (40 mg, 0.18 mmol) and 1 eq commercially available p-SCN-Bn-NOTA HCl salt (100 mg, 0.18 mmol) dissolved in CH<sub>2</sub>Cl<sub>2</sub> (2 mL). To the suspension was added 3 eq TEA (0.11 mL) and the reaction was allowed to stir under room temperature for 18 hours and monitored by FIA. Upon completion, the crude product was purified by prep-HPLC and **4-24** was isolated by preparative HPLC (62 mg, 0.09 mmol, 50 %) as cotton-like solid. <sup>1</sup>H NMR (700 MHz, D<sub>2</sub>O) δ 1.19-1.21 (m, 6 H), 1.24 (t, *J* = 7.21 Hz, 1 H), 1.32-1.36 (m, 1 H), 1.46-1.51 (m, 1 H), 1.57-1.61 (m, 1 H), 1.67-1.74 (m, 2 H), 1.82-1.83 (m, 1 H), 1.87-1.91 (m, 1 H), 2.06-2.09 (m, 2 H), 2.15-2.17 (m, 1 H), 2.73 (m, 1 H), 2.93 (m 2 H), 3.11-3.14 (m, 4 H), 3.31-3.37 (m, 6 H), 3.47 (m, 1 H), 3.51 (m, 1 H), 3.64 (m, 3 H), 3.72-3.81 (m, 6 H), 3.93 (s, 2 H), 4.29 (s, 1 H), 7.17 (d, *J* = 7.35 Hz, 2 H), 7.32 (s, 1 H). <sup>13</sup>C NMR (176 MHz, D<sub>2</sub>O) δ 6.5, 8.2, 20.0, 25.7, 29.0, 33.8, 41.5, 46.6, 52.1, 52.4, 67.5, 73.7, 91.1, 103.7, 126.2, 130.5, 172.7. HRMS (TOF) [M + H]<sup>+</sup> *m/z* calcd. for C<sub>32</sub>H<sub>47</sub>N<sub>6</sub>O<sub>8</sub>S<sup>+</sup>: 675.3171, found 675.3184. (Δ = 1.9 ppm).

### **Biotin-Triazine-Linker-Drug-NOTA Construct (4-25)**

To a microwave vial was added **4-5** (81 mg, 43 μmol) and 1 equivalent **4-24** (29 mg, 43 μmol) dissolved methanol/distilled water=3:1 (total 4 mL). The vial was sealed and heated to 100 °C for 10 minutes under microwave condition. Then the product **4-25** was purified by preparative HPLC as white solid (56 mg, 22 μmol, 51 %). <sup>1</sup>H NMR (700 MHz, MeOD) δ 0.99 (m, 2 H), 1.03 (m, 1 H), 1.09 (m, 1 H), 1.19 (s, 4 H), 1.27 (m, 3 H), 1.38 (d, *J* = 6.65 Hz, 2 H), 1.43 (s, 9 H), 1.60-1.65 (m, 4 H), 1.67 (s, 3 H), 1.76-1.78 (d, *J* = 14.7 Hz, 2 H), 1.81 (m, 3 H), 1.91 (m, 1 H), 1.94 (s, 2 H), 2.05 (m, 2 H), 2.14 (m, 1 H), 2.21 (t, *J* = 5.2 Hz, 2 H), 2.27 (m, 3 H), 2.40 (s, 2 H), 2.46 (m, 2 H), 2.61 (m, 2 H), 2.70 (d, *J* = 12.7 Hz, 2 H), 2.72 (m, 1 H), 2.87 (m, 3 H), 2.91 (dd, *J<sub>a</sub>* = 4.9 Hz, *J<sub>b</sub>* = 12.7 Hz, 2 H), 3.05 (m, 2 H), 3.19 (m, 3 H), 3.22 (m, 3 H), 3.36 (m, 3 H), 3.47 (m, 2 H), 3.54-3.65 (m, 20 H), 3.73 (m, 1 H), 3.81 (broad, 2 H), 3.86 (t, *J* = 7.35 Hz, 2 H), 3.95 (m, 2 H), 3.99 (m, 1 H), 4.02 (m, 2 H), 4.11 (m, 2 H), 4.20 (q, *J* = 8.05 Hz, 2 H), 4.30 (m, 1 H), 4.34 (m, 1 H), 4.47 (m, 3 H), 4.60 (m, 2 H), 5.02 (m, 2 H), 5.29 (s, 1 H), 5.68 (t, *J* = 7.14 Hz, 2 H), 6.15 (s, 1 H), 6.47 (s, 1 H), 7.27 (m, 3 H), 7.33 (m, 2 H), 7.52 (t, *J* = 7.63 Hz, 2 H), 7.64 (t, *J* = 7.35 Hz, 1 H), 7.81 (t, 1 H), 8.14 (d, *J* = 7.56 Hz, 2 H). <sup>13</sup>C NMR (176 MHz, MeOD) δ 7.7, 7.8, 9.0, 11.7, 12.4, 13.7, 15.6, 15.7, 15.8, 15.9, 16.0, 17.2, 19.6, 20.2, 20.9, 21.4, 21.8, 24.7, 25.1, 25.4, 25.5, 26.4, 27.4, 28.1, 28.3, 31.2, 32.9, 33.0, 35.3, 36.1, 38.1, 38.9, 39.6, 43.1, 46.6, 54.4, 55.6, 55.9, 56.0, 56.1, 57.8, 60.2, 61.9, 67.8, 69.1, 69.5, 69.8, 69.9, 70.0, 70.1, 70.2, 70.9, 74.9, 75.1, 75.3, 76.0, 77.6, 79.0, 80.9, 84.4, 119.8, 124.5, 127.5, 128.0, 128.2, 129.7, 130.0, 131.0, 133.1, 133.4, 135.4, 137.2, 137.3, 141.1, 143.6, 164.6, 166.2, 168.9, 170.0, 173.6, 174.6, 203.7. HRMS (TOF) [M + H]<sup>+</sup> *m/z* calcd. for C<sub>121</sub>H<sub>175</sub>N<sub>20</sub>O<sub>33</sub>S<sub>4</sub><sup>+</sup>: 2564.1508, found 855.7223, 1283.0791, deconvolution result 2564.1445. (Δ = -2.5 ppm).

### **Biotin-Triazine-Linker-Drug-NOTA-Cu Construct (4-26)**

To an empty container was added **4-25** (6 mg, 2.3 μmol) dissolved in acetonitrile/distilled water=1:1 (2 mL total). To this solution was added 1 eq colorless copper (II) chloride (0.3 mg, 2.3 μmol) solution in 300 μL distilled water, and the reaction changed to blue upon addition of CuCl<sub>2</sub> (aq). The reaction was allowed to stir under room temperature monitored by FIA. Upon

completion, the crude mixture was purified by preparative HPLC to yield product **4-26** as blue solid (6 mg, 2.3  $\mu\text{mol}$ , 85 %).  $^1\text{H}$  NMR (700 MHz, 85 %  $\text{ACN-d}_3$  + 15 %  $\text{D}_2\text{O}$ )  $\delta$  0.97 (m, 4 H), 1.03 (m, 2 H), 1.09 (m, 12 H), 1.19 (s, 8 H), 1.35 (m, 19 H), 1.57 (m, 16 H), 1.66-1.70 (m, 22 H), 1.82 (m, 6 H), 1.96 (m, 36 H), 2.15 (m, 8 H), 2.31 (s, 5 H), 2.34 (m, 1 H), 2.41 (s, 1 H), 2.65 (d,  $J$  = 12.25 Hz, 1 H), 2.79 (m, 1 H), 2.85 (m, 3 H), 2.97 (m, 1 H), 3.10 (m, 1 H), 3.16 (m, 2 H), 3.24 (m, 3 H), 3.28 (m, 4 H), 3.48-3.56 (m, 58 H), 3.82 (broad, 4 H), 3.92 (m, 3 H), 3.98 (m, 3 H), 4.14 (m, 3 H), 4.21-4.26 (m, 3 H), 4.40 (m, 1 H), 4.50 (m, 1 H), 4.83 (m, 2 H), 4.86 (s, 1 H), 4.97 (d,  $J$  = 8.82 Hz, 1 H), 5.18 (s, 1 H), 5.57 (d,  $J$  = 6.86 Hz, 1 H), 6.04 (s, 1 H), 6.33 (s, 1 H), 7.27 (s, 3 H), 7.35 (s, 2 H), 7.52 (t,  $J$  = 7.42 Hz, 4 H), 7.58 (broad, 2 H), 7.64 (t,  $J$  = 7.21 Hz, 2 H), 7.78 (s, 2 H), 8.06 (d,  $J$  = 7.14 Hz, 4 H).  $^{13}\text{C}$  NMR (176 MHz, 85 %  $\text{ACN-d}_3$  + 15 %  $\text{D}_2\text{O}$ )  $\delta$  8.1, 8.4, 9.4, 12.7, 13.9, 17.6, 19.8, 20.3, 21.2, 21.4, 22.0, 22.2, 23.5, 25.0, 25.3, 25.9, 26.3, 27.6, 27.9, 28.1, 31.1, 33.0, 33.1, 33.8, 35.4, 35.9, 38.3, 38.8, 39.9, 43.1, 43.7, 46.0, 46.5, 47.7, 48.7, 55.3, 57.9, 60.0, 61.7, 67.9, 69.0, 69.2, 69.6, 69.7, 69.8, 70.1, 70.9, 71.5, 74.8, 74.9, 75.1, 75.2, 76.1, 77.7, 80.7, 84.2, 119.5, 125.8, 127.8, 128.6, 128.7, 129.7, 129.8, 130.0, 130.1, 131.2, 133.3, 133.4, 133.7, 135.6, 137.3, 137.4, 137.8, 140.9, 143.8, 155.5, 164.3, 166.2, 169.0, 170.5, 171.1, 171.9, 174.1, 175.0, 181.1, 204.0. HRMS (TOF)  $[\text{M} + \text{H}]^+$   $m/z$  calcd. for  $\text{C}_{121}\text{H}_{172}\text{CuN}_{20}\text{O}_{33}\text{S}_4$ : 2626.6000, found 876.3606, 1314.0368, deconvolution result 2626.0593. ( $\Delta$  = -205 ppm).

#### Biotin-NOTA Construct (4-27)

To a microwave vial was added **3-21** (6.6 mg, 15  $\mu\text{mol}$ ) and 1 equivalent **4-24** (10 mg, 15  $\mu\text{mol}$ ) dissolved in 1 mL methanol. The vial was sealed and heated to 100  $^\circ\text{C}$  for 10 minutes under microwave condition. Then the solid was filtered out and the product **4-27** was purified as white solid (8 mg, 7.2  $\mu\text{mol}$ , 48 %) by preparative HPLC.  $^1\text{H}$  NMR (700 MHz,  $\text{D}_2\text{O}$ )  $\delta$  1.31 (m, 1 H), 1.44-1.49 (quint,  $J$  = 7.6 Hz, 2 H), 1.66 (m, 6 H), 1.73-1.80 (m, 3 H), 2.07 (q,  $J$  = 6.1 Hz, 1 H), 2.22-2.30 (m, 4 H), 2.71 (d,  $J$  = 12.7 Hz, 1 H), 2.88-2.90 (m, 1 H), 2.93 (dd,  $J_a$  = 4.95 Hz,  $J_b$  = 12.7 Hz, 1 H), 3.03 (m, 1 H), 3.22 (quint,  $J$  = 4.4 Hz, 1 H), 3.33-3.34 (quint,  $J$  = 1.6 Hz, 4 H), 3.36 (t,  $J$  = 5.5 Hz, 2 H), 3.44 (m, 1 H), 3.55-3.59 (m, 10 H), 3.78 (t,  $J$  = 5.15 Hz, 1 H), 3.84 (m, 1 H), 3.96-3.99 (m, 2 H), 4.04 (t,  $J$  = 5.65 Hz, 2 H), 4.32 (m, 1 H), 4.37 (t,  $J$  = 5.05 Hz, 1 H), 4.51 (m, 1 H), 4.92-5.00 (m, 2 H), 5.52 (s, 2 H), 7.39 (t,  $J$  = 7.05 Hz, 2 H), 7.59 (d,  $J$  = 7.85 Hz, 2 H), 7.96 (t,  $J$  = 7.75 Hz, 2 H), 8.88 (m, 2 H).  $^{13}\text{C}$  NMR (176 MHz,  $\text{D}_2\text{O}$ )  $\delta$  8.1, 20.3, 21.3, 24.7, 25.1, 26.2, 27.7, 27.9, 33.6, 35.4, 38.9, 39.7, 46.6, 47.5, 55.3, 60.2, 62.0, 67.6, 68.8, 68.9, 69.4, 69.5, 69.6, 69.9, 75.3, 125.9, 130.4, 136.3, 143.9, 165.2, 176.7, 179.8. HRMS (TOF)  $[\text{M} + \text{H}]^+$   $m/z$  calcd. for  $\text{C}_{50}\text{H}_{79}\text{N}_{12}\text{O}_{13}\text{S}_2^+$ : 1119.5325, found 560.2706, 1119.5334. ( $\Delta$  = 0.8 ppm).

#### Biotin-NOTA-Cu Construct (4-28)

To a microwave vial was added **4-27** (6 mg, 5.4  $\mu\text{mol}$ ) dissolved in 1 mL distilled water. To this solution was added 1 eq colorless copper (II) chloride (0.7 mg, 5.4  $\mu\text{mol}$ ) solution in 200  $\mu\text{L}$  distilled water, and the reaction changed to blue upon addition of  $\text{CuCl}_2$  (aq). The reaction was allowed to stir under room temperature monitored by FIA. Upon completion, the crude mixture was purified by preparative HPLC to yield product **4-28** as blue solid (6 mg, 5.1  $\mu\text{mol}$ , 94 %).  $^1\text{H}$  NMR (700 MHz,  $\text{D}_2\text{O}$ )  $\delta$  1.19-1.21 (m, 2 H), 1.25 (m, 1 H), 1.53-1.70 (m, 8 H), 2.07 (m, 2 H), 2.17 (m, 2 H), 2.64 (s, 1 H), 2.68 (m, 1 H), 2.80 (m, 1 H), 2.89 (m, 2 H), 3.11 (m, 1 H), 3.24 (m, 3 H), 3.51 (m, 10 H), 3.87 (m, 2 H), 4.01 (m, 2 H), 4.32 (m, 2 H), 4.51 (m, 2 H), 4.99 (m, 1 H), 7.50 (m, 2 H), 8.29 (m, 4 H).  $^{13}\text{C}$  NMR (176 MHz,  $\text{D}_2\text{O}$ )  $\delta$  6.5, 8.2, 20.5, 21.5, 25.0, 25.2, 26.3, 27.8,

28.0, 35.5, 38.7, 39.0, 39.9, 46.6, 55.5, 60.2, 62.0, 62.4, 68.9, 69.0, 69.5, 69.6, 69.7, 70.0, 75.2, 127.6, 135.5, 136.8, 165.2, 172.8, 176.7. HRMS (TOF)  $[M + H]^+$  m/z calcd. for  $C_{50}H_{77}CuN_{12}O_{13}S_2^+$ : 1180.4465, found 590.7268, 1180.4458. ( $\Delta = -0.6$  ppm).

#### §4.8 References

- (1) Rahmim, A.; Zaidi, H. PET versus SPECT: strengths, limitations and challenges. *Nucl. Med. Commun.* **2008**, *29*, 193-207.
- (2) Morais, G. R.; Paulo, A.; Santos, I. Organometallic Complexes for SPECT Imaging and/or Radionuclide Therapy. *Organometallics* **2012**, *31*, 5693-5714.
- (3) Khalil, M. M.; Tremoleda, J. L.; Bayomy, T. B.; Gsell, W. Molecular SPECT Imaging: An Overview. *Int J Mol Imaging* **2011**, 15 pages.
- (4) Pascu, S.; Dilworth, J. Recent developments in PET and SPECT imaging. *J Labelled Comp Radiopharm* **2014**, *57*, 191-194.
- (5) Ametamey, S. M.; Honer, M.; Schubiger, P. A. Molecular Imaging with PET. *Chem. Rev.* **2008**, *108*, 1501-1516.
- (6) <http://www.cellsighttech.com/technology/pet.html>.
- (7) Miller, P. W.; Long, N. J.; Vilar, R.; Gee, A. D. Synthesis of  $^{11}C$ ,  $^{18}F$ ,  $^{15}O$ , and  $^{13}N$  Radiolabels for Positron Emission Tomography. *Angew. Chem. Int. Ed.* **2008**, *47*, 8998-9033.
- (8) Alehyani, S. H. A. Application of single photon emission computed tomography (SPECT) parameters for bone scintigraphy. *Journal of King Saud University - Science* **2009**, *21*, 109-117.
- (9) Wolf, A. P.; Redvanly, C. S. Carbon-11 and radiopharmaceuticals. *Int J Appl Radiat Is* **1977**, *28*, 29-48.
- (10) Ferrieri R, A.; Wolf A, P. In *Radiochimica Acta* 1983; Vol. 34, p 69.
- (11) Miller, J. C. Neuroimaging for Dementia and Alzheimer's Disease. *Radiology Rounds* **2006**, *4*.
- (12) Wadas, T. J.; Wong, E. H.; Weisman, G. R.; Anderson, C. J. Coordinating Radiometals of Copper, Gallium, Indium, Yttrium, and Zirconium for PET and SPECT Imaging of Disease. *Chem. Rev.* **2010**, *110*, 2858-2902.
- (13) Anderson, C. J., Green, M. A., and Fujibayashi, Y. Chemistry of copper radionuclides and radiopharmaceutical products, Handbook of Radiopharmaceuticals: Radiochemistry and Applications (Welch, M. J., and Redvanly, C., Eds.) pp 401-422, John Wiley & Sons, Ltd. **2003**.
- (14) Zhou, Y.; Liu, S.  $^{64}Cu$ -Labeled Phosphonium Cations as PET Radiotracers for Tumor Imaging. *Bioconj. Chem.* **2011**, *22*, 1459-1472.
- (15) Banerjee, S.; Ambikalmajan Pillai, M. R.; Ramamoorthy, N. Evolution of Tc-99m in diagnostic radiopharmaceuticals. *Semin. Nucl. Med.* **2001**, *31*, 260-277.
- (16) Moffat, F. L.; Pinsky, C. M.; Hammershaimb, L.; Petrelli, N. J.; Patt, Y. Z.; Whaley, F. S.; Goldenberg, D. M. Clinical utility of external immunoscintigraphy with the IMMUN-4 technetium-99m Fab' antibody fragment in patients undergoing surgery for carcinoma of the colon and rectum: results of a pivotal, phase III trial. The Immunomedics Study Group. *J. Clin. Oncol.* **1996**, *14*, 2295-2305.
- (17) Gratz, S.; Schipper, M. L.; Dorner, J.; Hoffken, H.; Becker, W.; Kaiser, J. W.; Behe, M.; Behr, T. M. LeukoScan for Imaging Infection in Different Clinical Settings: A Retrospective Evaluation and Extended Review of the Literature. *Clin. Nucl. Med.* **2003**, *28*, 267-276.
- (18) Tait, J. F.; Cerqueira, M. D.; Dewhurst, T. A.; Fujikawa, K.; Ritchie, J. L.; Stratton, J. R.

- Evaluation of annexin V as a platelet-directed thrombus targeting agent. *Thromb. Res.* **1994**, *75*, 491-501.
- (19) Danielsson, R.; Bååth, M.; Svensson, L.; Forslöv, U.; Kölbeck, K.-G. Imaging of regional lymph node metastases with  $^{99m}\text{Tc}$ -depreotide in patients with lung cancer. *Eur. J. Nucl. Med. Mol. Imag.* **2005**, *32*, 925-931.
- (20) Blankenberg, F. G.; Strauss, H. W. Nuclear medicine applications in molecular imaging. *J. Magn. Reson. Im.* **2002**, *16*, 352-361.
- (21) Tisato, F.; Porchia, M.; Bolzati, C.; Refosco, F.; Vittadini, A. The preparation of substitution-inert  $^{99}\text{Tc}$  metal-fragments: Promising candidates for the design of new  $^{99m}\text{Tc}$  radiopharmaceuticals. *Coord. Chem. Rev.* **2006**, *250*, 2034-2045.
- (22) Waibel, R.; Alberto, R.; Willuda, J.; Finnern, R.; Schibli, R.; Stichelberger, A.; Egli, A.; Abram, U.; Mach, J.-P.; Pluckthun, A.; Schubiger, P. A. Stable one-step technetium-99m labeling of His-tagged recombinant proteins with a novel Tc(I)-carbonyl complex. *Nat Biotech* **1999**, *17*, 897-901.
- (23) Egli, A.; Alberto, R.; Tannahill, L.; Schibli, R.; Abram, U.; Schaffland, A.; Waibel, R.; Tourwé, D.; Jeannin, L.; Iterbeke, K.; Schubiger, P. A. Organometallic  $^{99m}\text{Tc}$ -Aquaion Labels Peptide to an Unprecedented High Specific Activity. *J. Nucl. Med.* **1999**, *40*, 1913-1917.
- (24) Morris, R. T.; Joyrich, R. N.; Naumann, R. W.; Shah, N. P.; Maurer, A. H.; Strauss, H. W.; Uszler, J. M.; Symanowski, J. T.; Ellis, P. R.; Harb, W. A. Phase II study of treatment of advanced ovarian cancer with folate-receptor-targeted therapeutic (vintafolide) and companion SPECT-based imaging agent ( $^{99m}\text{Tc}$ -etarfolatide). *Ann. Oncol.* **2014**, *25*, 852-858.
- (25) Betzel, T.; Müller, C.; Groehn, V.; Müller, A.; Reber, J.; Fischer, C. R.; Krämer, S. D.; Schibli, R.; Ametamey, S. M. Radiosynthesis and Preclinical Evaluation of 3'-Aza-2'-[ $^{18}\text{F}$ ]fluorofolic Acid: A Novel PET Radiotracer for Folate Receptor Targeting. *Bioconj. Chem.* **2013**, *24*, 205-214.
- (26) Leamon, C. P.; Parker, M. A.; Vlahov, I. R.; Xu, L.-C.; Reddy, J. A.; Vetzal, M.; Douglas, N. Synthesis and Biological Evaluation of EC20: A New Folate-Derived,  $^{99m}\text{Tc}$ -Based Radiopharmaceutical. *Bioconj. Chem.* **2002**, *13*, 1200-1210.
- (27) Bettio, A.; Honer, M.; Müller, C.; Brühlmeier, M.; Müller, U.; Schibli, R.; Groehn, V.; Schubiger, A. P.; Ametamey, S. M. Synthesis and Preclinical Evaluation of a Folic Acid Derivative Labeled with  $^{18}\text{F}$  for PET Imaging of Folate Receptor-Positive Tumors. *J. Nucl. Med.* **2006**, *47*, 1153-1160.
- (28) Claesener, M.; Breyholz, H.-J.; Hermann, S.; Faust, A.; Wagner, S.; Schober, O.; Schäfers, M.; Kopka, K. Efficient synthesis of a fluorine-18 labeled biotin derivative. *Nucl. Med. Biol.*, *39*, 1189-1194.
- (29) Kudo, T.; Ueda, M.; Konishi, H.; Kawashima, H.; Kuge, Y.; Mukai, T.; Miyano, A.; Tanaka, S.; Kizaka-Kondoh, S.; Hiraoka, M.; Saji, H. PET Imaging of Hypoxia-Inducible Factor-1-Active Tumor Cells with Pretargeted Oxygen-Dependent Degradable Streptavidin and a Novel  $^{18}\text{F}$ -Labeled Biotin Derivative. *Mol. Imag. Biol.* **2011**, *13*, 1003-1010.
- (30) Vineberg, J. G.; Zuniga, E. S.; Kamath, A.; Chen, Y.-J.; Seitz, J. D.; Ojima, I. Design, Synthesis, and Biological Evaluations of Tumor-Targeting Dual-Warhead Conjugates for a Taxoid-Camptothecin Combination Chemotherapy. *J. Med. Chem.* **2014**, *57*, 5777-5791.
- (31) Vineberg, J. G.; Wang, T.; Zuniga, E. S.; Ojima, I. Design, Synthesis, and Biological Evaluation of Theranostic Vitamin-Linker-Taxoid Conjugates. *J. Med. Chem.* **2015**, *58*, 2406-2416.
- (32) Kneeland, D. M.; Ariga, K.; Lynch, V. M.; Huang, C. Y.; Anslyn, E. V. Bis(alkylguanidinium) receptors for phosphodiesterases: effect of counterions, solvent mixtures, and cavity flexibility on

- complexation. *J. Am. Chem. Soc.* **1993**, *115*, 10042-10055.
- (33) Jensen, K. B.; Braxmeier, T. M.; Demarcus, M.; Frey, J. G.; Kilburn, J. D. Synthesis of Guanidinium-Derived Receptor Libraries and Screening for Selective Peptide Receptors in Water. *Chem.-Eur. J.* **2002**, *8*, 1300-1309.
- (34) Goswami, L. N.; Houston, Z. H.; Sarma, S. J.; Jalisatgi, S. S.; Hawthorne, M. F. Efficient synthesis of diverse heterobifunctionalized clickable oligo(ethylene glycol) linkers: potential applications in bioconjugation and targeted drug delivery. *Org. Biomol. Chem.* **2013**, *11*, 1116-1126.
- (35) Schwabacher, A. W.; Lane, J. W.; Schiesher, M. W.; Leigh, K. M.; Johnson, C. W. Desymmetrization Reactions: Efficient Preparation of Unsymmetrically Substituted Linker Molecules. *J. Org. Chem.* **1998**, *63*, 1727-1729.
- (36) Banerjee, P. S.; Zuniga, E. S.; Ojima, I.; Carrico, I. S. Targeted and armed oncolytic adenovirus via chemoselective modification. *Bioorg. Med. Chem. Lett.* **2011**, *21*, 4985-4988.
- (37) Agard, N. J.; Baskin, J. M.; Prescher, J. A.; Lo, A.; Bertozzi, C. R. A Comparative Study of Bioorthogonal Reactions with Azides. *ACS Chem. Biol.* **2006**, *1*, 644-648.
- (38) Bernardin, A.; Cazet, A.; Guyon, L.; Delannoy, P.; Vinet, F.; Bonnaffé, D.; Texier, I. Copper-Free Click Chemistry for Highly Luminescent Quantum Dot Conjugates: Application to in Vivo Metabolic Imaging. *Bioconj. Chem.* **2010**, *21*, 583-588.
- (39) Evans, H. L.; Slade, R. L.; Carroll, L.; Smith, G.; Nguyen, Q.-D.; Iddon, L.; Kamaly, N.; Stockmann, H.; Leeper, F. J.; Aboagye, E. O.; Spivey, A. C. Copper-free click-a promising tool for pre-targeted PET imaging. *Chem. Commun.* **2012**, *48*, 991-993.
- (40) Lazarova, N.; James, S.; Babich, J.; Zubieta, J. A convenient synthesis, chemical characterization and reactivity of  $[\text{Re}(\text{CO})_3(\text{H}_2\text{O})_3]\text{Br}$ : the crystal and molecular structure of  $[\text{Re}(\text{CO})_3(\text{CH}_3\text{CN})_2\text{Br}]$ . *Inorg. Chem. Commun.* **2004**, *7*, 1023-1026.
- (41) Cox, C.; Ferraris, D.; Murthy, N. N.; Lectka, T. Copper(II)-Catalyzed Amide Isomerization: Evidence for N-Coordination. *J. Am. Chem. Soc.* **1996**, *118*, 5332-5333.
- (42) Barrera, I. F.; Maxwell, C. I.; Neverov, A. A.; Brown, R. S. Cu(II)-Promoted Methanolysis of N,N-Dipicolylacetamide. Multistep Activation by Decoupling of  $>\ddot{\text{N}}-\text{C}=\text{O}$  Resonance via Cu(II)-N Binding, Delivery of the Cu(II):(-OCH<sub>3</sub>) Nucleophile, and Metal Ion Assistance of the Departure of the Leaving Group. *J. Org. Chem.* **2012**, *77*, 4156-4160.
- (43) Niklas, N.; Hampel, F.; Liehr, G.; Zahl, A.; Alsfasser, R. The Reactivity of N-Coordinated Amides in Metallopeptide Frameworks: Molecular Events in Metal-Induced Pathogenic Pathways? *Chem.-Eur. J.* **2001**, *7*, 5135-5142.
- (44) Gasser, G.; Sosniak, A. M.; Leonidova, A.; Braband, H.; Metzler-Nolte, N. Towards the preparation of novel  $\text{Re}^{99\text{mTc}}$  tricarbonyl-containing peptide nucleic acid bioconjugates. *Aust. J. Chem.* **2011**, *64*, 265-272.
- (45) Yamanaka, S.; Ōkawa, H.; Motoda, K.-i.; Yonemura, M.; Fenton, D. E.; Ebadi, M.; Lever, A. B. P. Tetracopper Assembly Complexes Comprised of One Dimetallic Core and Two Monometallic Auxiliaries: Intramolecular Electron-Transfer Relevant to Multicopper Oxidases. *Inorg. Chem.* **1999**, *38*, 1825-1830.
- (46) Pimentel, L. C. F.; de Souza, A. L. F.; Fernández, T. L.; Wardell, J. L.; Antunes, O. A. C. Microwave-assisted synthesis of N,N-bis-(2-pyridylmethyl)amine derivatives. Useful ligands in coordination chemistry. *Tetrahedron Lett.* **2007**, *48*, 831-833.
- (47) Borcard, F. o.; Godinat, A. I.; Staedler, D.; Comas Blanco, H.; Dumont, A.-L.; Chapuis-Bernasconi, C.; Scaletta, C.; Applegate, L. A.; Krauss Juillerat, F.; Gonzenbach, U. T.; Gerber-

- Lemaire, S.; Juillerat-Jeanneret, L. Covalent Cell Surface Functionalization of Human Fetal Osteoblasts for Tissue Engineering. *Bioconj. Chem.* **2011**, *22*, 1422-1432.
- (48) Hoigebazar, L.; Jeong, J. M.; Choi, S. Y.; Choi, J. Y.; Shetty, D.; Lee, Y.-S.; Lee, D. S.; Chung, J.-K.; Lee, M. C.; Chung, Y. K. Synthesis and Characterization of Nitroimidazole Derivatives for <sup>68</sup>Ga-Labeling and Testing in Tumor Xenografted Mice. *J. Med. Chem.* **2010**, *53*, 6378-6385.
- (49) Liu, Z.; Yan, Y.; Liu, S.; Wang, F.; Chen, X. <sup>18</sup>F, <sup>64</sup>Cu, and <sup>68</sup>Ga Labeled RGD-Bombesin Heterodimeric Peptides for PET Imaging of Breast Cancer. *Bioconj. Chem.* **2009**, *20*, 1016-1025.
- (50) Yang, C.-T.; Kim, Y.-S.; Wang, J.; Wang, L.; Shi, J.; Li, Z.-B.; Chen, X.; Fan, M.; Li, J.-J.; Liu, S. <sup>64</sup>Cu-labeled 2-(diphenylphosphoryl)ethyldiphenylphosphonium cations as highly selective tumor imaging agents: effects of linkers and chelates on radiotracer biodistribution characteristics. *Bioconj. Chem.* **2008**, *19*, 2008-2022.
- (51) Dissoki, S.; Hagooly, A.; Elmachily, S.; Mishani, E. Labeling approaches for the GE11 peptide, an epidermal growth factor receptor biomarker. *J Labelled Comp Radiopharm* **2011**, *54*, 693-701.
- (52) Mistry, S. N.; Baker, J. G.; Fischer, P. M.; Hill, S. J.; Gardiner, S. M.; Kellam, B. Synthesis and in Vitro and in Vivo Characterization of Highly  $\beta_1$ -Selective  $\beta$ -Adrenoceptor Partial Agonists. *J. Med. Chem.* **2013**, *56*, 3852-3865.

## Chapter 5

### Novel Asymmetric Bow-Tie Dendrimer-based Drug Delivery System

§5.1 Nanomedicine .....	143
§5.1.1 Introduction: Dendritic Polymer (Dendrimer).....	144
§5.1.2 Preparation .....	149
§5.1.3 Active and Passive Targeting Strategies .....	150
§5.2 Original Design of Asymmetric Bow-Tie Dendrimer (ABTD) Drug Delivery System...	152
§5.2.1 Rational Design .....	155
§5.2.2 Proof of Concept .....	156
§5.2.3 First Attempt towards ABTD Conjugate .....	160
§5.3 Modified Design of a Novel Versatile ABTD Drug Delivery System.....	162
§5.3.1 Solubility Improvement with PEG Oligomer Spacer.....	164
§5.3.2 Biotinylated PEGylated G3 PAMAM Dendrimer .....	165
§5.3.3 Click-ready PEGylated G1 PAMAM Dendrimer.....	167
§5.3.4 Bis(maleicimido) PEGylated Linker .....	169
§5.3.5 Synthesis of Click-ready Intermediates.....	170
§5.3.6 Synthesis of ABTD Conjugates.....	171
§5.3.7 Internalization Study via RME and Multi-binding Effect .....	173
§5.3.8 Cytotoxicity Measurements.....	174
§5.4 Tribrached Dendrimer Incorporating Imaging Agents.....	176
§5.4.1 Design and Synthesis Fluorescent Tribranched Linker.....	176
§5.5 Extended Multi-binding Effect Study .....	180
§5.6 Second Generation Versatile ABTD Drug Delivery System Design .....	183
§5.7 Summary.....	188
§5.8 Experimental Section.....	188
§5.8.1 Caution.....	188
§5.8.2 General Information.....	189
§5.8.3 Materials.....	190
§5.8.4 Experimental Procedure.....	191
§5.9 References.....	206



## §5.1 Nanomedicine

As the expanding development on the medical application of nanotechnology, nanomedicine has newly emerged with enormous potential for drug delivery and cancer treatment. To distinguish nanomedicine from biotech products which have inherent nanoscale size, such as proteins and antibodies, the European Science Foundation's Forward Look on Nanomedicine defined nanomedicines as "nanometer size scale complex systems, consisting of at least two components, one of which being the active ingredient".<sup>1</sup> The development of nanomedicine depends on the innovative nanotechnology to better understand disease pathophysiology and identify new target for therapeutic intervention. This nanotechnology involves design of new nanoscale devices or systems for use as diagnostic, biosensors, imaging agents and drug delivery nanocarriers.<sup>2</sup>

Nanocarriers have unique properties such as nanoscale size, high surface-to-volume ratio, and favorable physico-chemical characteristics.<sup>3</sup> Thus developing nanomedicine products have certain advantages in drug delivery for cancer therapy. A common application of nanocarrier is to increase the solubility of anti-cancer drugs. Usually the poor water solubility limits the bioavailability of a good anti-cancer drug candidate, and incorporation with a hydrophilic nanocarrier can markedly increase their uptake as well as *in vivo* stability.<sup>3</sup> Wortmannin (PI3K inhibitor and radiosensitizer) is a good example for a drug which is once postponed due to poor solubility and chemical instability, but re-launched by incorporating a lipid-based nanocarrier resulting in increased solubility from 4 mg/L to 20 g/L.<sup>4</sup> Moreover, nanocarriers can be designed to help to improve drug distribution in which both active and passive targeting strategies can be used to improve drug penetration into tumor tissue.<sup>3</sup> In addition, targeted nanomedicine therapeutics may also decrease tumor resistance against drugs by extending the drug circulation time, bypassing Pgp and MDR/ATP efflux pump, and allowing for selective and controlled drug release.<sup>3</sup> (Figure 5.1)

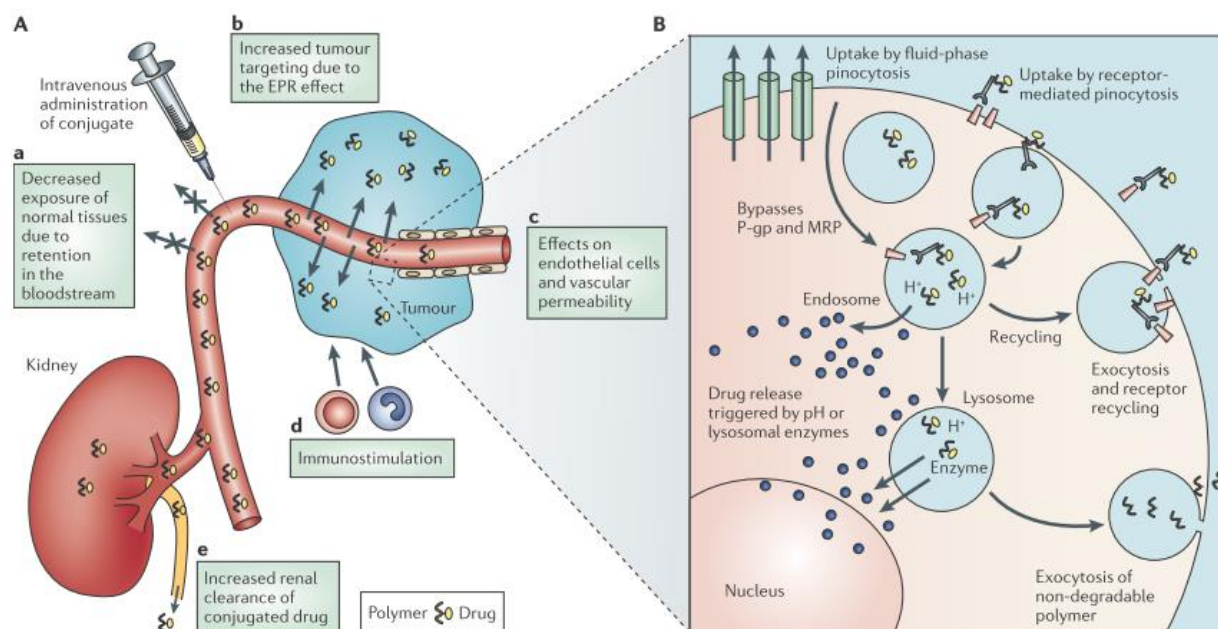


**Figure 5.1** Mechanism of action of nanocarrier-drug with improved features (reprinted from reference 2)<sup>2</sup>

Currently various types of nanocarriers (**Figure 5.2**) have been developed for cancer research, including viral vectors, drug conjugates (ADCs and polymer-drug conjugates), lipid-based nanocarriers (liposome), natural/synthetic polymer-based nanocarriers (polymeric micelle and polymeric nanoparticles) and inorganic nanocarriers (silica and metal nanoparticles).<sup>3</sup> Many organic/inorganic nanoscale platforms have been reported as nanocarrier for cancer therapy, such as carbon nanotube, graphene, gold nanoparticle, TiO<sub>2</sub> nanoparticle, and long chain or dendritic polymers.

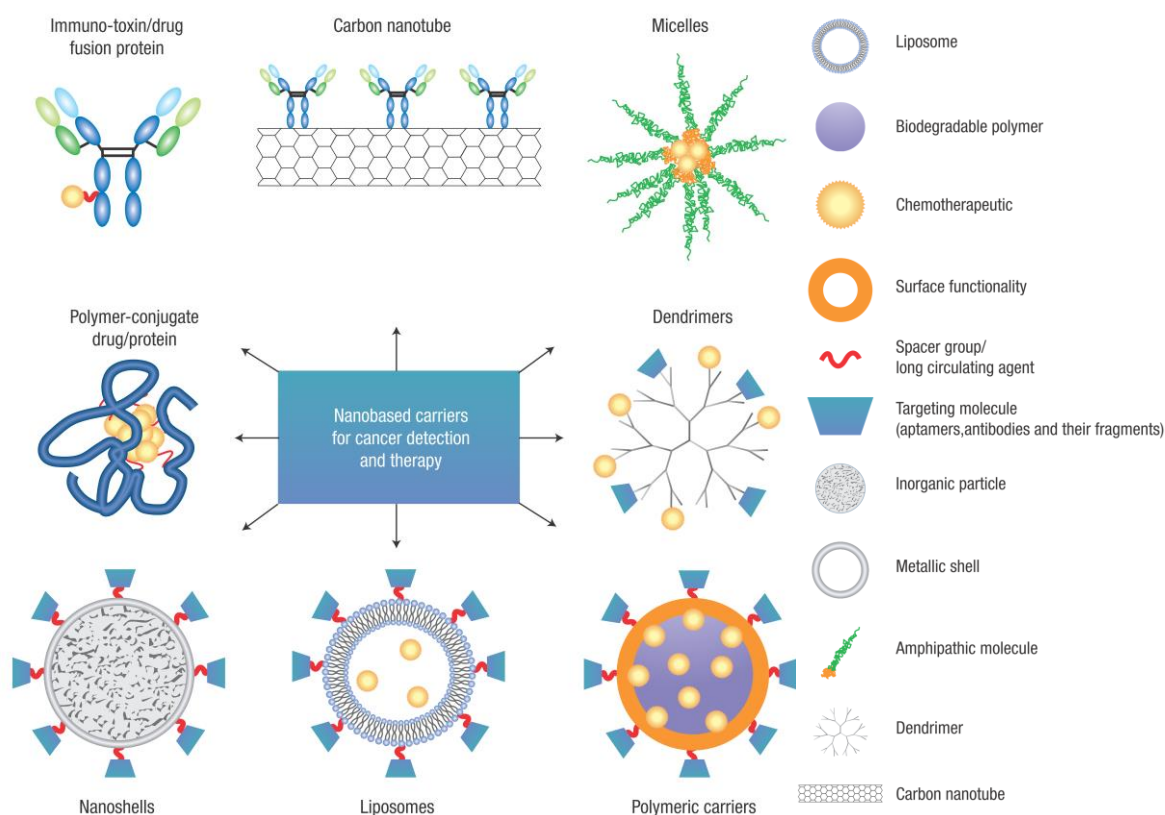


**Figure 5.2** A whole range of nanocarriers for targeting cancer (reprinted from reference 5)<sup>5</sup>

### §5.1.1 Introduction: Dendritic Polymer (Dendrimer)

Dendritic polymer present a very important class of nanoparticle (NP) delivery vehicles. The term “dendrimer” often refers to branched or dendrimeric polymer.<sup>6</sup> Dendrimer has stimulated wide interest in the field of chemistry and biology, especially in applications like drug delivery, thus it is often referred to as the “Polymers of the 21<sup>st</sup> century”.<sup>7</sup>

Dendrimer is a class of polymers which is often called starburst polymers because of their shapes.<sup>8</sup> In general, dendrimer has a tree-like molecular architecture with an interior core, interior layers (frequently referred to as “generations”) which consists of repeating units regularly attached to the core, and an exterior surface of terminal groups attached to the outermost generation.<sup>8</sup> (**Figure 5.3**) Generation number (usually abbreviated to G #) is determined by the number of focal points going from the core towards the surface. The size of dendrimer largely depends on the repeating units in interior layers and resulting intramolecular interaction. The surface functional

group which is the most exposed to outside environment determines the chemical property of the dendrimer as well as physical property such as solubility. The successive addition of generations results in highly amplified, organized, well-defined surface site and internal void channels. (**Figure 5.4**)

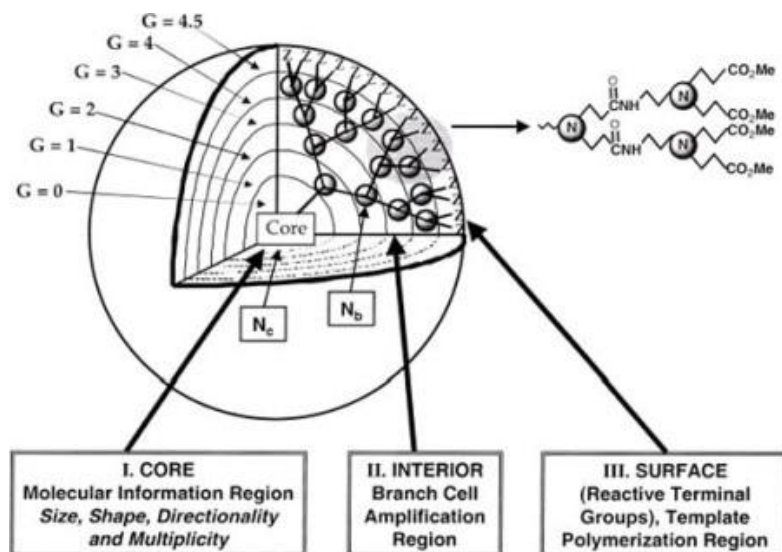


**Figure 5.3** The 3D projection of dendrimer core-shell architecture (reprinted from reference 9)<sup>9</sup>

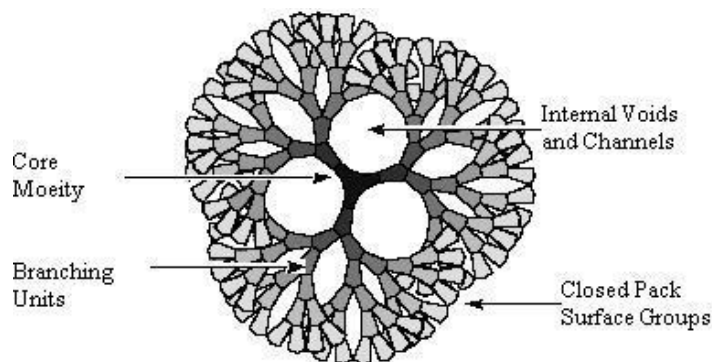
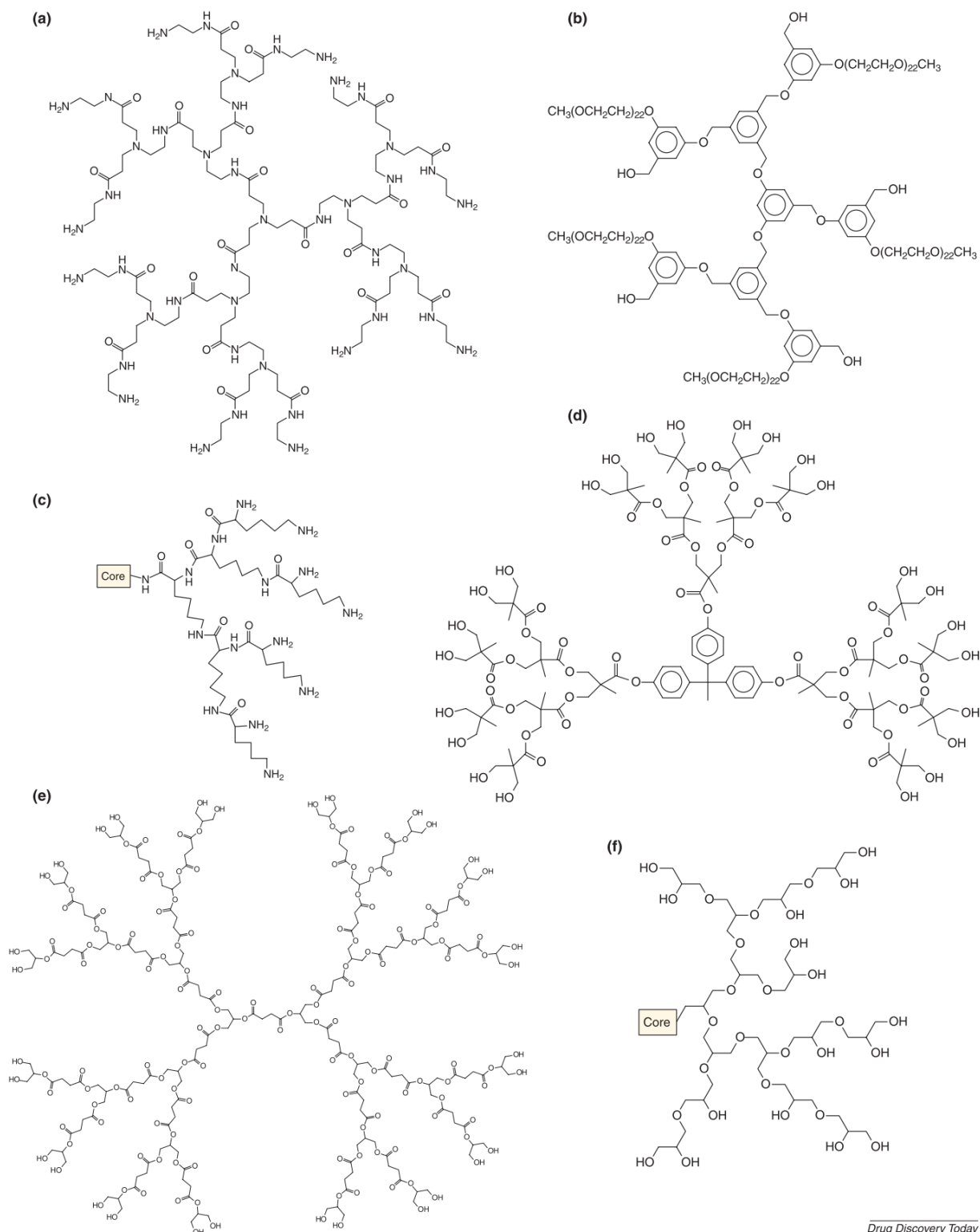


**Figure 5.4** The dendritic structure (reprinted from reference 10)<sup>10</sup>

Dendrimers could be divided to various classification depending on the different types of interior core and interior layer, as well as the shape and function, such as PAMAMOS (poly (amidoamine-organosilicon) dendrimers), PPI (poly (propylene imine)), amphiphilic dendrimer, chiral dendrimer, multilingual dendrimer, micellar dendrimer, Tecto dendrimer and Frechet type dendrimer.<sup>7</sup> Several examples of biocompatible dendrimers are shown in **Figure 5.5**. One of the commonly applied dendrimers as carrier on medicinal field is PAMAM (poly (amidoamine) dendrimer) (**Figure 5.6**). PAMAM dendrimer is commercially available, usually existing in methanol solutions. PAMAM dendrimer products can reach up to generation 7 with molecular weight over 930,000 g/mol have been obtained. They could be purchased from Center for Biologic Nanotechnology, University of Michigan or Dendritic Nanotechnologies, Inc<sup>®</sup> (DNT) from Mount Pleasant, Michigan, USA (**Figure 5.7**). *Starburst dendrimers* is applied as a trademark name for a sub-class of PAMAM dendrimers based on a tris-aminoethylene-imine core.<sup>7</sup> The name refers to the starlike pattern observed when looking at the structure of the high-generation dendrimers of this type in two-dimensions.



*Drug Discovery Today*

**Figure 5.5** Structures of biocompatible dendrimers that have been tested for drug delivery applications. (a) PAMAM dendrimer (b) Polyaryl ether dendrimer (c) Polylysine dendron (d) Polyester dendrimer based on 2,2-bis(hydroxymethyl)propionic acid (e) Polyester dendrimer based on glycerol and succinic acid (f) Dendritic polyglycerol (reprinted from reference 11)<sup>11</sup>

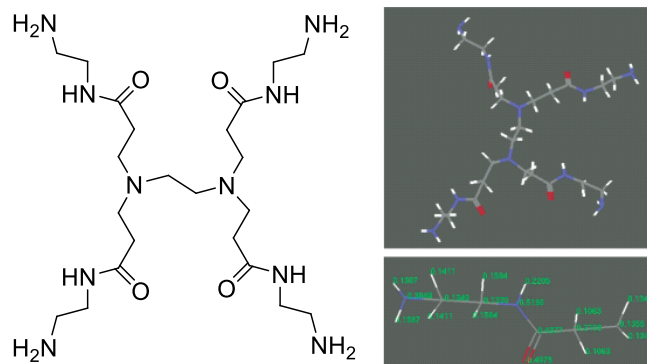


**Figure 5.6** Generation 0 of ethylenediamine (EDA) cored PAMAM dendrimer (reprinted from reference 12)<sup>12</sup>

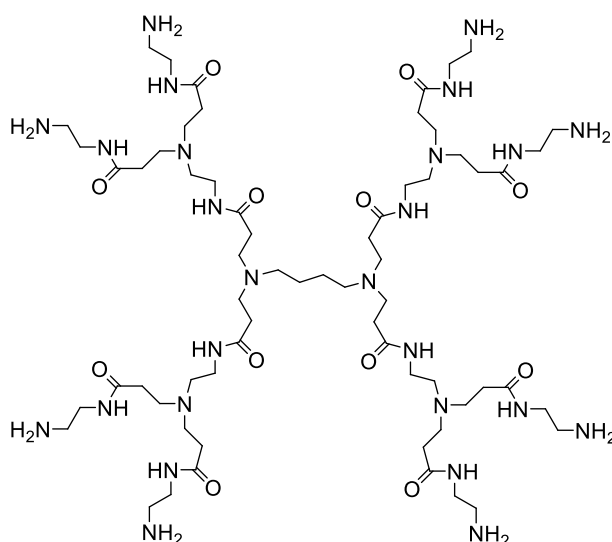


**Figure 5.7** Generation 1 diaminobutane core PAMAM dendrimer (DNT-102)

Significantly PAMAM dendrimers have size range of 2.3 nm in Generation 2 (G2) to 5.3 nm in G5.<sup>12-13</sup> The surface groups of dendrimer increases and becomes crowded and leads to tightly packed form as generation goes higher. It turns out that lower generation dendrimers have more open planar–elliptical shapes with transition to more compact spherical shapes for higher generations (**Figure 5.8**).

The dendrimer's unique physical and chemical properties mainly depend on its structure and external functional groups which contribute to its potential for being used as macromolecular vehicle of drug delivery. For instance, the multiple interactions between surface amine and nucleic acid phosphate are crucial for the formation of dendrimers and DNA complexes. On the other hand, dendrimer's solubility is also strongly influenced by its surface group. Dendrimer terminated in hydrophilic groups are soluble in polar solvents, while hydrophobic ended ones are soluble in non-polar solvents. Therefore, based on specific ending group, dendrimer can exist in changing conformation in different solvents. (**Figure 5.9**)

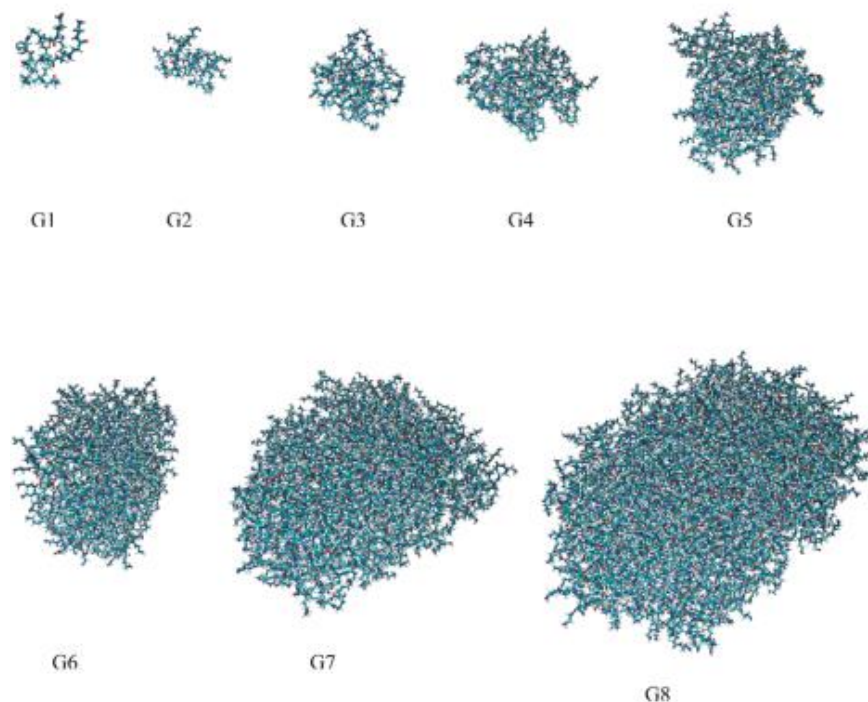


**Figure 5.8** Instantaneous snapshots of G1-G8 EDA core PAMAM dendrimers after long MD simulations at  $T = 300$  K. All figures are to the same scale (reprinted from reference 12)<sup>12</sup>

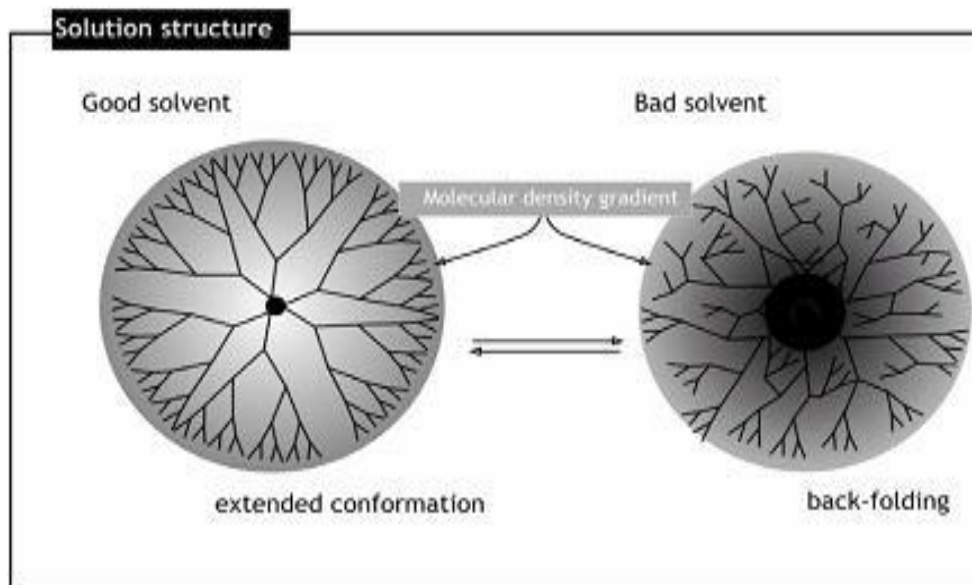


**Figure 5.9** Dendrimer conformation based on different solvents (reprinted from reference 9)<sup>9</sup>

In solution, lower generation dendrimers form a tightly packed ball. For PAMAM dendrimer, due to its chemical structures including basic interiors containing tertiary amines and free amines as surface groups, the low pH region generally leads to extended conformations due to electrostatic repulsion between the positively charged ammonium groups. At low pH value ( $\text{pH} < 4$ ), the interior area is getting “hollow” as a result of repulsion between the positively charged tertiary amines. At neutral conditions, back-folding may occur probably because of the hydrogen

bonding between the interior amine and surface positively charged amine groups. At high pH (pH>10), the repulsive forces between the interior groups and surface groups reach a minimum and form a more spherical (globular) structure. (**Figure 5.10**)

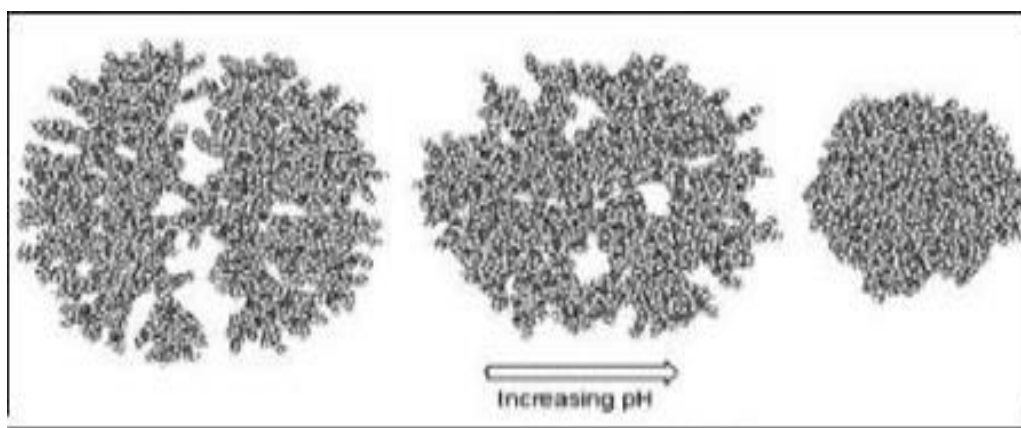
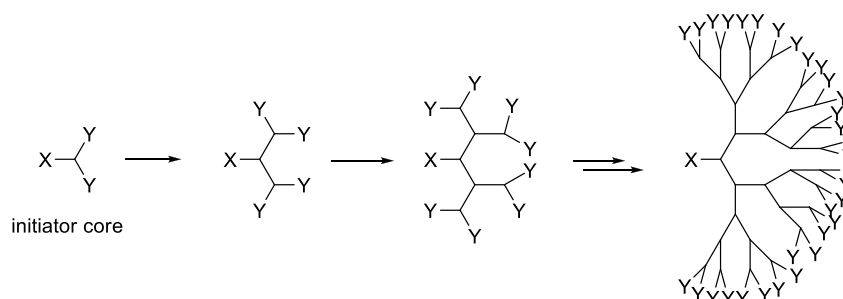


**Figure 5.10** PAMAM dendrimer's conformation under different pH condition (reprinted from reference 9)<sup>9</sup>

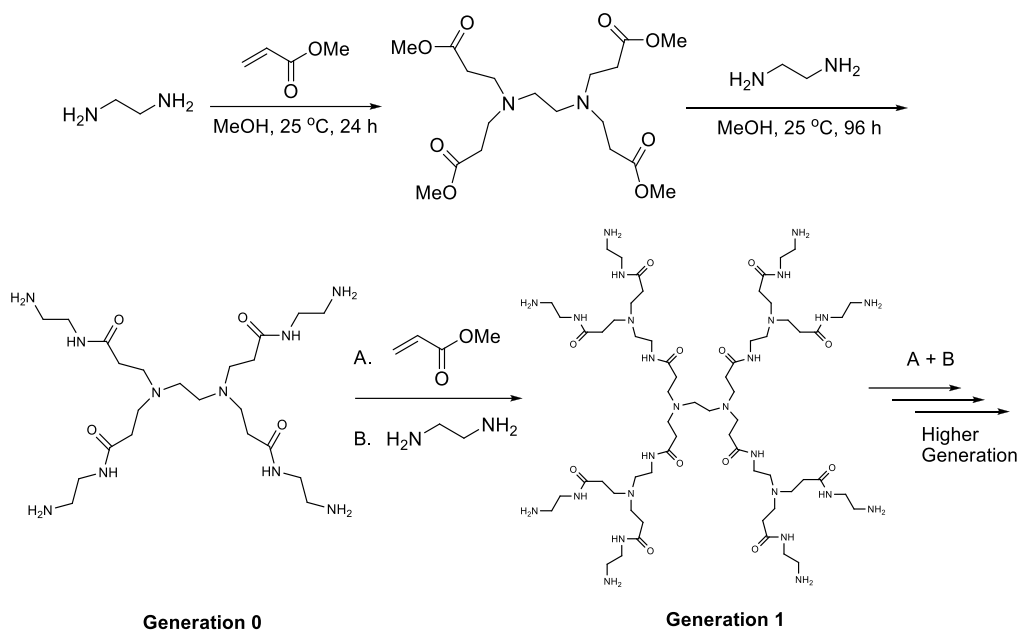
### §5.1.2 Preparation

Dendrimer chemistry was first introduced by Fritz Vogtle and coworkers by synthesizing the first “cascade molecules” in 1978.<sup>14</sup> In 1980s, Donald A. Tomalia, synthesized the first family of dendrimers with controlled molecular weight building, controlled branching and versatility in design and modification of the reactive terminal end groups.<sup>15</sup>

To synthetically build up the higher generation complicated dendrimer architecture, and more importantly to almost control over the critical molecular design parameters such as size, shape, surface/interior chemistry, flexibility and topology, two methods are usually applied on the basis of the starting point. In the early dendrimer syntheses, the methodology was employed as the “divergent” approach which the dendrimer grew outwards from the core, diverging into space.<sup>12</sup> (**Scheme 5.1**) More specifically, the first synthesized PAMAM dendrimer can be prepared follow a serial repetitive reaction sequences of Michael addition of methyl acrylate and condensation (amidation) of the resulting ester.<sup>8,16</sup> (**Scheme 5.2**)



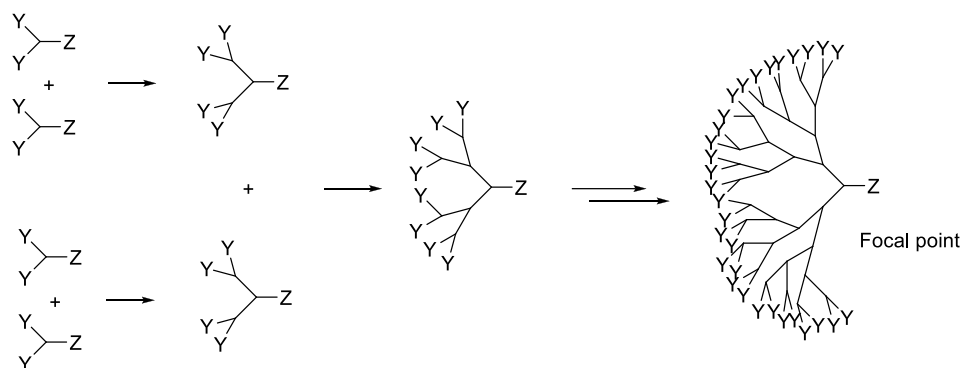
**Scheme 5.1** Schematic of divergent synthesis of dendrimers



**Scheme 5.2** PAMAM dendrimer growth from core to high generation

This synthetic methodology relies on extremely efficient reactions in order to ensure low polydispersities, or else it will be impossible to isolate pure product from side products with close molecular weight.

Another method, called “convergent” approach, was developed as a response to the weaknesses of divergent syntheses. It starts from the end-up parts and gradually accumulates inwards (**Scheme 5.3**). Only two simultaneous reactions are required for any generation-adding step so the purification step is relative easier. But due to the steric effect, problem occurs when the formation of high generation and this method suffers from low yield.



**Scheme 5.3** Schematic of convergent synthesis of dendrimers

### §5.1.3 Active and Passive Targeting Strategies

Tumor-targeting prodrug delivery strategies are based on active or passive targeting. Active targeting relies on the difference of tumor-associated cell surface biomarkers expression, such as antigen or receptor, between cancer and normal tissue. In past, numerous research efforts have



focused on conjugating the anticancer drugs with antibodies through a linker to construct a tumor-targeting drug conjugate for drug delivery. For example, monoclonal antibodies (mAbs) were intensively investigated in active targeting approaches because of their high binding affinity for the responding antigens. Another more challenging strategy classified as passive targeting aims on employing macromolecules including polymers or nanoparticles as inactive carriers or vehicles. These macromolecules are not directly interacting with tumor cells, but strongly influence the accumulation, transportation and biodistribution of their drug conjugates in tumor tissue due to the enhanced permeability and retention (EPR) effect. This concept was firstly elucidated by Maeda and co-workers in 1980s.<sup>17</sup> In principle, tumor cell clusters induce angiogenesis which is essential for their increasing demands of oxygen and nutrition. **(Figure 5.11)** The new blood vessels generated by the tumor often have irregular shape and large size pore, compared to the healthy tissue. The leaky and defective vessels make the vasculature of tumor tissue permeable to macromolecules which hardly pass the endothelial barrier of the blood vessels of healthy tissue. In addition, the enhanced uptake of macromolecules in tumor tissue is also relating to its increased retention in the tumor. If the molecular weight achieves the 40KDa criteria,<sup>18</sup> macromolecules are shown in the decreased clearance from the tumor due to the defective lymphatic drainage system. **(Figure 5.12)**

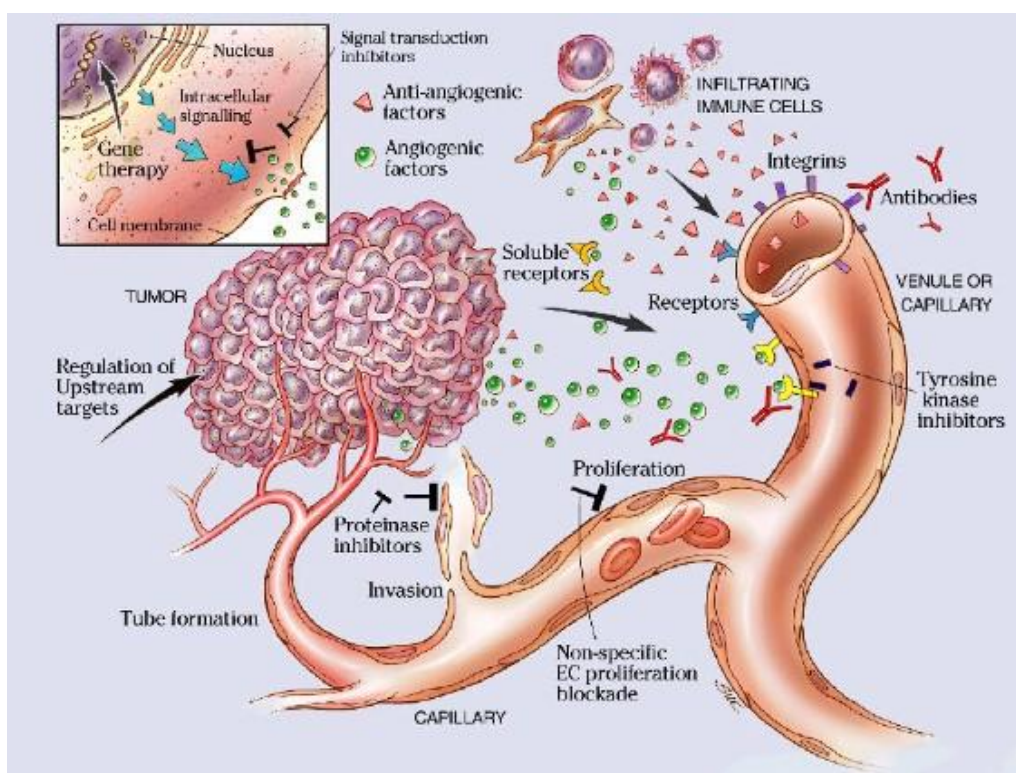


**Figure 5.11** Angiogenesis (reprinted from reference 19)<sup>19</sup>

Dendrimer-based nanocarrier are suitable for both active and passive strategies in tumor-targeted drug delivery. With higher generation dendrimer as vehicles, the molecular weight and size of entire dendrimer-based drug conjugates after incorporating with different functionalities (tumor-targeting modules, drugs, imaging agents, etc.) can be easily increased to exceed 40KDa to utilize EPR effect. Moreover, higher generation dendrimer also provide exponentially higher number of functional group to afford multiple types of functionalities within one dendrimer-based

carrier.

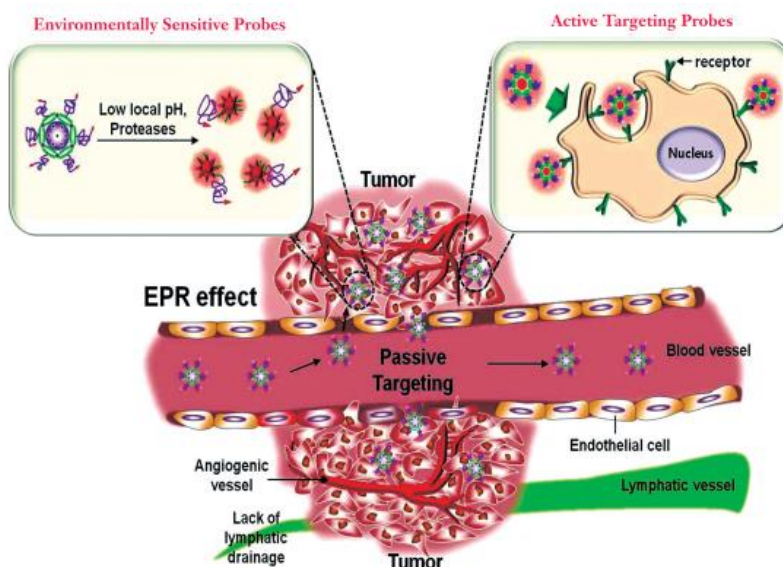


**Figure 5.12** Active and passive targeting approaches of nanocarriers in tumor-targeted drug delivery (reprinted from reference 20)<sup>20</sup>

## §5.2 Original Design of Asymmetric Bow-Tie Dendrimer (ABTD) Drug Delivery System (DDS)

As one of the macromolecular material, dendrimers have been investigated as carrier molecules for tumor-targeted drug delivery. Therapeutic agents can either be encapsulated within the dendrimers to form so-called “dendritic box” which can reduce not only the therapeutic agents’ hydrophobicity, but also their systemic toxicity and side-effect,<sup>21-22</sup> or covalently bound to its multivalent surface. The drug loading can be adjusted by increasing the generation of the dendrimer, and release can be controlled by incorporating degradable linkages between the drug and the dendrimer. Furthermore, the high density of surface groups permits attachment of additional targeting groups or functionality that may modify the solution behavior or toxicity of dendrimers.

To date, the most common and feasible strategy for dendrimer-based DDS design<sup>16,23-24</sup> is to use dendrimer as multivalent platform to carry multiple components including a drug, a cancer-detecting agent, and a fluorescent sensing agent. (**Figure 5.13**) Due to existence of tertiary amino groups in the interior region and the primary amino groups on the surface, PAMAM dendrimers are pH sensitive and responsible for low pH-triggered nonspecifically targeted drug delivery.<sup>25-26</sup> Therefore certain number of primary amino group on the PAMAM dendrimer surface can be partially acetylated depending on the reaction condition (equivalence, temperature, reaction time, concentration, etc.) to neutralize the dendrimer surface which will prevent side reactions and nonspecific targeting. Partial acetylation can also control the number of functional amino group and increase the solubility of the resulting functionalized dendrimer-based nanocarrier. For higher than generation 3 dendrimers, fully functionalization of at least 128 surface amino groups with hydrophobic molecules may resulting in dramatic decreased solubility. Thus by partially blocking the dendrimer, the remaining nonacetylated primary amino groups can efficiently attach various functional molecules including targeting agents, imaging agents, and therapeutic drugs.

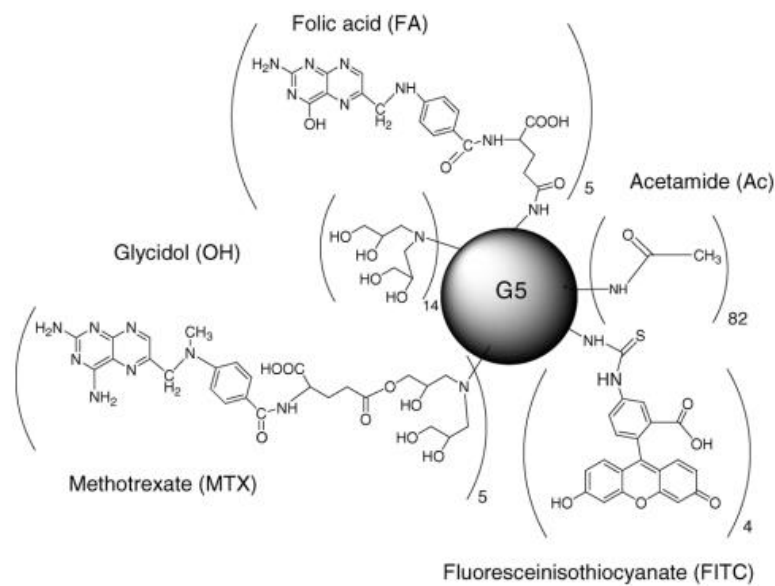


**Figure 5.13** Structure of multi-functional generation 5 PAMAM dendrimer conjugate bearing different functional molecules (Ac, FITC, FA, OH, and MTX) with approximate average number (reprinted from reference 23)<sup>23</sup>

However, several critical issues relating to the dendrimer-based drug delivery system require full investigations. First, the structural defects during the synthesis of the dendrimer has been identified and described as the purification and analysis problem.<sup>27</sup> (**Figure 5.14**) Occurrences of undesirable side reactions during the successive steps result in macromolecular polydispersity.<sup>28</sup> The resulting mixture contains a wide range of polymers with similar molecular weight and little regional structural difference which are impossible for separation. In addition, the amount and existing form of defect dendrimer may be very different for each batch of commercial available or lab-synthesized product. Thus it is not easy to conclude the purity and quality of resulting dendrimer drug conjugate. No reproducible or reliable biological evaluations can be expected.

Regardless of the defect structures, functionalization with different classes of functionalities on single dendrimer core may end up with uneven distribution on the surface which is referred as heterogeneity.<sup>29</sup> Heterogeneity of distribution is determined by the reaction conditions including temperature, local concentration, and equivalence of reagents. In a quantitative assessment of dendrimer-ligand distribution study, it was found that the distributions of dendrimer-ligand species possessed means between 0.4 and 13 ligands per dendrimer and average structure is not sufficient to reflect the sample diversity.<sup>29</sup> In many cases, the dendrimer-ligand species with the same number of ligands as the mean number is not even the most abundant species.<sup>29</sup> Based on the HPLC analysis results, a theoretical calculation was given to simulate the distribution. (**Figure 5.15**)

Overall, the present dendrimer-based multivalent macromolecular drug conjugates are represented by the average number of each type of functional molecules regardless of their distribution on the surface, and the quality of final conjugate of each batch was not guaranteed to be identical, resulting in inconsistent and unreliable biological evaluation results. The number of

each functionality vary from each batch, mainly depending on the reaction conditions, and also related to the dendrimer derivatives derived from the defect starting material.

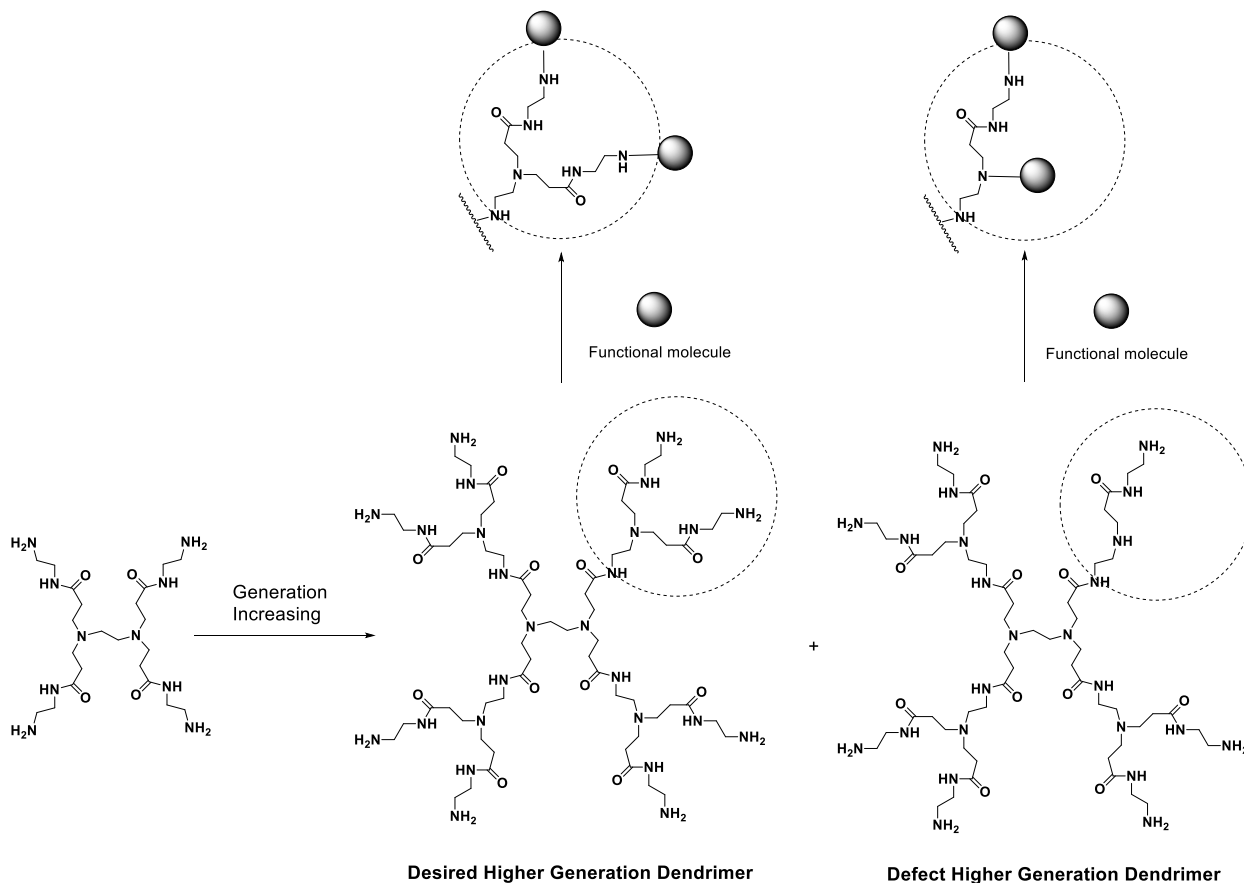


**Figure 5.14** Example of defect dendrimer formation and further functionalization

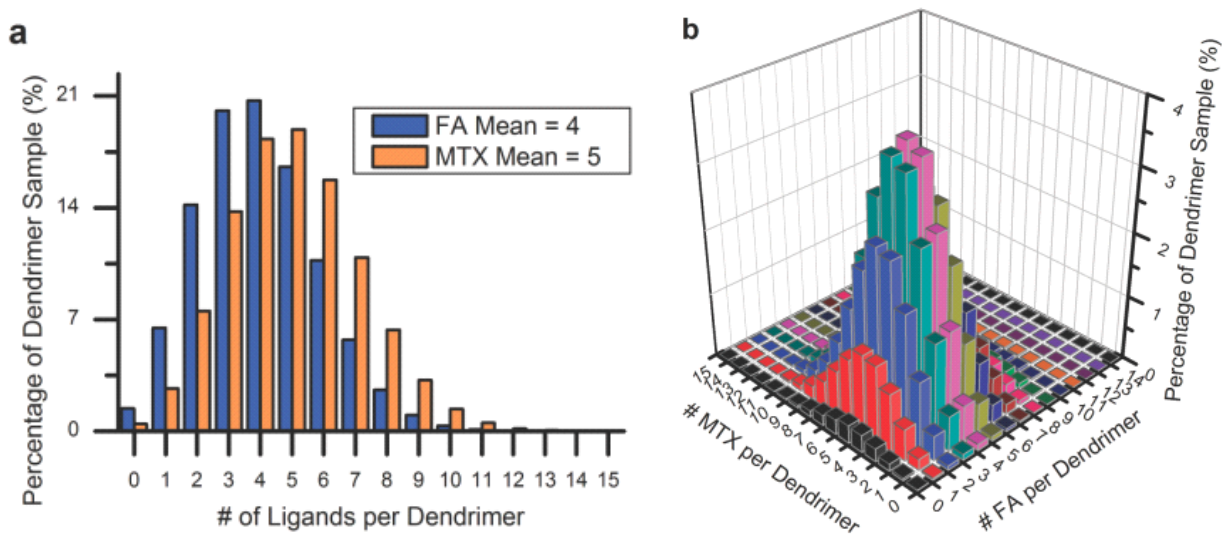


**Figure 5.15** Theoretical distribution of dendrimer species with a mean of 4 folic acid and 5 methotrexate molecules per dendrimer (reprinted from reference 29)<sup>29</sup>

## §5.2.1 Rational Design

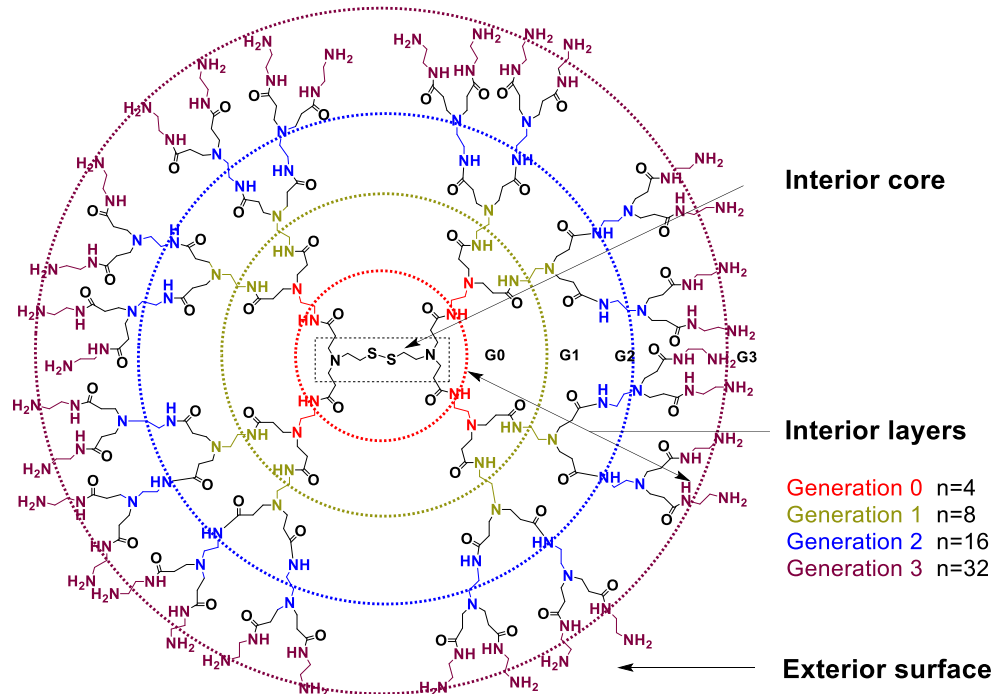


**Figure 5.16** Chemical structure of PAMAM dendrimer architecture bearing cleavable core

To solve this problem mentioned above, we selected a type of PAMAM dendrimer with cleavable cystamine core. (**Figure 5.16**) Upon fully functionalization of different functionalities on different generation dendrimers, the pure desired products can be purified and isolated, followed by the cleavage of the fully functionalized dendrimer to generate two half dendrons. Then the two half dendrons could be re-coupled through a linker to construct an asymmetric bow-tie dendrimer-based construct (**Figure 5.17**).

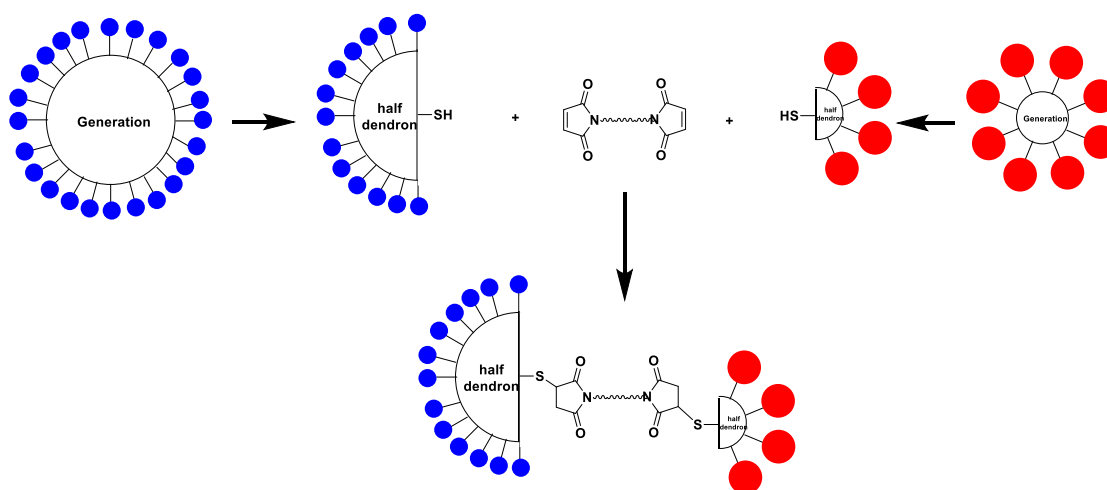


**Figure 5.17** Strategy of construction of asymmetric bow-tie dendrimer scaffold using fully functionalized half dendrons

This novel design was proposed by Dr. Gary Teng in his PhD research proposal in 2010. Soon later a comparable example based on the use of cleavable dendrimer was published in 2011. Hartley group designed a symmetric robust and versatile PAMAM dendrimer-based platform for vaccine delivery applications. A peptide array and a mannose array were fully functionalized on two different generation 3 PAMAM dendrimer with cleavable cystamine core to generate heterodendrimers, followed by orthogonally re-attachment through a di-block linker incorporating with a fluorescein probe for imaging purpose.<sup>30</sup> (Figure 5.18)

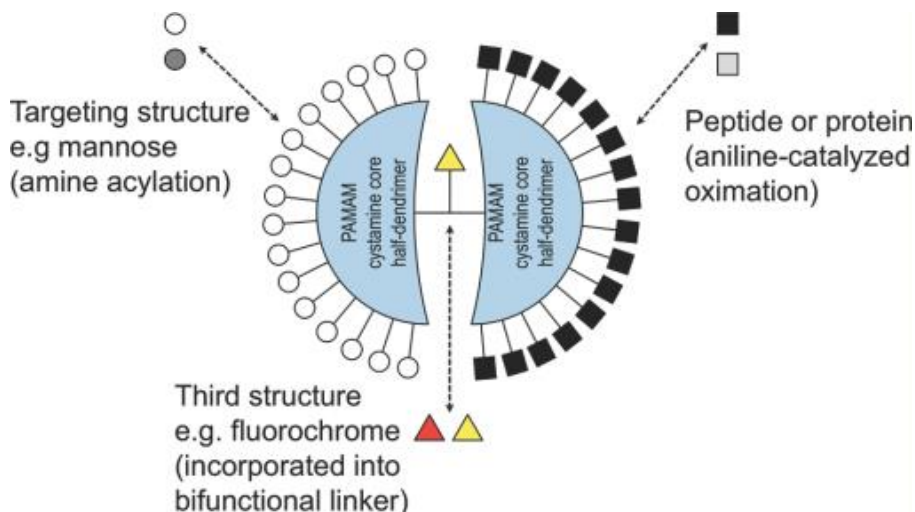
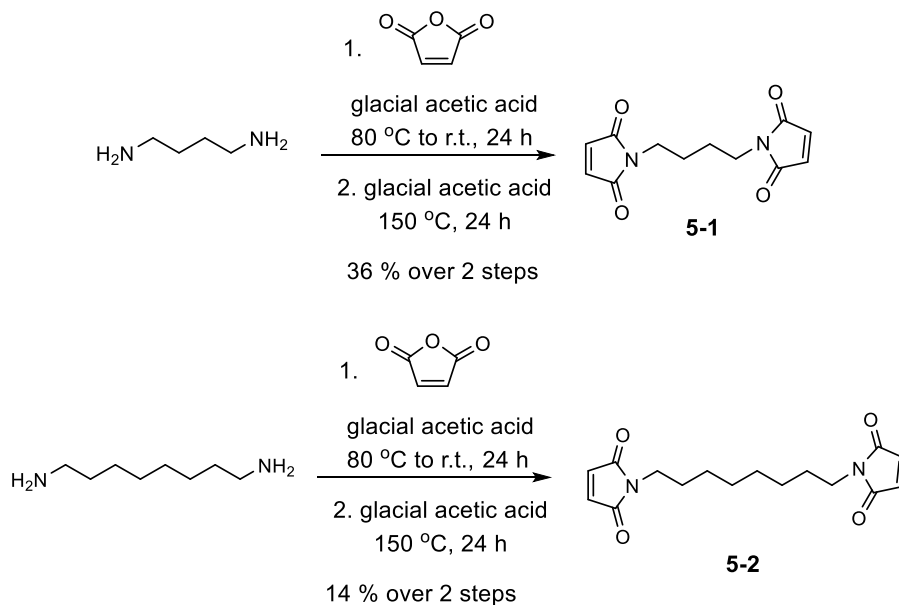


**Figure 5.18** A robust and versatile bioactive dendrimer diblock platform (reprinted from reference 30)<sup>30</sup>

### §5.2.2 Proof of Concept



**Scheme 5.4** Synthesis of bis(maleimido) butane and octane linkers

To evaluate the strategy for homo-cleavage a dendrimer compound with cystamine core, and recouple two half dendrons to a suitable linker, a simplest ABTD model and a bis(maleimido) alkane linker were designed and synthesized. Based on the feasible 1,4-Michael addition between  $\alpha$ ,  $\beta$ -unsaturated ketone and  $-SH$  as nucleophile, the bis(maleimido) alkane was designed to link two cleaved half dendrons to obtain the asymmetric conjugate. Two linkers were obtained starting from 1,4-diamino butane and 1,8-diamino octane reacting with maleic acid anhydride in the presence of glacial acetic acid as dehydrating agent to give **5-1** and **5-2** (Scheme 5.4).

Before coupling of the two half dendrons to obtain the final asymmetric conjugate, sulfhydryl addition experiments were carried for model 1,4-Michael addition investigation. To simply represent generation 1 dendrimer, generation 3 dendrimer and their derivatives, two half circles with surface amino groups connected with a disulfide bond was used to illustrate dendrimer structures. (Figure 5.19)

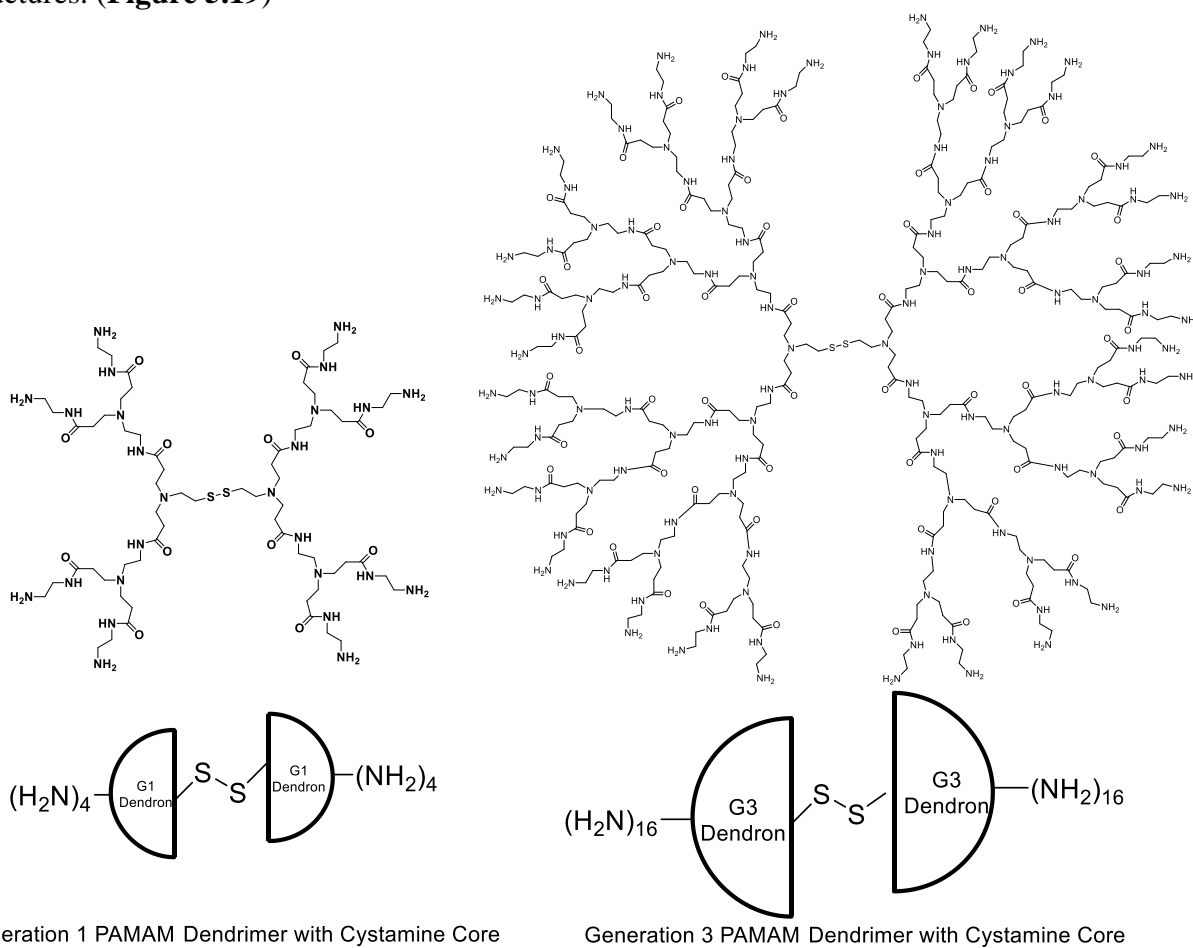
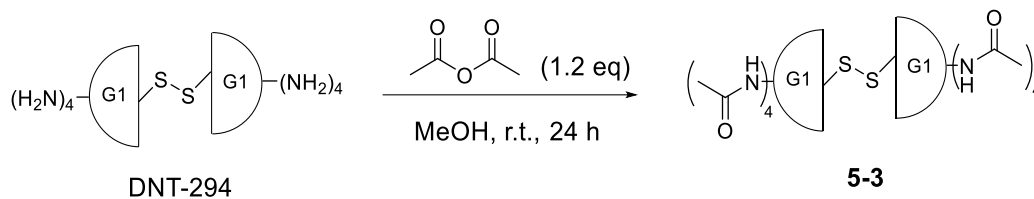


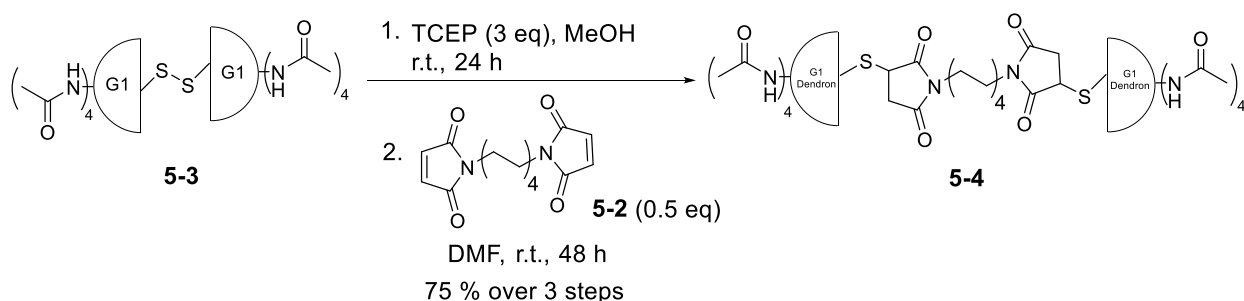
**Figure 5.19** A robust and versatile bioactive dendrimer diblock platform

Therefore, G1 dendrimer was used to be fully acetylated to give **5-3**. (Scheme 5.5)



**Scheme 5.5** Acylation of G1 dendrimer

Then interior disulfide bond was cleaved to generate two half dendrons with sulfhydryl group, followed by addition of bis(maleimido) octane linker to give the symmetric acetylated G1 dendrimer connected with bis(maleimido) octane linker **5-4** in good yield (**Scheme 5.6**). From MALDI analysis, it was clearly observed that not only the existence of peak corresponding to molecular weight of desired product **5-4** ( $m/z$  2165.43), but also its corresponding fragmentations ( $m/z$  896.62 and 1236.79 for half dendron species with C-S bond cleavage and half dendron with linker, respectively) (**Figure 5.20**). On the basis of analytical results of **5-4**, it indicated that two half dendrons could be recoupled through a bis(maleimido) linker. Defect structures were observed but not fully characterized.



**Scheme 5.6** Synthesis of acetylated G1 PAMAM dendrimer with bis(maleimido) octane linker (**5-4**)

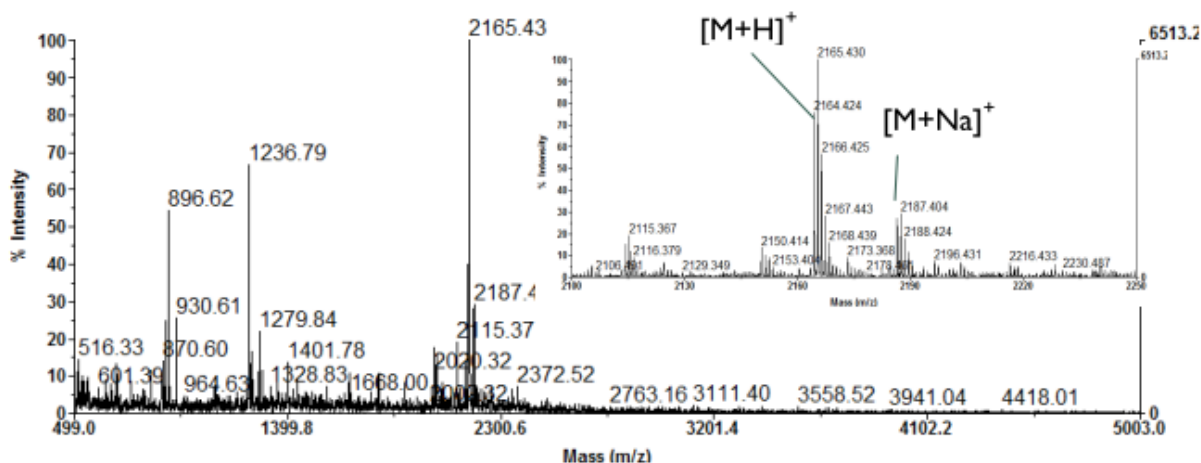


**Figure 5.20** MALDI-TOF of symmetric G1 PAMAM dendrimer with bis(maleimido) octane linker (**5-4**)

Another concern was whether the primary amino group on G1 PAMAM (8 amino groups in total) dendrimer and G3 PAMAM dendrimer (32 amino groups in total) can be fully



functionalized due to the potential steric hindrance on the surface, especially for G3 dendrimer, and solubility problem. Biotin, as tumor-targeting module for the dendrimer final conjugates, its NHS activated ester **3-20** was directly used to functionalize G1 and G3 dendrimer to give **5-5** and **5-6** (Scheme 5.7) (Figure 5.21). The amount of biotin added to the dendrimer was determined based on the number of the primary amine group on the surface of dendrimer. MALDI-TOF showed biotin was successfully coupled to dendrimer scaffold for both G1 and G3 (Figure 5.22 and 5.23). Compared to the G1 dendrimer, G3 dendrimer functionalized with biotin showed more peaks with slightly decreased mass values near the expected molecular weight indicating much defect derivatives existing in higher generation dendrimer. Purification was carried out either by molecular weight cut-off filter combined with centrifuge, or by using dialysis tubing membrane followed by lyophilization to remove solvents.

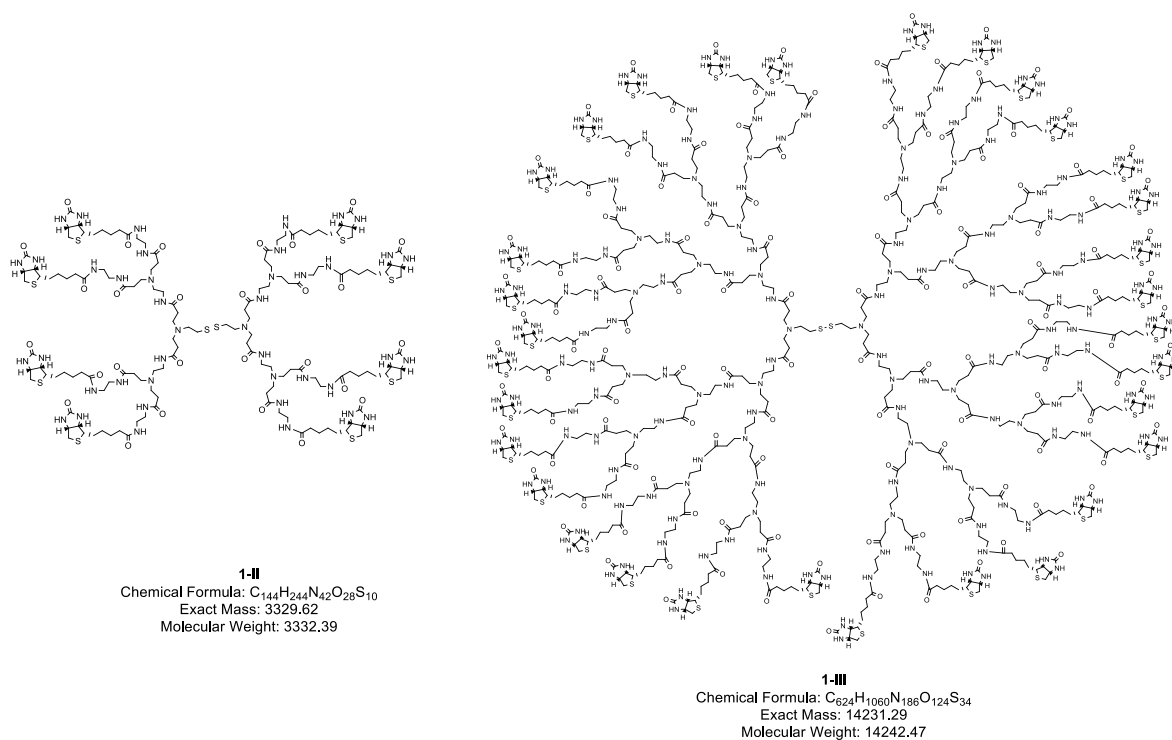
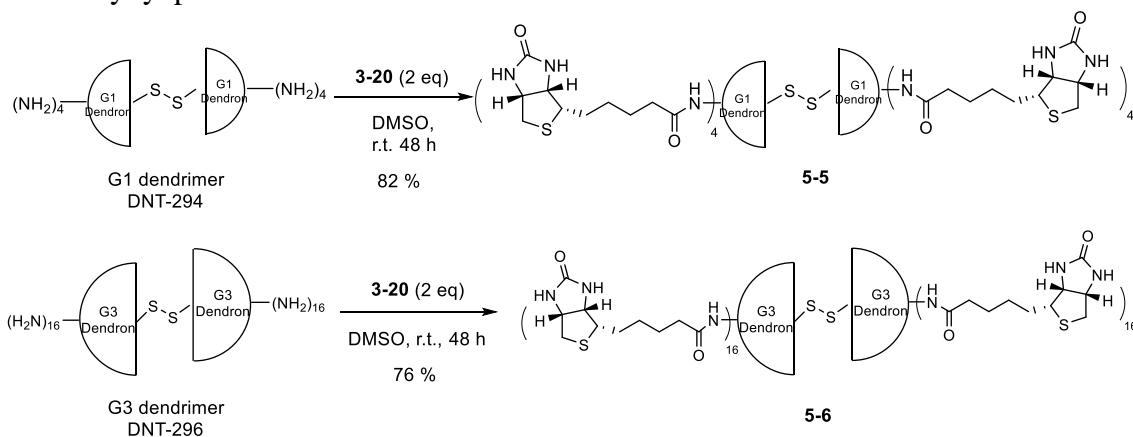


**Figure 5.21** Chemical structures and molecular weights of two fully biotinylated dendrimers **5-5** and **5-6**

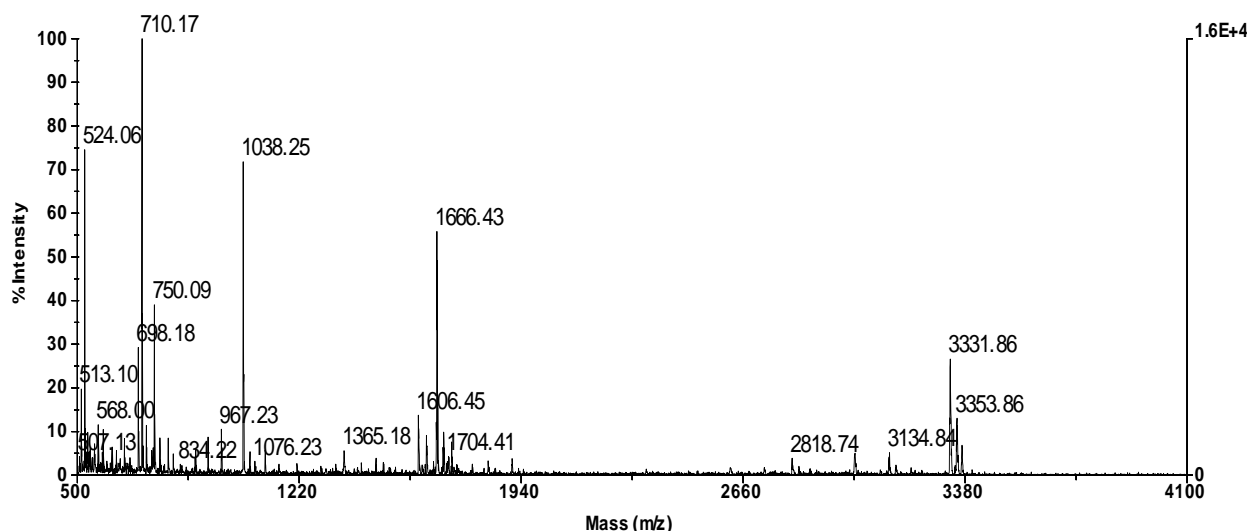


**Figure 5.22** MALDI-TOF of fully biotinylated G1 dendrimer **5-5**

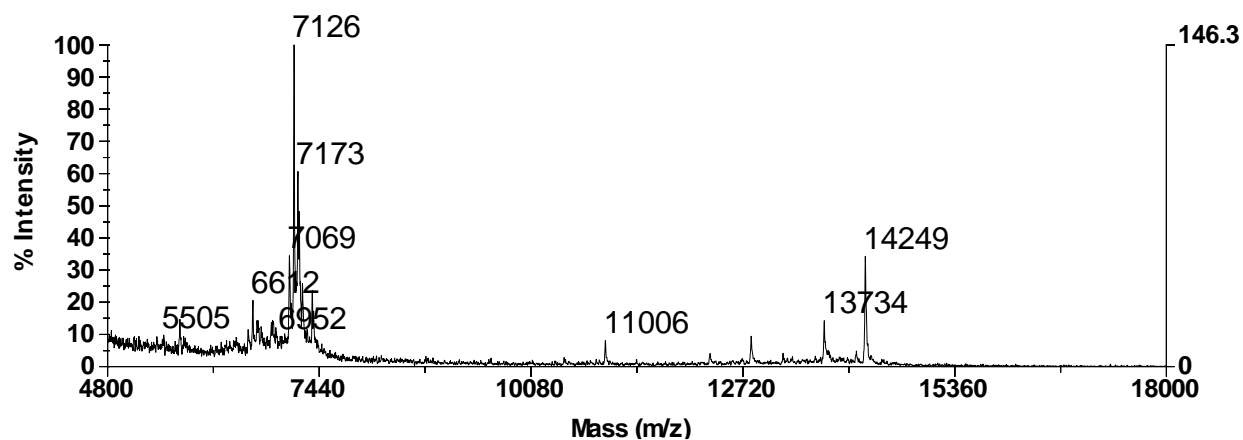
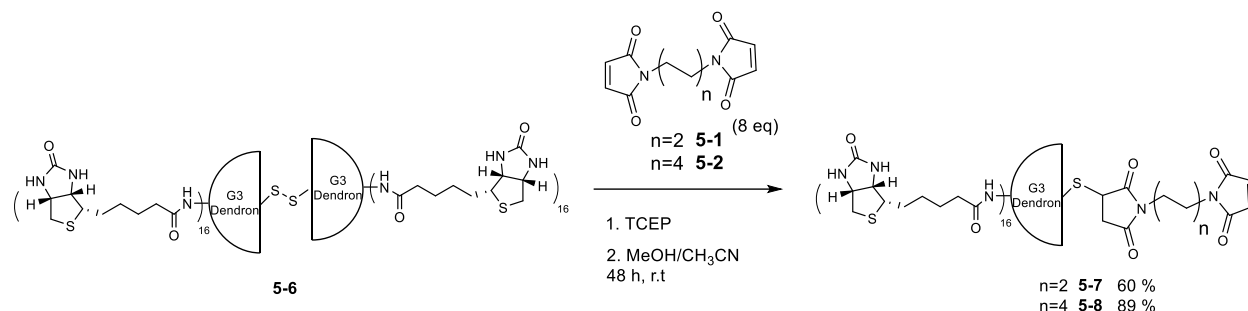


**Figure 5.23** MALDI-TOF of fully biotinylated G3 dendrimer **5-6**

### §5.2.3 First Attempt towards ABTD Conjugate

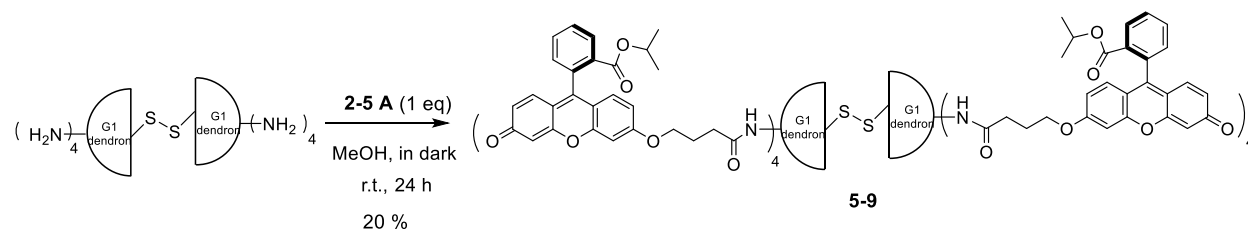
The asymmetric multi-functionalized dendrimer conjugate contains 3 major components: a half dendron functionalized by biotin as tumor-targeting moiety, a half dendron functionalized by fluorescein derivatives as fluorescent agent, and a bis(maleimido) linker to connect the two half dendrons.

To obtain the biontin functionalized dendron which was used to form the asymmetric dendrimer conjugate, TCEP (Tris (2-carboxy-ethyl) phosphine hydrochloride) was used to cleave the disulfide bond of the cystamine core to generate half dendron each with sulfhydryl group. Due to the stability issue of the  $-SH$  group after the disulfide bond, the resulting half dendron was consumed immediately by reacting with the bis(maleimido) linker *in situ* to avoid the oxidation of free  $-SH$  group. (**Scheme 5.8**) To decrease the side reaction which two half dendrons couple to one linker diluted reaction condition and excess of bis(maleimido) linker were applied. MALDI result indicated that only the mono addition product was generated.



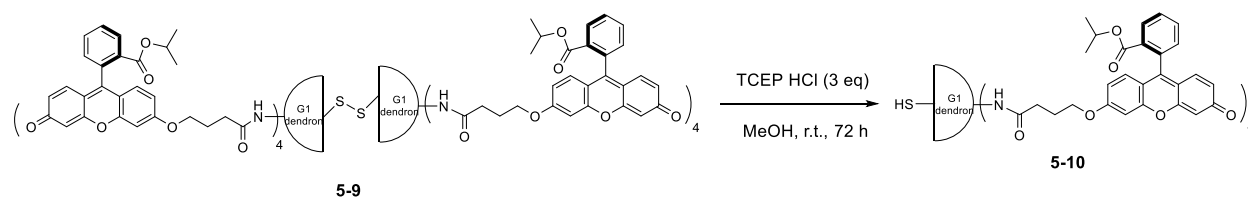
**Scheme 5.8** Formation of fully biotinylated half dendrons with linker mono adduct intermediate

On the other hand, to measure the internalization of drug-fluorescence agent conjugate into tumor cells, *in vivo* bioanalysis involves fluorescence detection in the early stage. At first several attempts using FITC (fluorescein isothiocyanate) as fluorescein probe were tried to covalently bond to dendrimer. FITC contains isothiocyanate functional group which is supposed to easily react with nucleophiles, such as amines on the surface of dendrimer. However, according to the MALDI-TOF results, the peaks relating to the expected molecular weight were never found around the corresponding range. So an alternative isopropyl protected fluorescein derivative **2-9 A** was tried to fully functionalize G1 dendrimer (**Scheme 5.9**)



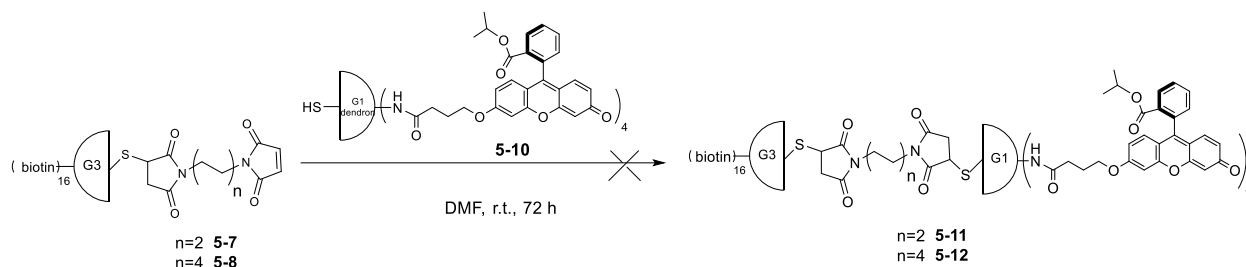
**Scheme 5.9** Synthesis of fluorescein functionalized G1 dendrimer **5-9**

The disulfide bond was also cleaved by using TCEP HCl (Tris (2-carboxy-ethyl) phosphine hydrochloride) to generate sulfhydryl group of half dendron **5-10**. (**Scheme 5.10**)

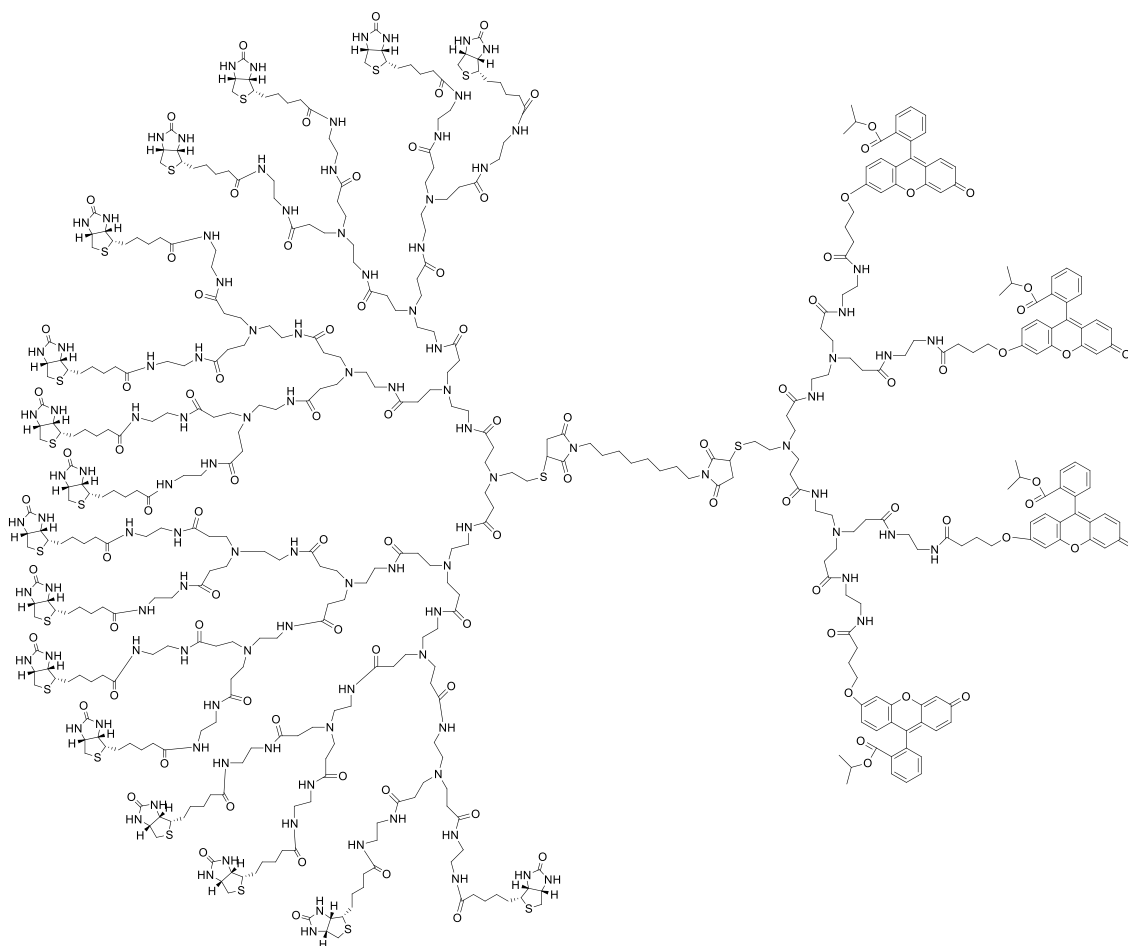


**Scheme 5.10** Synthesis of fluorescein functionalized half dendron

The final asymmetric conjugates were carried out by using mono adduct precursor **5-7** and **5-8**, and fluorescein functionalized half dendron **5-10**, followed by the dialysis purification against distilled water and methanol to obtain yellow solid. (**Scheme 5.11**) However, MALDI result did not show the corresponding molecular weight mass peak, but only some fragment peaks were observed maybe due to the thiol ether bond cleavage. This failure towards the final conjugates were resulted from solubility issue, especially on the 16 biotin moiety on the generation 3 dendrimer hardly dissolve in any solvents.



**Scheme 5.11** Attempts towards asymmetric PAMAM dendrimer conjugates



Chemical Formula:  $\text{C}_{468}\text{H}_{706}\text{N}_{108}\text{O}_{96}\text{S}_{18}$

Exact Mass: 9950.87

Molecular Weight: 9958.45

m/z: 9955.88 (100.0%), 9954.88 (84.3%), 9953.88 (70.7%), 9956.89 (68.1%), 9957.88 (49.7%), 9952.87 (38.8%),  
 9956.87 (30.5%), 9951.87 (18.8%), 9955.87 (12.8%), 9958.88 (12.3%), 9950.87 (7.9%)

Elemental Analysis: C, 56.44; H, 7.15; N, 15.19; O, 15.42; S, 5.80

**Figure 5.24** Structural information of asymmetric PAMAM dendrimer conjugate **5-12**

### §5.3 Modified Design of a Novel Versatile ABTD Drug Delivery System (DDS)

Based on the experimental results from the first attempt, the solubility of dendrimer derivatives after functionalization especially the biotinylated G3 dendrimer need to be improved.

To increase the solubility of the macromolecular conjugates, a PEG short oligomer was inserted to each dendrimer arm, as well as the interior bis(maleicimido) linker. Another major modification involved the novel design an ABTD versatile platform. Instead of fully functionalizing the G1 dendrimer with functional molecules in early assembly stage, a PEGylated terminal alkyne moiety was left on each arm of G1 dendrimer, allowing for the coupling of drug or imaging agent via click chemistry in the final step. (**Figure 5.25**) Different functionalities can be orthogonally and efficiently installed to the ABTD drug delivery system. With the modification and rational design, a novel asymmetric PAMAM dendrimer-based platform has been synthesized and applied on constructing a series of Asymmetric Bow-Tie Dendrimer-based (ABTD) conjugates (**Figure 5.26**) which bearing a biotin moiety as tumor-targeting module, a new generation taxoid as cytotoxic agent, and/or a fluorescein derivative as imaging module.

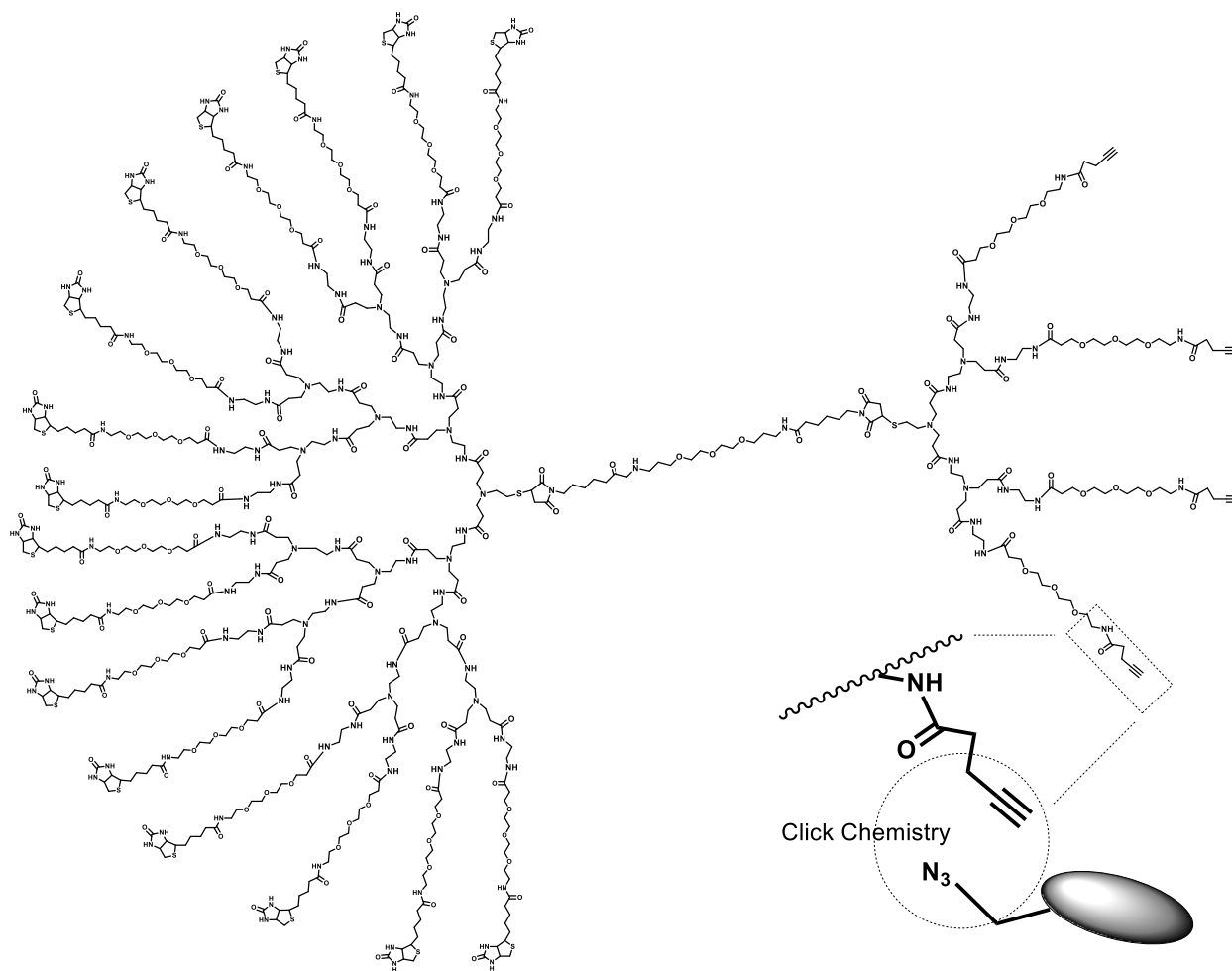


**Figure 5.25** Chemical structure of modified ABTD versatile platform

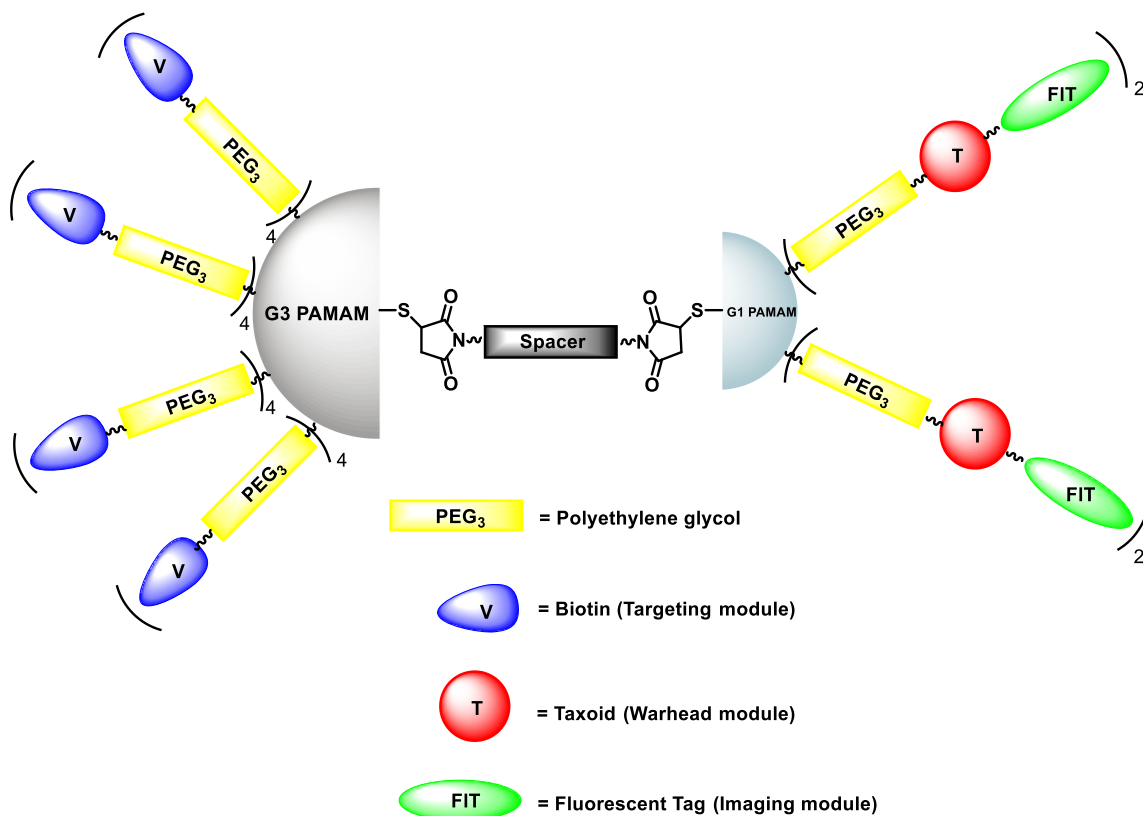
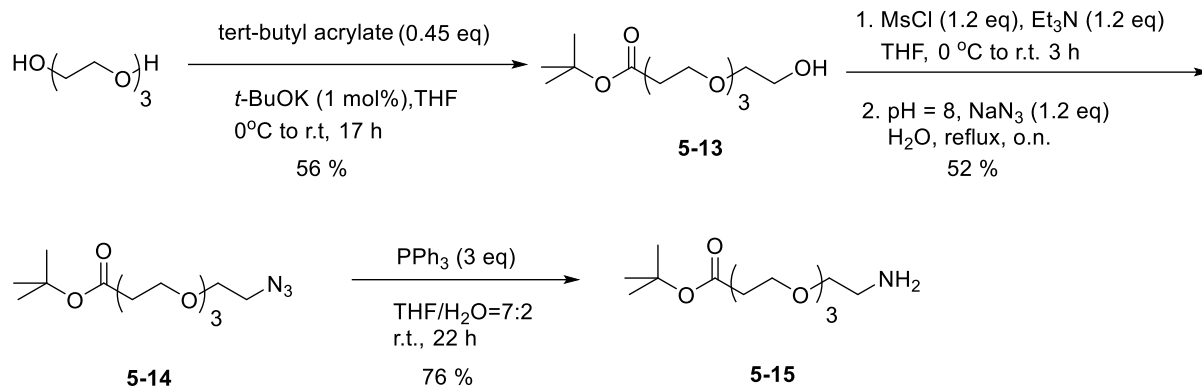


**Figure 5.26** Model structure of Asymmetric Bow-Tie Dendrimer-based (ABTD) conjugates

### §5.3.1 Solubility Improvement with PEG Oligomer Spacer

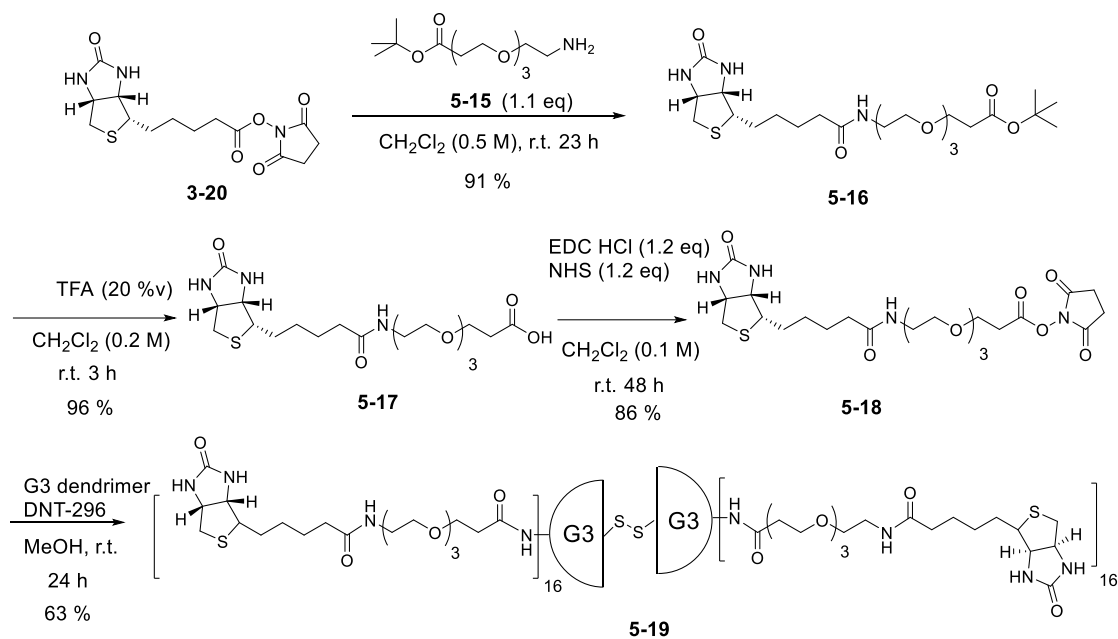
Polyethylene glycol (PEG) polymers have been commonly used in drug development to enhance the *in vivo* efficacy of potential therapeutic agents. PEGylation can enhance the pharmaceutical properties in a number of ways including: (1) half-life extension due to an increase in the apparent molecular size leading to decreased rate of renal filtration, (2) increased stability to proteolytic enzymes and (3) shielding of possible immunogenic epitopes.<sup>31</sup> Previous design which directly decorated the dendrimer with functionalities, especially the biotin moiety, resulted in limited solubility of the generated intermediate. To increase the molecular weight and solubility, various PEG multifunctional spacers were synthesized from PEG trimer and tetramer (Chapter 2). Commercially available *tert*-butyl 12-amino-4,7,10-trioxadodecanoate **5-13** can be readily prepared by Michael addition from triethylene glycol and *tert*-butyl acrylate in the presence of potassium *tert*-butoxide.<sup>32</sup> (Scheme 5.12)



**Scheme 5.12** Modification of PEG oligomer spacer

### §5.3.2 Biotinylated PEGylated G3 PAMAM Dendrimer

As mentioned, biotin was selected as the tumor-targeting molecule to be fully functionalized to each arm (totally 32) on the surface of generation 3 dendrimer. Due to the poor solubility towards commonly used organic solvents, a PEG short chain spacer was inserted into each arm to enhance the solubility. Biotin-PEG<sub>3</sub>-NHS ester could either be purchased from commercial available product or be readily prepared from biotin and commercially available *tert*-butyl 12-amino-4,7,10-trioxadodecanoate **5-15** through amide coupling, followed by TFA deprotection to remove *tert*-butyl moiety,<sup>33</sup> and activated with NHS to yield **5-18**. Then **5-18** was directly used to react with commercial generation 3 PAMAM dendrimer with cystamine core (DNT-296, from Dendritic Nanotechnologies, Inc.). (**Scheme 5.13**) Due to the limited solubility of compound **5-19**, the purification was mainly done by dialysis in methanol using MWCO 6000-8000 tubing membrane to remove the unreacted starting material. The purity of isolated product was confirmed by MALDI-TOF using 2,5-dihydroxybenzoic acid (DHB) as matrix. The desired peak 20748.3 could be assigned to the product. The highest ionic peak 10378.6 corresponds to the interior disulfide bond cleaved half dendron generated during the MALDI measurement. This result indicated that the fully functionalized desired product was successfully obtained in good quality. (**Figure 5.27**)



**Scheme 5.13** Fully functionalization with PEGylated biotin on generation 3 PAMAMA dendrimer

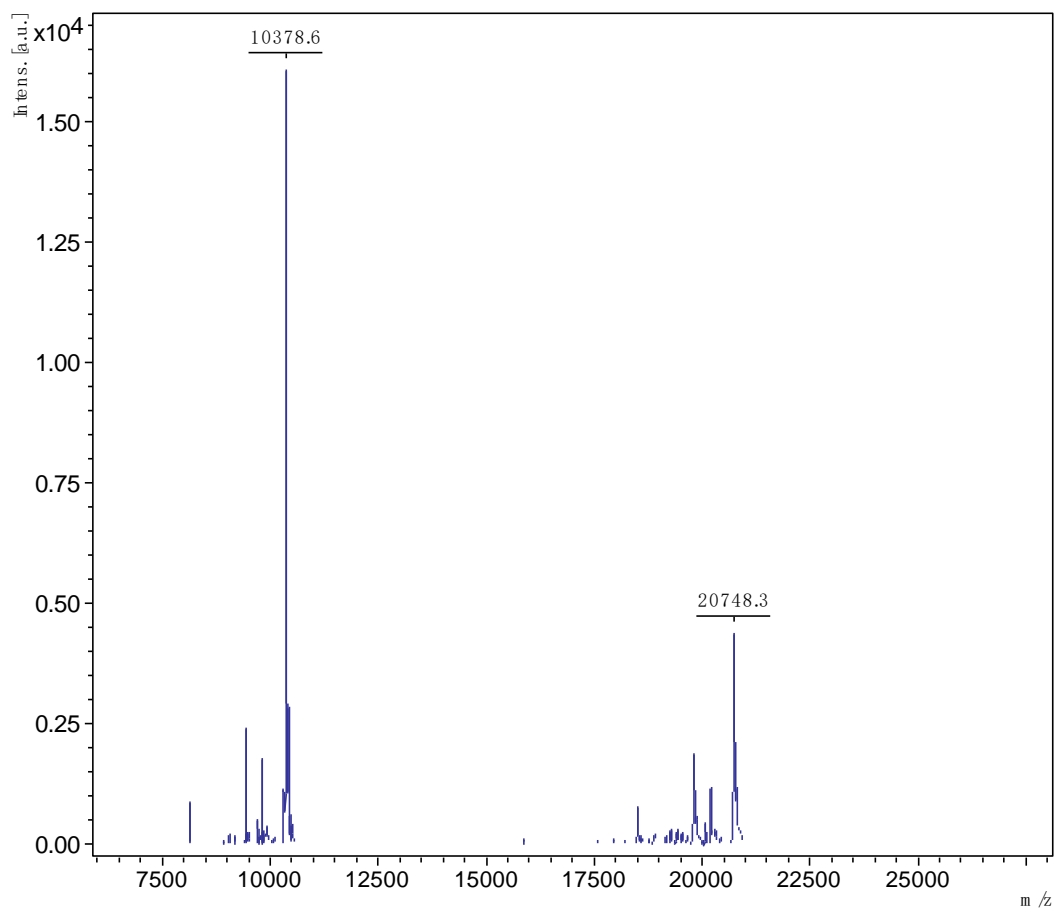
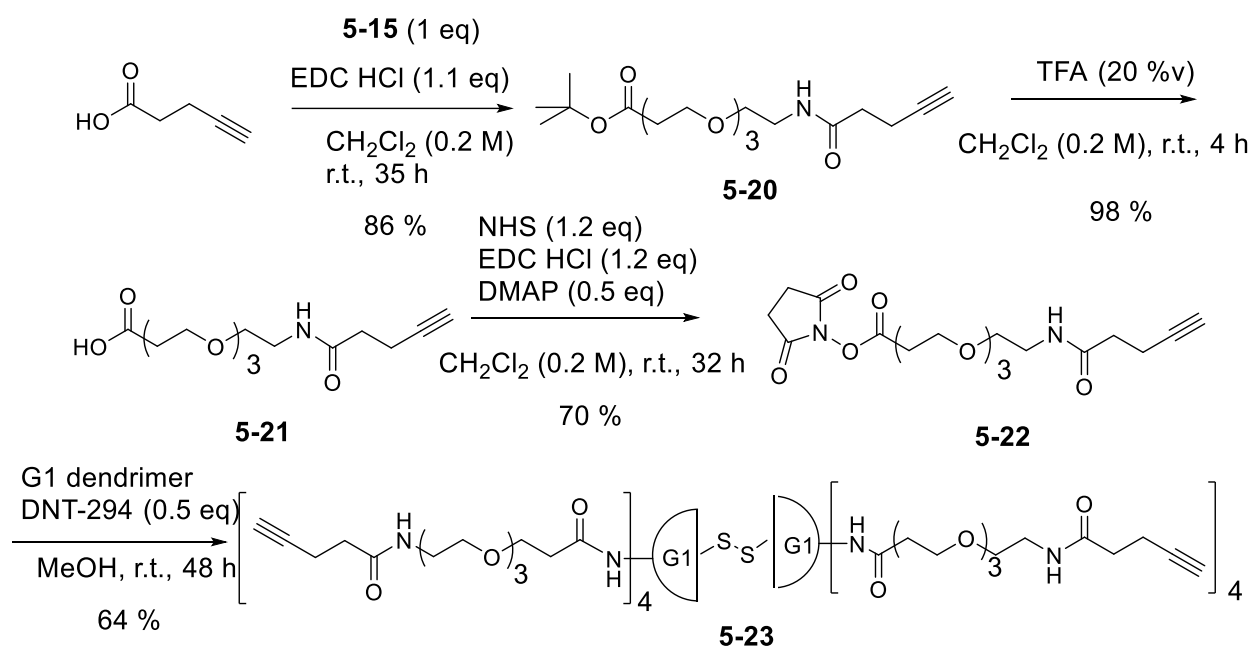


**Figure 5.27** MALDI-TOF result of purified fully functionalized generation 3 PAMAMA dendrimer



### §5.3.3 Click-ready PEGylated G1 PAMAM Dendrimer

4-pentynoic acid was treated with **5-15** to give **5-20** and deprotection of *tert*-butyl group using TFA to afford **5-21**, followed by activation using NHS to form its activated ester **5-22**. Then fully functionalization occur by amidation of generation 1 dendrimer bearing cleavable cystamine core (DNT-294, from Dendritic Nanotechnologies, Inc.) to generate **5-23** leaving terminal alkyne for orthogonal conjugation through a click reaction. (**Scheme 5.14**) Compound **5-23** was purified and isolated by preparative HPLC using C18 column. The purity of **5-23** was confirmed by MALDI analysis and LC-UV-TOF. The highest ionic peak 1895.205 was corresponding to the interior disulfide bond cleaved half dendron generated during the MALDI measurement. (**Figure 5.28-5.31**) And the 3788.202 was the non-cleaved mono charged desired peak value. After purification, LC-UV-TOF result clearly showed a major peak with retention time around 21.8 min under 215 nm UV absorption which was also the major peak in TIC trace. By mass analysis, this peak gave 1895.0713 ( $M+2H^+$ )<sup>2+</sup>/<sub>2</sub>, 1263.7156 ( $M+3H^+$ )<sup>3+</sup>/<sub>3</sub>, 948.0384 ( $M+4H^+$ )<sup>4+</sup>/<sub>4</sub>, 758.6320 ( $M+5H^+$ )<sup>5+</sup>/<sub>5</sub> which could be deconvoluted to the designed mass number 3788.13. These results indicated that the fully functionalized desired product **5-23** was successfully obtained in good quality.



**Scheme 5.14** Fully functionalization with click-ready PEGylated terminal alkyne on generation 1 PAMAMA dendrimer

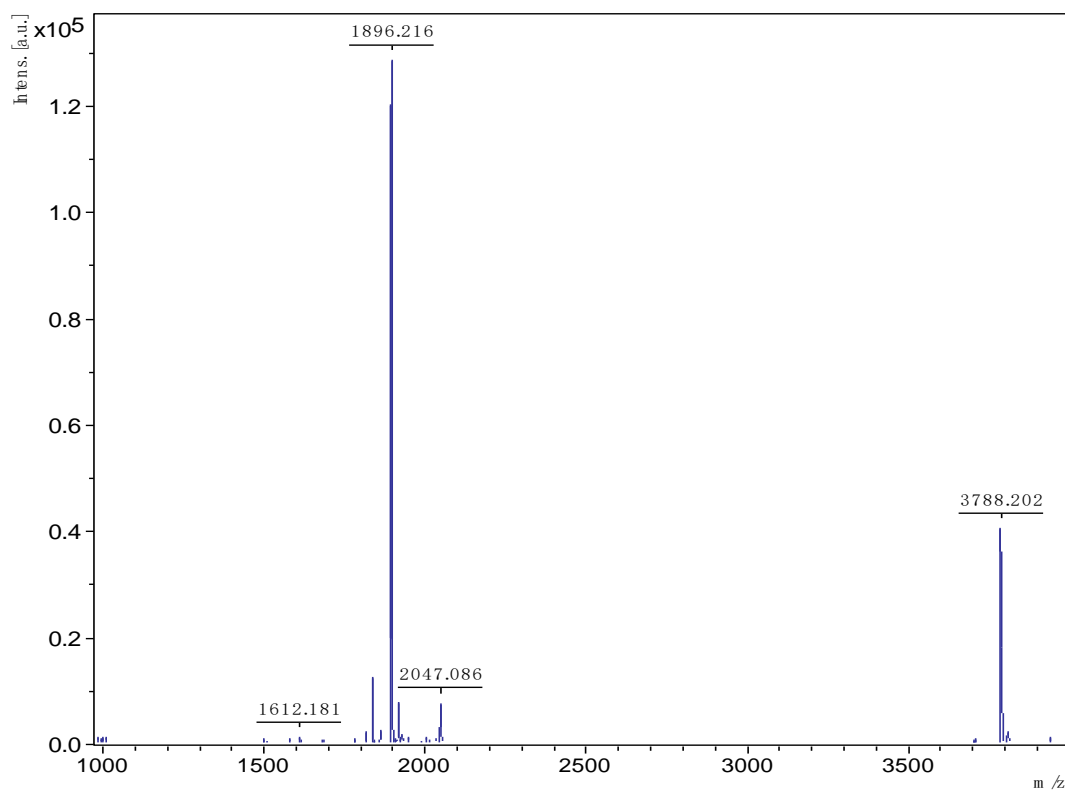


**Figure 5.28** MALDI-TOF result of purified fully functionalized generation 1 PAMAM dendrimer

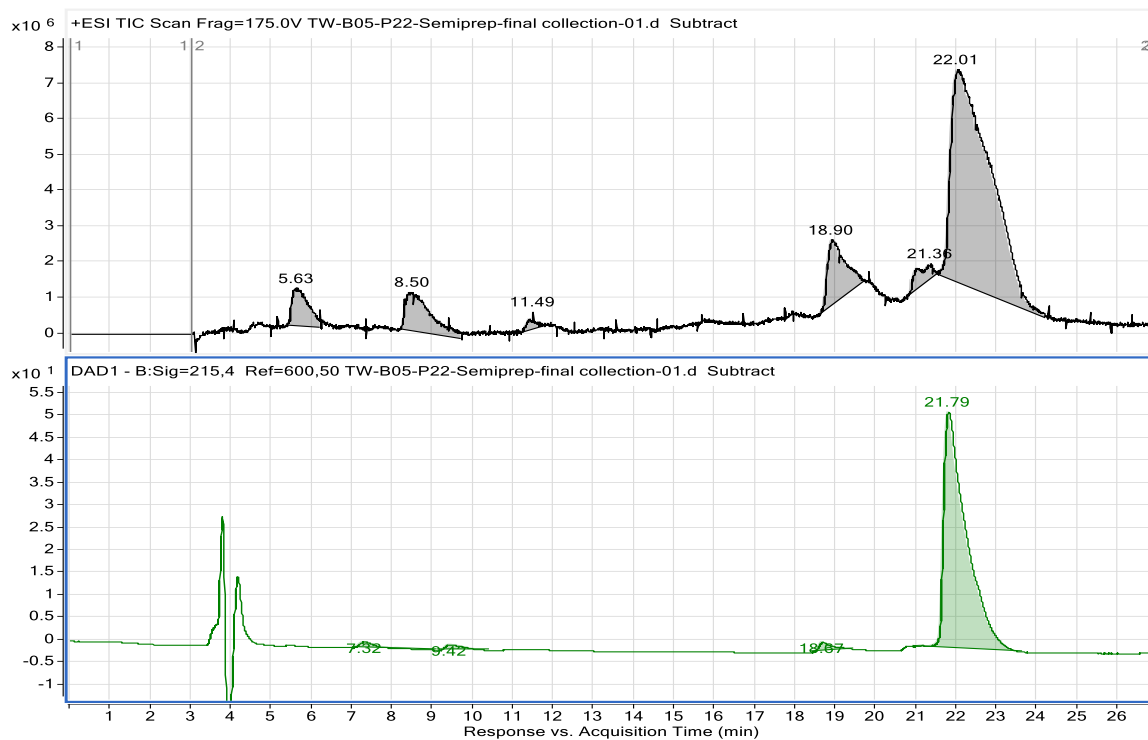


**Figure 5.29** LC-UV-TOF results for purified fully functionalized generation 1 PAMAM dendrimer

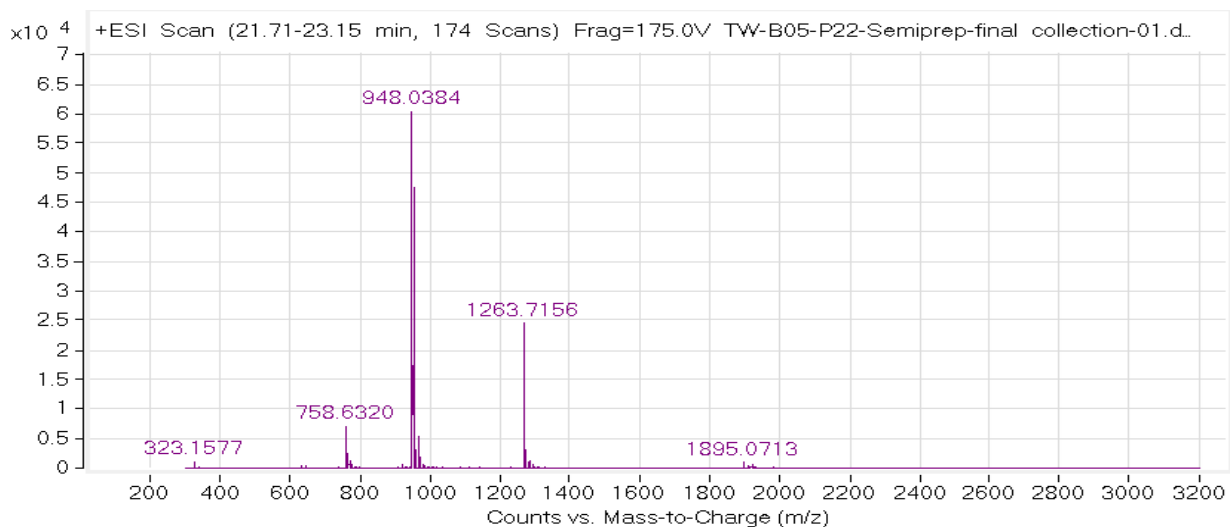


**Figure 5.30** LC-UV-TOF mass analysis results for purified fully functionalized generation 1 PAMAM dendrimer

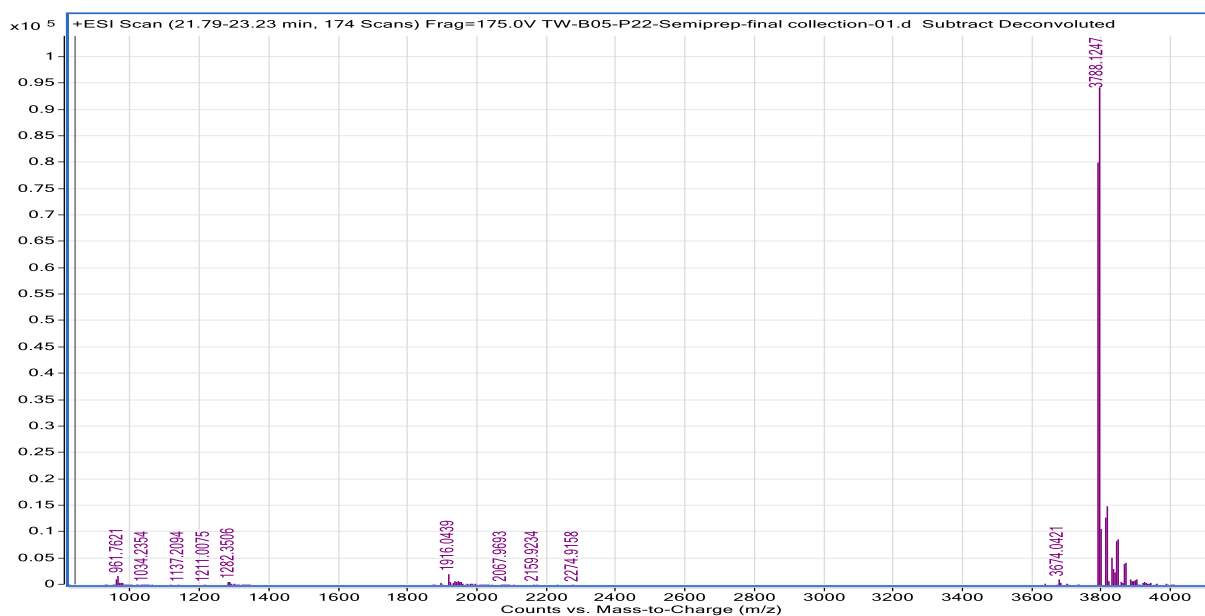


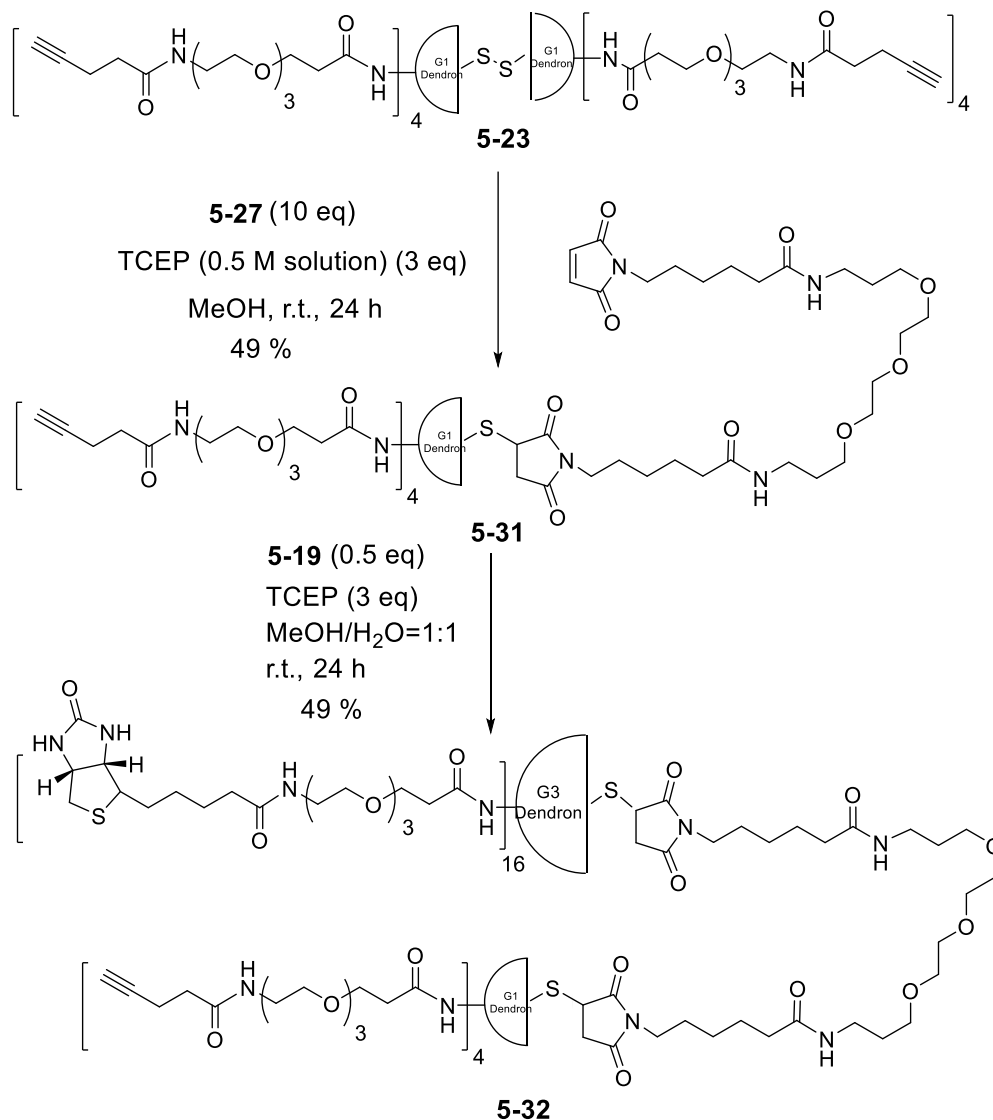
**Figure 5.31** LC-UV-TOF mass deconvolution results for purified fully functionalized generation 1 PAMAM dendrimer

### §5.3.4 Bis(maleicimido) PEGylated Linker

Since sulfhydryl group will be generated upon the cleavage of interior disulfide bond of **5-19** and **5-23**, a typical 1,4-Michael addition was applied here to stepwise couple the fully functionalized generation 1 and generation 3 half dendrons to a bis(maleicimido) linker. To synthesize this linker, 6-aminocaproic acid was treated with maleic anhydride in acetic acid<sup>34-35</sup> to generate the ring-open product **5-24**, followed by heat to reflux condition to form the cyclic condensation product **5-25**. Then in the presence of *N*-methylmorpholine, carboxylic acid group of **5-25** was activated by isobutyl chloroformate and give **5-26**. To increase the solubility of the linker, as well as the length of the linker so that the first half dendron on the linker will not embed



### §5.3.6 Synthesis of ABTD Conjugates

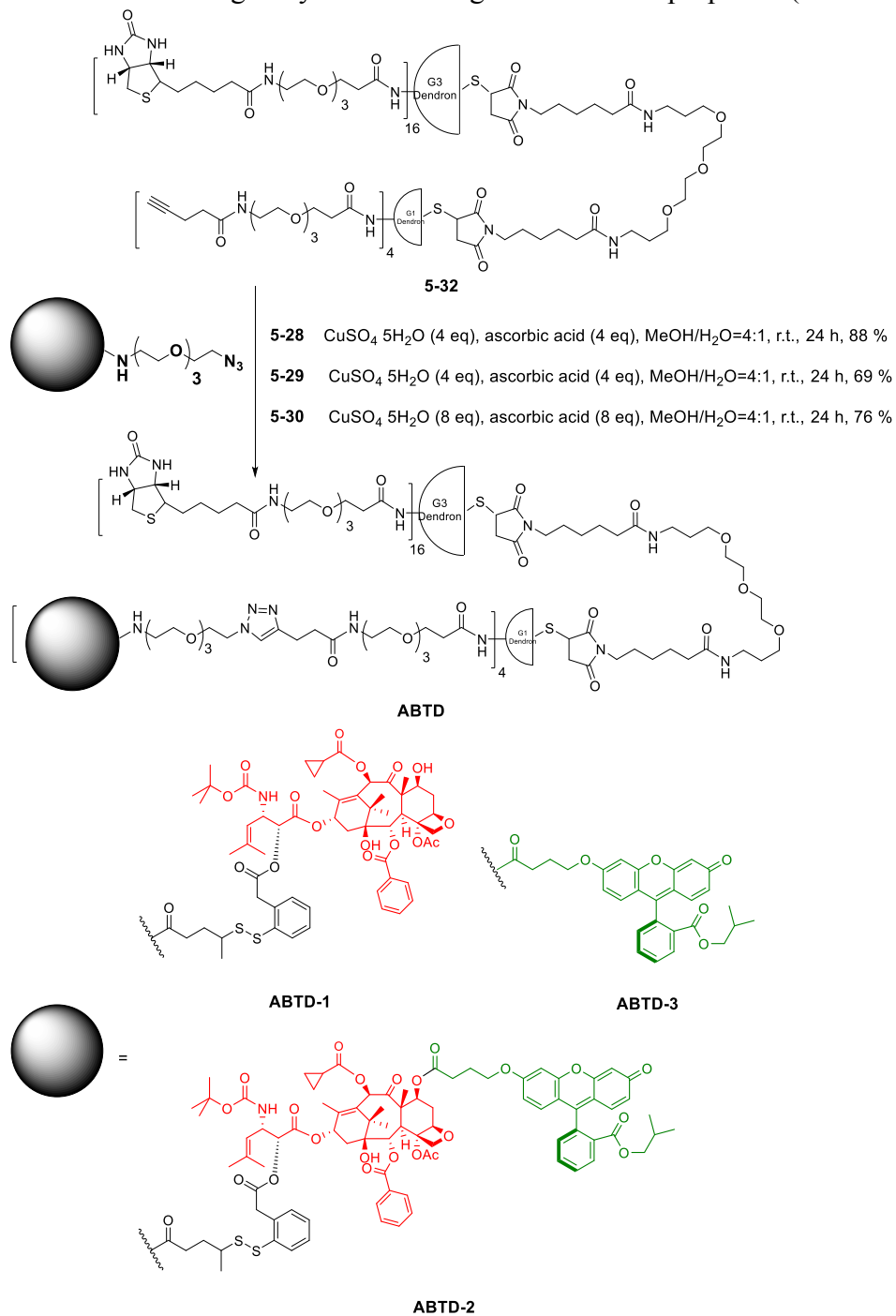


**Scheme 5.17** Synthesis of asymmetric bow-tie dendrimer click-ready scaffold

To construct the “click-ready” dendrimer scaffold bearing four PEGylated terminal alkyne arms and sixteen PEGylated biotin arms, fully functionalized G1 dendrimer **5-23** and G3 dendrimer **5-19** were required to be cleaved to form two half dendrons, followed by re-coupled through the bis(maleimido) linker **5-27** stepwise. The fully functionalized G1 dendrimer **5-23** was selected to first couple with **5-27** for reasons: (1) **5-23** has better solubility than **5-19** so purification with preparative HPLC was feasible and (2) the molecular weight difference was significant from **5-31** to **5-32** due to the dominant contribution of **5-19** so that dialysis as the most applicable purification method could be carried out for purifying **5-32**. (**Scheme 5.17**)

Purification of **5-31** was done by preparative HPLC using Jupiter C18 column. Solvents were water with 0.1 % TFA (solvent A) and acetonitrile with 0.1 % TFA (solvent B). We were able to remove the impurities and defect derivatives to solely isolate the desired product as single

component. The purity could be confirmed by MALDI-TOF and LC/UVMS-TOF. Formation of **5-31** was confirmed by the LC/UVMS-TOF analysis. Compound **5-32** was also purified by preparative HPLC and the formation of compound **5-32** was confirmed by mass analysis. Then three “click-ready” intermediates were synthesized via click reaction with **5-32** to give **ABTD-1**, **ABTD-2** and **ABTD-3** in good yield for biological evaluation purposes. (Scheme 5.18)



**Scheme 5.18** Synthesis Diagram of Asymmetric Bow-tie Dendrimer-based (ABTD) Conjugates

### §5.3.7 Internalization Study via RME and Multi-binding Effect

Here we describe a mechanistic study to prove the dendrimer-based platform an efficient drug delivery system by investigating (1) the internalization through receptor-mediated endocytosis (RME), (2) multi-binding effect resulting from the multi targeting moiety on each dendrimer-based drug conjugate, (3) increased loading capacity and delivery efficiency of anti-cancer drug, and (4) drug release through self-immolation of disulfide linker triggered by intracellular glutathione (GSH). Three different cells lines including ID-8 and MX-1 as biotin-receptor overexpressed cancer cell lines and WI-38 as normal human cell line which does not express vitamin receptor have been used to evaluate the efficacy and cell-specificity of the dendrimer-based drug conjugates bearing multiple biotin modules.

Internalization of **ABTD-3** was monitored by confocal fluorescence microscopy (CFM) and the fluorescence was quantified by flow cytometry, using ca. 10 000 treated live ID-8 and MX-1 cells, overexpressing biotin receptor. (**Figure 5.32**)

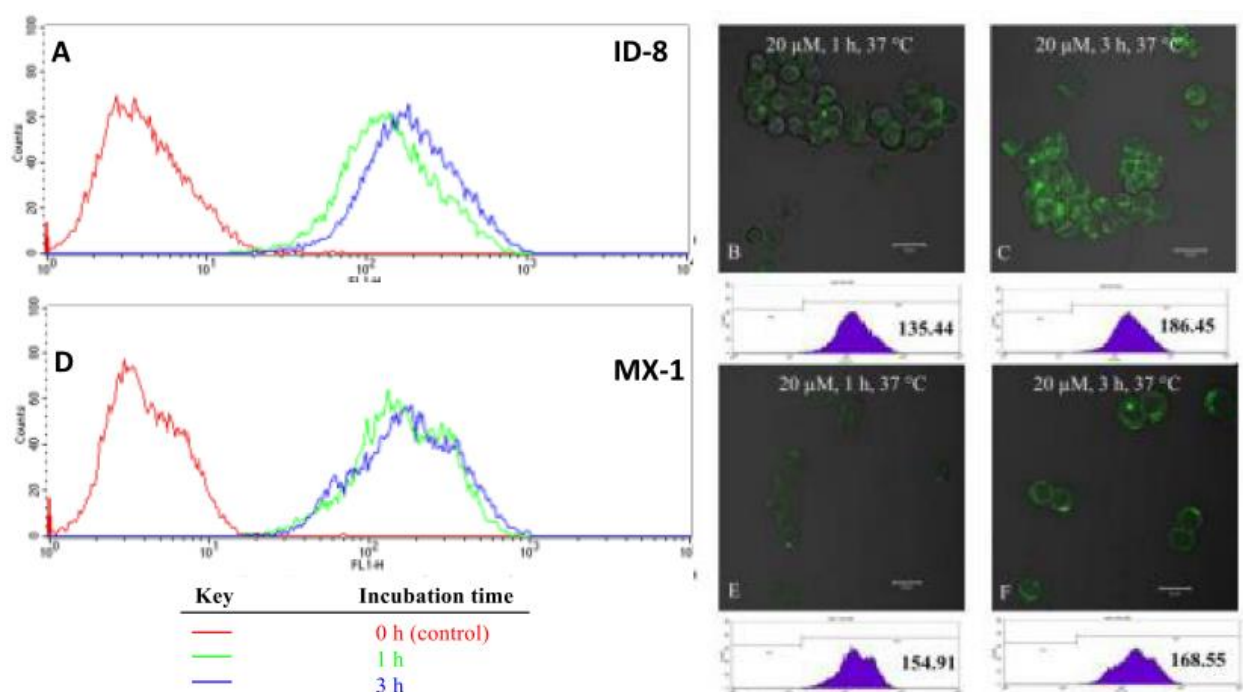


**Figure 5.32** CFM images and flow cytometry analysis of different types of cells after incubation with the **ABTD-3** at the final concentration of 20  $\mu\text{M}$  at 37  $^{\circ}\text{C}$  for different periods: (A) flow cytometry analysis of **ABTD-3** in ID-8 at 0 h (red, control), 1 h (green), and 3 h (blue); (B,C) CFM images and flow cytometry analysis in ID8 at 1 and 3 h, respectively; (D) flow cytometry analysis of **ABTD-3** in MX-1 at 0 h (red, control), 1 h (green), and 3 h (blue); (E,F) CFM images and flow cytometry analysis in MX-1 at 1 and 3 h, respectively.

**Figure 5.32** clearly showed the efficient internalization of **ABTD-3** via RME using CFM. Flow cytometry also indicates that at 20  $\mu\text{M}$  concentration, the internalization of **ABTD-3** reaches saturation since the fluorescein signal intensity slightly increases from 1 hour to 3 hours incubation period.

The multiple TTM (16 biotin modules in this case) on a single ABTD macromolecular drug conjugate are expected to increase its targeting ability and affinity to get internalized through RME via multi-binding to the biotin receptors, which are overexpressed on the surface of cancer cells. Consequently, to prove this hypothesis, small molecule Biotin-PEG-Fluorescein **3-25** (Biotin-PEG<sub>3</sub>-(CH<sub>2</sub>)<sub>2</sub>-Fluorescein) which only have one biotin moiety for one fluorescent moiety (TTM/fluorescein ratio is 1) was used as comparison to the ABTD-3 which have 16 biotin moiety for 4 fluorescent moiety (TTM/fluorescein ratio is 4).

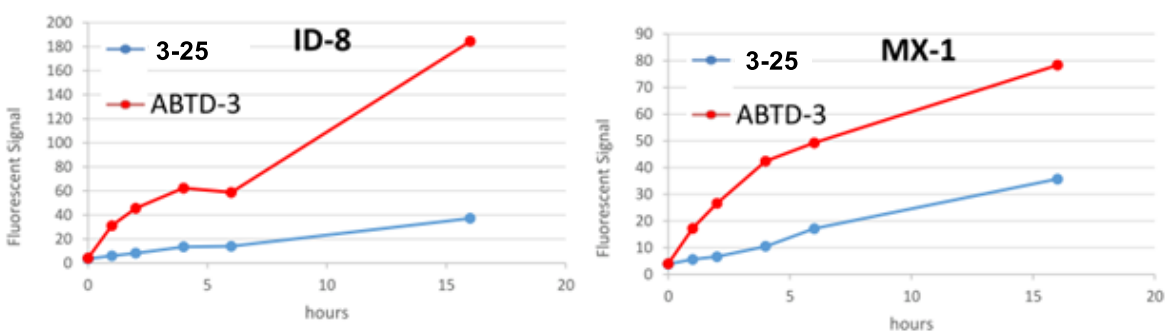


**Figure 5.33** Time dependent RME rate comparison between a small fluorescent probe Biotin-PEG-Fluorescein (**3-25**) (in red) and **ABTD-3** (in blue). Curves were drawn based on the flow cytometry results by incubation of **ABTD-3** at the concentration of 10  $\mu$ M at 37  $^{\circ}$ C for 0 h (control), 1 h, 2 h, 4 h, 6 h and 16 h, in ID-8 (left) and MX-1 (right), respectively.

**Figure 5.33** clearly showed that at 10  $\mu$ M concentration of probes, with incubation time increasing, **3-25** and **ABTD-3** both can be internalized via RME against two different cancer cell lines (ID-8 and MX-1) overexpressing biotin receptors. It also reveals that at the initial stage the RME rate of ABTD is higher than **3-25**, which indicates the multiple TTM can increase the targeting ability and affinity to the cancer cells. In addition, for each time point, considering the different number of inherited fluorescein of **ABTD-3** and **3-25**, the fluorescein signal intensity of **ABTD-3** is still more than 4 times of **3-25** against ID-8 cell line, suggesting that the multiple TTM can enhance the cell uptake of the whole conjugate via RME, resulting in more probes internalized at the end.

### §5.3.8 Cytotoxicity Measurements

Cytotoxicity assays of ABTD conjugates using MTT method against ID-8, MX-1, and WI-38 cell lines were performed. For comparison purpose, paclitaxel and free taxoid SB-T-1214 (**1-10**) with its fluorescein probe (**2-8**) and BLT-S (**3-23**) were assayed as well. Results are summarized in **Table 5.1**.

**Table 5.1** Cytotoxicity (IC<sub>50</sub>, nM) of paclitaxel, SB-T-1214, SB-T-1214-fluorescein, BLT-S and ABTD conjugates

	ID-8	MX-1	WI-38
Paclitaxel	21.2 $\pm$ 4.30	3.83 $\pm$ 0.59	175 $\pm$ 51.6
SB-T-1214 ( <b>1-10</b> )	1.89 $\pm$ 0.30	2.90 $\pm$ 0.47	4.14 $\pm$ 0.82
SB-T-1214-fluorescein ( <b>2-8</b> )	846 $\pm$ 112	N.D.	519 $\pm$ 156



BLT-S (3-23)	7.84 ± 1.85	26.7 ± 3.44	519 ± 90.3
BLT-S (3-23) + GSH-OEt*	5.91 ± 0.32	1.52 ± 0.34	N.D.
ABTD-1	0.66 ± 0.03	2.05 ± 0.91	582 ± 48.8
ABTD-1 + GSH-OEt*	0.62 ± 0.07	0.12 ± 0.05	N.D.
ABTD-2	> 5000	3630 ± 1300	N.D.
ABTD-2 + GSH-OEt*	651 ± 169	411 ± 80.9	N.D.
ABTD-3	> 5000	> 5000	N.D.

The concentration of cytotoxic compounds that inhibit 50 % (IC<sub>50</sub>, nM) of different types of cells after 72 hours of drug exposure at 37 °C under 5 % CO<sub>2</sub> was examined.

\*24 hours of drug exposure, followed by thorough washing with DPBS, and 48 hours incubation with 6 equivalents of glutathione-OEt at 37 °C under 5 % CO<sub>2</sub>.

N.D. = not determined

As **Table 5.1** shows, the IC<sub>50</sub> values of SB-T-1214 against ID-8, MX-1 and WI-38 are 1.89 nM, 2.90 nM and 4.14 nM, respectively, which is 1 to 2 order of magnitude more potent than paclitaxel (IC<sub>50</sub> 21.2 nM, 3.83 nM and 175 nM, respectively). SB-T-1214 exhibited very similar IC<sub>50</sub> values against these three cell lines. Paclitaxel showed small differences in their IC<sub>50</sub> values against the three cell lines. Thus, we can conclude that paclitaxel has appreciable selectivity difference between cancer cells and normal cells, but SB-T-1214 does not distinguish targeted cancer cells from normal cells, as anticipated. **Table 5.1** also shows that SB-T-1214-fluorescein (**2-8**) with modification at the C7 position exhibits 2 to 3 order of magnitude less potency than SB-T-1214. Similar results were also observed from the comparison between ABTD-1 and ABTD-2 against ID-8 (IC<sub>50</sub> 0.66 nM, > 5,000 nM, respectively) and MX-1 (IC<sub>50</sub> 2.05 nM, 3,630 nM, respectively).

**ABTD-1** exhibits extraordinary potency (IC<sub>50</sub> 0.66 nM), three times more potent compared to SB-T-1214 (IC<sub>50</sub> 1.89 nM) against ID-8, overexpressing biotin receptors, indicating the high efficiency of this ABTD platform to deliver cytotoxic agent, which is in consistent with the CFM and flow cytometry results (Figures 4 and 5). With addition of 6 equivalents of glutathione-ethyl ester to fully cleave the linker and release all the warhead, the IC<sub>50</sub> did not change too much (IC<sub>50</sub> 0.62 nM), indicating endogenous glutathione level (and possibly some other thiols) was sufficient to cleave all the internalized ABTD conjugate in 72 hours incubation. **ABTD-1** shows similar potency as SB-T-1214 against MX-1 (IC<sub>50</sub> 2.05 nM, 2.90 nM, respectively) without addition of glutathione-ethyl ester. However, as anticipated, **ABTD-1** exhibited 1 order of magnitude higher potency (IC<sub>50</sub> 0.12 nM) once 6 equivalents of glutathione-ethyl ester were added after 24 hours and incubated for another 48 hours, indicating the insufficient endogenous glutathione level in MX-1 cells. **ABTD-1** and BLT-S exhibit a similar weak potency against WI-38 cell line (biotin receptor is not overexpressed), which indicates that excellent tumor-targeting efficiency using biotin receptor a tumor-specific target via RME was clearly achieved by these conjugates. However, **ABTD-1** exhibited more than two orders of magnitude weaker cytotoxicity against WI-38 (IC<sub>50</sub> 582 nM), which demonstrates that **ABTD-1** has even higher (more than 10 times) cancer cell selectivity than that of BLT-S. Moreover, **ABTD-1** exhibits ca. 10 times higher potency than BLT-S (single TTM with single warhead conjugate) against ID-8 cell line (IC<sub>50</sub> 0.66 nM, 2.05 nM, respectively), and MX-1 cell line (IC<sub>50</sub> 7.84 nM, 26.7 nM, respectively). Same trend was also observed with addition of 6 equivalents of glutathione-ethyl ester. Therefore, we can conclude that

higher intracellular concentration of warhead was achieved by utilizing the ABTD platform with multiple warhead moieties, resulting in the higher potency of drug conjugate with lower dosage. To assess a possible cytotoxicity of dendrimer itself as macromolecular vehicle, cytotoxicity assay, using **ABTD-3** which only has TTM and fluorescein moiety without warhead, was performed. As **Table 5.1** clearly shows, the  $IC_{50}$  values of **ABTD-3** against ID-8 and MX-1 are both over 5,000 nM, indicating the cytotoxicity of dendrimer platform is non-toxic and biocompatible.

#### §5.4 Tribranched Dendrimer Incorporating Imaging Agents

From Table 1, it clearly showed that with modification on C7 of taxoid, the potency was significantly decreased, which was consistent to previous result.<sup>36</sup> Therefore, a modified maleimido linker was designed. Instead of two maleimido groups for coupling with two half Dendron with -SH group, an additional arm was used to incorporate an imaging group (e.g. fluorescent probe, PET/SPECT tracer, or MRI contrast agent without interfering the potency by chemically modified the taxoid structure. Two model structures were proposed in 2011 (**Figure 5.34**) for construct tribranched dendrimer-based theranostic conjugates bearing a fluorescent probe or MRI contrast agent (Gd-DOTA).

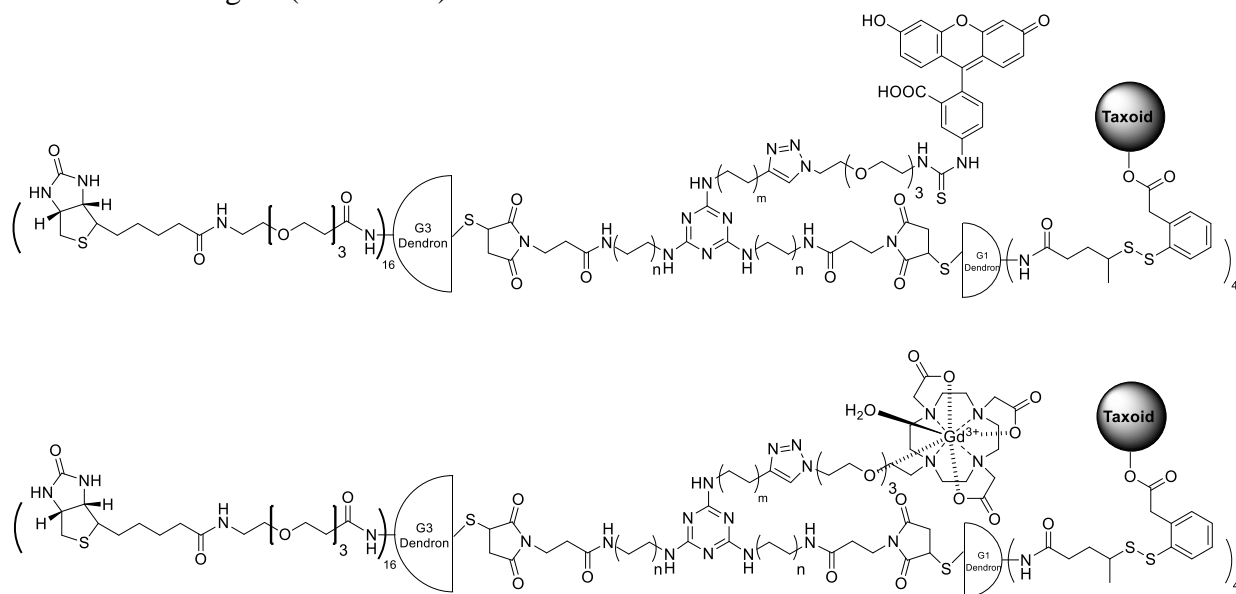


**Figure 5.34** Design of dendrimer-based theranostic tribranched conjugates

##### §5.4.1 Design and Synthesis Fluorescent Tribranched Linker

On the basis of the previously designed tri-branched triazine core, the original tribranched dendrimer-based theranostic conjugates bearing a fluorescent probe was modified and finalized as shown in **Figure 5.35**.

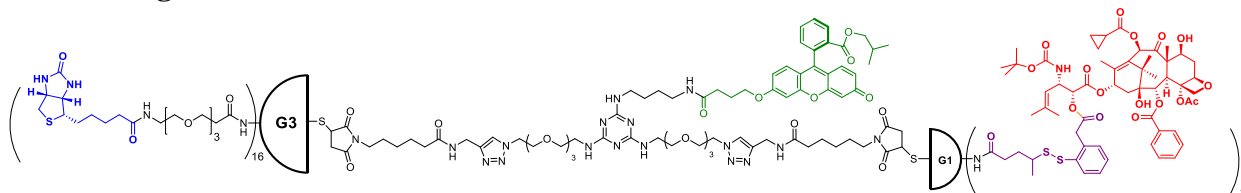


**Figure 5.35** Tribranched dendrimer-based theranostic conjugates bearing a fluorescent probe

To synthesize the tribranched linker, a PEGylated tribranched triazine core with fluorescent probe will be first formed which also has two orthogonal functional azido groups. (**Figure 5.36**) Then a double-click reaction was applied in the presence of copper catalyst to install two maleimide groups simultaneously for later use.

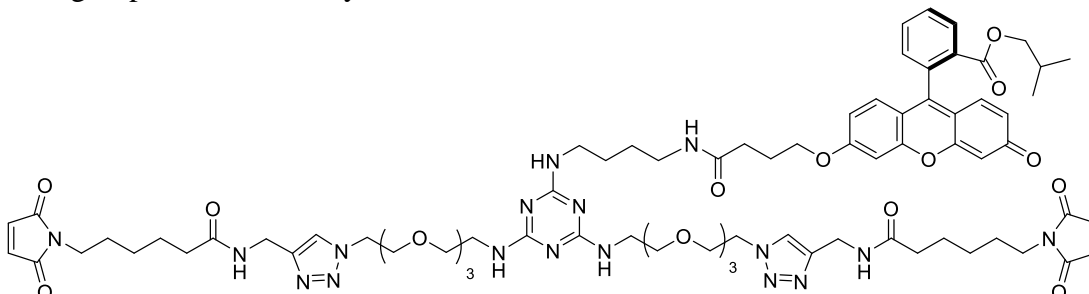
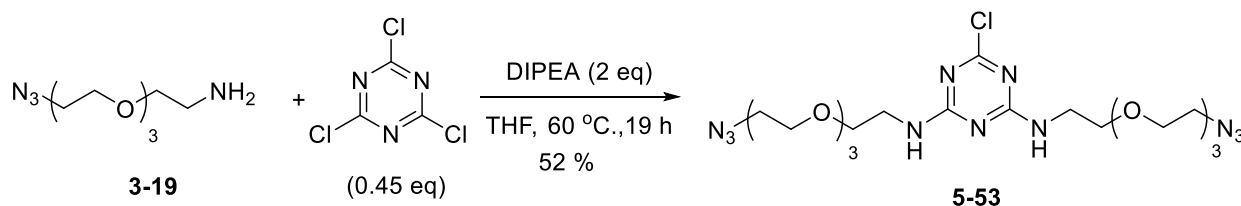


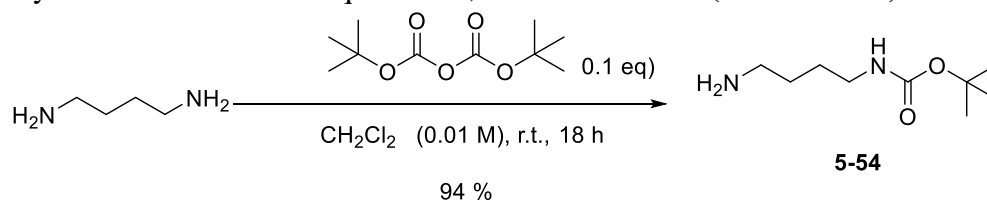
**Figure 5.36** Structure of modified PEGylated tri-branched core

Previously made 2-(2-(2-(2-azidoethoxy)ethoxy)ethoxy)ethanamine **3-19** was used as the arm in the lower moiety. In the presence of DIPEA, 2 eq of azido-PEG-amine **3-19** substitute two chloro group to form the intermediate **5-53**. (**Scheme 5.19**)

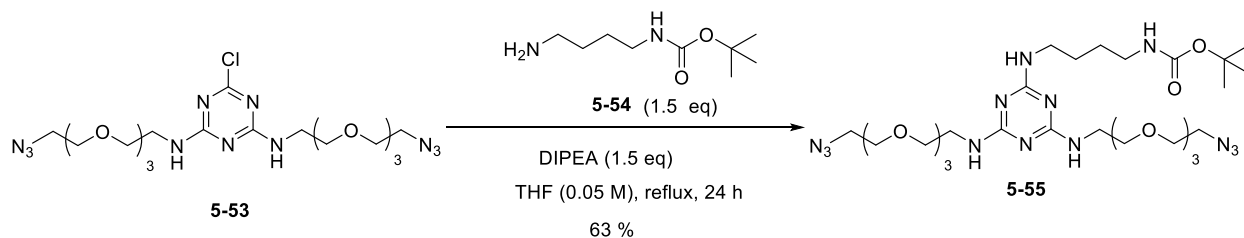


**Scheme 5.19** Synthesis of intermediate **5-53**

The top arm was a mono-Boc protected butane diamine. This arm was synthesized from the Boc anhydride treated with 10 eq excess 1,4-diaminobutane. (**Scheme 5.20**)

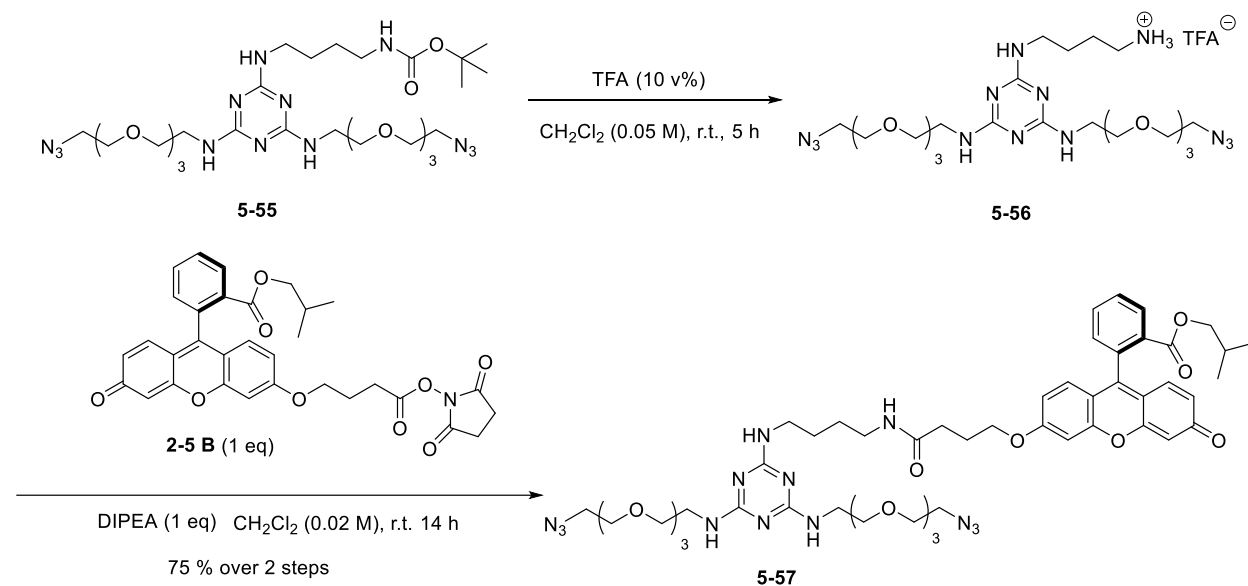


**Scheme 5.20** Synthesis of intermediate **3-53**



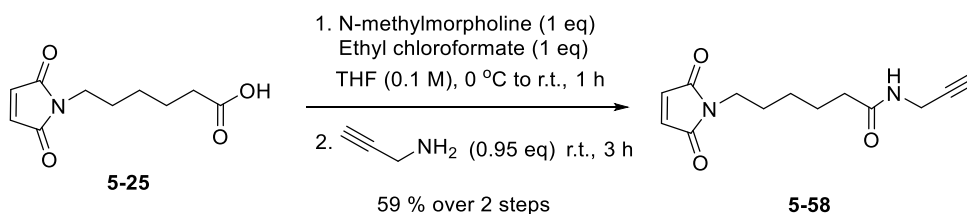
**Scheme 5.21** Third arm installation on intermediate **5-55**

Then **5-54** was used to substitute the chloro group on **5-53** to form the intermediate **5-55** (Scheme 5.21), followed by the Boc deprotection in the presence of TFA (Scheme 5.22). The crude **5-56** was taken forward to react with previously made fluorescent probe activated OSu ester in the presence of DIPEA to form the click-ready intermediate **5-57**. (Scheme 5.22)



**Scheme 5.22** Synthesis of click-ready intermediate **5-57**

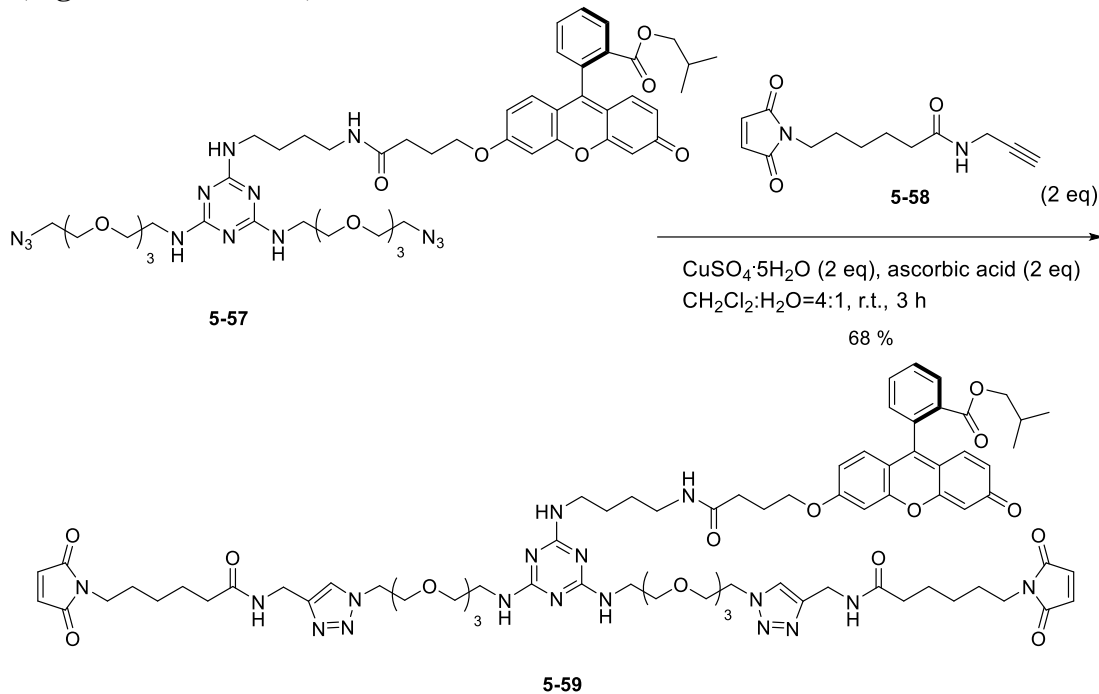
The maleimide moiety with a clickable alkyne group was synthesized from the **5-25**. Direct amidation between the acid group and propargylamine was not successful due to the by-product formation which was the Michael addition product between the maleimide group and the amino group. Activation of the carboxylic acid group was done by treating with ethyl chloroformate in the presence of base, then the crude product was taken forward for the next step which around 1 eq propargylamine was used to react with the activated intermediate to generate the product as white crystal solid. (Scheme 5.23)



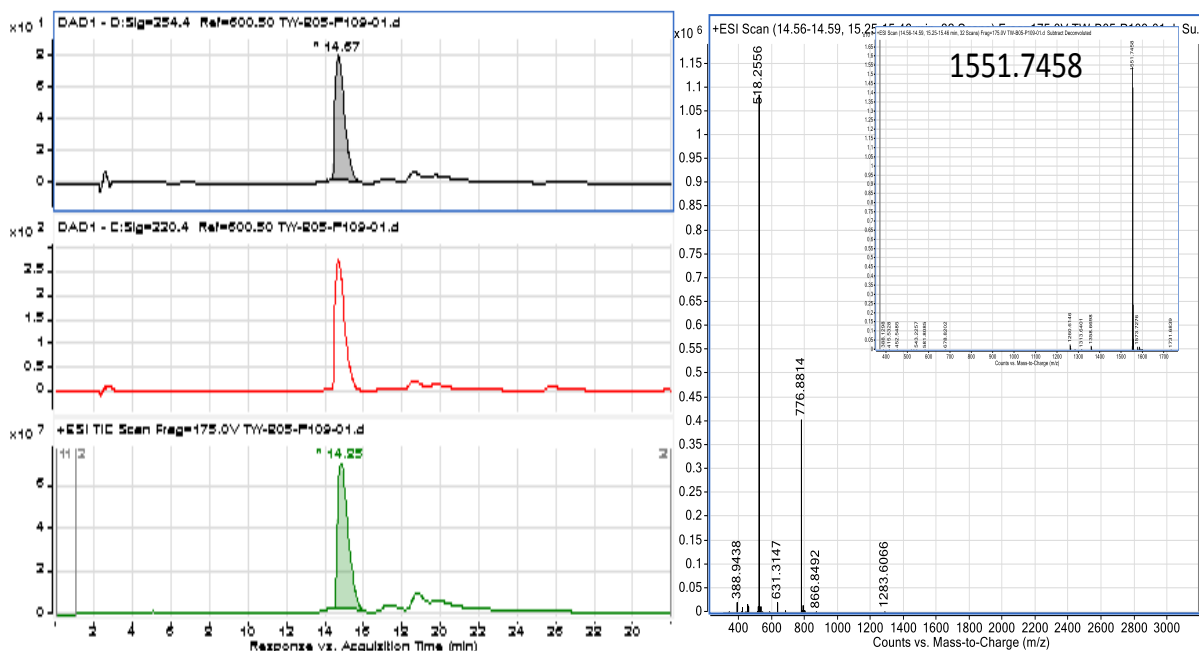
**Scheme 5.23** One pot reaction of synthesis of intermediate **5-58**

Then the copper-catalyzed double click reaction was carried out between the intermediate **5-57** and **5-58**. (Scheme 5.24) CuSO<sub>4</sub> 5H<sub>2</sub>O and ascorbic acid generated Cu<sup>+</sup> which formed the active species with acetylene then cyclize with azido group. Firstly the combination of THF and distilled water with ratio of 4 to 1 were used as solvents to dissolve each components, however, resulted in the THF adduct to the desired product observed from mass spectrum. To avoid the THF adduct, CH<sub>2</sub>Cl<sub>2</sub> and distilled water were used as the combined solvents with ratio of 4 to 1. By deconvolution, the desired was clearly formed as major product without any other by-products.

LC/UV/MS-TOF and MALDI-TOF result also confirmed that the desired product was successfully made. (Figure 5.37 and 5.38)



**Scheme 5.24** Double click reaction towards the final compound **5-59**



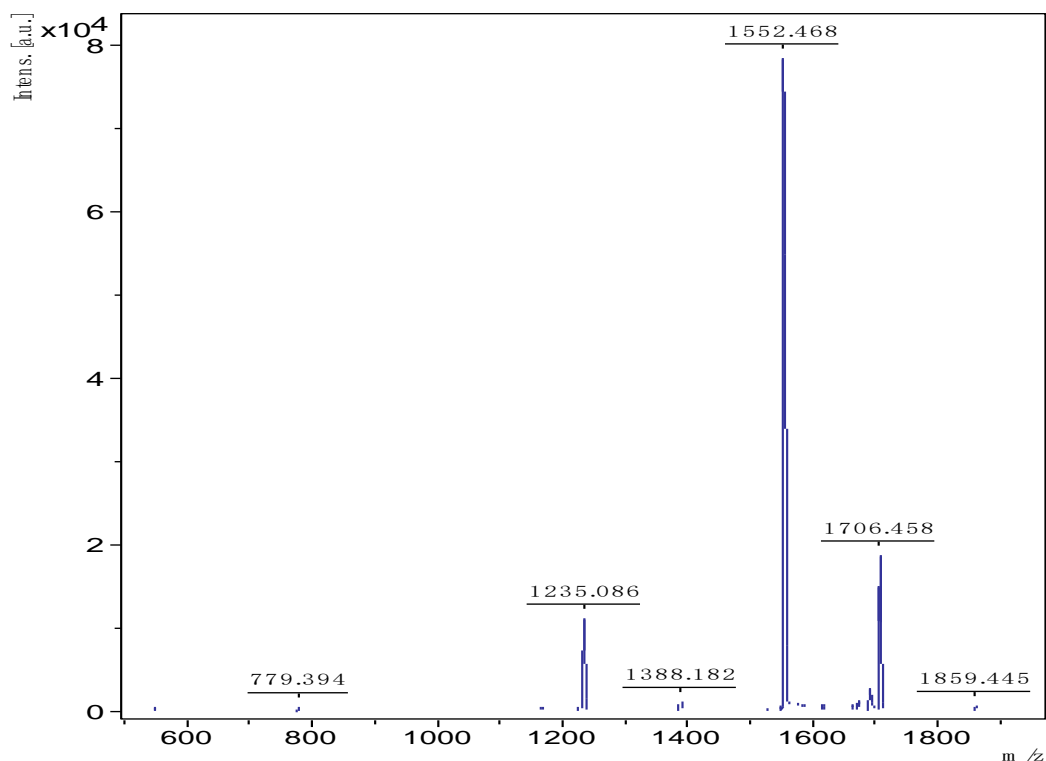


**Figure 5.38** MALDI-TOF analysis of **5-59**

### §5.5 Extended Multi-binding Effect Study

It is generally known that higher binding affinity increases targeting efficacy.<sup>29</sup> In addition to enhanced affinity, multivalent binding effects (or avidity) may also be used to improve targeting. The collective binding in a multivalent interaction is much stronger than monovalent binding. For example, dendrimer nanocarriers conjugated to 3–15 folate molecules showed a 2,500–170,000-fold enhancement in dissociation constants (KD) over free folate when attaching to folate-binding proteins immobilized on a surface.<sup>29</sup> It was attributed to the avidity of the multiple folic acid groups on the periphery of the dendrimers. In the **Figure 5.33**, the ABTD-3 also showed enhanced uptake compared to a small molecule Biotin-PEG-Fluorescein. But quantitative evidence to estimate the optimized ratio of TTM per nanocarrier has not been well studied. Thus the different generations of half dendrons fully functionalized with biotin (TTM) were designed to attach only one fluorescent probe (imaging agent) *via* click reaction to investigate the multi-binding effect of multiple targeting modules. For each fluorescent probe, numerous TTM are combined depending on the generation (*n*) of dendrimer (TTM/Fluorescein= $2^{n+1}$ :1), and a single biotin-FITC molecule is synthesized as control (TTM/Fluorescein=1:1). (**Figure 5.39**)

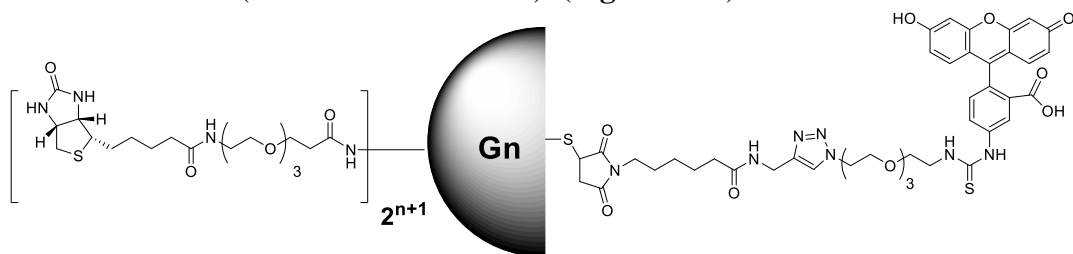
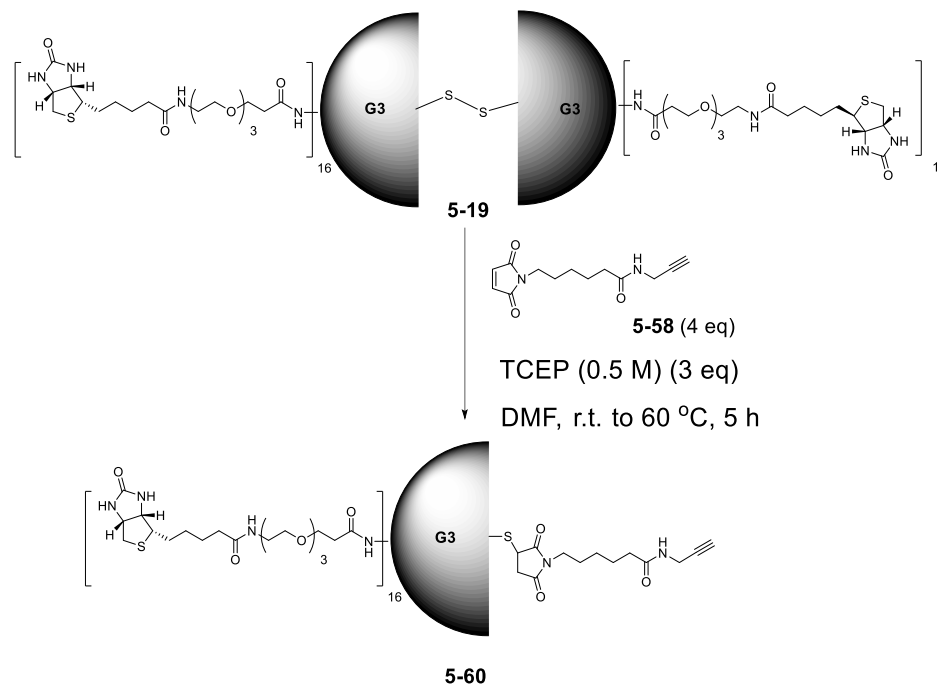


**Figure 5.39** 2<sup>nd</sup> generation di-branched dendrimer-based drug delivery system

A G3 half dendron fully functionalized with biotin moiety (16 modules) was attached to a maleimido-alkyne tether through a 1,4-Michael addition, then connected to an azido-PEGylated FITC via click reaction to afford the G3-FITC probe. The cleavage of cystamine bond of G3-PEG-biotin precursor was performed in DMF followed by 3 eq TCEP addition. (**Scheme 5.25**) MALDI analyzed result clearly showed the consumption of biotin-PEG-G3 and formation of **5-60** with sodium adduct corresponding to the detected mass 10645 ( $C_{469}H_{819}N_{111}O_{129}S_{17}$ , calc. MW 10622.3790). (**Figure 5.40**)



**Scheme 5.25** Synthesis of G3-PEG-biotin half dendron with click-ready alkyne moiety

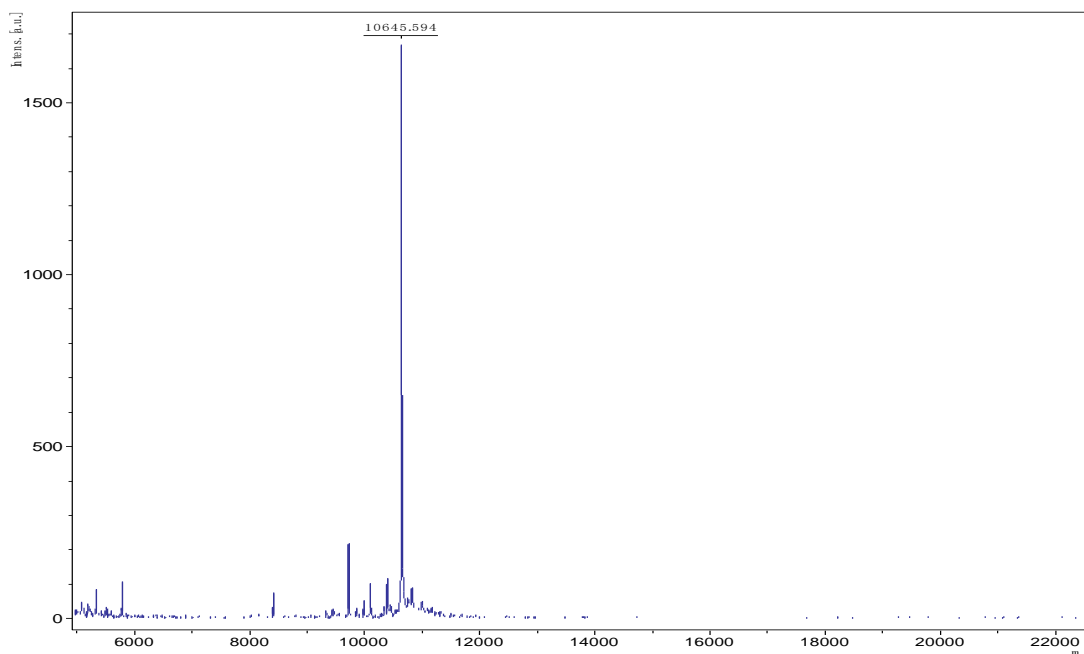


**Figure 5.40** MALDI result for G3-PEG-biotin half dendron with click-ready alkyne moiety





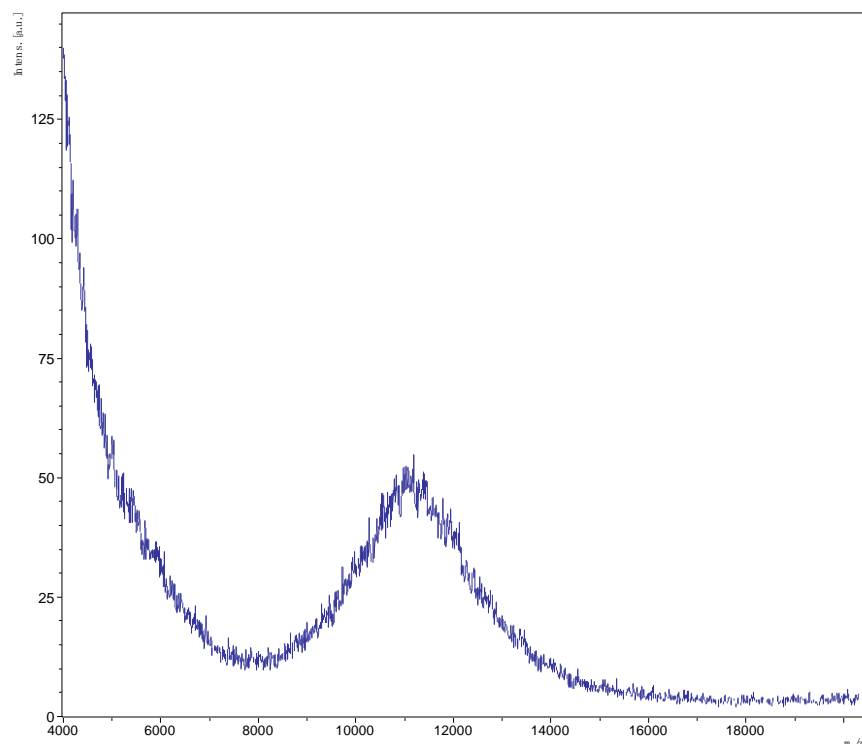


**Figure 5.41** MALDI result for 5-62

## §5.6 Second Generation Versatile ABTD Drug Delivery System Design

On the basis of previous experimental results, the first generation dendrimer-based drug delivery system was designed and applied for three ABTD conjugates. Take ABTD-2 as example, the first generation dendrimer-based drug delivery system is consist of biotin as a tumor-targeting moiety, fully functionalized generation 1 and generation 3 half dendrons connected by a PEGylated bis(maleimido) linker as versatile platform, and linker-drug/fluorescent probe as cytotoxic agent/imaging agent. Numerous PEG chains were used to increase the solubility of the final dendritic conjugate to overcome the hydrophobicity of the taxoid once it get coupled on. (**Figure 5.42**)

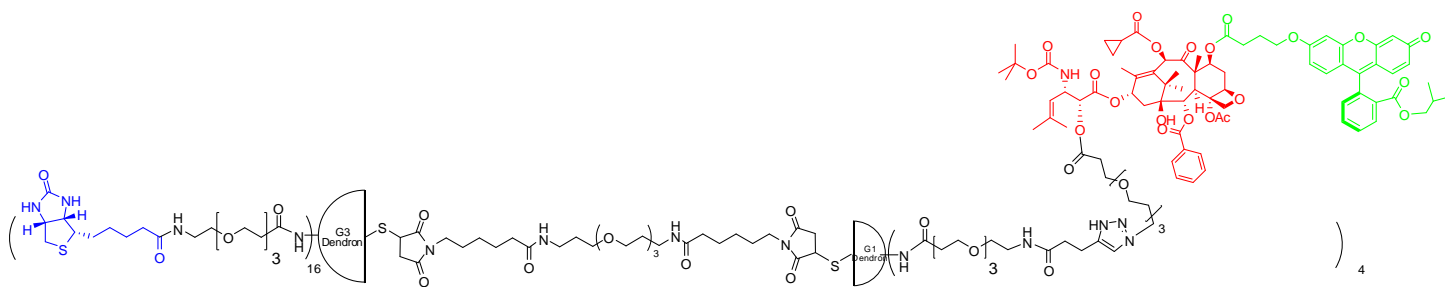


**Figure 5.42** Example of 1<sup>st</sup> generation di-branched dendrimer-based drug delivery system (ABTD-2)

Although excellent biological evaluations results have been obtained to prove the enhanced tumor cell uptake through biotin receptor-mediated endocytosis by means of CFM and FACS, as

well as extraordinary cytotoxicity measurement results showing good specificity, selectivity and efficiency, the first generation dendrimer-based drug delivery system (DDS) can be modified to extend its application and improve its drug delivery efficiency. Several aspects can be taken account on the basis of molecular design of 1<sup>st</sup> generation dendrimer-based DDS: 1. The tumor-targeting moiety (biotin) was used to functionalize the G3 dendrimer before attachment with G1 part through an amide bond. If different tumor-targeting module (TTM), such as folate, need to be investigated, it will have to be incorporated with the system in very early stage, therefore might increase the solubility issue in terms of the isolation and purification difficulties. 2. The G3-G1 combination of 1<sup>st</sup> dendrimer-based DDS will only reach 15KD to 20KD molecular size as the final drug conjugates, which is far less the 40KD criteria for EPR effect. However, the molecular weight of final drug conjugates can be easily increased by replacement of higher generation dendrimer since the number of functional arms will exponentially increase. Accordingly, the G1 part of 1<sup>st</sup> generation dendrimer-based DDS can be switched to G2 or G3, and the final conjugate derived from G3 will just reach the 40KD if taxoid-linker moiety remains. 3. The design of strategy may be improved by a G3-G3 scaffold. 1<sup>st</sup> generation dendrimer-based DDS had the “versatile dendrimer platform” design, which used a terminal alkyne moiety on the G1 part allowing different taxoid with or without imaging probes to be incorporated into the final conjugates through a CuAAC click reaction in the very last steps. A better versatile platform can be achieved by a smart design, therefore the tumor-targeting moiety and the drug-imaging moiety can be sequentially incorporated orthogonally in the last stage, and the accumulation of the versatile dendrimer-based platform will be applicable.

So the 2<sup>nd</sup> generation dendrimer-based DDS was proposed in **Figure 5.43 and 5.44**. Both half dendrons were derived from G3 dendrimer which can provide 16 arms for incorporation of functionalities. The interior linker is the bis(maleic)imido PEG linker that was used previously. On the surface of platform, besides the terminal alkyne moiety that was also from previous design, an additional cyclooctyne moiety can afford another type of conjugate method through a copper catalyst-free click reaction, which is also known as SPAAC (Strain-Promoted Alkyne-Azide Cycloaddition) click process. This platform allows a controlled catalyst-based regioselectivity when different functionalities are conjugated to it. Without addition of copper catalyst, only the G3-cyclooctyne part will react with the reactant bearing azide group. And this type of platform also allows more combinations of different TTM and drugs, thus a series of library of drug conjugates will be easily built up. In addition, a good amount of this platform should be easily prepared and accumulated in large scale.

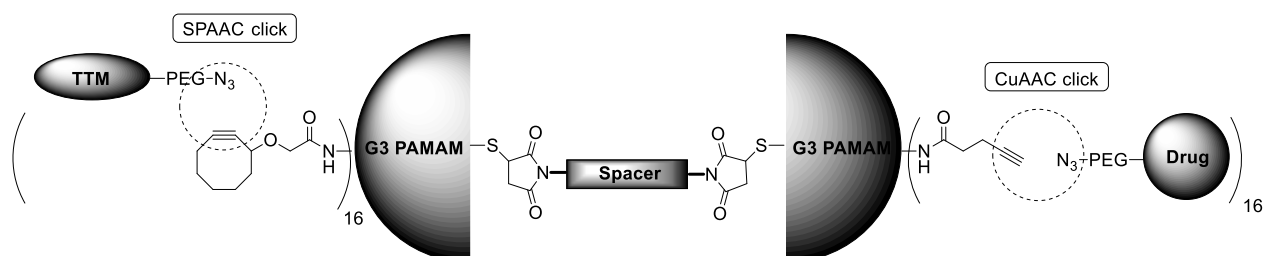


**Figure 5.43** 2<sup>nd</sup> generation di-branched dendrimer-based drug delivery system

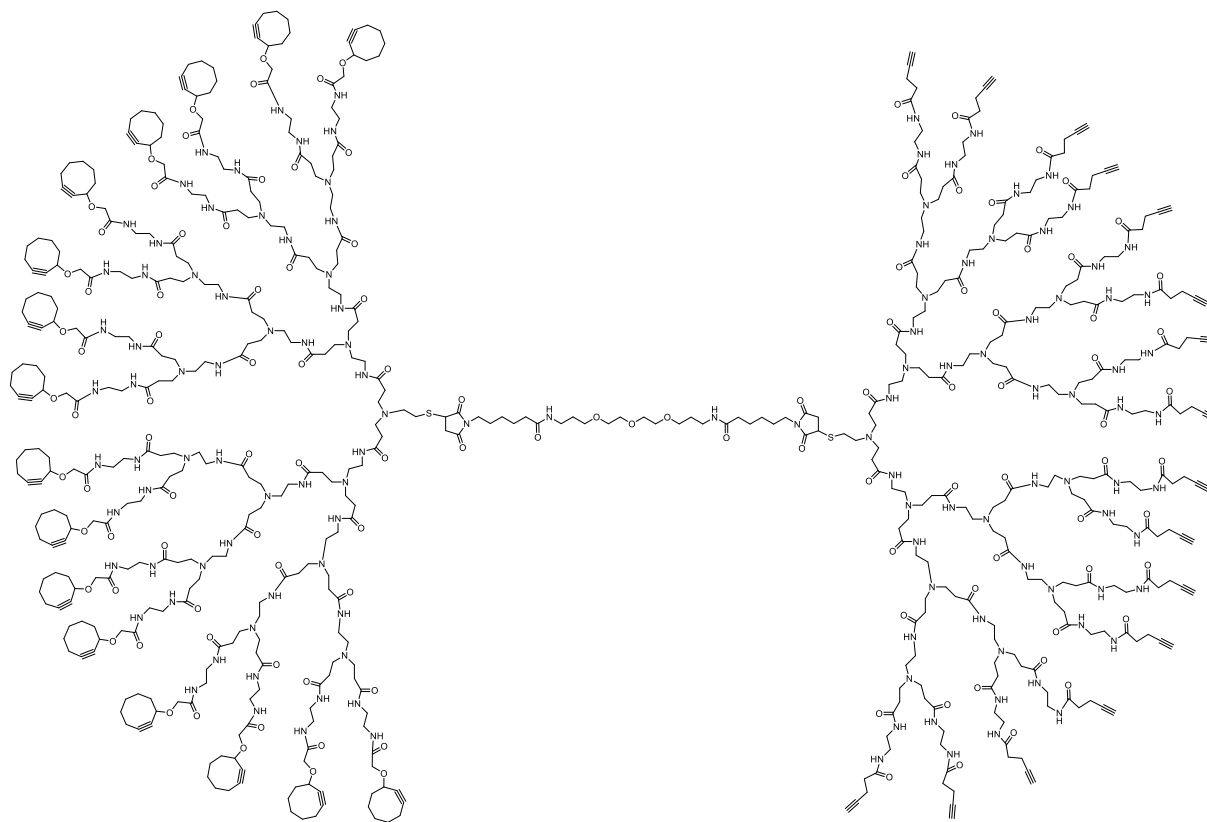
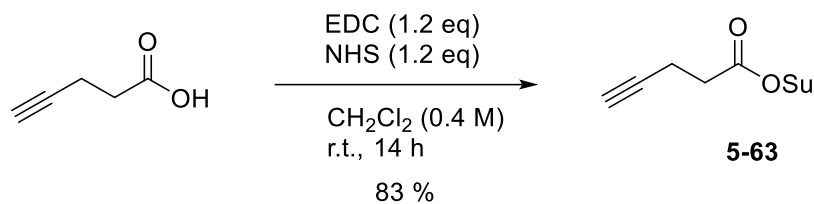
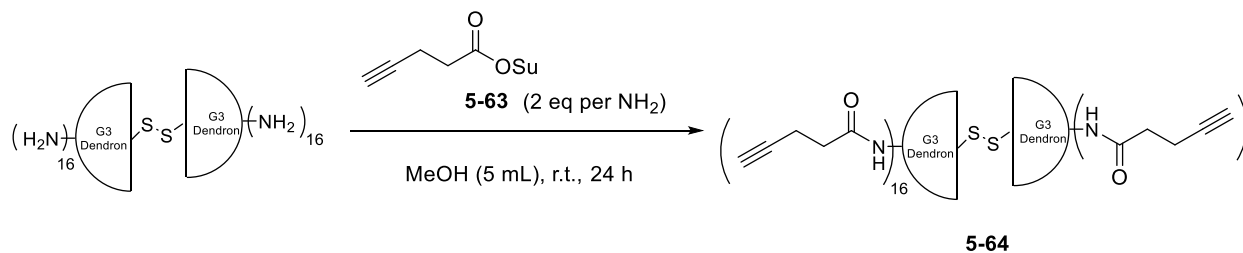


**Figure 5.44** Structure of 2<sup>nd</sup> generation dendrimer-based drug delivery system versatile platform

To fully functionalize the G3 dendrimer with alkyne moiety, the 4-pentynoic acid was firstly activated by NHS through EDC coupling condition, (**Scheme 5.28**) then directly treated with G3 dendrimer with primary amino group on surface. (**Scheme 4**)



**Scheme 5.28** NHS activation of 4-pentynoic acid



**Scheme 5.29** Fully functionalization on G3 dendrimer

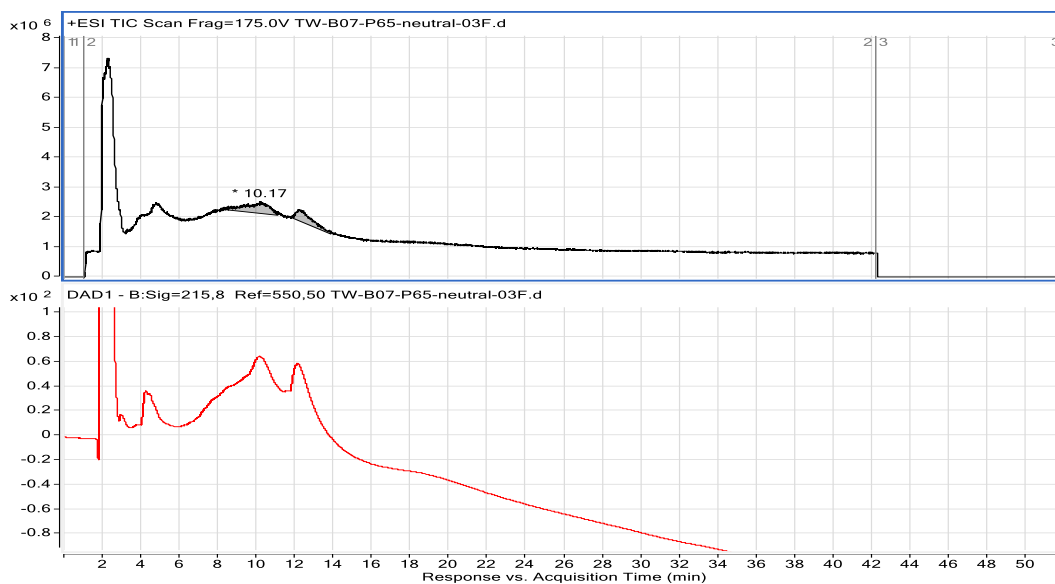


**Figure 5.45** LC-MS-TOF trace of crude **5-64** under neutral condition

Due to the defect structures existing in the dendrimer starting material, the crude **5-64** was firstly analyzed by LC-MS-TOF to identify the purity, and establish the isolation method. Neutral and acidic conditions were measured to eluent the crude product. Poor separation was observed under neutral condition, mainly due to the relatively high ratio of defect structure in G3 starting material, resulting in the inseparable fractions with the desired product. (**Figure 5.45**) The desired product **5-64** and major defect impurity were identified by mass analysis as peaks with retention times of 12 min, and 10 min, respectively. (**Figure 5.46 and 5.47**) Deconvolution results clearly showed the presence of defect structure derived from the impure starting material. (**Figure 5.48**) Then acidic condition was also tried to improve the separation of the desired and defect structures. (**Figure 5.49**)

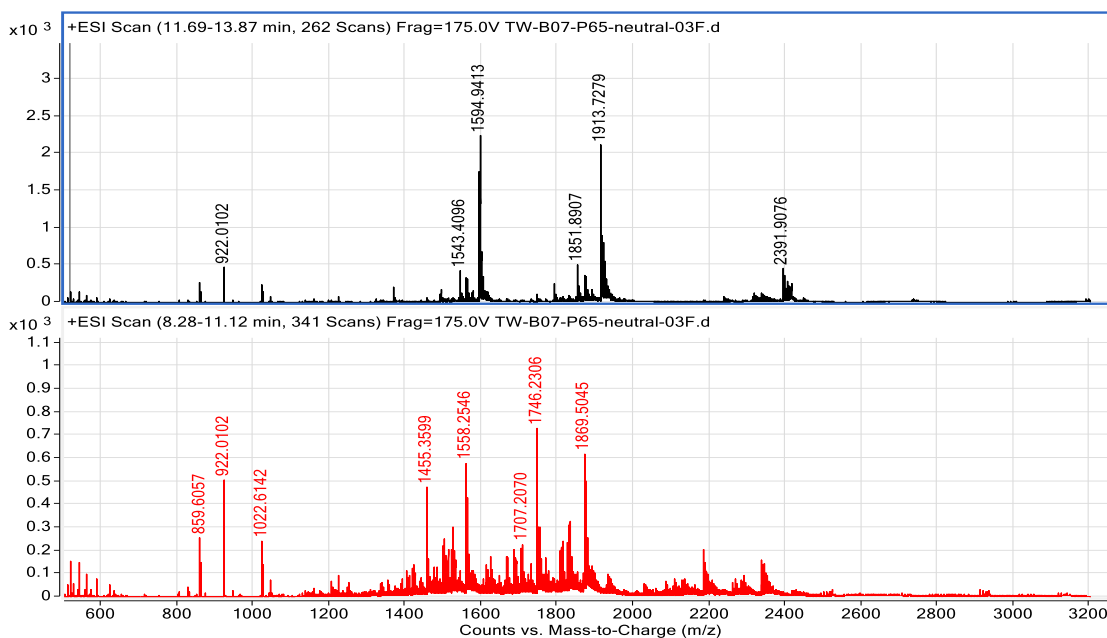


**Figure 5.46** Mass analysis result of LC-MS-TOF trace

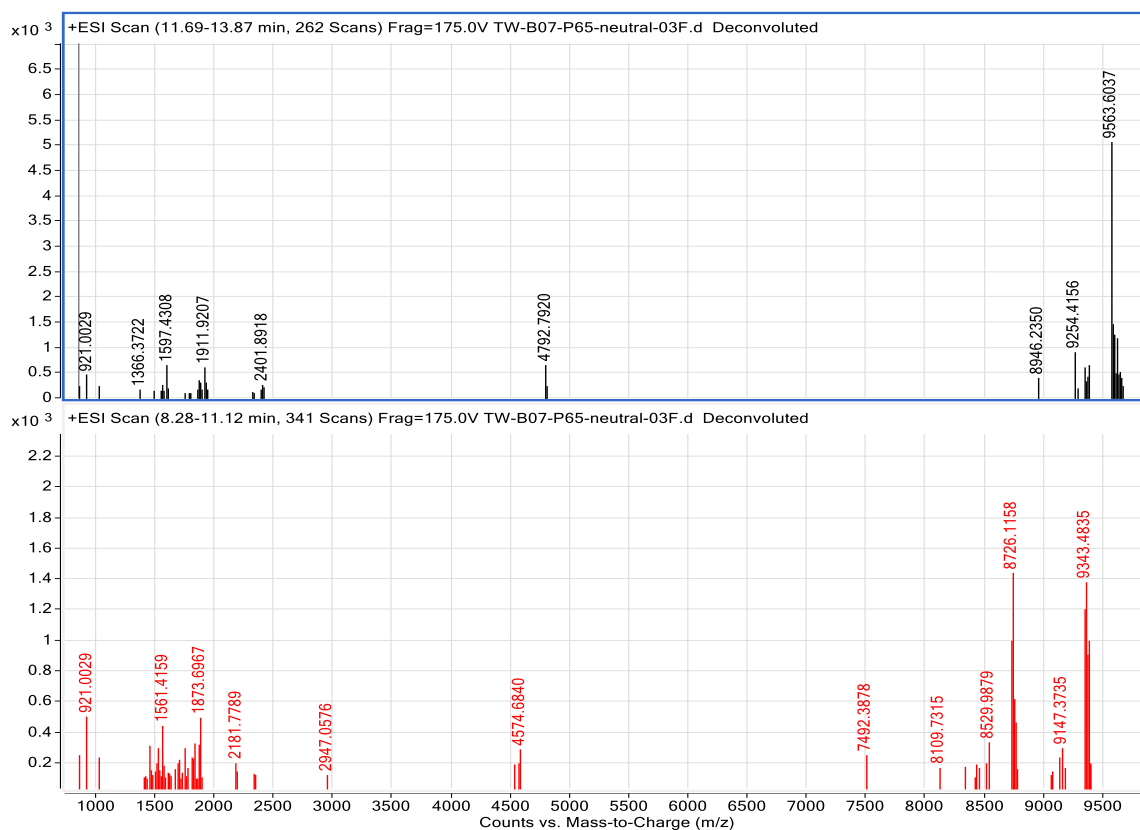


**Figure 5.47** Deconvolution mass analysis result of LC-MS-TOF trace

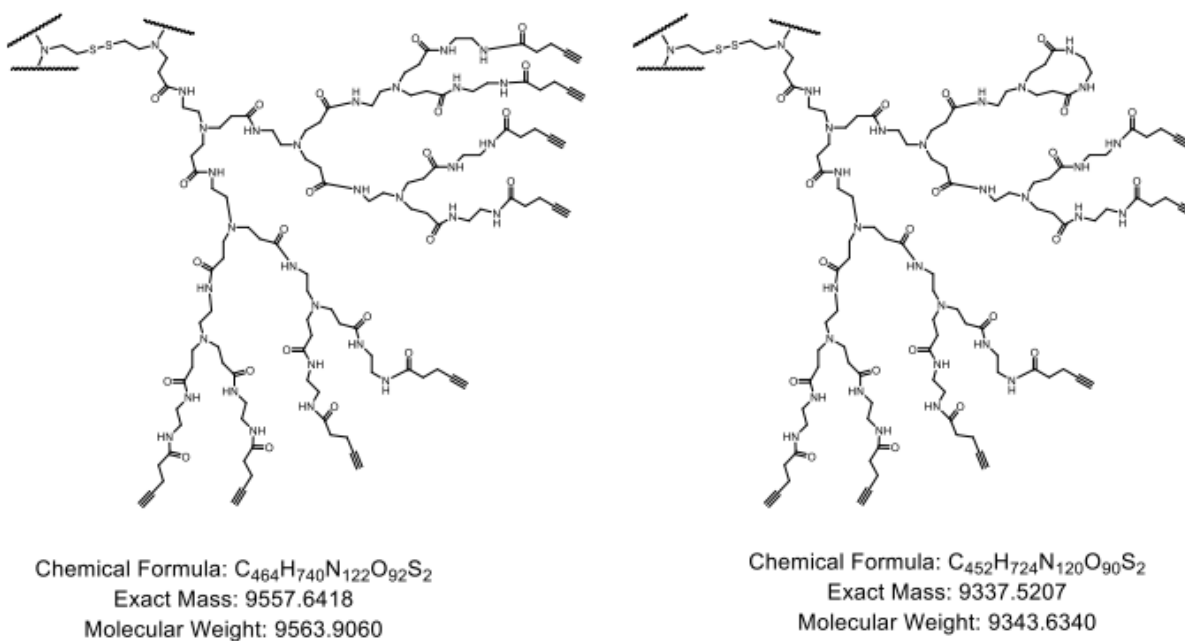


**Figure 5.48** Structures and molecular weights of desired product and defect impurity

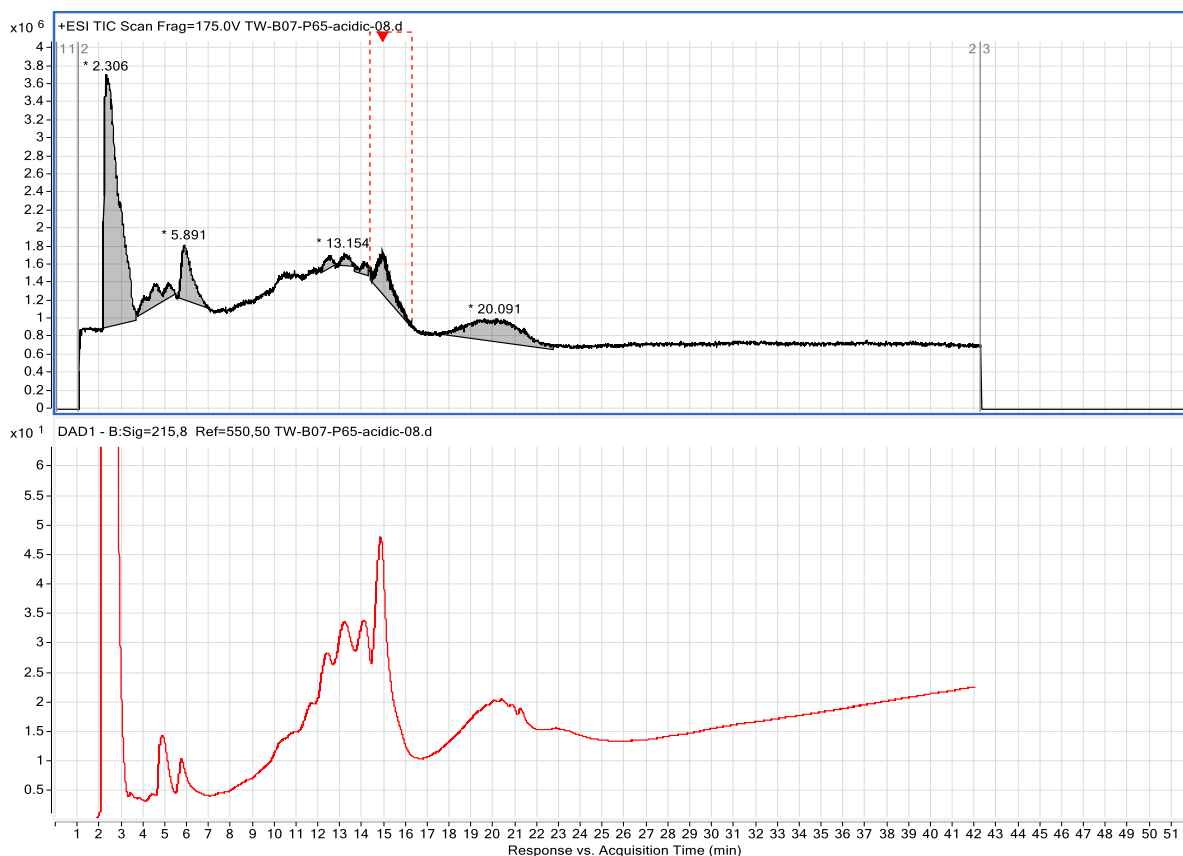


**Figure 5.49** LC-MS-TOF trace of crude **5-64** under acidic condition

## §5.7 Summary

Asymmetric Bow-Tie PAMAM Dendrimer-based (ABTD) platform as a novel tumor-targeting drug delivery system have been designed and three ABTD conjugates have been successfully synthesized. Purification and characterization methods have been developed and successfully established. The ABTD conjugates can be obtained in good purity and reproduced with consistent biological evaluation results. By means of flow cytometry and confocal fluorescence microscopy, we confirmed that this macromolecular drug delivery system could be internalized into cancer cells through RME. We also disclosed the multi-binding effect of this platform by the comparison of RME internalization rate and the fluorescein signal intensity between **ABTD-3** and a small fluorescent probe (**3-25**). The  $IC_{50}$  values observed for **ABTD-1** clearly showed the high efficiency of this dendrimer-based drug delivery system compared to paclitaxel or SB-T-1214 and a small drug conjugate (BLT-S). And the  $IC_{50}$  values observed for **ABTD-3** indicated the non-toxicity and biocompatibility of this platform. Further studies will include changing different tumor-targeting molecules as well as newer generation toxoids with higher potency.

## §5.8 Experimental Sections

### §5.8.1 Caution

Taxoids have been classified as potent cytotoxic agents. Thus, all drugs and structurally related compounds and derivatives must be considered as mutagens and potential reproductive hazards for both males and females. Silver perchlorate should be stored away from heat and direct sunlight. Appropriate precautions (i.e. use of gloves, goggles, lab coat and fume hood) must be taken while handling these compounds.

### §5.8.2 General Methods

$^1\text{H}$  NMR and  $^{13}\text{C}$  NMR spectra were measured on a Varian 300 or 500 MHz spectrometer or a Bruker 400 MHz, 500 MHz, or 700 MHz NMR spectrometer. Melting points were measured on a Thomas–Hoover capillary melting point apparatus and are uncorrected. TLC analyses were performed on Sorbent Technologies aluminum-backed Silica G TLC plates (Sorbent Technologies, 200  $\mu\text{m}$ , 20 cm  $\times$  20 cm) and were visualized with UV light and stained with sulfuric acid-EtOH, 10 % PMA-EtOH, 10 % Vanillin-EtOH with 1% sulfuric acid or Ninhydrin-butanol with 10 % AcOH. Column chromatography was carried out on silica gel 60 (Merck; 230-400 mesh ASTM). Chemical purity was determined with a Shimadzu L-2010A HPLC HT series HPLC assembly, using a Kinetex PFP column (4.6 mm  $\times$  100 mm, 2.6  $\mu\text{m}$ ), employing  $\text{CH}_3\text{CN}$ /water as the solvent system with a flow rate of 1 mL/min. High resolution mass spectrometry analysis was carried out on an Agilent LC-UV-TOF mass spectrometer using Jupiter C18 analytical column with 2.6  $\mu\text{m}$ , 100 A, 2.1  $\times$  100 mm, with 0.1% TFA in water (optima grade) as solvent A and 0.1% TFA in  $\text{CH}_3\text{CN}$  (optima grade) as solvent B, running temperature 25  $^\circ\text{C}$  and flow rate 0.5 mL/min, at the Institute of Chemical Biology and Drug Discovery (ICB&DD), Stony Brook, NY or at the Mass Spectrometry Laboratory, University of Illinois at Urbana–Champaign, Urbana, IL. Purification were also performed using Jupiter C18 semi-preparative HPLC column (5  $\mu\text{m}$ , 300 A, 250  $\times$  10 mm) or Jupiter C18 preparative HPLC column (5  $\mu\text{m}$ , 300 A, 250  $\times$  21.2 mm) on a Shimadzu CBM-10AW VP communications bus module, Shimadzu SPD-10A VP UV-Vis detector, and Shimadzu LC-6AD liquid chromatography assembly. Matrix-assisted laser desorption/ionization (MALDI)-TOF analysis for determination of molecular weight was facilitated by ICB&DD using DHB (2, 5-dihydroxybenzoic acid) as matrix.

**Cell Culture.** ID-8 (ovary), MX-1 (breast) and WI-38 (human lung fibroblast) cell lines were cultured as monolayers on 100 mm tissue culture dishes in the RPMI-1640 cell culture medium (Gibco) supplemented with 10% (v/v) heat-inactivated fetal bovine serum (FBS) as well as 1% (v/v) penicillin and streptomycin (P/S) at 37  $^\circ\text{C}$  in a humidified atmosphere with 5%  $\text{CO}_2$ . The cells were harvested and collected by centrifugation at 950 rpm for 5 min, and finally suspended in fresh cell culture medium containing different cell densities for subsequent biological experiments and analysis.

**Incubation of Cells with the Biotin-PEG-Fluorescein (3-25) and ABTD-3.** The cell suspension at  $5 \times 10^5$  cells/well was split into each well of a 6-well plate with 3 mL RPMI-1640 cell culture medium and allowed to grow for 24 hours. The fluorescent probe in DMSO was diluted in RPMI-1640 cell culture medium (3 mL) at final concentration of 10  $\mu\text{M}$  or 20  $\mu\text{M}$  for multi-binding effect study and internalization through RME study, respectively, and was used to replace the medium in each well followed by incubated at 37  $^\circ\text{C}$  for different periods (16 h, 6 h, 4 h, 2 h, 1 h for multi-binding effect study, and 3 h, 1h for internalization through RME study, respectively). One well with cells was incubated without any fluorescent probes as control for different periods

(16 h for multi-binding effect study, and 3 h for internalization through RME study). After incubation, the medium was aspirated and the cells were washed twice with DPBS buffer, collected by centrifugation, and resuspended in 300  $\mu$ L PBS for flow cytometry fluorescein measurement and confocal microscopy imaging.

**Flow Cytometry Fluorescent Measurements of the Cells.** Flow cytometry analysis of the treated cells was performed with a flow cytometer, FACSCalibur, operating at a 488 nm excitation wavelength and detecting emission wavelengths with a 530/30 nm bandpass filter. At least 10,000 cells were counted for each experiment using CellQuest 3.3 software (Becton Dickinson) and the distribution of FITC fluorescence was analyzed using WinMDI 2.8 freeware (Joseph Trotter, Scripps Research Institute). Propidium iodide staining was used in all experiments to rule out dead cell count in the analysis.

**Confocal Microscopy Imaging of the Treated Cells.** Cells treated as described above were dropped onto an uncoated glass dish (MatTek Corp.). Confocal fluorescence microscopy (CFM) experiments were performed using a Zeiss LSM 510 META NLO two-photon laser scanning confocal microscope system, operating at a 488 nm excitation wavelength and at 527 (23 nm detecting emission wavelength using a 505-550 nm bandpass filter. Images were captured using a C-Apochromat 63  $\times$  /1.2 water (corr.) objective or a Plan-Apochromat 100  $\times$  /1.45 oil objective. Acquired data were analyzed using LSM 510 META software.

***In Vitro* Cytotoxicity Assay.** The cytotoxicity of paclitaxel, SB-T-1214 (**1-10**), SB-T-1214-fluorescein (**2-8**), biotin-PEG<sub>3</sub>-linker-SB-T-1214 (**3-23**), **ABTD-1**, **ABTD-2** and **ABTD-3** were evaluated in vitro against ID-8 (ovary) and MX-1 (breast) cancer cell lines with biotin receptor overexpression (BR+), as well as WI-38 (human lung fibroblast cell line, normal), by means of a quantitative colorimetric assay using a tetrazolium salt-based analysis (“MTT assay”; MTT = 3-(4,5-dimethylthiazol-2-yl)-2,5-diphenyltetrazolium bromide; Sigma Chemical Co.). The inhibitory activity of each compound is represented by the IC<sub>50</sub> value, which is defined as the concentration required for inhibiting 50% of the cell growth. Cells were harvested, collected, and resuspended in 200  $\mu$ L medium at a concentration of  $\sim 0.5 \times 10^6$  cells (ID-8) or  $\sim 1.5 \times 10^6$  (MX-1 and WI-38) per well over a 96-well plate. Cells were allowed to descend to the bottom of the plates overnight and fresh medium was added to each well upon removal of the old medium. A drug or drug conjugate in DMSO stock solution listed above was diluted to a series of concentrations in the cell culture medium to prepare test solutions. These test solutions at different concentrations ranging from 500 pM to 5  $\mu$ M (100  $\mu$ L each) were added to the wells in the 96-well plate and cells were subsequently cultured for 72 h. After removing the old medium by aspiration, 50  $\mu$ L DPBS buffer containing MTT (0.5 mg/mL) was added to each well and incubated at 37  $^{\circ}$ C for 3 h. The resulting DPBS buffer was then removed and as-produced insoluble violet formazan crystals were dissolved into 50  $\mu$ L 0.1 N HCl in isopropanol to give a violet solution. The plate was allowed to shake for 8 minutes to fully dissolve the violet formazan crystal, then the spectrophotometric absorbance measurement of each well in the 96-well plate was run at 568 nm. The IC<sub>50</sub> values and their standard errors were calculated from the viability-concentration curve using the Four Parameter Logistic Model of Sigmaplot. The concentration of DMSO per well was  $\leq 1\%$  in all cases.

### §5.8.3 Materials



The chemicals were purchased from Sigma Aldrich, Fisher Scientific or VWR International and used as received or purified before use by standard methods. Dichloromethane and methanol were dried before use by distillation over calcium hydride under nitrogen. Ether and THF were dried before use by distillation over sodium-benzophenone kept under nitrogen. 10-Deacetylbaccatin III was obtained from Indena, SpA, Italy. Reaction flasks were dried in a 100 °C oven and allowed to cool to room temperature in a desiccator over “Drierite” (calcium sulfate) and assembled under an inert nitrogen gas atmosphere. The generation 1 and generation 3 dendrimers stored in MeOH were purchased from Dendritic Nanotechnologies, Inc<sup>®</sup> (DNT). Biological materials including RPMI-1640 cell culture media, DPBS buffer, fetal bovine serum, PenStrep, and TrypLE were obtained from Gibco and VWR International, and used as received for cell-based assays.

#### §5.8.4 Experimental Procedure

##### 1,4-Bis (maleimido) butane (5-1)<sup>37</sup>

To a 100 mL round bottomed flask were added 1,4-diaminobutane (600 mg, 6.8 mmol) and glacial acetic acid (3 mL) as solvent. A white solid precipitate formed upon addition of glacial acetic acid. Then solution was heated to 80 °C to dissolve the solid while stirring. The resulting solution was then allowed to cool to room temperature and suspension started to show up. To a separate round bottom flask was added maleic acid anhydride (1.3 g, 13.6 mmol) followed by 8 mL glacial acetic acid. Then it was slowly added to the first round bottom flask and the resulting solution turned to yellow and clear. The resulting solution was stirred for 24 hours which formed a white cloudy solution. To the cloudy solution, 6 mL glacial acetic acid was added and then refluxed at 150 °C for 24 hours. The reaction was monitored by TLC. After completion, the resulting solution was concentrated *in vacuo*. Then crude product **5-1** was done by chromatography with sample dry loading method on silica gel with increasing methanol in dichloromethane to afford a white solid **5-1** (612 mg, 2.5 mmol) in 36 % yield for 2 steps. <sup>1</sup>H NMR (300 MHz, CDCl<sub>3</sub>) δ 1.57 (t, 4 H), 3.53 (t, 4 H), 6.68 (s, 4 H). All data are in agreement with literature values.<sup>37</sup>

##### 1,8-Bis (maleimido) octane (5-2)<sup>37</sup>

To a 100 mL round bottom flask were added 1,8-diaminobutane (800 mg, 5.6 mmol) and glacial acetic acid (3 mL) as solvent. Then solution was heated to 80 °C to dissolve the solid while stirring. The resulting solution was then allowed to cool to room temperature and suspension started to show up. To a separate round bottom flask was added maleic acid anhydride (1.1 g, 11.1 mmol) followed by 8 mL glacial acetic acid. Then it was slowly added to the first flask. The resulting solution was stirred for 24 hours. To the resulting solution, 5 mL glacial acetic acid was added and then refluxed at 150 °C for 24 hours. The reaction was monitored by TLC. After completion, the resulting solution was concentrated *in vacuo* to yield light yellow sticky liquid. Then crude product **5-2** was done by chromatography loaded as a dry powder on silica gel with increasing methanol in dichloromethane to afford a white solid **5-2** (228 mg, 0.75 mmol) in 14 % yield for 2 steps. Melting point: 119-120 °C. <sup>1</sup>H NMR (300 MHz, CDCl<sub>3</sub>) δ 1.27 (m, 8 H), 1.55 (m, 4 H), 3.49 (t, *J* = 7.5 Hz, 4 H), 6.67 (s, 4 H). All data are in agreement with literature values.<sup>37</sup>

##### Acetylated G1 PAMAM Dendrimer (5-3)

To an empty 5 mL round bottomed flask was added generation 1 dendrimer-methanol solution (Dendritic Nanotechnologies Inc. Item # DNT-294, 21.99 % solid in methanol, MW: 1532 g/mol), then dried *in vacuo* to remove most methanol and calculate weight of inside formed solid (9.3 mg, 6  $\mu$ mol). The dendrimer was dissolved in methanol (1 mL). Then 1.2 eq acetic acid anhydride (5.9 mg, 58  $\mu$ mol, 5  $\mu$ L) and 1.2 eq triethylamine (5.9 mg, 58  $\mu$ mol, 8  $\mu$ L) were added dropwise and stirred at room temperature for 24 hours. The solvent and excess acetic acid were removed by lyophilization to give a yellow sticky solid. The crude **5-3** was taken for next step. ESI-MSD calcd. for  $C_{80}H_{149}N_{26}O_{20}S_2^+ [M+H]^+$  1859.3535, found multiple charged ions  $[M + 2H]^{2+}/2$  930.0,  $[M + 3H]^{3+}/3$  620.2,  $[M + 4H]^{4+}/4$  465.4,  $[M + 5H]^{5+}/5$  372.5.

### Acetylated G1 PAMAM Dendrimer with Bis(maleimido) Octane Linker (5-4)

Crude **5-3** and 3 eq TCEP HCl (Tris (2-carboxy-ethyl) phosphine hydrochloride) (4.2 mg, 18  $\mu$ mol) were dissolved in methanol (1 mL) to form yellow solution. The resulting solution was allowed to stir under room temperature for 24 hours. Then to this solution was added 0.5 eq **5-2** dissolved in DMF (1 mL) to form yellow solution. The resulting solution was allowed to stir under room temperature for 48 hours and solvent was removed by lyophilization for 24 hours to give **5-4** (9.7 mg, 4.5  $\mu$ mol, 75 % over 3 steps) as light yellow sticky solid. MALDI-TOF-MS calcd. for  $C_{96}H_{171}N_{28}O_{24}S_2^+ [M+H]^+$  2164.2457, found 2165.43, 1236.79, 930.61, 896.62 (Fragment relating to thio-ester bond cleavage).

### G1 Biotinylated PAMAM Dendrimer (5-5)

To an empty 10 mL round bottomed flask was added generation 1 PAMAM dendrimer-methanol solution (Dendritic Nanotechnologies Inc. Item # DNT-294, 21.99 % solid in methanol, MW: 1532 g/mol), then dried *in vacuo* to remove most methanol and calculate weight of inside formed solid (7.2 mg, 4.7  $\mu$ mol). Then 2 eq of primary amine of **3-20** (26 mg, 0.079 mmol) and DMSO (3 mL) were added and the resulting solution was stirred for 48 hours under room temperature. After completion, 15 mL purified water was added and white solid crushed out, followed by continuous filtration through a 1 KDa molecular weight cut-off filtered by centrifugation at 900 rpm for 1 day while keep changing filters. The residue was then washed with distilled water into a tube and lyophilized to give **5-5** (12.8 mg, 3.8  $\mu$ mol, 82 %) as white solid. MALDI-TOF-MS calcd. for  $C_{144}H_{245}N_{42}O_{28}S_{10}^+ [M+H]^+$  3332.62, found 3331.86, 1666.43.

### G3 Biotinylated PAMAM Dendrimer (5-6)

To an empty 10 mL round bottomed flask was added generation 3 cystamine dendrimer-methanol solution (Dendritic Nanotechnologies Inc. Item # DNT-296, 20.1 % solid in methanol, MW: 6969 g/mol), then dried *in vacuo* to remove most methanol and calculate weight of inside formed solid (58.8 mg, 8.4  $\mu$ mol). Then 2 eq of primary amine of **3-20** (183 mg, 0.5 mmol) and DMSO (2 mL) were added and the resulting solution was stirred for 48 hours under room temperature. After completion 15 mL distilled water was added and white solid crushed out, followed by dialysis. The resulting solution was transferred into a clamped tubing membrane with capacity of 6.74 mL/cm, followed by stirring for 2 days and removal of the solvent to give **5-6** (91 mg, 6.4  $\mu$ mol,

76 %) as white solid. MALDI-TOF-MS calcd. for  $C_{624}H_{1061}N_{186}O_{124}S_{34}^+$   $[M+H]^+$  14243.47, found 14242.47, 7126.

#### **Mono Biotinylated G3 PAMAM Half Dendron-1,4-Bis(maleimido) Butane Linker Conjugate (5-7)**

To a small round bottomed flask were added **5-6** (60.3 mg, 4.2  $\mu$ mol), 8 eq 1,4-Bis(maleimido) butane linker **5-1** (8.3 mg, 33.6  $\mu$ mol) and 3 eq TCEP·HCl (Tris (2-carboxy-ethyl) phosphine hydrochloride) (3.6 mg, 12.7  $\mu$ mol). The mixture was dissolved in MeOH/CH<sub>3</sub>CN (1:1) (4 mL) stirring for 2 days under room temperature. Purification was done by removal of solvent and concentrated using lyophilization, followed by transfer into dialysis tubing membrane for 4 days and concentrated under lyophilization to give **5-7** (37 mg, 5  $\mu$ mol, 60 %) as light yellow solid.

#### **Mono Biotinylated G3 PAMAM Half Dendron-1,8-Bis(maleimido) Octane Linker Conjugate (5-8)**

To a small round bottomed flask were added **5-6** (53.8 mg, 3.8  $\mu$ mol), 8 eq of 1,8-Bis (maleimido) octane linker **5-2** (9.2 mg, 30  $\mu$ mol) and 3 eq TCEP·HCl (Tris (2-carboxy-ethyl) phosphine hydrochloride) (4.2 mg, 18  $\mu$ mol). The mixture was dissolved in MeOH/CH<sub>3</sub>CN (1:1) (4 mL) stirring for 2 days under room temperature, followed by evaporation of solvent and freezer drier. The crude was washed by using 10 % methanol in dichloromethane and filter to give **5-8** (50 mg, 6.7  $\mu$ mol, 89 %) as white solid. MALDI-TOF-MS calcd. for  $C_{328}H_{552}N_{95}O_{66}S_{17}^+$   $[M+H]^+$  7427.6425, found. 7429.5, 7122.4 (fragment relating to thio-ester bond cleavage), 6916.7, 6007.8.

#### **G1 Fluorescein Functionalized PAMAM Dendrimer (5-9)**

To an empty 10 mL round bottom flask was added generation 1 dendrimer-methanol solution (Dendritic Nanotechnologies Inc. Item # DNT-294, 21.99 % solid in methanol, MW: 1532 g/mol), then dried *in vacuo* to remove most methanol and calculate weight of inside formed solid (26.6 mg, 17  $\mu$ mol). Then 1 eq of primary amine of **2-5 A** (41 mg, 73.6  $\mu$ mol) and MeOH (2 mL) were added and the resulting solution was stirred for 24 hours in dark under room temperature. After completion the solution was transferred into dialysis tubing membrane against MeOH through 10 days, followed by removal of solvent by lyophilization to give **5-9** (35 mg, 7  $\mu$ mol, 20 %) foam orange solid.

#### **G1 Fluorescein Functionalized PAMAM Half Dendron (5-10)**

To a small round bottomed flask were added **5-9** (15 mg, 3  $\mu$ mol) and 3 eq of TCEP·HCl (Tris (2-carboxy-ethyl) phosphine hydrochloride) (2.6 mg, 9  $\mu$ mol) dissolved in methanol (2 mL) under room temperature and nitrogen protection. The resulting solution was stirred for 3 days followed by removal of solvent to yield crude **5-10**. The crude **5-10** was divided to two portions and taken for next step immediately.

#### **Asymmetric biotinylated and fluorescein functionalized PAMAM dendrimer conjugate (5-11)**

To a small round bottomed flask were added **5-7** (22.1 mg, 3  $\mu\text{mol}$ ) and **5-10** (3  $\mu\text{mol}$ ) and dissolved in 0.7 mL DMF. The resulting solution was stirred for 3 days under room temperature, followed by freezer drier to remove the solvent. Purification was done by dialysis against distilled water first and dialysis against methanol and then concentrate under freezer drier to obtain 31 mg unidentified orange solid. MALDI-TOF-MS:  $[\text{M}+\text{H}]^+$ : no observed mass near 10,000 Da (calculated mass 9903 Da). Other major fragments: 7378.4 (fragment relating to thio-ester bond cleavage on the fluorescein half dendron), 7128.1 (fragment relating to thio-ester bond cleavage on the biotin half dendron), 5067.0 (fragment relating to fluorescein fully functionalized dendrimer).

### **Asymmetric biotinylated and fluorescein functionalized PAMAM dendrimer conjugate (5-12)**

To a small round bottomed flask were added **5-8** (22.3 mg, 3  $\mu\text{mol}$ ) and **5-10** (3  $\mu\text{mol}$ ) and dissolved in 0.7 mL DMF. The resulting solution was stirred for 3 days under room temperature, followed by freezer drier to remove the solvent. Purification was done by dialysis against distilled water first and dialysis against methanol and then concentrate under freezer drier to obtain 32 mg unidentified orange solid.

### **12-Hydroxy-4,7,10-trioxadodecanoic acid-tert-butylester (5-13)<sup>38-39</sup>**

To a 250 mL round bottomed flask was added triethylene glycol (15 g, 100 mmol, 13 mL) dissolved in dry THF (50 mL). 1 mol% of potassium *tert*-butoxide (100 mg, 0.9 mmol) was slowly added into the solution. After potassium *tert*-butoxide completely dissolved, 0.45 eq of *tert*-butyl acrylate (6.4 g, 50 mmol, 7 mL) was dissolved in dry THF (50 mL) and added through an addition funnel, and the mixture was stirred at room temperature for 17 h. After remove the solvent by rotary evaporation, the resulting residue was purified *via* column chromatography on silica gel with increasing amounts of eluent (hexane:ethyl acetate) to yield **5-13** (7.79 g, 28 mmol) as a colorless oil in 56 % yield.  $^1\text{H}$  NMR (500 MHz,  $\text{CDCl}_3$ )  $\delta$  1.43 (s, 9 H), 2.50 (t,  $J = 2.7$  Hz, 2 H), 3.58-3.73 (m, 14 H).  $^{13}\text{C}$  NMR (125 MHz,  $\text{CDCl}_3$ )  $\delta$  28.0, 36.2, 61.7, 66.8, 70.3, 70.4, 70.6, 72.5, 76.8, 77.0, 77.3, 80.5, 170.9. All data are in agreement with literature values.<sup>38-39</sup>

### ***tert*-Butyl 3-(2-(2-(2-azidoethoxy)ethoxy)ethoxy)propanoate (5-14)<sup>38-39</sup>**

To a 25 mL round bottomed flask was added an aliquot of **5-13** (2.3 g, 8.3 mmol) dissolved in 1 M THF (8.3 mL) in an ice-bath. The resulting solution was allowed to stir under 0  $^\circ\text{C}$  for 10 minutes, then 1.2 eq methanesulfonyl chloride (1.2 g, 10 mmol, 0.8 mL) was slowly added, followed by addition of 1.2 eq triethyl amine (1 g, 10 mmol, 1.4 mL) dropwise. White precipitate was formed while TEA was adding. Then the ice-bath was removed and the suspension solution was stirred for 3 hours. Then the organic solvent was removed by rotary evaporation and the yellow residue was dissolved in distilled water (15 mL). The aqueous solution was allowed to stir in a chilled ice-bath and sodium bicarbonate (solid) was used to adjust the pH to 8. Then 1.2 eq sodium azide (650 mg, 10 mmol) was added slowly and the suspension solution was allowed to reflux overnight. Upon completion, the product was extract with ether (100 mL), then washed with brine (30 mLx3), dried over anhydrous  $\text{MgSO}_4$  and concentrated *in vacuo*. Purification was done *via* column chromatography on silica gel with increasing amounts of eluent (hexane:ethyl acetate) to

**5-14** (1.3 g, 4.3 mmol, 52 % yield) in light oil.  $^1\text{H}$  NMR (700 MHz,  $\text{CDCl}_3$ )  $\delta$  1.44 (s, 9 H), 2.49 (t,  $J = 6.6$  Hz, 2 H), 3.38 (t,  $J = 4.5$  Hz, 2 H), 3.59-3.72 (m, 12 H).  $^{13}\text{C}$  NMR (176 MHz,  $\text{CDCl}_3$ )  $\delta$  28.0, 36.2, 50.6, 66.8, 76.8, 77.0, 77.2, 80.4, 170.9. All data are in agreement with literature values.<sup>38-39</sup>

***tert*-Butyl 3-(2-(2-(2-aminoethoxy)ethoxy)ethoxy)propanoate (5-15)**<sup>38-39</sup>

To a 100 mL round bottomed flask was added **5-14** (1.2 g, 3.96 mmol) and dissolved in THF/ $\text{H}_2\text{O}$  in 7:2 (80 mL total) under room temperature. To this solution was added 3 eq triphenylphosphine (3.12 g, 11.9 mmol) and reaction was stirred for 22 hours. Upon completion, the solvents were removed by rotary evaporation and white solid was formed. The white solid was filtered out and washed with cold ether. The solvent was combined and remove in vacuum to yield crude **5-15** (831 mg, 3 mmol, 76 %) in yellow oil.  $^1\text{H}$  NMR (500 MHz,  $\text{CDCl}_3$ )  $\delta$  1.43 (s, 9 H), 2.49 (t,  $J = 6.6$  Hz, 2 H), 2.86 (t,  $J = 5.1$  Hz, 2 H), 3.50 (t,  $J = 5.4$  Hz, 2 H), 3.60-3.63 (m, 8 H), 3.70 (t,  $J = 6.6$  Hz, 2 H).  $^{13}\text{C}$  NMR (125 MHz,  $\text{CDCl}_3$ )  $\delta$  28.0, 36.2, 41.8, 66.9, 70.3, 70.5, 73.5, 80.4, 170.8. All data are in agreement with literature values.<sup>38-39</sup>

***tert*-Butoxy-3-(3,6,9-triethoxy-(5-(2-oxohexahydro-1H-thieno[3,4-d]imidazol-4-yl)pentanamido)decanoxy)propanoate (5-16)**<sup>40</sup>

To a 10 mL round bottomed flask was added **3-20** (853 mg, 2.5 mmol) and 1.1 equivalent *tert*-butyl-12-amino-4,7,10-trioxadodecanoate **5-15** (747 mg, 2.7 mmol) dissolved in 0.1 M  $\text{CH}_2\text{Cl}_2$  (25 mL). The resulting solution was allowed to stir under room temperature for 23 hours. The reaction was monitored *via* TLC and stained with DAKA. Upon completion, the resulting solution was concentrated to remove solvent and purified *via* column chromatography on silica gel with increasing amounts of eluent (dichloromethane:methanol) to yield **5-16** (1.14 g, 2.3 mmol) in 91 % yield.  $^1\text{H}$  NMR (500 MHz,  $\text{CDCl}_3$ )  $\delta$  1.44 (s, 9 H), 1.69 (m, 4 H), 2.24 (t,  $J = 7.2$  Hz, 2 H), 2.49 (t,  $J = 6.6$  Hz, 2 H), 2.77 (d,  $J = 12.9$  Hz, 1 H), 2.89 (dd, 1 H), 3.13 (m, 1 H), 3.43 (t,  $J = 4.5$  Hz, 2 H), 3.56 (t,  $J = 4.8$  Hz, 2 H), 3.61 (s, 8 H), 3.70 (t,  $J = 6.3$  Hz, 2 H), 4.30 (m, 1 H), 4.49 (m, 1 H).  $^{13}\text{C}$  NMR (125 MHz,  $\text{CDCl}_3$ )  $\delta$  25.5, 28.1, 35.9, 36.2, 39.1, 40.5, 55.4, 60.1, 61.7, 66.9, 69.9, 70.1, 70.3, 70.4, 80.6, 163.6, 170.9, 173.1. All data are in agreement with literature values.<sup>40</sup>

**3-(3,6,9-triethoxy-(5-(2-oxohexahydro-1H-thieno[3,4-d]imidazol-4-yl)pentanamido)decanoxy)propanoic acid (5-17)**<sup>40</sup>

To a 5 mL round bottomed flask was added **5-16** (1.12 g, 2.2 mmol) dissolved in 0.2 M  $\text{CH}_2\text{Cl}_2$  (11 mL). To the solution, 2.2 mL TFA was slowly added and the resulting solution was allowed to stir under room temperature for 3 hours. The reaction was monitored *via* TLC and stained with DAKA. Upon completion, the resulting solution was concentrated to remove solvent and purified *via* column chromatography on silica gel with increasing amounts of eluent (dichloromethane:methanol) to yield **5-17** (950 mg, 2.1 mmol) in 96 % yield.  $^1\text{H}$  NMR (500 MHz, MeOD)  $\delta$  1.23-1.27 (m, 2 H), 1.42-1.49 (m, 2 H), 1.63-1.80 (m, 4 H), 2.27 (t,  $J = 7.2$  Hz, 2 H), 2.59 (t,  $J = 5.7$  Hz, 2 H), 2.70 (d,  $J = 12.6$  Hz, 1 H), 2.89 (dd, 1 H), 3.13 (m, 1 H), 3.42 (m, 2 H), 3.55 (t,  $J = 4.5$  Hz, 2 H), 3.62 (s, 8 H), 3.76 (t,  $J = 6.3$  Hz, 2 H), 4.34 (m, 1 H), 4.51 (m, 1 H).  $^{13}\text{C}$  NMR (125 MHz, MeOD)  $\delta$  25.4, 28.1, 28.3, 34.4, 35.3, 38.9, 39.6, 55.6, 60.2, 61.9, 66.4, 69.2, 69.8, 69.9, 70.0, 70.2, 164.7, 173.9, 174.7. All data are in agreement with literature values.<sup>40</sup>

### **2,5-dioxopyrrolidin-1-yl-3-(3,6,9-triethoxy-(5-(2-oxohexahydro-1H-thieno[3,4-d]imidazol-4-yl)pentanamido)decanoxy)propanoate (5-18)**

To a 25 mL two-neck round bottomed flask were added **5-17** (950 mg, 2.12 mmol), 1.2 eq of EDC HCl (487 mg, 2.54 mmol) and 1.2 eq NHS (293 mg, 2.54 mmol) dissolved in 0.1 M dichloromethane (21 mL). Then the resulting solution under room temperature for 48 hours. The reaction was monitored *via* TLC and stained with DAKA. Upon completion, the resulting solution was concentrated to remove solvent and purified *via* column chromatography on silica gel with increasing amounts of eluent (dichloromethane:methanol) to yield **5-18** (977 mg, 1.8 mmol) in 86 % yield. <sup>1</sup>H NMR (500 MHz, CDCl<sub>3</sub>) δ 1.25 (m, 1 H), 1.41 (m, 2 H), 1.64 (m, 4 H), 2.21 (t, *J* = 7.2 Hz, 2 H), 2.60 (t, *J* = 4.2 Hz, 1 H), 2.70 (d, 1 H), 2.85 (s, 4 H), 2.90 (t, 2 H), 3.14 (m, 1 H), 3.43 (m, 2 H), 3.55 (t, *J* = 5.1 Hz, 2 H), 3.62-3.65 (s, 8 H), 3.82 (t, *J* = 6.3 Hz, 2 H), 4.32 (m, 1 H), 4.50 (m, 1 H). <sup>13</sup>C NMR (125 MHz, CDCl<sub>3</sub>) δ 11.4, 14.1, 14.3, 18.7, 19.6, 20.7, 22.6, 25.2, 25.4, 25.5, 25.6, 28.0, 28.2, 29.0, 31.6, 34.5, 34.6, 34.8, 35.9, 36.0, 39.1, 40.5, 51.7, 53.4, 55.6, 60.3, 61.8, 65.7, 66.6, 69.8, 69.9, 70.1, 70.3, 70.4, 70.7, 164.3, 166.8, 169.1, 172.0, 172.9, 173.4. HRMS (TOF) [M + H]<sup>+</sup> calcd. for C<sub>23</sub>H<sub>37</sub>N<sub>4</sub>O<sub>9</sub>S<sup>+</sup> 545.2276, found 545.2276. (Δ = 0 ppm).

### **Biotinylated PEGylated generation 3 PAMAM dendrimer (5-19)**

To a solution of generation 3 cystamine dendrimer-methanol 1.88 g solution (Dendritic Nanotechnologies Inc. Item # DNT-296, 10.1 % solid in methanol, 188 mg, 27 μmol, MW: 7001 g/mol) was added 2 eq (per amino group on G3 dendrimer) biotin-PEG<sub>3</sub>-NHS ester **5-18** (937 mg, 1.7 mmol) dissolved 19 mL methanol. The resulting solution was stirred for 2 days under room temperature. Purification was done by dialysis against methanol for 24 hours, followed by removal of solvent by lyophilizer under -49 °C to give product **5-19** as a white solid (435 mg, 0.11 mmol) in 64 % yield. <sup>1</sup>H NMR (700 MHz, CD<sub>3</sub>OD) δ 1.22 (d, *J* = 7 Hz, 7 H), 1.32 (d, *J* = 7 Hz, 30 H), 1.46 (m, 69 H), 1.61 (m, 39 H), 1.66 (m, 65 H), 1.76 (m, 32 H), 2.24 (t, *J* = 7 Hz, 70 H), 2.39 (m, 134 H), 2.49 (t, *J* = 7 Hz, 67 H), 2.61 (m, 68 H), 2.74 (d, *J* = 14 Hz, 35 H), 2.83 (m, 138 H), 2.95 (dd, *J<sub>a</sub>* = 7 Hz, *J<sub>b</sub>* = 14 Hz, 40 H), 3.24 (m, 42 H), 3.37 (s, 16 H), 3.38 (t, *J* = 7 Hz, 66 H), 3.56 (t, *J* = 7 Hz, 70 H), 3.64 (m, 268 H), 3.70 (s, 10 H), 3.75 (t, *J* = 7 Hz, 68 H), 4.34 (m, 32 H), 4.53 (m, 32 H). <sup>13</sup>C NMR (176 MHz, CD<sub>3</sub>OD) δ 20.0, 21.3, 25.4, 25.5, 28.1, 28.2, 28.3, 28.4, 33.3, 34.3, 35.3, 35.4, 36.3, 37.2, 38.7, 38.9, 39.0, 39.6, 39.8, 48.4, 49.6, 49.7, 50.7, 52.1, 53.4, 55.5, 55.7, 60.2, 61.9, 66.2, 66.9, 69.1, 69.2, 69.8, 69.9, 70.0, 70.1, 70.2, 164.6, 172.4, 172.6, 173.2, 173.6, 174.5, 174.7. MALDI-TOF-MS [M + H]<sup>+</sup> calcd. for C<sub>912</sub>H<sub>1605</sub>N<sub>218</sub>O<sub>252</sub>S<sub>34</sub><sup>+</sup> 20747.1855, found 20748.3, 10378.6.

### **12-N-(4-Pentynoate)-4,7,10-trioxadodecanoic acid-tert-butylester (5-20)**

To a solution of 4-pentynoic acid (1.04 g, 5.35 mmol) dissolved in 0.2 M CH<sub>2</sub>Cl<sub>2</sub> (27 mL) was added 1.1 eq **5-15** (1.63 g, 5.88 mmol) and 1.1 eq EDC HCl salt (1.12 g, 5.88 mmol). The resulting solution was allowed to stir under room temperature for 35 hours. The reaction was monitored *via* TLC. Upon completion, the resulting solution was concentrated to remove solvent and purified *via* column chromatography on silica gel with increasing amounts of eluent (hexane:ethyl acetate) to yield **5-20** as a light yellow oil (1.64 g, 4.6 mmol) in 86 % yield. <sup>1</sup>H NMR (500 MHz, CDCl<sub>3</sub>) δ 1.44 (s, 9 H), 2.00 (t, *J* = 2.52 Hz, 1 H), 2.38 (t, *J* = 7.24 Hz, 2 H), 2.48-2.52 (t+dt overlapped, 4 H), 3.44 (q, *J* = 5.16 Hz, 2 H), 3.54 (t, *J* = 5.2 Hz, 2 H), 3.62 (m, 8 H), 3.69 (t, *J* = 6.52 Hz, 2 H). <sup>13</sup>C NMR (125 MHz, CDCl<sub>3</sub>) δ 14.8, 28.1, 35.2, 36.2, 39.3, 66.9, 69.2, 69.8, 70.3, 70.3, 70.5, 70.5,

80.6, 83.0, 170.9, 170.9. HRMS (TOF)  $[M + H]^+$  calcd. for  $C_{18}H_{32}NO_6^+$  358.2224, found 358.2231. ( $\Delta = 1.9$  ppm).

### **12-N-(4-Pentynoate)-4,7,10-trioxadodecanoic acid (5-21)**

To a solution of **5-20** (1.56 g, 4.36 mmol) dissolved in 0.2 M  $CH_2Cl_2$  (22 mL) was slowly added 4.4 mL TFA and the resulting solution was allowed to stir under room temperature for 4 hours. The reaction was monitored *via* TLC. Upon completion, the resulting solution was concentrated to remove solvent and purified *via* column chromatography on silica gel with increasing amounts of eluent (dichloromethane:methanol) to yield **5-21** as a yellow oil (950 mg, 2.1 mmol) in 96 % yield.  $^1H$  NMR (500 MHz,  $CDCl_3$ )  $\delta$  2.02 (t,  $J = 2.55$  Hz, 1 H), 2.46 (t,  $J = 6.45$  Hz, 2 H), 2.51 (dt,  $J_a = 6.05$  Hz,  $J_b = 2.35$  Hz, 2 H), 2.62 (t,  $J = 5.95$  Hz, 2 H), 3.47 (q,  $J = 5.1$  Hz, 2 H), 3.58 (t,  $J = 5.25$  Hz, 2 H), 3.64-3.67 (m, 8 H), 3.77 (t,  $J = 5.95$  Hz, 2 H).  $^{13}C$  NMR (125 MHz,  $CDCl_3$ )  $\delta$  14.9, 34.8, 35.0, 39.6, 66.3, 69.5, 69.8, 70.0, 70.2, 70.2, 70.5, 82.7, 172.5. HRMS (TOF)  $[M - H]^-$  calcd. for  $C_{14}H_{22}NO_6^-$  300.1453, found 300.1465. ( $\Delta = 4.0$  ppm).

### **2, 5-Dioxopyrrolidin-1-yl-12-N-(4-pentynoate)-4,7,10-trioxadodecanoate (5-22)**

To a round bottomed flask were added **5-21** (1.35 g, 4.48 mmol), 1.2 equivalent NHS (618 mg, 5.37 mmol) and 1.2 equivalent EDC HCl salt (1.03 g, 5.37 mmol) and dissolved in 0.2 M  $CH_2Cl_2$  (22 mL). The resulting solution was allowed to stir under room temperature for 19 hours. The reaction was monitored *via* TLC. Upon completion, the resulting solution was concentrated to remove solvent and purified *via* column chromatography on silica gel with increasing amounts of eluent (dichloromethane:methanol) to yield **5-22** as a yellow oil (1.22 g, 3.1 mmol) in 70 % yield.  $^1H$  NMR (500 MHz,  $CDCl_3$ )  $\delta$  2.01 (t,  $J = 2.6$  Hz, 1 H), 2.38 (t,  $J = 7.35$  Hz, 2 H), 2.50 (dt,  $J_a = 7.15$  Hz,  $J_b = 2.55$  Hz, 2 H), 2.83 (broad, 4 H), 2.89 (t,  $J = 6.35$  Hz, 2 H), 3.44 (q,  $J = 5.25$  Hz, 2 H), 3.54 (t,  $J = 5.2$  Hz, 2 H), 3.62 (m, 4 H), 3.65 (s, 4 H), 3.83 (t,  $J = 6.3$  Hz, 2 H), 6.25 (broad, 1 H).  $^{13}C$  NMR (125 MHz,  $CDCl_3$ )  $\delta$  14.8, 25.6, 32.1, 35.2, 39.3, 53.4, 65.7, 69.3, 69.8, 70.3, 70.4, 70.6, 70.7, 83.1, 166.7, 169.0, 171.0. HRMS (TOF)  $[M + H]^+$  calcd. for  $C_{18}H_{27}N_2O_8^+$  399.1762, found 399.1783. ( $\Delta = 5.2$  ppm).

### **PEGylated “click-ready” generation 1 PAMAM dendrimer (5-23)**

To a solution of generation 1 dendrimer-methanol 1.36 g solution (Dendritic Nanotechnologies Inc. Item # DNT-294, 20.1 % solid in methanol, 271 mg, 0.18 mmol, MW: 1522 g/mol) was added 3 equivalent (per amino group on G1 dendrimer) **5-22** (1.14 g, 2.86 mmol) dissolved in 27 mL methanol and the resulting solution was allowed to stir for 2 days under room temperature. Purification was done by dialysis against methanol for 2 days, and concentrate by lyophilization to generate **5-23** (435 mg, 0.11 mg, 64 %) as a sticky yellow solid. Further purification was done by Jupiter-C18 preparative chromatography column (5  $\mu m$ , 300 A, 250 x 21.2 mm). Solvent A:  $H_2O + 0.1\%$  TFA, solvent B: ACN + 0.1% TFA, increased from 20 % B to 35 % B. Flow rate is 10 mL/min. The fractions containing product was combined and concentrated to give **5-23**.  $^1H$  NMR (700 MHz, MeOD)  $\delta$  2.28 (t,  $J = 2.45$  Hz, 8 H), 2.36-2.43 (t,  $J = 6.45$  Hz, 16 H), 2.43 (t,  $J = 6.1$  Hz, 36 H), 2.73 (t, 16 H), 2.88 (t, 8 H), 3.25-3.34 (m, 76 H), 3.39 (m, 9 H), 3.49-3.51 (m, 36 H), 3.59-3.60 (m, 81 H), 3.68-3.72 (m+t, 32 H).  $^{13}C$  NMR (176 MHz, MeOD)  $\delta$  14.3, 28.0, 28.4, 34.1, 34.5, 36.2, 38.1, 39.0, 39.0, 48.0, 50.0, 52.0, 52.2, 66.9, 69.1, 69.8, 69.9, 70.0, 70.1, 171.3,

172.2, 172.7, 172.9. MALDI-TOF-MS  $[M + H]^+$  calcd. for  $C_{176}H_{301}N_{34}O_{52}S_2^+$  3789.6495, found 1895.205, 3788.202. LC/MS/UV-TOF  $t_R = 21.93$  min.

#### ***N*-(5-Carboxy-*n*-pentyl)maleamic acid (5-24)<sup>34-35</sup>**

To a 250 mL round bottomed flask was added maleic anhydride (11 g, 0.11 mol) dissolved in glacial acetic acid (80 mL) under room temperature, followed by addition of 1 eq of 6-aminocaproic acid (15 g, 0.11 mol) to form clear solution. After addition, white precipitate started to form about 30 mins. The reaction was allowed to stir under room temperature for 3 hours and the white precipitate was filter out and recrystallized from methanol to get white crystal **5-24** (25.42 g, 0.10 mol) in 96 % yield.  $^1H$  NMR (500 MHz, MeOD+KOH)  $\delta$  1.36 (m, 2 H), 1.54 (m, 4 H), 2.17 (t,  $J = 7.2$  Hz, 2 H), 3.23 (t,  $J = 4.2$  Hz, 2 H), 3.30 (q,  $J = 7.2$  Hz, 1 H), 5.82 (d,  $J = 12.3$  Hz, 1 H), 6.33 (d,  $J = 12.3$  Hz, 1 H).  $^{13}C$  NMR (125 MHz, MeOD+KOH)  $\delta$  25.9, 26.7, 28.6, 37.7, 38.9, 124.1, 137.1, 166.5, 173.7, 181.7. m.p. 162-163 °C. All data are in agreement with literature values.<sup>34-35</sup>

#### ***N*-(5-Carboxypentyl)maleimide (5-25)<sup>34-35</sup>**

To a 50 mL round bottomed flask was added **5-24** (10.2 g, 44.5 mmol) dissolved in glacial acetic acid (20 mL). The resulting solution was allowed to reflux for 90 mins then cool down to room temperature. The solution turned to brown color. The reaction mixture was evaporated to remove excess acetic acid and the residual was purified *via* column chromatography on silica gel with increasing amounts of eluent (dichloromethane:methanol) to yield the product **5-25** as white solid (3.1 g, 14.7 mmol) in 33 % yield.  $^1H$  NMR (500 MHz,  $CDCl_3$ )  $\delta$  1.36 (m, 2 H), 1.61 (m, 4 H), 2.36 (t,  $J = 7.5$  Hz, 2 H), 3.53 (t,  $J = 7.2$  Hz, 2 H), 6.72 (s, 2 H).  $^{13}C$  NMR (125 MHz,  $CDCl_3$ )  $\delta$  24.1, 26.1, 28.1, 33.6, 37.6, 134.0, 170.8, 178.5. All data are in agreement with literature values.<sup>34-35</sup>

#### **6-(2,5-Dioxo-2,5-dihydro-1H-pyrrol-1-yl)hexanoic propionic anhydride (5-26)**

To a cooled solution of *N*-(5-carboxypentyl)maleimide **5-25** (1.1 mg, 5.4 mmol) and 1 eq *N*-methylmorpholine (546 mg, 5.4 mmol, 0.6 mL) dissolved in 0.25 M THF (20 mL) was slowly added 1 eq isobutyl chloroformate (738 mg, 5.4 mmol, 0.7 mL). White precipitate was immediately generated. The reaction was allowed to warm to room temperature for 3 hours and monitored by TLC. Upon completion, the precipitate was filtered out and the resulting THF solution containing crude product **5-26** was immediately taken for next step due to it can be easily hydrolyzed under aqueous condition. A small portion of the crude product in THF was concentrated for NMR characterization.  $^1H$  NMR (500 MHz,  $CDCl_3$ )  $\delta$  0.95 (d,  $J = 6.75$  Hz, 6 H), 1.32 (m, 2 H), 1.58 (quint,  $J = 7.6$  Hz, 2 H), 1.67 (quint,  $J = 7.4$  Hz, 2 H), 1.99 (sept,  $J = 6.7$  Hz, 1 H), 2.43 (t,  $J = 7.45$  Hz, 2 H), 3.49 (t,  $J = 7.25$  Hz, 2 H), 4.02 (d,  $J = 6.7$  Hz, 2 H), 6.68 (s, 2 H).  $^{13}C$  NMR (125 MHz,  $CDCl_3$ )  $\delta$  18.7, 23.6, 25.9, 27.6, 28.1, 33.9, 37.5, 75.5, 134.0, 149.2, 167.7, 170.8.

#### ***N,N'*-(3,3'-(2,2'-oxybis(ethane-2,1-diyl)bis(oxy))bis(propane-3,1-diyl))bis(6-(2,5-dioxo-2,5-dihydro-1H-pyrrol-1-yl)hexanamide) (5-27)**

To a cooled solution of crude **5-26** in THF was slowly added 0.5 eq 4,7,10-trioxa-1,13-tridecanediamine (595 mg, 2.7 mmol). The resulting solution was allowed to warm to room temperature for 22 hours and monitored *via* TLC. Upon completion, the solvent was removed and purification was done *via* column chromatography on silica gel with increasing amounts of eluent



(dichloromethane:methanol) to yield **5-27** as a white foam-like solid (814 mg, 1.3 mmol) in 50 % yield for successive 2 steps. <sup>1</sup>H NMR (500 MHz, CDCl<sub>3</sub>) δ 1.23 (quint, *J* = 8.85 Hz, 4 H), 1.50-1.63 (2 quint, 8 H), 1.71 (quint, *J* = 7.75 Hz, 4 H), 2.09 (t, *J* = 9.4 Hz, 4 H), 3.27 (q, *J* = 7.55 Hz, 4 H), 3.45 (t, *J* = 9 Hz, 4 H), 3.50 (t, *J* = 7.25 Hz, 4 H), 3.53-3.55 (m, 4 H), 3.58-3.60 (m, 4 H), 6.64 (s, 4 H). <sup>13</sup>C NMR (125 MHz, CDCl<sub>3</sub>) δ 25.1, 26.3, 28.2, 29.0, 36.4, 37.6, 37.7, 69.9, 70.0, 70.4, 134.0, 170.8, 172.7. HRMS (TOF) [M + H]<sup>+</sup> calcd. for C<sub>30</sub>H<sub>47</sub>N<sub>4</sub>O<sub>9</sub><sup>+</sup> 607.3338, found 607.3334. (Δ = -0.6 ppm).

#### Click-ready SB-T-1214-(SS-Linker)-PEG<sub>3</sub>-N<sub>3</sub> (**5-28**)

An aliquot of the deprotected drug-linker compound **3-11** (114 mg, 0.1 mmol) was dissolved in 0.01 M CH<sub>2</sub>Cl<sub>2</sub> (10 mL). To this solution was added 1 eq **3-19** (21.5 mg, 0.1 mmol) in 2 mL CH<sub>2</sub>Cl<sub>2</sub> dropwise under room temperature for 23 h. Upon completion, the solvent was evaporated and the residual was purified *via* column chromatography on silica gel with increasing amounts of eluent (dichloromethane:methanol) to give **5-28** (118 mg, 0.082 mmol, 85 % yield). <sup>1</sup>H NMR (500 MHz, MeOD) δ 1.12 (s, 3 H), 1.22 (s, 3 H), 1.25 (d, 3 H), 1.32 (s, 9 H), 1.63 (s, 3 H), 1.68 (d, 6 H), 1.72 (m, 1 H), 1.88 (s, 6 H), 2.16-2.20 (m, 2 H), 2.33 (s, 3 H), 2.46-2.53 (m, 1 H), 2.68 (broad, 1 H), 2.86-2.91 (m, 1 H), 3.34-3.37 (m, 4 H), 3.48-3.50 (q, *J* = 3 Hz, 2 H), 3.59 (d, *J* = 3.75 Hz, 3 H), 3.63-3.65 (m, 10 H), 3.77 (d, *J* = 7 Hz, 3 H), 3.92-3.96 (dd, 1 H), 4.06-4.09 (d, 1 H), 4.14 (d, *J* = 8.4 Hz, 1 H), 4.37 (q, *J* = 6.85 Hz, 1 H), 4.92 (m, 4 H), 5.08 (m, 1 H), 5.63 (d, *J* = 7.1 Hz, 1 H), 6.03 (m, 1 H), 6.14 (t, *J* = 8.9 Hz, 1 H), 6.26 (s, 1 H), 7.21-7.32 (m, 2 H), 7.44 (t, *J* = 7.75 Hz, 2 H), 7.57 (t, *J* = 7.45 Hz, 1 H), 7.77 (d, *J* = 7.7 Hz, 1 H), 8.07 (d, *J* = 7.75 Hz, 2 H). <sup>13</sup>C NMR (125 MHz, MeOD) δ 9.1, 9.3, 9.5, 13.0, 14.8, 18.5, 20.6, 20.7, 22.2, 22.4, 25.7, 26.6, 28.2, 31.2, 33.4, 33.5, 35.4, 35.5, 38.7, 38.8, 39.2, 43.1, 45.6, 46.2, 46.3, 49.0, 50.6, 58.4, 69.7, 70.0, 70.2, 70.5, 70.6, 70.6, 70.7, 71.7, 72.1, 75.0, 75.2, 75.4, 76.3, 79.2, 79.7, 80.9, 84.4, 119.9, 127.8, 128.3, 128.6, 129.3, 130.1, 130.4, 130.5, 130.9, 131.0, 132.4, 133.3, 133.6, 137.4, 137.5, 137.7, 143.3, 155.0, 166.9, 168.1, 169.6, 170.3, 172.1, 175.0, 204.1. HRMS (TOF) [M + H]<sup>+</sup> calcd. for C<sub>66</sub>H<sub>90</sub>N<sub>5</sub>O<sub>20</sub>S<sub>2</sub><sup>+</sup> 1336.5615, found 1336.5620. (Δ = 0.4 ppm).

#### Click-ready 7-Fluorescein-SB-T-1214-(SS-Linker)-PEG<sub>3</sub>-N<sub>3</sub> (**5-29**)

To a solution of **3-14** (73 mg, 0.043 mmol) dissolved in 0.01 M CH<sub>2</sub>Cl<sub>2</sub> (4 mL) was slowly added **3-19** (9.4 mg, 0.043 mmol) dissolved in 2 mL CH<sub>2</sub>Cl<sub>2</sub> under room temperature for 21 hours. Upon completion, the solvent was evaporated and the residual was purified *via* column chromatography on silica gel with increasing amounts of eluent (dichloromethane:methanol) to yield **5-29** as an orange solid (57 mg, 0.03 mmol) in 70 % yield. <sup>1</sup>H NMR (500 MHz, MeOD) δ 0.66-0.69 (m, 6 H), 0.81-0.91 (m, 11 H), 0.94 (m, 1 H), 1.05 (m, 2 H), 1.15 (s, 3 H), 1.21 (s, 3 H), 1.24-1.29 (m, 10 H), 1.34 (s, 9 H), 1.48 (m, 1 H), 1.58 (m, 2 H), 1.69 (d, *J* = 9.6 Hz, 6 H), 1.77 (s, 3 H), 1.85 (m, 2 H), 1.95 (s, 3 H), 2.02-2.12 (m, 3 H), 2.17 (m, 2 H), 2.36 (s, 3 H), 2.47 (m, 2 H), 2.56 (m, 1 H), 2.87 (quint, *J* = 6.55 Hz, 1 H), 3.35 (t, 3 H), 3.49 (m, 2 H), 3.63-3.65 (m, 10 H), 3.70-3.80 (m, 2 H), 3.93 (m, 2 H), 4.06 (m, 3 H), 4.14 (d, *J* = 8.4 Hz, 1 H), 4.29 (d, *J* = 8.45 Hz, 1 H), 4.93 (s, 3 H), 5.09 (d, 1 H), 5.56 (q, *J* = 7.2 Hz, 1 H), 5.66 (d, *J* = 6.9 Hz, 1 H), 6.06 (broad, 1 H), 6.12 (t, *J* = 8.55 Hz, 1 H), 6.27 (s, 1 H), 6.44 (s, 1 H), 6.52 (d, *J* = 9.7 Hz, 1 H), 6.71 (d, *J* = 8.85 Hz, 1 H), 6.85 (t, *J* = 9.9 Hz, 2 H), 6.94 (t, *J* = 2.3 Hz, 1 H), 7.21-7.28 (m, 3 H), 7.44 (t, *J* = 7.65 Hz, 2 H), 7.57 (t, *J* = 7.4 Hz, 1 H), 7.64 (t, *J* = 7.55 Hz, 1 H), 7.69 (t, *J* = 7.35 Hz, 1 H), 7.77 (d, *J* = 7.8 Hz, 1 H), 8.08 (d, *J* = 7.55 Hz, 2 H), 8.24 (d, *J* = 7.75 Hz, 1 H). <sup>13</sup>C NMR (125 MHz, MeOD) δ 8.7, 8.8, 10.8, 11.4, 12.8, 14.1, 14.3, 14.5, 18.5, 18.7, 18.8, 18.9, 20.4, 20.6, 20.7, 21.4,

22.3, 22.6, 23.7, 25.2, 25.4, 25.4, 25.7, 26.2, 27.5, 27.6, 28.0, 28.2, 29.0, 29.7, 30.3, 31.2, 31.6, 33.3, 33.4, 33.5, 34.5, 34.6, 35.3, 36.0, 38.7, 39.2, 41.3, 43.2, 46.2, 46.3, 46.8, 49.0, 50.6, 56.0, 68.0, 69.6, 69.8, 70.0, 70.2, 70.5, 70.6, 70.7, 71.5, 71.7, 71.8, 74.6, 75.0, 76.3, 78.7, 79.7, 80.6, 83.9, 100.7, 105.7, 114.0, 114.7, 117.5, 119.9, 127.8, 128.3, 128.6, 128.9, 129.2, 129.6, 129.8, 130.1, 130.3, 130.4, 130.5, 130.5, 130.8, 131.0, 131.3, 132.1, 132.5, 133.3, 133.6, 134.2, 137.4, 137.5, 137.8, 141.8, 150.5, 154.4, 155.0, 159.0, 163.6, 165.5, 166.8, 168.2, 169.5, 170.1, 171.7, 172.1, 172.8, 185.7, 202.5. HRMS (TOF)  $[M + H]^+$  calcd. for  $C_{94}H_{114}N_5O_{26}S_2^+$  1792.7188, found 1792.7177. ( $\Delta = -0.6$  ppm).

### Click-ready Fluorescein-PEG<sub>3</sub>-(CH<sub>2</sub>)<sub>2</sub>N<sub>3</sub> (5-30)

To a solution of **2-4 B** (116 mg, 0.24 mmol), 1.2 eq EDC HCl salt (55 mg, 0.29 mmol), and 0.5 eq DMAP (14.7 mg, 0.29 mmol) dissolved in 0.02 M CH<sub>2</sub>Cl<sub>2</sub> (12 mL) was slowly added 1.2 eq 11-azido-3,6,9-trioxadecan-1-amine **3-19** (63 mg, 0.29 mmol) dissolved in 2 mL CH<sub>2</sub>Cl<sub>2</sub> and the resulting solution was allowed to stir under room temperature for 24 hours. Upon completion, the solvent was evaporated and the residual was purified via column chromatography on silica gel with increasing amounts of eluent (dichloromethane:methanol) to yield **5-30** as a sticky orange solid (136 mg, 0.20 mmol) in 82 % yield. <sup>1</sup>H NMR (500 MHz, MeOD)  $\delta$  0.62 (m, 6 H), 0.77 (m, 6 H), 2.08 (m, 2 H), 2.32 (m, 2 H), 3.28 (m, 2 H), 3.37 (m, 2 H), 3.47-3.56 (m, 12 H), 3.65-3.70 (m, 2 H), 4.04 (m, 2 H), 4.19 (m, 1 H), 6.33 (s, 1 H), 6.42 (m, 1 H), 6.65 (d,  $J = 8.9$  Hz, 1 H), 6.81 (m, 2 H), 6.86 (s, 1 H), 7.20 (m, 1 H), 7.43 (s, 1 H), 7.63 (m, 2 H), 8.16 (m, 1 H). <sup>13</sup>C NMR (125 MHz, MeOD)  $\delta$  18.8, 19.0, 24.7, 27.4, 32.2, 39.2, 50.5, 68.0, 69.7, 69.9, 70.1, 70.4, 70.5, 70.6, 71.7, 100.9, 105.5, 113.6, 114.7, 117.4, 128.7, 129.0, 129.6, 130.3, 130.4, 130.6, 130.9, 131.2, 132.6, 134.1, 150.6, 154.2, 158.9, 163.5, 165.4, 167.6, 172.0, 185.5. HRMS (TOF)  $[M + H]^+$  calcd for  $C_{36}H_{43}N_4O_9^+$  675.3025, found 675.3064. ( $\Delta = 5.7$  ppm).

### PEGylated “click-ready” Generation 1 PAMAM Half Dendron Linker Construct (5-31)

To a solution of **5-23** (66 mg, 17  $\mu$ mol) and 10 eq bis(maleicimido) linker **5-27** (103 mg, 170  $\mu$ mol) dissolved in 3 mL methanol was slowly added 3 eq 0.5 M TCEP (51  $\mu$ mol, 0.1 mL). Upon addition, the solution turned cloudy. The resulting solution was allowed to stir under room temperature and kept be monitoring by FIA. Upon completion, the reaction mixture was diluted with 1 mL distilled water and purified by Jupiter-C18 preparative chromatography column (5  $\mu$ m, 300 A, 250 x 21.2 mm). Acidic solvent A: H<sub>2</sub>O + 0.1% TFA, solvent B: Acetonitrile+ 0.1% TFA, increased from 45 % B to 55 % B. Flow rate is 10 mL/min. The fractions containing product was combined and concentrated to yield **5-31** as a sticky yellow solid (21 mg, 8.4  $\mu$ mol) in 49 % yield. <sup>1</sup>H NMR (500 MHz, CD<sub>3</sub>OD)  $\delta$  1.28-1.34 (m, 6 H), 1.58-1.61 (m, 6 H), 1.62-1.64 (m, 6 H), 1.74-1.79 (m, 6 H), 2.17-2.20 (q,  $J = 5.7$  Hz, 6 H), 2.31 (t,  $J = 5.1$  Hz, 4 H), 2.41 (t,  $J = 7.2$  Hz, 10 H), 2.47 (t,  $J = 5.6$  Hz, 20 H), 2.76 (t,  $J = 6.1$  Hz, 10 H), 2.94 (m, 5 H), 3.26-2.8 (m, 8 H), 3.30-3.31 (m, 12 H), 3.32-3.33 (m, 21 H), 3.35-3.37 (m, 9 H), 3.37 (t,  $J = 5.6$  Hz, 10 H), 3.43 (t,  $J = 5.4$  Hz, 4 H), 3.49-3.51 (m, 6 H), 3.52-3.56 (m, 26 H), 3.60-3.61 (m, 6 H), 3.63-3.66 (m, 50 H), 3.75-3.77 (t,  $J = 6.0$  Hz, 10 H), 5.50 (s, 4 H), 6.82 (s, 2 H). <sup>13</sup>C NMR (125 MHz, CD<sub>3</sub>OD)  $\delta$  14.3, 25.1, 25.9, 26.9, 27.8, 28.0, 28.3, 29.0, 34.1, 34.5, 35.2, 35.4, 35.5, 36.2, 36.4, 37.0, 38.0, 38.4, 38.9, 39.0, 39.5, 50.0, 50.1, 52.3, 52.6, 53.4, 66.8, 68.5, 69.0, 69.1, 69.8, 69.9, 70.0, 70.1, 82.2, 133.9, 161.0, 171.2, 171.3, 172.5, 172.6, 172.9, 174.3, 174.4, 175.0, 177.6. MALDI-TOF-MS  $[M + H]^+$  calcd. for  $C_{118}H_{198}N_{21}O_{35}S^+$  2503.0535, found 2499.6. LC-UV-TOF  $[M + H]^+$  calcd. for

C<sub>118</sub>H<sub>198</sub>N<sub>21</sub>O<sub>35</sub>S<sup>+</sup> 2503.0535, found 657.3406, 835.4750, 1252.7086, deconvolution result 2503.40. LC-UV-TOF t = 13.57 min.

### G1 Half Dendron-Linker-G3 Half Dendron Construct (5-32)

To a solution of **5-31** (21 mg, 8.4 μmol) and 0.5 eq G3-PEG<sub>3</sub>-biotin **5-19** (87 mg, 4.2 μmol) dissolved in MeOH/H<sub>2</sub>O in 1:1 (2mL) was added 3 eq 0.5 M TCEP (25.2 μmol, 50 μL) under room temperature. The resulting solution was allowed to stir overnight. The reaction was monitored by FIA until the starting material was consumed. Then the solution was transferred to dialysis tubing membrane (MWCO 6000-8000) against methanol for 48 hours. The inside solution was lyophilized to give **5-32** as a sticky yellow solid (53 mg, 4.1 μmol) in 49 % yield. <sup>1</sup>H NMR (700 MHz, CD<sub>3</sub>OD) δ 0.86 (m, 33 H), 1.27 (m, 26 H), 1.34-1.35 (d, 64 H), 1.42 (m, 34 H), 1.59 (m, 30 H), 1.66 (m, 30 H), 1.72 (m, 22 H), 1.80 (m, 8 H), 2.07 (m, 60 H), 2.16 (m, 10 H), 2.21 (m, 24 H), 2.27 (m, 6 H), 2.35-2.39 (m, 62 H), 2.44-2.46 (m, 104 H), 2.57-2.58 (m, 24 H), 2.62 (m, 8 H), 2.71 (m, 12 H), 2.84 (s, 28 H), 2.91-2.93 (m, 16 H), 2.98 (s, 30 H), 3.19 (m, 24 H), 3.33 (s, 12 H), 3.35 (m, 32 H), 3.51 (m, 40 H), 3.60-3.62 (m, 141 H), 3.65 (m, 26 H), 3.71 (m, 35 H), 4.30 (m, 18 H), 4.48 (m, 18 H). <sup>13</sup>C NMR (700 MHz, CD<sub>3</sub>OD) δ 11.8, 14.3, 16.6, 23.5, 23.9, 24.7, 25.1, 25.4, 25.5, 26.9, 28.0, 28.1, 28.3, 28.4, 29.0, 30.2, 33.2, 33.3, 34.3, 34.4, 35.5, 36.3, 37.2, 38.6, 38.9, 39.0, 39.6, 39.7, 39.8, 42.2, 48.4, 49.6, 49.7, 50.7, 52.0, 54.2, 55.5, 55.6, 60.2, 61.9, 66.2, 66.8, 68.5, 69.0, 69.1, 69.2, 69.7, 69.8, 69.9, 70.0, 70.1, 82.2, 128.4, 130.9, 132.1, 163.4, 164.6, 164.7, 172.4, 172.6, 172.7, 173.3, 173.6, 173.7, 174.6, 174.7, 177.7. LC-UV-TOF [M + H]<sup>+</sup> calcd. for C<sub>574</sub>H<sub>1001</sub>N<sub>130</sub>O<sub>161</sub>S<sub>18</sub><sup>+</sup> 12877.1505, found 1840.4098, 2146.9901, deconvolution result (neutral form M) 12876.20. LC-UV-TOF t = 14.44 min.

### ABTD-1

To a round bottomed flask were added **5-32** (4 mg, 0.3 μmol), 4 eq **5-28** (1.7 mg, 1.24 μmol), 4 eq copper sulfate pentylhydrate (0.3 mg, 1.24 μmol) and 4 eq sodium ascorbic acid (0.2 mg, 1.24 μmol) dissolved in MeOH/distilled water in 4:1 ratio (1.6 mL/0.4 mL). The resulting reaction mixture was allowed to stir for 24 hours and monitored by FIA. Purification was done by dialysis using MWCO 3000-3500 tubing membrane for 48 hours. The inside solution was filtrated to remove insoluble solid and the solution was lyophilized to give **ABTD-1** as a light yellow sticky solid (5 mg, 0.26 μmol) in 88 % yield. <sup>1</sup>H NMR 700 MHz, CD<sub>3</sub>OD) δ 0.08-0.09 (m, 16 H), 0.86-0.89 (m, 24 H), 0.97-0.98 (m, 24 H), 1.07 (m, 14 H), 1.17 (s, 58 H), 1.27 (dd, *J*<sub>a</sub> = 1.95 Hz, *J*<sub>b</sub> = 4.85 Hz, 58 H), 1.40 (s, 116 H), 1.65 (s, 90 H), 1.73 (d, *J* = 9.95 Hz, 102 H), 1.91 (s, 40 H), 2.22 (m, 60 H), 2.37 (s, 38 H), 2.45 (m, 60 H), 2.56 (m, 42 H), 2.71 (m, 28 H), 3.33 (s, 20 H), 3.35 (t, 60 H), 3.49-3.73 (m, 313 H), 3.77 (m, 52 H), 3.84 (d, *J* = 5 Hz, 22 H), 3.99-4.02 (dd, *J*<sub>a</sub> = 3.25 Hz, *J*<sub>b</sub> = 12 Hz, 16 H), 4.10-4.12 (d, *J* = 12.25 Hz, 16 H), 4.17 (q, *J* = 6 Hz, 25 H), 4.30 (q, *J* = 5 Hz, 32 H), 4.50 (m, 35 H), 4.92 (s, 18 H), 4.99 (d, *J* = 6.85 Hz, 12 H), 5.27 (broad, 12 H), 5.66 (d, *J* = 5.1 Hz, 12 H), 6.13 (m, 14 H), 6.45 (s, 11 H), 6.82 (m, 9 H), 7.26 (m, 10 H), 7.31 (m, 18 H), 7.49 (t, *J* = 5.55 Hz, 20 H), 7.61 (t, *J* = 5.35 Hz, 12 H), 7.71 (m, 4 H), 7.79 (m, 16 H), 7.99 (m, 6 H), 8.12 (d, *J* = 5.35 Hz, 20 H). <sup>13</sup>C NMR (176 MHz, CD<sub>3</sub>OD) δ 7.7, 9.0, 12.3, 13.5, 17.2, 19.4, 19.5, 20.9, 21.8, 24.6, 25.5, 27.3, 28.1, 28.4, 31.3, 32.7, 32.9, 35.4, 36.1, 36.3, 38.1, 38.9, 39.8, 43.1, 45.8, 45.9, 46.6, 48.4, 50.3, 55.7, 57.8, 60.2, 61.9, 66.9, 69.1, 69.2, 69.7, 69.8, 70.1, 70.2, 70.9, 71.5, 74.9, 75.1, 75.3, 76.0, 77.7, 79.0, 80.9, 84.4, 119.8, 127.5, 127.9, 128.2, 129.7, 130.0, 130.1, 130.2, 130.9, 131.0, 133.1, 133.4, 133.6, 137.2, 137.3, 141.2, 156.0, 164.6, 166.2, 168.8, 170.0, 170.9, 172.7, 173.6, 173.7, 174.6, 203.7.

## ABTD-2

To a round bottom flask were added **5-32** (7.5 mg, 0.58  $\mu\text{mol}$ ), 4 eq **5-29** (4.2 mg, 2.3  $\mu\text{mol}$ ) 4 eq copper sulfate pentahydrate (0.6 mg, 2.3  $\mu\text{mol}$ ) and 4 eq sodium ascorbic acid (0.4 mg, 2.3  $\mu\text{mol}$ ) dissolved in MeOH/distilled water in 4:1 ratio (2 mL/0.5 mL). The resulting reaction mixture was allowed to stir for 24 hours and monitored by FIA. Purification was done by dialysis using MWCO 3000-3500 tubing membrane for 48 hours. The inside solution was filtrated to remove insoluble solid and the solution was lyophilized to yield **ABTD-2** as a yellow/orange sticky solid (8 mg, 0.4  $\mu\text{mol}$ ) in 69 % yield.  $^1\text{H}$  NMR (700 MHz, MeOD)  $\delta$  0.65 (t,  $J = 4.35$  Hz, 20 H), 0.86-0.88 (m, 36 H), 1.13-1.17 (m, 26 H), 1.26 (m, 46 H), 1.40 (s, 32 H), 1.57 (m, 24 H), 1.65 (m, 16 H), 1.73 (m, 32 H), 1.86 (s, 16 H), 2.22 (m, 18 H), 2.46 (s, 10 H), 2.54 (m, 32 H), 2.70 (d, 11 H), 2.97 (m, 34 H), 3.34 (m, 28 H), 3.53-3.62 (m, 124 H), 3.71 (m, 27 H), 3.93 (d, 6 H), 4.10-4.12 (d,  $J = 12.25$  Hz, 16 H), 4.17 (m, 12 H), 4.21 (m, 8 H), 4.49 (broad, 10 H), 4.93 (s, 6 H), 4.99 (d,  $J = 6.85$  Hz, 6 H), 5.27 (broad, 6 H), 5.60 (t, 4 H), 5.65 (d,  $J = 4.95$  Hz, 6 H), 6.13 (broad, 4 H), 6.29 (s, 4 H), 6.50 (s, 5 H), 6.57 (d,  $J = 6.8$  Hz, 5 H), 6.95 (d,  $J = 6.6$  Hz, 5 H), 7.04 (m, 7 H), 7.26 (m, 8 H), 7.31 (m, 6 H), 7.41 (d,  $J = 5.25$  Hz, 4 H), 7.49 (t,  $J = 5.5$  Hz, 8 H), 7.61 (m, 6 H), 7.71 (m, 4 H), 7.78 (m, 8 H), 7.82 (t,  $J = 5.2$  Hz, 4 H), 8.12 (d,  $J = 5.35$  Hz, 8 H), 8.28 (d,  $J = 5.75$  Hz, 4 H).  $^{13}\text{C}$  NMR (176 MHz, MeOD)  $\delta$  7.7, 10.0, 12.2, 13.0, 13.7, 16.9, 17.2, 17.8, 19.4, 19.5, 20.7, 21.2, 21.7, 22.3, 23.4, 24.6, 25.0, 25.1, 25.4, 25.5, 25.7, 27.3, 27.4, 28.1, 28.4, 28.8, 29.0, 29.2, 29.3, 29.8, 31.6, 32.9, 34.9, 35.1, 35.2, 35.9, 36.3, 38.6, 28.7, 38.9, 39.7, 43.2, 45.8, 45.9, 49.7, 50.3, 55.6, 55.8, 56.9, 60.2, 61.9, 66.9, 67.4, 68.1, 68.5, 69.0, 69.1, 69.2, 69.7, 69.9, 70.1, 70.2, 70.5, 71.4, 71.7, 74.5, 75.0, 75.8, 77.5, 79.0, 80.5, 83.7, 100.7, 104.1, 114.8, 116.7, 119.8, 127.6, 127.9, 128.2, 128.4, 129.4, 129.7, 130.2, 130.3, 130.5, 130.9, 131.0, 131.2, 132.6, 133.2, 133.6, 137.2, 137.3, 154.8, 155.0, 160.1, 161.4, 161.6, 161.8, 164.6, 165.0, 166.1, 167.8, 168.8, 170.1, 172.6, 173.1, 173.7, 174.6, 185.8, 202.5.

## ABTD-3

To a round bottom flask were added **5-32**(11 mg, 0.85  $\mu\text{mol}$ ), 4 eq **5-30** (2.3 mg, 3.4  $\mu\text{mol}$ ), 8 eq copper sulfate pentahydrate (1.7 mg, 6.8  $\mu\text{mol}$ ) and 8 eq sodium ascorbic acid (1.2 mg, 6.8  $\mu\text{mol}$ ) dissolved in MeOH/distilled water in 4:1 ratio (2 mL/0.5 mL). The resulting reaction mixture was allowed to stir for 24 hours and monitored by FIA. Purification was done by dialysis using MWCO 3000-3500 tubing membrane for 48 hours. The inside solution was filtrated to remove insoluble solid and the solution was lyophilized to yield **ABTD-3** as a yellow sticky solid (10 mg, 0.64  $\mu\text{mol}$ ) in 76 % yield.  $^1\text{H}$  NMR (700 MHz, MeOD)  $\delta$  0.65 (m, 20 H), 0.85 (m, 32 H), 1.17 (m, 10 H), 1.28 (m, 10 H), 1.43 (s, 12 H), 1.52 (m, 16 H), 1.86 (m, 58 H), 2.22 (m, 8 H), 2.51 (m, 32 H), 2.66 (d, 12 H), 3.44 (m, 28 H), 3.57 (m, 124 H), 3.74 (m, 16 H), 4.20 (m, 16 H), 4.25 (m, 8 H), 4.93 (s, 16 H), 4.99 (m, 8 H), 6.50 (s, 8 H), 6.66 (m, 5 H), 6.94 (m, 2 H), 7.06 (m, 27 H), 7.30 (m, 4 H), 7.49 (m, 8 H), 7.62 (m, 4 H), 7.74 (m, 4 H), 8.15 (m, 4 H), 8.21 (m, 4 H).  $^{13}\text{C}$  NMR (176 MHz, MeOD)  $\delta$  7.5, 9.9, 11.2, 11.3, 16.7, 17.8, 19.2, 21.3, 21.7, 22.3, 24.8, 25.0, 25.1, 25.2, 25.9, 27.2, 27.4, 28.1, 28.4, 28.8, 29.2, 29.3, 29.5, 35.4, 35.8, 38.9, 39.7, 43.2, 50.3, 55.6, 55.8, 56.9, 60.2, 61.9, 66.9, 67.5, 68.4, 68.5, 69.0, 69.2, 69.7, 69.9, 70.1, 70.2, 100.7, 128.4, 129.4, 129.7, 130.2, 130.3, 130.4, 130.9, 132.0, 131.7, 132.6, 163.6, 164.9, 166.1, 166.8, 170.1, 172.6, 174.7, 174.6.

**N2,N4-Bis(2-(2-(2-(2-azidoethoxy)ethoxy)ethoxy)ethyl)-6-chloro-1,3,5-triazine-2,4-diamine (5-53)**

To a 25 mL round bottomed flask was added **3-19** (520 mg, 2.39 mmol) and 0.45 eq cyanuric chloride (198 mg, 1.07 mmol) dissolved in 0.1 M THF (24 mL) under room temperature. The resulting solution was allowed to heat to 60 °C followed by addition of 2 eq DIPEA (4.78 mmol, 618 mg, 0.83 mL) for 19 hours. The reaction was monitored by TLC. Upon completion, the solvent was removed by rotary evaporation and residue was purified *via* column chromatography on silica gel firstly with increasing amounts of eluent (dichloromethane:methanol) to give **5-53** (305 mg, 0.56 mmol, 52 %) as pale yellow sticky solid. <sup>1</sup>H NMR (500 MHz, CDCl<sub>3</sub>) δ 3.30-3.32 (t, *J* = 8.8 Hz, 4 H), 3.52-3.61 (m, 28 H), 5.86-6.25 (1 H), 6.42 (1 H). <sup>13</sup>C NMR (125 MHz, CDCl<sub>3</sub>) δ 40.5, 40.6, 40.76, 50.1, 50.6, 61.3, 61.6, 69.3, 69.7, 70.0, 70.2, 70.4, 70.6, 165.3, 165.6, 166.0, 168.2, 169.0. HRMS calcd. for C<sub>19</sub>H<sub>35</sub>ClN<sub>11</sub>O<sub>6</sub><sup>+</sup> [M+H]<sup>+</sup> 548.2455, found 548.2461. (Δ = 1.1 ppm).

**tert-Butyl (4-aminobutyl)carbamate (5-54)**

To a solution of 1,4-diaminobutane dissolved in 0.04 M CH<sub>2</sub>Cl<sub>2</sub> (1.25 L) in 2 L three neck round bottomed flask, 0.1 eq Boc anhydride dissolved in 100 mL CH<sub>2</sub>Cl<sub>2</sub> was added dropwise through 4 hours. The reaction was completed in 18 hours and white precipitate was formed. Then the solvent was rotary evaporated to form white sticky solid. The residue was redissolved in distilled water, and extracted with CH<sub>2</sub>Cl<sub>2</sub>. The organic layers were combined and dried with MgSO<sub>4</sub>. The organic layers were concentrated to form the sticky solid **5-54** in 94 % yield. <sup>1</sup>H NMR (500 MHz, MeOD) δ 1.43 (s, 9 H), 1.51 (m, 4 H), 2.73 (m, 2 H), 3.11 (m, 2 H), 4.71 (m, 1 H). <sup>13</sup>C NMR (125 MHz, MeOD) δ 27.5, 28.5, 40.4, 41.7, 79.1, 156.1.

**Tert-butyl(4-((4,6-bis((2-(2-(2-(2-azidoethoxy)ethoxy)ethoxy)ethyl)amino)-1,3,5-triazin-2-yl)amino)butyl)carbamate (5-55)**

To a 25 mL round bottom flask was added **5-53** (305 mg, 0.56 mmol) and 1.5 eq **5-54** (157 mg, 0.84 mmol) dissolved in 0.05 M THF (11 mL) under room temperature. Then 1.5 eq DIPEA (0.84 mmol, 109 mg, 0.15 mL) was slowly added. The starting material was not fully dissolved so few drops of DMF was added and the resulting solution was allowed to heat to reflux for 24 hours. The reaction was monitored by TLC. Upon completion, the solvent was removed by rotary evaporation and residue was purified *via* column chromatography on silica gel with increasing amounts of eluent (dichloromethane:methanol) to yield pure **5-55** (243 mg, 0.35 mmol, 63 %) as yellow sticky solid. <sup>1</sup>H NMR (500 MHz, CDCl<sub>3</sub>) δ 1.43 (s, 9 H), 1.52-1.54 (m, 4 H), 3.13-3.14 (m, 2 H), 3.35 (m, 2 H), 3.37-3.39 (t, *J* = 5 Hz, 4 H), 3.54-3.68 (m, 24 H), 4.91 (1 H). <sup>13</sup>C NMR (125 MHz, CDCl<sub>3</sub>) δ 28.5, 37.8, 40.1, 40.4, 50.7, 70.1, 70.2, 70.4, 70.6, 70.7, 79.1, 156.0, 156.1, 161.3, 165.9. HRMS calcd. for C<sub>28</sub>H<sub>54</sub>N<sub>13</sub>O<sub>8</sub><sup>+</sup> [M+H]<sup>+</sup> 700.4213, found 700.4218. (Δ = 0.7 ppm).

**N2-(4-Aminobutyl)-N4,N6-bis(2-(2-(2-(2-azidoethoxy)ethoxy)ethoxy)ethyl)-1,3,5-triazine-2,4,6-triamine TFA salt (5-56)**

To a 10 mL round bottomed flask was added **5-55** (181 mg, 0.26 mmol) dissolved in 0.05 M CH<sub>2</sub>Cl<sub>2</sub> (5 mL) under room temperature. Then 10 v% TFA (0.52 mL) was slowly added. The reaction was allowed to stir under room temperature for 5 hours and monitored by TLC. Upon completion, the solvent was removed by rotary evaporation and residue was lyophilized overnight

to yield crude **5-56** (228 mg) as yellow sticky solid.  $^1\text{H}$  NMR (500 MHz,  $\text{CD}_3\text{OD}$ )  $\delta$  1.74 (m, 4 H), 3.00 (m, 2 H), 3.39-3.40 (m, 4 H), 3.48-3.52 (m, 2 H), 3.60 (m, 2 H), 3.68 (m, 24 H).  $^{13}\text{C}$  NMR (125 MHz,  $\text{CD}_3\text{OD}$ )  $\delta$  24.4, 24.5, 25.6, 25.9, 36.7, 38.9, 39.5, 39.9, 40.2, 40.3, 40.7, 50.4, 68.6, 68.7, 68.9, 69.7, 70.0, 70.1, 70.2, 113.2, 115.5, 117.8, 120.2, 155.0, 156.0, 156.2, 161.2, 161.5, 161.7, 162.6, 163.1, 163.4, 165.9. HRMS calcd. for  $\text{C}_{23}\text{H}_{46}\text{N}_{13}\text{O}_6^+$   $[\text{M}+\text{H}]^+$  600.3689, found 600.3694. ( $\Delta = 0.8$  ppm).

### **Tribrached Triazine-Fluorescein Construct (5-57)**

To a 25 mL round bottomed flask was added crude **5-56** and fluorescent probe OSu activated ester **2-5 B** (131 mg, 0.23 mmol) dissolved in 0.02 M  $\text{CH}_2\text{Cl}_2$  (12 mL) under room temperature, followed by addition of 1 eq DIPEA (0.23 mmol, 30 mg, 0.04 mL). The reaction was allowed to stir under room temperature for 14 hours. Upon completion, the solvent was removed by rotary evaporation and residue was purified *via* column chromatography on silica gel with increasing amounts of eluent (dichloromethane:methanol) to give **5-57** (205 mg, 0.19 mmol, 75 % for 2 steps) as red sticky solid.  $^1\text{H}$  NMR (500 MHz,  $\text{CDCl}_3$ )  $\delta$  0.68-0.72 (t,  $J = 6.7$  Hz, 6 H), 0.82-0.88 (m, 1 H), 1.24 (s, 1 H), 1.55 (s, 4 H), 1.59-1.68 (m, 1 H), 2.12-2.19 (quint,  $J = 6.4$  Hz, 3 H), 2.34-2.38 (t,  $J = 7.1$  Hz, 3 H), 3.27-3.28 (m, 2 H), 3.37-3.39 (t,  $J = 9.2$  Hz, 4 H), 3.54 (m, 4 H), 3.57-3.58 (m, 4 H), 3.62-3.68 (m, 20 H), 3.74-3.3.82 (m, 2 H), 4.1 (t,  $J = 6.2$  Hz, 2 H), 5.1 (broad, 1 H), 5.2 (s, 1 H), 5.3 (broad, 1 H), 5.9 (broad, 1 H), 6.4 (t,  $J = 1.5$  Hz, 1 H), 6.5 (dt,  $J_a = 9.7$  Hz,  $J_b = 1.7$  Hz, 1 H), 6.7 (dd,  $J_a = 8.9$  Hz,  $J_b = 2.4$  Hz, 1 H), 6.9 (t,  $J = 9.7$  Hz, 2 H), 6.9 (d,  $J = 2.1$  Hz, 1 H), 7.3 (d,  $J = 7.4$  Hz, 1 H), 7.6 (t,  $J = 7.5$  Hz, 1 H), 7.7 (t,  $J = 7.5$  Hz, 1 H), 8.2 (d,  $J = 7.7$  Hz, 1 H).  $^{13}\text{C}$  NMR (125 MHz,  $\text{CDCl}_3$ )  $\delta$  18.8, 18.9, 24.9, 26.9, 27.2, 27.5, 29.7, 32.5, 39.2, 40.0, 40.4, 50.7, 68.0, 70.0, 70.1, 70.3, 70.7, 71.8, 101.0, 105.8, 113.5, 114.9, 117.6, 129.0, 129.7, 129.9, 130.3, 130.5, 130.8, 131.3, 132.6, 134.2, 150.3, 154.3, 159.0, 163.4, 165.5, 171.9, 185.7. HRMS calcd. for  $\text{C}_{51}\text{H}_{70}\text{N}_{13}\text{O}_{12}^+$   $[\text{M}+\text{H}]^+$  1056.5257, found 1056.5258. ( $\Delta = 0.6$  ppm).

### **6-(2,5-Dioxo-2,5-dihydro-1H-pyrrol-1-yl)-N-(prop-2-yn-1-yl)hexanamide (5-58)**

To a 50 mL round bottomed flask was added **5-25** (400 mg, 1.9 mmol) dissolved in 0.1 M THF (19 mL) under 0 °C. To the solution was slowly added 1 eq N-methylmorpholine (192 mg, 1.9 mmol, 0.21 mL), followed by the addition of 1 eq ethyl chloroformate (206 mg, 1.9 mmol, 0.18 mL) dropwise. White precipitate was forming during the addition. The reaction mixture was allowed to warm to room temperature for 1 hour. The reaction was monitored by TLC. Then 0.95 eq propargylamine (100 mg, 1.81 mmol) was dissolved in 2 mL THF and slowly added. The reaction run for 3 hours and was monitored by TLC. Upon completion, the solid was filtered out and solvent was removed by rotary evaporation and residue was purified *via* column chromatography on silica gel with increasing amounts of eluent (hexanes:ethyl acetate) to yield pure **5-58** (266 mg, 1.1 mmol, 59 % for 2 steps) as white crystal solid. M.P. 104-105 °C.  $^1\text{H}$  NMR (500 MHz,  $\text{CDCl}_3$ )  $\delta$  1.28-1.34 (m, 2 H), 1.57-1.70 (m, 6 H), 2.17-2.20 (t,  $J = 7.6$  Hz, 2 H), 2.22-2.23 (t,  $J = 2.6$  Hz, 1 H), 3.49-3.52 (t,  $J = 7.3$  Hz, 2 H), 4.03-4.05 (q,  $J = 2.6$  Hz, 2.6 H), 5.65 (s, 1 H), 6.68 (s, 2 H).  $^{13}\text{C}$  NMR (125 MHz,  $\text{CDCl}_3$ )  $\delta$  24.9, 26.2, 28.2, 29.2, 36.1, 37.6, 71.6, 79.6, 134.1, 170.9, 172.3. HRMS calcd. for  $\text{C}_{13}\text{H}_{17}\text{N}_2\text{O}_3^+$   $[\text{M}+\text{H}]^+$  249.1234, found 249.1239. ( $\Delta = 2$  ppm).

### **Tribrached Triazine-Fluorescein Tripod Linker (5-59)**

To a 10 mL round bottomed flask was added intermediate **5-57** (116 mg, 0.11 mmol) and 2 eq **5-58** (55 mg, 0.22 mmol). 2 eq copper sulfate pentyl hydrate (55 mg, 0.22 mmol) and 2 eq ascorbic acid (39 mg, 0.22 mmol) were added, followed by the addition of CH<sub>2</sub>Cl<sub>2</sub> and distilled water as combined solvents with ration of 4:1 (0.75 mL/3.75 mL). The heterogeneous reaction was allowed to stir for 3 hours and monitored by FIA. Upon completion, the two portion of crude reaction mixture were combined, then separated using separated funnel and the organic layers were combined, dried with MgSO<sub>4</sub> and concentrated. The residue was purified *via* column chromatography on alumina gel with increasing amounts of eluent (dichloromethane:methanol) to yield pure **5-59** (125 mg, 0.08 mmol, 68 %) as red sticky solid. <sup>1</sup>H NMR (400 MHz, CDCl<sub>3</sub>) δ 0.69-0.72 (t, *J* = 6.9 Hz, 6 H), 0.84-0.89 (m, 2 H), 1.24-1.31 (m, 8 H), 1.53-1.67 (m, 14 H), 1.85 (broad, 8 H), 2.14-2.19 (m, 6 H), 2.36-2.40 (t, *J* = 7.0 Hz, 2 H), 3.27-3.28 (m, 2 H), 3.46-3.49 (t, *J* = 7.3 Hz, 4 H), 3.6 (m, 21 H), 3.71-3.3.82 (m, 2 H), 3.86-3.88 (t, *J* = 5.1 Hz, 4 H), 4.1 (t, *J* = 6.3 Hz, 2 H), 4.48 (d, *J* = 5.5 Hz, 4 H), 4.52-4.53 (t, *J* = 5.0 Hz, 2 H), 6.42 (d, *J* = 1.9 Hz, 1 H), 6.51-6.54 (dd, *J*<sub>a</sub> = 9.7 Hz, *J*<sub>b</sub> = 1.9 Hz, 1 H), 6.67 (s, 4 H), 6.70-6.73 (dd, *J*<sub>a</sub> = 9.0 Hz, *J*<sub>b</sub> = 2.5 Hz, 1 H), 6.85 (t, *J* = 9.4 Hz, 2 H), 6.94 (d, *J* = 2.4 Hz, 1 H), 7.28 (dd, *J*<sub>a</sub> = 7.2 Hz, *J*<sub>b</sub> = 0.8 Hz, 1 H), 7.64-7.69 (dt, *J*<sub>a</sub> = 1.2 Hz, *J*<sub>b</sub> = 7.5 Hz, 1 H), 7.70-7.74 (m, 1 H + 2 H), 8.24-8.26 (dd, *J*<sub>a</sub> = 8.0 Hz, *J*<sub>b</sub> = 1.3 Hz, 1 H). <sup>13</sup>C NMR (400 MHz, CDCl<sub>3</sub>) δ 18.9, 24.9, 25.0, 25.9, 26.0, 26.4, 26.8, 27.1, 27.2, 27.3, 27.5, 28.2, 29.4, 29.7, 32.2, 32.4, 34.9, 36.1, 37.6, 38.3, 38.5, 39.1, 40.1, 40.3, 43.1, 44.3, 50.2, 53.4, 68.0, 68.6, 68.7, 69.4, 69.9, 70.2, 70.5, 71.8, 78.7, 100.9, 105.6, 113.6, 114.8, 117.5, 123.3, 129.0, 129.6, 129.8, 130.3, 130.5, 130.7, 131.2, 132.5, 134.0, 134.2, 144.5, 150.5, 154.2, 159.0, 163.5, 165.5, 170.8, 172.1, 172.9, 176.8, 176.9, 177.5, 178.3, 185.6. HRMS calcd. for C<sub>77</sub>H<sub>102</sub>N<sub>17</sub>O<sub>18</sub><sup>+</sup> [M+H]<sup>+</sup> 1552.7501, found 776.8811, 518.2564, deconvolution result 1552.7477. (Δ = -3.4 ppm). MALDI-ESI calcd. for C<sub>77</sub>H<sub>102</sub>N<sub>17</sub>O<sub>18</sub><sup>+</sup> [M+H]<sup>+</sup> 1552.7501, found 1552.4682.

### G3-PEG-biotin half dendron with click-ready alkyne moiety construct (**5-60**)

To a 5 mL round bottomed flask was added **5-19** (11 mg, 0.53 μmol) and 4 eq **5-58** (1.1 mg, 2.1 μmol) dissolved in 1 mL DMF. To this suspension was added 0.5 M TCEP solution (3 μL) and this resulting solution was allowed to heat to 60 °C for 5 hours. The reaction was monitored by MALDI-MS. Then the reaction mixtures was purified by dialysis using MWCO 6000-8000 dialysis membrane and lyophilized to yield **5-60** (16 mg) as light yellow sticky solid. <sup>1</sup>H NMR (700 MHz, DMSO-*d*<sub>6</sub>) δ 1.24 (m, 32 H), 1.48 (m, 48 H), 1.61 (m, 16 H), 1.93 (m, 4 H), 2.06 (m, 32 H), 2.19 (m, 52 H), 2.31 (m, 32 H), 2.42 (m, 32 H), 2.50 (m, 24 H), 2.57 (m, 20 H), 2.65 (m, 48 H), 2.81 (m, 16 H), 3.08 (s, 96 H), 3.17 (m, 32 H), 3.44 (m, 116 H), 3.58 (m, 32 H), 4.13 (m, 16 H), 4.31 (m, 16 H), 6.38 (s, 16 H), 6.45 (s, 16 H), 7.81 (m, 8 H), 7.85 (m, 16 H), 7.90 (d, 32 H). <sup>13</sup>C NMR (176 MHz, DMSO-*d*<sub>6</sub>) δ 25.7, 28.4, 28.6, 33.6, 35.5, 36.5, 38.7, 38.9, 49.9, 52.6, 55.8, 59.6, 61.5, 67.2, 69.6, 69.9, 70.0, 70.1, 163.2, 170.7, 171.7, 172.0, 172.6. MALDI-TOF-MS [M+H]<sup>+</sup> for C<sub>469</sub>H<sub>820</sub>N<sub>111</sub>O<sub>129</sub>S<sub>17</sub><sup>+</sup>, calcd. 10622.3790, found 10645.594 as [M+Na]<sup>+</sup>.

### Azido-PEG<sub>3</sub>-FITC (**5-61**)

To a 25 mL round bottomed flask were added FITC (100 mg, 0.26 mmol) and 1.2 eq **3-19** (72 mg, 0.33 mmol) dissolved in 0.03 M DCM/DMF=4:1 (9 mL). The reaction was allowed to stir for 16 hours, and the resulting crude product was concentrated and purified by preparative HPLC to give

**5-61** as orange solid (111 mg, 0.18 mmol) in 73 % yield. <sup>1</sup>H NMR (500 MHz, DMSO-*d*6) δ 3.38 (s, 2 H), 3.56-3.37 (m, 14 H), 6.60 (m, 3 H), 6.70 (s, 2 H), 7.19 (d, *J* = 7.8 Hz, 1 H), 7.77 (s, 1 H), 8.14 (s, 1 H), 8.32 (s, 1 H), 10.10 (s, 1 H). <sup>13</sup>C NMR (125 MHz, DMSO-*d*6) δ 44.2, 50.4, 55.3, 68.9, 69.7, 70.1, 70.2, 102.7, 110.3, 113.2, 116.9, 124.6, 127.3, 129.5, 129.7, 141.8, 147.1, 152.4, 160.2, 169.0, 181.0. HRMS [M+H]<sup>+</sup> for C<sub>29</sub>H<sub>30</sub>N<sub>5</sub>O<sub>8</sub>S<sup>+</sup> calcd. 608.1810, found 608.1814. (Δ = 0.6 ppm).

### G3-PEG-biotin half dendron-FITC construct (5-62)

To a 5 mL round bottomed flask was added **5-60** (14 mg, 1.32 μmol), 1.5 eq **5-61** (1.2 mg, 2 μmol), 1.5 eq CuSO<sub>4</sub> 5H<sub>2</sub>O (0.5 mg, 2 μmol) and 1.5 eq ascorbic acid (0.35 mg, 2 μmol) dissolved in DMF/H<sub>2</sub>O=1:1 (2 mL). The resulting solution was allowed to stir under room temperature in dark and monitored by MALDI-TOF-MS. After 24 hours, the reaction mixture was purified by dialysis using MWCO 6000-8000 dialysis membrane and lyophilized to yield **5-62** (3 mg). <sup>1</sup>H NMR (700 MHz, DMSO-*d*6) δ 1.23 (m, 35 H), 1.49 (m, 30 H), 1.60 (m, 12 H), 2.06 (m, 25 H), 2.19 (m, 26 H), 2.30 (m, 18 H), 2.65 (m, 22 H), 2.81 (m, 16 H), 3.08 (m, 48 H), 3.18 (m, 22 H), 3.33 (m, 86 H), 3.38 (m, 20 H), 3.49 (m, 56 H), 3.58 (m, 24 H), 4.13 (m, 16 H), 4.31 (m, 16 H), 6.38 (d, 24 H), 6.53 (m, 16 H), 7.84 (m, 45 H), 10.12 (m, 13 H). <sup>13</sup>C NMR (176 MHz, DMSO-*d*6) δ 25.7, 28.4, 28.6, 33.6, 35.5, 36.5, 37.3, 38.7, 38.9, 49.9, 52.6, 55.8, 59.6, 61.5, 67.2, 69.6, 61.5, 67.2, 69.6, 69.9, 70.0, 70.1, 70.3, 163.2, 170.7, 171.6, 172.0, 172.6. MALDI-TOF-MS [M+H]<sup>+</sup> for C<sub>498</sub>H<sub>849</sub>N<sub>116</sub>O<sub>137</sub>S<sub>18</sub><sup>+</sup>, calcd. 11230.0170, found broad peak within this range.

### 2,5-Dioxopyrrolidin-1-yl pent-4-ynoate (5-63)

To a 25 mL round bottomed flask was added 4-pentynoic acid (500 mg, 5.1 mmol), 1.2 eq NHS (703 mg, 6.1 mmol), and 1.2 eq EDC HCl salt (1.16 g, 6.1 mmol) dissolved in 0.4 M CH<sub>2</sub>Cl<sub>2</sub> (12 mL). The resulting solution was allowed to stir under room temperature for 14 hours. The reaction was monitored *via* TLC. Upon completion, the resulting solution was concentrated to remove solvent and purified *via* column chromatography on silica gel with increasing amounts of eluent (hexane:ethyl acetate) to yield **5-63** (830 mg, 4.2 mmol) as white crystal in 83 % yield. M.P. 71-73 °C. <sup>1</sup>H NMR (500 MHz, CDCl<sub>3</sub>) δ 2.07 (m, 1 H), 2.63 (m, 2 H), 2.87 (s, 4 H), 2.89 (m, 2 H). <sup>13</sup>C NMR (125 MHz, CDCl<sub>3</sub>) δ 14.1, 25.5, 30.3, 70.0, 80.8, 167.0, 168.9. HRMS (TOF) [M + H]<sup>+</sup> calcd. for C<sub>9</sub>H<sub>10</sub>NO<sub>4</sub><sup>+</sup> 196.0604, found 196.0621. (Δ = 8.7 ppm).

### G3 dendrimer functionalized with PEGylated alkyne (5-64)

To a 10 mL round bottomed flask was added generation 3 cystamine dendrimer-methanol solution (Dendritic Nanotechnologies Inc. Item # DNT-296, 10.1 % solid in methanol, MW: 7001 g/mol) (100 mg, 0.014 mmol). Then 2 eq (based on the primary amine of dendrimer surface) **5-63** (179 mg, 0.91 mmol) and 5 mL methanol were added and the resulting solution was stirred for 24 hours under room temperature. The crude product was directly injected and analyzed by LC-MS-TOF under two conditions: 1. Neutral condition: Jupiter-C18, 3μm, 300Å, 250x2mm, SolvA2-H<sub>2</sub>O+0.25% ammonium acetate, SolvB2-CH<sub>3</sub>CN, T=25°C; 0.35 mL/min; t=0-40', B2=25-40%; t=40-45', B2=40-95%; t=45-50', B2=95-96%; t=50-52', B2=96-25%; 2. Acidic condition: Jupiter-C18, 3μm, 300Å, 250x2mm, SolvA2-H<sub>2</sub>O+0.1% TFA, SolvB2-CH<sub>3</sub>CN+0.1% TFA, T=25°C; 0.35 mL/min; t=0-40', B2=25-40%; t=40-45', B2=40-95%; t=45-50', B2=95-96%; t=50-



52', B2=96-25%. LC/UV/MS-TOF  $t_R$  = 12.21 min.

## §5.10 Reference

- (1) European Science Foundation. European Science Foundation Forward Look on Nanomedicine. European Science Foundation <http://www.esf.org/publication/196/ESPB23.pdf> (2005).
- (2) Duncan, R. Polymer conjugates as anticancer nanomedicines. *Nat. Rev. Cancer* **2006**, *6*, 688-701.
- (3) Wicki, A.; Witzigmann, D.; Balasubramanian, V.; Huwyler, J. Nanomedicine in cancer therapy: Challenges, opportunities, and clinical applications. *J. Controlled Release* **2015**, *200*, 138-157.
- (4) Karve, S.; Werner, M. E.; Sukumar, R.; Cummings, N. D.; Copp, J. A.; Wang, E. C.; Li, C.; Sethi, M.; Chen, R. C.; Pacold, M. E.; Wang, A. Z. Revival of the abandoned therapeutic wortmannin by nanoparticle drug delivery. *Proc Natl Acad Sci* **2012**, *109*, 8230-8235.
- (5) Peer, D.; Karp, J. M.; Hong, S.; Farokhzad, O. C.; Margalit, R.; Langer, R. Nanocarriers as an emerging platform for cancer therapy. *Nat Nano* **2007**, *2*, 751-760.
- (6) Min, Y.; Caster, J. M.; Eblan, M. J.; Wang, A. Z. Clinical Translation of Nanomedicine. *Chem. Rev.* **2015**.
- (7) Trivedi, V. Dendrimer: polymer of 21st century. *IJPRBS* **2012**, *1*, 1-21.
- (8) Kannan, R. M.; Kannan, S.; Romero, R.; Navath, R. S.; Dai, H.; Menjoge, A. R.; **2012**, US20120003155 A1.
- (9) B.Pavan Kumar, I. S., B.Bhavya, Sravanthi.U, Sindhuri.M Dendrimer: a complete drug carrier. *IJPRR* **2011**, *1*, 25-39.
- (10) Prajapat R , S. B., Jain S , Bhandari. A Dendrimer: a polymer of 21st century. *WebmedCentral Pharmaceutical Sciences* **2010**, *1*, WMC00745.
- (11) Gillies, E. R.; Fréchet, J. M. J. Dendrimers and dendritic polymers in drug delivery. *Drug Discov Today*. **2005**, *10*, 35-43.
- (12) Maiti, P. K.; Çağın, T.; Wang, G.; Goddard, W. A. Structure of PAMAM Dendrimers: Generations 1 through 11. *Macromolecules* **2004**, *37*, 6236-6254.
- (13) Svenson, S.; Tomalia, D. A. Dendrimers in biomedical applications—reflections on the field. *Adv. Drug Del. Rev.* **2005**, *57*, 2106-2129.
- (14) Buhleier, E.; Wehner, W.; Vögtle, F. "Cascade"- and "Nonskid-Chain-like" Syntheses of Molecular Cavity Topologies. *Synthesis* **1978**, *2*, 155-158.
- (15) Tomalia, D. A.; Baker, H.; Dewald, J.; Hall, M.; Kallos, G.; Martin, S.; Roeck, J.; Ryder, J.; Smith, P. A New Class of Polymers: Starburst-Dendritic Macromolecules. *Polym. J.* **1985**, *17*, 117-132.
- (16) Majoros, I. J.; Thomas, T. P.; Mehta, C. B.; Baker, J. R. Poly(amidoamine) Dendrimer-Based Multifunctional Engineered Nanodevice for Cancer Therapy. *J. Med. Chem.* **2005**, *48*, 5892-5899.
- (17) Matsumura, Y.; Maeda, H. A New Concept for Macromolecular Therapeutics in Cancer Chemotherapy: Mechanism of Tumor-tropic Accumulation of Proteins and the Antitumor Agent Smancs. *Cancer Res.* **1986**, *46*, 6387-6392.
- (18) Noguchi, Y.; Wu, J.; Duncan, R.; Strohalm, J.; Ulbrich, K.; Akaike, T.; Maeda, H. Early Phase Tumor Accumulation of Macromolecules: A Great Difference in Clearance Rate between Tumor and Normal Tissues. *Jpn. J. Cancer Res.* **1998**, *89*, 307-314.
- (19) Ellis, L. M.; Liu, W.; Fan, F.; Reinmuth, N.; Shaheen, R. M.; Jung, Y. D.; Ahmad, S. Role of angiogenesis inhibitors in cancer treatment. *Oncology (Williston Park)* **2001**, *15*, 39-46.

- (20) Park, K. Polysaccharide-based near-infrared fluorescence nanoprobe for cancer diagnosis. *Quant Imaging Med Surg.* **2012**, *2*, 106-113.
- (21) Jansen, J. F. G. A.; de Brabander-van den Berg, E. M. M.; Meijer, E. W. Encapsulation of Guest Molecules into a Dendritic Box. *Science* **1994**, *266*, 1226-1229.
- (22) Hawker, C. J.; Wooley, K. L.; Frechet, J. M. J. Unimolecular micelles and globular amphiphiles: dendritic macromolecules as novel recyclable solubilization agents. *J. Chem. Soc., Perkin Trans. 1* **1993**, 1287-1297.
- (23) Islam, M. T.; Majoros, I. J.; Baker Jr, J. R. HPLC analysis of PAMAM dendrimer based multifunctional devices. *J. Chromatogr. B* **2005**, *822*, 21-26.
- (24) Thomas, T. P.; Majoros, I. J.; Kotlyar, A.; Kukowska-Latallo, J. F.; Bielinska, A.; Myc, A.; Baker, J. R. Targeting and Inhibition of Cell Growth by an Engineered Dendritic Nanodevice. *J. Med. Chem.* **2005**, *48*, 3729-3735.
- (25) Paleos, C. M.; Tsiourvas, D.; Sideratou, Z.; Tziveleka, L. Acid- and Salt-Triggered Multifunctional Poly(propylene imine) Dendrimer as a Prospective Drug Delivery System. *Biomacromolecules* **2004**, *5*, 524-529.
- (26) Malik, N.; Evagorou, E. G.; Duncan, R. Dendrimer-platinate: a novel approach to cancer chemotherapy. *Anticancer Drugs* **1999**, *10*, 767-776.
- (27) Tomalia, D. A.; Naylor, A. M.; Goddard, W. A. Starburst Dendrimers: Molecular-Level Control of Size, Shape, Surface Chemistry, Topology, and Flexibility from Atoms to Macroscopic Matter. *Angew. Chem. Int. Ed.* **1990**, *29*, 138-175.
- (28) Peterson, J.; Allikmaa, V.; Subbi, J.; Pehk, T.; Lopp, M. Structural deviations in poly(amidoamine) dendrimers: a MALDI-TOF MS analysis. *Eur. Polym. J.* **2003**, *39*, 33-42.
- (29) Mullen, D. G.; Fang, M.; Desai, A.; Baker, J. R.; Orr, B. G.; Banaszak Holl, M. M. A Quantitative Assessment of Nanoparticle-Ligand Distributions: Implications for Targeted Drug and Imaging Delivery in Dendrimer Conjugates. *ACS Nano* **2010**, *4*, 657-670.
- (30) Gaertner, H. F.; Cerini, F.; Kamath, A.; Rochat, A.-F. o.; Siegrist, C.-A.; Menin, L.; Hartley, O. Efficient Orthogonal Bioconjugation of Dendrimers for Synthesis of Bioactive Nanoparticles. *Bioconjugate Chem.* **2011**, *22*, 1103-1114.
- (31) Mezo, A. R.; Low, S. C.; Hoehn, T.; Palmieri, H. PEGylation enhances the therapeutic potential of peptide antagonists of the neonatal Fc receptor, FcRn. *Bioorg. Med. Chem. Lett.* **2011**, *21*, 6332-6335.
- (32) Goswami, L. N.; Houston, Z. H.; Sarma, S. J.; Jalisatgi, S. S.; Hawthorne, M. F. Efficient synthesis of diverse heterobifunctionalized clickable oligo(ethylene glycol) linkers: potential applications in bioconjugation and targeted drug delivery. *Org. Biomol. Chem.* **2013**, *11*, 1116-1126.
- (33) Carter, R. L.; Johnson, B. F.; Sood, A.; Rishel, M. J.; Valliant, J. F.; Stephenson, K. A.; Wu, T.; Yang, Y. **2013**, *US20130261311A1*, 20pp.
- (34) Prodhomme, E. J. F.; Tutt, A. L.; Glennie, M. J.; Bugg, T. D. H. Multivalent Conjugates of Poly- $\gamma$ -d-glutamic Acid from *Bacillus licheniformis* with Antibody F(ab') and Glycopeptide Ligands. *Bioconjugate Chem.* **2003**, *14*, 1148-1155.
- (35) Han, J.; Sun, L.; Chu, Y.; Li, Z.; Huang, D.; Zhu, X.; Qian, H.; Huang, W. Design, Synthesis, and Biological Activity of Novel Dicoumarol Glucagon-like Peptide 1 Conjugates. *J. Med. Chem.* **2013**, *56*, 9955-9968.
- (36) Chen, S.; Zhao, X.; Chen, J.; Chen, J.; Kuznetsova, L.; Wong, S. S.; Ojima, I. Mechanism-Based Tumor-Targeting Drug Delivery System. Validation of Efficient Vitamin Receptor-Mediated

Endocytosis and Drug Release. *Bioconjugate Chem.* **2010**, *21*, 979-987.

(37) Goussé, C.; Gandini, A. Diels–Alder polymerization of difurans with bismaleimides. *Polym. Int.* **1999**, *48*, 723-731.

(38) Bradshaw, C. W.; Doppalapudi, V. R.; Lai, J.-Y.; Rizzo, J. **2006**, *WO2006094269A2*, 299pp.

(39) Bradshaw, C.; Sakamuri, S.; Fu, Y.; Oates, B.; Desharnais, J.; Tumelty, D. **2008**, *WO2008081418A1*, 227 pp.

(40) Carter, R. L.; Johnson, B. F.; Sood, A.; Rishel, M. J.; Valliant, J. F.; Stephenson, K. A.; Wu, T.; Yang, Y. **2013**, *US20130261311A1*, 20pp.; Chemical Indexing Equivalent to 159:577037 (WO).

## Chapter 6

### Hyaluronic Acid-Linker-Taxoid (HALT) Conjugate for Targeting Cancer Stem Cell

§6.1 Introduction-Cancer Stem Cell and Hyaluronic Acid .....	211
§6.2 Synthesis and Biological Evaluations.....	212
§6.2.1 Synthesis of Hyaluronic Acid-Linker-Taxoid (HALT) Conjugate .....	212
§6.2.2 Expression of Biotin Receptor and HA Receptor on CSC Surface .....	213
§6.2.3 Cytotoxicity Assay of Biotin-Linker-Taxoid against CSC .....	215
§6.3 Summary.....	217
§6.4 Experimental Section.....	217
§6.4.1 Caution.....	217
§6.4.2 General Information.....	217
§6.4.3 Materials.....	219
§6.4.4 Experimental Procedure.....	219
§6.5 References.....	220

## §6.1 Introduction-Cancer Stem Cell and Hyaluronic Acid

Current anti-cancer drug development makes a slow progress due to the existence of a rare, highly drug resistant, slow proliferating cell and tumor-driving cell population called cancer initiate cells (CICs) or cancer stem cells (CSCs).<sup>1</sup> After initial discovery and isolation of cancer stem cells, it was evident that the CSCs are responsible for tumor sustaining, recurrence, metastasis and resistance to treatment.<sup>1</sup> Although there was no conclusive statement on definition of universal or highly specific cell surface markers for CSCs, several markers were successfully used for prospective isolation of the tumor-initiating cells from diverse tumor type, including CD166, Musashi-1, CD29, CD24, leucine-rich repeat-containing G-protein-coupled receptor 5 (Lgr5), CD133 (also known as AC133 and prominin-1), and CD44 receptor.<sup>2</sup> Among these markers, CD133 is a cell-surface glycoprotein comprising five trans-membrane domains and two large glycosylated extracellular loops, and is found enriched in many types of CSCs, including cancer stem cells in brain, kidney, liver, colon and pancreatic carcinomas.<sup>1</sup> Another commonly used marker for CSCs is CD44. As a cell surface adhesion molecule, CD44 gets involved in cell-cell and cell-matrix interactions, stemness and tumour development.<sup>2</sup> And recently more and more experimental results indicated that the combination of different CSC markers can lead to better enrichment of cells with either exclusive or highly increased tumorigenicity compared to their bulk counterparts.<sup>2</sup>

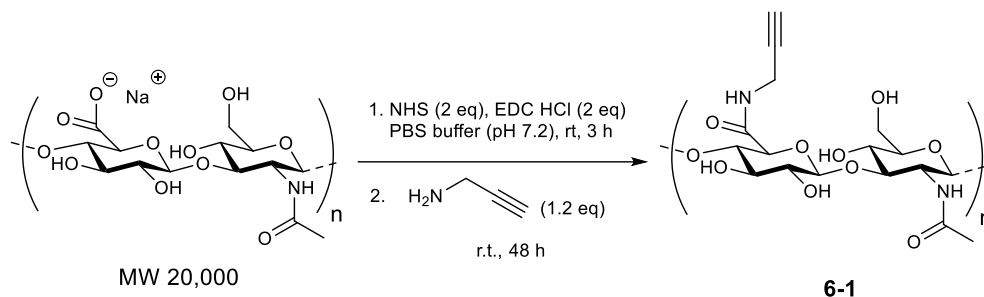
Besides the biotin discussed in previous chapter, hyaluronic acid or hyaluronan (HA) also represents great promise as a tumor-targeting moiety for cancer stem cell-targeted drug delivery. As a water-soluble polysaccharide, HA is commonly found in the extracellular tissue matrix of vertebrates, such as connective tissue,<sup>3-4</sup> and it plays a significant role in cell proliferation and participates in a number of cell surface receptor interactions. HA usually contains a single polysaccharide chain without peptide. The polysaccharide chain has repeating units, and functional groups such as hydroxyl and carboxyl groups. Its molecular weight can reach  $10^5$ - $10^7$ ,<sup>3</sup> for example, in normal synovial fluid, the weight-average is around  $7 \times 10^6$ , which would extend 15  $\mu\text{m}$  if straightened.<sup>3</sup> It has been reported that HA-based nanoparticles showed prolonged circulation and high accumulation in tumor tissue, based on their efficient penetration through vasculature in angiogenic tumor site with not well-established lymphatic drainage system, also called enhanced permeation and retention (EPR) effect.<sup>5</sup> This makes HA available for a good macromolecular vehicle or platform for tumor-targeted drug delivery towards CSCs. Numerous studies have demonstrated that the ratio of CD133<sup>+</sup> and CD44<sup>+</sup> cells correlates with tumor aggressiveness, histologic grade and clinical outcome,<sup>6-9</sup> however, both CD133<sup>+</sup> and CD44<sup>+</sup> CSCs are highly drug resistant due to multiple mechanisms, including their relative quiescence, profound capacity for DNA repair, activation of the ATP-binding cassette (ABC) transporters, resistance to apoptosis and others.<sup>10-12</sup> To achieve the optimized effectiveness, the anti-cancer drug conjugate must be specifically targeted toward CSCs, not only to bulk tumor cells.<sup>1</sup> Accordingly, HA can serve as a CSC-targeting moiety based on its affinity with CD44 marker, as well as a macromolecular platform which can be used to afford multiple anti-cancer drugs, such as highly potent newer generation taxoid. As it was mentioned in previous chapter, the taxoid will be connected through a self-immolative disulfide bond with HA scaffold to ensure the drug release will only occur inside the CSC after the HA conjugate get internalized to avoid systemic cytotoxicity. This hyaluronic acid-linker-taxoid (HALT) conjugate can be described as a “Trojan horse” type drug conjugate. For each HA single chain, it is readily to increase the drug-linker

payload and release them only inside the CSCs after the triggered linker cleavage. This novel CSC-targeted drug delivery system will focus on circumventing multi-drug resistance (MDR) and eliminating cancer relapse.

## §6.2 Synthesis and Biological Evaluation

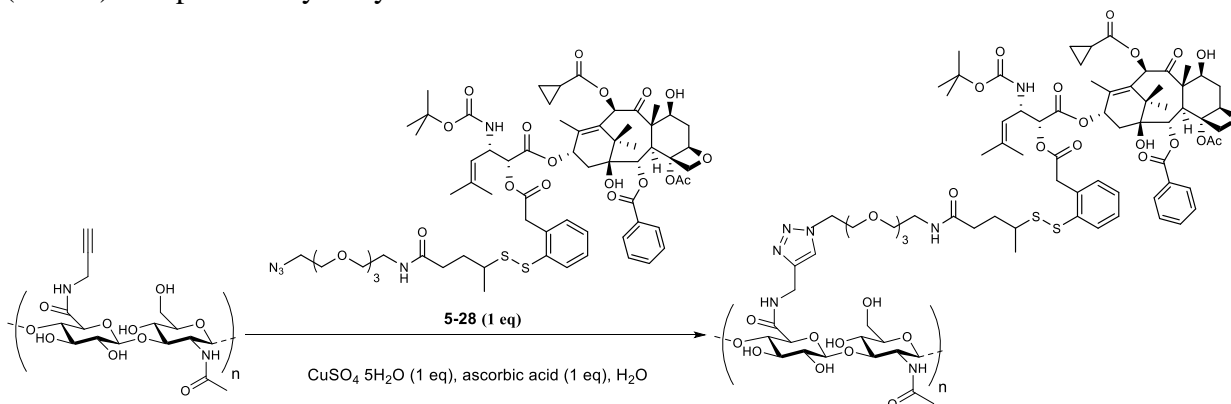
### §6.2.1 Synthesis of Hyaluronic Acid-Linker-Taxoid (HALT) Conjugate

To synthesize this CSC-targeted prodrug, a mechanism-based “smart” disulfide linker connected with a cytotoxic warhead (SB-T-1214) was previously synthesized and conjugated with HA under a copper-catalyzed azide-alkyne [3+2] click condition. The carboxylic groups of HA were firstly converted to alkyne by reacting with propargylamine. The reaction of the hyaluronic acid sodium salt with excess NHS in the presence of excess EDC-HCl salt converted the carboxylic acid into its activated OSu ester. Subsequently, excess propargylamine allowed a terminal acetylene to be installed on HA through amide bond formation to create a click-ready product (**Scheme 6.1**).



**Scheme 6.1** Synthesis of HA-alkyne intermediate

Then, through copper-catalyzed azide-alkyne [3+2] cycloaddition, the purified click-ready HA-alkyne was coupled with SB-T-1214-(PEG)<sub>3</sub>-linker-azide (**5-28**) in the presence of copper sulfate pentahydrate and ascorbic acid (**Scheme 6.2**). The resulting hyaluronic acid-linker-taxoid (HALT) was purified by dialysis membrane and characterized.



**Scheme 6.2** Synthesis of HALT through click chemistry

In the future, modification using propargylamine for COOH group of HA will be controlled to only 10% since the free COOH groups play a critical role in promoting mucoadhesive properties

through hydrogen bonds formation with components of the biological substrate.<sup>13</sup> Conversion of all COOH groups may hamper the affinity between the HA and its receptor on cancer stem cells.

### §6.2.2 Expression of Biotin Receptor and HA Receptor on CSC Surface

Two fluorescent probes were used for flow cytometry and confocal microscopy studies against cancer stem cell lines. Biotin-PEG<sub>3</sub>-FITC was previously synthesized by directly reacting biotin-PEG<sub>3</sub>-NH<sub>2</sub> with FITC. Another fluorescent probe HA-FITC was purchased from Sigma Aldrich and the payload of FITC on HA is around 5 mol%. (**Figure 6.1**)

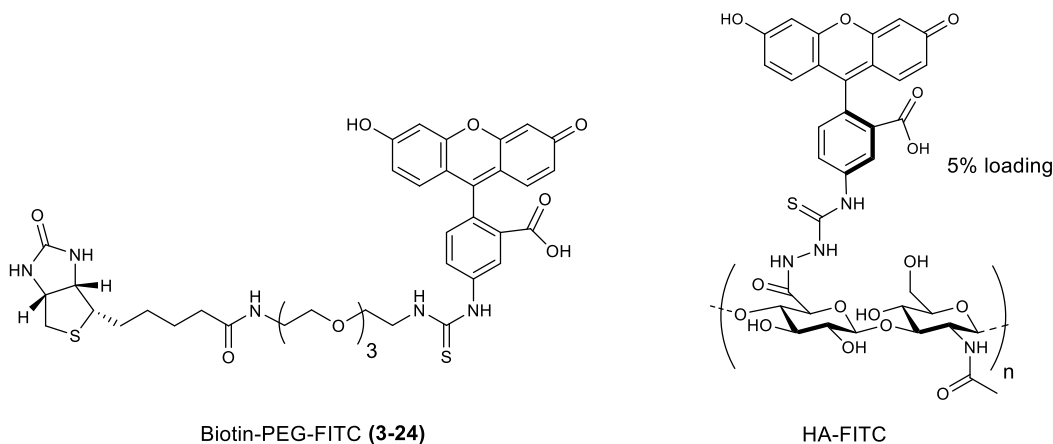


**Figure 6.1** Structures of two fluorescent probes

Receptor-mediated endocytosis of biotin into CSCs was confirmed by means of confocal microscopy and flow cytometry. Juxtaposed against the >99% negative control for PPT2 primary prostate CSCs and HCT116 colon cancer spheroids (**Figure 6.2**), the 96% (20,000/20,837 signal intensity in PPT2) and 82% (9,271/10,125 signal intensity in HCT116) overexpression of biotin receptors was displayed by a significant right shift in the FACS graph. Biotin receptors are overexpressed on nearly all CSCs and spheroids, and a prodrug conjugate utilizing biotin as a TTM is capable of undergoing RME to infiltrate the cell. Furthermore, analysis of CD133 and CD44 receptors revealed the discovery of their CD133<sup>++</sup>/CD44<sup>+++</sup> expression on the particular cell surfaces of PPT2 CSCs and HCT116 spheroids. 67% (8319/10,000 signal intensity for HCT116) and 70% (20,000/20,869 signal intensity for PPT2) CD133<sup>++</sup>/CD44<sup>+++</sup> coexpression was quantified. The immunofluorescent merge qualitatively indicated colocalization of CSC biomarkers, not only with each other, but also with biotin, on the cell surfaces of PPT2 and HCT116 (**Figure 6.2**). Thus, the CSC and spheroid cell lines were identified to contain populations overexpressing the putative CD133<sup>++</sup>/CD44<sup>+++</sup> stem-like cell surface markers.

There appear to be two populations of cells sorted by flow cytometry, indicating slightly different microenvironments within stem-like 3-D spheroids and CSCs. Furthermore, there was 65% biotin binding to CD133, as opposed to 99% Biotin<sup>++</sup>/CD44<sup>++</sup> coexpression in PPT2 (**Table 6.1**). Meanwhile, nearly a third of the cancer-initiating cells were negative for CD133 and CD44, indicating the lack of stem-like ability in what may be progenitor cells programmed to differentiate and proliferate as mature prostate and colon cancer cells.<sup>14</sup> Taken together, the data indicate both cell lines' potential for intratumoral heterogeneity.<sup>15</sup> This study is the first to strongly demonstrate

biotin's ability to overcome such intratumoral heterogeneity by binding to its uniformly overexpressed receptors and undergoing RME in both cancer cells and CSCs. Accordingly, this study indicates the high potential of a biotin-linked prodrug as a successful CSC-targeted drug delivery system.

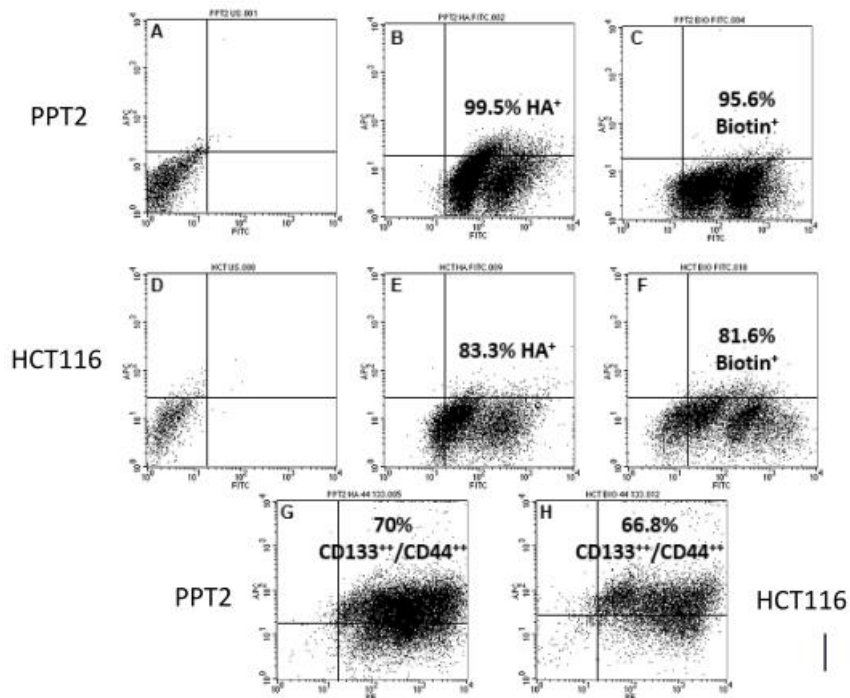


**Figure 6.2** Flow cytometry analysis of different receptors in prostate (PPT2) CSCs and colon (HCT116) spheroids Structures of two fluorescent probes. (A, D) PPT2 and HCT116 unstained; (B, C, E, F) Uniform expression of HA and Biotin-PEG-FITC (3-24) in PPT2 and HCT116; (G, H) Coexpression of CSC biomarkers CD44 and CD133

**Table 6.1** Summary of biotin and hyaluronic acid binding to TTM receptors, CD133, and CD44 receptors in PPT2 and HCT116, as shown by flow cytometry

	Unstained (control)	Biotin <sup>++</sup>	HA <sup>++</sup>	Biotin <sup>++</sup> /CD133 <sup>++</sup>	Biotin <sup>++</sup> /CD44 <sup>++</sup>	HA <sup>++</sup> /CD133 <sup>++</sup>	HA <sup>++</sup> /CD44 <sup>++</sup>	CD133 <sup>++</sup> /CD44 <sup>++</sup>
<b>PPT2</b>	>99%	96%	99%	65%	97%	72%	99%	70%
<b>HCT116</b>	>99%	82%	83%	62%	58%	67%	75%	67%

Additionally, it is implicated that extruded hyaluronic acid interacts multivalently with CD44 in CSCs to induce signaling domains, which drive oncogenic pathways such as the MAP kinase and PI3 kinase and enrich multidrug transporters such as P-gp.<sup>16,17</sup> Previously, it was unclear whether HA would be capable of binding to its CD44 receptors and specific hyaluronic acid receptor for endocytosis (HARE) in cell lines studied.<sup>18</sup> This report demonstrates the lack of competition between HA receptors and CD44 mAbs for their respective receptors, as indicated by 99% of PPT2 CSCs and 75% HCT116 spheroids binding to both HA and CD44, and their colocalization as depicted by CFM (**Figure 6.3**). The aforementioned visual and quantified data indicate the presence of mature cancer cells and intratumor heterogeneity in the given CSC



types.<sup>14-15</sup> This study demonstrates that a prodrug conjugate utilizing HA as a TTM is capable of directly targeting both CD44 and HARE, allowing for cancer cell specificity, CSC-selectivity, and circumvention of P-gp<sup>+</sup>-mediated multidrug resistance.

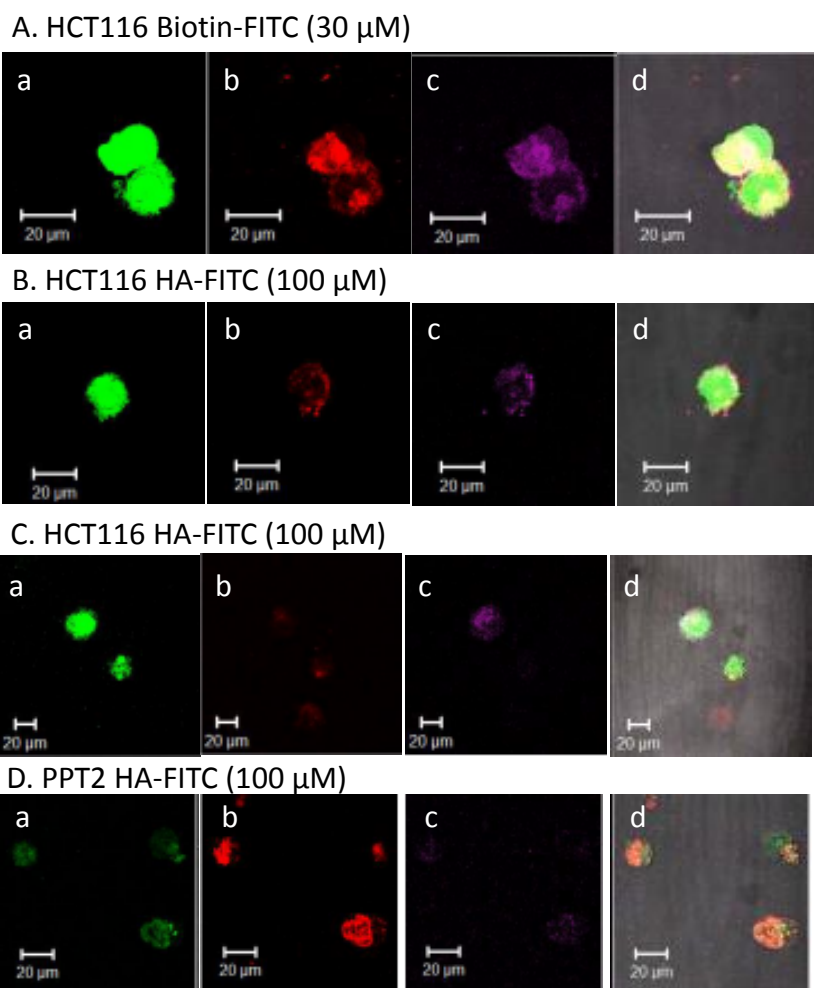
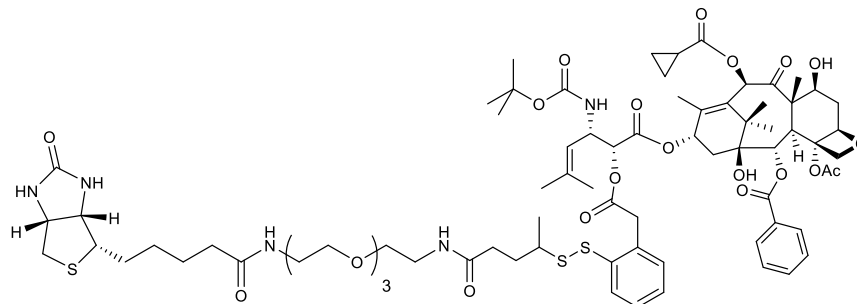


**Figure 6.3** Colocalization of receptors depicted by confocal microscopy. (A) HCT116 cells with Biotin FITC, (B) HCT116 stained with HA-FITC, (C) PPT2 stained for Biotin-FITC, (D) PPT2 stained for HA-FITC. (a) high expression of either TTM, Biotin or HA, (b) CD133-APC, (c) CD44-PE, (d) Colocalization of TTM, CD133, and CD44 receptors

### §6.2.3 Cytotoxicity Assay of Biotin-Linker-Taxoid against CSC

BLT-S (**3-25**) is composed of biotin as its TTM, a self-immolative disulfide linker, a PEG spacer, and the second-generation taxoid SB-T-1214, which was synthesized previously (**Figure 6.4**).<sup>19</sup>



3-23 (BLT-S)

**Figure 6.4** Chemical structure of BLT-S (3-25)

In this study, the FDA-approved drug paclitaxel induced apoptosis of 50% PPT2 CSCs (41.9 nM), while in previous studies paclitaxel was effective against L1210FR (biotin receptor<sup>++</sup>), L1210, and WI38 only at high concentrations above 100 nM (**Table 6.2**). The results indicate that paclitaxel would induce more widespread systemic toxicity when administered to cancer patients. Meanwhile, the free drug SB-T-1214 was over 7 times more effective against PPT2 CSCs, with an IC<sub>50</sub> value of only 5.77 nM, and SB-T-1214 demonstrated a similarly high level of efficacy against both leukemia cell lines. These data reveal SB-T-1214's release and cytotoxicity. Furthermore, SB-T-1214 is reported to surpass FDA-approved drugs such as paclitaxel and docetaxel by exhibiting efficacy and potency against multidrug resistant Pgp<sup>+</sup> human breast carcinoma cell lines.<sup>21</sup> Against colon cancer cell lines, it efficiently inhibited the expression of a majority of stem cell-related genes, including several key regulators of pluripotency and self-renewal of embryonic stem cells.<sup>22</sup> Despite these promising results, SB-T-1214 was an entire order of magnitude more cytotoxic than paclitaxel against healthy lung fibroblasts, thus revealing its inability to distinguish between cancerous and non-carcinogenic cells. These data indicate the necessity of using a more selective drug delivery method.

**Table 6.2** Cytotoxicities (IC<sub>50</sub>, nM) of paclitaxel, SB-T-1214, and BLT-S against various cell lines (WI38 lung fibroblast are negative for biotin) New cytotoxicities ascertained for PPT2 and HCT116 CSC lines, determined by MTT assays on cell viability

Drug/Drug Conjugate	PPT2	HCT116	WI38
Paclitaxel	41.9 ± 4.85	41.3 ± 9.83	157
SB-T-1214	5.77 ± 1.36	41.1 ± 7.46	10.7
BLT-S	3.07 ± 1.93	8.02 ± 3.88	570

In contrast to the MTT assay results with paclitaxel and SB-T-1214, BLT-S was discovered to be efficaciously potent against PPT2 CSCs and HCT116 spheroids. In this study, paclitaxel and SB-T-1214 exhibited nearly identical cytotoxicity levels (41 nM) against HCT116, suggesting that both drugs met with exceptionally high Pgp<sup>+</sup>-mediated resistance in addition resistance mediated by aberrant signaling interactions. On the other hand, compared to paclitaxel and SB-T-1214, BLT-S exhibits high efficiency against HCT116 with a lower IC<sub>50</sub> value (8 nM). This data is supplemented by BLT-S' IC<sub>50</sub> values against PPT2 (3.07 nM) and L1210FR (8.8 nM), both >13 times more sensitive. As such, BLT-S demonstrates its ability to overcome various mechanisms of resistance by selectively targeting not only cancer cells, but also CSCs. However, against L1210

(leukemia) and WI38 (lung fibroblast), both of which are negative for biotin receptor overexpression, BLT-S was two orders of magnitude less potent, requiring 59 and 65 times higher drug concentration to perform at the same level of efficacy. BLT-S therefore has selectivity based on its receptors' overexpression on cancer cells. Furthermore, new data indicate that BLT-S is even more efficient against the resistant CSCs. As such, this study presents BLT-S for consideration as a highly effective and potent as a new generation CSC-targeted drug delivery system.

### §6.3 Summary

HA can serve as a CSC-targeting moiety based on its affinity with CD44 marker which is biomarker of MDR cancer cells, as well as a macromolecular platform which can be used to afford multiple anti-cancer drugs. This type of HA-based conjugate will selectively accumulate in the tumor site with prolonged retention time due to EPR effect. To conceptually prove HALT type conjugate, HA-FITC probes as well as a biotin bearing fluorescent probe, were evaluated by confocal fluorescein microscopy and flow cytometry to visualize the internalization and enhanced uptake of HA, and the coexpression of HA receptor and biotin receptor on the surface of selected cancer stem cell. The modified synthetic route toward HALT is being developed and currently underway.

### §6.4 Experimental Sections

#### §6.4.1 Caution

Taxoids have been classified as potent cytotoxic agents. Thus, all drugs and structurally related compounds and derivatives must be considered as mutagens and potential reproductive hazards for both males and females. Appropriate precautions (i.e. use of gloves, goggles, lab coat and fume hood) must be taken while handling these compounds.

#### §6.4.2 General Methods

$^1\text{H}$  NMR and  $^{13}\text{C}$  NMR were measured on a Bruker 500 MHz or 700 MHz NMR spectrometer. Matrix-assisted laser desorption/ionization (MALDI)-TOF analysis for determination of the molecular weight of the HA-alkyne intermediate was facilitated by ICB&DD. LC-TOF analysis for determination of the molecular weight was facilitated by ICB&DD, using Kinetex C18 analytical column with 2.6  $\mu\text{m}$ , 100 A, 2.1x100 mm. Solvent A was 0.1% Ac-0.02% TFA and solvent B was  $\text{CH}_3\text{CN}$ . Running temperature was 35  $^\circ\text{C}$ ; flow rate was 0.5 mL/min.

#### Cell Culturing

Primary prostate (PPT2) CSC-enriched cell line was cultured *in vitro* on type-I collagen-coated dishes (Biocoat; Becton Dickenson, Bedford, MA) in Stemline Pluripotent Basal Medium (SPCM; Sigma-Aldrich); the colon (HCT116) cancer cells were cultured in Dulbecco's Modified Eagle's Medium (Gibco, USA) containing 10% fetal bovine serum (Gibco, USA) and 1% penicillin streptomycin (Invitrogen, Grand Island, NY, USA), respectively. Additionally, 3D floating spheroids were induced by HCT116 and serially propagated with Mesenchymal Stem Cell Basal

Media (Lonza) in ) the Ultra-Low Attachment (ULA) 6-well plate (Corning, Lowell, MA) in serum-free MSCB medium (Lonza) or Stemline Pluripotent Stem Cell Culture media (SPCM; Sigma) containing 5-15% of type I collagen gel. Both cell lines were cultured and maintained at 37.5 °C in a humidified atmosphere (5% CO<sub>2</sub>).

### **Quantitative Analysis: Flow Cytometry (FACS)**

PPT2 and HCT116 CSCs were dissociated and split into a 24-well ultra low attachment plate (Corning, Lowell, MA). PPT2 cells (330 uL) were added to 7 wells (P1-P7), 340 uL of HCT116 cells were added to an additional 7 wells (H1-H7). HA-FITC (Sigma-Aldrich) (1 uM, 40 uL) was added to P2 and H2. Previously prepared Biotin-(PEG)<sub>3</sub>-FITC (30 uM, 12 uL) were added to P3 and H3 (**Fig. 2**). Blocking Reagent (Miltenyi Biotec) (15 uL), 15 uL of anti-human CD133/2-APC (clone 293C3; Miltenyi Biotec, CA, USA), 11 uL of CD44-PE (clone F10-44-2; Invitrogen/Biosources, USA), and the same amount of HA-FITC was added to P4 and H4. The same amounts of CD133-APC mAb, CD44-PE mAb, and Biotin-(PEG)<sub>3</sub>-FITC were added to P5 and H5. CD133-APC mAb and HA-FITC were added to P6 and H6. CD133-APC and Biotin-(PEG)<sub>3</sub>-FITC were added to P7 and H7. After incubation with the fluorescent probes for 24 hours, the cells were transferred to 15 mL tubes, with 400 uL of 1% formalin added to each. Stained cells were sorted and analyzed with FACSCalibur, and at least 10,000 cells were counted for each experiment using CellQuest 3.3 software (Becton Dickinson, CA).

### **Qualitative Analysis: Confocal Fluorescence Microscopy**

PPT2 and HCT116 CSCs were cultured on collagen-I coated glass microslides, encased by sterile Petri dishes for incubation. 24 hours later, 10 uL Blocking Reagent, 10 uL CD133-APC, 10 uL CD44-PE were added to two PPT2 slides, while 12 uL Biotin-(PEG)<sub>3</sub>-FITC (30 uM) and 20 uL HA-FITC (1 uM) were split into distinct slides. The procedure was repeated for HCT116. Following 24-hour incubation with fluorescent probes, cells were fixed with ~400-500 uL 1% formalin, transferred to vials, then centrifuged for 3 min at 2000 rpm. Cells were washed with 500 uL HPLC H<sub>2</sub>O, centrifuged again, then maintained in 100 uL HPLC H<sub>2</sub>O. For CFM, fixed cells were dropped onto a uncoated microslide with a coverslip. The CFM instrument used includes the Zeiss LSM 510 META NLO two-photon laser scanning confocal microscope system, operating at a 488 nm excitation wavelength and at 527 ± 23 nm detecting emission wavelength using a 505–550 nm bandpass filter. Images were captured using a C-Apochromat 63x/1.2 water objective.

### **MTT Cell Proliferation Assay**

Cells were cultured until confluent and counted with a hemacytometer using 10 uL of a solution 10 uL cells, and 10 uL TrypanBlue (Gibco, USA) stain. 10 million cells were split into each 96-well-plate in DMEM, treated at 70% confluency, and incubated for 48 hours. The 96-well-plate treatment scheme was divided into four 4X6 sections, allowing for drug treatment of Paclitaxel, SB-T-1214, BLT-S, and one repeat. Paclitaxel, SB-T-1214, and BLT-S were prepared in DMEM at 5 uM, 500 nM, 50 nM, 5 nM, and 500 pM through serial dilution from a 1 mM stock solution. 200 uL of each drug was administered to each well, while the sixth and seventh well columns served as controls containing 200 uL DMEM. Post-treatment, media was aspirated and cells were incubated for 3 hours with 50uL/well of a 1mg/2mL solution of MTT, or 3-(4, 5-

dimethylthiazolyl-2)-2, 5-diphenyltetrazolium bromide, after which 50 uL/well of HCl was added. Absorbance was recorded at 570 nM using a Labsystems Multiskan Ascent microplate reader. IC<sub>50</sub> values were calculated from the viability–concentration curve using the Four Parameter Logistic Model of SigmaPlot.

### §6.4.3 Materials

The chemicals were purchased from Sigma Aldrich Company, Fischer Company or Acros Organic Company. Hyaluronic acid (20K) sodium salt was purchased from Lifecore Biomedical in Chaska, Minnesota. Hyaluronic acid-FITC (5mol% loading) was purchased from Sigma Aldrich. Dry DMF was purchased from EMD chemical company, and used without further purification. Reaction flasks were dried in a 100 °C oven and allowed to cool to room temperature in a desiccator over “Drierite” (calcium sulfate) and assembled under an inert nitrogen gas atmosphere.

### §6.4.4 Experimental Procedure

#### HA-Alkyne Intermediate (6-1)

To generate the HA-alkyne construct, 50 mg hyaluronic acid sodium salt (MW~20,000 g/mol, Lifecore Biomedical) were dissolved in 5 mL PBS buffer (pH = 7.2), 2 equivalents of *N*-hydroxysuccinimide (NHS) were added, followed by the addition of 2 equivalents of 1-ethyl-3-(3-dimethylaminopropyl)carbodiimide (EDC) HCl salt. This step was allowed to run under room temperature for 3 hours, then 1.2 equivalent propargylamine was added and the reaction was allowed to run for 48 hours to generate the product. Purification was done by dialysis using molecular weight cut-off (MWCO 3500~4000, Fisher brand) dialysis tubing membrane against distilled water for 48 hours. Upon completion, the resulting solution was lyophilized *in vacuo* to yield a 73 mg product **6-1** as a cotton-like white solid: <sup>1</sup>H NMR (700 MHz, D<sub>2</sub>O) δ 1.94 (s, 6 H), 2.80 (s, 1 H), 2.82 (t, *J* = 13.1 Hz, 1 H), 3.26 (m, 3 H), 3.40-3.44 (m, 6 H), 3.50 (m, 3 H), 3.67 (m, 8 H), 3.75 (d, *J* = 2.55 Hz, 2 H), 3.81-3.83 (m, 2 H), 4.39 (s, 2 H), 4.47 (s, 2 H). <sup>13</sup>C NMR (176 MHz, D<sub>2</sub>O) δ 14.3, 22.4, 24.9, 28.9, 34.9, 36.3, 42.6, 54.2, 55.3, 60.4, 68.3, 72.4, 73.6, 74.7, 75.3, 76.4, 79.9, 82.5, 100.5, 103.1, 173.2, 174.9.

#### HALT (HA-Linker-Taxoid) Conjugate (6-2)

Then, through “click chemistry” or copper(I)-catalyzed azide-alkyne [3+2] cycloaddition (CuAAC), HA-alkyne was conjugated to taxoid-linker-(PEG)<sub>3</sub>-azide. In the presence of ascorbic acid, Cu(II) was reduced to Cu(I). The reactive alkyne formed a copper acetylide, followed by the azide displacing a ligand and binding to copper. To a round bottom flask, 20 mg HA-alkyne (**6-1**), 1 equivalent previously made SB-T-1214-linker-PEG<sub>3</sub>-azide (**5-28**) (1.3 mg), 1 equivalent copper sulfate pentahydrate (0.24 mg), and 1 equivalent ascorbic acid (0.17 mg) were added. The flask was sealed and 1 mL distilled water was added to the flask. The resulting solution was allowed to stir under room temperature for 22 hours. Upon completion, the crude product was purified by molecular weight cut-off dialysis tubing membrane for 24 hours and the resulting solution was lyophilized *in vacuo* to yield the desired HALT product **6-2** as a 10 mg white solid: <sup>1</sup>H NMR (700 MHz, D<sub>2</sub>O) δ 0.95 (m, 1 H), 1.01 (s, 1 H), 1.12 (m, 1 H), 1.30 (s, 2 H), 1.47 (s, 1

H), 1.56 (s, 1 H), 1.64 (m, 1 H), 1.73 (s, 1 H), 1.83 (broad, 3 H), 2.25 (s, 1 H), 2.72 (s, 1 H), 2.97 (m, 1 H), 3.24 (m, 3 H), 3.38 (m, 1 H), 3.50 (m, 3 H), 3.65 (m, 2 H), 3.92 (m, 1 H), 5.45 (d,  $J = 7.7$  Hz, 1 H), 5.95 (s, 1 H), 6.27 (s, 1 H), 6.95 (m, 1 H), 7.21 (m, 1 H), 7.31 (m, 1 H), 7.45 (t,  $J = 8.05$  Hz, 1 H), 7.59 (t,  $J = 7.1$  Hz, 1 H), 7.69 (d,  $J = 7.5$  Hz, 1 H), 7.80 (m, 1 H), 7.96 (d,  $J = 8.3$  Hz, 1 H).  $^{13}\text{C}$  NMR (176 MHz,  $\text{D}_2\text{O}$ )  $\delta$  0.64, 0.71, 13.3, 14.3, 22.4, 23.6, 24.9, 28.9, 29.3, 34.9, 35.1, 35.2, 35.7, 35.9, 36.3, 38.1, 42.6, 42.7, 48.8, 54.2, 54.9, 55.3, 60.4, 68.3, 71.3, 72.3, 72.6, 73.6, 74.7, 75.3, 76.4, 79.9, 82.5, 100.6, 103.2, 160.5, 171.8, 173.8, 174.9.

## §6.5 References

- (1) Galina I Botchkina, E. S. Z., Manisha Das, Yuan Wang, Haichao Wang, Shu Zhu, Anne G Savitt, Rebecca A Rowehl, Yan Leyfman, Jingfang Ju, Kenneth Shroyer and Iwao Ojima New-generation taxoid SB-T-1214 inhibits stem cell-related gene expression in 3D cancer spheroids induced by purified colon tumor-initiating cells. *Mol. Cancer* **2010**, *9*, 192.
- (2) Galina Botchkina, I. O.; InTech, Prostate and Colon Cancer Stem Cells as a Target for Anti-Cancer Drug Development. *Cancer Stem Cells Theories and Practice*, Chapter 8. 2011.
- (3) Fraser, J. R. E.; Laurent, T. C.; Laurent, U. B. G. Hyaluronan: its nature, distribution, functions and turnover. *J. Intern. Med.* **1997**, *242*, 27-33.
- (4) Lim, S. T.; Martin, G. P.; Berry, D. J.; Brown, M. B. Preparation and evaluation of the in vitro drug release properties and mucoadhesion of novel microspheres of hyaluronic acid and chitosan. *J. Controlled Release* **2000**, *66*, 281-292.
- (5) Yoon, H. Y.; Koo, H.; Choi, K. Y.; Chan Kwon, I.; Choi, K.; Park, J. H.; Kim, K. Photocrosslinked hyaluronic acid nanoparticles with improved stability for in vivo tumor-targeted drug delivery. *Biomaterials* **2013**, *34*, 5273-5280.
- (6) Al-Hajj, M.; Wicha, M. S.; Benito-Hernandez, A.; Morrison, S. J.; Clarke, M. F. Prospective identification of tumorigenic breast cancer cells. *Proc. Natl. Acad. Sci.* **2003**, *100*, 3983-3988.
- (7) Zeppernick, F.; Ahmadi, R.; Campos, B.; Dictus, C.; Helmke, B. M.; Becker, N.; Lichter, P.; Unterberg, A.; Radlwimmer, B.; Herold-Mende, C. C. Stem Cell Marker CD133 Affects Clinical Outcome in Glioma Patients. *Clin. Cancer Res.* **2008**, *14*, 123-129.
- (8) Maeda, S.; Shinchi, H.; Kurahara, H.; Mataka, Y.; Maemura, K.; Sato, M.; Natsugoe, S.; Aikou, T.; Takao, S. CD133 expression is correlated with lymph node metastasis and vascular endothelial growth factor-C expression in pancreatic cancer. *Br. J. Cancer* **2008**, *98*, 1389-1397.
- (9) Horst, D.; Kriegl, L.; Engel, J.; Kirchner, T.; Jung, A. CD133 expression is an independent prognostic marker for low survival in colorectal cancer. *Br. J. Cancer* **2008**, *99*, 1285-1289.
- (10) Dean, M.; Fojo, T.; Bates, S. Tumour stem cells and drug resistance. *Nat. Rev. Cancer* **2005**, *5*, 275-284.
- (11) Donnenberg, V. S.; Donnenberg, A. D. Multiple Drug Resistance in Cancer Revisited: The Cancer Stem Cell Hypothesis. *J. Clin. Pharmacol.* **2005**, *45*, 872-877.
- (12) Mimeault, M.; Batra, S. K. Recent progress on normal and malignant pancreatic stem/progenitor cell research: therapeutic implications for the treatment of type 1 or 2 diabetes mellitus and aggressive pancreatic cancer. *Gut* **2008**, *57*, 1456-1468.
- (13) Sau-Hung Spence, L.; Robinson, J. R. The contribution of anionic polymer structural features to mucoadhesion. *J. Controlled Release* **1987**, *5*, 223-231.
- (14) Bao, B. A., A.; Azmi, A.; Ali, S.; Sarkar, F. et al. Cancer Stem Cells (CSCs) and Mechanisms of Their Regulation: Implications for Cancer Therapy. *Curr Protoc. Pharmacol.* **2013**, *14*, 1-32.
- (15) Gerlinger, M. e. a. Intratumor Heterogeneity and Branched Evolution Revealed by

Multiregion Sequencing. *New Engl. J. Med.* **2012**, 336, 883-892.

(16) Toole, B. Hyaluronan-CD44 Interactions in Cancer: Paradoxes and Possibilities. *Clin. Cancer Res.* **2009**, 15, 7462-7468.

(17) Miletti-Gonzalez, K. C., S.; Muthukamaran, N.; et al The CD44 Receptor Interacts with P-Glycoprotein to Promote Cell Migration and Invasion in Cancer. *Cancer Res.* **2005**, 65, 6660-6667.

(18) Qhattal, H. S. S.; Liu, X. Characterization of CD44-Mediated Cancer Cell Uptake and Intracellular Distribution of Hyaluronan-Grafted Liposomes. *Mol. Pharm.* **2011**, 8, 1233-1246.

(19) Ojima, I. S., J.; Michaud, E.; Kuduk, S.; Bounaud, P.; Vrignaud, P.; Bissery, M.; Veith, J.; Pera, P.; Bernacki, R. Syntheses and structure-activity relationships of the second-generation antitumor taxoids: exceptional activity against drug-resistant cancer cells. *J. Med. Chem.* **1996**, 39, 3889-3896.

(20) Ojima, I. Z., E.; Berger, W.; Seitz, J. Tumor-targeting drug delivery of new-generation taxoids. *Future Med. Chem.* **2012**, 4, 33-50.

(21) Kuznetsova, L. C., J.; Sun, L. Wu, X.; Pepe, A.; Veith, J.; Pera, P.; Bernacki, R.; Ojima, I. Syntheses and evaluation of novel fatty acid-second-generation taxoid conjugates as promising anticancer agents. *Bioorg. Med. Chem. Lett.* **2006**, 16, 974-977.

(22) Botchkina, G. e. a. New-generation taxoid SB-T-1214 inhibits stem cell-related gene expression in 3D cancer spheroids induced by purified colon tumor-initiating cells. *Mol. Cancer* **2010**, 9, 192-204.

## Perspective

### *Future directions of the ongoing projects*

With presented research progress and results, efforts should be continually made on the following directions in the future.

For the  $^{11}\text{C}$ -labeled SB-T-1214 radiotracer for PET imaging study in Chapter 2, all synthesized new taxoid-based derivatives will need to be purified and determine retention times to compare the corresponding peaks from the crude reaction mixture. Measurement of retention time of alkyne-taxoid (**2-15**) will determine the other unknown isolated taxoid-based product other than Tc-taxoid (**2-11**) in **Scheme 2.11**. Larger amount synthesis of Tc-taxoid (**2-11**), Ph-taxoid (**2-12**), allene-taxoid (**2-14**) and alkyne-taxoid (**2-15**) will need to be done for fully characterization including  $^1\text{H}$  NMR,  $^{13}\text{C}$  NMR and 2D NMR to determine the chemical structures and finalize the JOC paper for publication.

For the  $^{18}\text{F}$ -labeled biotin-PEG-F radiotracer for PET imaging study in Chapter 3, the key precursor biotin-PEG-OMs (**3-29**) will be sent out for collaboration to study the biodistribution and localization of biotin-bearing probe for *in vivo* biological evaluation.

For the 1,3,5-triazine-based tripod platform for PET/SPECT imaging studies in Chapter 4, modification on the imaging arm with DOTA moiety will enable the incorporation of Gd as MRI contrast agent. Thus this robust and versatile platform will be used for PET/SPECT/MRI studies. Moreover, the tripod platform can be used to construct dual-warhead conjugates (previously published by Dr. Edison Zuniga and Dr. Jacob Vineber) with one tumor-targeting module and two different types of cytotoxic agents, or dual tumor-targeted modules conjugate (previously designed by Dr. Jacob Vineberg) with two different types of tumor-targeting modules (such as folate and biotin) and one cytotoxic agent, or dual imaging agents diagnostic conjugate with one tumor-targeting module and two different imaging agents (fluorescent probe combined with PET/SPECT/MRI agents, or PET/MRI combination). With the established cold synthesis condition and purification/isolation HPLC methods, the radiolabing diagnostic probes biotin-triazine-NOTA- $^{65}\text{Cu}$  (**4-28**) and biotin-triazine-DPA( $sp^3\text{N}$ )- $^{185}\text{Re}(\text{CO})_3$  (**4-21**) can be used for PET and SPECT imaging studies, respectively. Similarly, the radiolabing theranostic probes biotin-triazine-linker-drug-NOTA- $^{65}\text{Cu}$  conjugate (**4-26**) and biotin-triazine-linker-drug-DPA( $sp^3\text{N}$ )- $^{185}\text{Re}(\text{CO})_3$  (**4-19**) will be readily used for PET and SPECT imaging studies, respectively. These research results will be published for another JOC paper.

For the ABTD project in Chapter 5, the mass spectrum analysis and HPLC purity analysis of final ABTD conjugates will need to be done for JACS publication. Furthermore, the actual size of this nano-sized macromolecular drug conjugates should be measured in any applicable biophysical methods. Imaging agents can be incorporated to the ABTD platform for *in vivo* imaging studies to validate the EPR effect. Different tumor-targeting modules and newer generation taxoids with higher potency can be used to construct new ABTD drug conjugates following the established synthetic protocol and purification methods. Two tribranched dendrimer-based theranostic drug conjugates bearing a fluorescent probe or MRI agent on the tribranched triazine core will be continued. Multi-binding effect will need to be done to estimate the number of multiple tumor



targeting module to achieve the optimized RME result, and once the number is fixed, the half dendron scaffold with multiple TTM can be used to deliver other types of agents for hyperthermia study.

For the “Trojan horse” hyaluronic acid-linker-taxoid (HALT) conjugate in Chapter 6, a revised strategy for 10 % loading on the HA chain will replace the synthetic strategy presented in this thesis. New characterization method, such as GPC, will be established for measurement of HA-based intermediates. The biological evaluations using synthesized HALT conjugates will be performed in different kinds of CSCs, and other biomarkers of CSC will be screened to develop new CSC-targeted drug delivery system.

## References

### References for General Introduction:

- (1) American Cancer Society, Inc. Cancer Statistics 2015: A Presentation from the American Cancer Society. **2015**.
- (2) American Cancer Society, Atlanta, Georgia. Cancer Facts & Figures. **2015**.
- (3) Atlanta: American Cancer Society. Global Cancer Facts & Figures 3rd Edition. **2015**.
- (4) Hanahan, D.; Weinberg, Robert A. Hallmarks of Cancer: The Next Generation. *Cell* **2011**, *144*, 646-674.
- (5) Hanahan, D.; Weinberg, R. A. The Hallmarks of Cancer. *Cell* **2000**, *100*, 57-70.
- (6) Gottesman, M. M.; Pastan, I. Biochemistry of Multidrug Resistance Mediated by the Multidrug Transporter. *Annu. Rev. Biochem.* **1993**, *62*, 385-427.
- (7) Druker, B. J.; Lydon, N. B. Lessons learned from the development of an Abl tyrosine kinase inhibitor for chronic myelogenous leukemia. *J. Clin. Invest.* **2000**, *105*, 3-7.
- (8) Jaracz, S.; Chen, J.; Kuznetsova, L. V.; Ojima, I. Recent advances in tumor-targeting anticancer drug conjugates. *Bioorg. Med. Chem.* **2005**, *13*, 5043-5054.
- (9) Ducry, L.; Stump, B. Antibody–Drug Conjugates: Linking Cytotoxic Payloads to Monoclonal Antibodies. *Bioconj. Chem.* **2009**, *21*, 5-13.
- (10) Ojima, I.; Zuniga, E. S.; Berger, W. T.; Seitz, J. D. Tumor-targeting drug delivery of new-generation taxoids. *Future Med. Chem.* **2012**, *4*, 33-50.
- (11) Ojima, I.; Zuniga, E. S.; Berger, W. T.; Seitz, J. D. Tumor-targeting drug delivery of new-generation taxoids. *Future Med Chem.* **2012**, *4*, 33-50.
- (12) Chen, J.; Jaracz, S.; Zhao, X.; Chen, S.; Ojima, I. Antibody–cytotoxic agent conjugates for cancer therapy. *Expert Opinion on Drug Delivery* **2005**, *2*, 873-890.
- (13) Wu, X.; Ojima, I. Tumor Specific Novel Taxoid-Monoclonal Antibody Conjugates. *Curr. Med. Chem.* **2004**, *11*, 429-438.
- (14) Ojima, I.; Geng, X.; Wu, X.; Qu, C.; Borella, C. P.; Xie, H.; Wilhelm, S. D.; Leece, B. A.; Bartle, L. M.; Goldmacher, V. S.; Chari, R. V. J. Tumor-Specific Novel Taxoid–Monoclonal Antibody Conjugates. *J. Med. Chem.* **2002**, *45*, 5620-5623.
- (15) Hamann, P. R.; Hinman, L. M.; Hollander, I.; Beyer, C. F.; Lindh, D.; Holcomb, R.; Hallett, W.; Tsou, H.-R.; Upešlaciš, J.; Shochat, D.; Mountain, A.; Flowers, D. A.; Bernstein, I. Gemtuzumab Ozogamicin, A Potent and Selective Anti-CD33 Antibody–Calicheamicin Conjugate for Treatment of Acute Myeloid Leukemia. *Bioconj. Chem.* **2001**, *13*, 47-58.
- (16) Chari, R. V. J. Targeted delivery of chemotherapeutics: tumor-activated prodrug therapy. *Adv. Drug Del. Rev.* **1998**, *31*, 89-104.
- (17) Bradley, M. O.; Webb, N. L.; Anthony, F. H.; Devanesan, P.; Witman, P. A.; Hemamalini, S.; Chander, M. C.; Baker, S. D.; He, L.; Horwitz, S. B.; Swindell, C. S. Tumor Targeting by Covalent Conjugation of a Natural Fatty Acid to Paclitaxel. *Clin. Cancer Res.* **2001**, *7*, 3229-3238.
- (18) Kuznetsova, L.; Chen, J.; Sun, L.; Wu, X.; Pepe, A.; Veith, J. M.; Pera, P.; Bernacki, R. J.; Ojima, I. Syntheses and evaluation of novel fatty acid-second-generation taxoid conjugates as promising anticancer agents. *Bioorg. Med. Chem. Lett.* **2006**, *16*, 974-977.
- (19) Chen, J.; Chen, S.; Zhao, X.; Kuznetsova, L. V.; Wong, S. S.; Ojima, I. Functionalized Single-Walled Carbon Nanotubes as Rationally Designed Vehicles for Tumor-Targeted Drug Delivery. *J. Am. Chem. Soc.* **2008**, *130*, 16778-16785.

- (20) Chen, S.; Zhao, X.; Chen, J.; Chen, J.; Kuznetsova, L.; Wong, S. S.; Ojima, I. Mechanism-Based Tumor-Targeting Drug Delivery System. Validation of Efficient Vitamin Receptor-Mediated Endocytosis and Drug Release. *Bioconjugate Chem.* **2010**, *21*, 979-987.
- (21) Leamon, C. P.; Reddy, J. A. Folate-targeted chemotherapy. *Adv. Drug Del. Rev.* **2004**, *56*, 1127-1141.
- (22) Lu, Y.; Low, P. S. Folate-mediated delivery of macromolecular anticancer therapeutic agents. *Adv. Drug Del. Rev.* **2002**, *54*, 675-693.
- (23) Wagner, E.; Curiel, D.; Cotten, M. Delivery of drugs, proteins and genes into cells using transferrin as a ligand for receptor-mediated endocytosis. *Adv. Drug Del. Rev.* **1994**, *14*, 113-135.
- (24) Nagy, A.; Schally, A. V.; Halmos, G.; Armatis, P.; Cai, R.-Z.; Csernus, V.; Kovács, M.; Koppán, M.; Szepesházi, K.; Kahán, Z. Synthesis and biological evaluation of cytotoxic analogs of somatostatin containing doxorubicin or its intensely potent derivative, 2-pyrrolinodoxorubicin. *Proc. Natl. Acad. Sci. U. S. A.* **1998**, *95*, 1794-1799.
- (25) Chu, T. C.; Marks, J. W.; Lavery, L. A.; Faulkner, S.; Rosenblum, M. G.; Ellington, A. D.; Levy, M. Aptamer:Toxin Conjugates that Specifically Target Prostate Tumor Cells. *Cancer Res.* **2006**, *66*, 5989-5992.
- (26) Luo, Y.; Bernshaw, N.; Lu, Z.-R.; Kopecek, J.; Prestwich, G. Targeted Delivery of Doxorubicin by HPMA Copolymer-Hyaluronan Bioconjugates. *Pharm. Res.* **2002**, *19*, 396-402.
- (27) Jaracz, S.; Chen, J.; Kuznetsova, L. V.; Ojima, I. Recent advances in tumor-targeting anticancer drug conjugates. *Bioorg. Med. Chem.* **2005**, *13*, 5043-5054.
- (28) Chen, J.; Jaracz, S.; Zhao, X.; Chen, S.; Ojima, I. Antibody-cytotoxic agent conjugates for cancer therapy. *Expert Opin. Drug Deliv.* **2005**, *2*, 873-890.

## References for Chapter 1:

- (1) Wani, M. C.; Taylor, H. L.; Wall, M. E.; Coggon, P.; McPhail, A. T. Plant antitumor agents. VI. Isolation and structure of taxol, a novel antileukemic and antitumor agent from *Taxus brevifolia*. *J. Am. Chem. Soc.* **1971**, *93*, 2325-2327.
- (2) Rowinsky, M., Eric K. The development and clinical utility of the taxane class of antimicrotubule chemotherapy agents. *Annu. Rev. Med.* **1997**, *48*, 353-374.
- (3) Bissery, M.-C.; Nohynek, G.; Sanderink, G.-J.; Lavelie, F. Docetaxel (Taxotere(R)) a review of preclinical and clinical experience. Part I: preclinical experience. *Anti-Cancer Drug.* **1995**, *6*, 339-355.
- (4) Galsky, M. D.; Dritselis, A.; Kirkpatrick, P.; Oh, W. K. Cabazitaxel. *Nat Rev Drug Discov* **2010**, *9*, 677-678.
- (5) Pivot, X.; Koralewski, P.; Hidalgo, J. L.; Chan, A.; Gonçalves, A.; Schwartzmann, G.; Assadourian, S.; Lotz, J. P. A multicenter phase II study of XRP6258 administered as a 1-h i.v. infusion every 3 weeks in taxane-resistant metastatic breast cancer patients. *Ann. Oncol.* **2008**, *19*, 1547-1552.
- (6) Holton, R. A.; Somoza, C.; Kim, H. B.; Liang, F.; Biediger, R. J.; Boatman, P. D.; Shindo, M.; Smith, C. C.; Kim, S. First total synthesis of taxol. 1. Functionalization of the B ring. *J. Am. Chem. Soc.* **1994**, *116*, 1597-1598.
- (7) Holton, R. A.; Kim, H. B.; Somoza, C.; Liang, F.; Biediger, R. J.; Boatman, P. D.; Shindo, M.; Smith, C. C.; Kim, S. First total synthesis of taxol. 2. Completion of the C and D rings. *J. Am. Chem. Soc.* **1994**, *116*, 1599-1600.
- (8) Nicolaou, K. C.; Nantermet, P. G.; Ueno, H.; Guy, R. K.; Couladouros, E. A.; Sorensen, E. J. Total Synthesis of Taxol. 1. Retrosynthesis, Degradation, and Reconstitution. *J. Am. Chem. Soc.* **1995**, *117*, 624-633.
- (9) Nicolaou, K. C.; Liu, J. J.; Yang, Z.; Ueno, H.; Sorensen, E. J.; Claiborne, C. F.; Guy, R. K.; Hwang, C. K.; Nakada, M.; Nantermet, P. G. Total Synthesis of taxol. 2. Construction of A and C ring intermediates and initial attempts to construct the ABC ring system. *J. Am. Chem. Soc.* **1995**, *117*, 634-644.
- (10) Nicolaou, K. C.; Yang, Z.; Liu, J. J.; Nantermet, P. G.; Claiborne, C. F.; Renaud, J.; Guy, R. K.; Shibayama, K. Total Synthesis of Taxol. 3. Formation of Taxol's ABC Ring Skeleton. *J. Am. Chem. Soc.* **1995**, *117*, 645-652.
- (11) Nicolaou, K. C.; Ueno, H.; Liu, J. J.; Nantermet, P. G.; Yang, Z.; Renaud, J.; Paulvannan, K.; Chadha, R. Total Synthesis of Taxol. 4. The Final Stages and Completion of the Synthesis. *J. Am. Chem. Soc.* **1995**, *117*, 653-659.
- (12) Danishefsky, S. J.; Masters, J. J.; Young, W. B.; Link, J. T.; Snyder, L. B.; Magee, T. V.; Jung, D. K.; Isaacs, R. C. A.; Bornmann, W. G.; Alaimo, C. A.; Coburn, C. A.; Di Grandi, M. J. Total Synthesis of Baccatin III and Taxol. *J. Am. Chem. Soc.* **1996**, *118*, 2843-2859.
- (13) Wender, P. A.; Badham, N. F.; Conway, S. P.; Floreancig, P. E.; Glass, T. E.; Gränicher, C.; Houze, J. B.; Jänichen, J.; Lee, D.; Marquess, D. G.; McGrane, P. L.; Meng, W.; Mucciario, T. P.; Mühlebach, M.; Natchus, M. G.; Paulsen, H.; Rawlins, D. B.; Satkofsky, J.; Shuker, A. J.; Sutton, J. C.; Taylor, R. E.; Tomooka, K. The Pinene Path to Taxanes. 5. Stereocontrolled Synthesis of a Versatile Taxane Precursor. *J. Am. Chem. Soc.* **1997**, *119*, 2755-2756.
- (14) Morihira, K.; Hara, R.; Kawahara, S.; Nishimori, T.; Nakamura, N.; Kusama, H.; Kuwajima, I. Enantioselective Total Synthesis of Taxol. *J. Am. Chem. Soc.* **1998**, *120*, 12980-12981.
- (15) Mukaiyama, T.; Shiina, I.; Iwadare, H.; Saitoh, M.; Nishimura, T.; Ohkawa, N.; Sakoh, H.;

- Nishimura, K.; Tani, Y.-i.; Hasegawa, M.; Yamada, K.; Saitoh, K. Asymmetric Total Synthesis of Taxol. *Chem.-Eur. J.* **1999**, *5*, 121-161.
- (16) Doi, T.; Fuse, S.; Miyamoto, S.; Nakai, K.; Sasuga, D.; Takahashi, T. A Formal Total Synthesis of Taxol Aided by an Automated Synthesizer. *Chem Asian J.* **2006**, *1*, 370-383.
- (17) Chauvière, G. G., D.; Picot, F.; Sénilh, V.; Potier, P. Structural Analysis and Biochemical Study of Isolated Products of the Yew: *Taxus Baccata* L. (Taxaceae). *C. R. Seances Acad. Sci., Ser 2* **1981**, *293*, 501-503.
- (18) American Cancer Society, Atlanta, Georgia. Cancer Facts & Figures. **2015**.
- (19) Guenard, D.; Gueritte-Voegelein, F.; Potier, P. Taxol and taxotere: discovery, chemistry, and structure-activity relationships. *Acc. Chem. Res.* **1993**, *26*, 160-167.
- (20) Denis, J. N.; Greene, A. E.; Guenard, D.; Gueritte-Voegelein, F.; Mangatal, L.; Potier, P. Highly efficient, practical approach to natural taxol. *J. Am. Chem. Soc.* **1988**, *110*, 5917-5919.
- (21) Ojima, I.; Habus, I.; Zhao, M.; Georg, G. I.; Jayasinghe, L. R. Efficient and practical asymmetric synthesis of the taxol C-13 side chain, N-benzoyl-(2R,3S)-3-phenylisoserine, and its analogs via chiral 3-hydroxy-4-aryl-.beta.-lactams through chiral ester enolate-imine cyclocondensation. *J. Org. Chem.* **1991**, *56*, 1681-1683.
- (22) Ojima, I.; Habus, I.; Zhao, M.; Zucco, M.; Park, Y. H.; Sun, C. M.; Brigaud, T. New and efficient approaches to the semisynthesis of taxol and its C-13 side chain analogs by means of  $\beta$ -lactam synthon method. *Tetrahedron* **1992**, *48*, 6985-7012.
- (23) Ojima, I.; Kuduk, S. D.; Pera, P.; Veith, J. M.; Bernacki, R. J. Synthesis and Structure-Activity Relationships of Nonaromatic Taxoids: Effects of Alkyl and Alkenyl Ester Groups on Cytotoxicity. *J. Med. Chem.* **1997**, *40*, 279-285.
- (24) Ojima, I.; Slater, J. C.; Kuduk, S. D.; Takeuchi, C. S.; Gimi, R. H.; Sun, C.-M.; Park, Y. H.; Pera, P.; Veith, J. M.; Bernacki, R. J. Syntheses and Structure-Activity Relationships of Taxoids Derived from 14 $\beta$ -Hydroxy-10-deacetylbaccatin III. *J. Med. Chem.* **1997**, *40*, 267-278.
- (25) Ojima, I.; Slater, J. C.; Michaud, E.; Kuduk, S. D.; Bounaud, P.-Y.; Vrignaud, P.; Bissery, M.-C.; Veith, J. M.; Pera, P.; Bernacki, R. J. Syntheses and Structure-Activity Relationships of the Second-Generation Antitumor Taxoids: Exceptional Activity against Drug-Resistant Cancer Cells. *J. Med. Chem.* **1996**, *39*, 3889-3896.
- (26) Kamath, A.; Ojima, I. Advances in the chemistry of  $\beta$ -lactam and its medicinal applications. *Tetrahedron* **2012**, *68*, 10640-10664.
- (27) Staudinger, H. Zur Kenntniss der Ketene. Diphenylketen. *Justus Liebigs Ann. Chem.* **1907**, *356*, 51-123.
- (28) Ojima, I.; Habus, I. Asymmetric synthesis of  $\beta$ -lactams by chiral ester enolate - imine condensation. *Tetrahedron Lett.* **1990**, *31*, 4289-4292.
- (29) Lopez, R.; Sordo, T. L.; Sordo, J. A.; Gonzalez, J. Torquoelectronic effect in the control of the stereoselectivity of ketene-imine cycloaddition reactions. *J. Org. Chem.* **1993**, *58*, 7036-7037.
- (30) Jiao, L.; Liang, Y.; Xu, J. Origin of the Relative Stereoselectivity of the  $\beta$ -Lactam Formation in the Staudinger Reaction. *J. Am. Chem. Soc.* **2006**, *128*, 6060-6069.
- (31) Brieva, R.; Crich, J. Z.; Sih, C. J. Chemoenzymic synthesis of the C-13 side chain of taxol: optically active 3-hydroxy-4-phenyl .beta.-lactam derivatives. *J. Org. Chem.* **1993**, *58*, 1068-1075.
- (32) Cragg, G. M., Kingston, D. G. I., Newman, D. J. Anticancer agents from natural products. CRC Press. **2011**.
- (33) Ojima, I.; Zuniga, E. S.; Berger, W. T.; Seitz, J. D. Tumor-targeting drug delivery of new-generation taxoids. *Future Med Chem.* **2012**, *4*, 33-50.

- (34) Al-Hajj, M.; Wicha, M. S.; Benito-Hernandez, A.; Morrison, S. J.; Clarke, M. F. Prospective identification of tumorigenic breast cancer cells. *Proc. Natl. Acad. Sci. U. S. A.* **2003**, *100*, 3983-3988.
- (35) Wilson, L.; Jordan, M. A. Microtubule dynamics: taking aim at a moving target. *Chem. Biol.* **1995**, *2*, 569-573.
- (36) Zhao, X. R. Design, synthesis and biological evaluation of novel taxane-based anticancer agents and their applications to tumor-targeting drug delivery systems (Doctoral Dissertation). *State University of New York at Stony Brook* **2009**.
- (37) Jordan, M. A.; Wilson, L. Microtubules as a target for anticancer drugs. *Nat Rev Cancer* **2004**, *4*, 253-265.
- (38) Schiff, P. B.; Fant, J.; Horwitz, S. B. Promotion of microtubule assembly in vitro by taxol. *Nature* **1979**, *277*, 665-667.
- (39) Holmes, F. A.; Walters, R. S.; Theriault, R. L.; Buzdar, A. U.; Frye, D. K.; Hortobagyi, G. N.; Forman, A. D.; Newton, L. K.; Raber, M. N. Phase II Trial of Taxol, an Active Drug in the Treatment of Metastatic Breast Cancer. *J. Natl. Cancer Inst.* **1991**, *83*, 1797-1805.
- (40) Weiss, R. B.; Donehower, R. C.; Wiernik, P. H.; Ohnuma, T.; Gralla, R. J.; Trump, D. L.; Baker, J. R.; Van Echo, D. A.; Von Hoff, D. D.; Leyland-Jones, B. Hypersensitivity reactions from taxol. *J Clin. Oncol.* **1990**, *8*, 1263-1268.
- (41) Rowinsky, E. K.; Donehower, R. C. Paclitaxel (Taxol). *N. Engl. J. Med.* **1995**, *332*, 1004-1014.
- (42) Gottesman, M. M.; Pastan, I. Biochemistry of Multidrug Resistance Mediated by the Multidrug Transporter. *Annu. Rev. Biochem.* **1993**, *62*, 385-427.
- (43) Szakacs, G.; Paterson, J. K.; Ludwig, J. A.; Booth-Genthe, C.; Gottesman, M. M. Targeting multidrug resistance in cancer. *Nat Rev Drug Discov* **2006**, *5*, 219-234.
- (44) Germann, U. A. P-glycoprotein—A mediator of multidrug resistance in tumour cells. *Eur. J. Cancer* **1996**, *32*, 927-944.
- (45) Ducry, L.; Stump, B. Antibody–Drug Conjugates: Linking Cytotoxic Payloads to Monoclonal Antibodies. *Bioconjugate Chem.* **2009**, *21*, 5-13.
- (46) Penson, R. T.; Oliva, E.; Skates, S. J.; Glyptis, T.; Fuller Jr, A. F.; Goodman, A.; Seiden, M. V. Expression of multidrug resistance-1 protein inversely correlates with paclitaxel response and survival in ovarian cancer patients: a study in serial samples. *Gynecol. Oncol.* **2004**, *93*, 98-106.
- (47) Martinez, L.; Falson, P. Multidrug resistance ATP-binding cassette membrane transporters as targets for improving oropharyngeal candidiasis treatment. *Advances in Cellular and Molecular Otolaryngology* **2014**, *2*, 23955.
- (48) Aller, S. G.; Yu, J.; Ward, A.; Weng, Y.; Chittaboina, S.; Zhuo, R.; Harrell, P. M.; Trinh, Y. T.; Zhang, Q.; Urbatsch, I. L.; Chang, G. Structure of P-Glycoprotein Reveals a Molecular Basis for Poly-Specific Drug Binding. *Science* **2009**, *323*, 1718-1722.
- (49) Lage, H.; Dietel, M. Multiple mechanisms confer different drug-resistant phenotypes in pancreatic carcinoma cells. *J. Cancer Res. Clin. Oncol.* **2002**, *128*, 349-357.
- (50) O'Driscoll, L.; Walsh, N.; Larkin, A.; Ballot, J.; Ooi, W. S.; Gullo, G.; O'Connor, R.; Clynes, M.; Crown, J.; Kennedy, S. MDR1/P-glycoprotein and MRP-1 Drug Efflux Pumps in Pancreatic Carcinoma. *Anticancer Res.* **2007**, *27*, 2115-2120.
- (51) Donnenberg, V. S.; Donnenberg, A. D. Multiple Drug Resistance in Cancer Revisited: The Cancer Stem Cell Hypothesis. *J Clin Pharmacol.* **2005**, *45*, 872-877.
- (52) Borcard, F.; Godinat, A.; Staedler, D.; Comas Blanco, H.; Dumont, A.-L.; Chapuis-

Bernasconi, C.; Scaletta, C.; Applegate, L. A.; Krauss Juillerat, F.; Gonzenbach, U. T.; Gerber-Lemaire, S.; Juillerat-Jeanneret, L. Covalent Cell Surface Functionalization of Human Fetal Osteoblasts for Tissue Engineering. *Bioconjugate Chem.* **2011**, *22*, 1422-1432.

(53) American Cancer Society, Inc. Cancer Statistics 2015: A Presentation from the American Cancer Society. **2015**.

(54) Ojima, I.; Duclos, O.; Kuduk, S. D.; Sun, C.-M.; Slater, J. C.; Lavelle, F.; Veith, J. M.; Bernacki, R. J. Synthesis and biological activity of 3'-alkyl- and 3'-alkenyl-3'-dephenyldocetaxels. *Bioorg. Med. Chem. Lett.* **1994**, *4*, 2631-2634.

(55) Ojima, I.; Fumero-Oderda, C. L.; Kuduk, S. D.; Ma, Z.; Kirikae, F.; Kirikae, T. Structure-activity relationship study of taxoids for their ability to activate murine macrophages as well as inhibit the growth of macrophage-like cells. *Bioorg. Med. Chem.* **2003**, *11*, 2867-2888.

(56) Kuznetsova, L. V.; Pepe, A.; Ungureanu, I. M.; Pera, P.; Bernacki, R. J.; Ojima, I. Syntheses and Structure-Activity Relationships of Novel 3'-Difluoromethyl and 3'-Trifluoromethyl-Taxoids. *J. Fluorine Chem.* **2008**, *129*, 817-828.

(57) Kuznetsova, L.; Ungureanu, I. M.; Pepe, A.; Zanardi, I.; Wu, X.; Ojima, I. Trifluoromethyl- and difluoromethyl- $\beta$ -lactams as useful building blocks for the synthesis of fluorinated amino acids, dipeptides, and fluoro-taxoids. *J. Fluorine Chem.* **2004**, *125*, 487-500.

## References for Chapter 2:

- (1) Li, X.; Barasoain, I.; Matesanz, R.; Fernando Díaz, J.; Fang, W.-S. Synthesis and biological activities of high affinity taxane-based fluorescent probes. *Bioorg. Med. Chem. Lett.* **2009**, *19*, 751-754.
- (2) Li, X.; Barasoain, I.; Matesanz, R.; Fernando Díaz, J.; Fang, W.-S. Synthesis and biological activities of high affinity taxane-based fluorescent probes. *Bioorg. Med. Chem. Lett.* **2009**, *19*, 751-754.
- (3) Vineberg, J. G.; Wang, T.; Zuniga, E. S.; Ojima, I. Design, Synthesis, and Biological Evaluation of Theranostic Vitamin-Linker-Taxoid Conjugates. *J. Med. Chem.* **2015**, *58*, 2406-2416.
- (4) Kiesewetter, D. O.; Jagoda, E. M.; Kao, C.-H. K.; Ma, Y.; Ravasi, L.; Shimoji, K.; Szajek, L. P.; Eckelman, W. C. Fluoro-, bromo-, and iodopaclitaxel derivatives: synthesis and biological evaluation. *Nucl. Med. Biol.* **2003**, *30*, 11-24.
- (5) Adamczyk, M.; Grote, J. Efficient fluorescein spirolactam and bis-spirolactam synthesis. *Synth. Commun.* **2001**, *31*, 2681-2690.
- (6) Mason, W. T., Ed. Fluorescent and Luminescent Probes for Biological Activity. *Wiley Interscience: New York*, **1983**, Chapter 2.
- (7) Adamczyk, M.; Grote, J. Synthesis of novel spirolactams by reaction of fluorescein methyl ester with amines. *Tetrahedron Lett.* **2000**, *41*, 807-809.
- (8) Brown, L.; Halling, P. J.; Johnston, G. A.; Suckling, C. J.; Valivety, R. H. The synthesis of some water insoluble dyes for the measurement of pH in water immiscible solvents. *J. Chem. Soc., Perkin Trans. 1* **1990**, 3349-3353.
- (9) Brown, L.; Halling, P. J.; Johnston, G. A.; Suckling, C. J.; Valivety, R. H. Water insoluble indicators for the measurement of pH in water immiscible solvents. *Tetrahedron Lett.* **1990**, *31*, 5799-5802.
- (10) Miller, P. W.; Long, N. J.; Vilar, R.; Gee, A. D. Synthesis of  $^{11}\text{C}$ ,  $^{18}\text{F}$ ,  $^{15}\text{O}$ , and  $^{13}\text{N}$  Radiolabels for Positron Emission Tomography. *Angew. Chem. Int. Ed.* **2008**, *47*, 8998-9033.
- (11) Ametamey, S. M.; Honer, M.; Schubiger, P. A. Molecular Imaging with PET. *Chem. Rev.* **2008**, *108*, 1501-1516.
- (12) Ravert, H. T.; Klecker, R. W.; Collins, J. M.; Mathews, W. B.; Pomper, M. G.; Wahl, R. L.; Dannals, R. F. Radiosynthesis of [ $^{11}\text{C}$ ]paclitaxel. *J. Labelled Comp Radiopharm.* **2002**, *45*, 471-477.
- (13) van Tilburg, E. W.; Franssen, E. J. F.; van der Hoeven, J. J. M.; van der Meij, M.; Elshove, D.; Lammertsma, A. A.; Windhorst, A. D. Radiosynthesis of [ $^{11}\text{C}$ ]docetaxel. *J. Labelled Comp Radiopharm.* **2004**, *47*, 763-777.
- (14) Mäding, P.; Zessin, J.; Pleiß, U.; Füchtner, F.; Wüst, F. Synthesis of a  $^{11}\text{C}$ -labelled taxane derivative by [ $1-^{11}\text{C}$ ]acetylation. *J. Labelled Compd. Radiopharmaceut.* **2006**, *49*, 357-365.
- (15) Seitz, J. D. The design, synthesis and biological evaluation of novel taxoid anticancer agents and their tumor-targeted drug conjugates. Doctoral Dissertation. Stony Brook University. **2013**.
- (16) Joshua D. Seitz, T. W., Jacob G. Vineberg and Iwao Ojima Synthesis of a next-generation taxoid by rapid methylation amenable for [ $^{11}\text{C}$ ] labeling. *To be submitted shortly*
- (17) Seitz, J. D.; Vineberg, J. G.; Wei, L.; Khan, J. F.; Lichtenthal, B.; Lin, C.-F.; Ojima, I. Design, synthesis and application of fluorine-labeled taxoids as  $^{19}\text{F}$  NMR probes for the metabolic stability assessment of tumor-targeted drug delivery systems. *J. Fluorine Chem.* **2015**, *171*, 148-161.



- (18) Borcard, F.; Godinat, A.; Staedler, D.; Comas Blanco, H.; Dumont, A.-L.; Chapuis-Bernasconi, C.; Scaletta, C.; Applegate, L. A.; Krauss Juillerat, F.; Gonzenbach, U. T.; Gerber-Lemaire, S.; Juillerat-Jeanneret, L. Covalent Cell Surface Functionalization of Human Fetal Osteoblasts for Tissue Engineering. *Bioconj. Chem.* **2011**, *22*, 1422-1432.
- (19) Vineberg, J. G.; Wang, T.; Zuniga, E. S.; Ojima, I. Design, Synthesis, and Biological Evaluation of Theranostic Vitamin–Linker–Taxoid Conjugates. *J. Med. Chem.* **2015**, *58*, 2406-2416.

### References for Chapter 3:

- (1) Zempleni, J.; Wijeratne, S. S. K.; Hassan, Y. I. Biotin. *BioFactors* **2009**, *35*, 36-46.
- (2) Leamon, C. P. Folate-targeted drug strategies for the treatment of cancer. *Curr Opin Investig Drugs* **2008**, *9*, 1277-1286.
- (3) Lu, Y.; Low, P. S. Folate-mediated delivery of macromolecular anticancer therapeutic agents. *Adv. Drug Delivery Rev.* **2012**, *64*, Supplement, 342-352.
- (4) Russell-Jones, G.; McTavish, K.; McEwan, J.; Rice, J.; Nowotnik, D. Vitamin-mediated targeting as a potential mechanism to increase drug uptake by tumours. *J. Inorg. Biochem.* **2004**, *98*, 1625-1633.
- (5) Vineberg, J. G.; Zuniga, E. S.; Kamath, A.; Chen, Y.-J.; Seitz, J. D.; Ojima, I. Design, Synthesis, and Biological Evaluations of Tumor-Targeting Dual-Warhead Conjugates for a Taxoid–Camptothecin Combination Chemotherapy. *J. Med. Chem.* **2014**, *57*, 5777-5791.
- (6) Ojima, I.; Zuniga, E. S.; Berger, W. T.; Seitz, J. D. Tumor-targeting drug delivery of new-generation taxoids. *Future Med Chem.* **2012**, *4*, 33-50.
- (7) Ojima, I.; Slater, J. C.; Michaud, E.; Kuduk, S. D.; Bounaud, P.-Y.; Vrignaud, P.; Bissery, M.-C.; Veith, J. M.; Pera, P.; Bernacki, R. J. Syntheses and Structure–Activity Relationships of the Second-Generation Antitumor Taxoids: Exceptional Activity against Drug-Resistant Cancer Cells. *J. Med. Chem.* **1996**, *39*, 3889-3896.
- (8) Harris, J. M.; Chess, R. B. Effect of pegylation on pharmaceuticals. *Nat Rev Drug Discov* **2003**, *2*, 214-221.
- (9) Vlashi, E.; Kelderhouse, L. E.; Sturgis, J. E.; Low, P. S. Effect of Folate-Targeted Nanoparticle Size on Their Rates of Penetration into Solid Tumors. *ACS Nano* **2013**, *7*, 8573-8582.
- (10) Ojima, I. Guided Molecular Missiles for Tumor-Targeting Chemotherapy—Case Studies Using the Second-Generation Taxoids as Warheads. *Acc. Chem. Res.* **2008**, *41*, 108-119.
- (11) Ojima, I. Use of Fluorine in the Medicinal Chemistry and Chemical Biology of Bioactive Compounds—A Case Study on Fluorinated Taxane Anticancer Agents. *ChemBioChem* **2004**, *5*, 628-635.
- (12) Seitz, J. D.; Vineberg, J. G.; Wei, L.; Khan, J. F.; Lichtenthal, B.; Lin, C.-F.; Ojima, I. Design, synthesis and application of fluorine-labeled taxoids as <sup>19</sup>F NMR probes for the metabolic stability assessment of tumor-targeted drug delivery systems. *J. Fluorine Chem.* **2015**, *171*, 148-161.
- (13) Chen, S.; Zhao, X.; Chen, J.; Chen, J.; Kuznetsova, L.; Wong, S. S.; Ojima, I. Mechanism-Based Tumor-Targeting Drug Delivery System. Validation of Efficient Vitamin Receptor-Mediated Endocytosis and Drug Release. *Bioconjugate Chem.* **2010**, *21*, 979-987.
- (14) Das, M. Design, Synthesis and Biological Evaluation of Novel Tumor-targeting Taxane-based Drug Delivery Systems. Doctoral Dissertation. Stony Brook University. **2011**.
- (15) Seitz, J. D. The design, synthesis and biological evaluation of novel taxoid anticancer agents and their tumor-targeted drug conjugates. Doctoral Dissertation. Stony Brook University. **2013**.
- (16) Vineberg, J. G. Design, synthesis, and biological evaluation of novel taxoid-based drug conjugates and theranostic imaging agents towards tumor-targeted chemotherapy. Doctoral Dissertation. Stony Brook University. **2014**.
- (17) Joshua D. Seitz, J. G. V., Tao Wang, and Iwao Ojima Synthesis of a Next-Generation Taxoid by Rapid Methylation Amenable for [<sup>11</sup>C]-Labeling. *J. Org. Chem.* *To be submitted shortly*
- (18) Claesener, M.; Breyholz, H.-J.; Hermann, S.; Faust, A.; Wagner, S.; Schober, O.; Schäfers, M.; Kopka, K. Efficient synthesis of a fluorine-18 labeled biotin derivative. *Nucl. Med. Biol.*, *39*,

1189-1194.

- (19) Mosmann, T. Rapid colorimetric assay for cellular growth and survival: Application to proliferation and cytotoxicity assays. *J. Inorg. Biochem.* **1983**, *65*, 55-63.
- (20) Bordwell, F. G.; Fried, H. E. Heterocyclic aromatic anions with  $4n + 2$  .pi.-electrons. *J. Org. Chem.* **1991**, *56*, 4218-4223.
- (21) Shaabani, A.; Tavasoli - Rad, F.; Lee, D. G. Potassium Permanganate Oxidation of Organic Compounds. *Synth. Commun.* **2005**, *35*, 571-580.
- (22) Widdison, W. C.; Wilhelm, S. D.; Cavanagh, E. E.; Whiteman, K. R.; Leece, B. A.; Kovtun, Y.; Goldmacher, V. S.; Xie, H.; Steeves, R. M.; Lutz, R. J.; Zhao, R.; Wang, L.; Blättler, W. A.; Chari, R. V. J. Semisynthetic Maytansine Analogues for the Targeted Treatment of Cancer. *J. Med. Chem.* **2006**, *49*, 4392-4408.
- (23) Banerjee, P. S.; Zuniga, E. S.; Ojima, I.; Carrico, I. S. Targeted and armed oncolytic adenovirus via chemoselective modification. *Bioorg. Med. Chem. Lett.* **2011**, *21*, 4985-4988.
- (24) Rich, D. H.; Gesellchen, P. D.; Tong, A.; Cheung, A.; Buckner, C. K. Alkylating derivatives of amino acids and peptides. Synthesis of N-maleoylamino acids, [1-(N-maleoylglycyl)cysteinyl]oxytocin, and [1-(N-maleoyl-11-aminoundecanoyl)cysteinyl]oxytocin. Effects on vasopressin-stimulated water loss from isolated toad bladder. *J. Med. Chem.* **1975**, *18*, 1004-1010.
- (25) Goswami, L. N.; Houston, Z. H.; Sarma, S. J.; Jalisatgi, S. S.; Hawthorne, M. F. Efficient synthesis of diverse heterobifunctionalized clickable oligo(ethylene glycol) linkers: potential applications in bioconjugation and targeted drug delivery. *Org. Biomol. Chem.* **2013**, *11*, 1116-1126.
- (26) Fusz, S.; Srivatsan, S. G.; Ackermann, D.; Famulok, M. Photocleavable Initiator Nucleotide Substrates for an Aldolase Ribozyme. *J. Org. Chem.* **2008**, *73*, 5069-5077.
- (27) Borcard, F.; Godinat, A.; Staedler, D.; Comas Blanco, H.; Dumont, A.-L.; Chapuis-Bernasconi, C.; Scaletta, C.; Applegate, L. A.; Krauss Juillerat, F.; Gonzenbach, U. T.; Gerber-Lemaire, S.; Juillerat-Jeanneret, L. Covalent Cell Surface Functionalization of Human Fetal Osteoblasts for Tissue Engineering. *Bioconjugate Chem.* **2011**, *22*, 1422-1432.
- (28) Luo, Z.; Ding, X.; Hu, Y.; Wu, S.; Xiang, Y.; Zeng, Y.; Zhang, B.; Yan, H.; Zhang, H.; Zhu, L.; Liu, J.; Li, J.; Cai, K.; Zhao, Y. Engineering a Hollow Nanocontainer Platform with Multifunctional Molecular Machines for Tumor-Targeted Therapy in Vitro and in Vivo. *ACS Nano* **2013**, *7*, 10271-10284.
- (29) Rong, L.; Liu, L.-H.; Chen, S.; Cheng, H.; Chen, C.-S.; Li, Z.-Y.; Qin, S.-Y.; Zhang, X.-Z. A coumarin derivative as a fluorogenic glycoproteomic probe for biological imaging. *Chem. Commun.* **2014**, *50*, 667-669.

## References for Chapter 4:

- (1) Rahmim, A.; Zaidi, H. PET versus SPECT: strengths, limitations and challenges. *Nucl. Med. Commun.* **2008**, *29*, 193-207.
- (2) Morais, G. R.; Paulo, A.; Santos, I. Organometallic Complexes for SPECT Imaging and/or Radionuclide Therapy. *Organometallics* **2012**, *31*, 5693-5714.
- (3) Khalil, M. M.; Tremoleda, J. L.; Bayomy, T. B.; Gsell, W. Molecular SPECT Imaging: An Overview. *Int J Mol Imaging* **2011**, 15 pages.
- (4) Pascu, S.; Dilworth, J. Recent developments in PET and SPECT imaging. *J Labelled Comp Radiopharm* **2014**, *57*, 191-194.
- (5) Ametamey, S. M.; Honer, M.; Schubiger, P. A. Molecular Imaging with PET. *Chem. Rev.* **2008**, *108*, 1501-1516.
- (6) <http://www.cellsighttech.com/technology/pet.html>.
- (7) Miller, P. W.; Long, N. J.; Vilar, R.; Gee, A. D. Synthesis of  $^{11}\text{C}$ ,  $^{18}\text{F}$ ,  $^{15}\text{O}$ , and  $^{13}\text{N}$  Radiolabels for Positron Emission Tomography. *Angew. Chem. Int. Ed.* **2008**, *47*, 8998-9033.
- (8) Alehyani, S. H. A. Application of single photon emission computed tomography (SPECT) parameters for bone scintigraphy. *Journal of King Saud University - Science* **2009**, *21*, 109-117.
- (9) Wolf, A. P.; Redvanly, C. S. Carbon-11 and radiopharmaceuticals. *Int J Appl Radiat Is* **1977**, *28*, 29-48.
- (10) Ferrieri R, A.; Wolf A, P. In *Radiochimica Acta* 1983; Vol. 34, p 69.
- (11) Miller, J. C. Neuroimaging for Dementia and Alzheimer's Disease. *Radiology Rounds* **2006**, *4*.
- (12) Wadas, T. J.; Wong, E. H.; Weisman, G. R.; Anderson, C. J. Coordinating Radiometals of Copper, Gallium, Indium, Yttrium, and Zirconium for PET and SPECT Imaging of Disease. *Chem. Rev.* **2010**, *110*, 2858-2902.
- (13) Anderson, C. J., Green, M. A., and Fujibayashi, Y. Chemistry of copper radionuclides and radiopharmaceutical products, Handbook of Radiopharmaceuticals: Radiochemistry and Applications (Welch, M. J., and Redvanly, C., Eds.) pp 401-422, John Wiley & Sons, Ltd. **2003**.
- (14) Zhou, Y.; Liu, S.  $^{64}\text{Cu}$ -Labeled Phosphonium Cations as PET Radiotracers for Tumor Imaging. *Bioconj. Chem.* **2011**, *22*, 1459-1472.
- (15) Banerjee, S.; Ambikalmajan Pillai, M. R.; Ramamoorthy, N. Evolution of Tc-99m in diagnostic radiopharmaceuticals. *Semin. Nucl. Med.* **2001**, *31*, 260-277.
- (16) Moffat, F. L.; Pinsky, C. M.; Hammershaimb, L.; Petrelli, N. J.; Patt, Y. Z.; Whaley, F. S.; Goldenberg, D. M. Clinical utility of external immunoscintigraphy with the IMMU-4 technetium-99m Fab' antibody fragment in patients undergoing surgery for carcinoma of the colon and rectum: results of a pivotal, phase III trial. The Immunomedics Study Group. *J. Clin. Oncol.* **1996**, *14*, 2295-2305.
- (17) Gratz, S.; Schipper, M. L.; Dorner, J.; Hoffken, H.; Becker, W.; Kaiser, J. W.; Behe, M.; Behr, T. M. LeukoScan for Imaging Infection in Different Clinical Settings: A Retrospective Evaluation and Extended Review of the Literature. *Clin. Nucl. Med.* **2003**, *28*, 267-276.
- (18) Tait, J. F.; Cerqueira, M. D.; Dewhurst, T. A.; Fujikawa, K.; Ritchie, J. L.; Stratton, J. R. Evaluation of annexin V as a platelet-directed thrombus targeting agent. *Thromb. Res.* **1994**, *75*, 491-501.
- (19) Danielsson, R.; Bååth, M.; Svensson, L.; Forslöv, U.; Kölbeck, K.-G. Imaging of regional lymph node metastases with  $^{99\text{m}}\text{Tc}$ -depreotide in patients with lung cancer. *Eur. J. Nucl. Med. Mol.*

*Imag.* **2005**, *32*, 925-931.

(20) Blankenberg, F. G.; Strauss, H. W. Nuclear medicine applications in molecular imaging. *J. Magn. Reson. Im.* **2002**, *16*, 352-361.

(21) Tisato, F.; Porchia, M.; Bolzati, C.; Refosco, F.; Vittadini, A. The preparation of substitution-inert  $^{99}\text{Tc}$  metal-fragments: Promising candidates for the design of new  $^{99\text{m}}\text{Tc}$  radiopharmaceuticals. *Coord. Chem. Rev.* **2006**, *250*, 2034-2045.

(22) Waibel, R.; Alberto, R.; Willuda, J.; Finnern, R.; Schibli, R.; Stichelberger, A.; Egli, A.; Abram, U.; Mach, J.-P.; Pluckthun, A.; Schubiger, P. A. Stable one-step technetium-99m labeling of His-tagged recombinant proteins with a novel Tc(I)-carbonyl complex. *Nat Biotech* **1999**, *17*, 897-901.

(23) Egli, A.; Alberto, R.; Tannahill, L.; Schibli, R.; Abram, U.; Schaffland, A.; Waibel, R.; Tourwé, D.; Jeannin, L.; Iterbeke, K.; Schubiger, P. A. Organometallic  $^{99\text{m}}\text{Tc}$ -Aquaion Labels Peptide to an Unprecedented High Specific Activity. *J. Nucl. Med.* **1999**, *40*, 1913-1917.

(24) Morris, R. T.; Joyrich, R. N.; Naumann, R. W.; Shah, N. P.; Maurer, A. H.; Strauss, H. W.; Uszler, J. M.; Symanowski, J. T.; Ellis, P. R.; Harb, W. A. Phase II study of treatment of advanced ovarian cancer with folate-receptor-targeted therapeutic (vintafolide) and companion SPECT-based imaging agent ( $^{99\text{m}}\text{Tc}$ -etarfolatide). *Ann. Oncol.* **2014**, *25*, 852-858.

(25) Betzel, T.; Müller, C.; Groehn, V.; Müller, A.; Reber, J.; Fischer, C. R.; Krämer, S. D.; Schibli, R.; Ametamey, S. M. Radiosynthesis and Preclinical Evaluation of 3'-Aza-2'-[ $^{18}\text{F}$ ]fluorofolic Acid: A Novel PET Radiotracer for Folate Receptor Targeting. *Bioconj. Chem.* **2013**, *24*, 205-214.

(26) Leamon, C. P.; Parker, M. A.; Vlahov, I. R.; Xu, L.-C.; Reddy, J. A.; Vetzal, M.; Douglas, N. Synthesis and Biological Evaluation of EC20: A New Folate-Derived,  $^{99\text{m}}\text{Tc}$ -Based Radiopharmaceutical. *Bioconj. Chem.* **2002**, *13*, 1200-1210.

(27) Bettio, A.; Honer, M.; Müller, C.; Brühlmeier, M.; Müller, U.; Schibli, R.; Groehn, V.; Schubiger, A. P.; Ametamey, S. M. Synthesis and Preclinical Evaluation of a Folic Acid Derivative Labeled with  $^{18}\text{F}$  for PET Imaging of Folate Receptor-Positive Tumors. *J. Nucl. Med.* **2006**, *47*, 1153-1160.

(28) Claesener, M.; Breyholz, H.-J.; Hermann, S.; Faust, A.; Wagner, S.; Schober, O.; Schäfers, M.; Kopka, K. Efficient synthesis of a fluorine-18 labeled biotin derivative. *Nucl. Med. Biol.*, *39*, 1189-1194.

(29) Kudo, T.; Ueda, M.; Konishi, H.; Kawashima, H.; Kuge, Y.; Mukai, T.; Miyano, A.; Tanaka, S.; Kizaka-Kondoh, S.; Hiraoka, M.; Saji, H. PET Imaging of Hypoxia-Inducible Factor-1-Active Tumor Cells with Pretargeted Oxygen-Dependent Degradable Streptavidin and a Novel  $^{18}\text{F}$ -Labeled Biotin Derivative. *Mol. Imag. Biol.* **2011**, *13*, 1003-1010.

(30) Vineberg, J. G.; Zuniga, E. S.; Kamath, A.; Chen, Y.-J.; Seitz, J. D.; Ojima, I. Design, Synthesis, and Biological Evaluations of Tumor-Targeting Dual-Warhead Conjugates for a Taxoid-Camptothecin Combination Chemotherapy. *J. Med. Chem.* **2014**, *57*, 5777-5791.

(31) Vineberg, J. G.; Wang, T.; Zuniga, E. S.; Ojima, I. Design, Synthesis, and Biological Evaluation of Theranostic Vitamin-Linker-Taxoid Conjugates. *J. Med. Chem.* **2015**, *58*, 2406-2416.

(32) Kneeland, D. M.; Ariga, K.; Lynch, V. M.; Huang, C. Y.; Anslyn, E. V. Bis(alkylguanidinium) receptors for phosphodiesterases: effect of counterions, solvent mixtures, and cavity flexibility on complexation. *J. Am. Chem. Soc.* **1993**, *115*, 10042-10055.

(33) Jensen, K. B.; Braxmeier, T. M.; Demarcus, M.; Frey, J. G.; Kilburn, J. D. Synthesis of Guanidinium-Derived Receptor Libraries and Screening for Selective Peptide Receptors in Water. *Chem.-Eur. J.* **2002**, *8*, 1300-1309.

- (34) Goswami, L. N.; Houston, Z. H.; Sarma, S. J.; Jalisatgi, S. S.; Hawthorne, M. F. Efficient synthesis of diverse heterobifunctionalized clickable oligo(ethylene glycol) linkers: potential applications in bioconjugation and targeted drug delivery. *Org. Biomol. Chem.* **2013**, *11*, 1116-1126.
- (35) Schwabacher, A. W.; Lane, J. W.; Schiesher, M. W.; Leigh, K. M.; Johnson, C. W. Desymmetrization Reactions: Efficient Preparation of Unsymmetrically Substituted Linker Molecules. *J. Org. Chem.* **1998**, *63*, 1727-1729.
- (36) Banerjee, P. S.; Zuniga, E. S.; Ojima, I.; Carrico, I. S. Targeted and armed oncolytic adenovirus via chemoselective modification. *Bioorg. Med. Chem. Lett.* **2011**, *21*, 4985-4988.
- (37) Agard, N. J.; Baskin, J. M.; Prescher, J. A.; Lo, A.; Bertozzi, C. R. A Comparative Study of Bioorthogonal Reactions with Azides. *ACS Chem. Biol.* **2006**, *1*, 644-648.
- (38) Bernardin, A.; Cazet, A.; Guyon, L.; Delannoy, P.; Vinet, F.; Bonnaffé, D.; Texier, I. Copper-Free Click Chemistry for Highly Luminescent Quantum Dot Conjugates: Application to in Vivo Metabolic Imaging. *Bioconj. Chem.* **2010**, *21*, 583-588.
- (39) Evans, H. L.; Slade, R. L.; Carroll, L.; Smith, G.; Nguyen, Q.-D.; Iddon, L.; Kamaly, N.; Stockmann, H.; Leeper, F. J.; Aboagye, E. O.; Spivey, A. C. Copper-free click-a promising tool for pre-targeted PET imaging. *Chem. Commun.* **2012**, *48*, 991-993.
- (40) Lazarova, N.; James, S.; Babich, J.; Zubieta, J. A convenient synthesis, chemical characterization and reactivity of  $[\text{Re}(\text{CO})_3(\text{H}_2\text{O})_3]\text{Br}$ : the crystal and molecular structure of  $[\text{Re}(\text{CO})_3(\text{CH}_3\text{CN})_2\text{Br}]$ . *Inorg. Chem. Commun.* **2004**, *7*, 1023-1026.
- (41) Cox, C.; Ferraris, D.; Murthy, N. N.; Lectka, T. Copper(II)-Catalyzed Amide Isomerization: Evidence for N-Coordination. *J. Am. Chem. Soc.* **1996**, *118*, 5332-5333.
- (42) Barrera, I. F.; Maxwell, C. I.; Neverov, A. A.; Brown, R. S. Cu(II)-Promoted Methanolysis of N,N-Dipicolylacetamide. Multistep Activation by Decoupling of  $>\ddot{\text{N}}-\text{C}=\text{O}$  Resonance via Cu(II)-N Binding, Delivery of the Cu(II): $(-\text{OCH}_3)$  Nucleophile, and Metal Ion Assistance of the Departure of the Leaving Group. *J. Org. Chem.* **2012**, *77*, 4156-4160.
- (43) Niklas, N.; Hampel, F.; Liehr, G.; Zahl, A.; Alsfasser, R. The Reactivity of N-Coordinated Amides in Metallopeptide Frameworks: Molecular Events in Metal-Induced Pathogenic Pathways? *Chem.-Eur. J.* **2001**, *7*, 5135-5142.
- (44) Gasser, G.; Sosniak, A. M.; Leonidova, A.; Braband, H.; Metzler-Nolte, N. Towards the preparation of novel  $\text{Re}^{99\text{m}}\text{Tc}$  tricarbonyl-containing peptide nucleic acid bioconjugates. *Aust. J. Chem.* **2011**, *64*, 265-272.
- (45) Yamanaka, S.; Ōkawa, H.; Motoda, K.-i.; Yonemura, M.; Fenton, D. E.; Ebadi, M.; Lever, A. B. P. Tetracopper Assembly Complexes Comprised of One Dimetallic Core and Two Monometallic Auxiliaries: Intramolecular Electron-Transfer Relevant to Multicopper Oxidases. *Inorg. Chem.* **1999**, *38*, 1825-1830.
- (46) Pimentel, L. C. F.; de Souza, A. L. F.; Fernández, T. L.; Wardell, J. L.; Antunes, O. A. C. Microwave-assisted synthesis of N,N-bis-(2-pyridylmethyl)amine derivatives. Useful ligands in coordination chemistry. *Tetrahedron Lett.* **2007**, *48*, 831-833.
- (47) Borcard, F. o.; Godinat, A. I.; Staedler, D.; Comas Blanco, H.; Dumont, A.-L.; Chapuis-Bernasconi, C.; Scaletta, C.; Applegate, L. A.; Krauss Juillerat, F.; Gonzenbach, U. T.; Gerber-Lemaire, S.; Juillerat-Jeanneret, L. Covalent Cell Surface Functionalization of Human Fetal Osteoblasts for Tissue Engineering. *Bioconj. Chem.* **2011**, *22*, 1422-1432.
- (48) Hoigebazar, L.; Jeong, J. M.; Choi, S. Y.; Choi, J. Y.; Shetty, D.; Lee, Y.-S.; Lee, D. S.; Chung, J.-K.; Lee, M. C.; Chung, Y. K. Synthesis and Characterization of Nitroimidazole Derivatives for

- <sup>68</sup>Ga-Labeling and Testing in Tumor Xenografted Mice. *J. Med. Chem.* **2010**, *53*, 6378-6385.
- (49) Liu, Z.; Yan, Y.; Liu, S.; Wang, F.; Chen, X. <sup>18</sup>F, <sup>64</sup>Cu, and <sup>68</sup>Ga Labeled RGD-Bombesin Heterodimeric Peptides for PET Imaging of Breast Cancer. *Bioconj. Chem.* **2009**, *20*, 1016-1025.
- (50) Yang, C.-T.; Kim, Y.-S.; Wang, J.; Wang, L.; Shi, J.; Li, Z.-B.; Chen, X.; Fan, M.; Li, J.-J.; Liu, S. <sup>64</sup>Cu-labeled 2-(diphenylphosphoryl)ethyl-diphenylphosphonium cations as highly selective tumor imaging agents: effects of linkers and chelates on radiotracer biodistribution characteristics. *Bioconj. Chem.* **2008**, *19*, 2008-2022.
- (51) Dissoki, S.; Hagooly, A.; Elmachily, S.; Mishani, E. Labeling approaches for the GE11 peptide, an epidermal growth factor receptor biomarker. *J Labelled Comp Radiopharm* **2011**, *54*, 693-701.
- (52) Mistry, S. N.; Baker, J. G.; Fischer, P. M.; Hill, S. J.; Gardiner, S. M.; Kellam, B. Synthesis and in Vitro and in Vivo Characterization of Highly  $\beta$ 1-Selective  $\beta$ -Adrenoceptor Partial Agonists. *J. Med. Chem.* **2013**, *56*, 3852-3865.

## References for Chapter 5:

- (1) European Science Foundation. European Science Foundation Forward Look on Nanomedicine. European Science Foundation <http://www.esf.org/publication/196/ESPB23.pdf> (2005).
- (2) Duncan, R. Polymer conjugates as anticancer nanomedicines. *Nat. Rev. Cancer* **2006**, *6*, 688-701.
- (3) Wicki, A.; Witzigmann, D.; Balasubramanian, V.; Huwyler, J. Nanomedicine in cancer therapy: Challenges, opportunities, and clinical applications. *J. Controlled Release* **2015**, *200*, 138-157.
- (4) Karve, S.; Werner, M. E.; Sukumar, R.; Cummings, N. D.; Copp, J. A.; Wang, E. C.; Li, C.; Sethi, M.; Chen, R. C.; Pacold, M. E.; Wang, A. Z. Revival of the abandoned therapeutic wortmannin by nanoparticle drug delivery. *Proc Natl Acad Sci* **2012**, *109*, 8230-8235.
- (5) Peer, D.; Karp, J. M.; Hong, S.; Farokhzad, O. C.; Margalit, R.; Langer, R. Nanocarriers as an emerging platform for cancer therapy. *Nat Nano* **2007**, *2*, 751-760.
- (6) Min, Y.; Caster, J. M.; Eblan, M. J.; Wang, A. Z. Clinical Translation of Nanomedicine. *Chem. Rev.* **2015**.
- (7) Trivedi, V. Dendrimer: polymer of 21st century. *IJPRBS* **2012**, *1*, 1-21.
- (8) Kannan, R. M.; Kannan, S.; Romero, R.; Navath, R. S.; Dai, H.; Menjoge, A. R.; **2012**, US20120003155 A1.
- (9) B.Pavan Kumar, I. S., B.Bhavya, Sravanthi.U, Sindhuri.M Dendrimer: a complete drug carrier. *IJPRR* **2011**, *1*, 25-39.
- (10) Prajapat R , S. B., Jain S , Bhandari. A Dendrimer: a polymer of 21st century. *WebmedCentral Pharmaceutical Sciences* **2010**, *1*, WMC00745.
- (11) Gillies, E. R.; Fréchet, J. M. J. Dendrimers and dendritic polymers in drug delivery. *Drug Discov Today*. **2005**, *10*, 35-43.
- (12) Maiti, P. K.; Çağın, T.; Wang, G.; Goddard, W. A. Structure of PAMAM Dendrimers: Generations 1 through 11. *Macromolecules* **2004**, *37*, 6236-6254.
- (13) Svenson, S.; Tomalia, D. A. Dendrimers in biomedical applications—reflections on the field. *Adv. Drug Del. Rev.* **2005**, *57*, 2106-2129.
- (14) Buhleier, E.; Wehner, W.; Vögtle, F. "Cascade"- and "Nonskid-Chain-like" Syntheses of Molecular Cavity Topologies. *Synthesis* **1978**, *2*, 155-158.
- (15) Tomalia, D. A.; Baker, H.; Dewald, J.; Hall, M.; Kallos, G.; Martin, S.; Roeck, J.; Ryder, J.; Smith, P. A New Class of Polymers: Starburst-Dendritic Macromolecules. *Polym. J.* **1985**, *17*, 117-132.
- (16) Majoros, I. J.; Thomas, T. P.; Mehta, C. B.; Baker, J. R. Poly(amidoamine) Dendrimer-Based Multifunctional Engineered Nanodevice for Cancer Therapy. *J. Med. Chem.* **2005**, *48*, 5892-5899.
- (17) Matsumura, Y.; Maeda, H. A New Concept for Macromolecular Therapeutics in Cancer Chemotherapy: Mechanism of Tumor-tropic Accumulation of Proteins and the Antitumor Agent Smancs. *Cancer Res.* **1986**, *46*, 6387-6392.
- (18) Noguchi, Y.; Wu, J.; Duncan, R.; Strohalm, J.; Ulbrich, K.; Akaike, T.; Maeda, H. Early Phase Tumor Accumulation of Macromolecules: A Great Difference in Clearance Rate between Tumor and Normal Tissues. *Jpn. J. Cancer Res.* **1998**, *89*, 307-314.
- (19) Ellis, L. M.; Liu, W.; Fan, F.; Reinmuth, N.; Shaheen, R. M.; Jung, Y. D.; Ahmad, S. Role of angiogenesis inhibitors in cancer treatment. *Oncology (Williston Park)* **2001**, *15*, 39-46.
- (20) Park, K. Polysaccharide-based near-infrared fluorescence nanoprobe for cancer diagnosis. *Quant Imaging Med Surg.* **2012**, *2*, 106-113.



- (21) Jansen, J. F. G. A.; de Brabander-van den Berg, E. M. M.; Meijer, E. W. Encapsulation of Guest Molecules into a Dendritic Box. *Science* **1994**, *266*, 1226-1229.
- (22) Hawker, C. J.; Wooley, K. L.; Frechet, J. M. J. Unimolecular micelles and globular amphiphiles: dendritic macromolecules as novel recyclable solubilization agents. *J. Chem. Soc., Perkin Trans. 1* **1993**, 1287-1297.
- (23) Islam, M. T.; Majoros, I. J.; Baker Jr, J. R. HPLC analysis of PAMAM dendrimer based multifunctional devices. *J. Chromatogr. B* **2005**, *822*, 21-26.
- (24) Thomas, T. P.; Majoros, I. J.; Kotlyar, A.; Kukowska-Latallo, J. F.; Bielinska, A.; Myc, A.; Baker, J. R. Targeting and Inhibition of Cell Growth by an Engineered Dendritic Nanodevice. *J. Med. Chem.* **2005**, *48*, 3729-3735.
- (25) Paleos, C. M.; Tsiourvas, D.; Sideratou, Z.; Tziveleka, L. Acid- and Salt-Triggered Multifunctional Poly(propylene imine) Dendrimer as a Prospective Drug Delivery System. *Biomacromolecules* **2004**, *5*, 524-529.
- (26) Malik, N.; Evagorou, E. G.; Duncan, R. Dendrimer-platinate: a novel approach to cancer chemotherapy. *Anticancer Drugs* **1999**, *10*, 767-776.
- (27) Tomalia, D. A.; Naylor, A. M.; Goddard, W. A. Starburst Dendrimers: Molecular-Level Control of Size, Shape, Surface Chemistry, Topology, and Flexibility from Atoms to Macroscopic Matter. *Angew. Chem. Int. Ed.* **1990**, *29*, 138-175.
- (28) Peterson, J.; Allikmaa, V.; Subbi, J.; Pehk, T.; Lopp, M. Structural deviations in poly(amidoamine) dendrimers: a MALDI-TOF MS analysis. *Eur. Polym. J.* **2003**, *39*, 33-42.
- (29) Mullen, D. G.; Fang, M.; Desai, A.; Baker, J. R.; Orr, B. G.; Banaszak Holl, M. M. A Quantitative Assessment of Nanoparticle–Ligand Distributions: Implications for Targeted Drug and Imaging Delivery in Dendrimer Conjugates. *ACS Nano* **2010**, *4*, 657-670.
- (30) Gaertner, H. F.; Cerini, F.; Kamath, A.; Rochat, A.-F. o.; Siegrist, C.-A.; Menin, L.; Hartley, O. Efficient Orthogonal Bioconjugation of Dendrimers for Synthesis of Bioactive Nanoparticles. *Bioconjugate Chem.* **2011**, *22*, 1103-1114.
- (31) Mezo, A. R.; Low, S. C.; Hoehn, T.; Palmieri, H. PEGylation enhances the therapeutic potential of peptide antagonists of the neonatal Fc receptor, FcRn. *Bioorg. Med. Chem. Lett.* **2011**, *21*, 6332-6335.
- (32) Goswami, L. N.; Houston, Z. H.; Sarma, S. J.; Jalisatgi, S. S.; Hawthorne, M. F. Efficient synthesis of diverse heterobifunctionalized clickable oligo(ethylene glycol) linkers: potential applications in bioconjugation and targeted drug delivery. *Org. Biomol. Chem.* **2013**, *11*, 1116-1126.
- (33) Carter, R. L.; Johnson, B. F.; Sood, A.; Rishel, M. J.; Valliant, J. F.; Stephenson, K. A.; Wu, T.; Yang, Y. **2013**, *US20130261311A1*, 20pp.
- (34) Prodhomme, E. J. F.; Tutt, A. L.; Glennie, M. J.; Bugg, T. D. H. Multivalent Conjugates of Poly- $\gamma$ -d-glutamic Acid from *Bacillus licheniformis* with Antibody F(ab') and Glycopeptide Ligands. *Bioconjugate Chem.* **2003**, *14*, 1148-1155.
- (35) Han, J.; Sun, L.; Chu, Y.; Li, Z.; Huang, D.; Zhu, X.; Qian, H.; Huang, W. Design, Synthesis, and Biological Activity of Novel Dicoumarol Glucagon-like Peptide 1 Conjugates. *J. Med. Chem.* **2013**, *56*, 9955-9968.
- (36) Chen, S.; Zhao, X.; Chen, J.; Chen, J.; Kuznetsova, L.; Wong, S. S.; Ojima, I. Mechanism-Based Tumor-Targeting Drug Delivery System. Validation of Efficient Vitamin Receptor-Mediated Endocytosis and Drug Release. *Bioconjugate Chem.* **2010**, *21*, 979-987.
- (37) Goussé, C.; Gandini, A. Diels–Alder polymerization of difurans with bismaleimides. *Polym.*

*Int.* **1999**, *48*, 723-731.

(38) Bradshaw, C. W.; Doppalapudi, V. R.; Lai, J.-Y.; Rizzo, J. **2006**, *WO2006094269A2*, 299pp.

(39) Bradshaw, C.; Sakamuri, S.; Fu, Y.; Oates, B.; Desharnais, J.; Tumelty, D. **2008**, *WO2008081418A1*, 227 pp.

(40) Carter, R. L.; Johnson, B. F.; Sood, A.; Rishel, M. J.; Valliant, J. F.; Stephenson, K. A.; Wu, T.; Yang, Y. **2013**, *US20130261311A1*, 20pp.; Chemical Indexing Equivalent to 159:577037 (WO).

## References for Chapter 6:

- (1) Galina I Botchkina, E. S. Z., Manisha Das, Yuan Wang, Haichao Wang, Shu Zhu, Anne G Savitt, Rebecca A Rowehl, Yan Leyfman, Jingfang Ju, Kenneth Shroyer and Iwao Ojima New-generation taxoid SB-T-1214 inhibits stem cell-related gene expression in 3D cancer spheroids induced by purified colon tumor-initiating cells. *Mol. Cancer* **2010**, *9*, 192.
- (2) Galina Botchkina, I. O.; InTech, Prostate and Colon Cancer Stem Cells as a Target for Anti-Cancer Drug Development. *Cancer Stem Cells Theories and Practice*, Chapter 8. 2011.
- (3) Fraser, J. R. E.; Laurent, T. C.; Laurent, U. B. G. Hyaluronan: its nature, distribution, functions and turnover. *J. Intern. Med.* **1997**, *242*, 27-33.
- (4) Lim, S. T.; Martin, G. P.; Berry, D. J.; Brown, M. B. Preparation and evaluation of the in vitro drug release properties and mucoadhesion of novel microspheres of hyaluronic acid and chitosan. *J. Controlled Release* **2000**, *66*, 281-292.
- (5) Yoon, H. Y.; Koo, H.; Choi, K. Y.; Chan Kwon, I.; Choi, K.; Park, J. H.; Kim, K. Photocrosslinked hyaluronic acid nanoparticles with improved stability for in vivo tumor-targeted drug delivery. *Biomaterials* **2013**, *34*, 5273-5280.
- (6) Al-Hajj, M.; Wicha, M. S.; Benito-Hernandez, A.; Morrison, S. J.; Clarke, M. F. Prospective identification of tumorigenic breast cancer cells. *Proc. Natl. Acad. Sci.* **2003**, *100*, 3983-3988.
- (7) Zeppernick, F.; Ahmadi, R.; Campos, B.; Dictus, C.; Helmke, B. M.; Becker, N.; Lichter, P.; Unterberg, A.; Radlwimmer, B.; Herold-Mende, C. C. Stem Cell Marker CD133 Affects Clinical Outcome in Glioma Patients. *Clin. Cancer. Res.* **2008**, *14*, 123-129.
- (8) Maeda, S.; Shinchi, H.; Kurahara, H.; Mataka, Y.; Maemura, K.; Sato, M.; Natsugoe, S.; Aikou, T.; Takao, S. CD133 expression is correlated with lymph node metastasis and vascular endothelial growth factor-C expression in pancreatic cancer. *Br. J. Cancer* **2008**, *98*, 1389-1397.
- (9) Horst, D.; Kriegl, L.; Engel, J.; Kirchner, T.; Jung, A. CD133 expression is an independent prognostic marker for low survival in colorectal cancer. *Br. J. Cancer* **2008**, *99*, 1285-1289.
- (10) Dean, M.; Fojo, T.; Bates, S. Tumour stem cells and drug resistance. *Nat. Rev. Cancer* **2005**, *5*, 275-284.
- (11) Donnenberg, V. S.; Donnenberg, A. D. Multiple Drug Resistance in Cancer Revisited: The Cancer Stem Cell Hypothesis. *J. Clin. Pharmacol.* **2005**, *45*, 872-877.
- (12) Mimeault, M.; Batra, S. K. Recent progress on normal and malignant pancreatic stem/progenitor cell research: therapeutic implications for the treatment of type 1 or 2 diabetes mellitus and aggressive pancreatic cancer. *Gut* **2008**, *57*, 1456-1468.
- (13) Sau-Hung Spence, L.; Robinson, J. R. The contribution of anionic polymer structural features to mucoadhesion. *J. Controlled Release* **1987**, *5*, 223-231.
- (14) Bao, B. A., A.; Azmi, A.; Ali, S.; Sarkar, F. et al. Cancer Stem Cells (CSCs) and Mechanisms of Their Regulation: Implications for Cancer Therapy. *Curr Protoc. Pharmacol.* **2013**, *14*, 1-32.
- (15) Gerlinger, M. e. a. Intratumor Heterogeneity and Branched Evolution Revealed by Multiregion Sequencing. *New Engl. J. Med.* **2012**, *336*, 883-892.
- (16) Toole, B. Hyaluronan-CD44 Interactions in Cancer: Paradoxes and Possibilities. *Clin. Cancer Res.* **2009**, *15*, 7462-7468.
- (17) Miletti-Gonzalez, K. C., S.; Muthukamaran, N.; et al The CD44 Receptor Interacts with P-Glycoprotein to Promote Cell Migration and Invasion in Cancer. *Cancer Res.* **2005**, *65*, 6660-6667.
- (18) Qhattal, H. S. S.; Liu, X. Characterization of CD44-Mediated Cancer Cell Uptake and

Intracellular Distribution of Hyaluronan-Grafted Liposomes. *Mol. Pharm.* **2011**, *8*, 1233-1246.

(19) Ojima, I. S., J.; Michaud, E.; Kuduk, S.; Bounaud, P.; Vrignaud, P.; Bissery, M.; Veith, J.; Pera, P.; Bernacki, R. Syntheses and structure-activity relationships of the second-generation antitumor taxoids: exceptional activity against drug-resistant cancer cells. *J. Med. Chem.* **1996**, *39*, 3889-3896.

(20) Ojima, I. Z., E.; Berger, W.; Seitz, J. Tumor-targeting drug delivery of new-generation taxoids. *Future Med. Chem.* **2012**, *4*, 33-50.

(21) Kuznetsova, L. C., J.; Sun, L. Wu, X.; Pepe, A.; Veith, J.; Pera, P.; Bernacki, R.; Ojima, I. Syntheses and evaluation of novel fatty acid-second-generation taxoid conjugates as promising anticancer agents. *Bioorg. Med. Chem. Lett.* **2006**, *16*, 974-977.

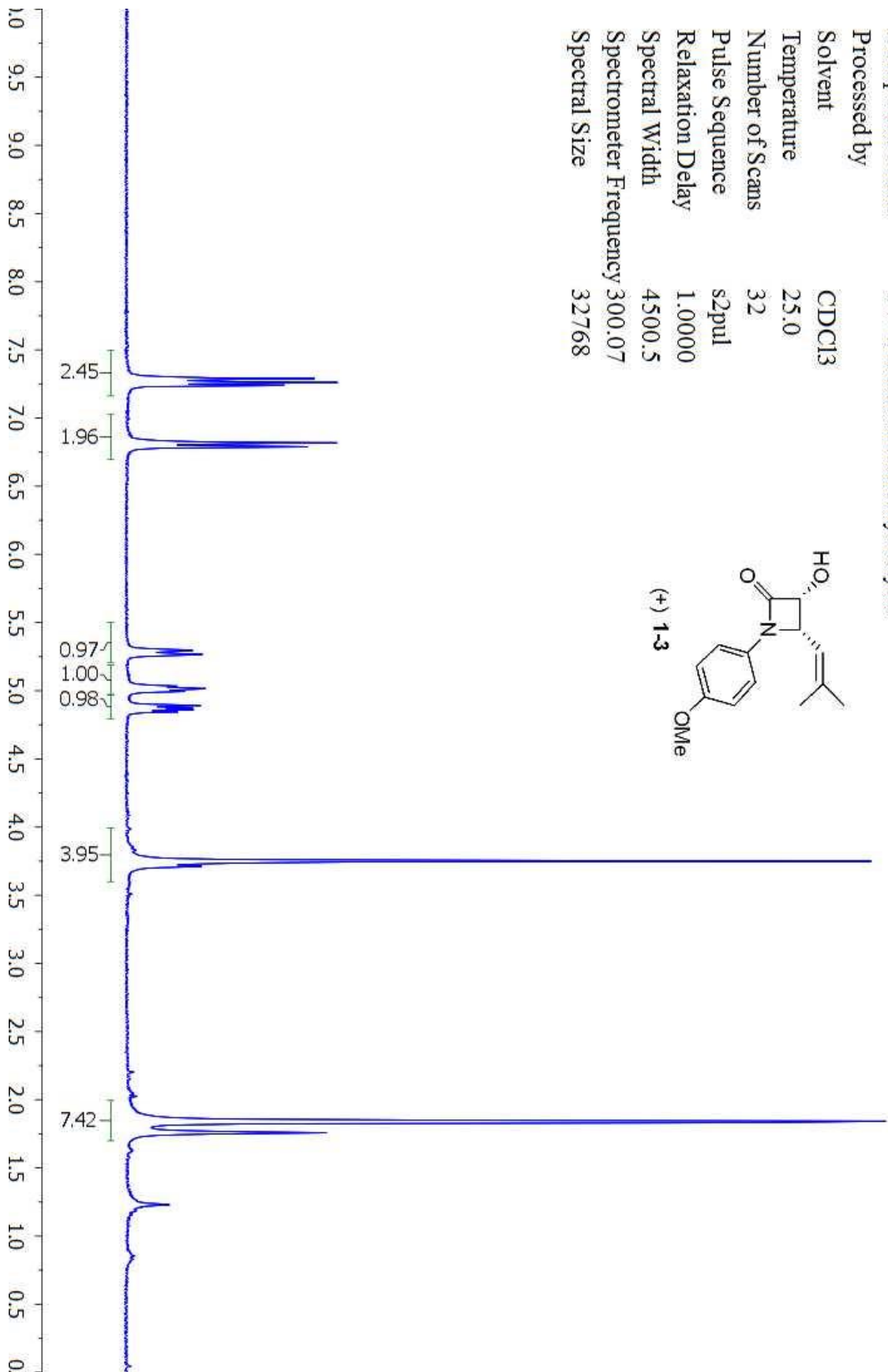
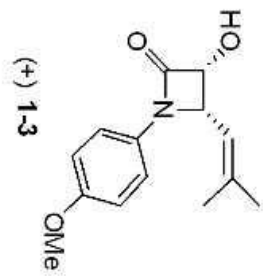
(22) Botchkina, G. e. a. New-generation taxoid SB-T-1214 inhibits stem cell-related gene expression in 3D cancer spheroids induced by purified colon tumor-initiating cells. *Mol. Cancer* **2010**, *9*, 192-204.

## Appendix

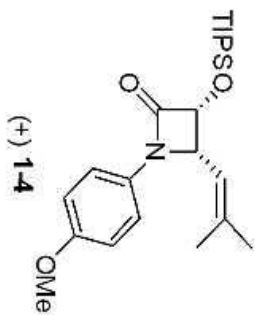
Appendix Chapter 1 NMR Spectra .....	A244-257
Appendix Chapter 2 NMR Spectra .....	A258-284
Appendix Chapter 3 NMR Spectra .....	A285-330
Appendix Chapter 4 NMR Spectra .....	A331-369
Appendix Chapter 5 NMR Spectra .....	A384-454
Appendix Chapter 6 NMR Spectra .....	A455-459

## Appendix Chapter 1 NMR Spectra

Compound Name TW-Plusalcoholafterhydrolysis  
Processed by  
Solvent CDCl3  
Temperature 25.0  
Number of Scans 32  
Pulse Sequence s2pul  
Relaxation Delay 1.0000  
Spectral Width 4500.5  
Spectrometer Frequency 300.07  
Spectral Size 32768

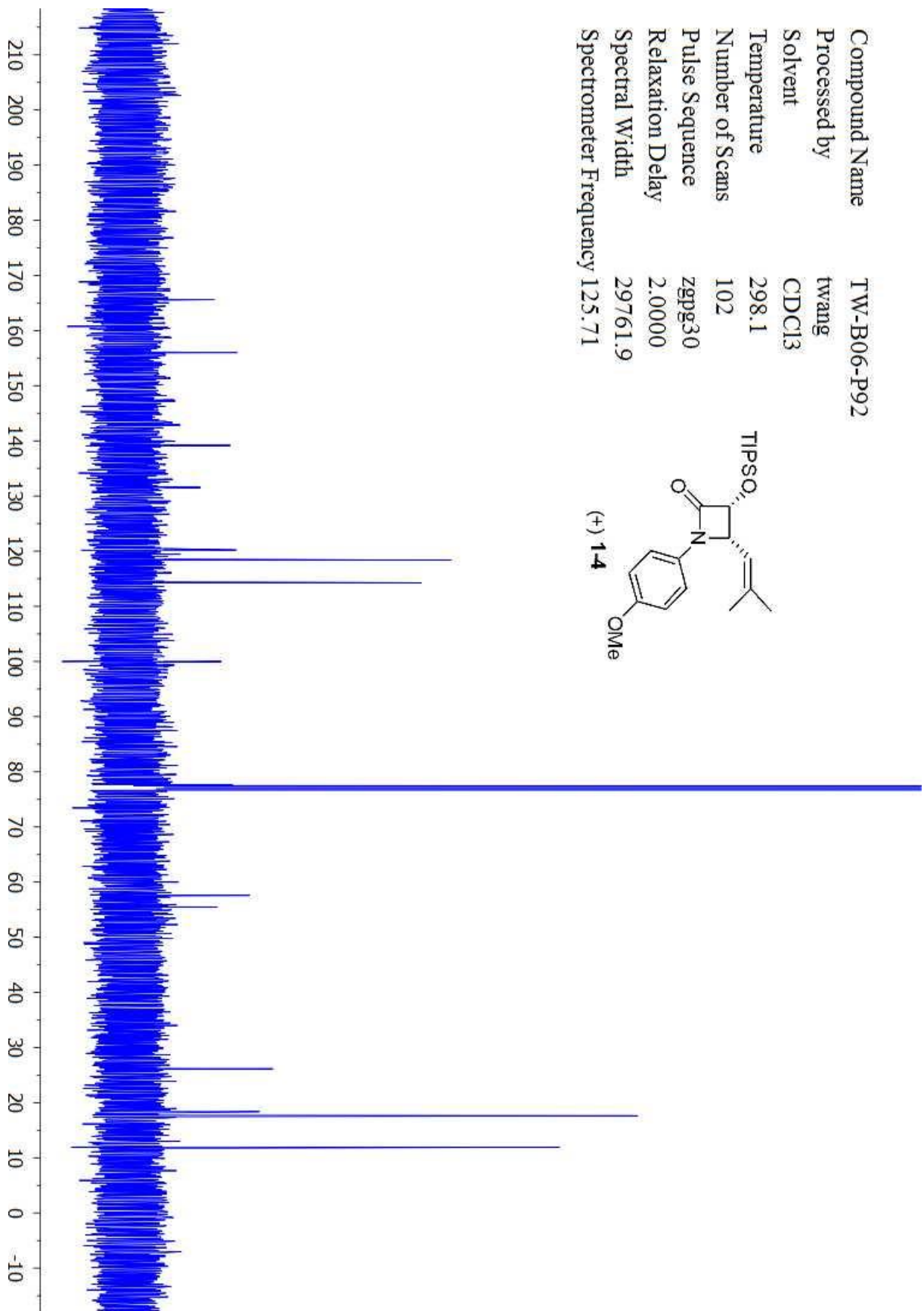
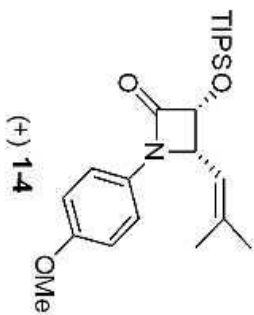


Compound Name TW-B06-P92  
Processed by twang  
Solvent CDCl3  
Temperature 298.1  
Number of Scans 16  
Pulse Sequence zg30  
Relaxation Delay 1.0000  
Spectral Width 10000.0  
Spectrometer Frequency 499.89

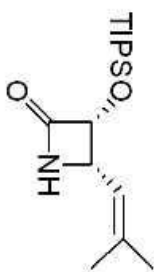




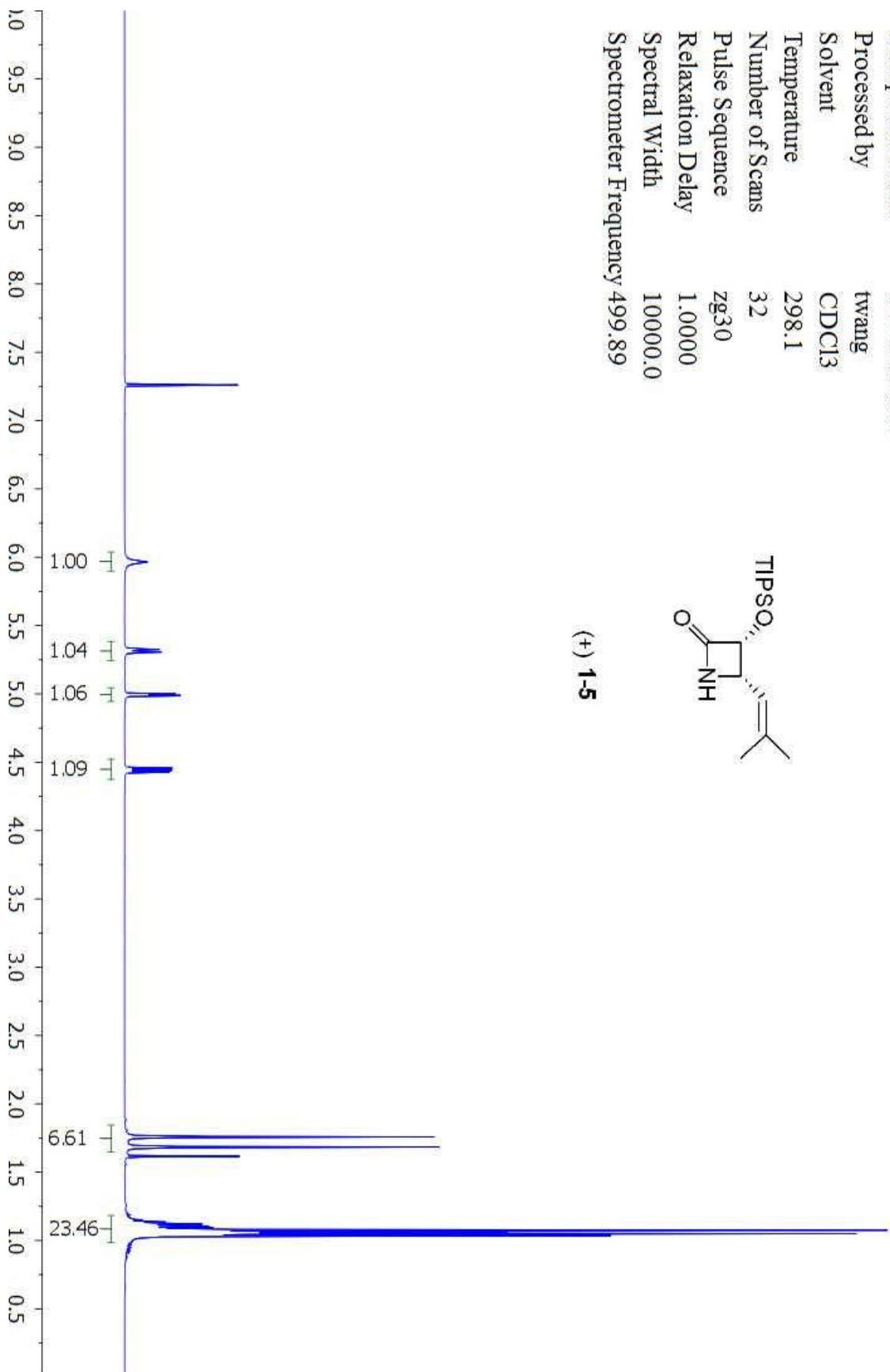
Compound Name TW-B06-P92  
Processed by twang  
Solvent CDCl3  
Temperature 298.1  
Number of Scans 102  
Pulse Sequence zgpg30  
Relaxation Delay 2.0000  
Spectral Width 29761.9  
Spectrometer Frequency 125.71



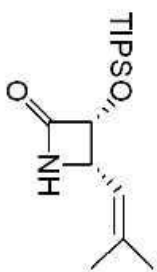
Compound Name TW-B06-P97  
Processed by twang  
Solvent CDCl3  
Temperature 298.1  
Number of Scans 32  
Pulse Sequence zg30  
Relaxation Delay 1.0000  
Spectral Width 10000.0  
Spectrometer Frequency 499.89



(+) 1-5



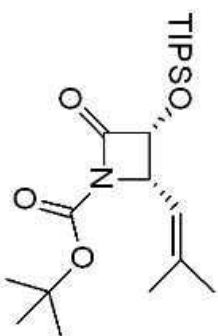
Compound Name TW-B06-P97  
Processed by twang  
Solvent CDCl3  
Temperature 298.2  
Number of Scans 57  
Pulse Sequence zgpg30  
Relaxation Delay 2.0000  
Spectral Width 29761.9  
Spectrometer Frequency 125.71



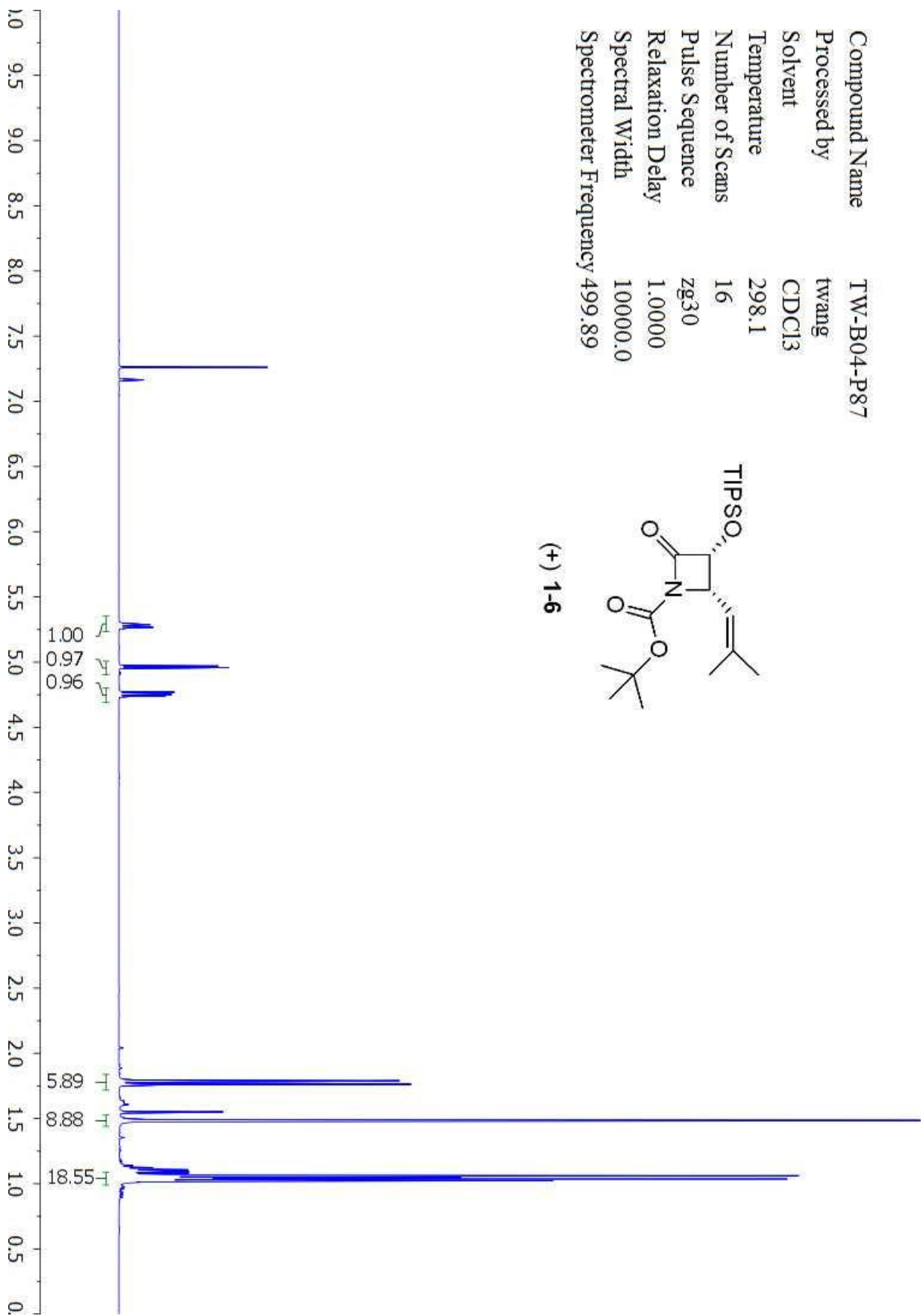
(+) 1-5



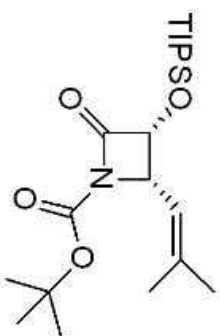
Compound Name TW-B04-P87  
Processed by twang  
Solvent CDCl3  
Temperature 298.1  
Number of Scans 16  
Pulse Sequence zg30  
Relaxation Delay 1.0000  
Spectral Width 10000.0  
Spectrometer Frequency 499.89



(+) 1-6



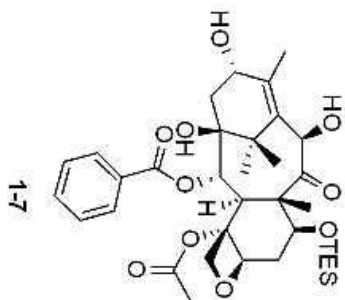
Compound Name TW-B04-P87  
Processed by twang  
Solvent CDCl3  
Temperature 298.2  
Number of Scans 203  
Pulse Sequence zgpg30  
Relaxation Delay 2.0000  
Spectral Width 29761.9  
Spectrometer Frequency 125.71



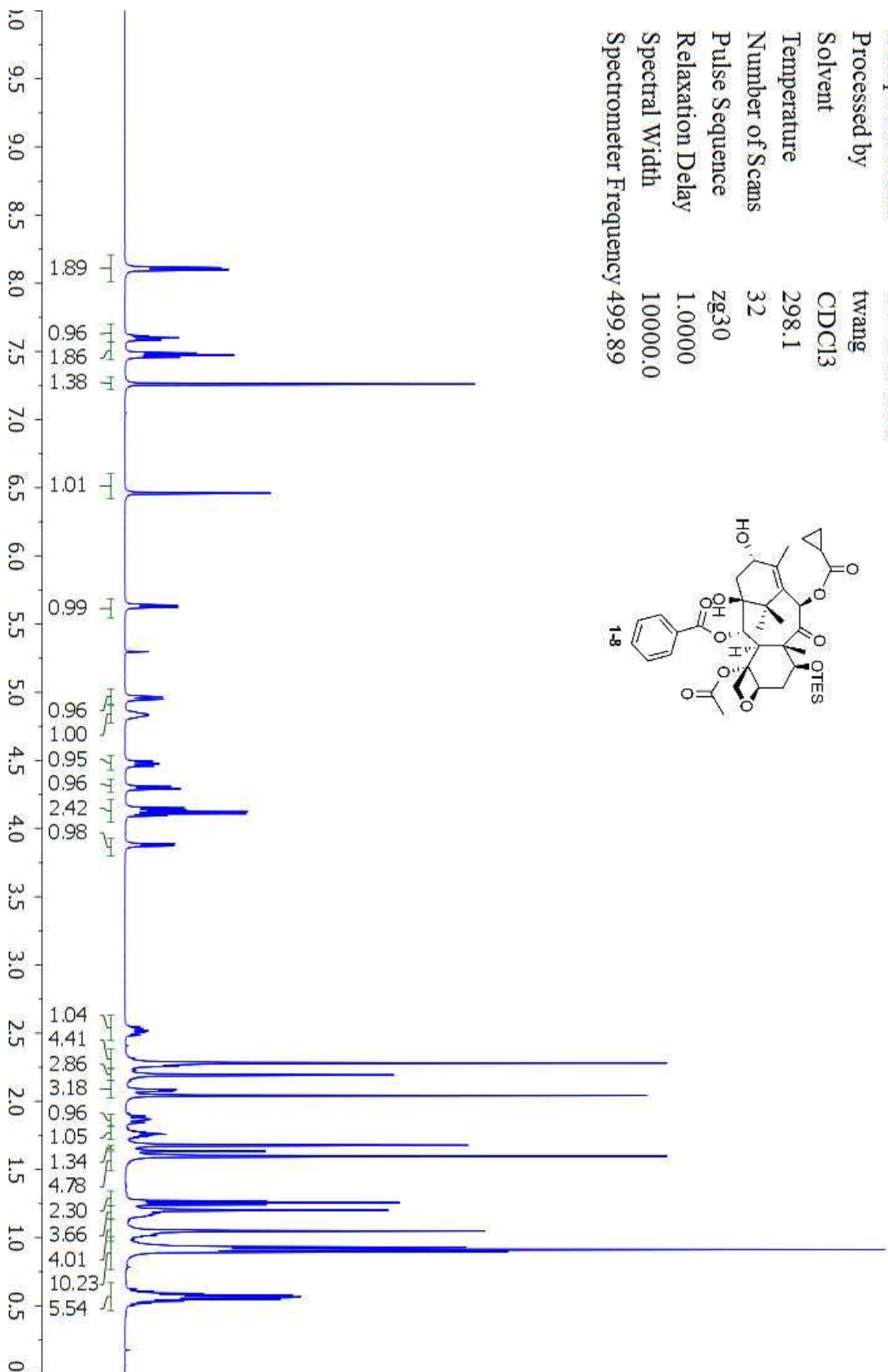
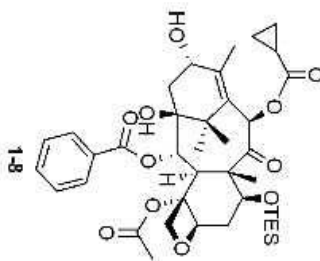
(+) 1-6



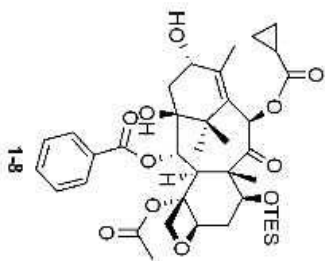
Compound Name TW-B02-1stcol  
 Processed by  
 Solvent CDCl3  
 Temperature 25.0  
 Number of Scans 32  
 Pulse Sequence s2pul  
 Relaxation Delay 1.0000  
 Spectral Width 4500.5  
 Spectrometer Frequency 300.07  
 Spectral Size 32768



Compound Name TW-B06-P06  
 Processed by twang  
 Solvent CDCl3  
 Temperature 298.1  
 Number of Scans 32  
 Pulse Sequence zg30  
 Relaxation Delay 1.0000  
 Spectral Width 10000.0  
 Spectrometer Frequency 499.89

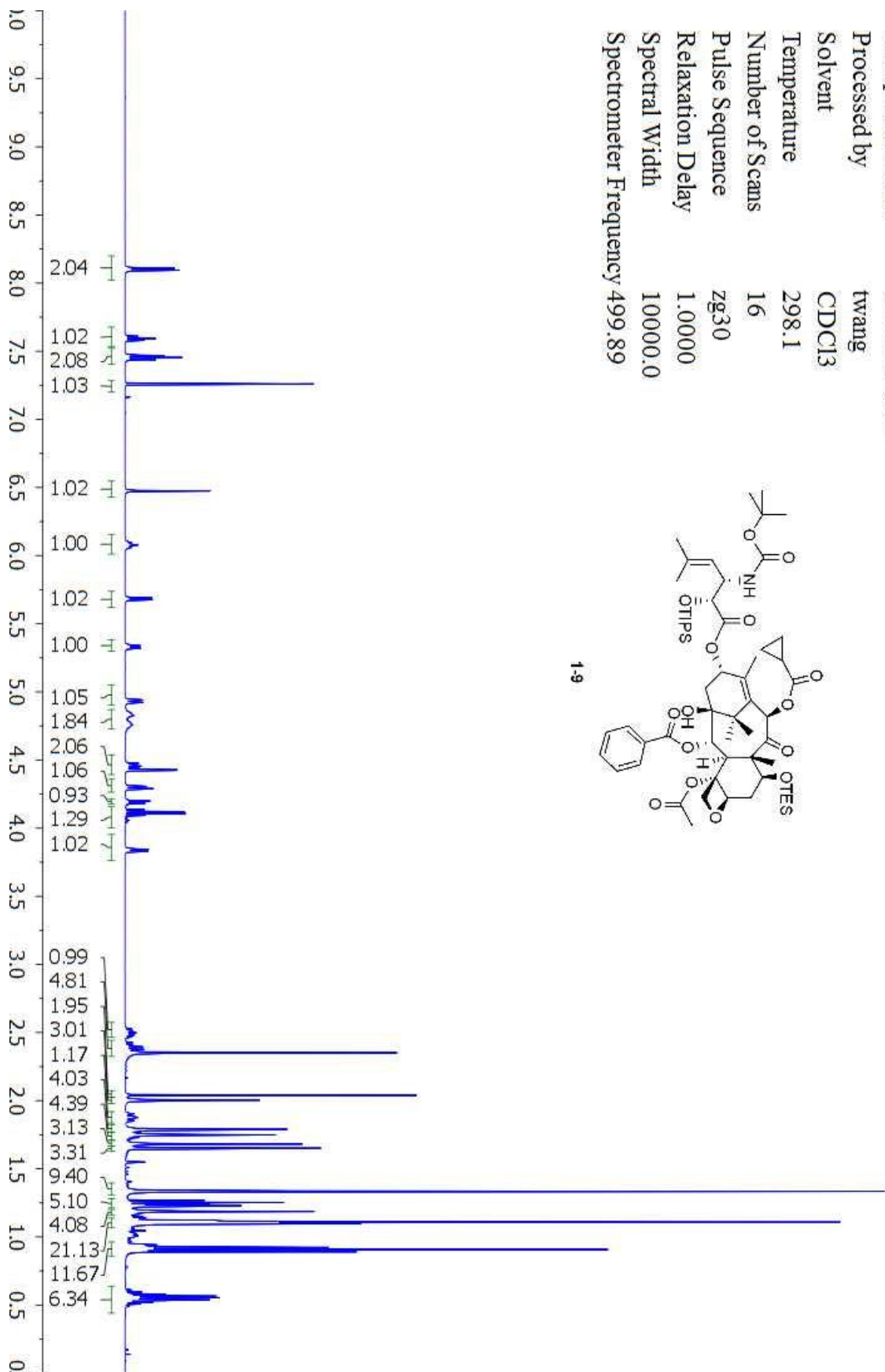
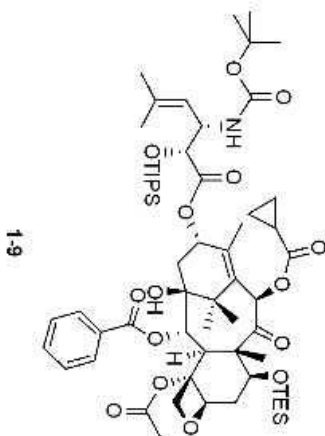


Compound Name TW-B06-P06  
Processed by twang  
Solvent CDCl3  
Temperature 298.1  
Number of Scans 200  
Pulse Sequence zgpg30  
Relaxation Delay 2.0000  
Spectral Width 29761.9  
Spectrometer Frequency 125.71

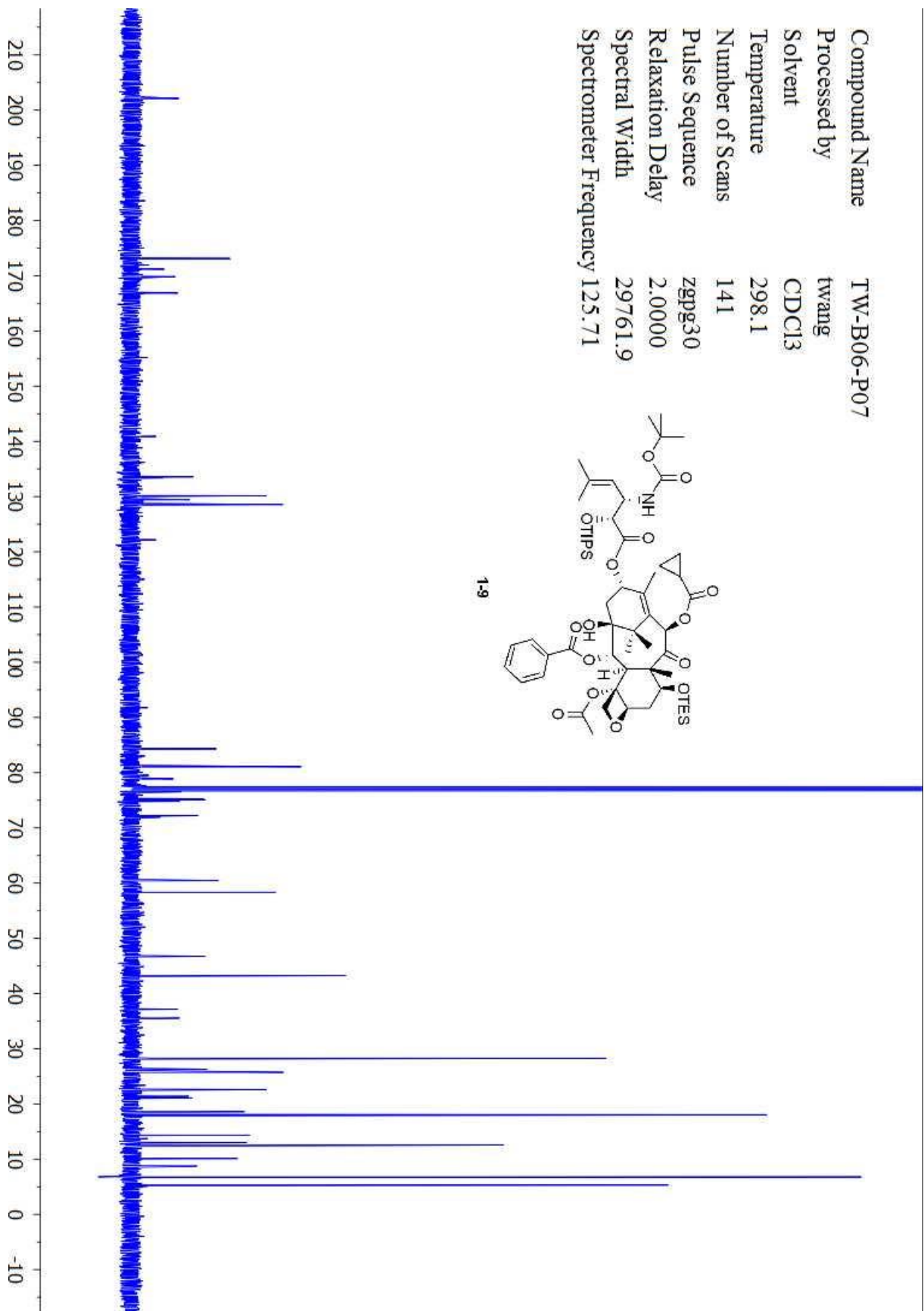
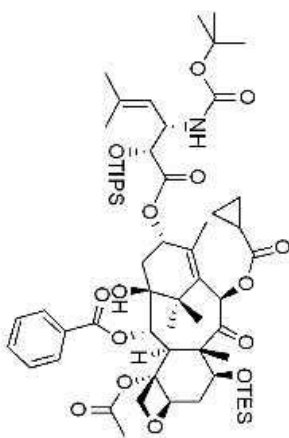




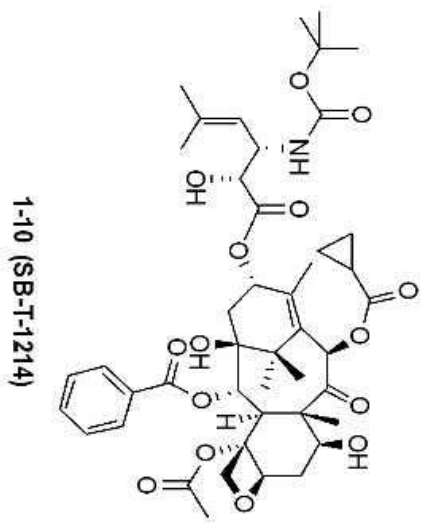
Compound Name TW-B06-P07  
 Processed by twang  
 Solvent CDCl3  
 Temperature 298.1  
 Number of Scans 16  
 Pulse Sequence zg30  
 Relaxation Delay 1.0000  
 Spectral Width 10000.0  
 Spectrometer Frequency 499.89



Compound Name TW-B06-P07  
Processed by twang  
Solvent CDCl3  
Temperature 298.1  
Number of Scans 141  
Pulse Sequence zgpg30  
Relaxation Delay 2.0000  
Spectral Width 29761.9  
Spectrometer Frequency 125.71

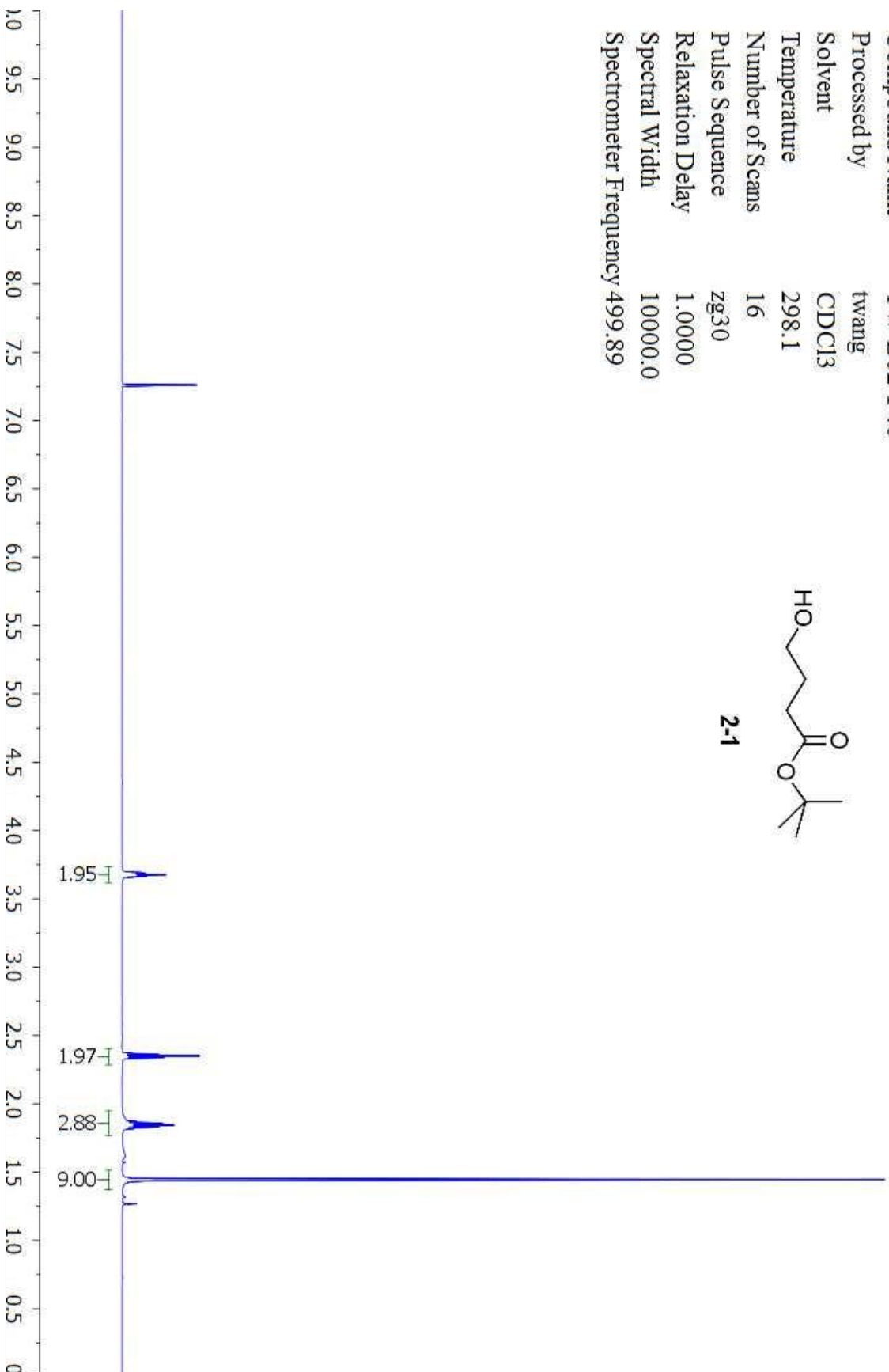
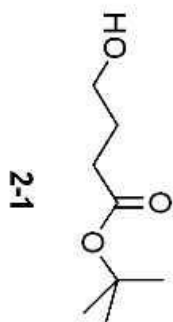


Compound Name TW-11-03-2010-SBT1214-2ndrun  
 Processed by  
 Solvent CDCl3  
 Temperature 25.0  
 Number of Scans 32  
 Pulse Sequence s2pul  
 Relaxation Delay 1.0000  
 Spectral Width 4500.5  
 Spectrometer Frequency 300.07  
 Spectral Size 32768

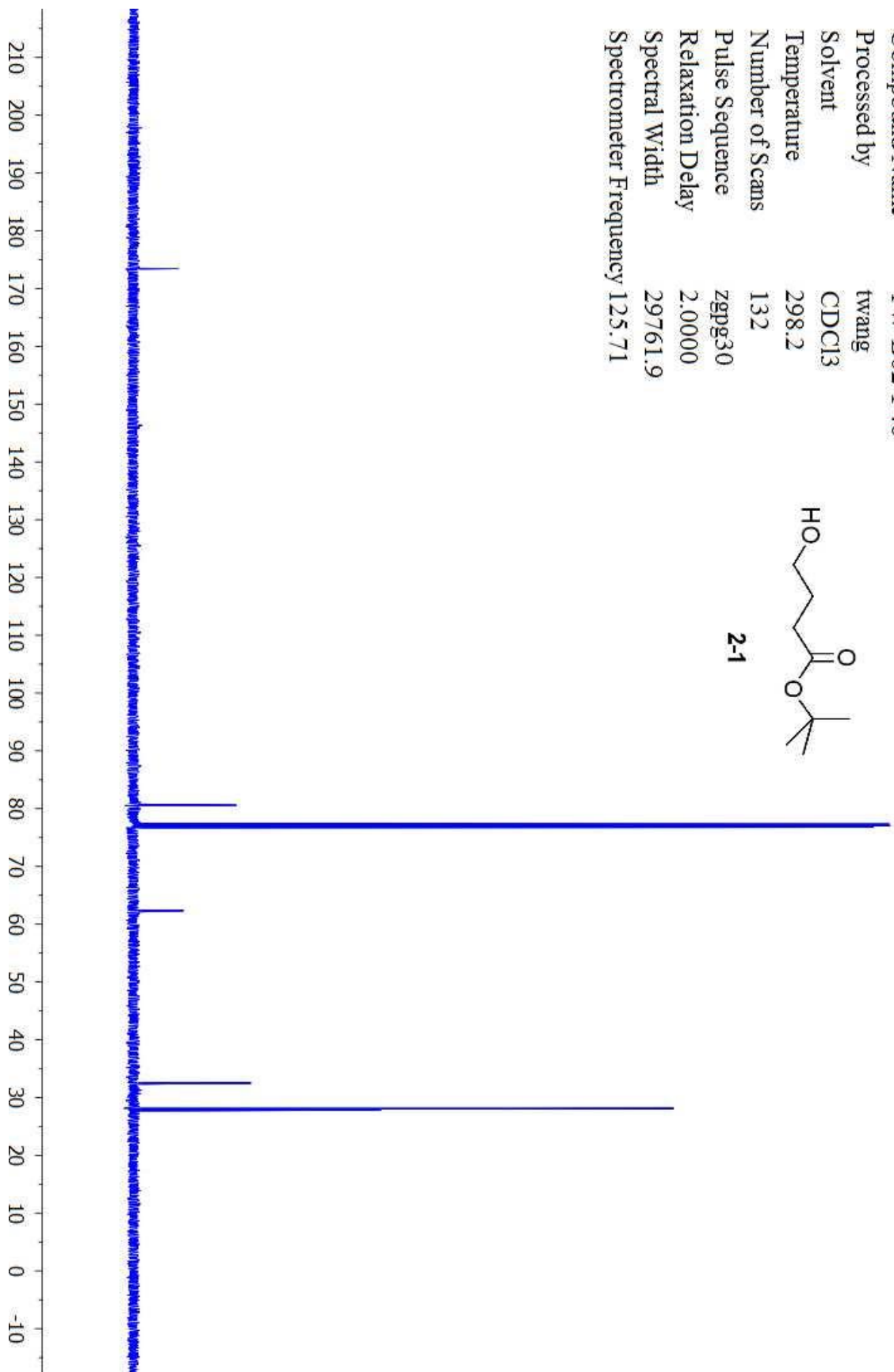
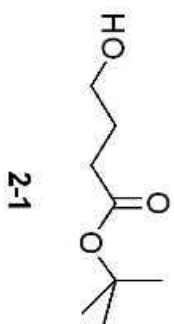


## Appendix Chapter 2 NMR Spectra

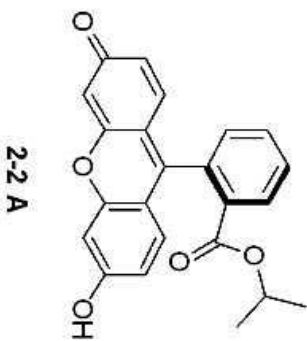
Compound Name TW-B02-P40  
Processed by twang  
Solvent CDCl3  
Temperature 298.1  
Number of Scans 16  
Pulse Sequence zg30  
Relaxation Delay 1.0000  
Spectral Width 10000.0  
Spectrometer Frequency 499.89



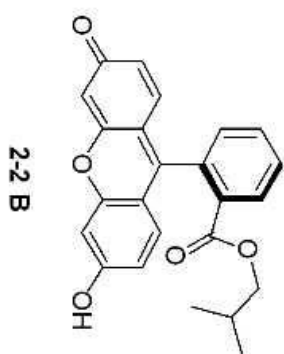
Compound Name TW-B02-P40  
Processed by twang  
Solvent CDCl3  
Temperature 298.2  
Number of Scans 132  
Pulse Sequence zgpg30  
Relaxation Delay 2.0000  
Spectral Width 29761.9  
Spectrometer Frequency 125.71



Compound Name TW-B02-P67-repurifiedSM1  
 Processed by  
 Solvent CD3OD  
 Temperature 25.0  
 Number of Scans 32  
 Pulse Sequence s2pul  
 Relaxation Delay 1.0000  
 Spectral Width 4500.5  
 Spectrometer Frequency 300.07  
 Spectral Size 32768

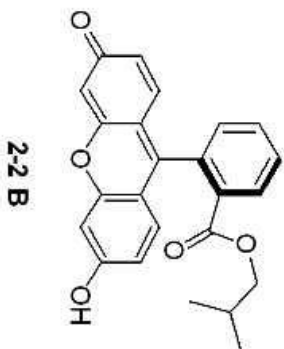


Compound Name TW-B02-P77  
Processed by twang  
Solvent CDCl3  
Temperature 298.2  
Number of Scans 32  
Pulse Sequence zg30  
Relaxation Delay 1.0000  
Spectral Width 10000.0  
Spectrometer Frequency 499.89

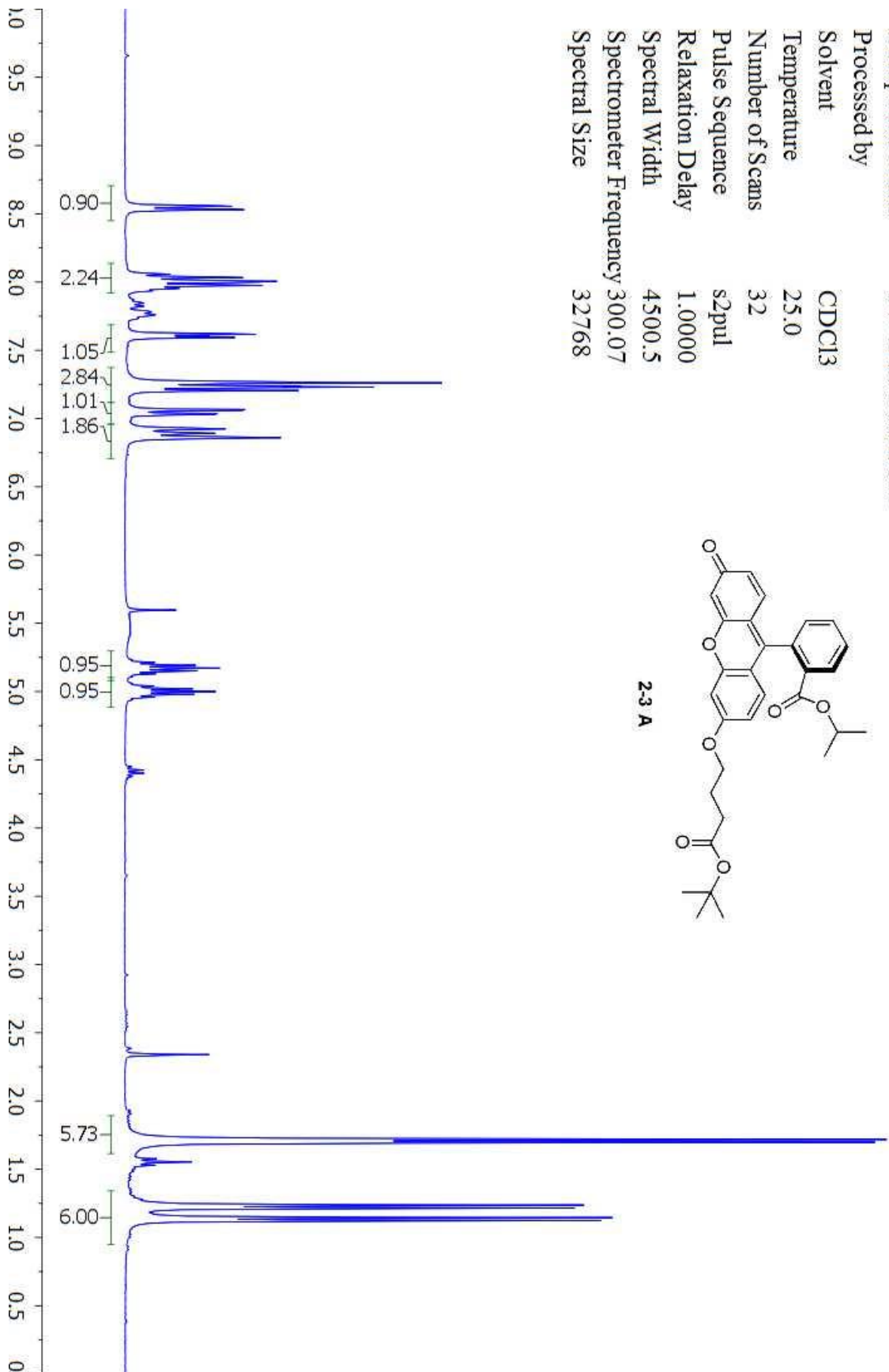
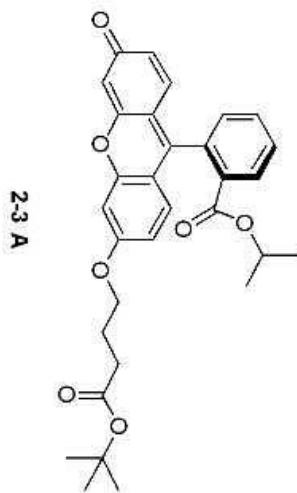




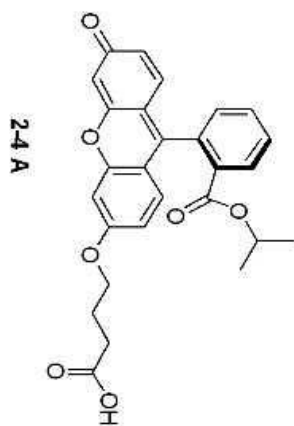
Compound Name TW-B02-P77  
Processed by twang  
Solvent CDCl3  
Temperature 298.2  
Number of Scans 722  
Pulse Sequence zgpg30  
Relaxation Delay 2.0000  
Spectral Width 29761.9  
Spectrometer Frequency 125.71



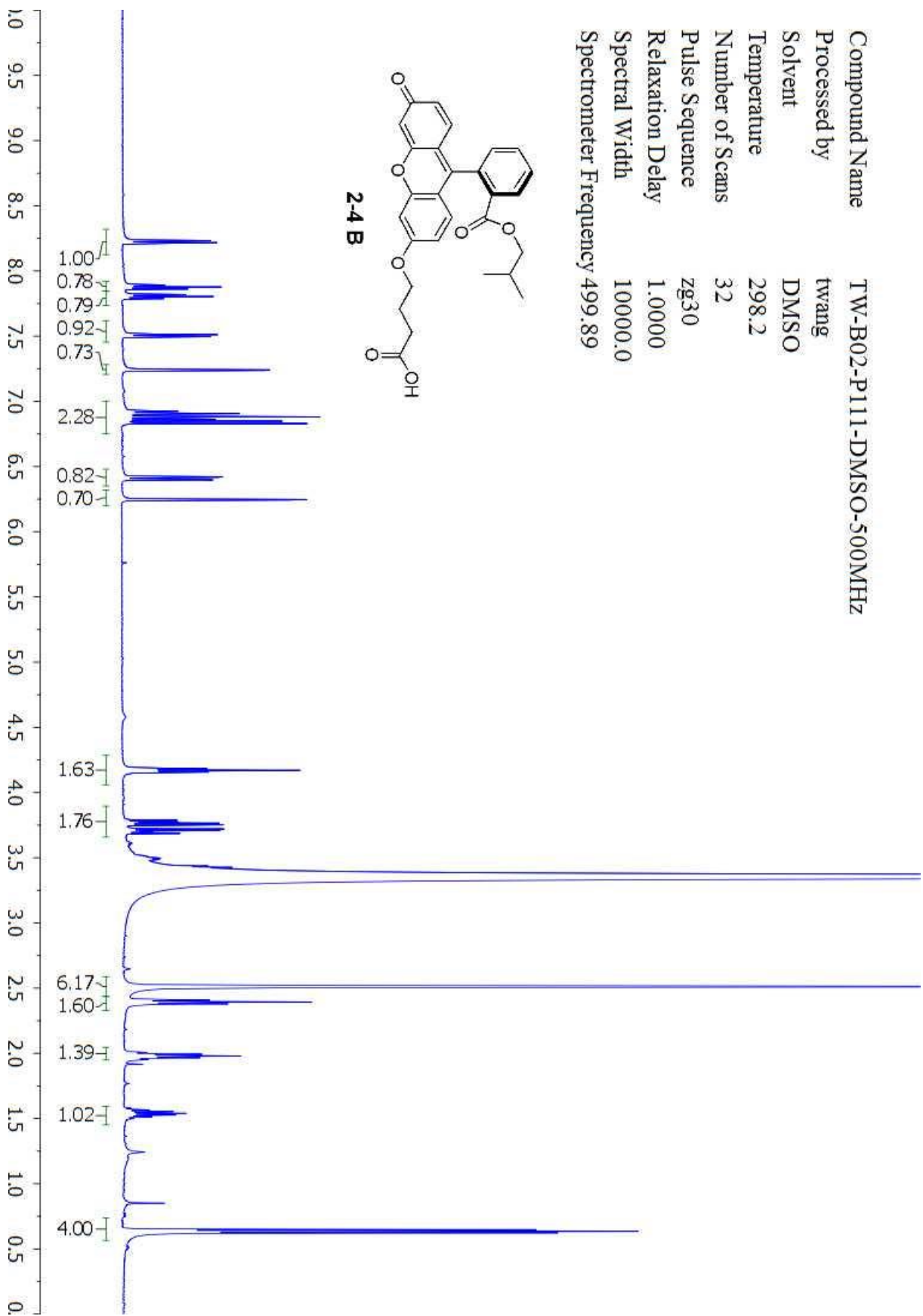
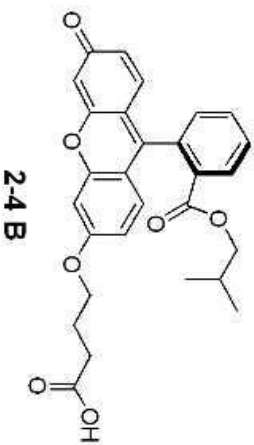
Compound Name TW-B02-P68-BSM  
 Processed by  
 Solvent CDCl3  
 Temperature 25.0  
 Number of Scans 32  
 Pulse Sequence s2pul  
 Relaxation Delay 1.0000  
 Spectral Width 4500.5  
 Spectrometer Frequency 300.07  
 Spectral Size 32768



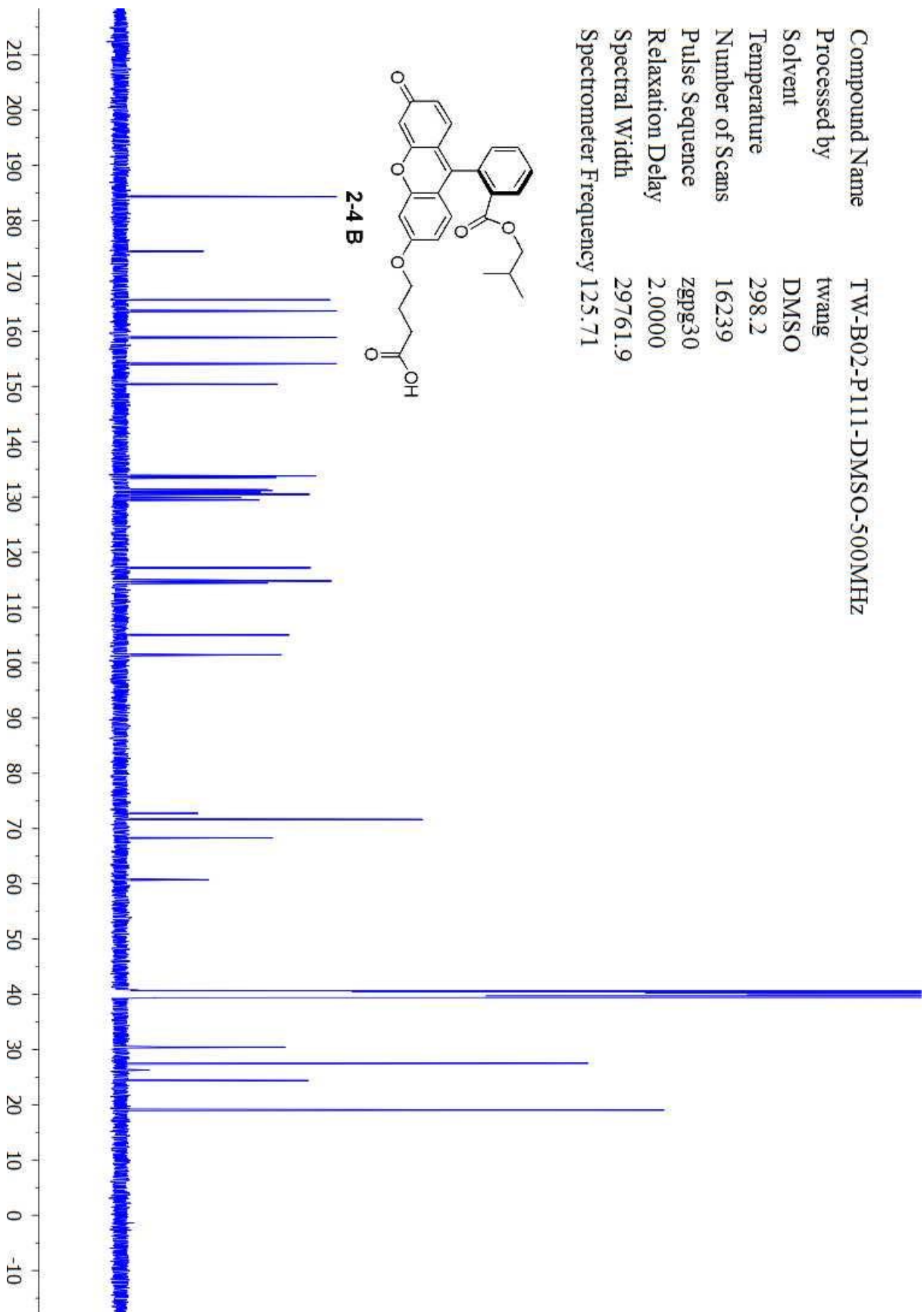
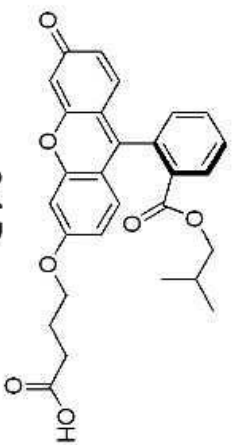
Compound Name TW-B02-P73-finalpurification  
Processed by  
Solvent CDCl3  
Temperature 25.0  
Number of Scans 32  
Pulse Sequence s2pul  
Relaxation Delay 1.0000  
Spectral Width 4500.5  
Spectrometer Frequency 300.07  
Spectral Size 32768



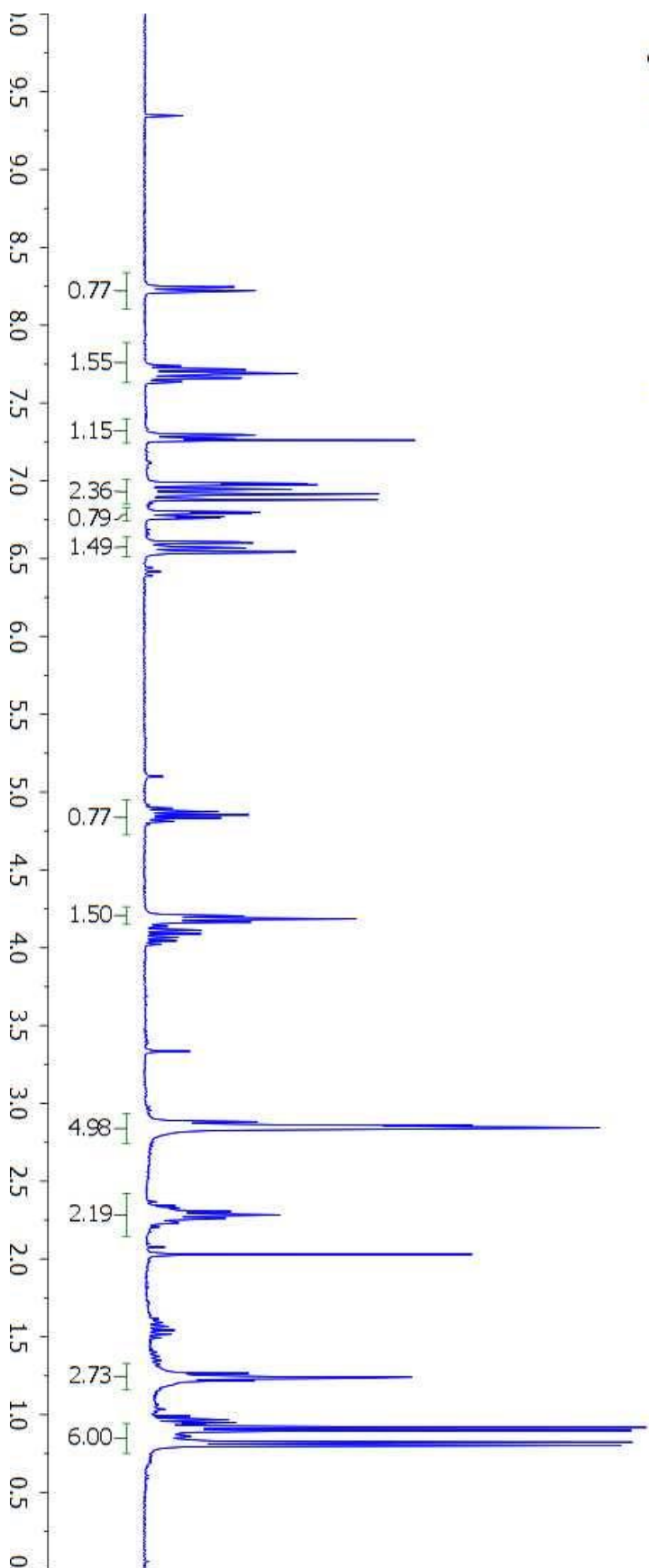
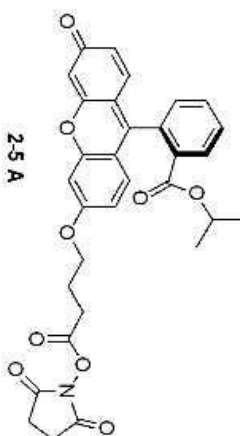
Compound Name TW-B02-P111-DMSO-500MHZ  
 Processed by twang  
 Solvent DMSO  
 Temperature 298.2  
 Number of Scans 32  
 Pulse Sequence zg30  
 Relaxation Delay 1.0000  
 Spectral Width 10000.0  
 Spectrometer Frequency 499.89



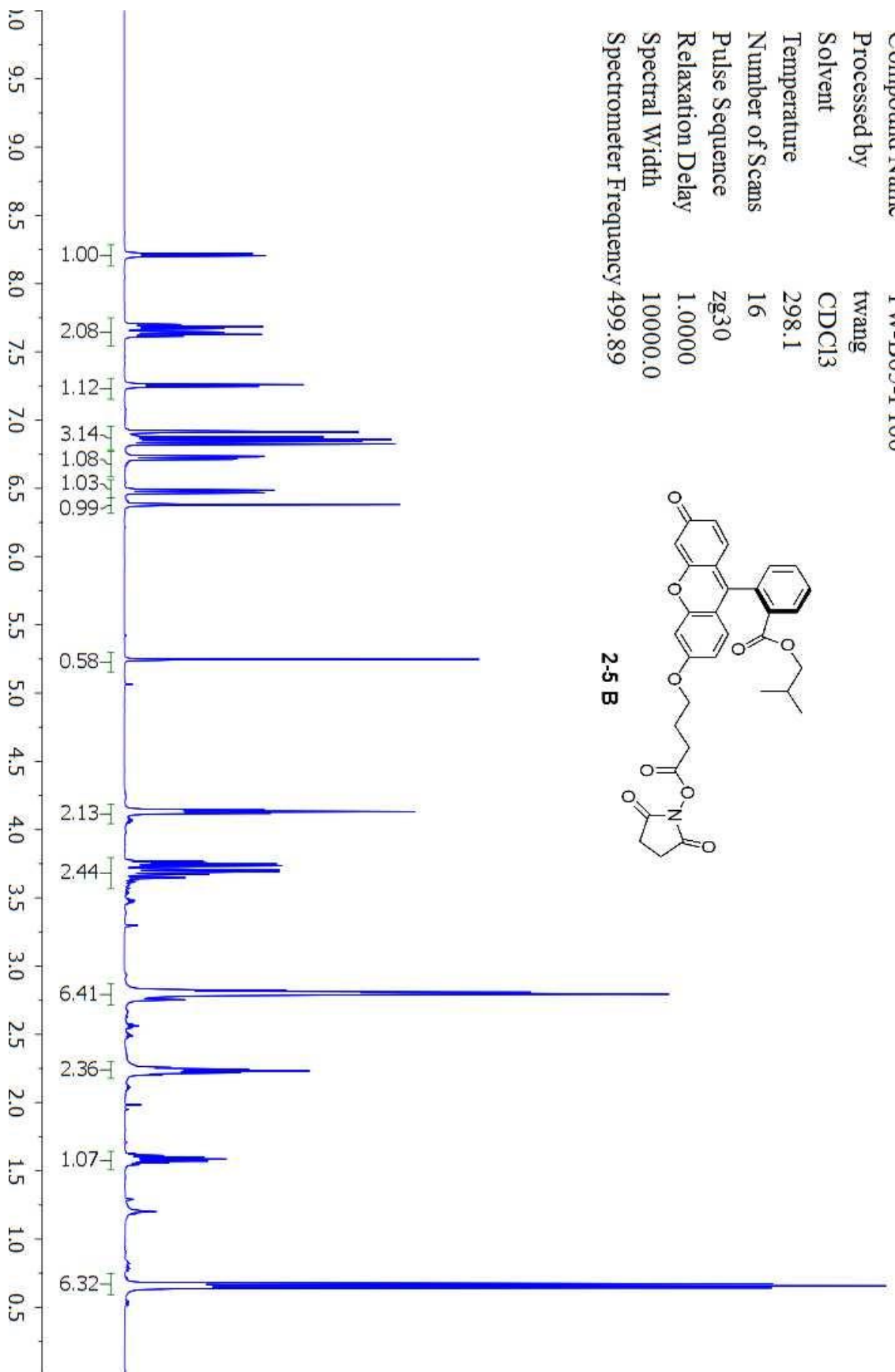
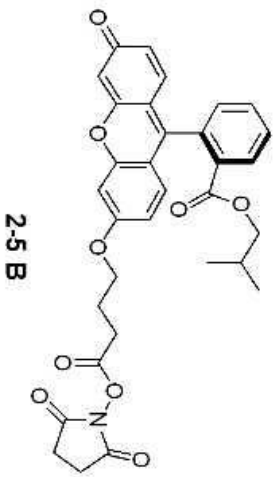
Compound Name TW-B02-P111-DMSO-500MHZ  
Processed by twang  
Solvent DMSO  
Temperature 298.2  
Number of Scans 16239  
Pulse Sequence zgpg30  
Relaxation Delay 2.0000  
Spectral Width 29761.9  
Spectrometer Frequency 125.71



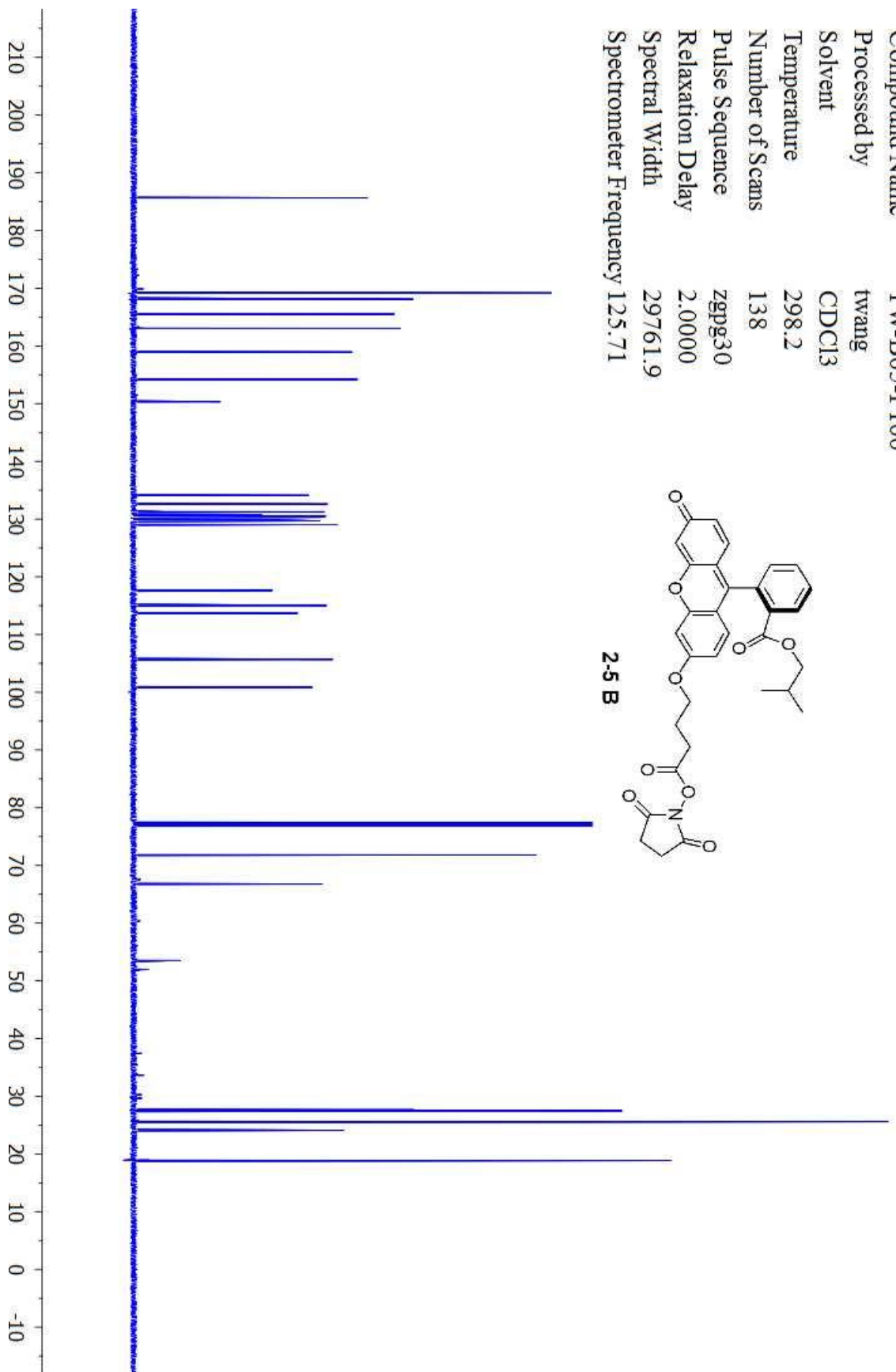
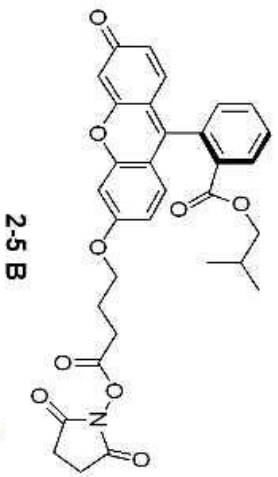
Compound Name TW-B02-P71-HOSU  
 Processed by  
 Solvent CDCl3  
 Temperature 25.0  
 Number of Scans 32  
 Pulse Sequence s2pul  
 Relaxation Delay 1.0000  
 Spectral Width 4500.5  
 Spectrometer Frequency 300.07  
 Spectral Size 32768



Compound Name TW-B05-P100  
 Processed by twang  
 Solvent CDCl3  
 Temperature 298.1  
 Number of Scans 16  
 Pulse Sequence zg30  
 Relaxation Delay 1.0000  
 Spectral Width 10000.0  
 Spectrometer Frequency 499.89

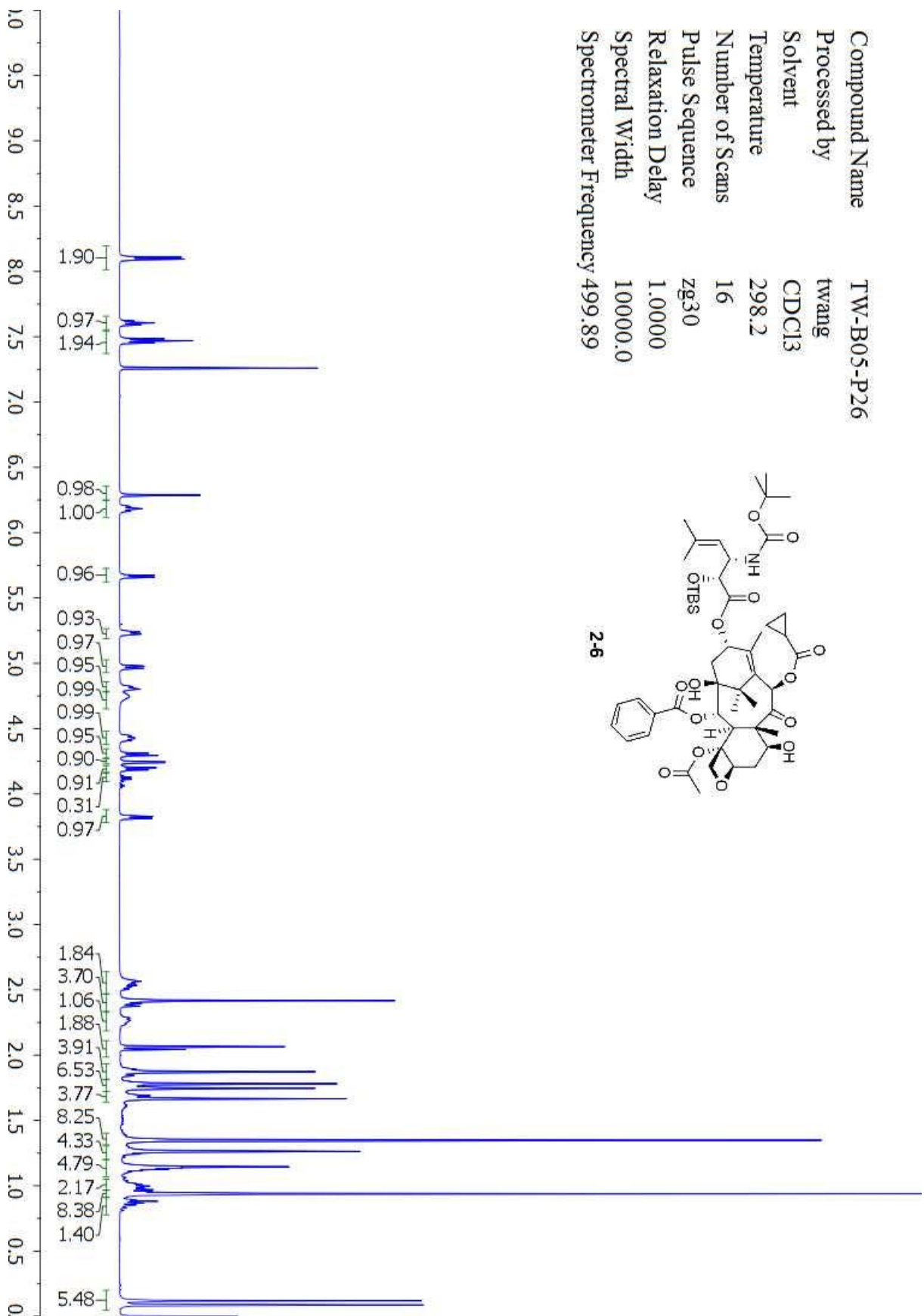
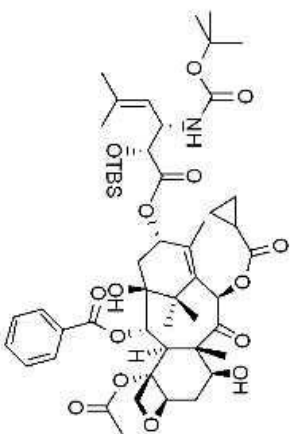


Compound Name TW-B05-P100  
Processed by twang  
Solvent CDCl3  
Temperature 298.2  
Number of Scans 138  
Pulse Sequence zgpg30  
Relaxation Delay 2.0000  
Spectral Width 29761.9  
Spectrometer Frequency 125.71

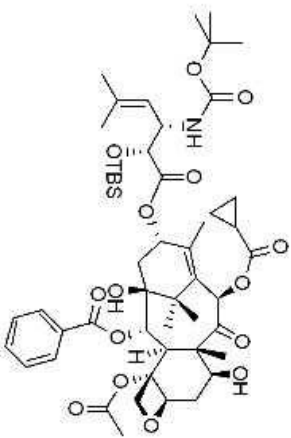




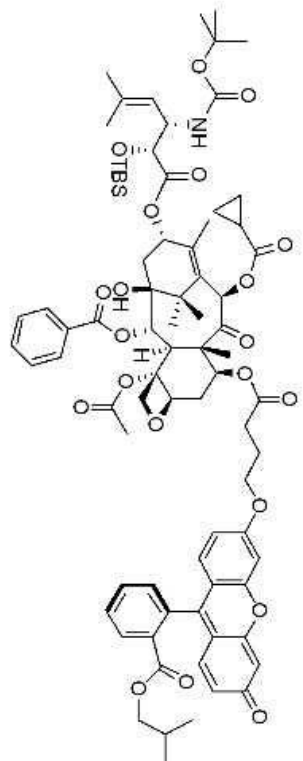
Compound Name TW-B05-P26  
 Processed by twang  
 Solvent CDCl3  
 Temperature 298.2  
 Number of Scans 16  
 Pulse Sequence zg30  
 Relaxation Delay 1.0000  
 Spectral Width 10000.0  
 Spectrometer Frequency 499.89



Compound Name TW-B05-P26  
Processed by twang  
Solvent CDCl3  
Temperature 298.2  
Number of Scans 450  
Pulse Sequence zgpg30  
Relaxation Delay 2.0000  
Spectral Width 29761.9  
Spectrometer Frequency 125.71





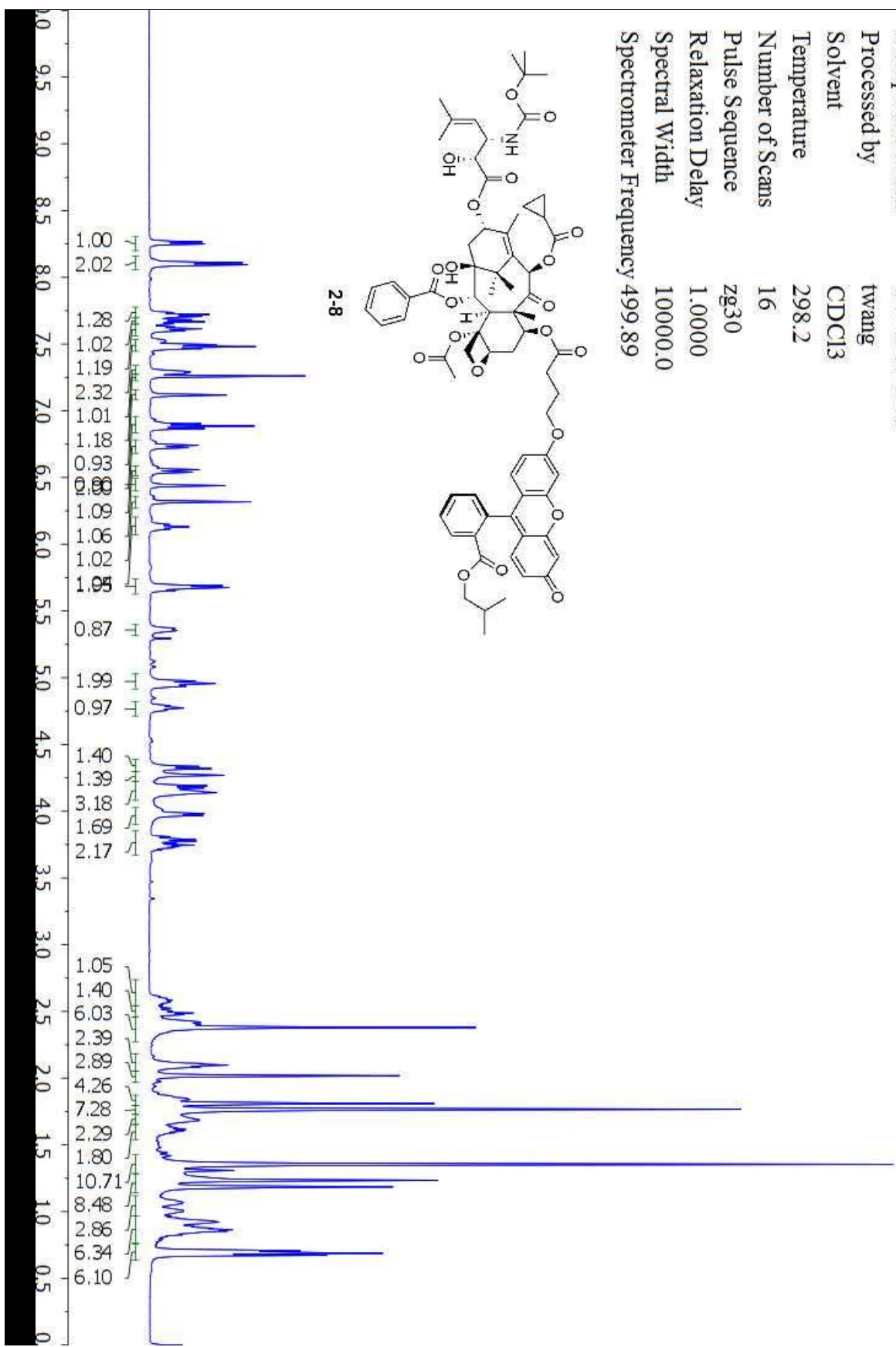
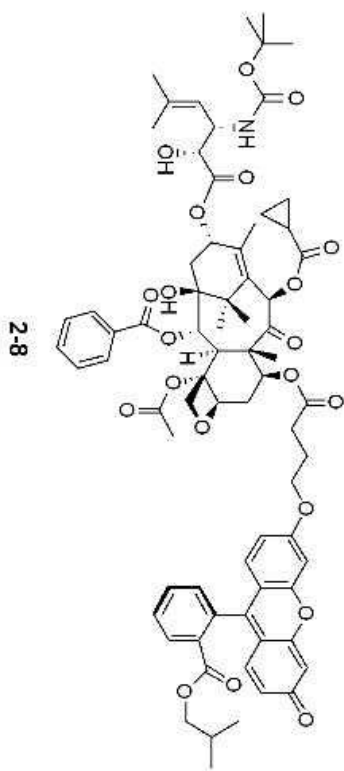


2-7

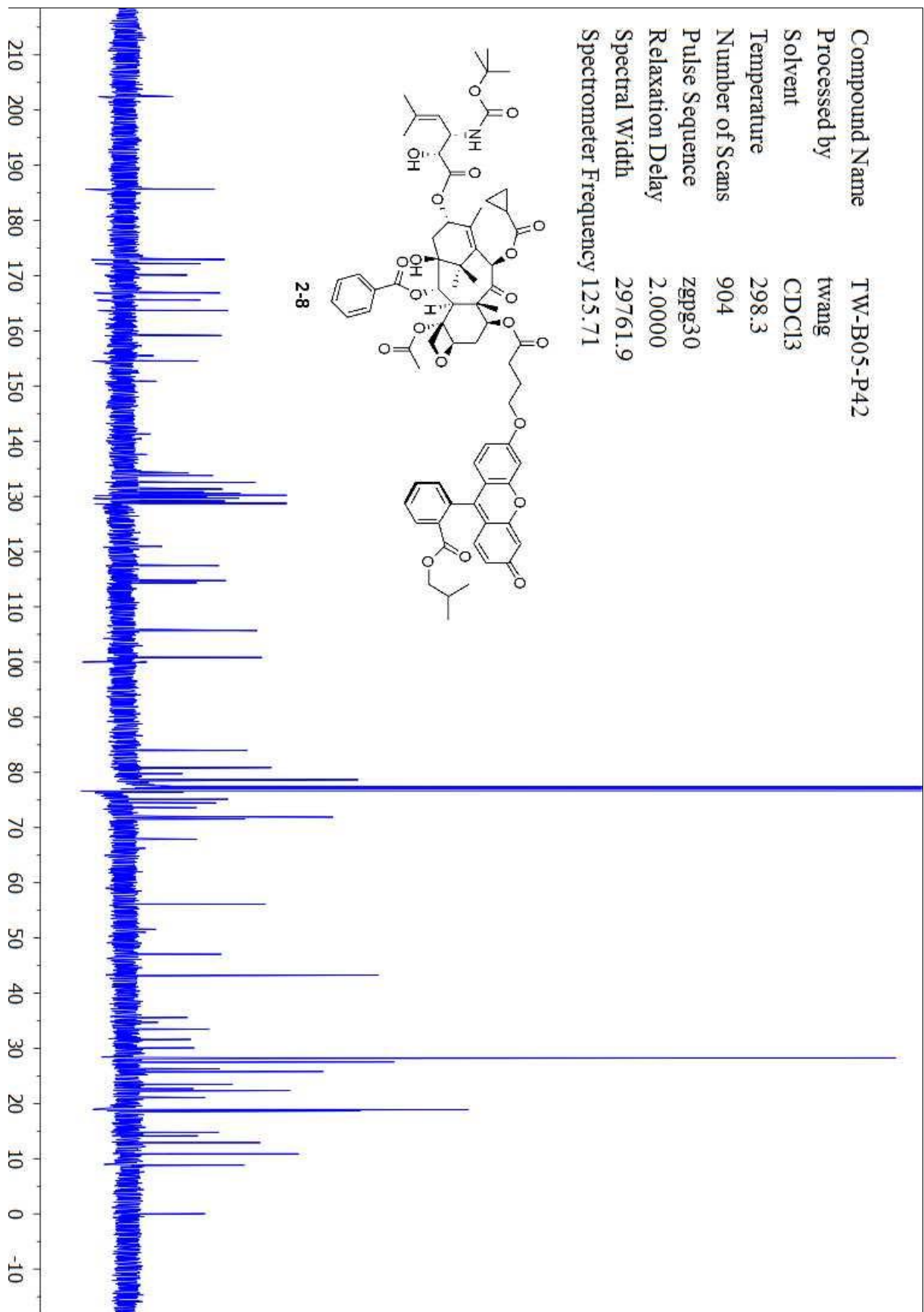
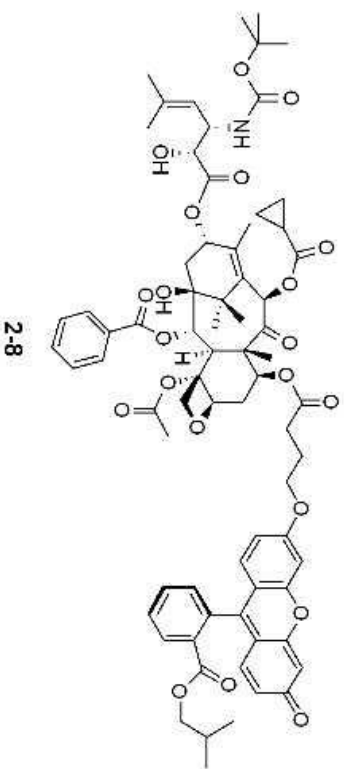
Compound Name TW-B05-P37  
 Processed by twang  
 Solvent CDCl3  
 Temperature 298.2  
 Number of Scans 203  
 Pulse Sequence zgpg30  
 Relaxation Delay 2.0000  
 Spectral Width 29761.9  
 Spectrometer Frequency 125.71



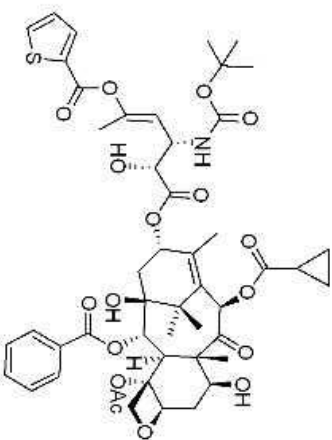
Compound Name TW-B05-P42  
 Processed by twang  
 Solvent CDCl3  
 Temperature 298.2  
 Number of Scans 16  
 Pulse Sequence zg30  
 Relaxation Delay 1.0000  
 Spectral Width 10000.0  
 Spectrometer Frequency 499.89



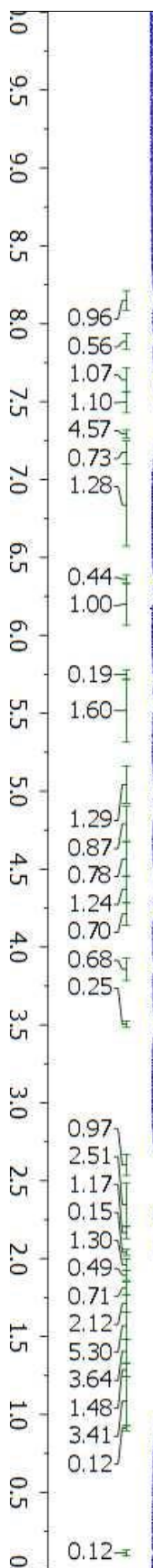
Compound Name TW-B05-P42  
Processed by twang  
Solvent CDCl3  
Temperature 298.3  
Number of Scans 904  
Pulse Sequence zgpg30  
Relaxation Delay 2.0000  
Spectral Width 29761.9  
Spectrometer Frequency 125.71



Compound Name TW-B07-P107-500MHz-Tc-Taxoid  
 Processed by twang  
 Solvent CDCl3  
 Temperature 298.2  
 Number of Scans 64  
 Pulse Sequence zg30  
 Relaxation Delay 1.0000  
 Spectral Width 10000.0  
 Spectrometer Frequency 499.89



2-11







Compound Name  
 Processed by  
 Solvent  
 Temperature  
 Number of Scans  
 Pulse Sequence  
 Relaxation Delay  
 Spectral Width  
 Spectrometer Frequency

TW-B08-P16-ph-taxoid-prep-500MHz-CDCl3

twang

CDCl3

298.1

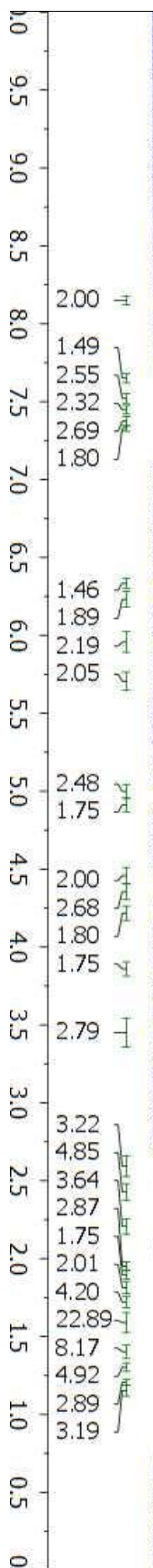
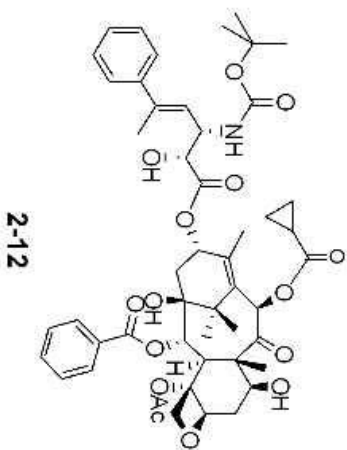
64

zg30

1.0000

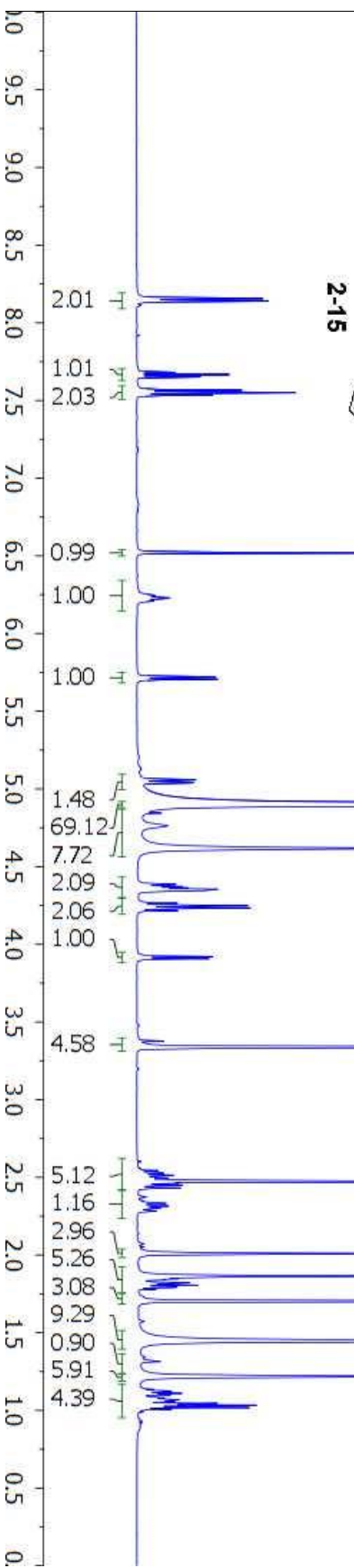
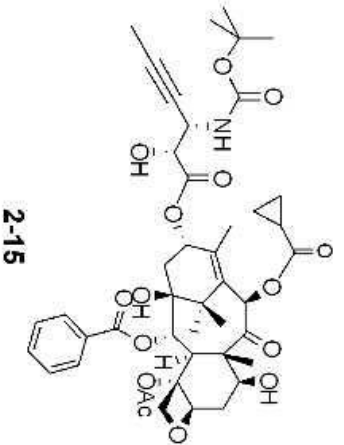
10000.0

499.89

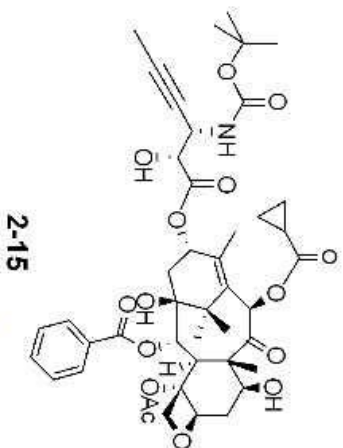




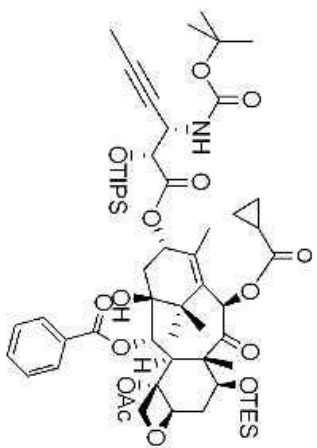
Compound Name TW-B08-P17-alkyne-taxoid-vial1 -500MHz-MeOD  
 Processed by twang  
 Solvent MeOD  
 Temperature 298.2  
 Number of Scans 32  
 Pulse Sequence zg30  
 Relaxation Delay 1.0000  
 Spectral Width 10000.0  
 Spectrometer Frequency 499.89



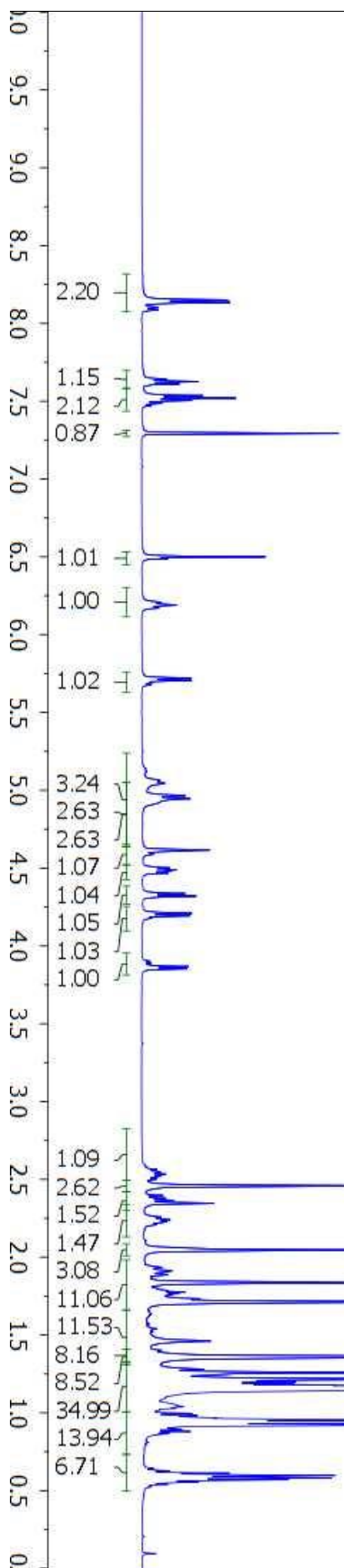
Compound Name TW-B08-P17-alkyne-taxoid-vial1-500MHz-MeOD  
 Processed by twang  
 Solvent MeOD  
 Temperature 298.1  
 Number of Scans 13911  
 Pulse Sequence zgpg30  
 Relaxation Delay 2.0000  
 Spectral Width 29761.9  
 Spectrometer Frequency 125.71



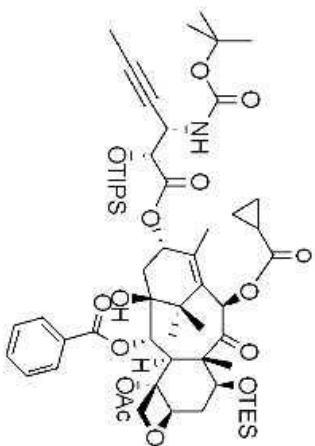
Compound Name TW-B07-P114-repurify-500MHz-CD3Cl  
 Processed by twang  
 Solvent CDCl3  
 Temperature 298.2  
 Number of Scans 29  
 Pulse Sequence zg30  
 Relaxation Delay 1.0000  
 Spectral Width 10000.0  
 Spectrometer Frequency 499.89



2-18

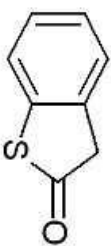


Compound Name TW-B07-P114-repurify-500MHz-CD3Cl  
Processed by twang  
Solvent CDCl3  
Temperature 298.1  
Number of Scans 197  
Pulse Sequence zgpg30  
Relaxation Delay 2.0000  
Spectral Width 29761.9  
Spectrometer Frequency 125.71



## Appendix Chapter 3 NMR Spectra

Compound Name TW-B06-P01  
Processed by twang  
Solvent CDCl3  
Temperature 298.1  
Number of Scans 16  
Pulse Sequence zg30  
Relaxation Delay 1.0000  
Spectral Width 10000.0  
Spectrometer Frequency 499.89

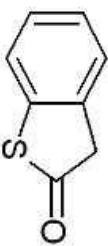


3-1

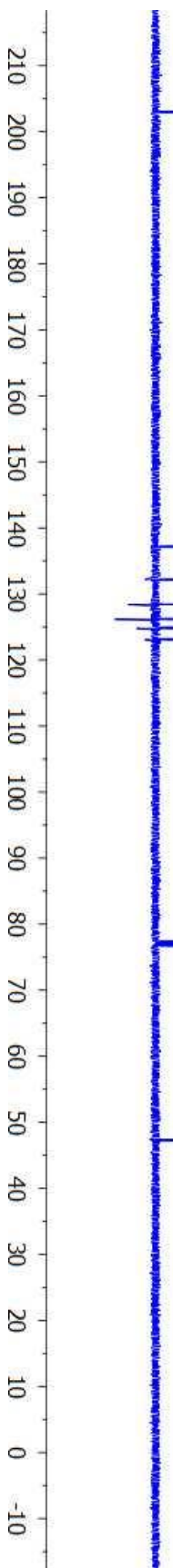




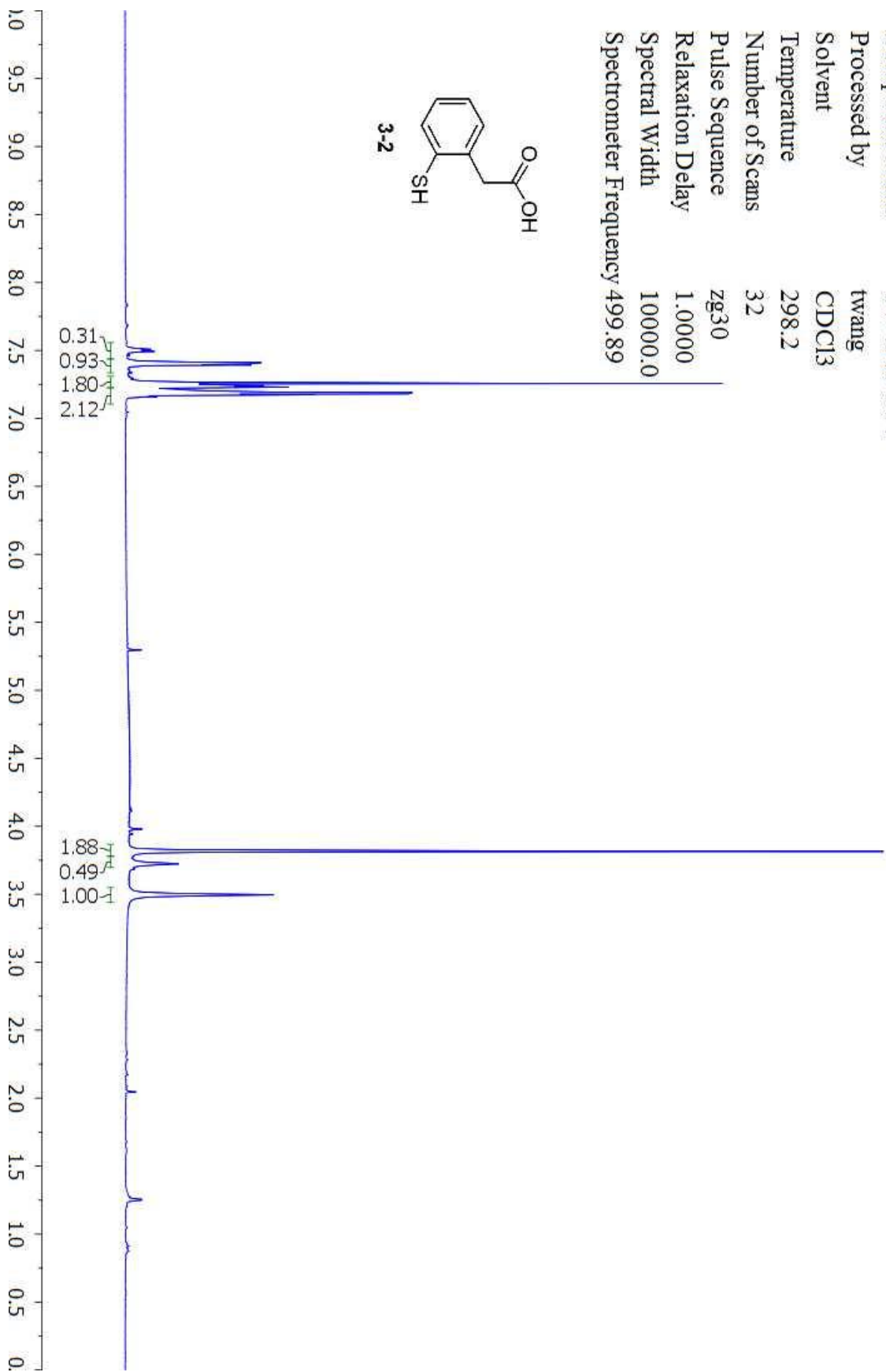
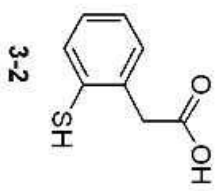
Compound Name TW-B06-P01  
Processed by twang  
Solvent CDCl3  
Temperature 298.1  
Number of Scans 118  
Pulse Sequence zgpg30  
Relaxation Delay 2.0000  
Spectral Width 29761.9  
Spectrometer Frequency 125.71



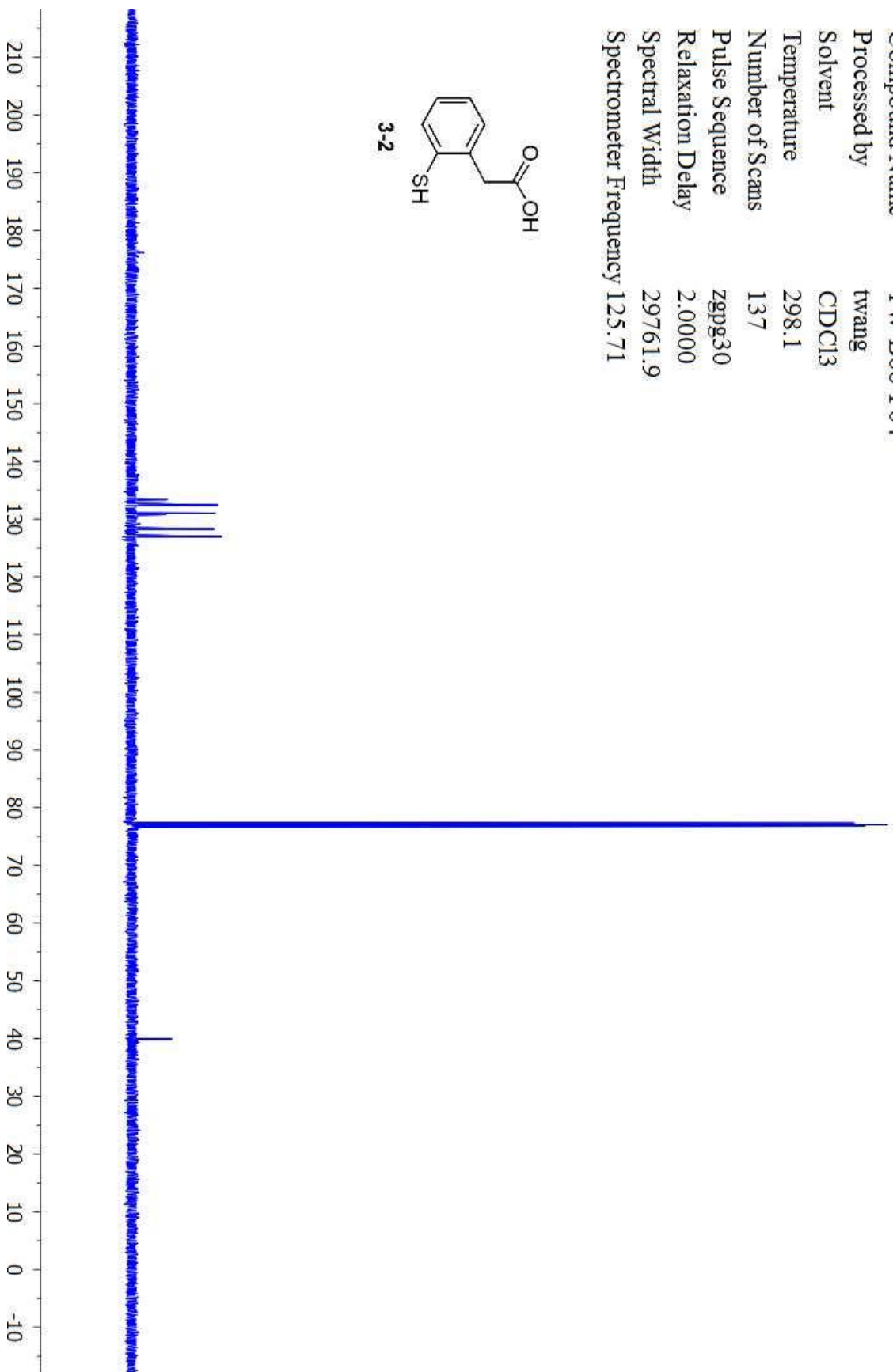
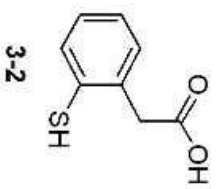
3-1



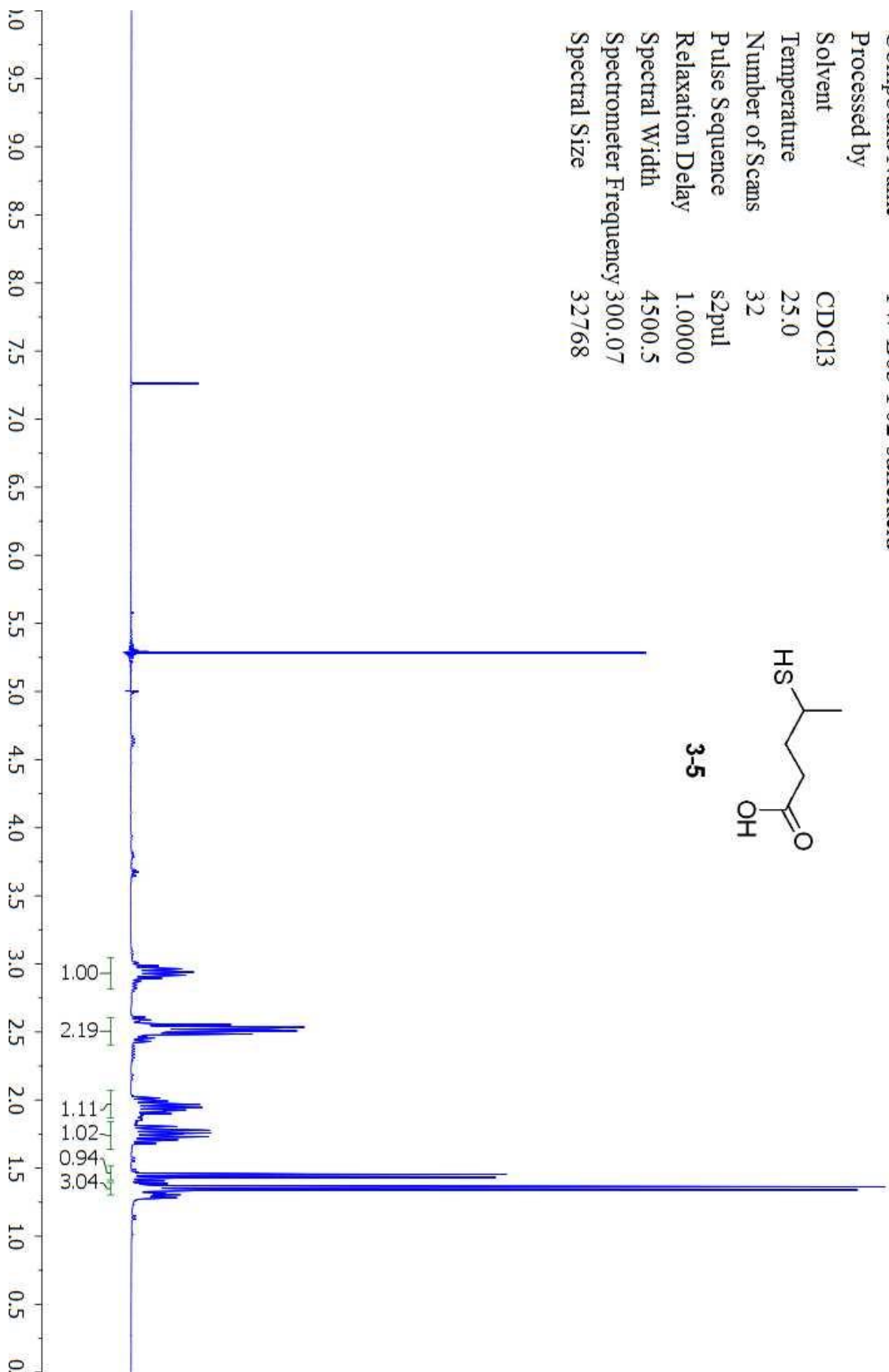
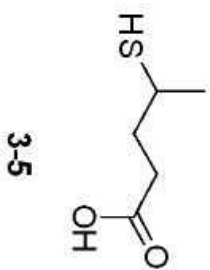
Compound Name TW-B06-P04  
Processed by twang  
Solvent CDCl3  
Temperature 298.2  
Number of Scans 32  
Pulse Sequence zg30  
Relaxation Delay 1.0000  
Spectral Width 10000.0  
Spectrometer Frequency 499.89



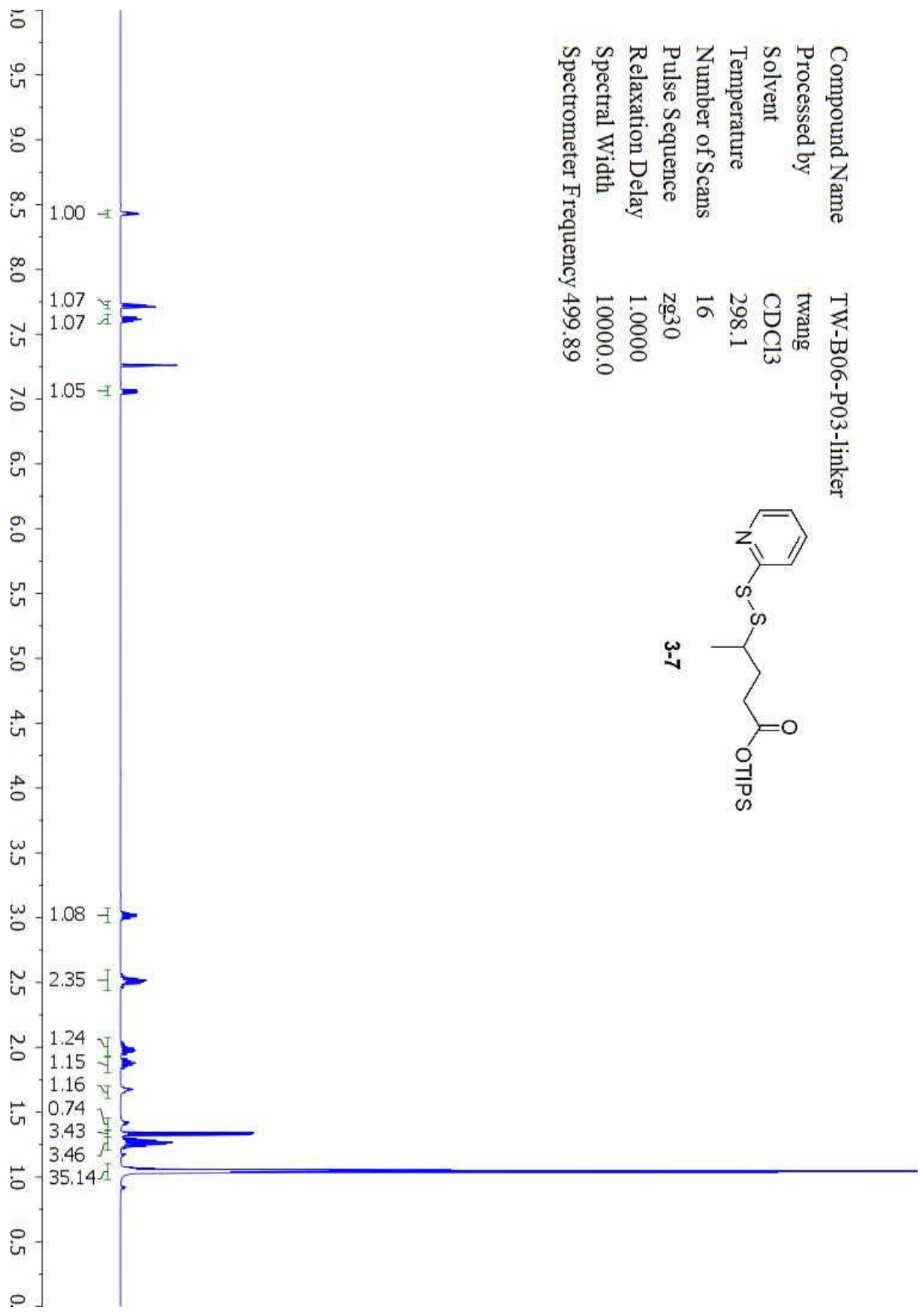
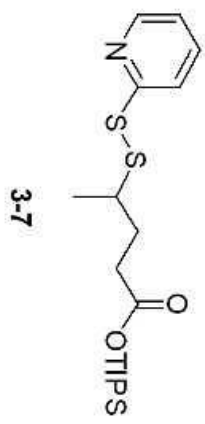
Compound Name TW-B06-P04  
Processed by twang  
Solvent CDCl3  
Temperature 298.1  
Number of Scans 137  
Pulse Sequence zgpg30  
Relaxation Delay 2.0000  
Spectral Width 29761.9  
Spectrometer Frequency 125.71



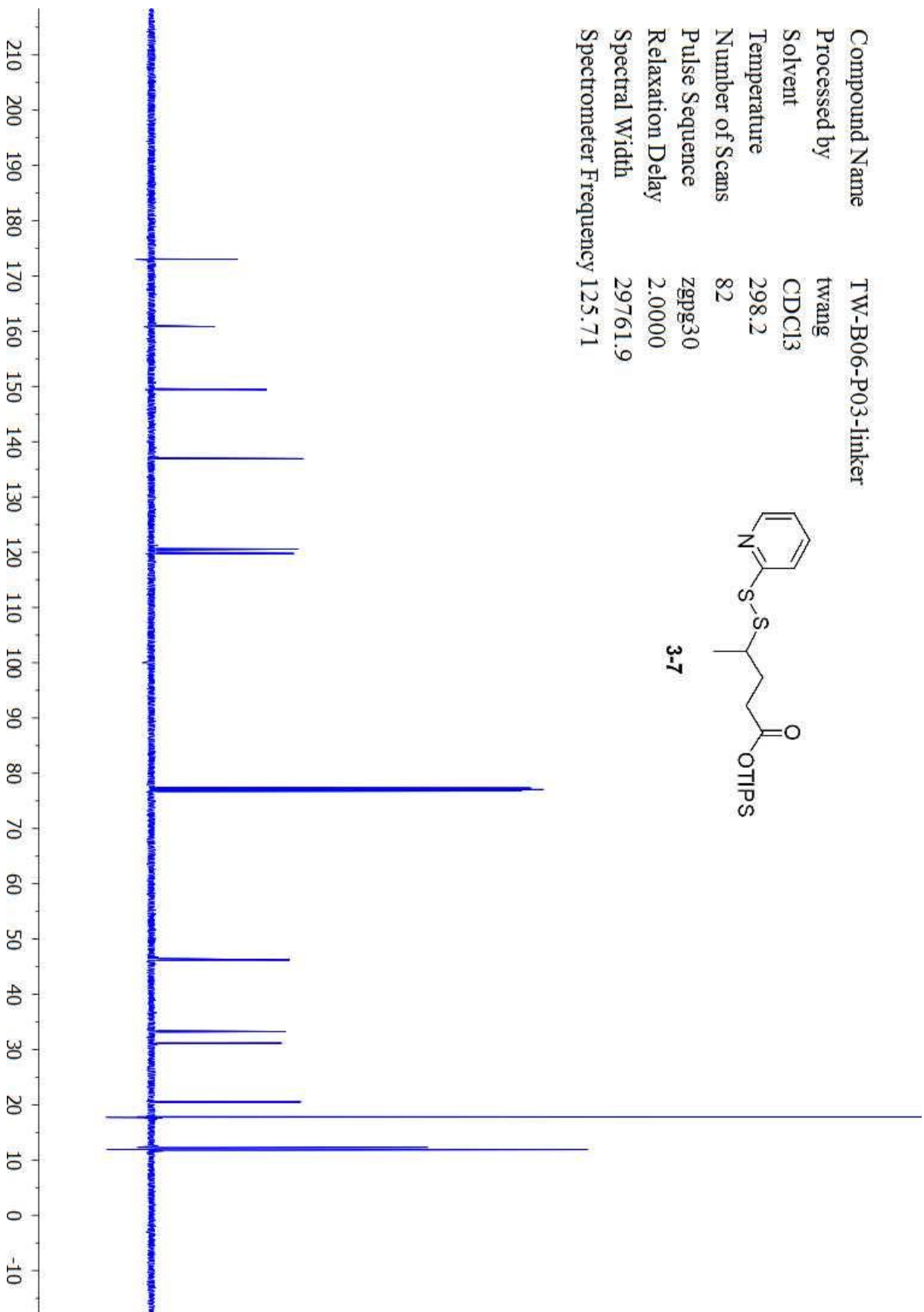
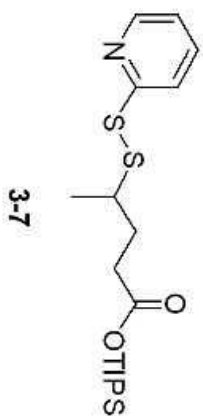
Compound Name TW-B03-P02-sulferacid  
Processed by  
Solvent CDCl3  
Temperature 25.0  
Number of Scans 32  
Pulse Sequence s2pul  
Relaxation Delay 1.0000  
Spectral Width 4500.5  
Spectrometer Frequency 300.07  
Spectral Size 32768



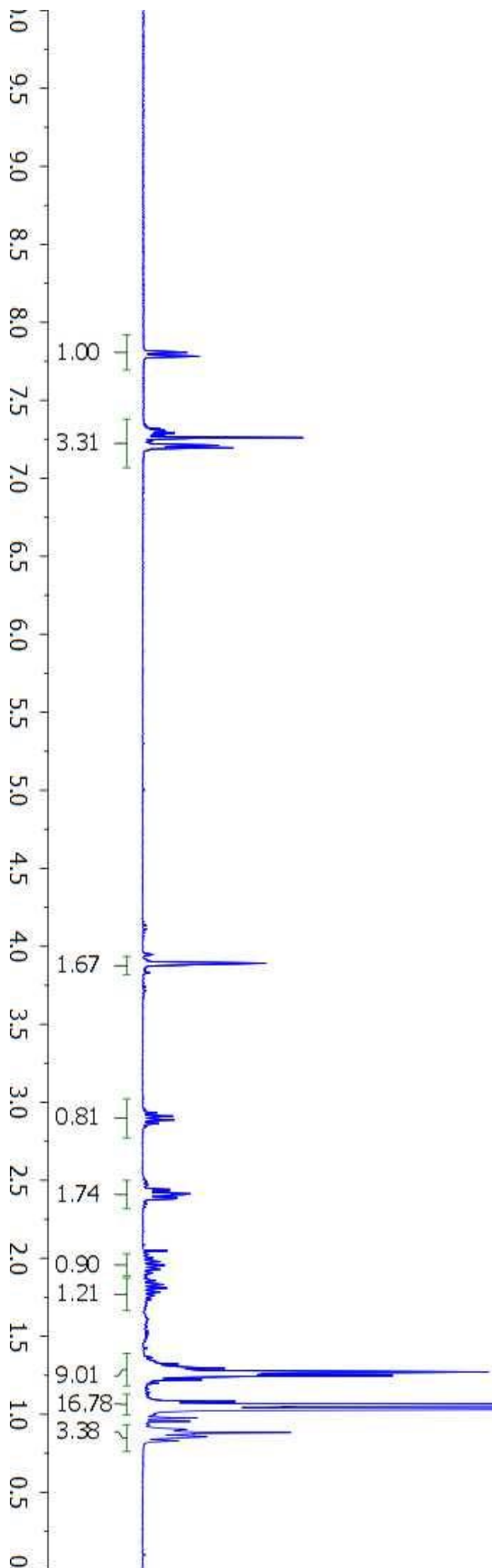
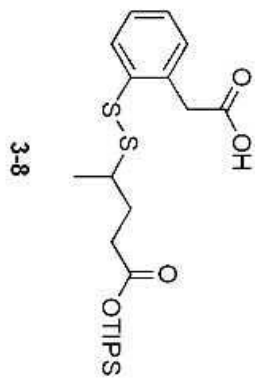
Compound Name TW-B06-P03-linker  
 Processed by twang  
 Solvent CDCl3  
 Temperature 298.1  
 Number of Scans 16  
 Pulse Sequence zg30  
 Relaxation Delay 1.0000  
 Spectral Width 10000.0  
 Spectrometer Frequency 499.89



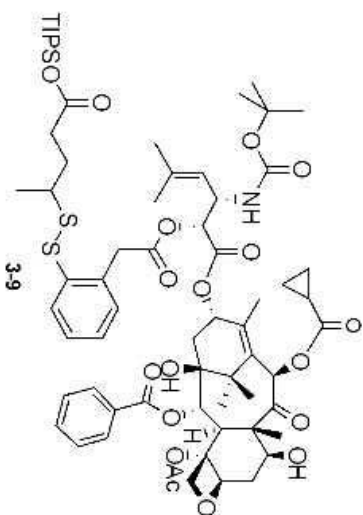
Compound Name TW-B06-P03-linker  
Processed by twang  
Solvent CDCl3  
Temperature 298.2  
Number of Scans 82  
Pulse Sequence zgpg30  
Relaxation Delay 2.0000  
Spectral Width 29761.9  
Spectrometer Frequency 125.71



Compound Name TW-B03-P47  
 Processed by  
 Solvent CDCl3  
 Temperature 25.0  
 Number of Scans 32  
 Pulse Sequence s2pul  
 Relaxation Delay 1.0000  
 Spectral Width 4500.5  
 Spectrometer Frequency 300.07  
 Spectral Size 32768

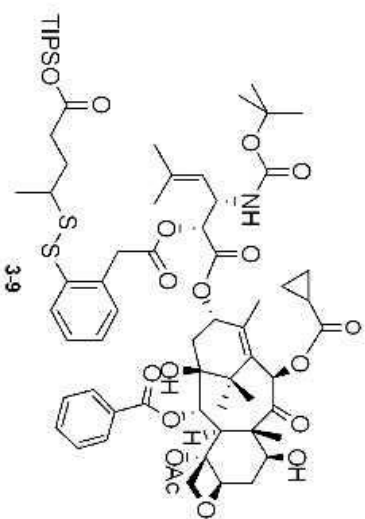


Compound Name TW-B05-P53  
 Processed by twang  
 Solvent CDCl3  
 Temperature 298.3  
 Number of Scans 16  
 Pulse Sequence zg30  
 Relaxation Delay 1.0000  
 Spectral Width 10000.0  
 Spectrometer Frequency 499.89

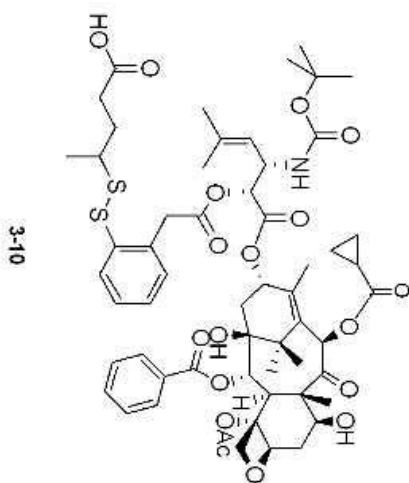




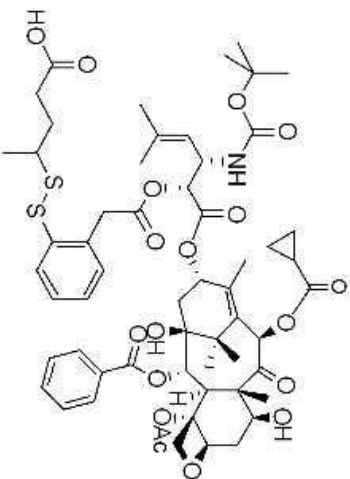
Compound Name TW-B05-P53  
Processed by twang  
Solvent CDCl3  
Temperature 298.3  
Number of Scans 1014  
Pulse Sequence zgpg30  
Relaxation Delay 2.0000  
Spectral Width 29761.9  
Spectrometer Frequency 125.71



Compound Name TW-B05-P55  
 Processed by twang  
 Solvent CDCl3  
 Temperature 298.2  
 Number of Scans 16  
 Pulse Sequence zg30  
 Relaxation Delay 1.0000  
 Spectral Width 10000.0  
 Spectrometer Frequency 499.89



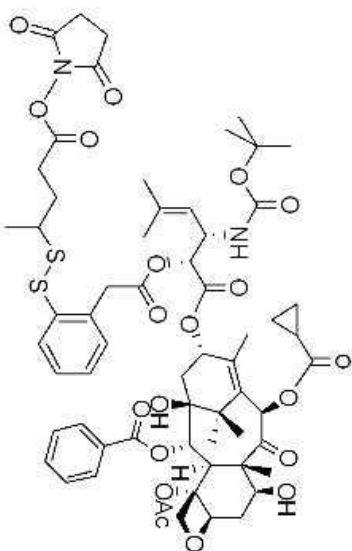
Compound Name TW-B05-P55  
Processed by twang  
Solvent CDCl3  
Temperature 298.2  
Number of Scans 312  
Pulse Sequence zgpg30  
Relaxation Delay 2.0000  
Spectral Width 29761.9  
Spectrometer Frequency 125.71



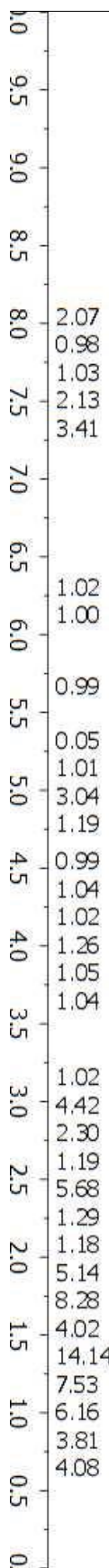
3-10



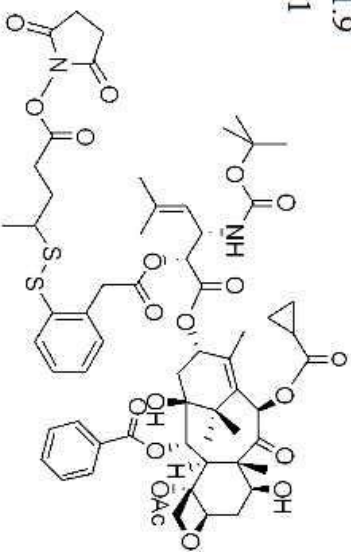
Compound Name TW-B05-P60  
 Processed by twang  
 Solvent CDCl3  
 Temperature 298.3  
 Number of Scans 32  
 Pulse Sequence zg30  
 Relaxation Delay 1.0000  
 Spectral Width 10000.0  
 Spectrometer Frequency 499.89



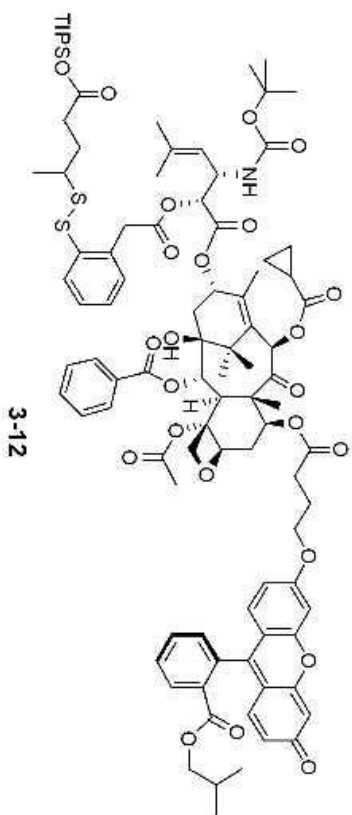
3-11



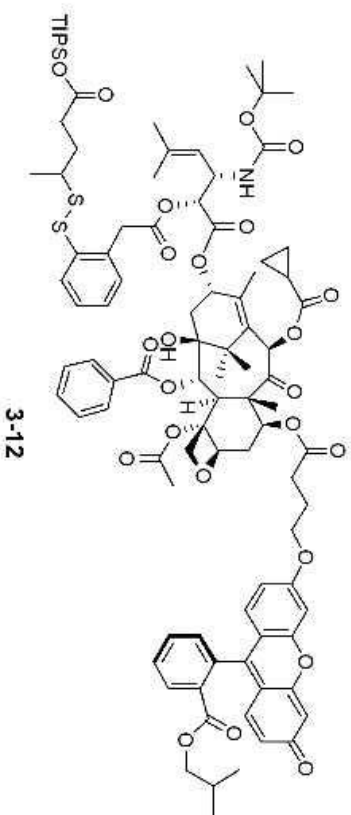
Compound Name TW-B05-P60  
Processed by twang  
Solvent CDCl3  
Temperature 298.3  
Number of Scans 314  
Pulse Sequence zgpg30  
Relaxation Delay 2.0000  
Spectral Width 29761.9  
Spectrometer Frequency 125.71



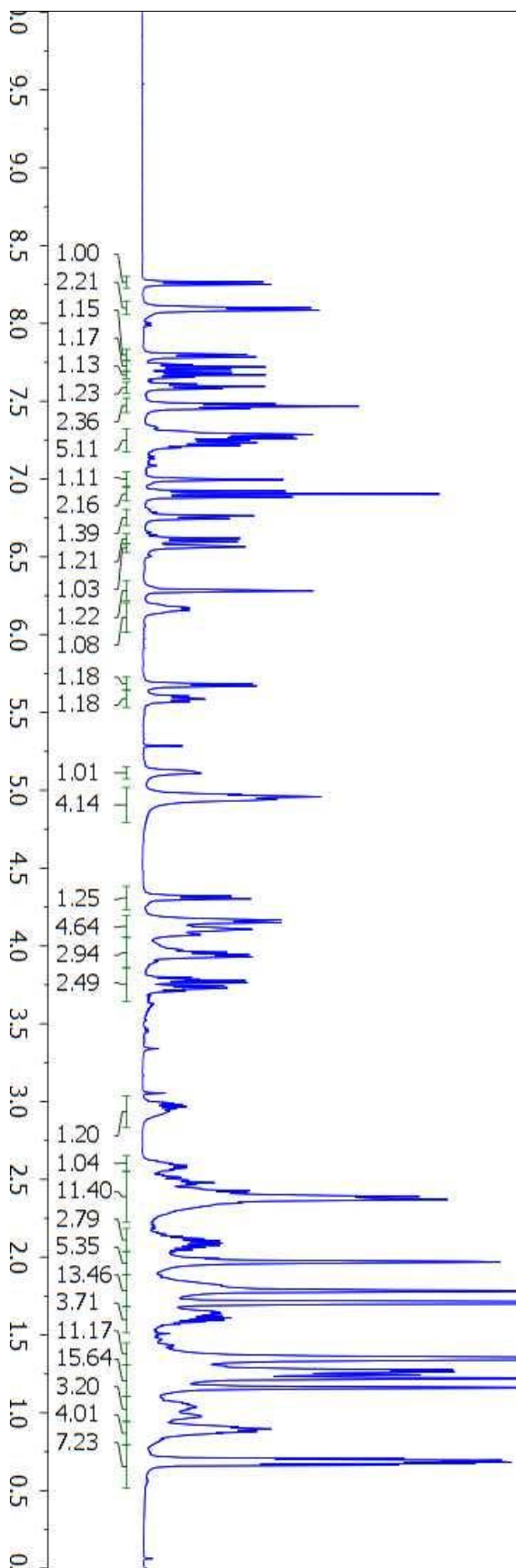
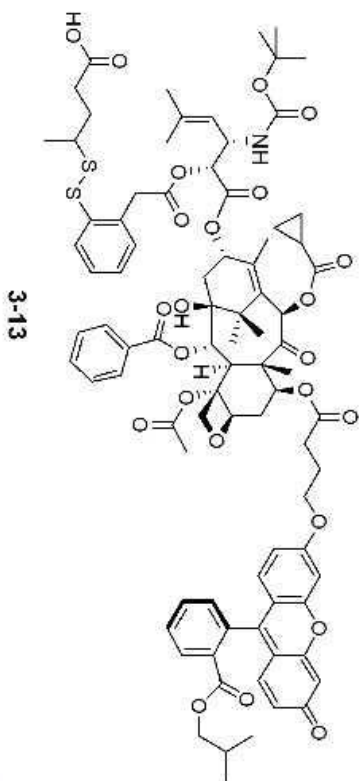
Compound Name TW-B05-P52  
 Processed by twang  
 Solvent CDCl3  
 Temperature 298.2  
 Number of Scans 16  
 Pulse Sequence zg30  
 Relaxation Delay 1.0000  
 Spectral Width 10000.0  
 Spectrometer Frequency 499.89



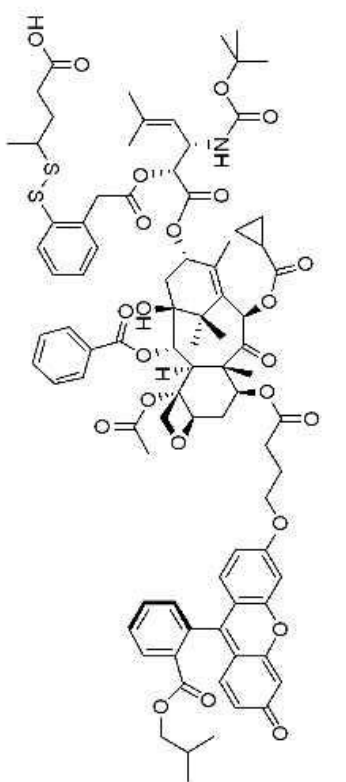
Compound Name TW-B05-P52  
Processed by twang  
Solvent CDCl3  
Temperature 298.3  
Number of Scans 1024  
Pulse Sequence zgpg30  
Relaxation Delay 2.0000  
Spectral Width 29761.9  
Spectrometer Frequency 125.71



Compound Name TW-B05-P57  
 Processed by twang  
 Solvent CDCl3  
 Temperature 298.2  
 Number of Scans 16  
 Pulse Sequence zg30  
 Relaxation Delay 1.0000  
 Spectral Width 10000.0  
 Spectrometer Frequency 499.89

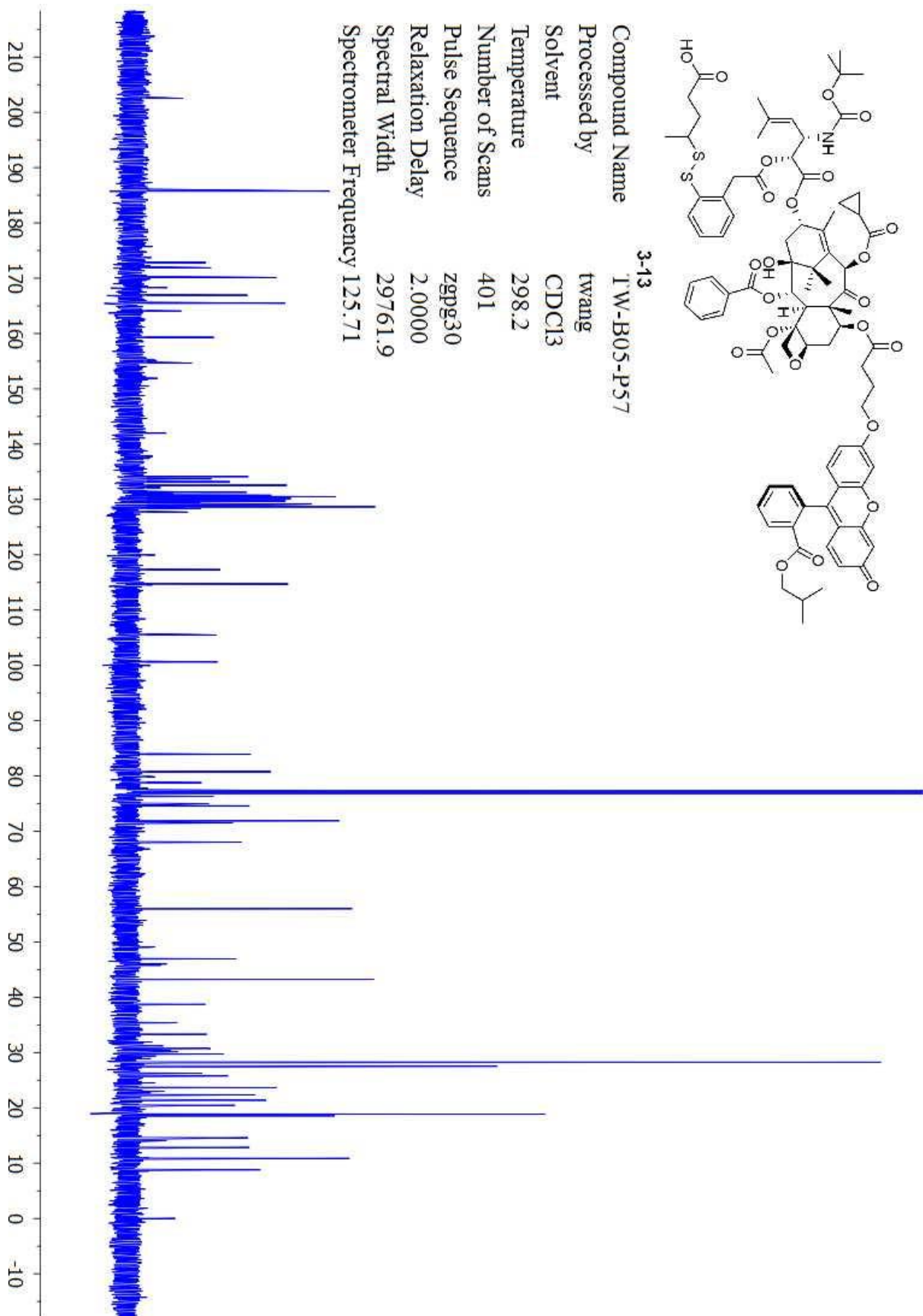




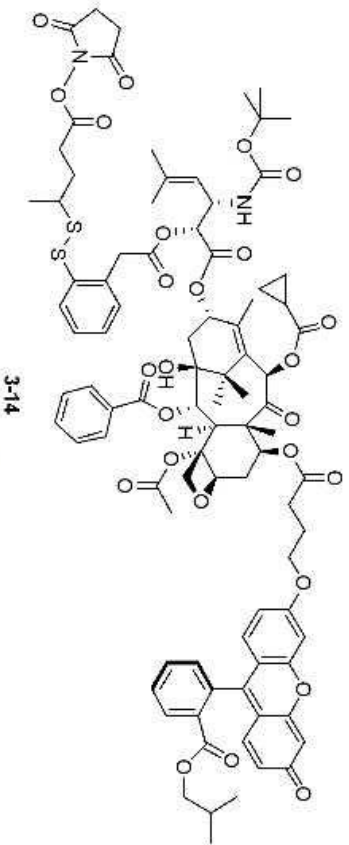


3-13

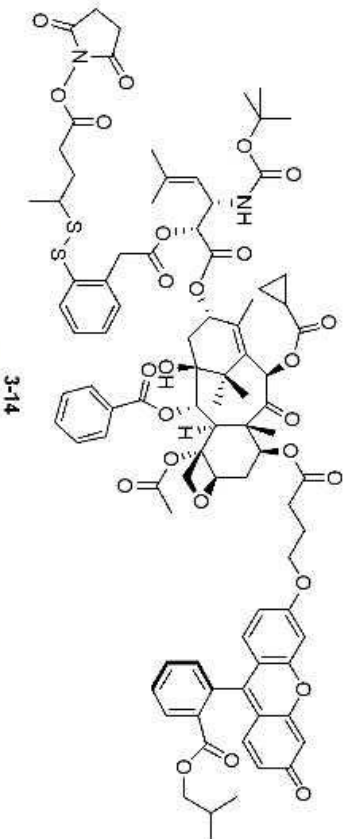
Compound Name      I'W-B05-P57  
 Processed by        twang  
 Solvent              CDCl3  
 Temperature        298.2  
 Number of Scans    401  
 Pulse Sequence     zgpg30  
 Relaxation Delay    2.0000  
 Spectral Width      29761.9  
 Spectrometer Frequency 125.71



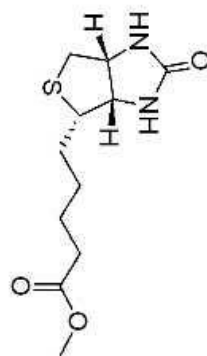
Compound Name TW-B05-P61  
 Processed by twang  
 Solvent CDCl3  
 Temperature 298.3  
 Number of Scans 32  
 Pulse Sequence zg30  
 Relaxation Delay 1.0000  
 Spectral Width 10000.0  
 Spectrometer Frequency 499.89



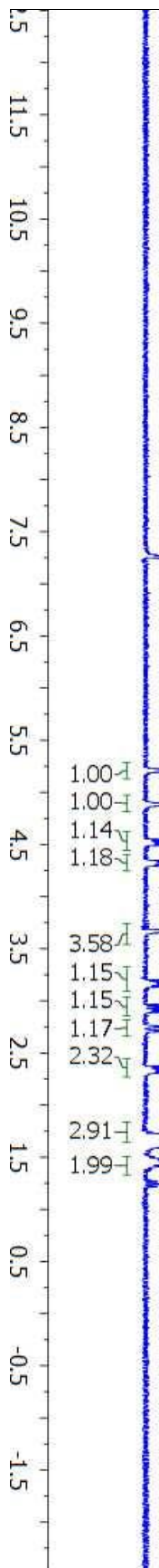
Compound Name TW-B05-P61  
Processed by twang  
Solvent CDCl3  
Temperature 298.3  
Number of Scans 951  
Pulse Sequence zgpg30  
Relaxation Delay 2.0000  
Spectral Width 29761.9  
Spectrometer Frequency 125.71



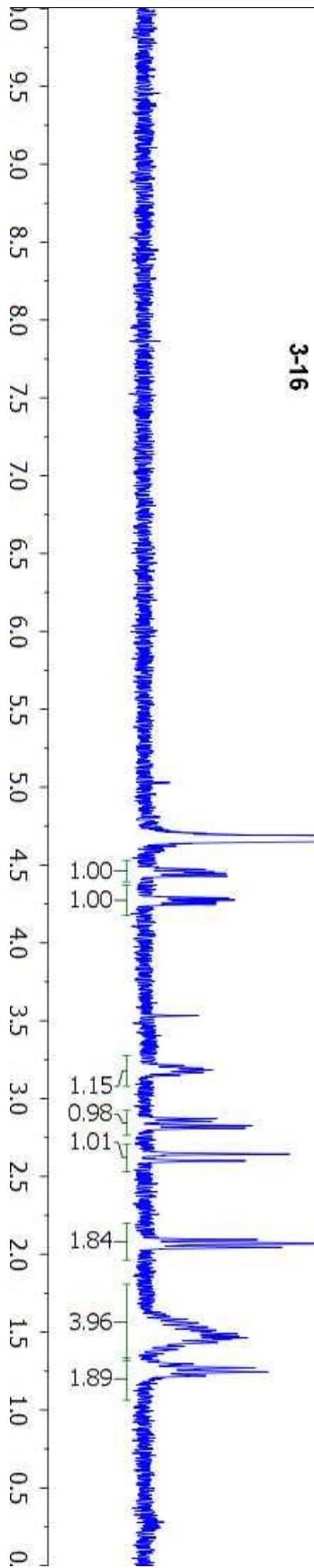
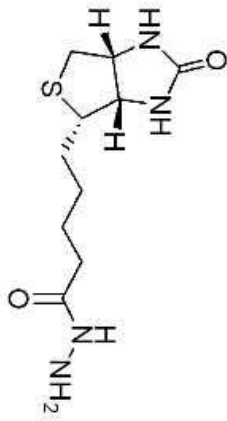
Compound Name TW-B04-P14-biotinOMe  
Processed by  
Solvent CDCl3  
Temperature 25.0  
Number of Scans 32  
Pulse Sequence s2pul  
Relaxation Delay 1.0000  
Spectral Width 4500.5  
Spectrometer Frequency 300.07  
Spectral Size 32768



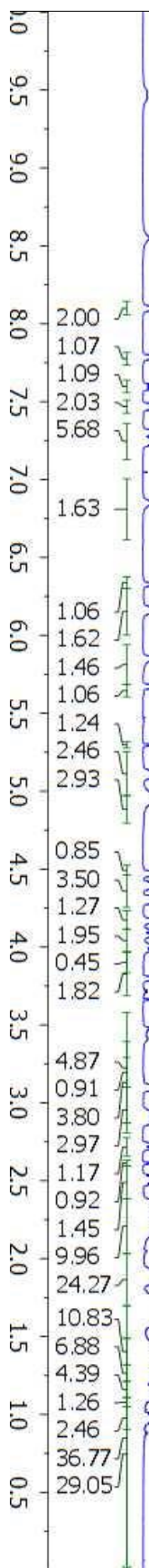
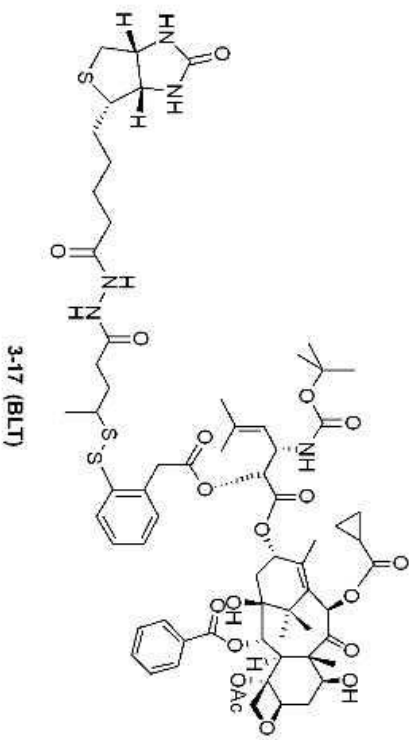
3-15



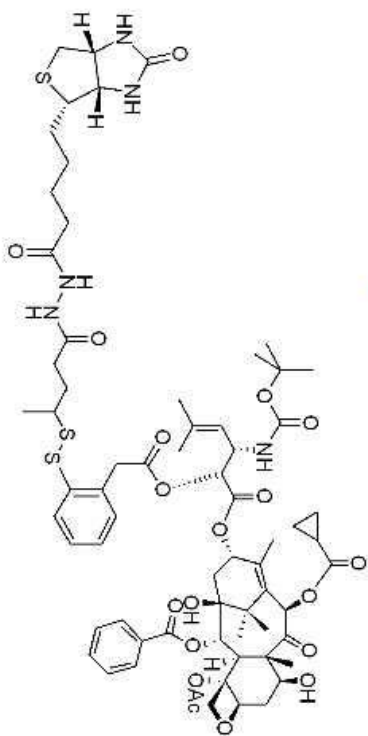
Compound Name TW-B04-P18-filtered  
Processed by  
Solvent D2O  
Temperature 25.0  
Number of Scans 32  
Pulse Sequence s2pul  
Relaxation Delay 1.0000  
Spectral Width 4500.5  
Spectrometer Frequency 300.07  
Spectral Size 32768



Compound Name TW-B04-P25  
 Processed by twang  
 Solvent CDCl3  
 Temperature 298.1  
 Number of Scans 32  
 Pulse Sequence zg30  
 Relaxation Delay 1.0000  
 Spectral Width 10000.0  
 Spectrometer Frequency 499.89



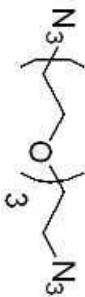
Compound Name TW-B04-P25-2  
 Processed by twang  
 Solvent CDCl3  
 Temperature 298.2  
 Number of Scans 1024  
 Pulse Sequence zgpg30  
 Relaxation Delay 2.0000  
 Spectral Width 29761.9  
 Spectrometer Frequency 125.71



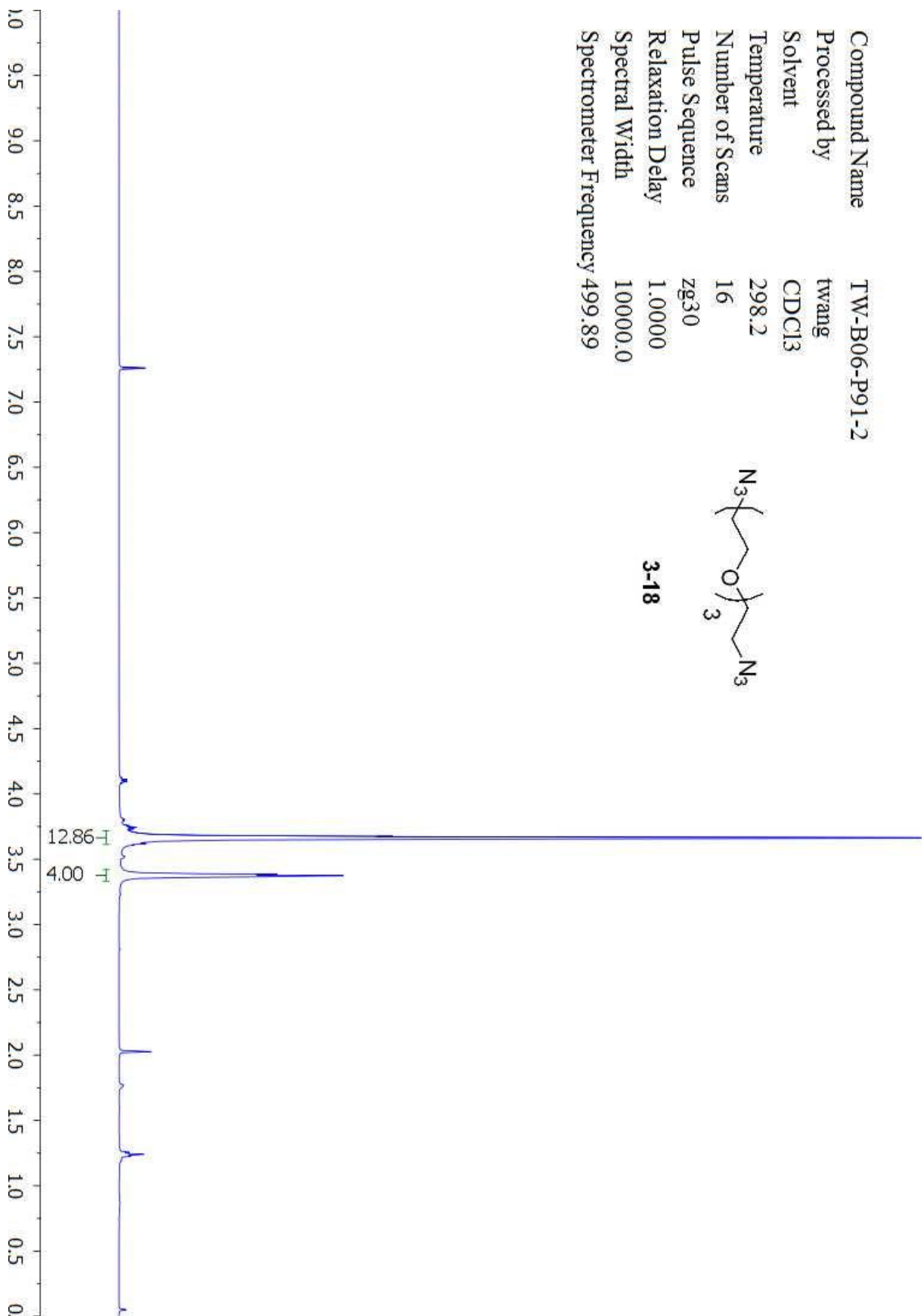
3-17 (BLT)



Compound Name TW-B06-P91-2  
Processed by twang  
Solvent CDCl3  
Temperature 298.2  
Number of Scans 16  
Pulse Sequence zg30  
Relaxation Delay 1.0000  
Spectral Width 10000.0  
Spectrometer Frequency 499.89



3-18





Compound Name TW-B06-P91-2  
Processed by twang  
Solvent CDCl3  
Temperature 298.2  
Number of Scans 39  
Pulse Sequence zgpg30  
Relaxation Delay 2.0000  
Spectral Width 29761.9  
Spectrometer Frequency 125.71



3-18



Compound Name TW-B06-P93  
Processed by twang  
Solvent CDCl3  
Temperature 298.2  
Number of Scans 16  
Pulse Sequence zg30  
Relaxation Delay 1.0000  
Spectral Width 10000.0  
Spectrometer Frequency 499.89



3-19



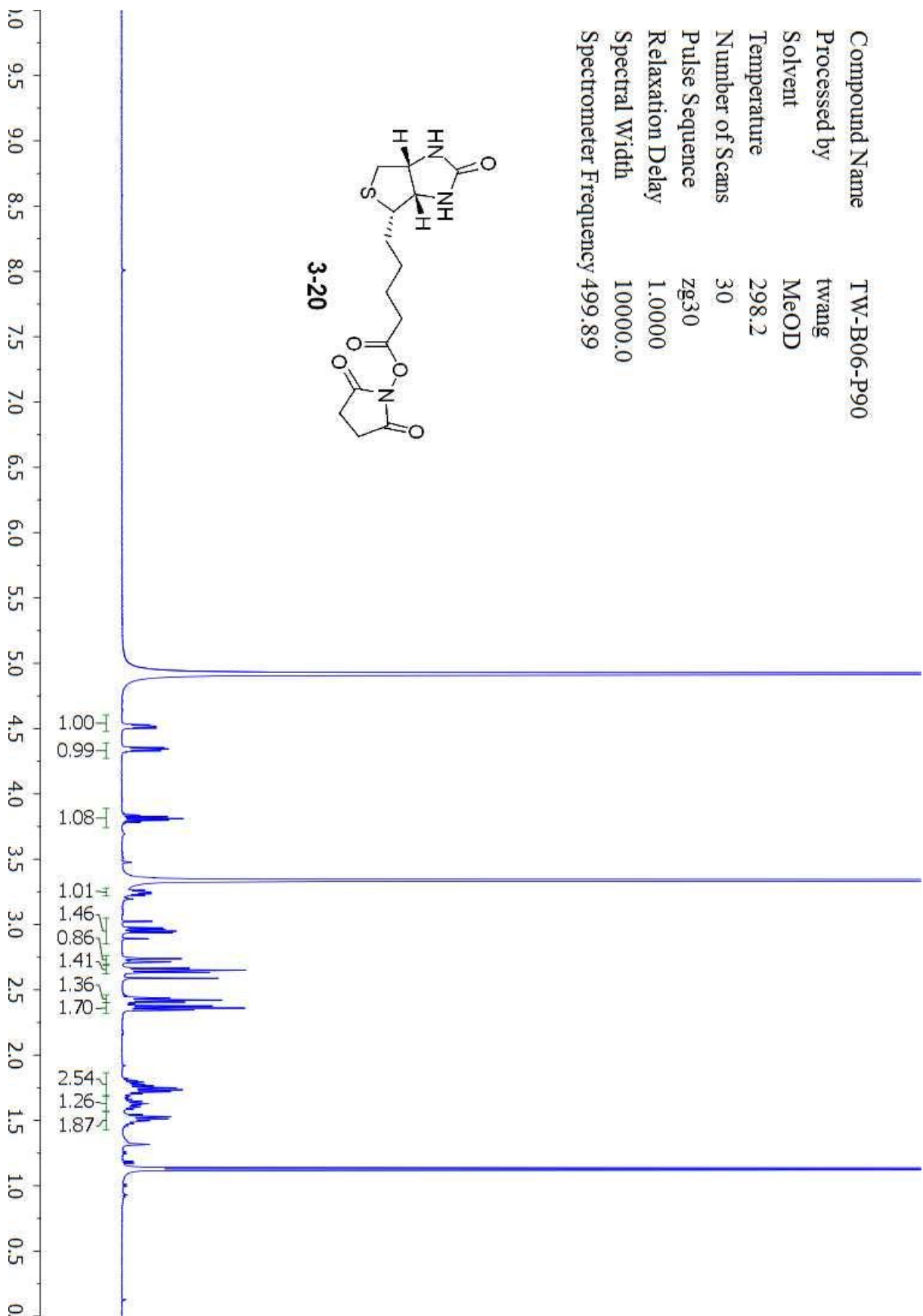
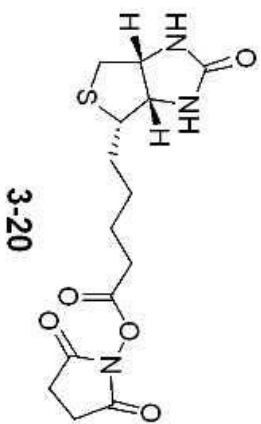
Compound Name TW-B06-P93  
Processed by twang  
Solvent CDCl3  
Temperature 298.1  
Number of Scans 55  
Pulse Sequence zgpg30  
Relaxation Delay 2.0000  
Spectral Width 29761.9  
Spectrometer Frequency 125.71



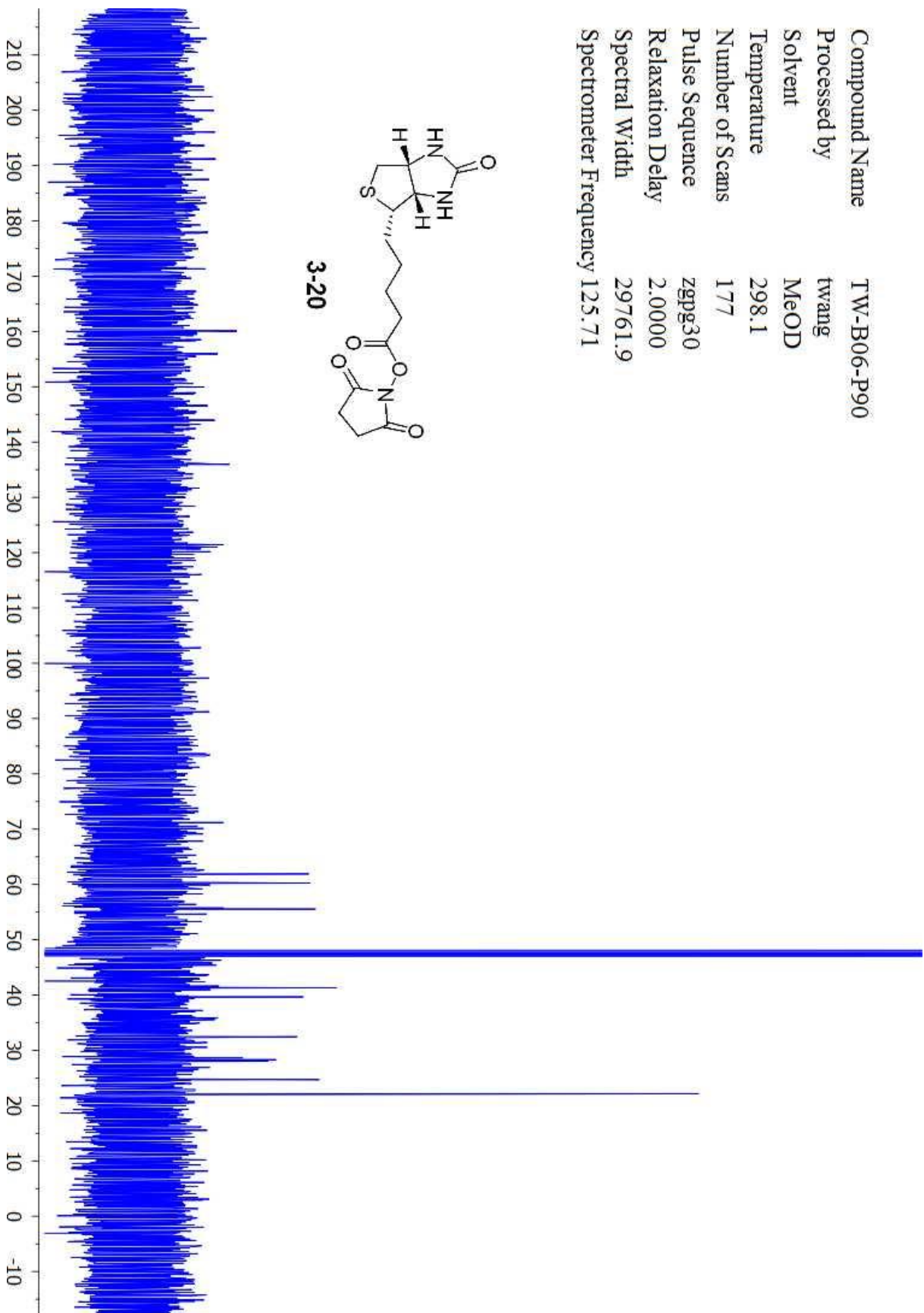
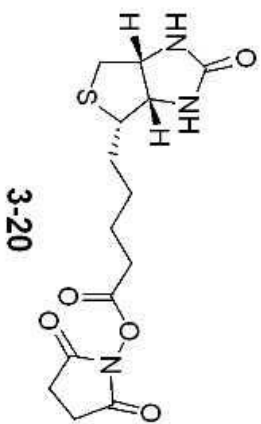
3-19



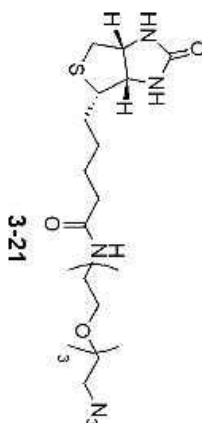
Compound Name TW-B06-P90  
 Processed by twang  
 Solvent MeOD  
 Temperature 298.2  
 Number of Scans 30  
 Pulse Sequence zg30  
 Relaxation Delay 1.0000  
 Spectral Width 10000.0  
 Spectrometer Frequency 499.89



Compound Name TW-B06-P90  
Processed by twang  
Solvent MeOD  
Temperature 298.1  
Number of Scans 177  
Pulse Sequence zgpg30  
Relaxation Delay 2.0000  
Spectral Width 29761.9  
Spectrometer Frequency 125.71



Compound Name TW-B06-P95  
 Processed by twang  
 Solvent CDCl3  
 Temperature 298.2  
 Number of Scans 16  
 Pulse Sequence zg30  
 Relaxation Delay 1.0000  
 Spectral Width 10000.0  
 Spectrometer Frequency 499.89



1.00

0.96

0.97

0.99

0.99

9.76

2.03

1.65

2.11

0.97

0.94

0.95

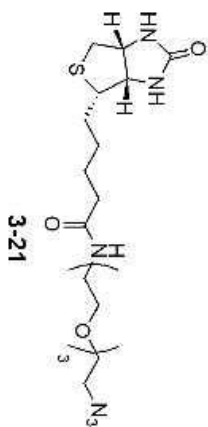
2.04

1.00

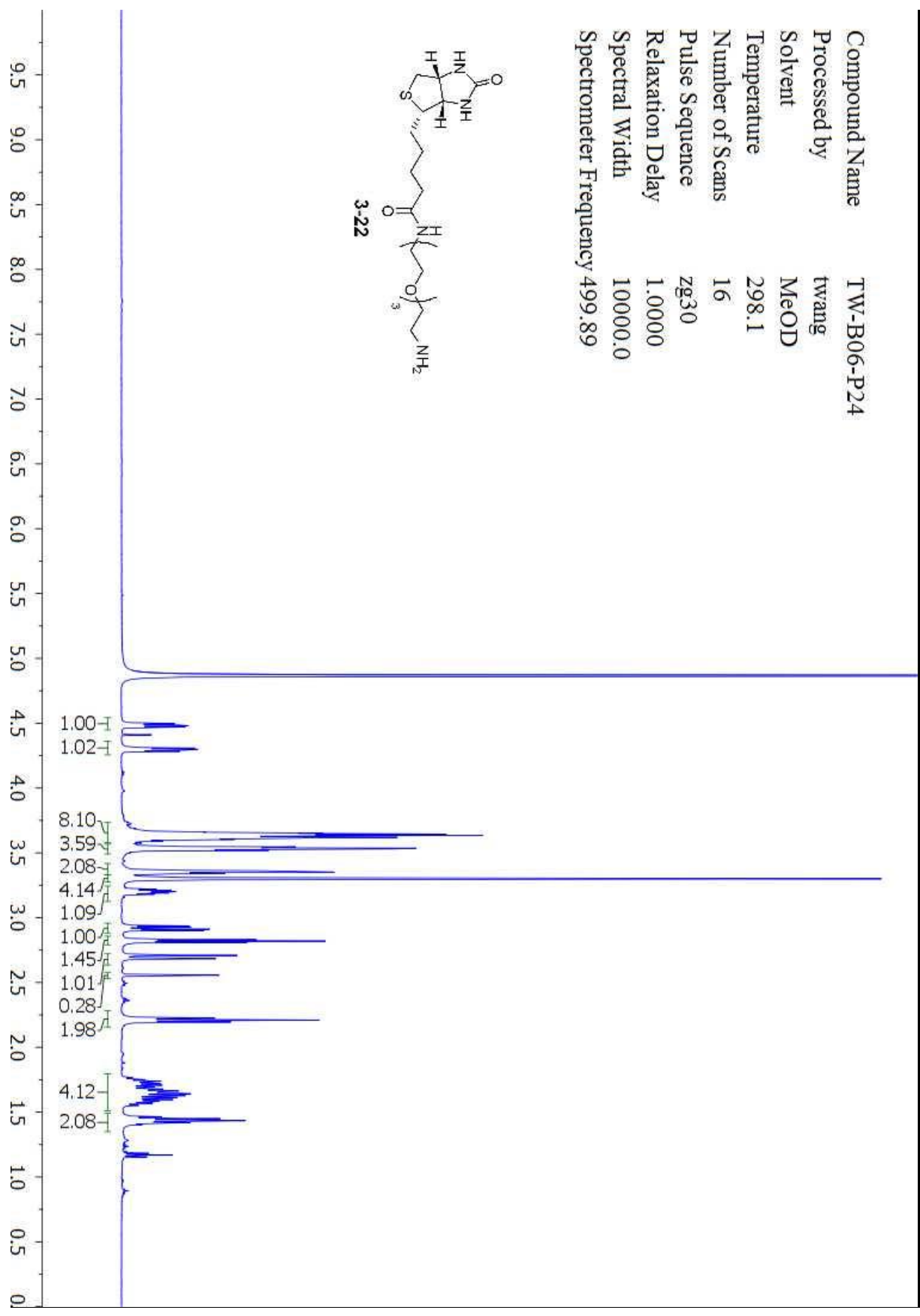
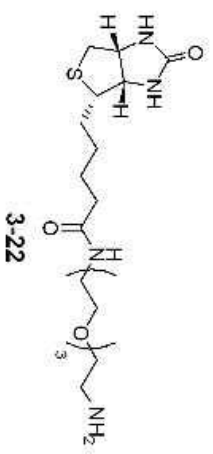
2.96

2.00

Compound Name TW-B06-P95  
Processed by twang  
Solvent CDCl3  
Temperature 298.1  
Number of Scans 130  
Pulse Sequence zgpg30  
Relaxation Delay 2.0000  
Spectral Width 29761.9  
Spectrometer Frequency 125.71

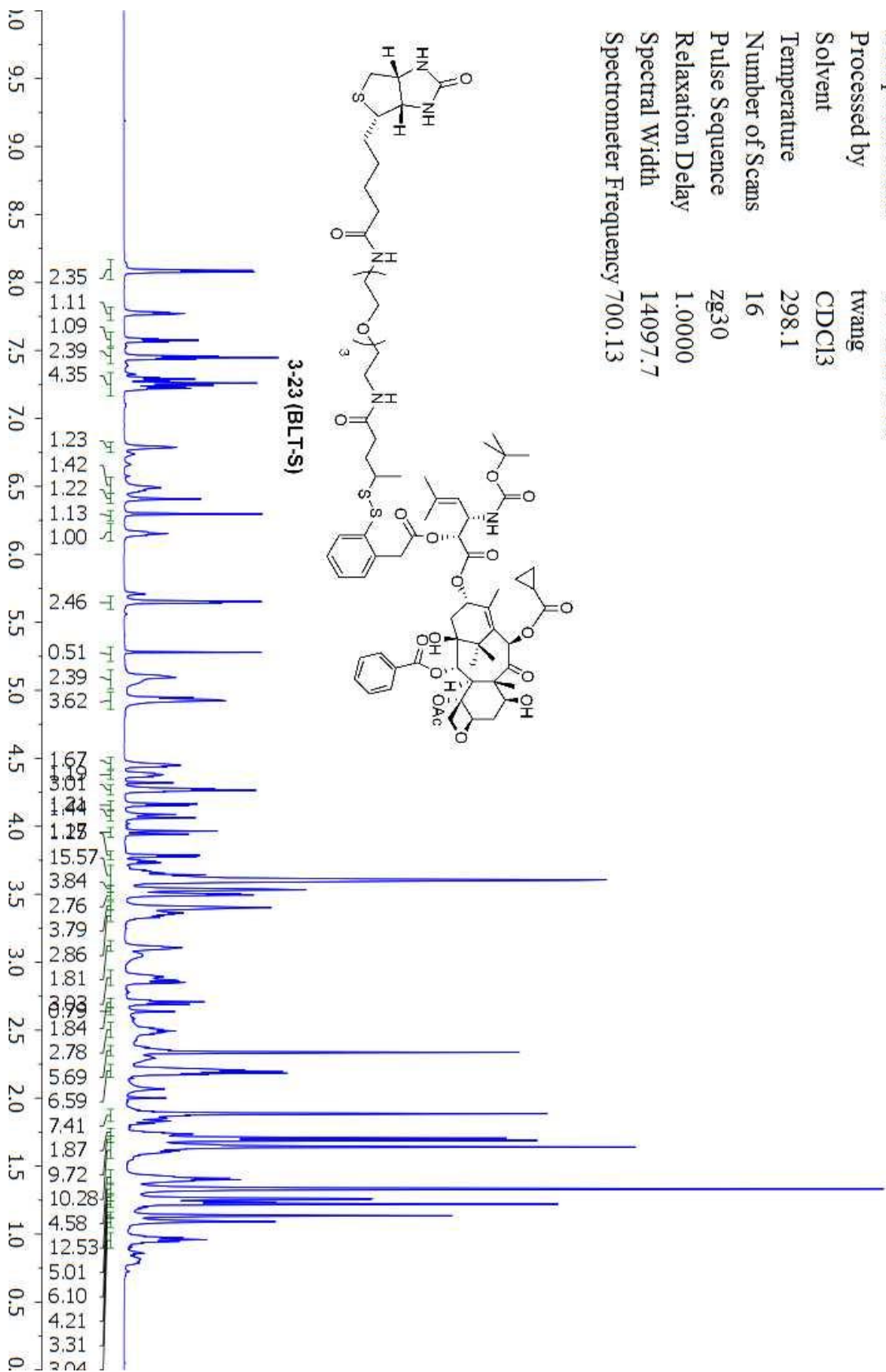


Compound Name TW-B06-P24  
 Processed by twang  
 Solvent MeOD  
 Temperature 298.1  
 Number of Scans 16  
 Pulse Sequence zg30  
 Relaxation Delay 1.0000  
 Spectral Width 10000.0  
 Spectrometer Frequency 499.89

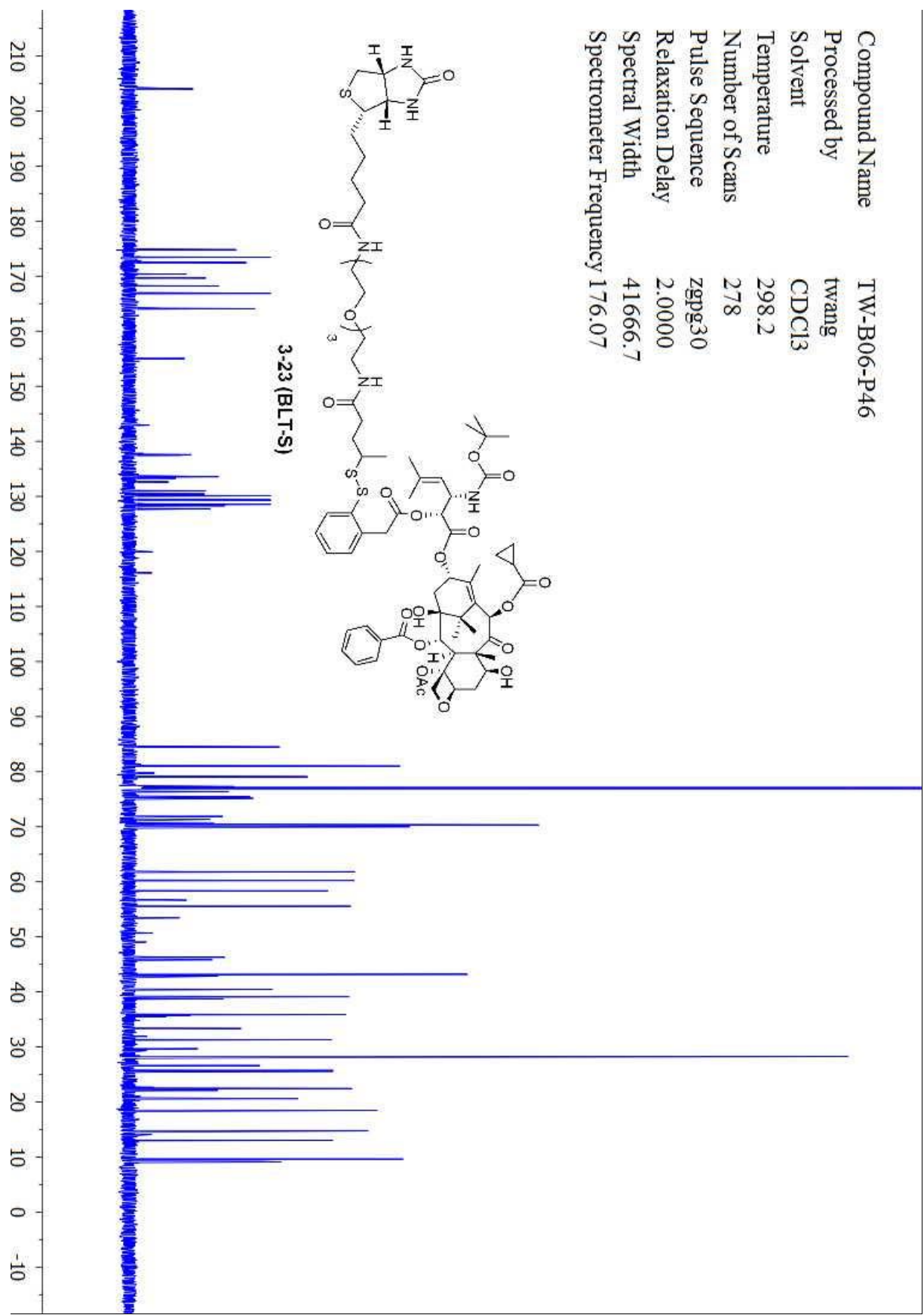
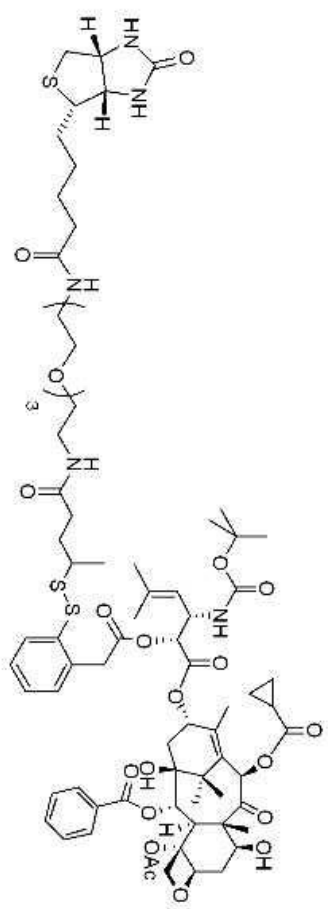




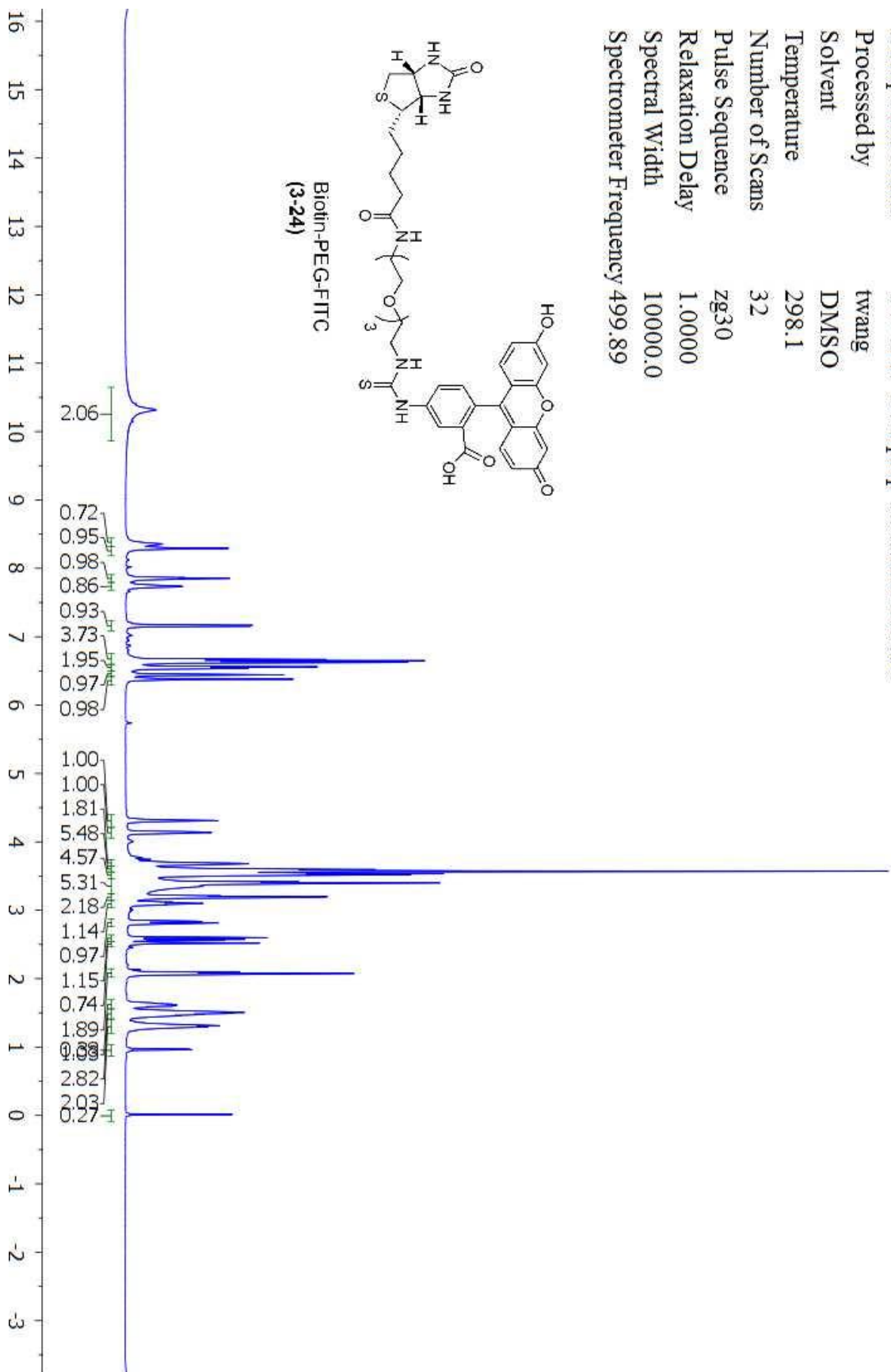
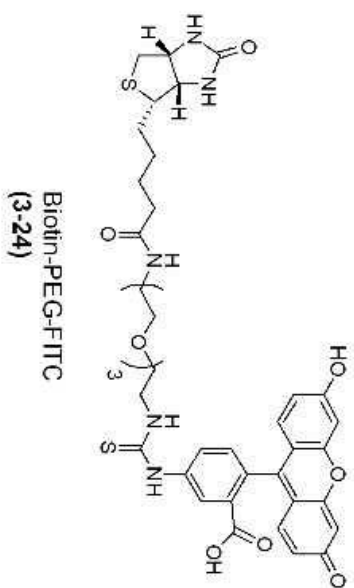
Compound Name TW-B06-P46  
 Processed by twang  
 Solvent CDCl3  
 Temperature 298.1  
 Number of Scans 16  
 Pulse Sequence zg30  
 Relaxation Delay 1.0000  
 Spectral Width 14097.7  
 Spectrometer Frequency 700.13



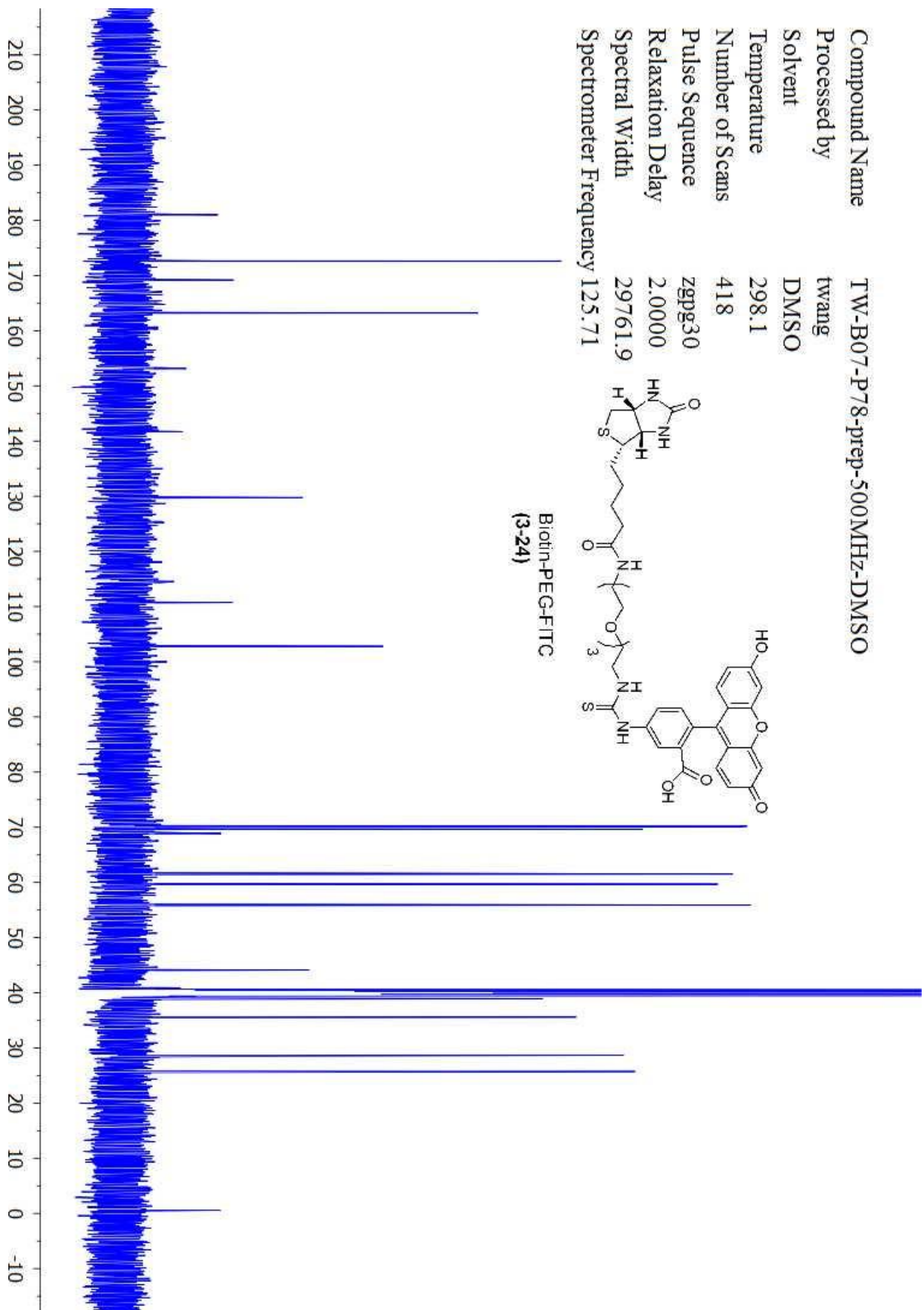
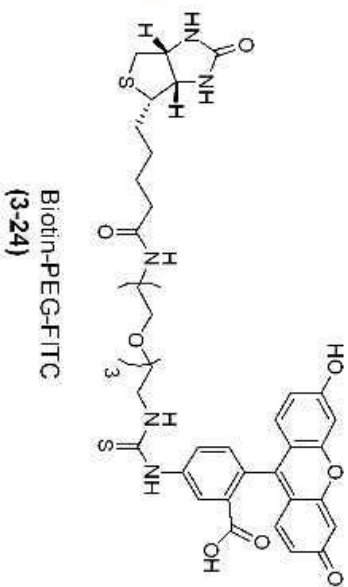
Compound Name TW-B06-P46  
 Processed by twang  
 Solvent CDCl3  
 Temperature 298.2  
 Number of Scans 278  
 Pulse Sequence zgpg30  
 Relaxation Delay 2.0000  
 Spectral Width 41666.7  
 Spectrometer Frequency 176.07



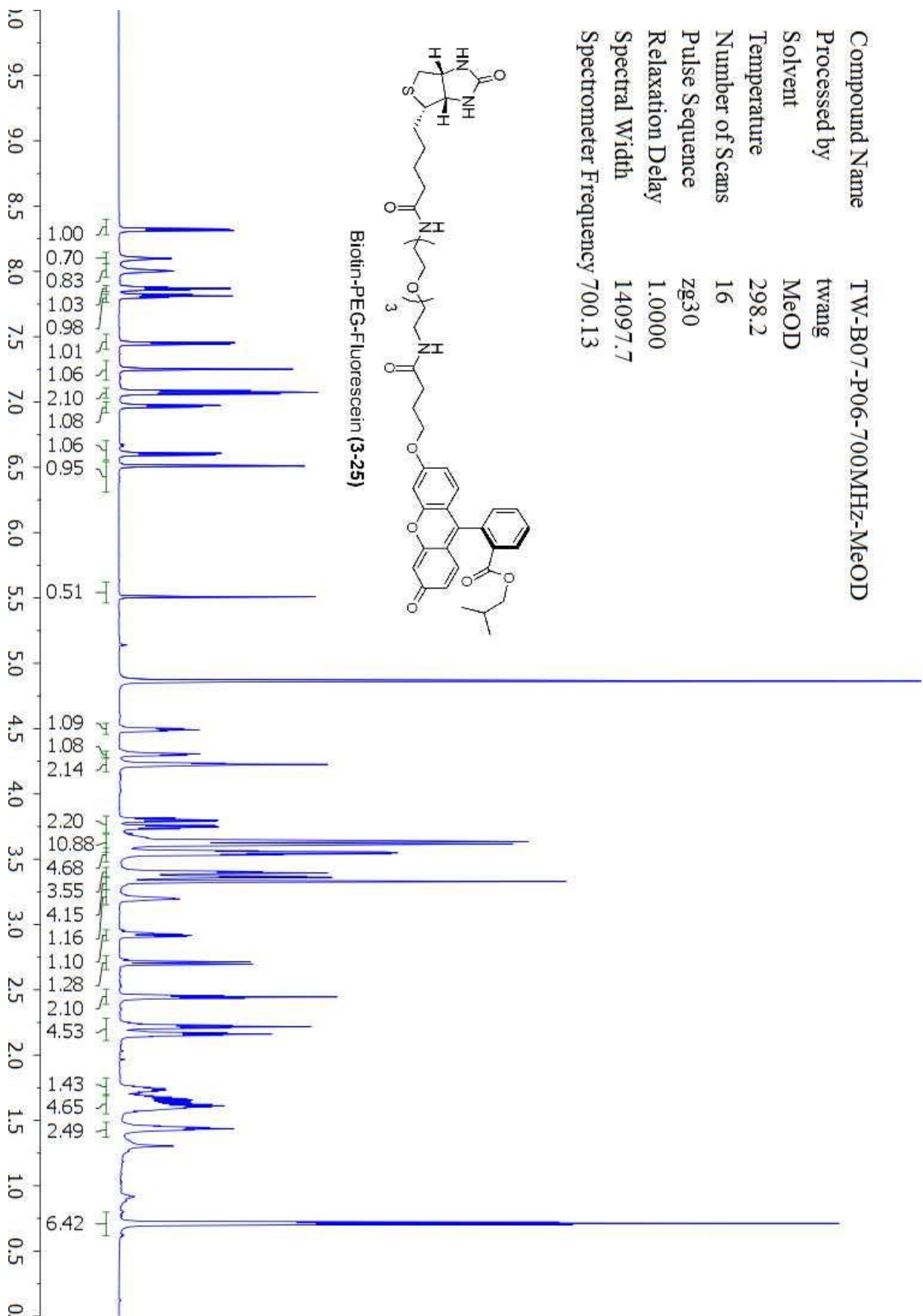
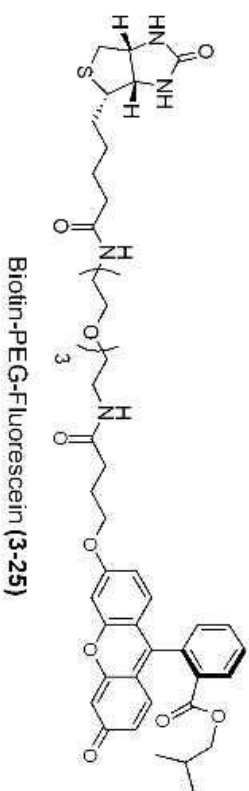
Compound Name TW-B07-P78-prep-500MHz-DMSO  
 Processed by twang  
 Solvent DMSO  
 Temperature 298.1  
 Number of Scans 32  
 Pulse Sequence zg30  
 Relaxation Delay 1.0000  
 Spectral Width 10000.0  
 Spectrometer Frequency 499.89



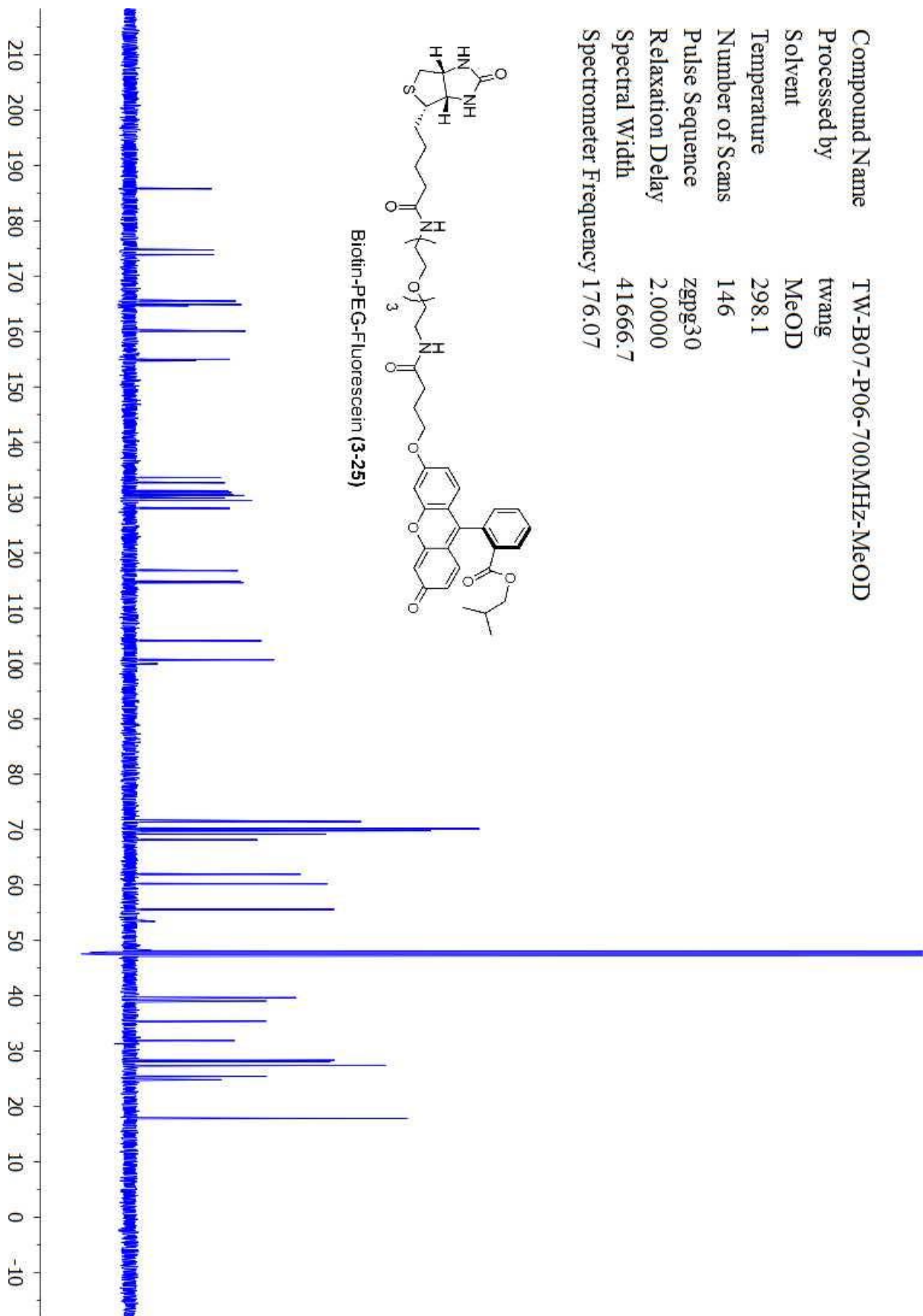
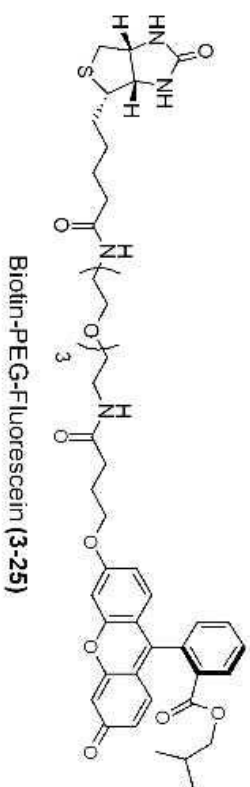
Compound Name TW-B07-P78-prep-500MHz-DMSO  
 Processed by twang  
 Solvent DMSO  
 Temperature 298.1  
 Number of Scans 418  
 Pulse Sequence zgpg30  
 Relaxation Delay 2.0000  
 Spectral Width 29761.9  
 Spectrometer Frequency 125.71



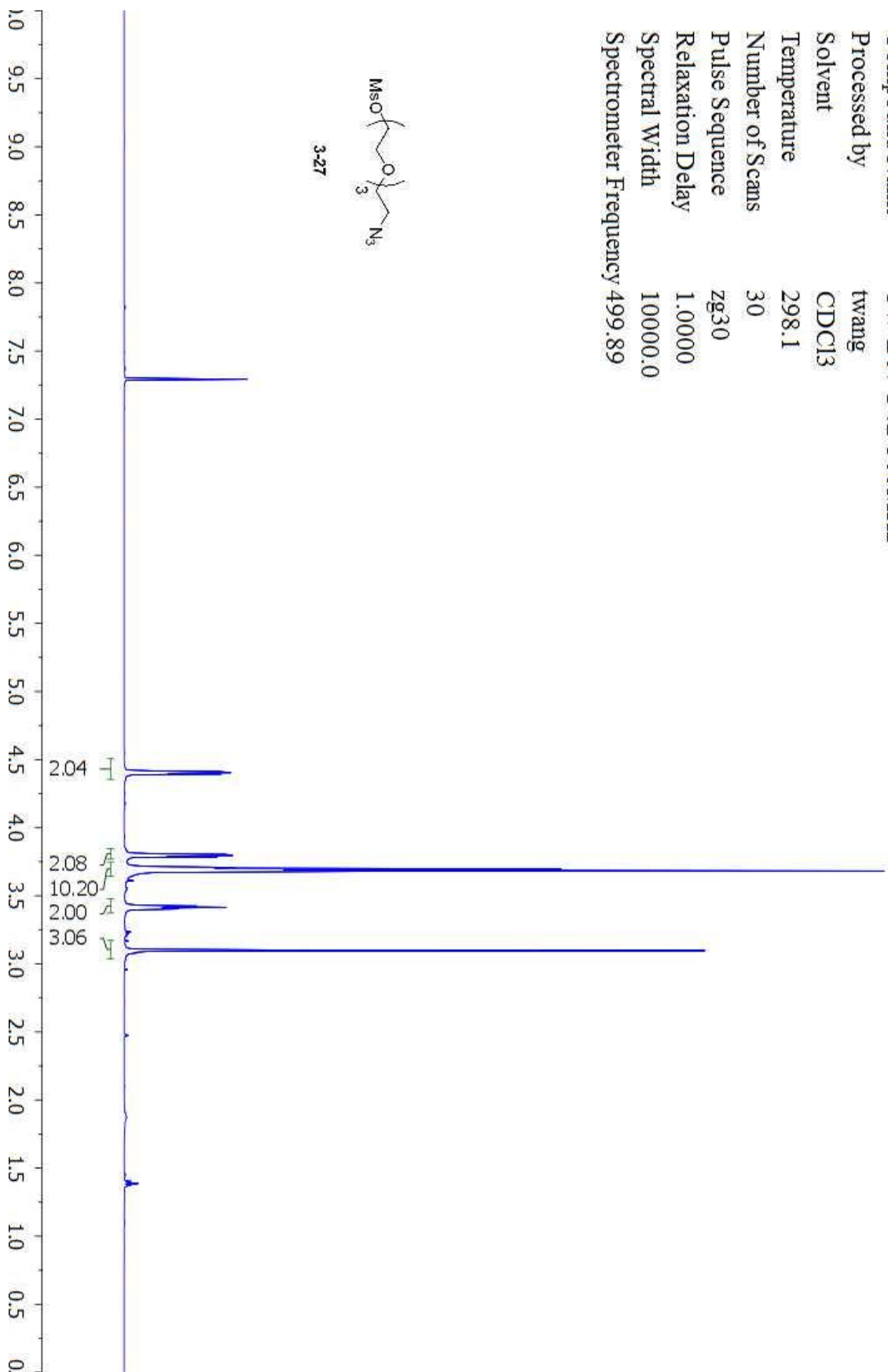
Compound Name TW-B07-P06-700MHz-MeOD  
 Processed by twang  
 Solvent MeOD  
 Temperature 298.2  
 Number of Scans 16  
 Pulse Sequence zg30  
 Relaxation Delay 1.0000  
 Spectral Width 14097.7  
 Spectrometer Frequency 700.13



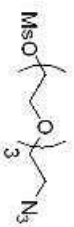
Compound Name TW-B07-P06-700MHz-MeOD  
 Processed by twang  
 Solvent MeOD  
 Temperature 298.1  
 Number of Scans 146  
 Pulse Sequence zgpg30  
 Relaxation Delay 2.0000  
 Spectral Width 41666.7  
 Spectrometer Frequency 176.07



Compound Name TW-B07-P42-500MHZ  
Processed by twang  
Solvent CDCl3  
Temperature 298.1  
Number of Scans 30  
Pulse Sequence zg30  
Relaxation Delay 1.0000  
Spectral Width 10000.0  
Spectrometer Frequency 499.89



Compound Name TW-B07-P42-500MHZ  
Processed by twang  
Solvent CDCl3  
Temperature 298.2  
Number of Scans 39  
Pulse Sequence zgpg30  
Relaxation Delay 2.0000  
Spectral Width 29761.9  
Spectrometer Frequency 125.71

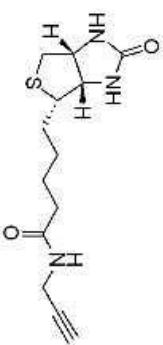


3-27

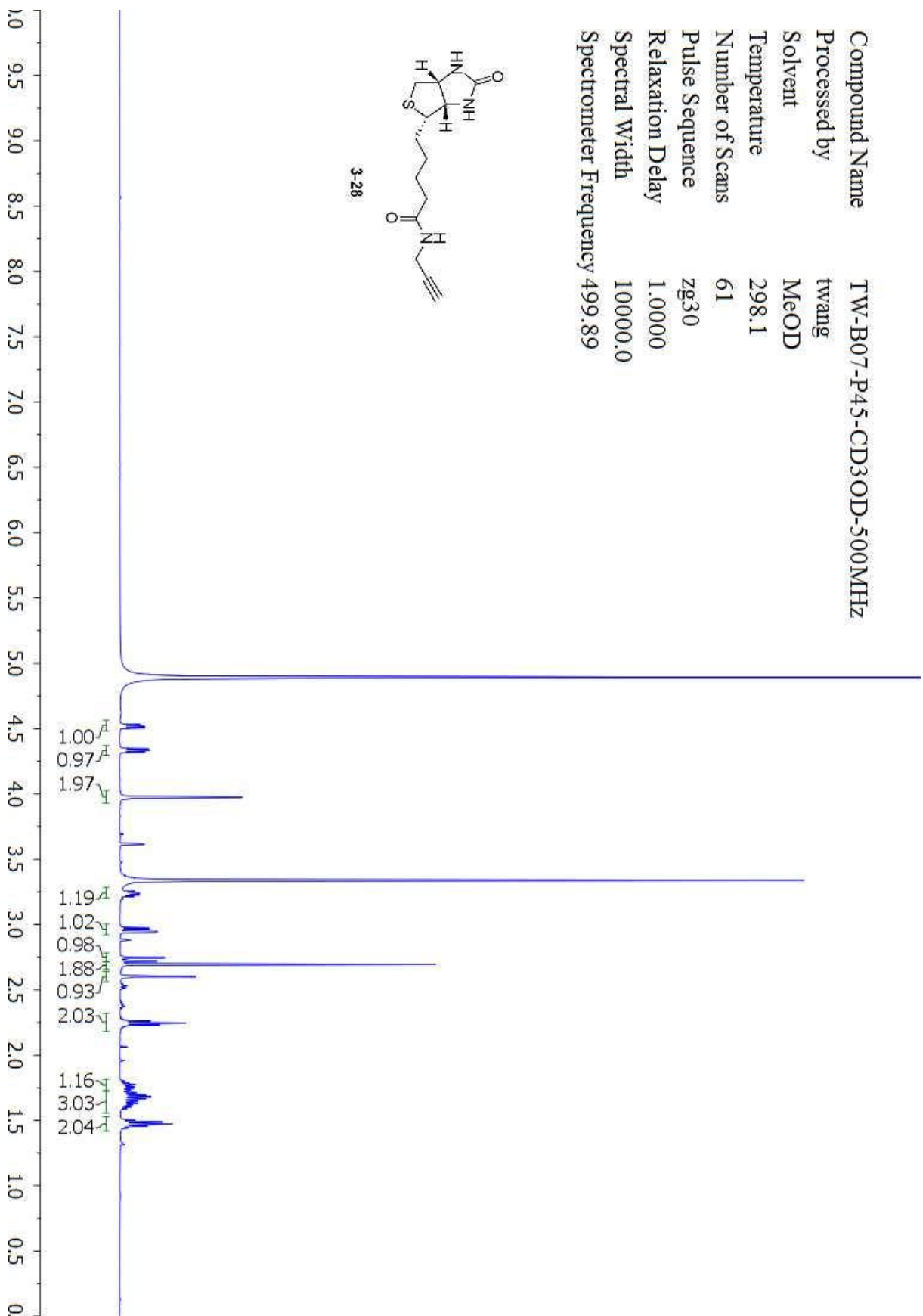




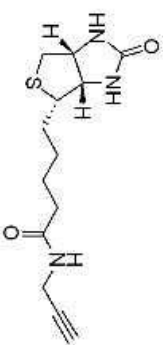
Compound Name TW-B07-P45-CD3OD-500MHZ  
 Processed by twang  
 Solvent MeOD  
 Temperature 298.1  
 Number of Scans 61  
 Pulse Sequence zg30  
 Relaxation Delay 1.0000  
 Spectral Width 10000.0  
 Spectrometer Frequency 499.89



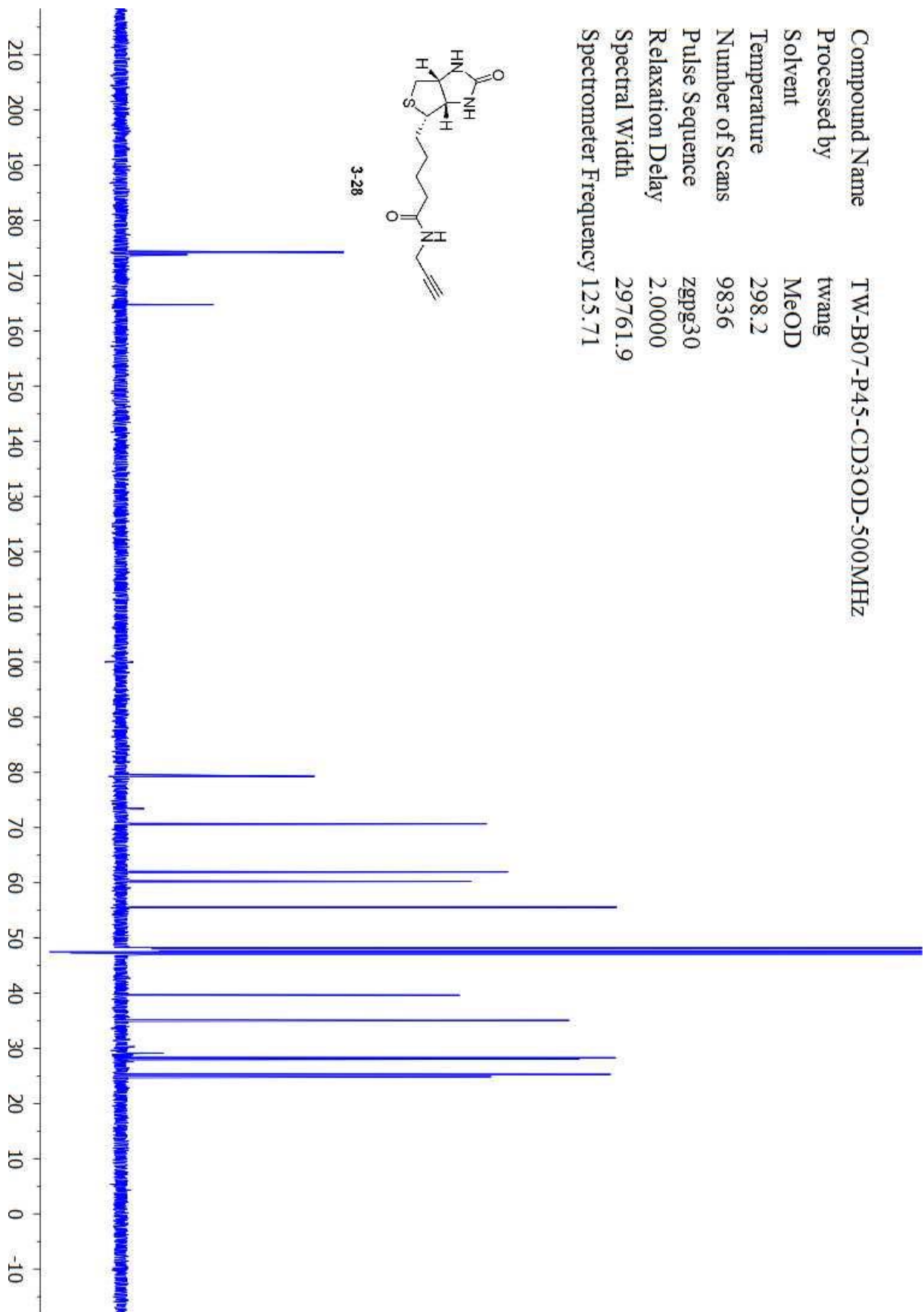
3-28



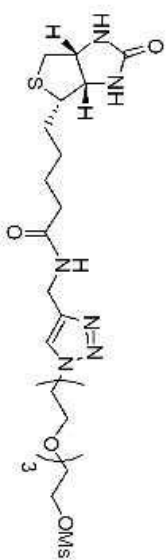
Compound Name TW-B07-P45-CD3OD-500MHZ  
Processed by twang  
Solvent MeOD  
Temperature 298.2  
Number of Scans 9836  
Pulse Sequence zgpg30  
Relaxation Delay 2.0000  
Spectral Width 29761.9  
Spectrometer Frequency 125.71



3-28



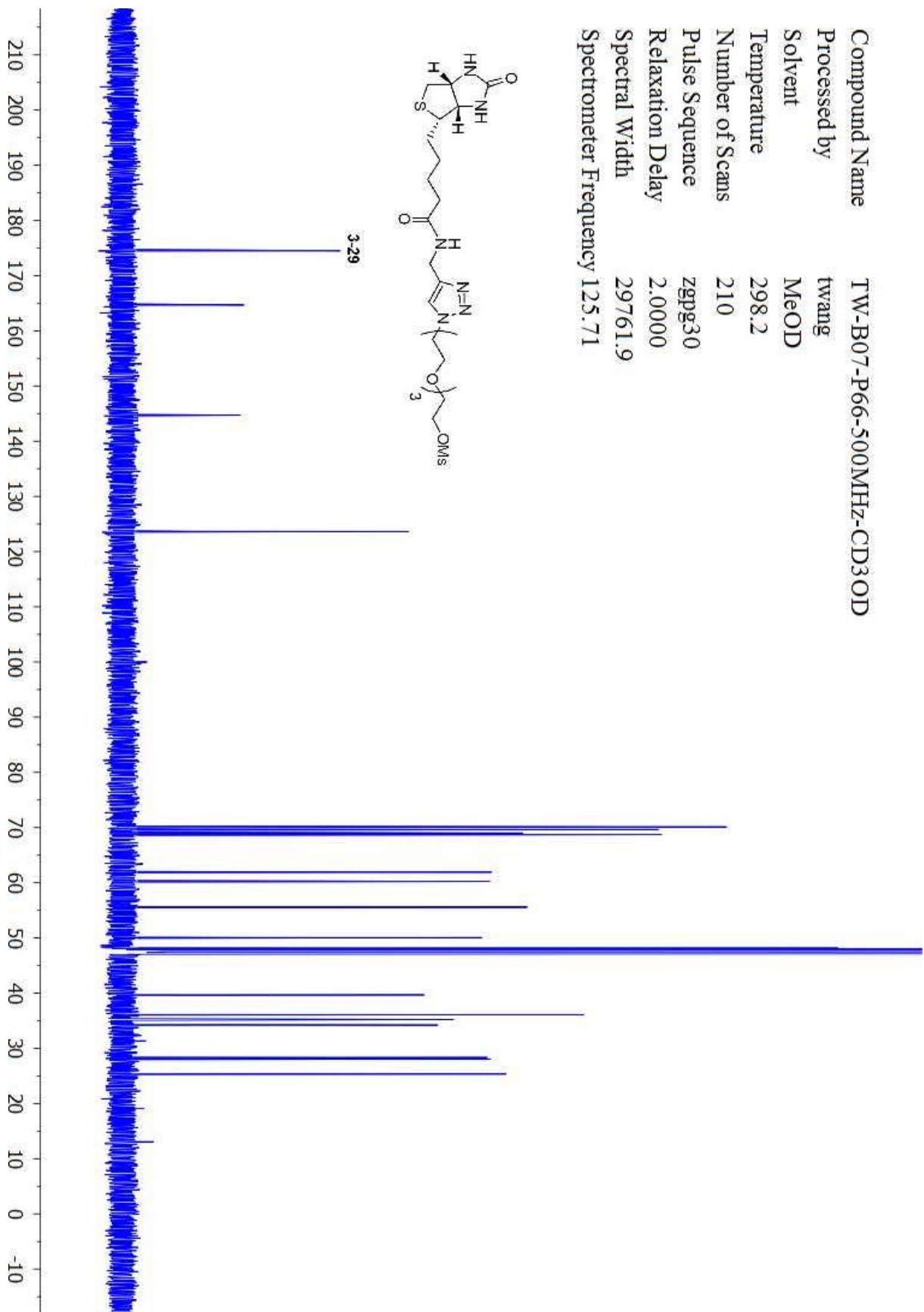
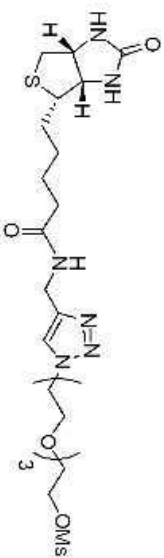
Compound Name TW-B07-P66-500MHz-CD3OD  
 Processed by twang  
 Solvent MeOD  
 Temperature 298.1  
 Number of Scans 32  
 Pulse Sequence zg30  
 Relaxation Delay 1.0000  
 Spectral Width 10000.0  
 Spectrometer Frequency 499.89



3-29

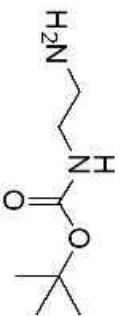


Compound Name TW-B07-P66-500MHz-CD3OD  
 Processed by twang  
 Solvent MeOD  
 Temperature 298.2  
 Number of Scans 210  
 Pulse Sequence zgpg30  
 Relaxation Delay 2.0000  
 Spectral Width 29761.9  
 Spectrometer Frequency 125.71

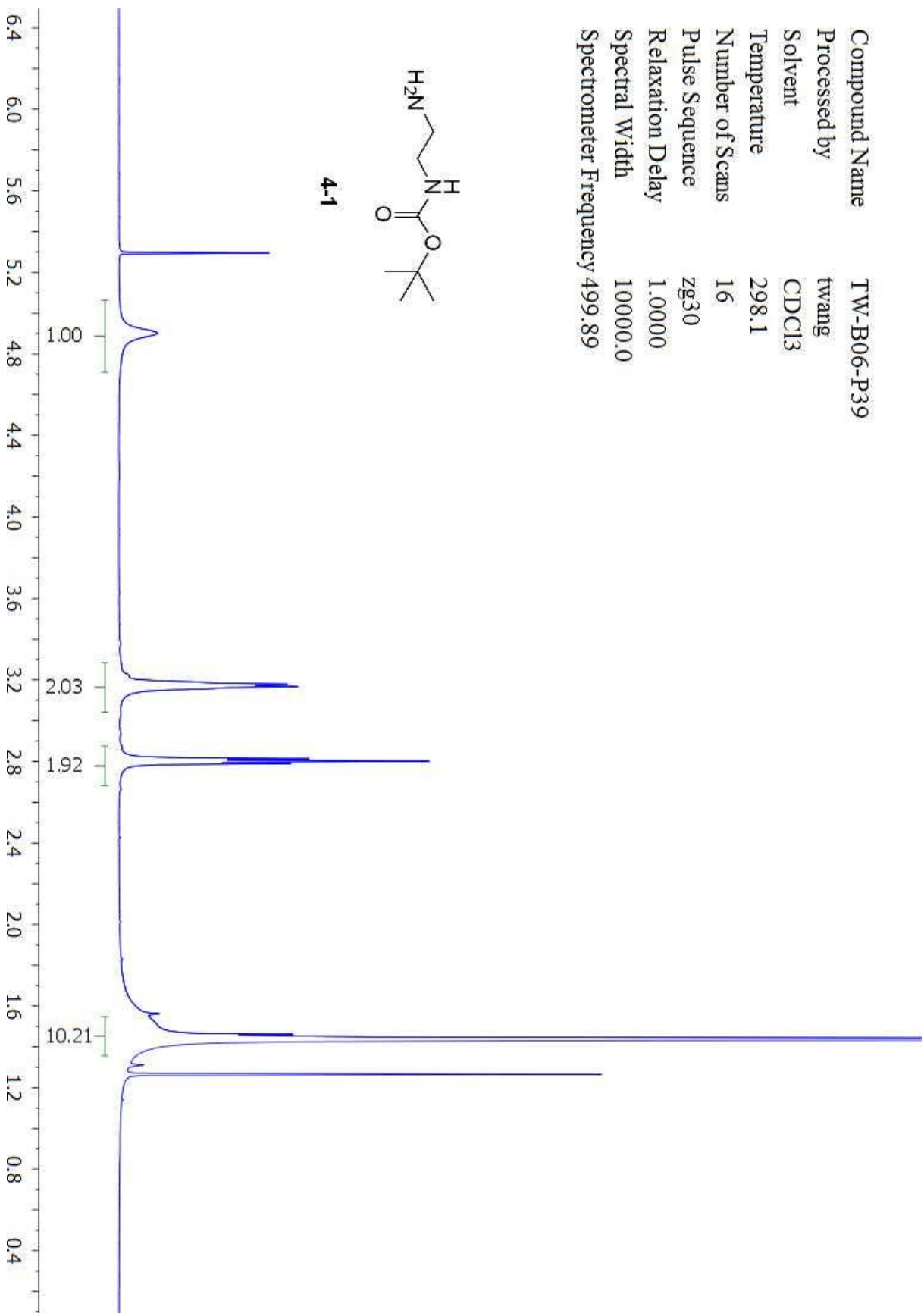


## Appendix Chapter 4 NMR Spectra

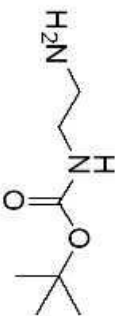
Compound Name TW-B06-P39  
Processed by twang  
Solvent CDCl3  
Temperature 298.1  
Number of Scans 16  
Pulse Sequence zg30  
Relaxation Delay 1.0000  
Spectral Width 10000.0  
Spectrometer Frequency 499.89



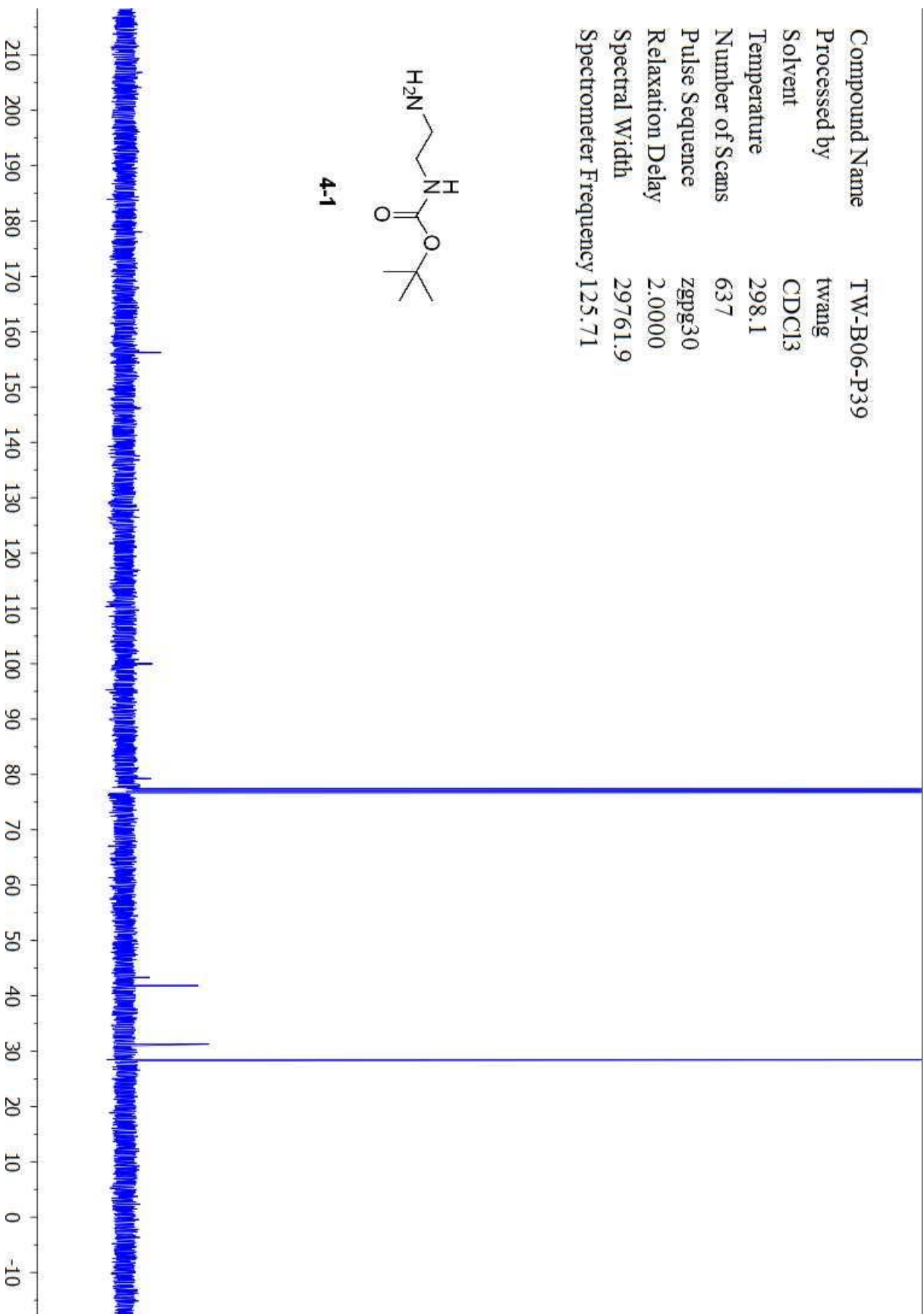
4-1



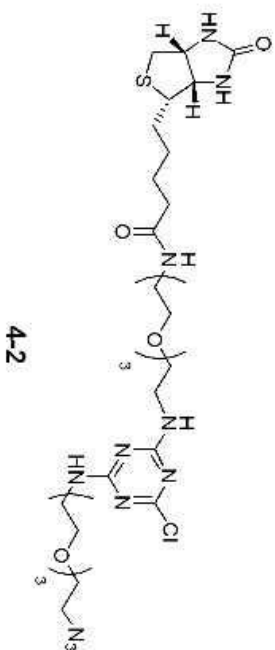
Compound Name TW-B06-P39  
Processed by twang  
Solvent CDCl3  
Temperature 298.1  
Number of Scans 637  
Pulse Sequence zgpg30  
Relaxation Delay 2.0000  
Spectral Width 29761.9  
Spectrometer Frequency 125.71



4-1

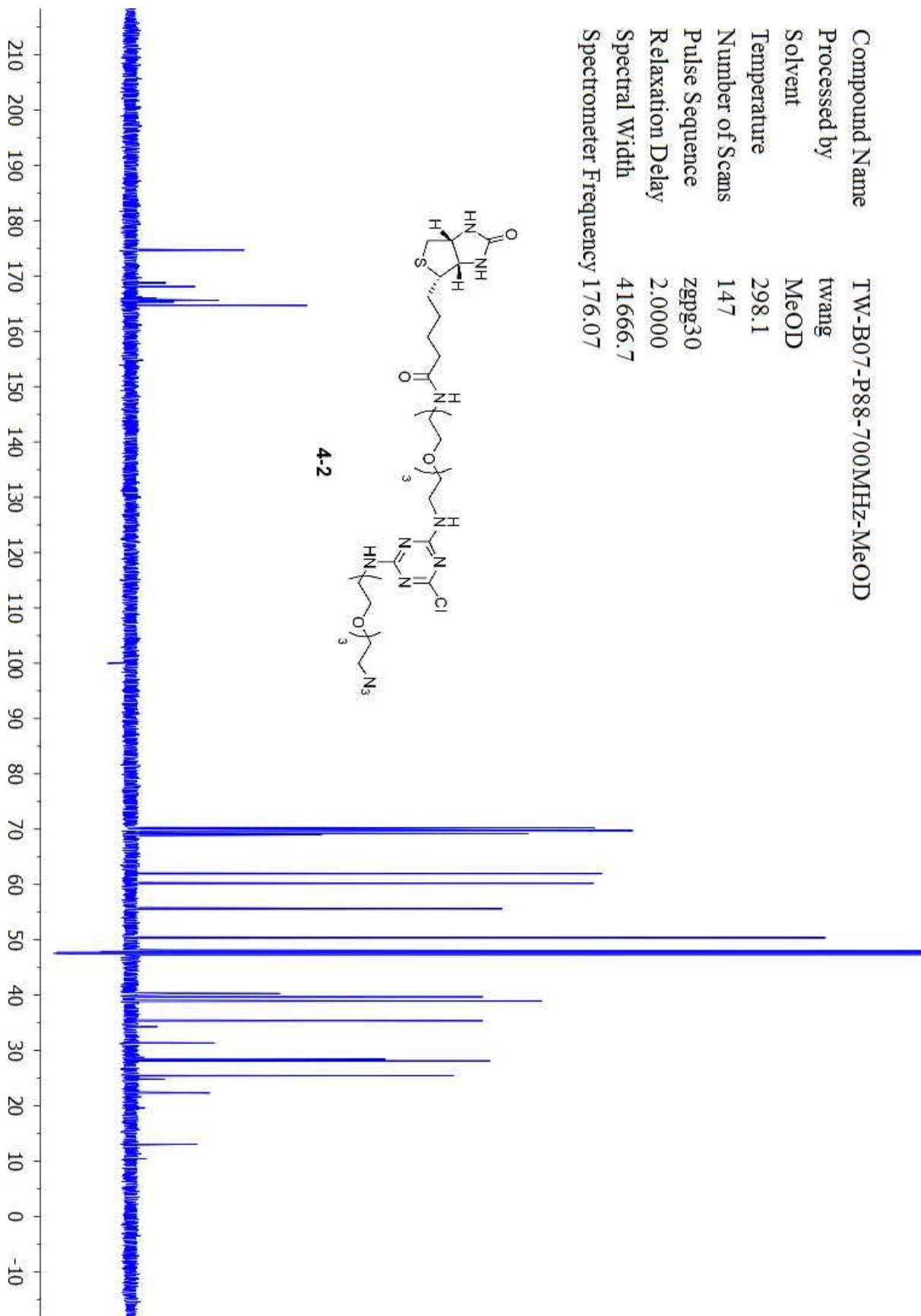
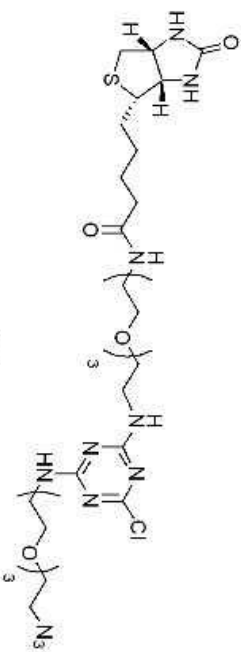


Compound Name TW-B07-P88-700MHz-MeOD  
 Processed by twang  
 Solvent MeOD  
 Temperature 298.2  
 Number of Scans 16  
 Pulse Sequence zg30  
 Relaxation Delay 1.0000  
 Spectral Width 14097.7  
 Spectrometer Frequency 700.13

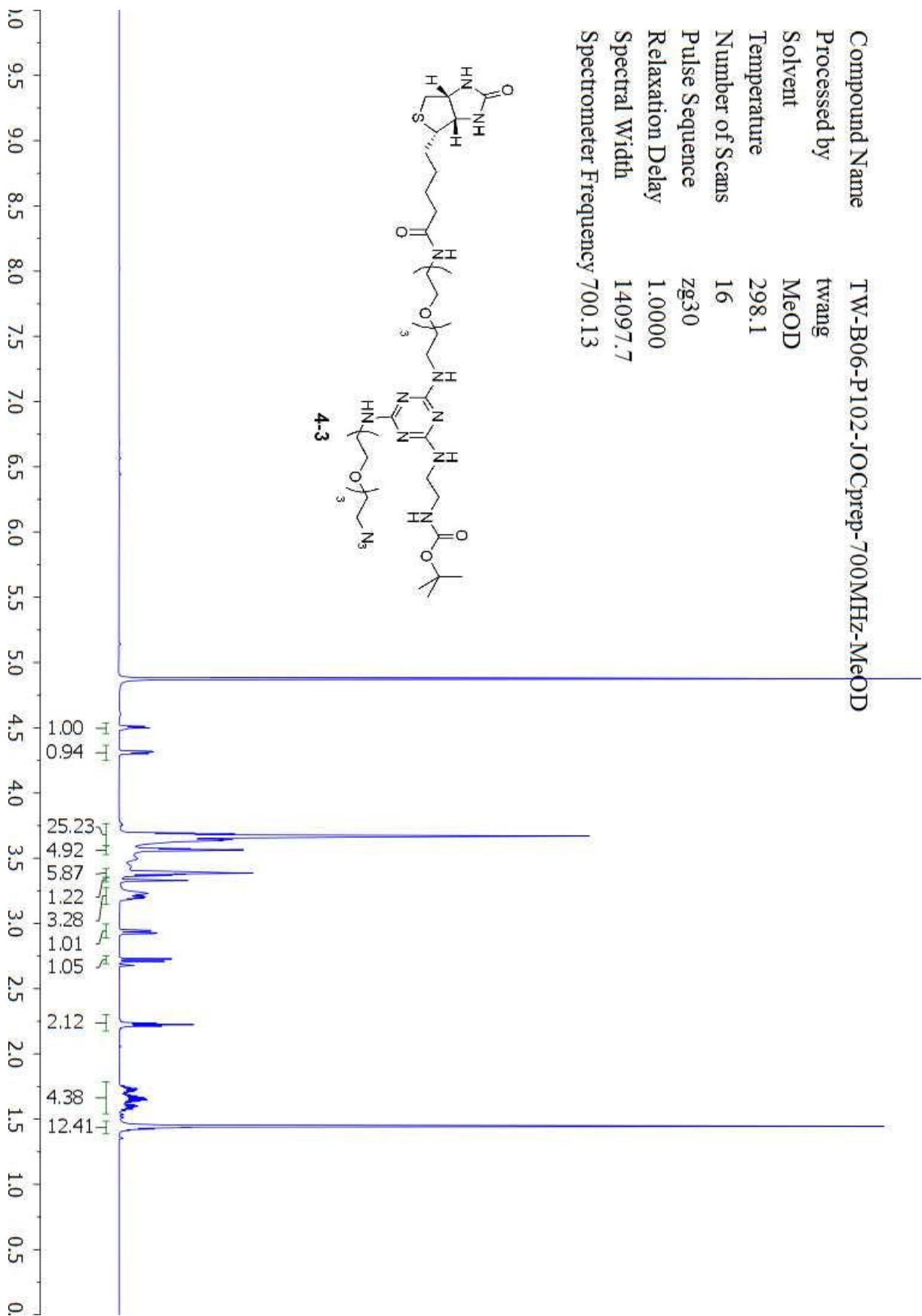
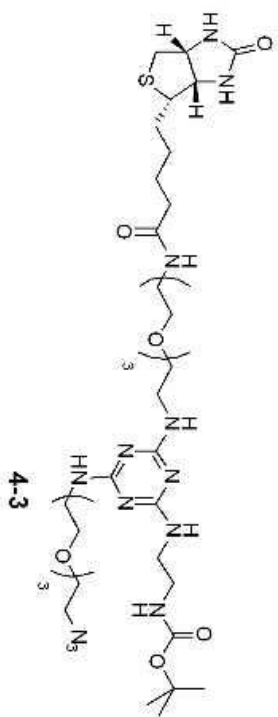




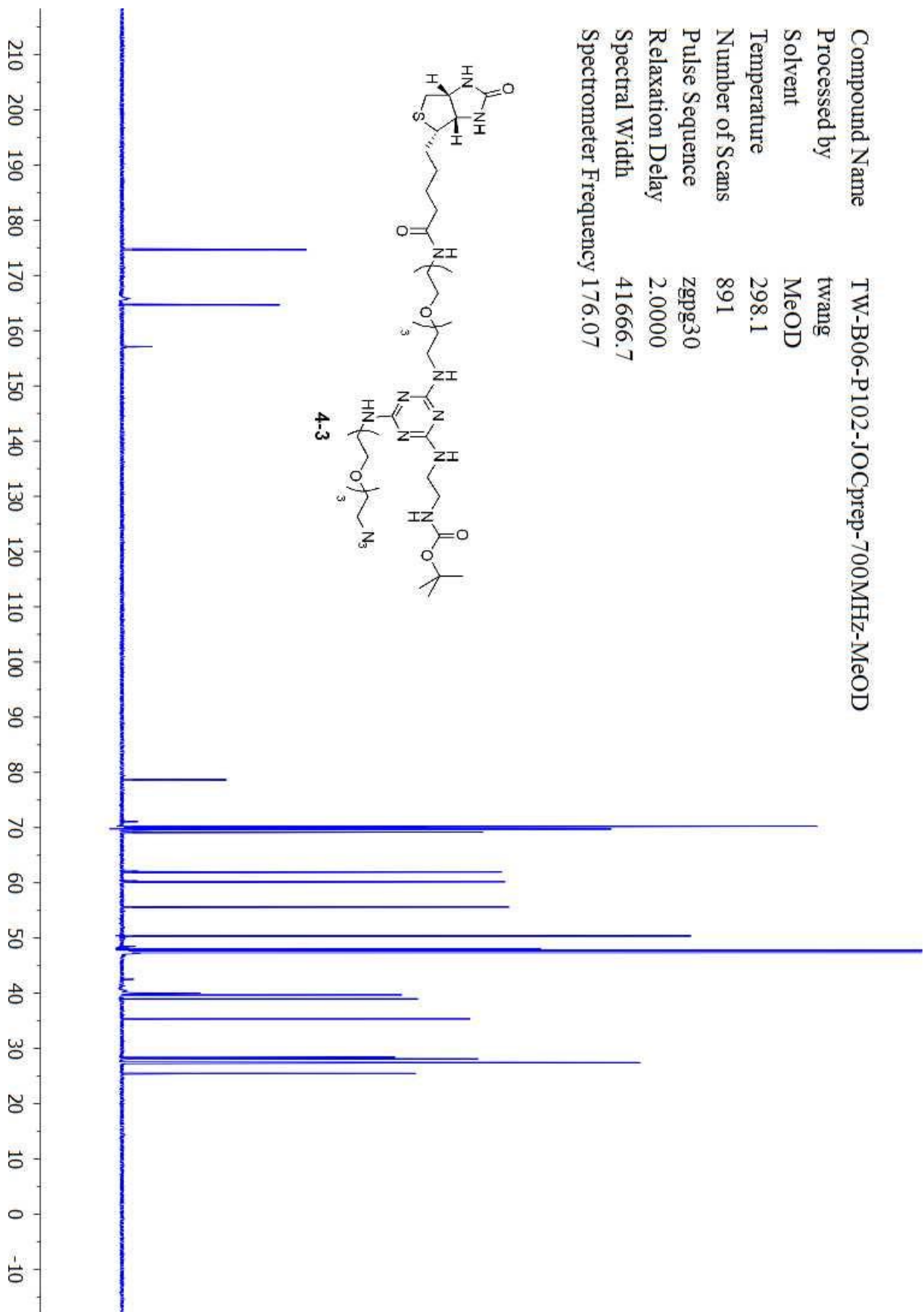
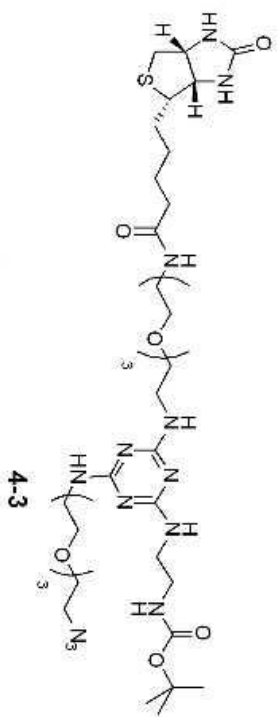
Compound Name TW-B07-P88-700MHz-MeOD  
 Processed by twang  
 Solvent MeOD  
 Temperature 298.1  
 Number of Scans 147  
 Pulse Sequence zgpg30  
 Relaxation Delay 2.0000  
 Spectral Width 41666.7  
 Spectrometer Frequency 176.07



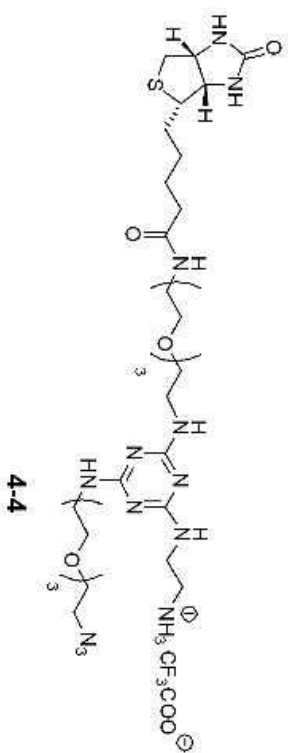
Compound Name TW-B06-P102-JOCprep-700MHz-MeOD  
 Processed by twang  
 Solvent MeOD  
 Temperature 298.1  
 Number of Scans 16  
 Pulse Sequence zg30  
 Relaxation Delay 1.0000  
 Spectral Width 14097.7  
 Spectrometer Frequency 700.13



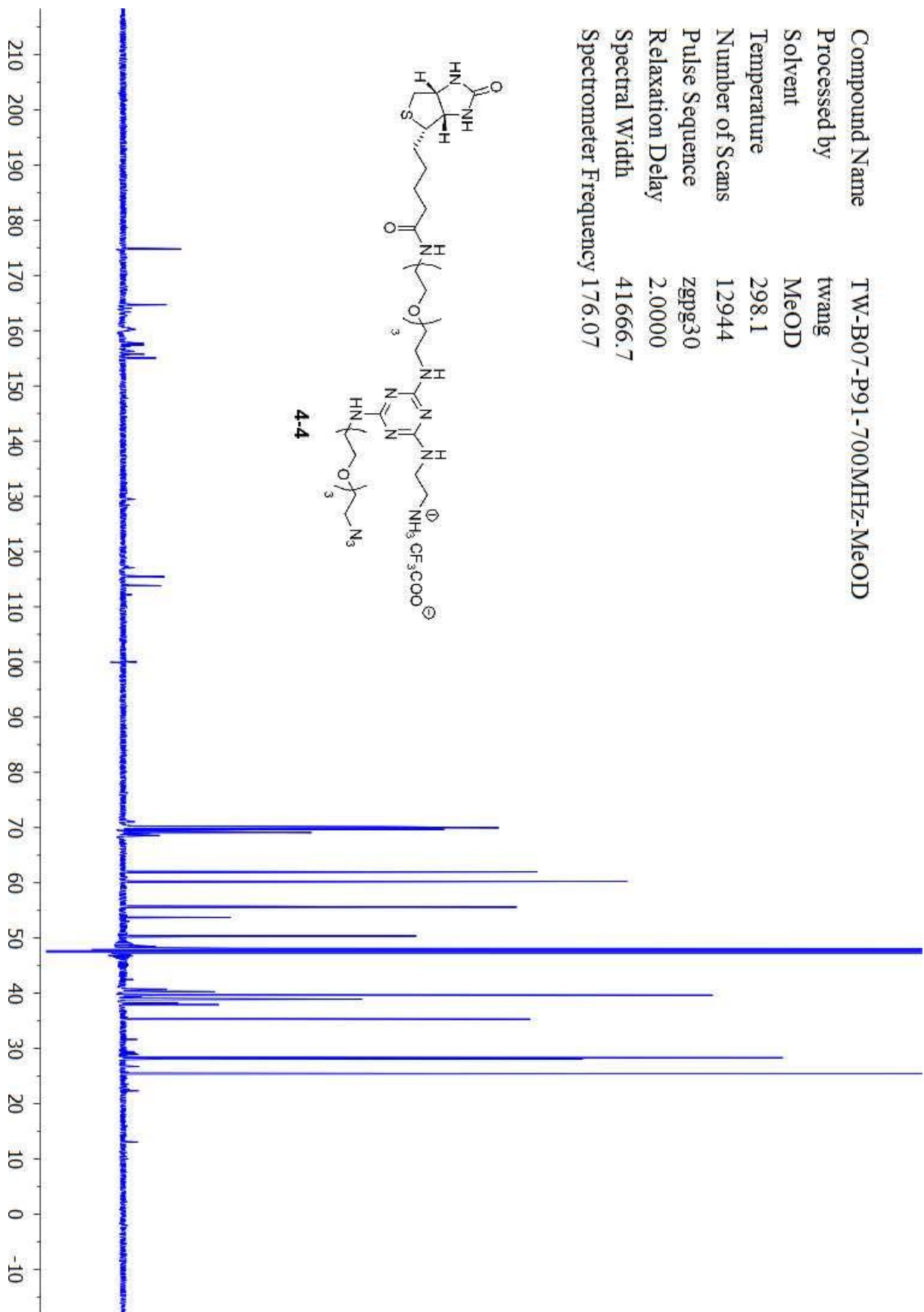
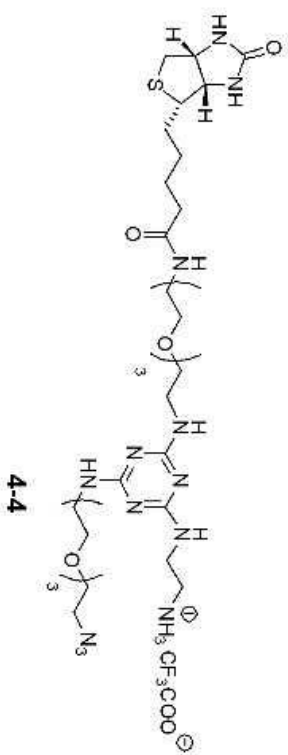
Compound Name TW-B06-P102-JOCprep-700MHz-MeOD  
 Processed by twang  
 Solvent MeOD  
 Temperature 298.1  
 Number of Scans 891  
 Pulse Sequence zgpg30  
 Relaxation Delay 2.0000  
 Spectral Width 41666.7  
 Spectrometer Frequency 176.07



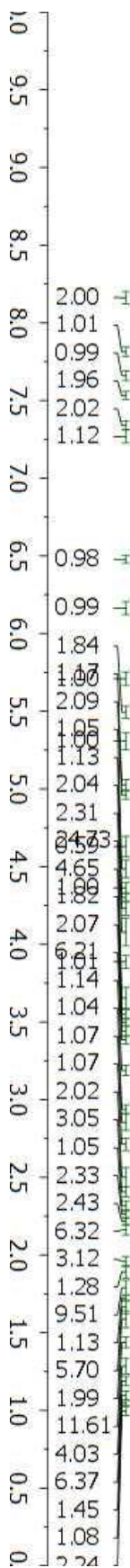
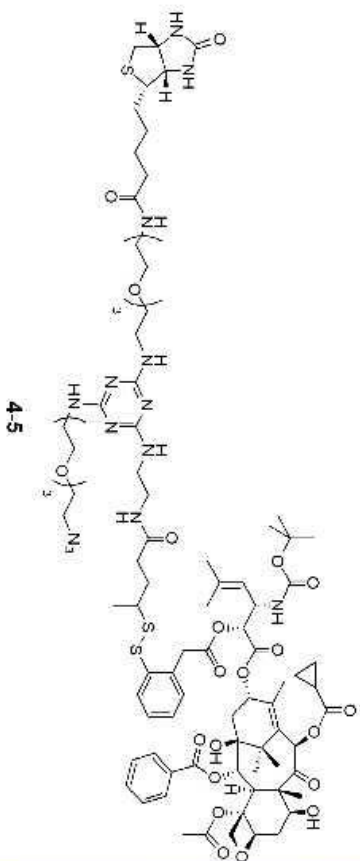
Compound Name TW-B07-P91-700MHz-MeOD  
 Processed by twang  
 Solvent MeOD  
 Temperature 298.1  
 Number of Scans 16  
 Pulse Sequence zg30  
 Relaxation Delay 1.0000  
 Spectral Width 14097.7  
 Spectrometer Frequency 700.13



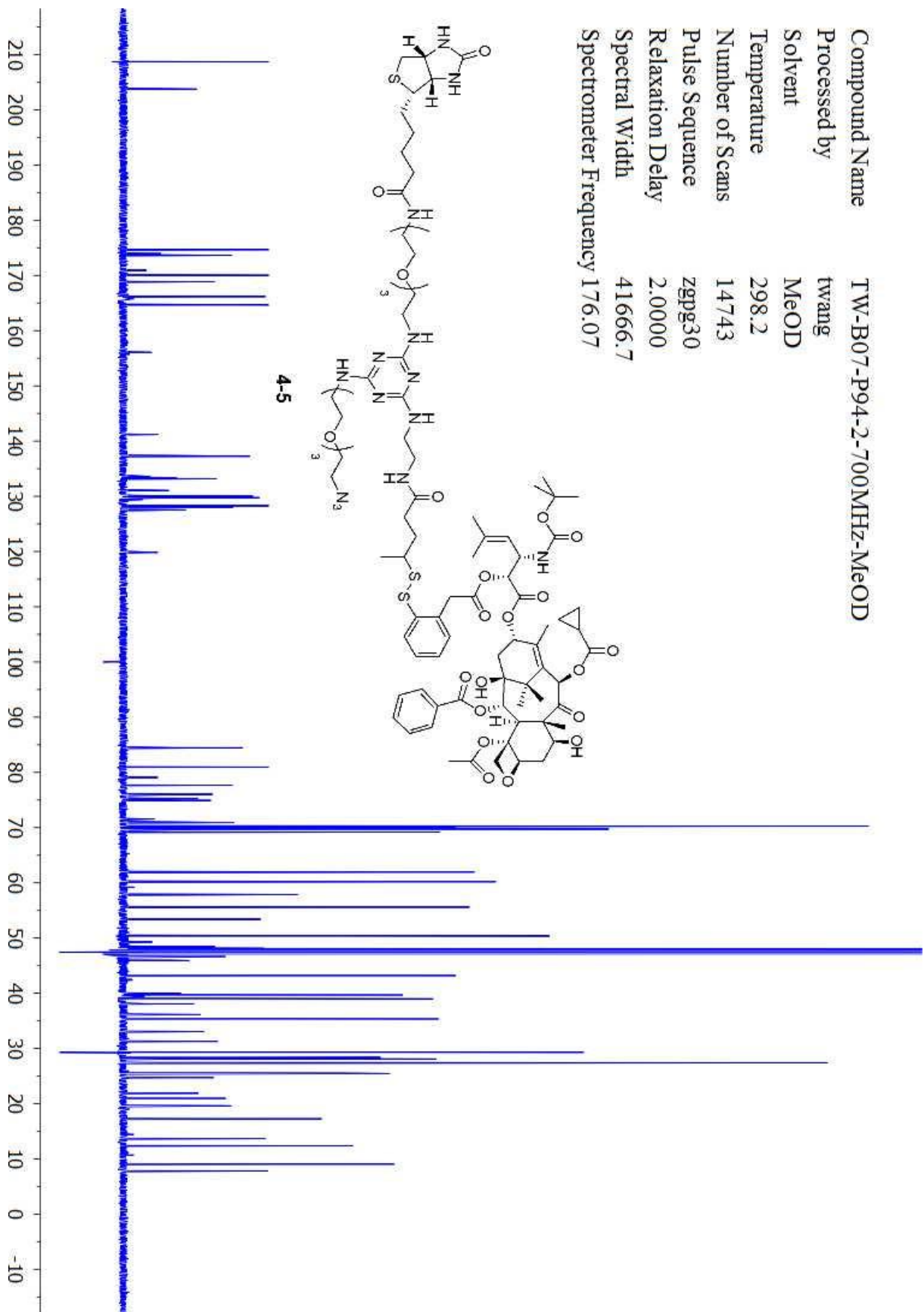
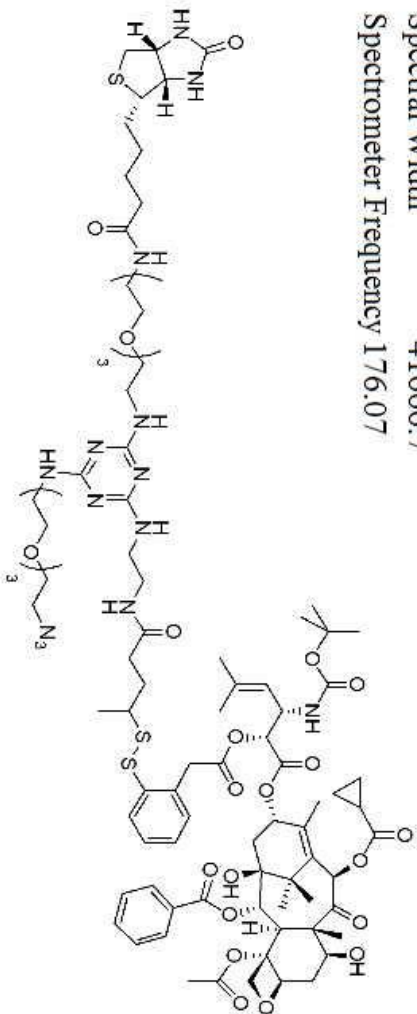
Compound Name TW-B07-P91-700MHz-MeOD  
 Processed by twang  
 Solvent MeOD  
 Temperature 298.1  
 Number of Scans 12944  
 Pulse Sequence zgpg30  
 Relaxation Delay 2.0000  
 Spectral Width 41666.7  
 Spectrometer Frequency 176.07



Compound Name TW-B07-P94-2-700MHz-MeOD  
 Processed by twang  
 Solvent MeOD  
 Temperature 298.1  
 Number of Scans 16  
 Pulse Sequence zg30  
 Relaxation Delay 1.0000  
 Spectral Width 14097.7  
 Spectrometer Frequency 700.13



Compound Name TW-B07-P94-2-700MHz-MeOD  
 Processed by twang  
 Solvent MeOD  
 Temperature 298.2  
 Number of Scans 14743  
 Pulse Sequence zgpg30  
 Relaxation Delay 2.0000  
 Spectral Width 41666.7  
 Spectrometer Frequency 176.07



Compound Name TW-B06-P101  
Processed by twang  
Solvent CDCl3  
Temperature 298.1  
Number of Scans 16  
Pulse Sequence zg30  
Relaxation Delay 1.0000  
Spectral Width 10000.0  
Spectrometer Frequency 499.89

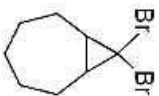


4-6

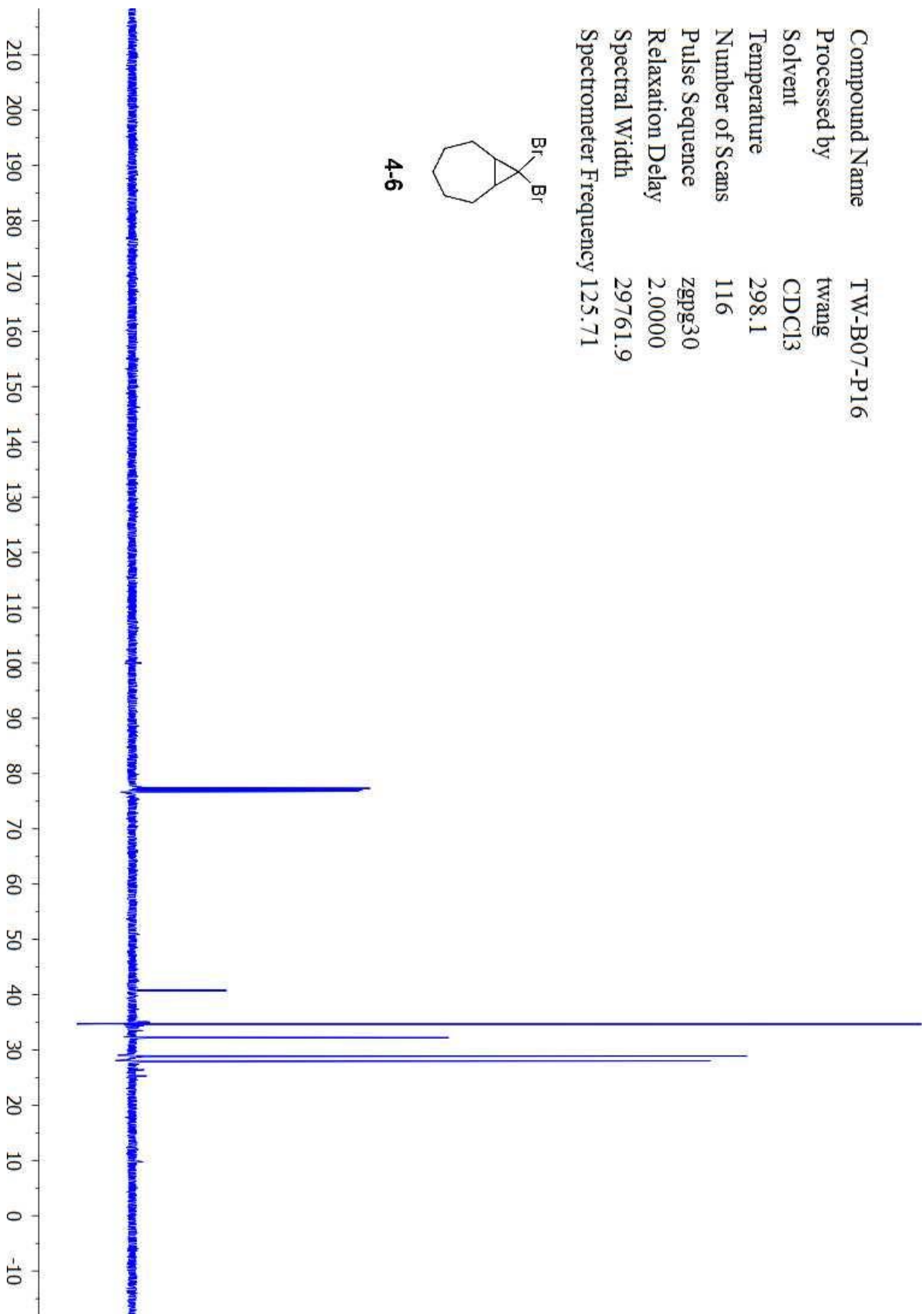




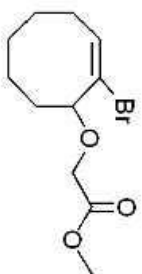
Compound Name TW-B07-P16  
Processed by twang  
Solvent CDCl3  
Temperature 298.1  
Number of Scans 116  
Pulse Sequence zgpg30  
Relaxation Delay 2.0000  
Spectral Width 29761.9  
Spectrometer Frequency 125.71



4-6



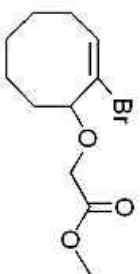
Compound Name TW-B06-P21  
Processed by twang  
Solvent CDCl3  
Temperature 298.1  
Number of Scans 16  
Pulse Sequence zg30  
Relaxation Delay 1.0000  
Spectral Width 10000.0  
Spectrometer Frequency 499.89



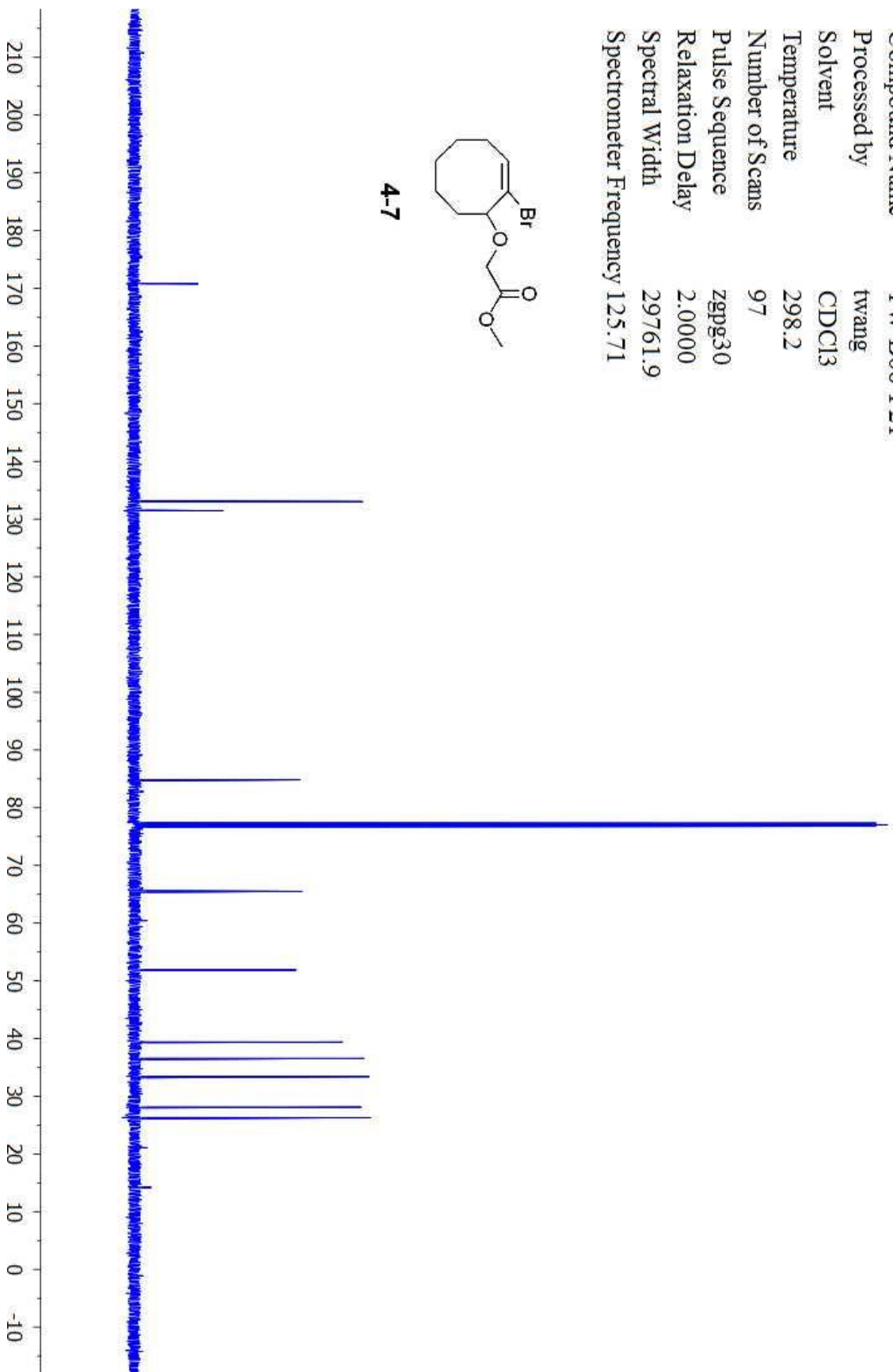
4-7



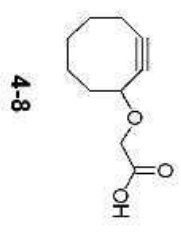
Compound Name TW-B06-P21  
Processed by twang  
Solvent CDCl3  
Temperature 298.2  
Number of Scans 97  
Pulse Sequence zgpg30  
Relaxation Delay 2.0000  
Spectral Width 29761.9  
Spectrometer Frequency 125.71



4-7

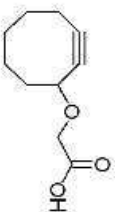


Compound Name TW-B07-P38+P39-700MHZ  
 Processed by twang  
 Solvent CDCl3  
 Temperature 298.1  
 Number of Scans 16  
 Pulse Sequence zg30  
 Relaxation Delay 1.0000  
 Spectral Width 14097.7  
 Spectrometer 700.13  
 Manufacturer

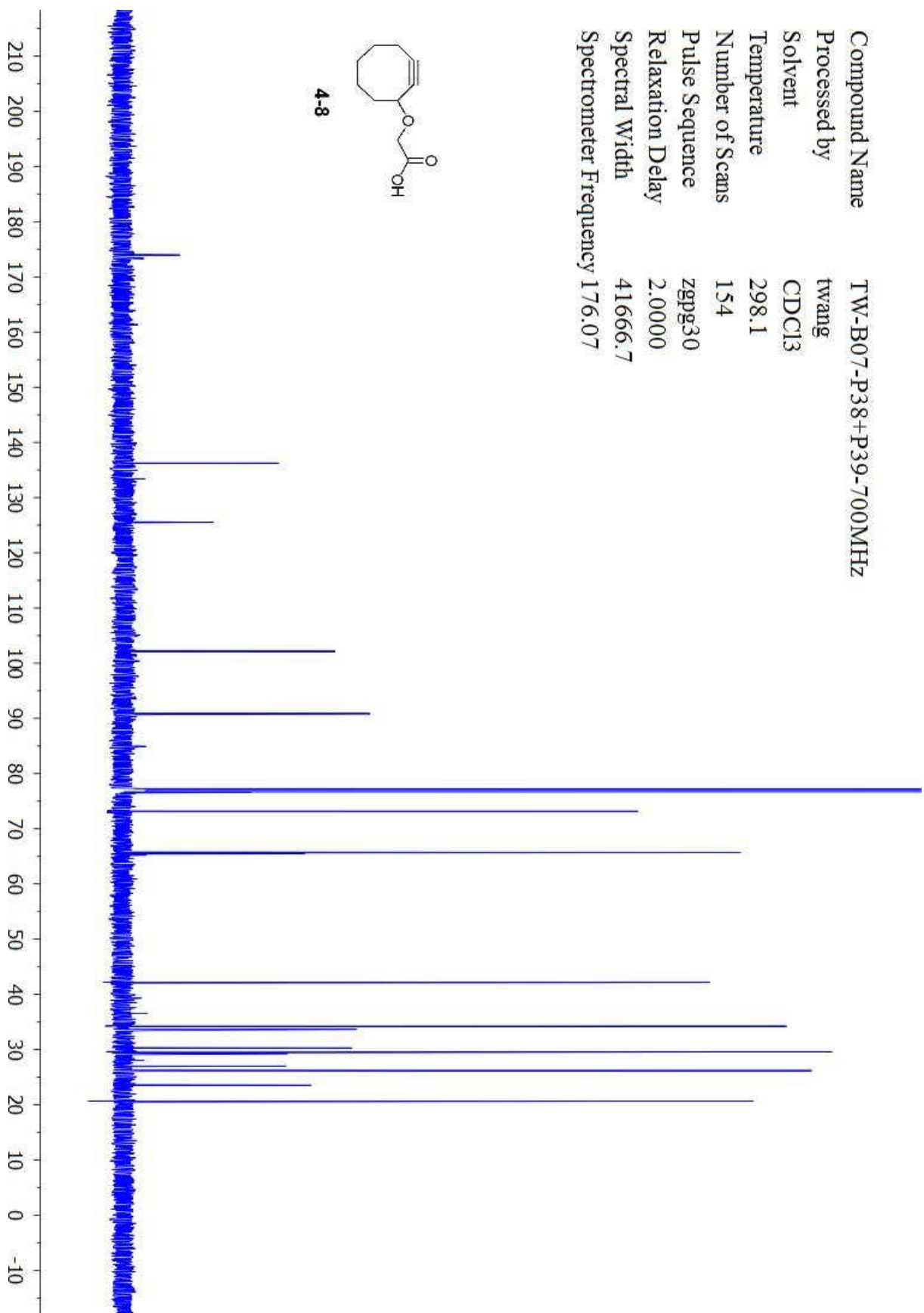


0.47  
 0.39  
 0.82  
 1.03  
 0.90  
 0.36  
 0.94  
 2.14  
 1.00  
 1.00  
 2.49  
 1.78  
 1.07  
 1.14

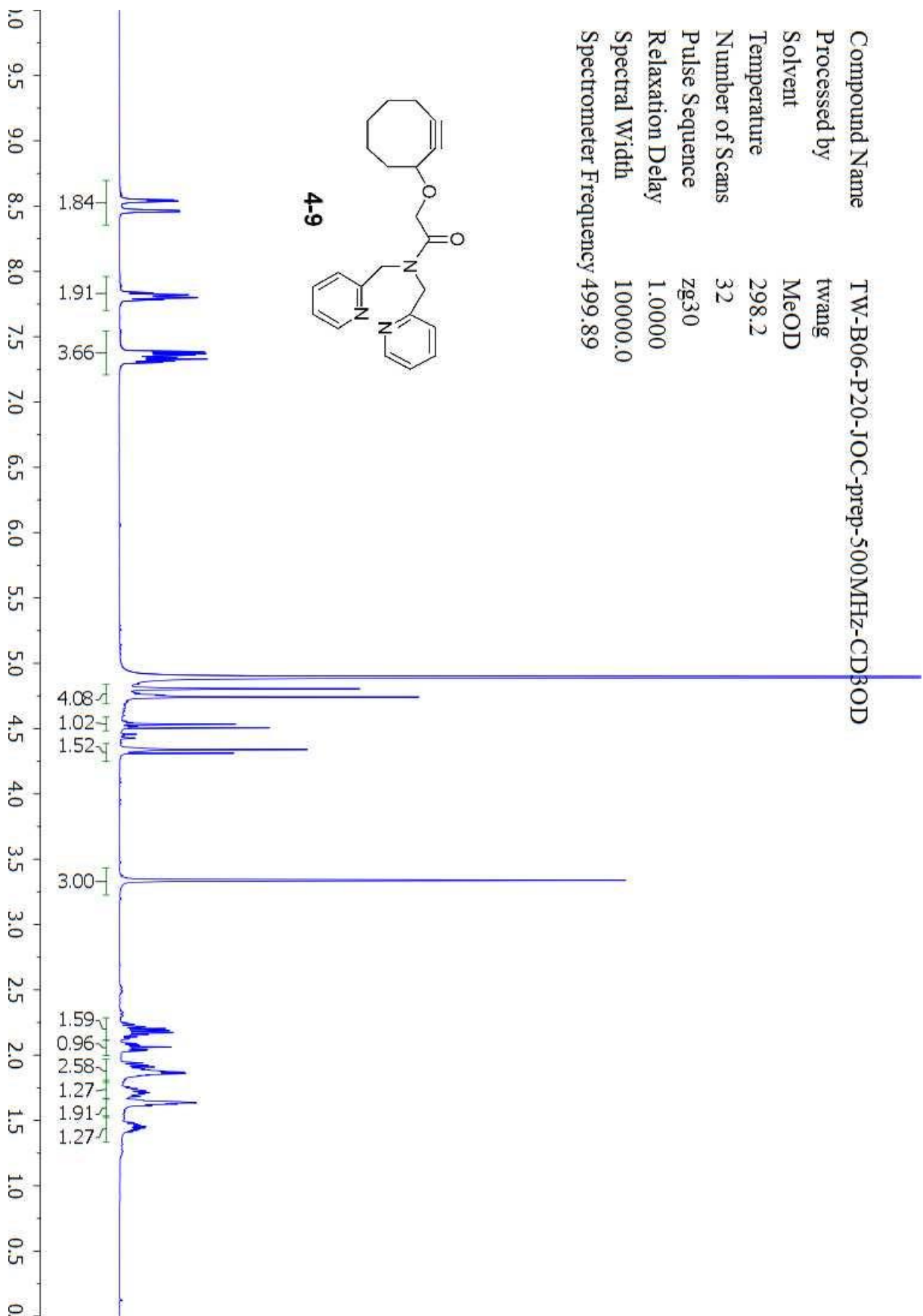
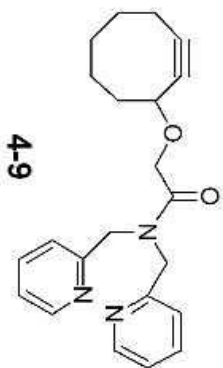
Compound Name TW-B07-P38+P39-700MHZ  
Processed by twang  
Solvent CDCl3  
Temperature 298.1  
Number of Scans 154  
Pulse Sequence zgpg30  
Relaxation Delay 2.0000  
Spectral Width 41666.7  
Spectrometer Frequency 176.07



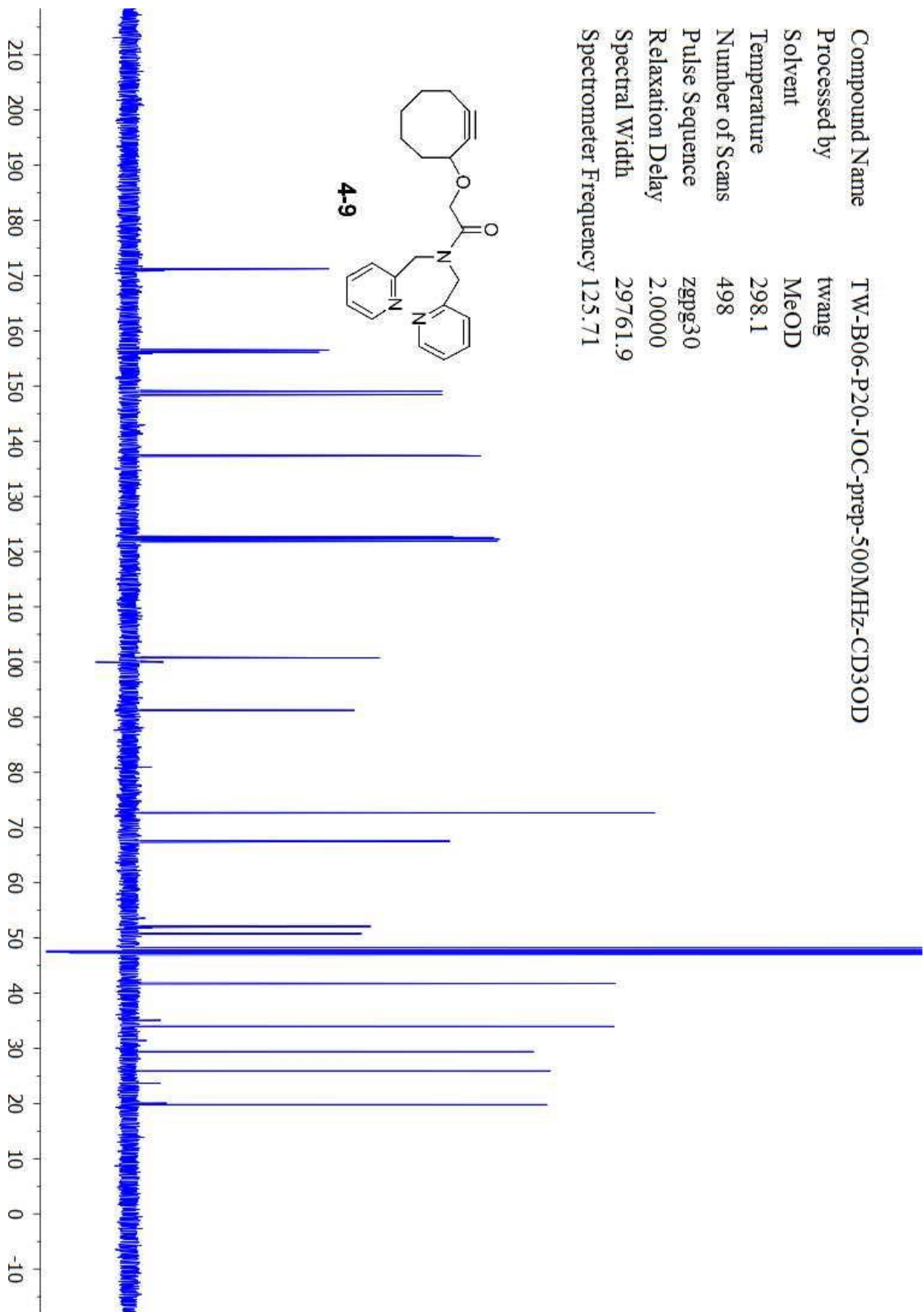
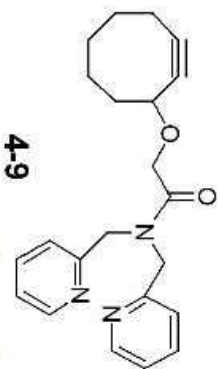
4-8



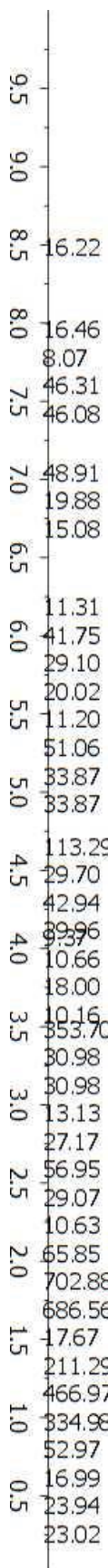
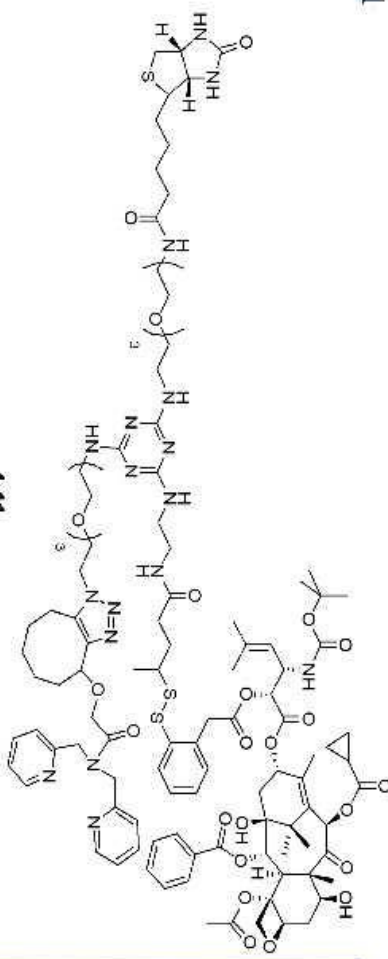
Compound Name TW-B06-P20-10C-prep-500MHz-CD3OD  
 Processed by twang  
 Solvent MeOD  
 Temperature 298.2  
 Number of Scans 32  
 Pulse Sequence zg30  
 Relaxation Delay 1.0000  
 Spectral Width 10000.0  
 Spectrometer Frequency 499.89



Compound Name TW-B06-P20-10C-prep-500MHz-CD3OD  
Processed by twang  
Solvent MeOD  
Temperature 298.1  
Number of Scans 498  
Pulse Sequence zgpg30  
Relaxation Delay 2.0000  
Spectral Width 29761.9  
Spectrometer Frequency 125.71

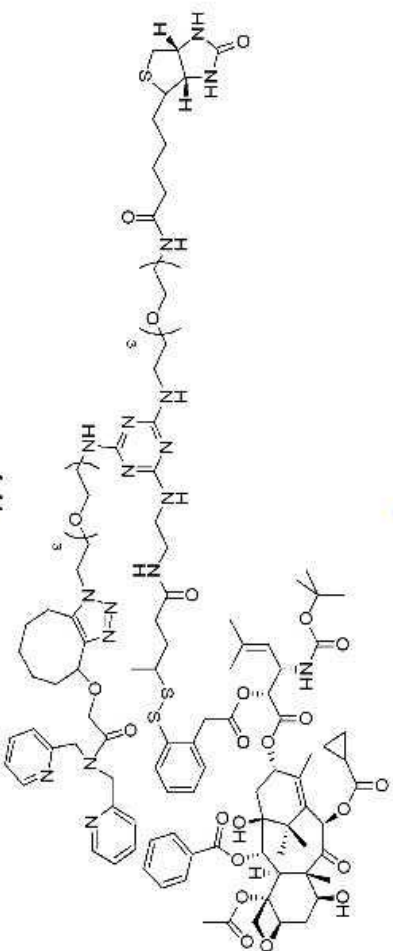


Compound Name TW-B06-P11  
 Processed by twang  
 Solvent CDCl3  
 Temperature 298.2  
 Number of Scans 32  
 Pulse Sequence zg30  
 Relaxation Delay 1.0000  
 Spectral Width 10000.0  
 Spectrometer Frequency 499.89

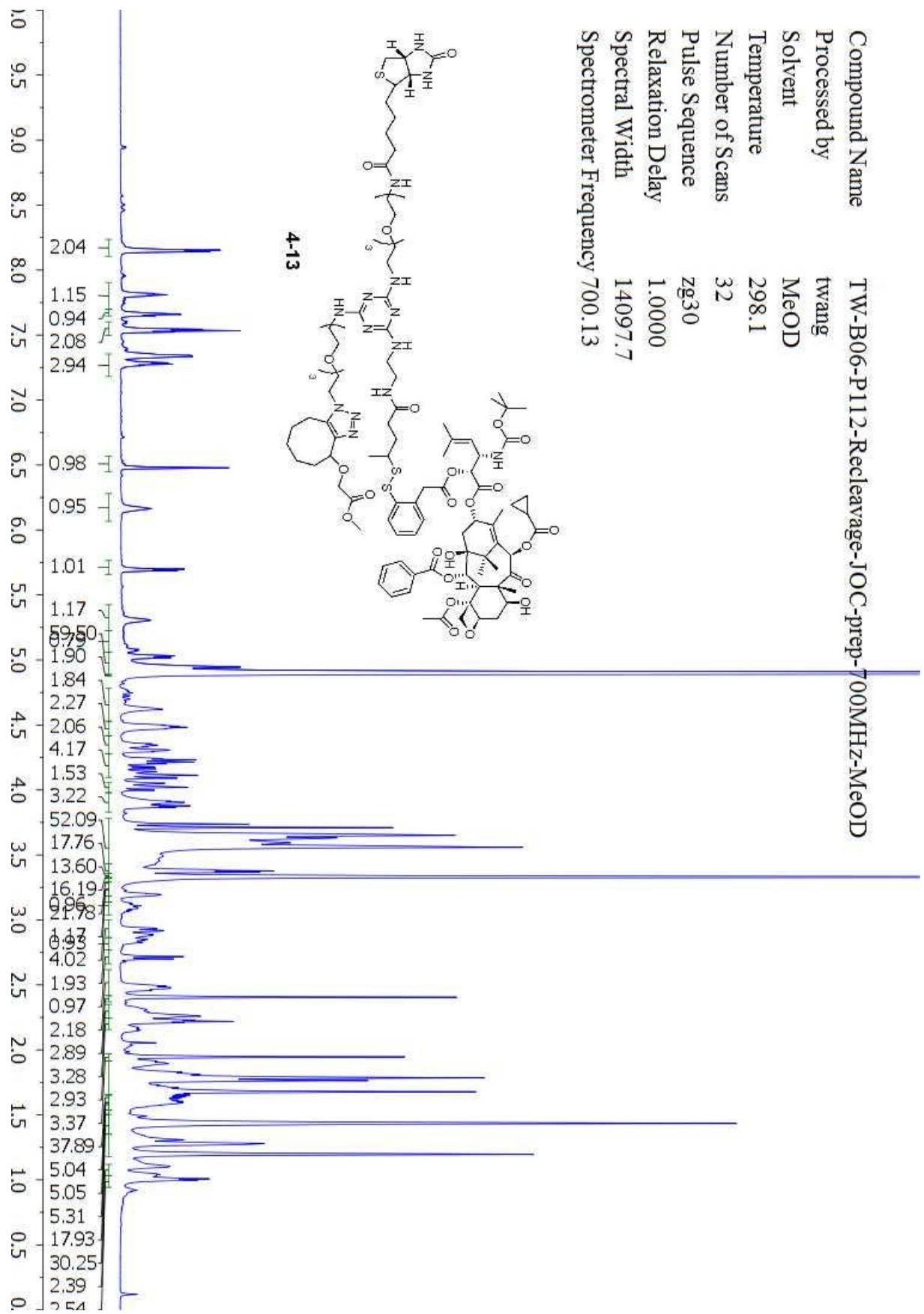




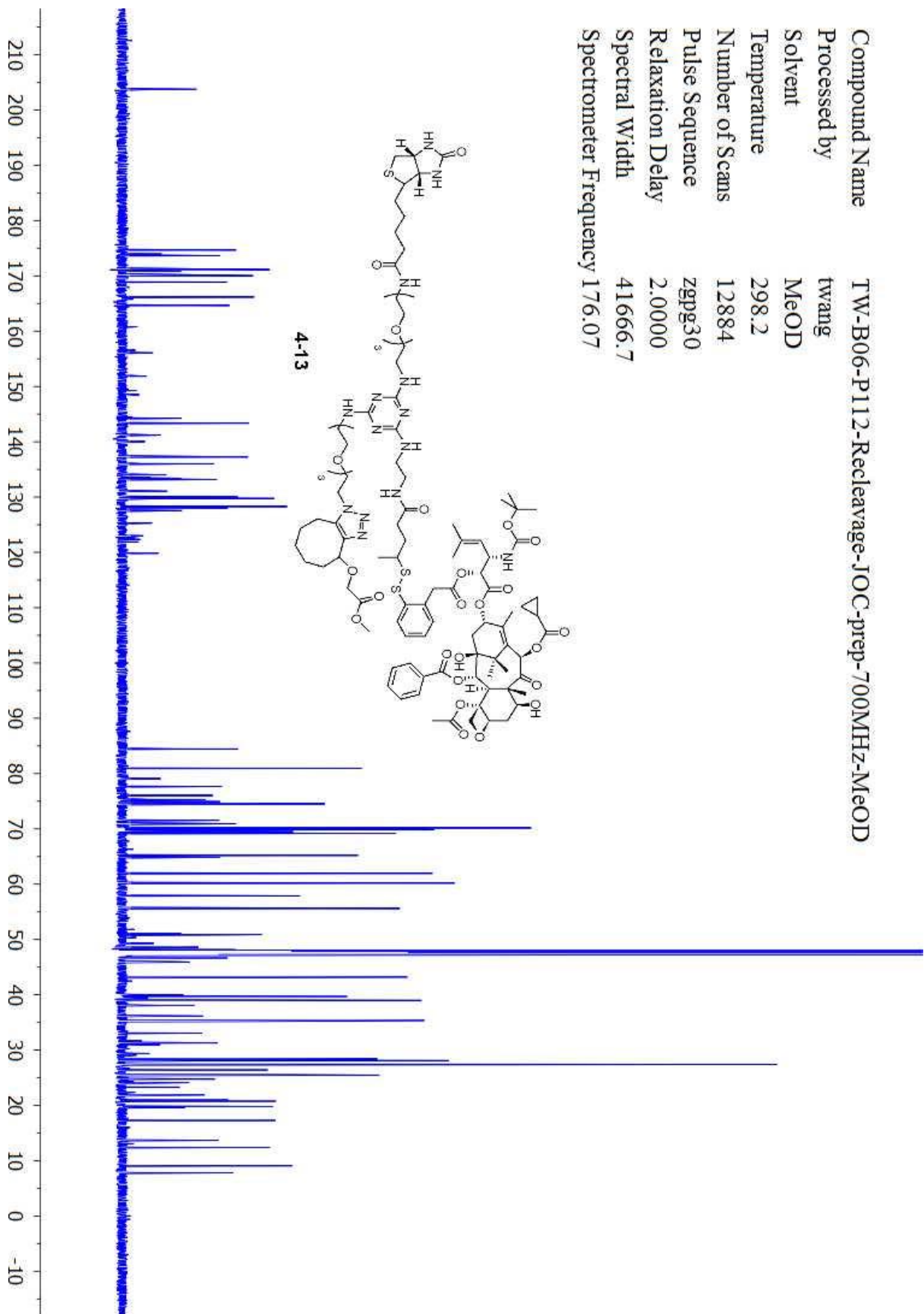
Compound Name TW-B06-P110  
Processed by twang  
Solvent CDCl3  
Temperature 298.2  
Number of Scans 198  
Pulse Sequence zgpg30  
Relaxation Delay 2.0000  
Spectral Width 29761.9  
Spectrometer Frequency 125.71



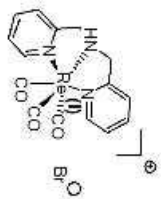
Compound Name TW-B06-P112-Recleavage-JOC-prep-700MHz-MeOD  
 Processed by twang  
 Solvent MeOD  
 Temperature 298.1  
 Number of Scans 32  
 Pulse Sequence zg30  
 Relaxation Delay 1.0000  
 Spectral Width 14097.7  
 Spectrometer Frequency 700.13



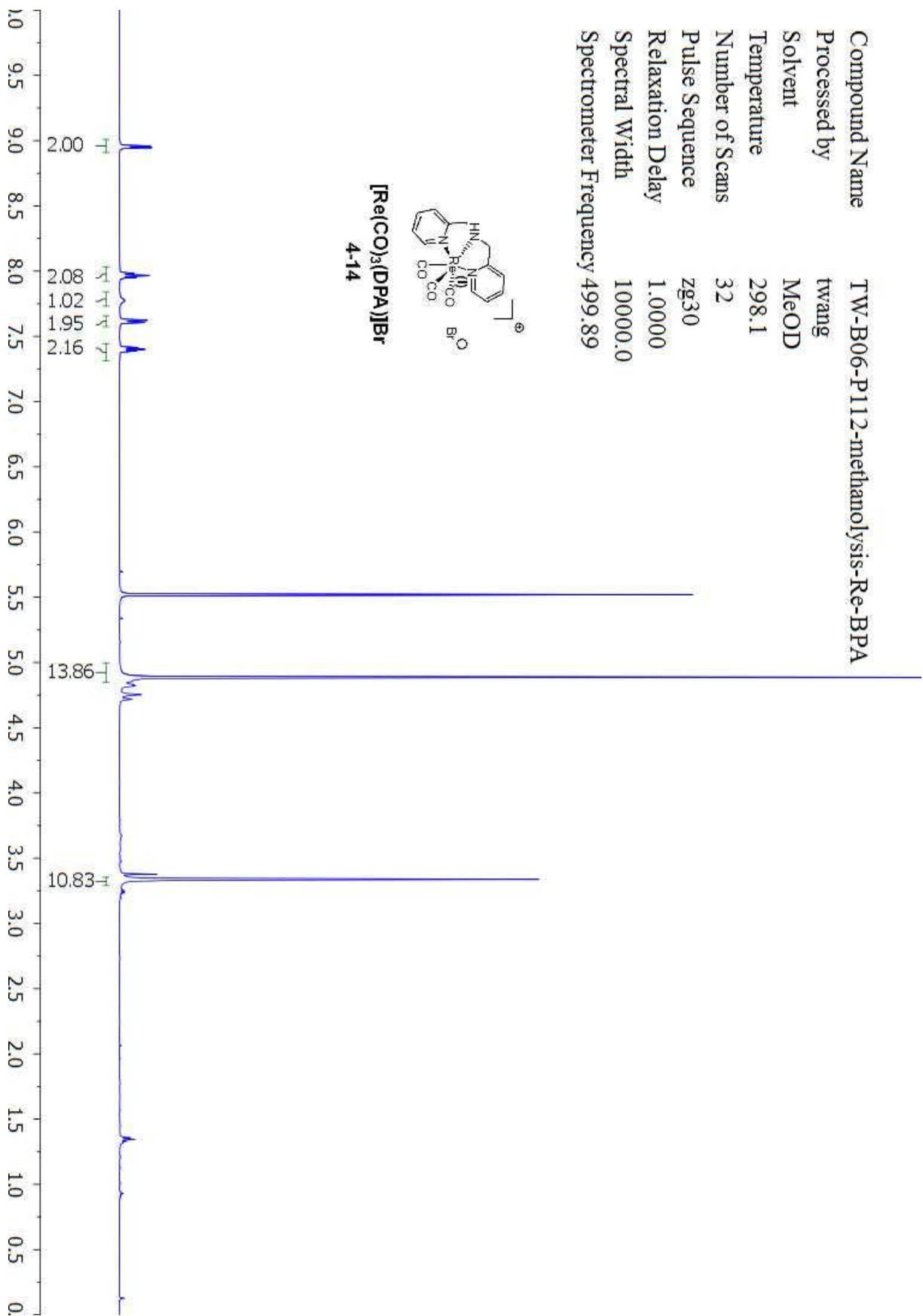
Compound Name TW-B06-P112-Releavage-IOC-prep-700MHz-MeOD  
 Processed by twang  
 Solvent MeOD  
 Temperature 298.2  
 Number of Scans 12884  
 Pulse Sequence zgpg30  
 Relaxation Delay 2.0000  
 Spectral Width 41666.7  
 Spectrometer Frequency 176.07



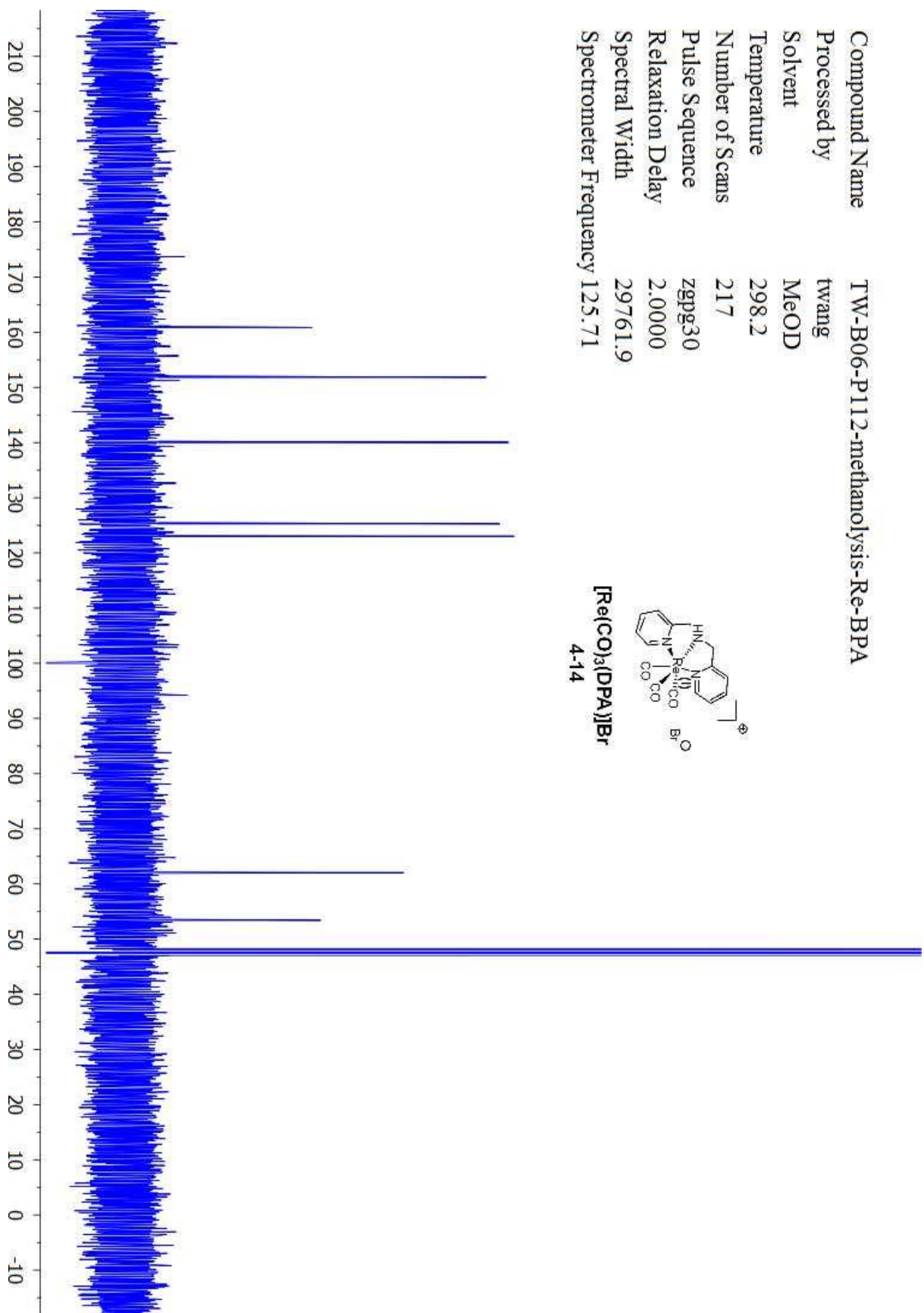
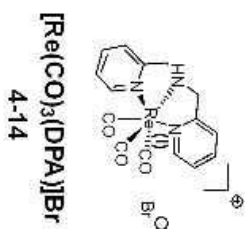
Compound Name TW-B06-P112-methanolysis-Re-BPA  
 Processed by twang  
 Solvent MeOD  
 Temperature 298.1  
 Number of Scans 32  
 Pulse Sequence zg30  
 Relaxation Delay 1.0000  
 Spectral Width 10000.0  
 Spectrometer Frequency 499.89



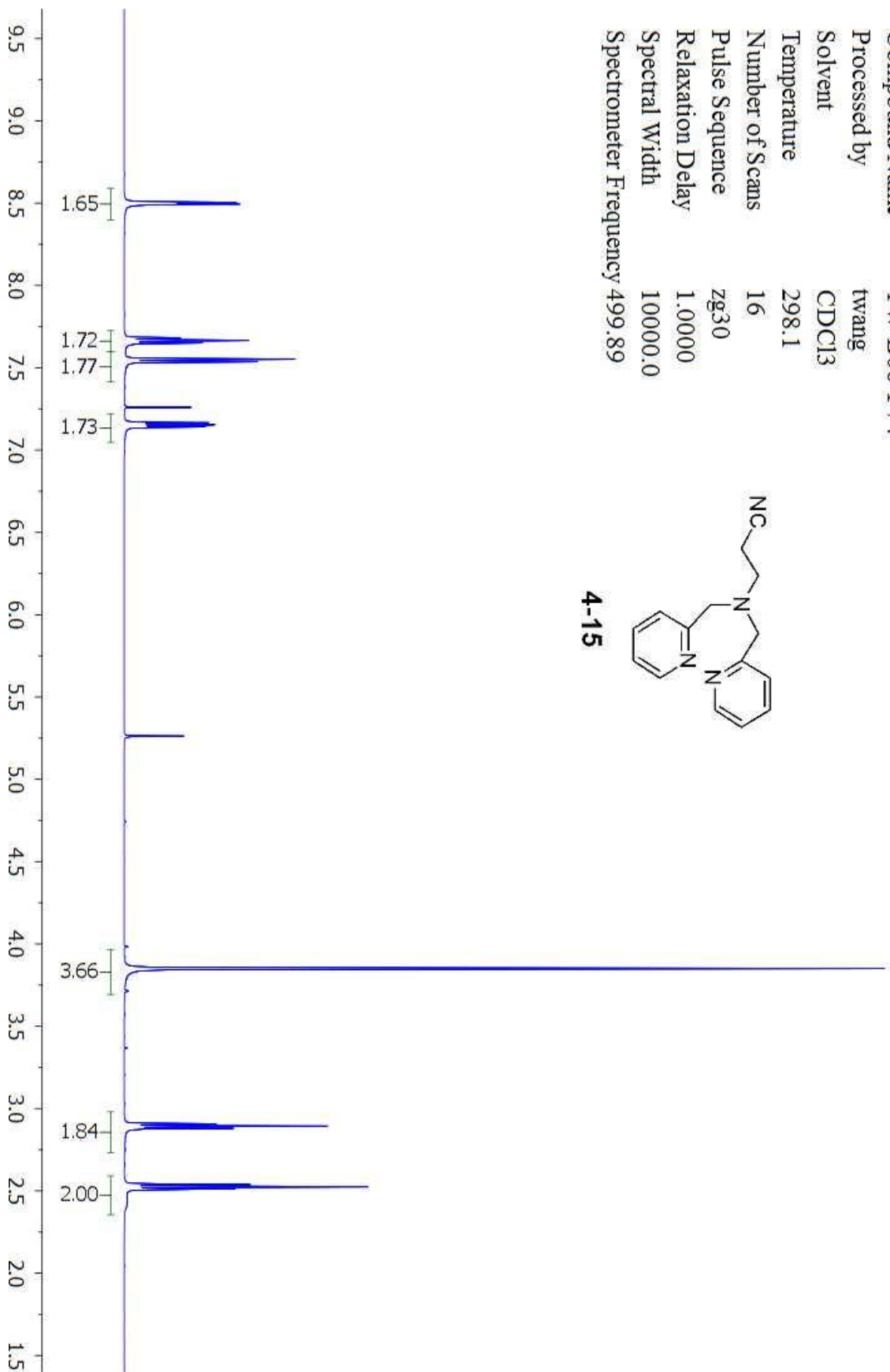
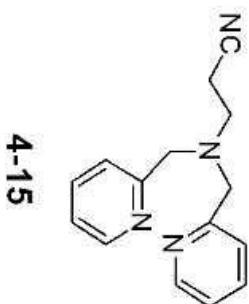
**[Re(CO)<sub>3</sub>(DPA)]Br**  
**4-14**



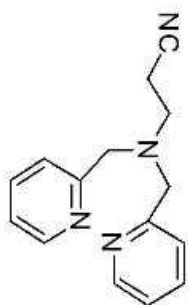
Compound Name TW-B06-P112-methanolysis-Re-BPA  
Processed by twang  
Solvent MeOD  
Temperature 298.2  
Number of Scans 217  
Pulse Sequence zgpg30  
Relaxation Delay 2.0000  
Spectral Width 29761.9  
Spectrometer Frequency 125.71



Compound Name TW-B06-P74  
Processed by twang  
Solvent CDCl3  
Temperature 298.1  
Number of Scans 16  
Pulse Sequence zg30  
Relaxation Delay 1.0000  
Spectral Width 10000.0  
Spectrometer Frequency 499.89



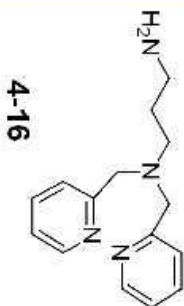
Compound Name TW-B06-P73  
Processed by twang  
Solvent CDCl3  
Temperature 298.1  
Number of Scans 94  
Pulse Sequence zgpg30  
Relaxation Delay 2.0000  
Spectral Width 29761.9  
Spectrometer Frequency 125.71



4-15

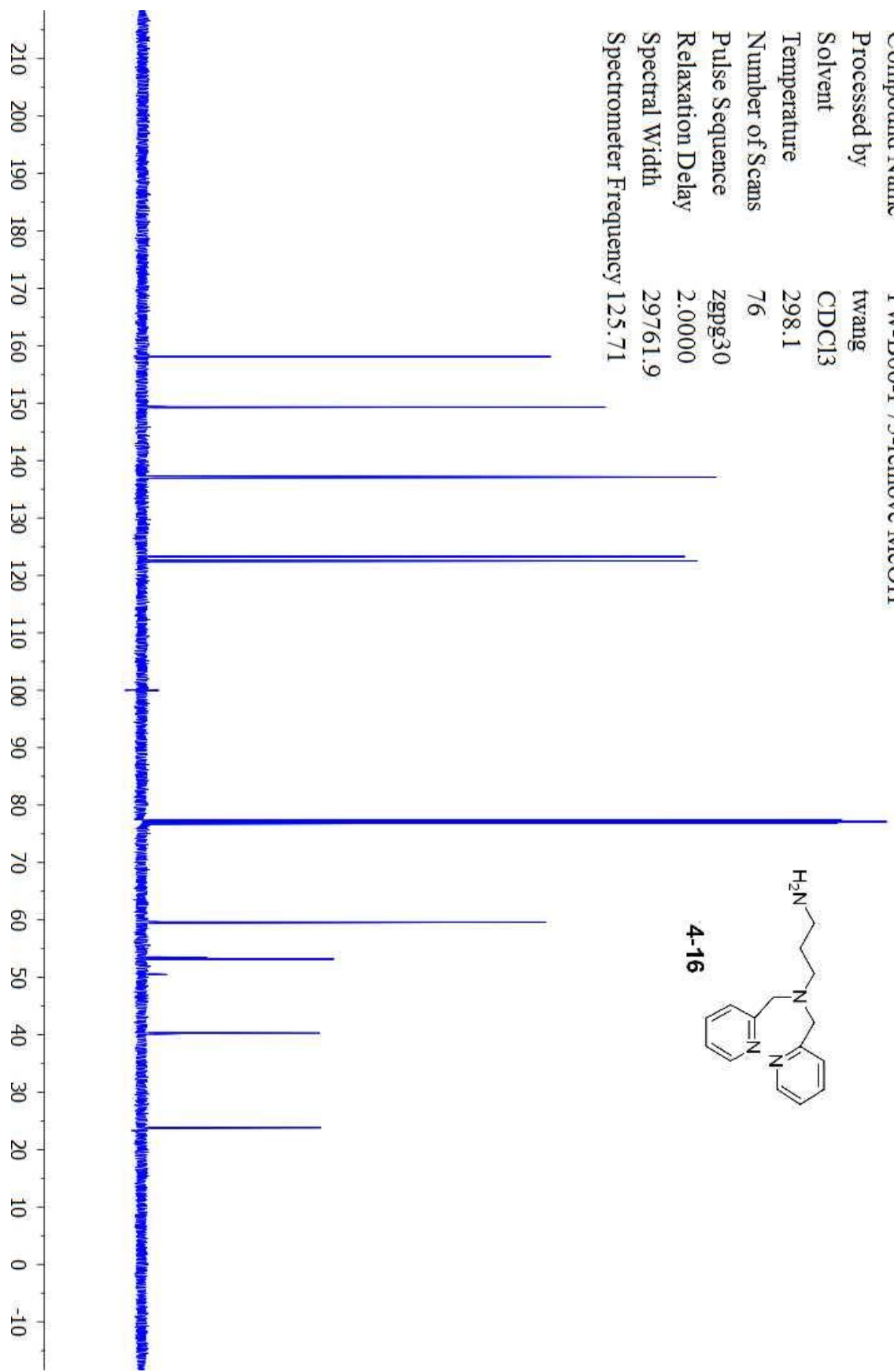
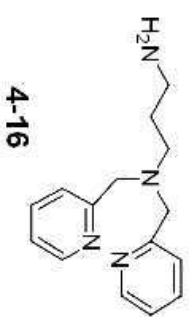


Compound Name TW-B06-P75-remove MeOH  
Processed by twang  
Solvent CDCl3  
Temperature 298.2  
Number of Scans 32  
Pulse Sequence zg30  
Relaxation Delay 1.0000  
Spectral Width 10000.0  
Spectrometer Frequency 499.89

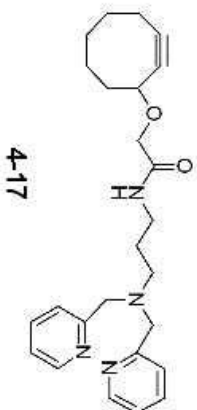




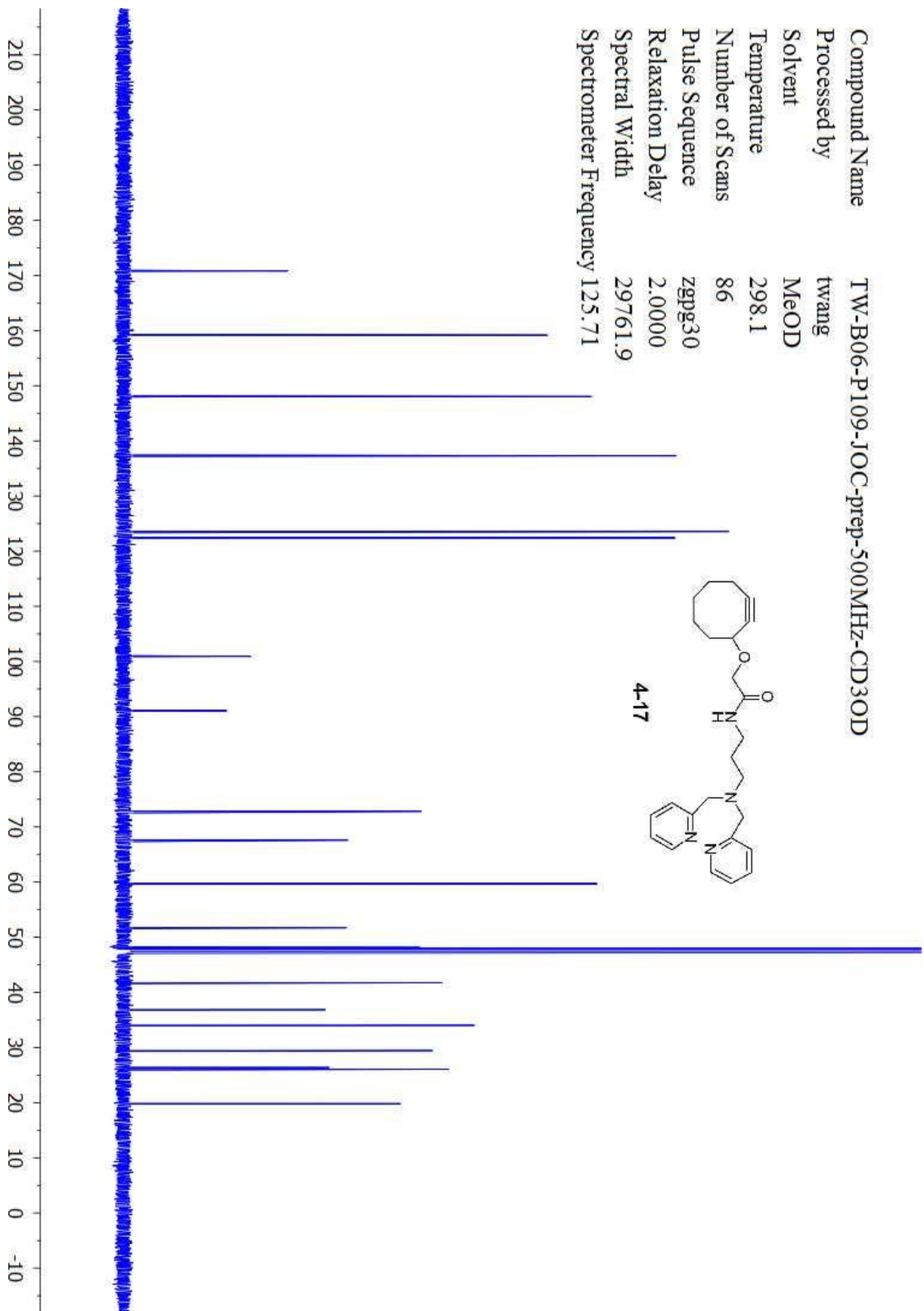
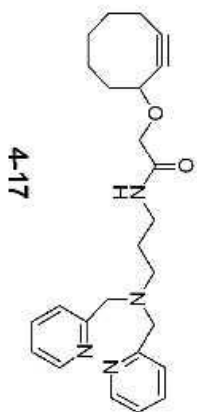
Compound Name TW-B06-P75-remove MeOH  
Processed by twang  
Solvent CDCl3  
Temperature 298.1  
Number of Scans 76  
Pulse Sequence zgpg30  
Relaxation Delay 2.0000  
Spectral Width 29761.9  
Spectrometer Frequency 125.71



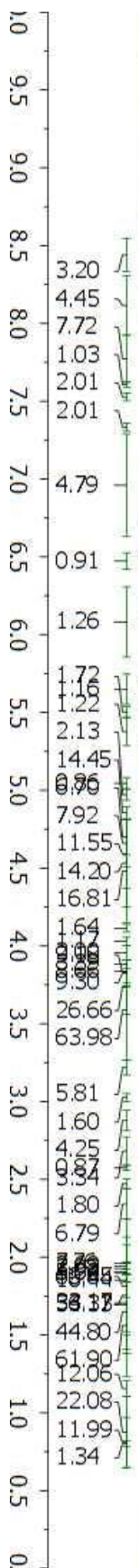
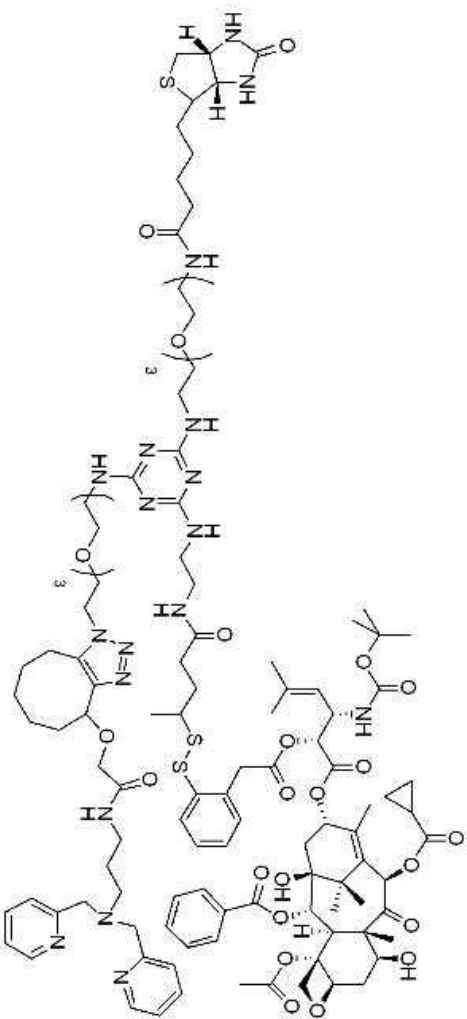
Compound Name TW-B06-P109-JOC-prep-500MHz-CD3OD  
 Processed by twang  
 Solvent MeOD  
 Temperature 298.2  
 Number of Scans 27  
 Pulse Sequence zg30  
 Relaxation Delay 1.0000  
 Spectral Width 10000.0  
 Spectrometer Frequency 499.89



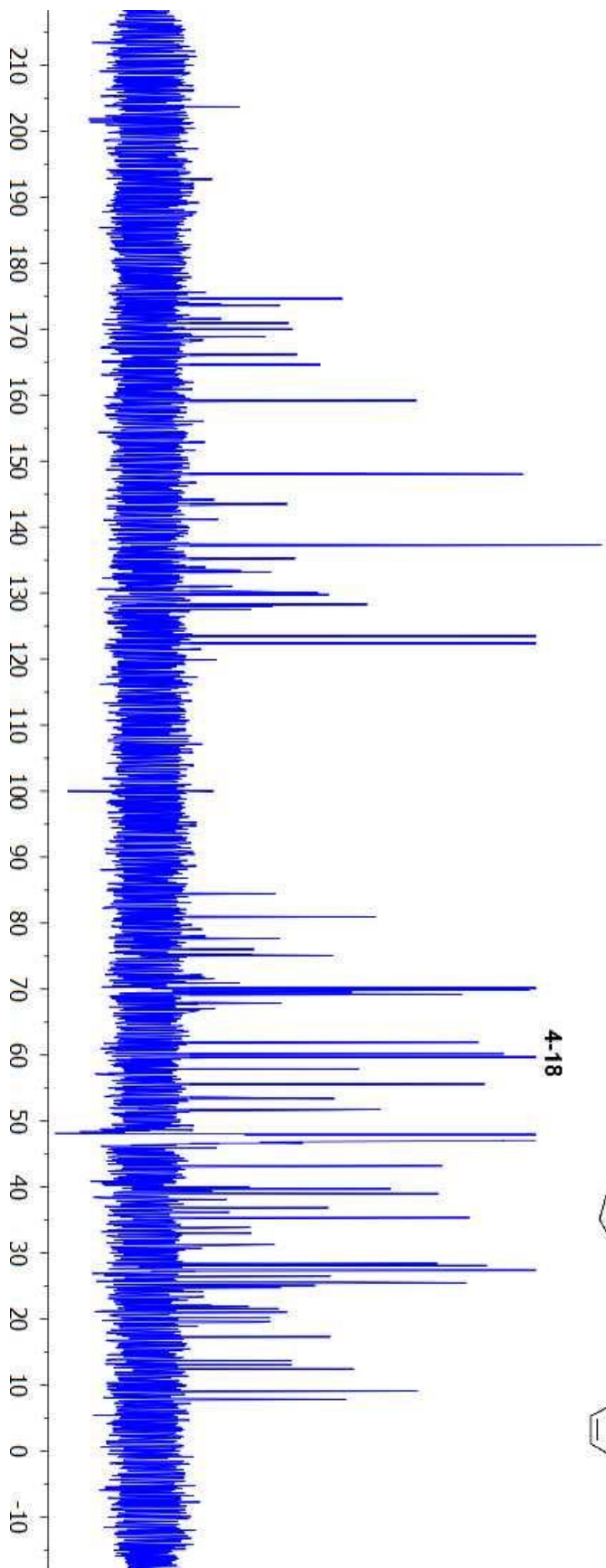
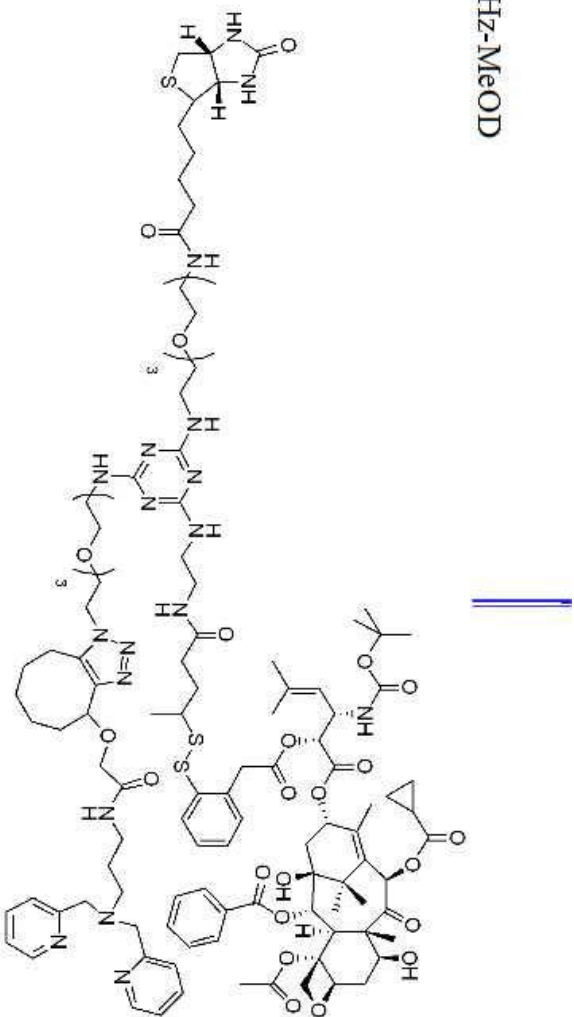
Compound Name TW-B06-P109-JOC-prep-500MHz-CD3OD  
Processed by twang  
Solvent MeOD  
Temperature 298.1  
Number of Scans 86  
Pulse Sequence zgpg30  
Relaxation Delay 2.0000  
Spectral Width 29761.9  
Spectrometer Frequency 125.71



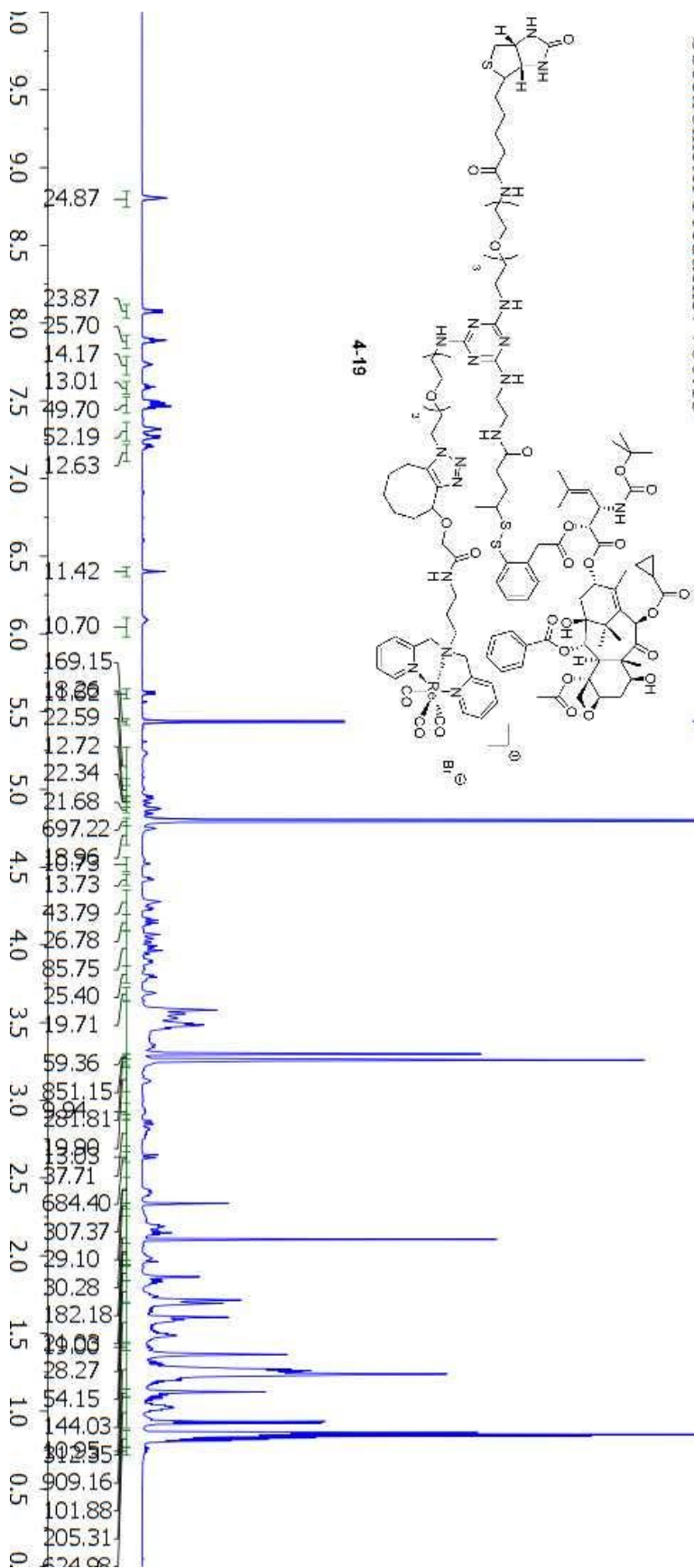
Compound Name TW-B07-P12-700MHz-MeOD  
 Processed by twang  
 Solvent MeOD  
 Temperature 298.1  
 Number of Scans 16  
 Pulse Sequence zg30  
 Relaxation Delay 1.0000  
 Spectral Width 14097.7  
 Spectrometer Frequency 700.13



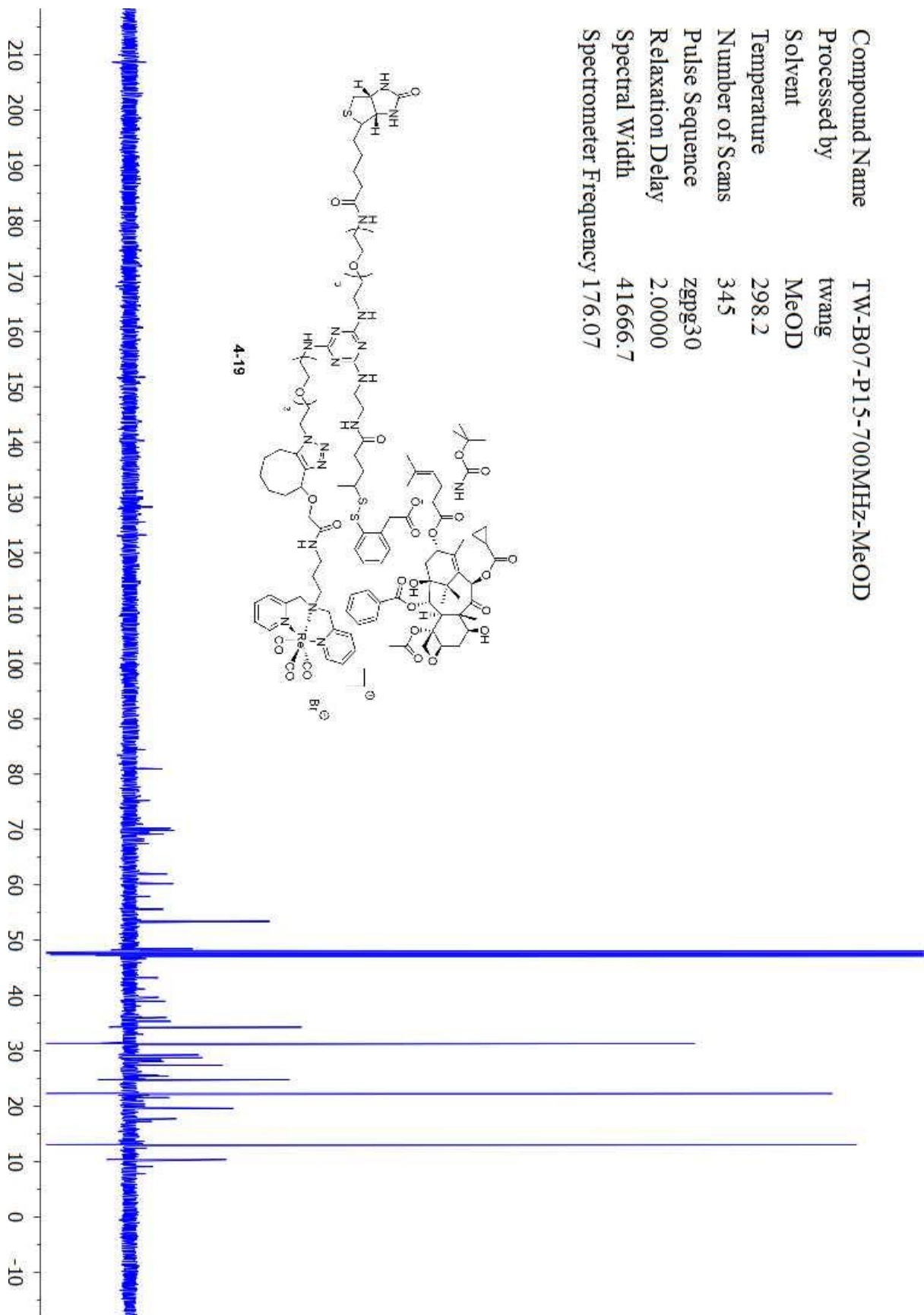
Compound Name TW-B07-P12-700MHz-MeOD  
 Processed by twang  
 Solvent MeOD  
 Temperature 298.1  
 Number of Scans 359  
 Pulse Sequence zgpg30  
 Relaxation Delay 2.0000  
 Spectral Width 41666.7  
 Spectrometer Frequency 176.07



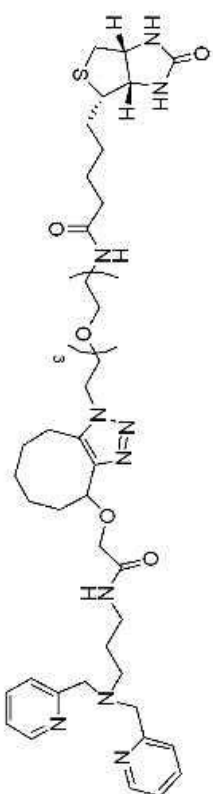
Compound Name TW-B07-P15-700MHz-MeOD  
 Processed by twang  
 Solvent MeOD  
 Temperature 298.2  
 Number of Scans 16  
 Pulse Sequence zg30  
 Relaxation Delay 1.0000  
 Spectral Width 14097.7  
 Spectrometer Frequency 700.13



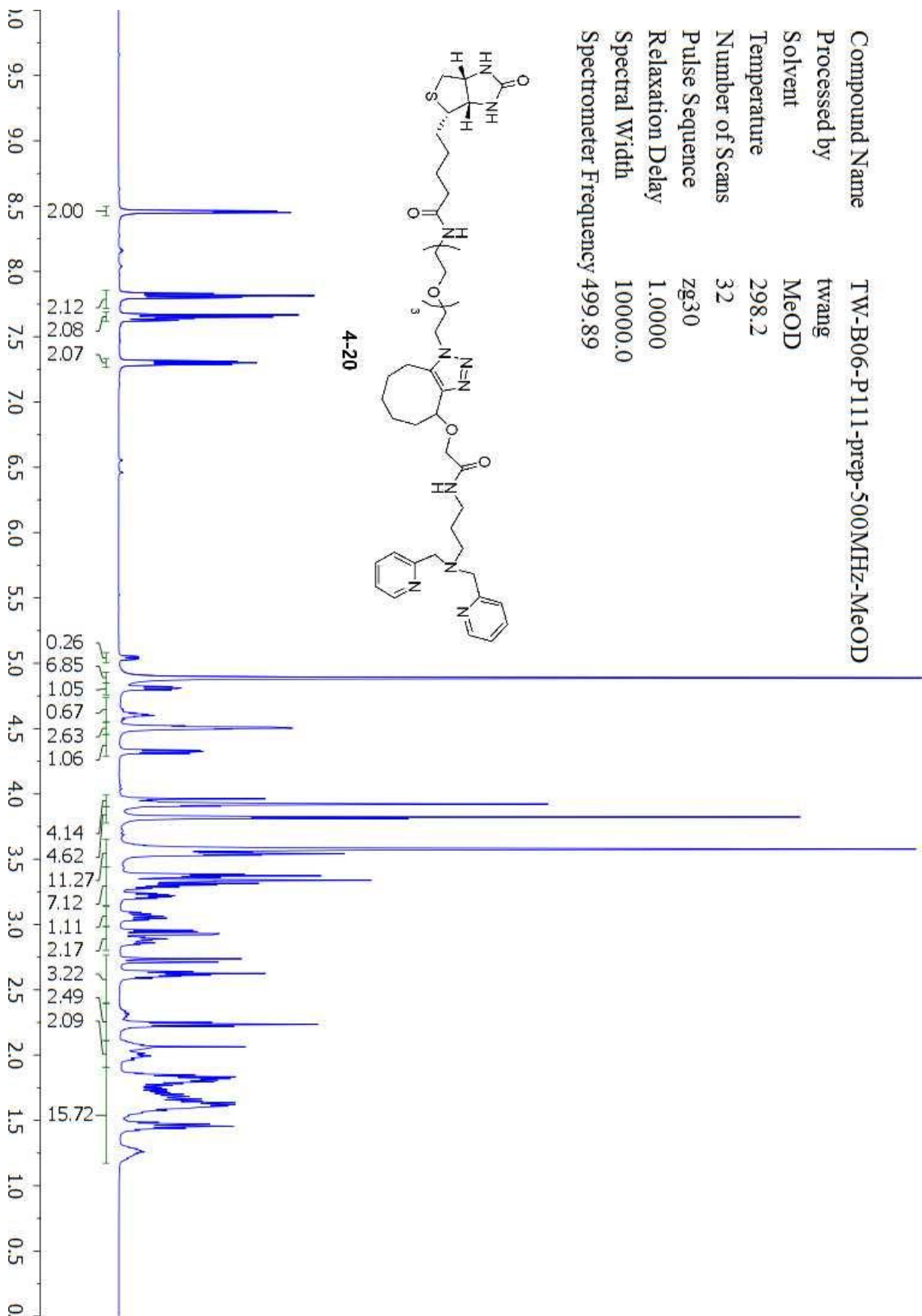
Compound Name TW-B07-P15-700MHz-MeOD  
 Processed by twang  
 Solvent MeOD  
 Temperature 298.2  
 Number of Scans 345  
 Pulse Sequence zgpg30  
 Relaxation Delay 2.0000  
 Spectral Width 41666.7  
 Spectrometer Frequency 176.07



Compound Name TW-B06-P111-prep-500MHz-MeOD  
 Processed by twang  
 Solvent MeOD  
 Temperature 298.2  
 Number of Scans 32  
 Pulse Sequence zg30  
 Relaxation Delay 1.0000  
 Spectral Width 10000.0  
 Spectrometer Frequency 499.89

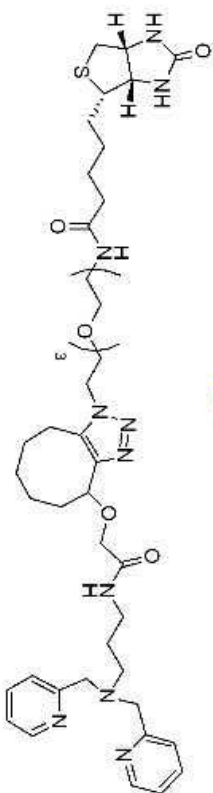


4-20

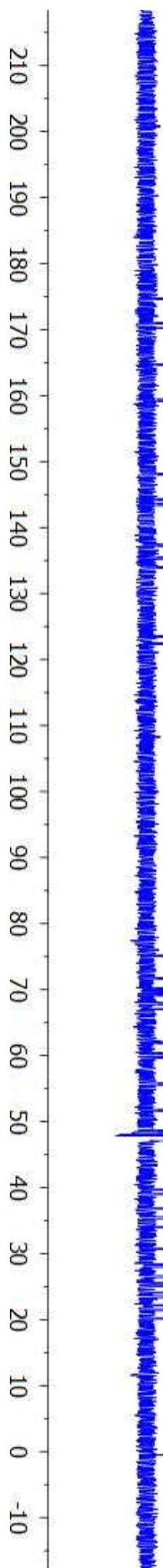




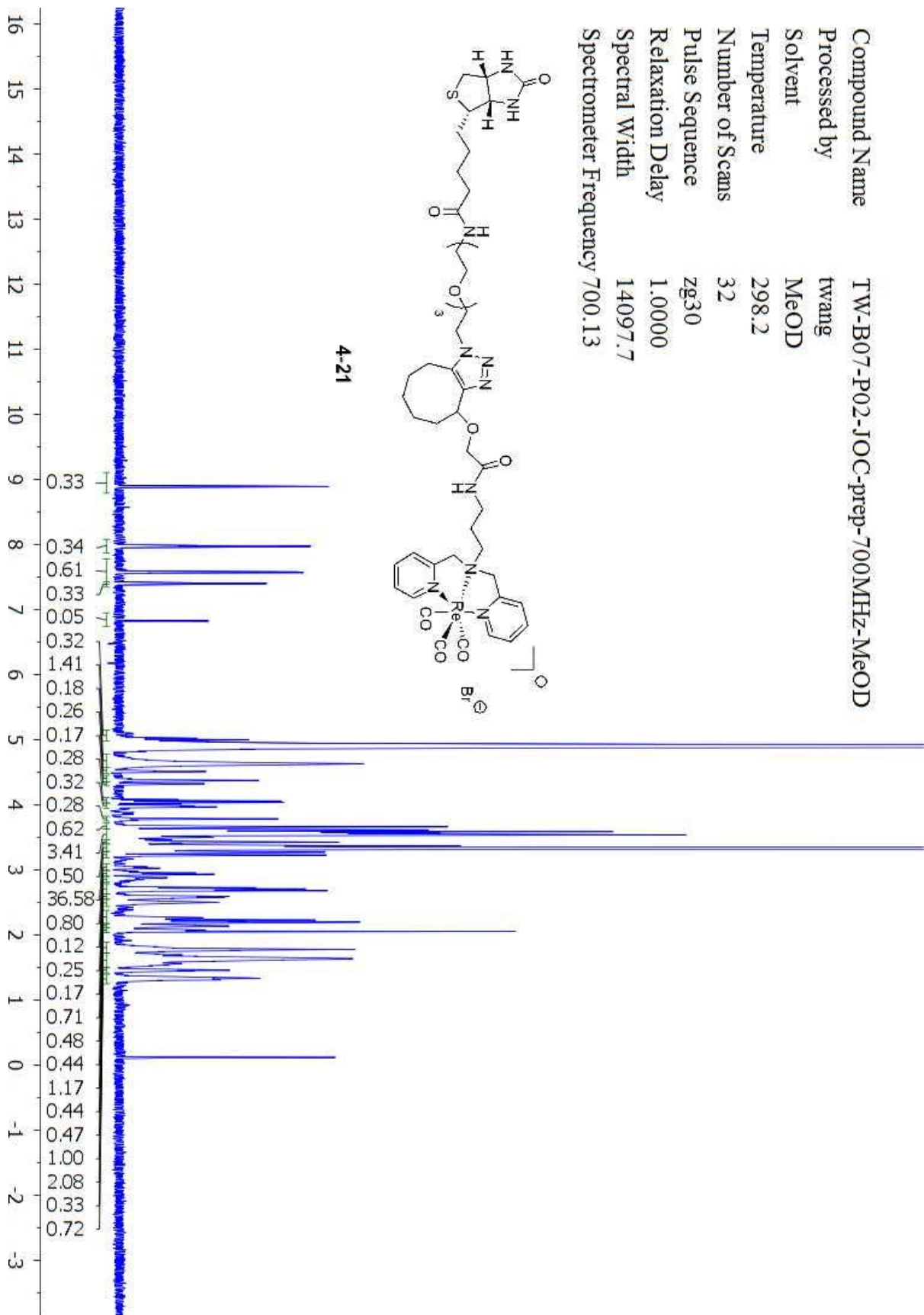
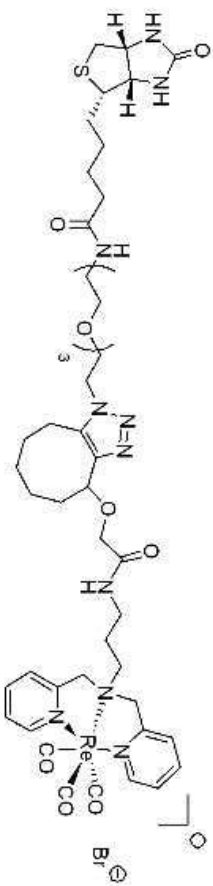
Compound Name TW-B06-P111-prep-500MHz-MeOD  
 Processed by twang  
 Solvent MeOD  
 Temperature 298.1  
 Number of Scans 203  
 Pulse Sequence zgpg30  
 Relaxation Delay 2.0000  
 Spectral Width 29761.9  
 Spectrometer Frequency 125.71



4-20

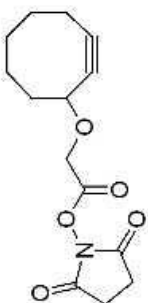


Compound Name TW-B07-P02-IOC-prep-700MHz-MeOD  
 Processed by twang  
 Solvent MeOD  
 Temperature 298.2  
 Number of Scans 32  
 Pulse Sequence zg30  
 Relaxation Delay 1.0000  
 Spectral Width 14097.7  
 Spectrometer Frequency 700.13

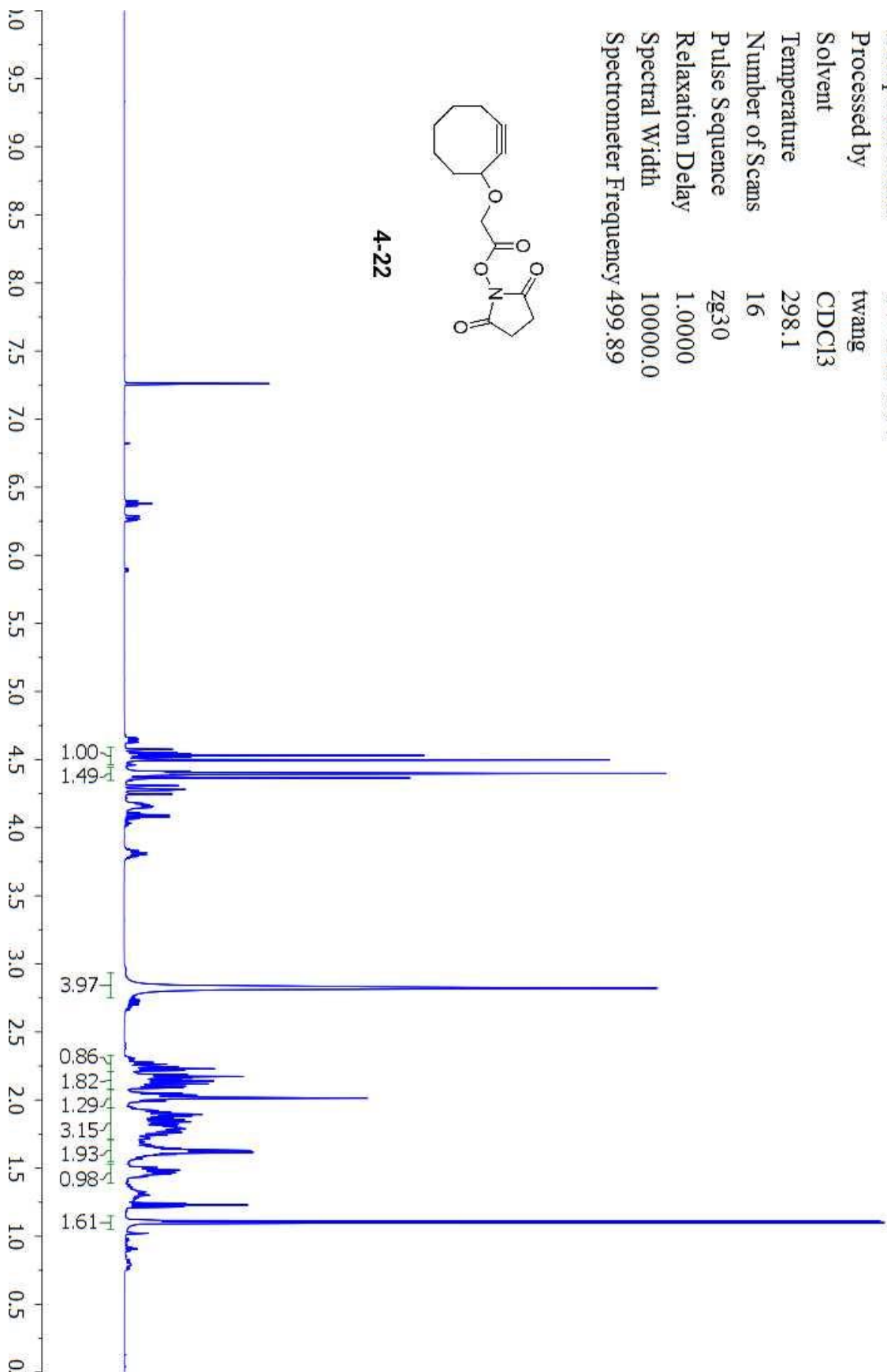




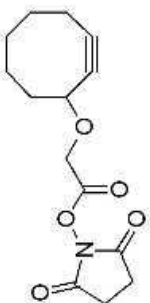
Compound Name TW-B06-P64  
Processed by twang  
Solvent CDCl3  
Temperature 298.1  
Number of Scans 16  
Pulse Sequence zg30  
Relaxation Delay 1.0000  
Spectral Width 10000.0  
Spectrometer Frequency 499.89



4-22



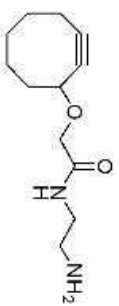
Compound Name TW-B06-P64  
Processed by twang  
Solvent CDCl3  
Temperature 298.2  
Number of Scans 88  
Pulse Sequence zgpg30  
Relaxation Delay 2.0000  
Spectral Width 29761.9  
Spectrometer Frequency 125.71



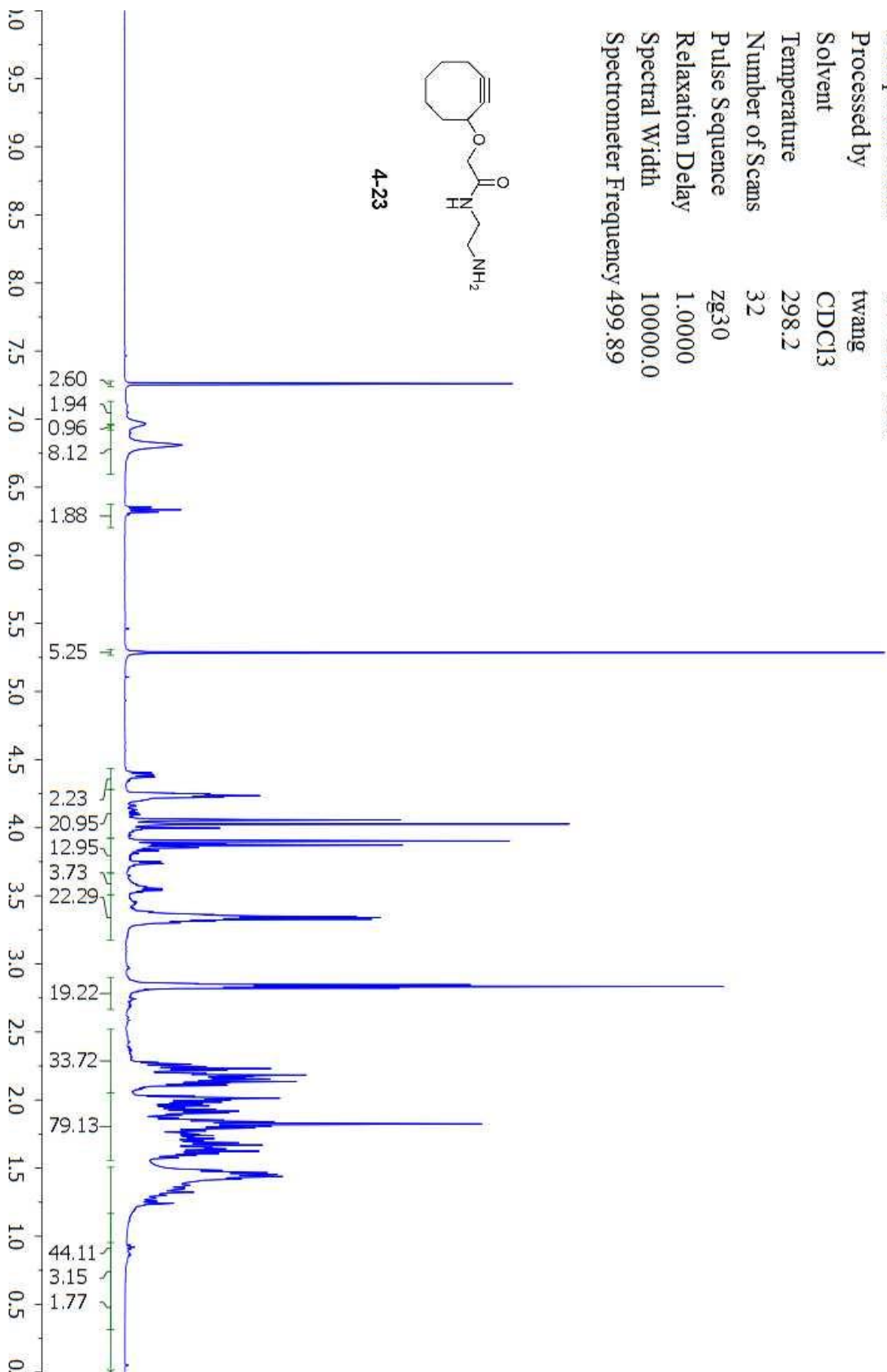
4-22



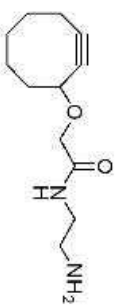
Compound Name TW-B07-P20  
 Processed by twang  
 Solvent CDCl3  
 Temperature 298.2  
 Number of Scans 32  
 Pulse Sequence zg30  
 Relaxation Delay 1.0000  
 Spectral Width 10000.0  
 Spectrometer Frequency 499.89



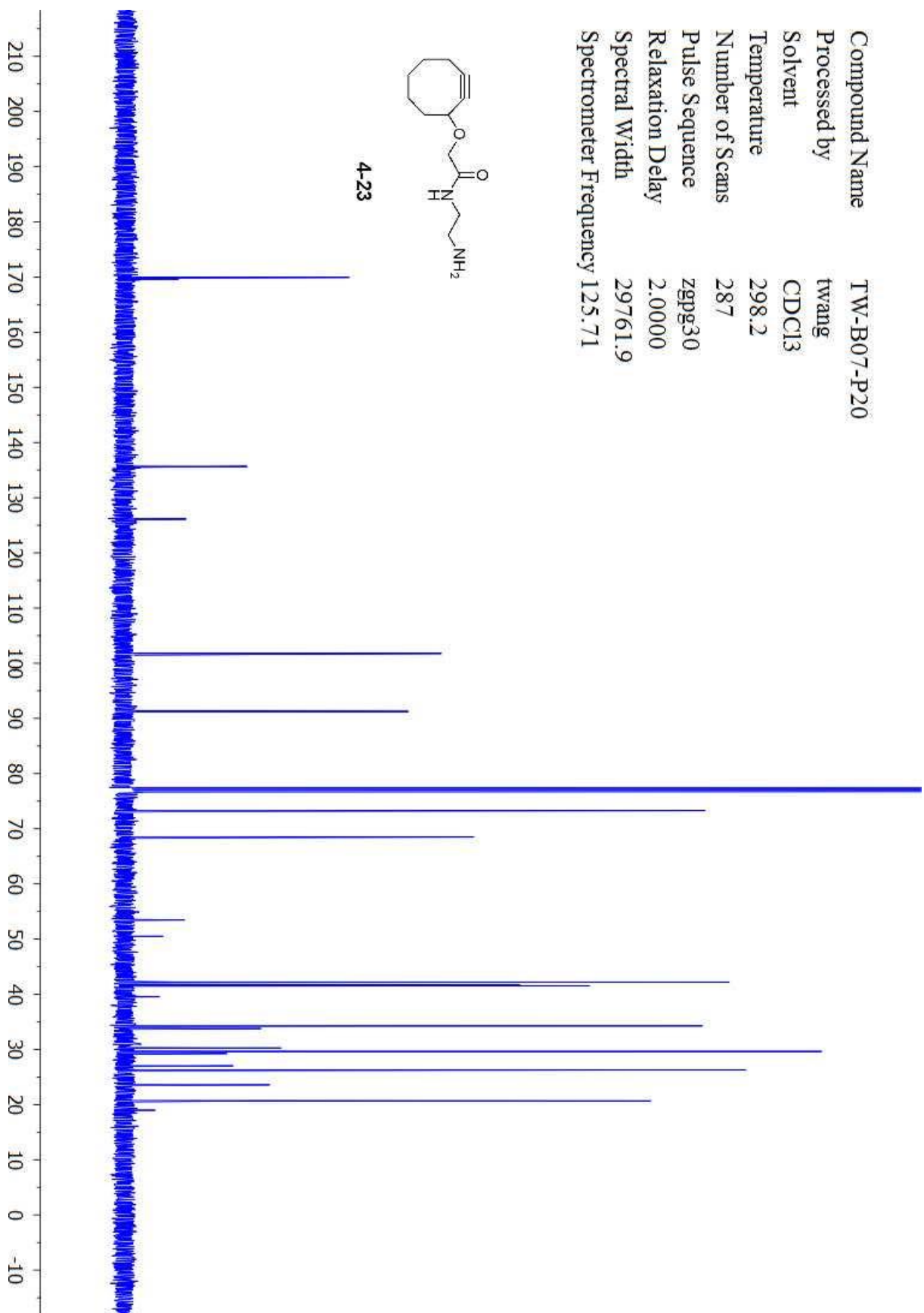
4.23



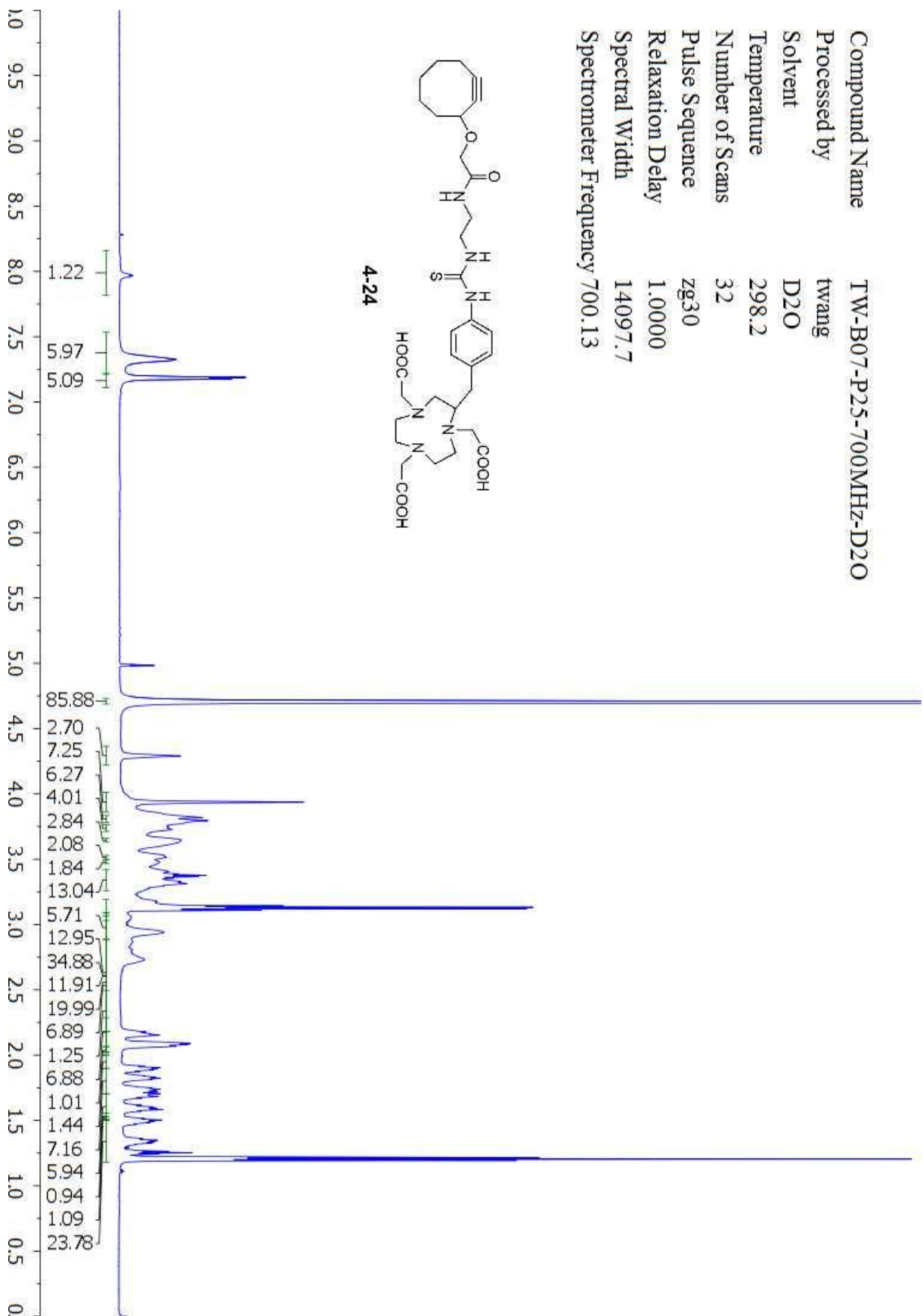
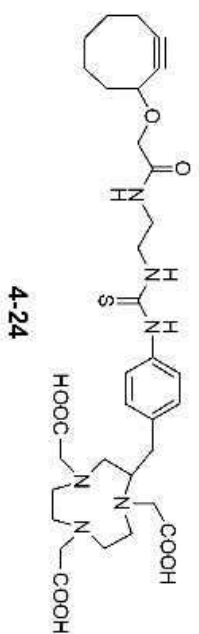
Compound Name TW-B07-P20  
Processed by twang  
Solvent CDCl3  
Temperature 298.2  
Number of Scans 287  
Pulse Sequence zgpg30  
Relaxation Delay 2.0000  
Spectral Width 29761.9  
Spectrometer Frequency 125.71



4-23

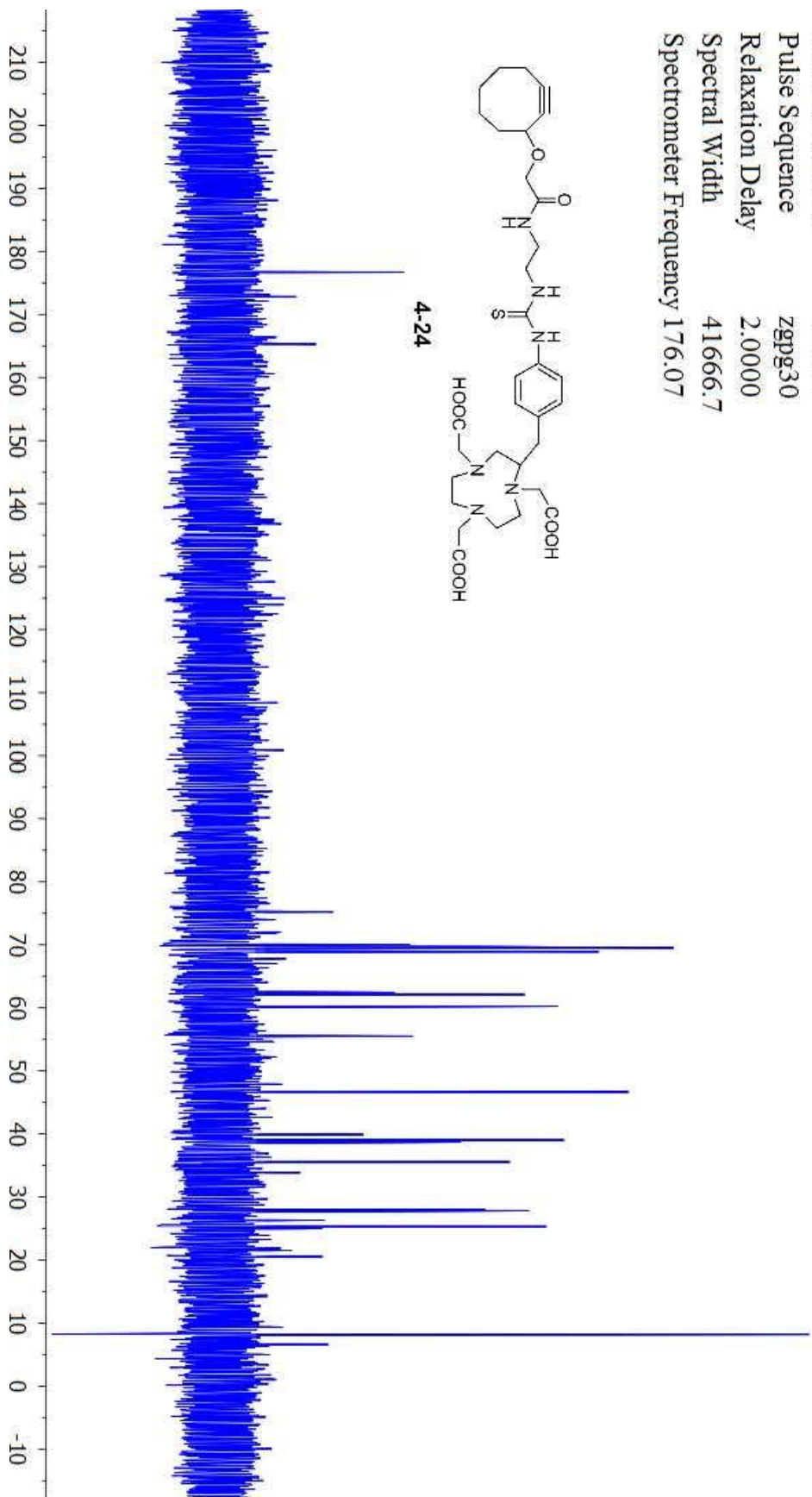
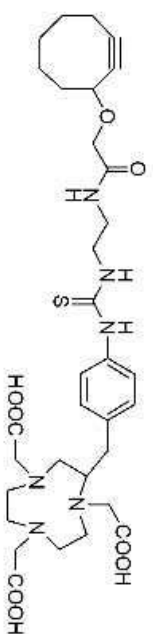


Compound Name TW-B07-P25-700MHz-D2O  
 Processed by twang  
 Solvent D2O  
 Temperature 298.2  
 Number of Scans 32  
 Pulse Sequence zg30  
 Relaxation Delay 1.0000  
 Spectral Width 14097.7  
 Spectrometer Frequency 700.13

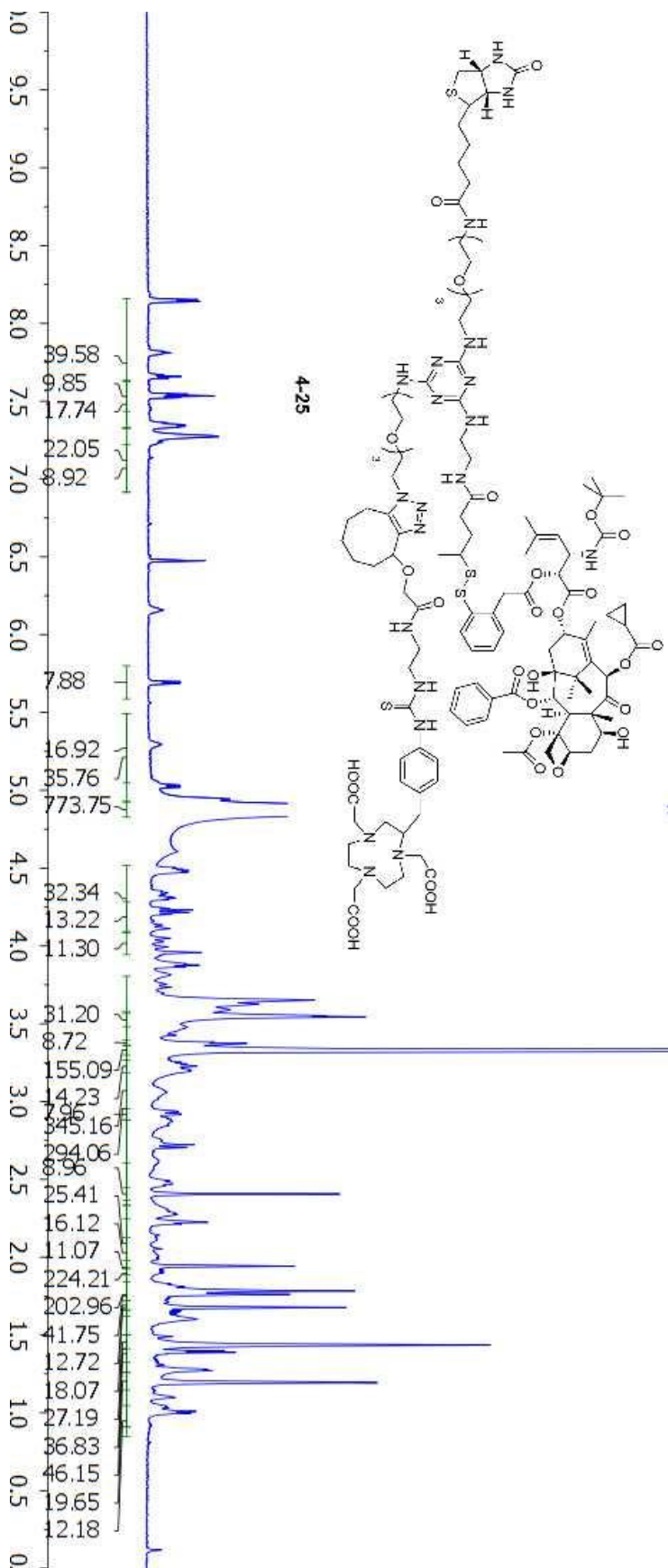




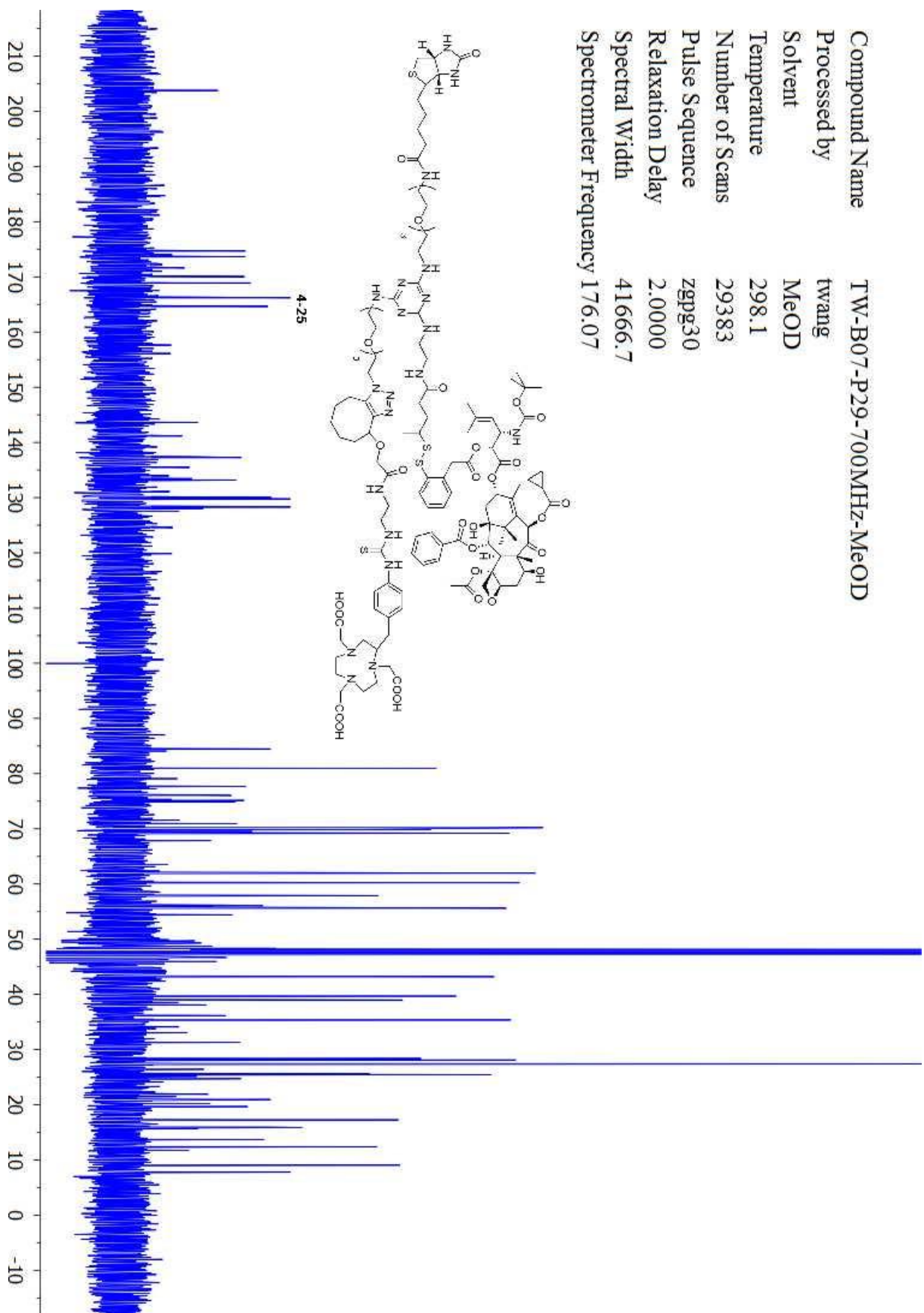
Compound Name TW-B07-P25-700MHz-D2O  
Processed by twang  
Solvent D2O  
Temperature 298.2  
Number of Scans 17877  
Pulse Sequence zgpg30  
Relaxation Delay 2.0000  
Spectral Width 41666.7  
Spectrometer Frequency 176.07



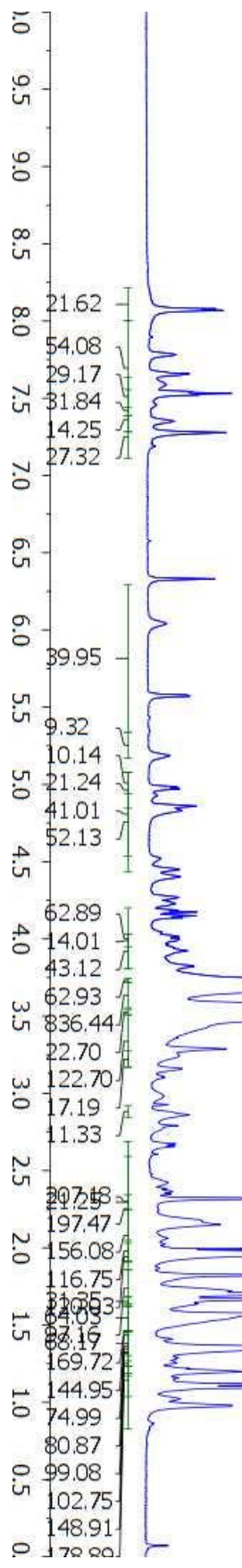
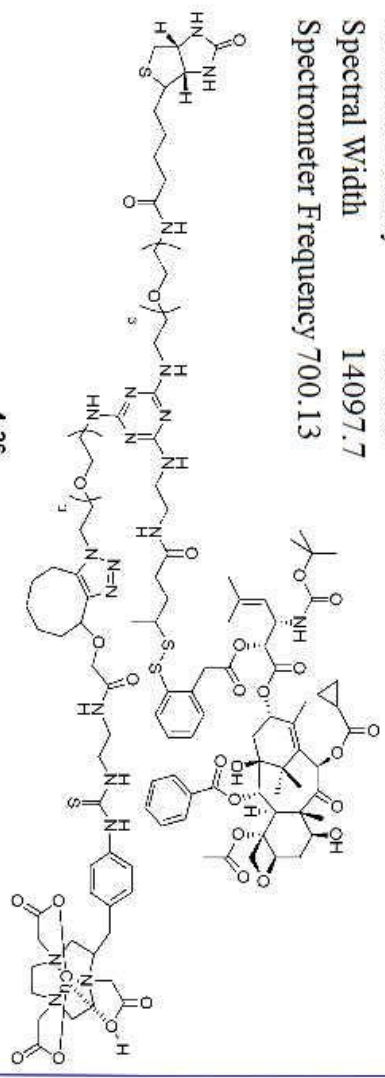
Compound Name TW-B07-P29-700MHz-MeOD  
 Processed by twang  
 Solvent MeOD  
 Temperature 298.1  
 Number of Scans 32  
 Pulse Sequence zg30  
 Relaxation Delay 1.0000  
 Spectral Width 14097.7  
 Spectrometer Frequency 700.13



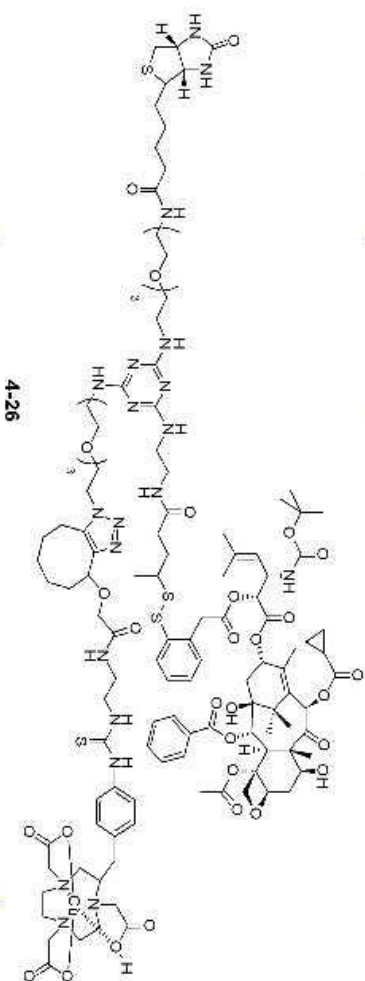
Compound Name TW-B07-P29-700MHz-MeOD  
Processed by twang  
Solvent MeOD  
Temperature 298.1  
Number of Scans 29383  
Pulse Sequence zgpg30  
Relaxation Delay 2.0000  
Spectral Width 41666.7  
Spectrometer Frequency 176.07



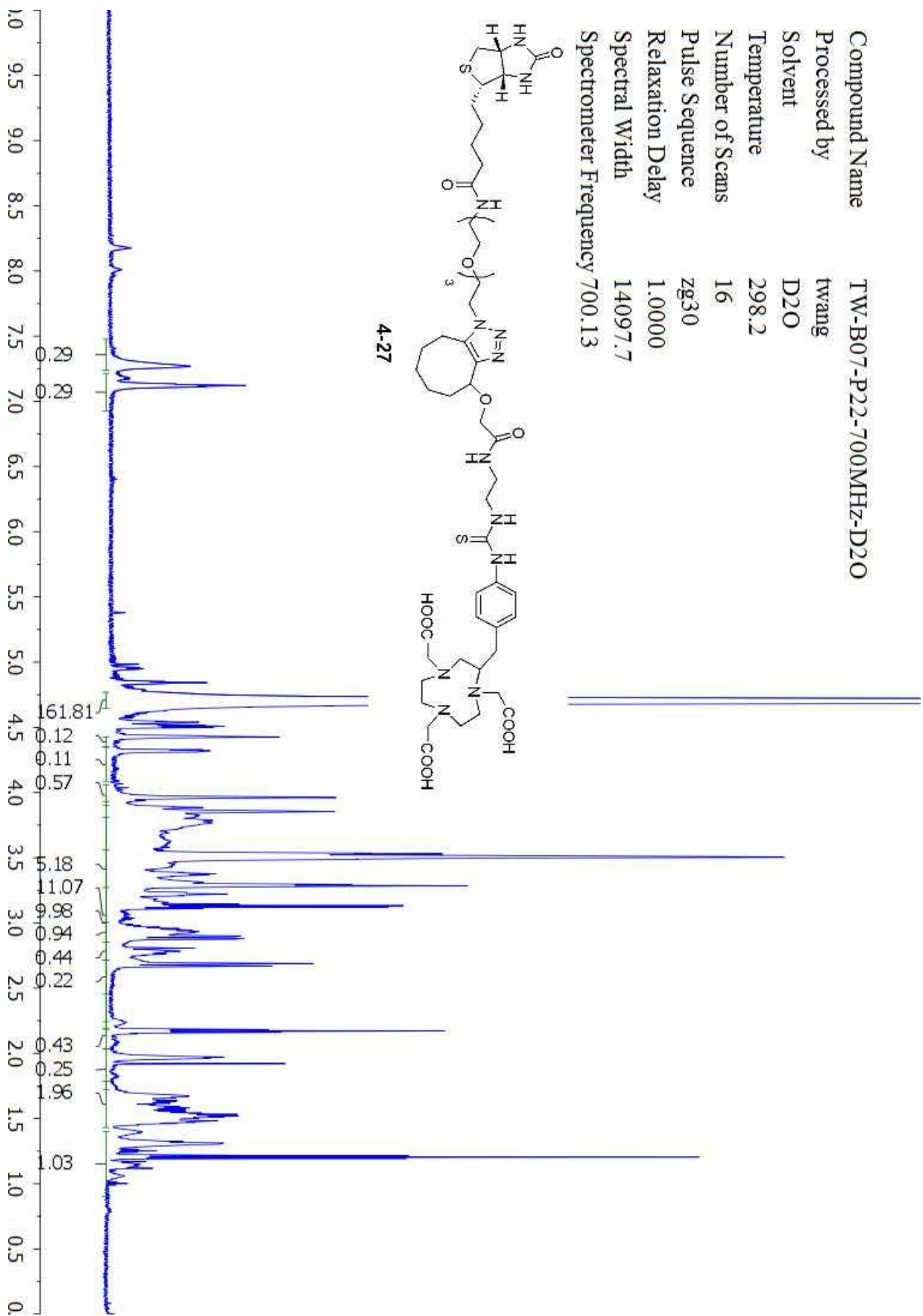
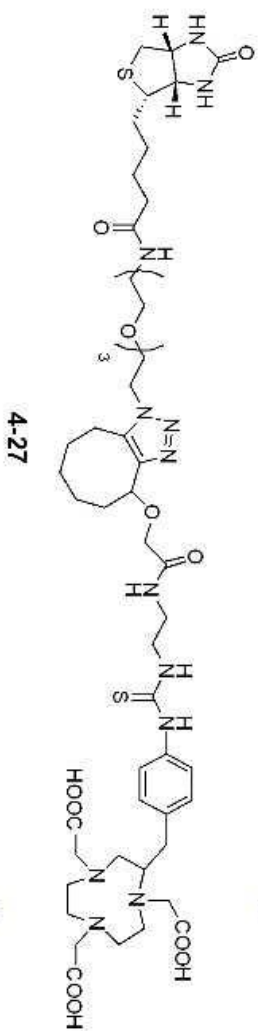
Compound Name TW-B07-P30--700MHz-85%ACND3+15%D2O  
 Processed by twang  
 Solvent CD3CN  
 Temperature 298.1  
 Number of Scans 64  
 Pulse Sequence zg30  
 Relaxation Delay 1.0000  
 Spectral Width 14097.7  
 Spectrometer Frequency 700.13



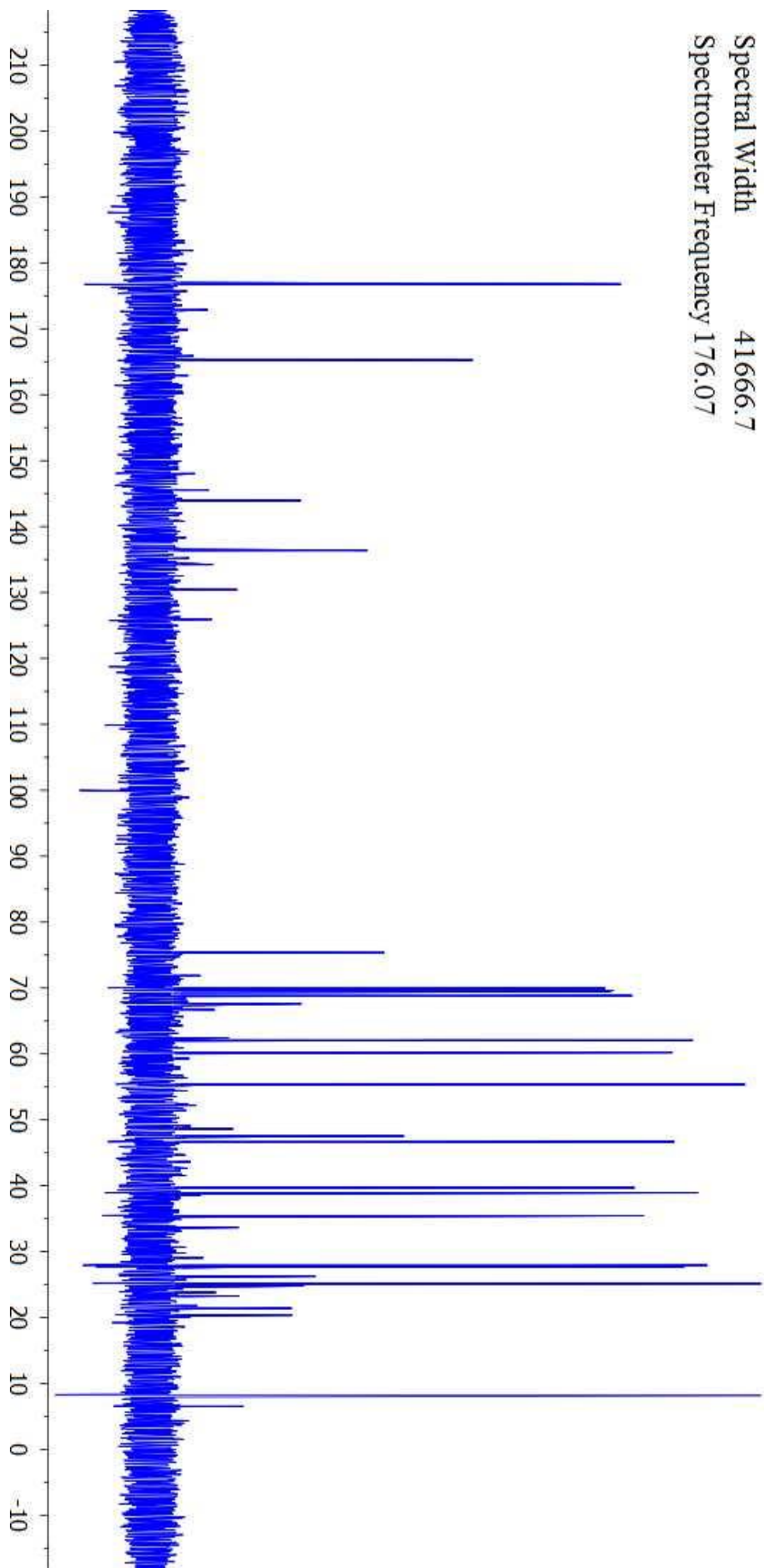
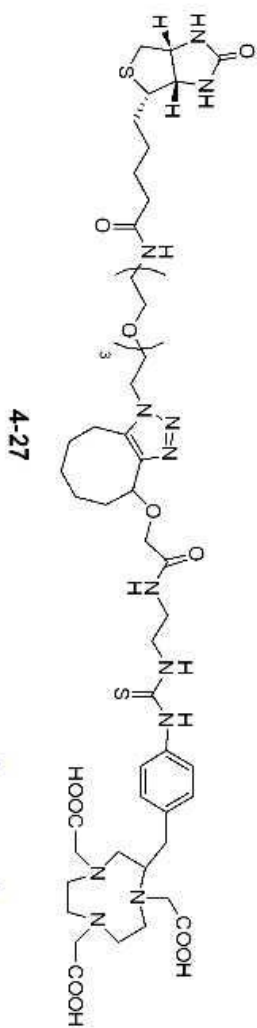
Compound Name TW-B07-P30--700MHz-8.5%ACND3+1.5%D2O  
 Processed by twang  
 Solvent CD3CN  
 Temperature 298.2  
 Number of Scans 30000  
 Pulse Sequence zgpg30  
 Relaxation Delay 2.0000  
 Spectral Width 41666.7  
 Spectrometer Frequency 176.07



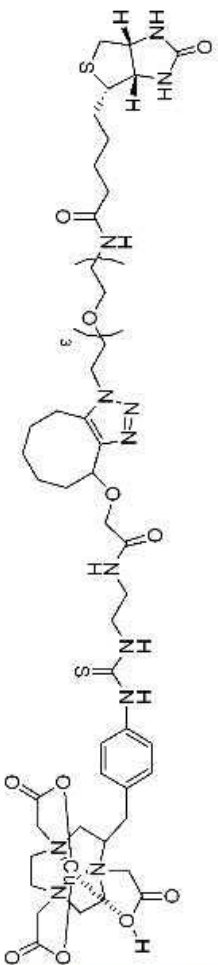
Compound Name TW-B07-P22-700MHz-D2O  
 Processed by twang  
 Solvent D2O  
 Temperature 298.2  
 Number of Scans 16  
 Pulse Sequence zg30  
 Relaxation Delay 1.0000  
 Spectral Width 14097.7  
 Spectrometer Frequency 700.13



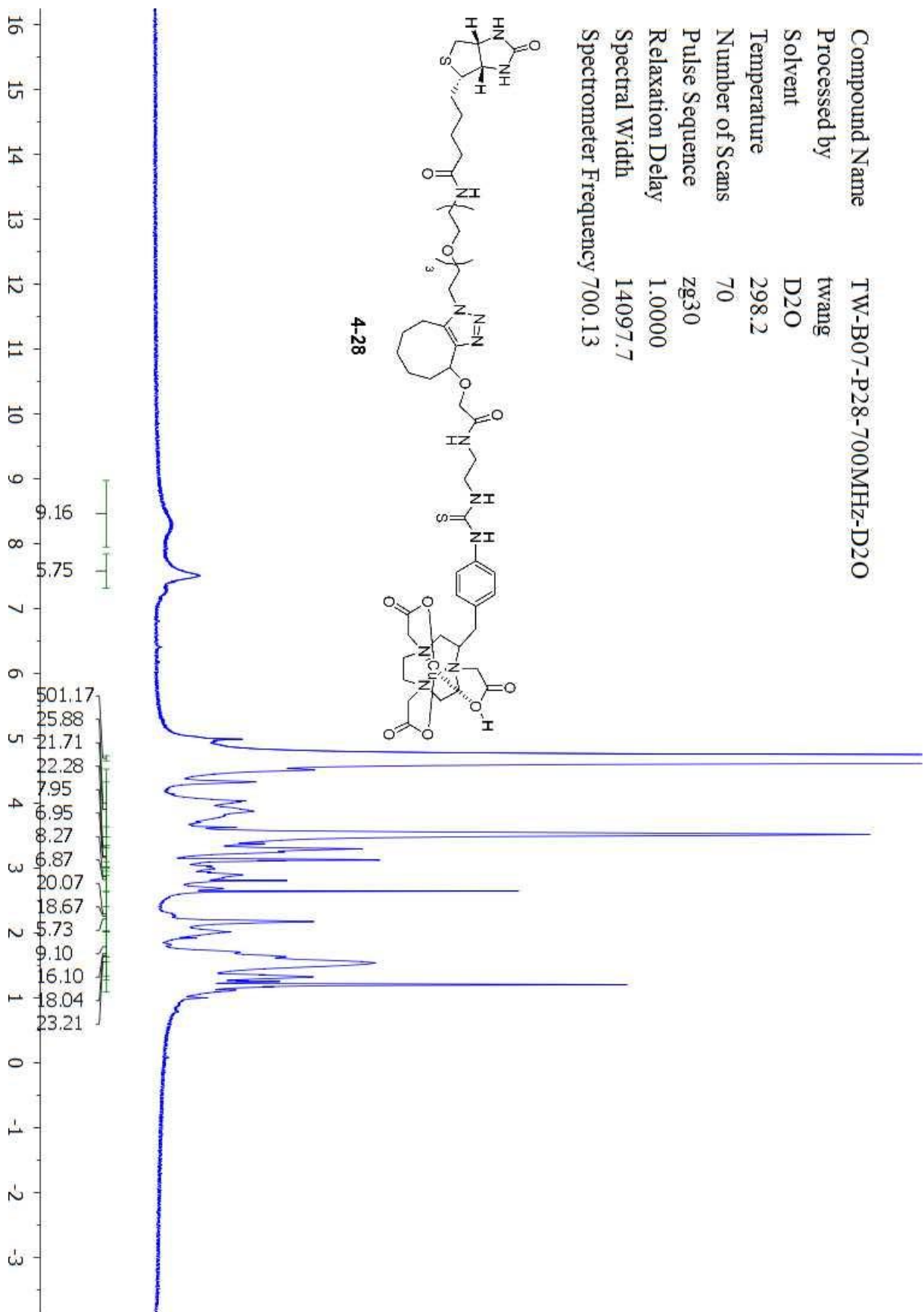
Compound Name TW-B07-P22-700MHz-D2O  
 Processed by twang  
 Solvent D2O  
 Temperature 298.2  
 Number of Scans 18429  
 Pulse Sequence zgpg30  
 Relaxation Delay 2.0000  
 Spectral Width 41666.7  
 Spectrometer Frequency 176.07



Compound Name TW-B07-P28-700MHz-D2O  
 Processed by twang  
 Solvent D2O  
 Temperature 298.2  
 Number of Scans 70  
 Pulse Sequence zg30  
 Relaxation Delay 1.0000  
 Spectral Width 14097.7  
 Spectrometer Frequency 700.13

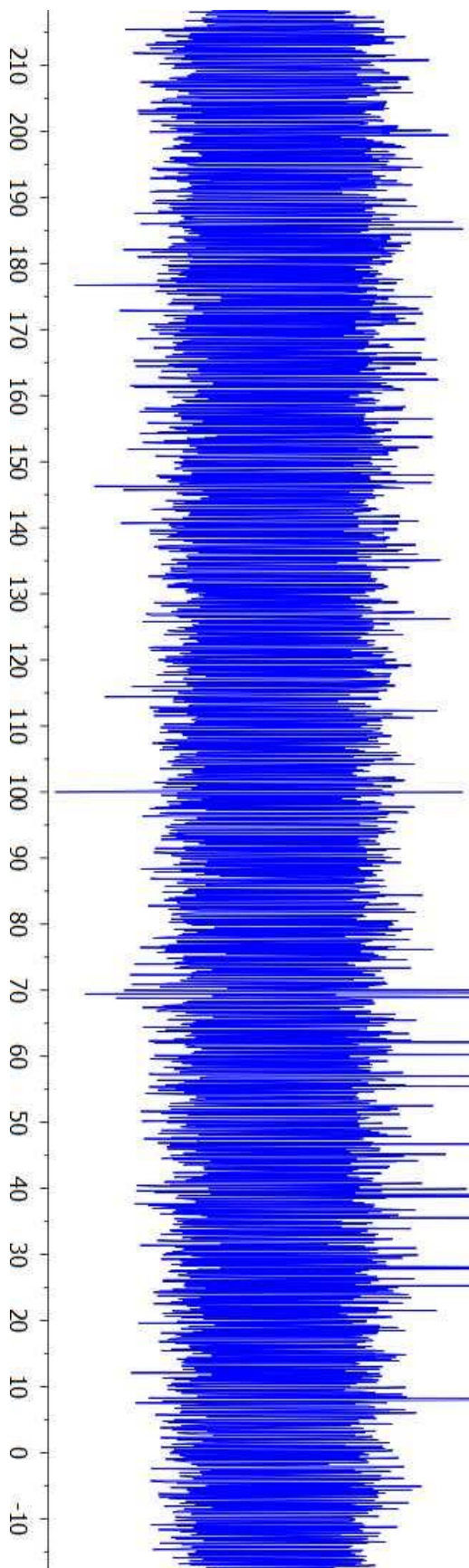
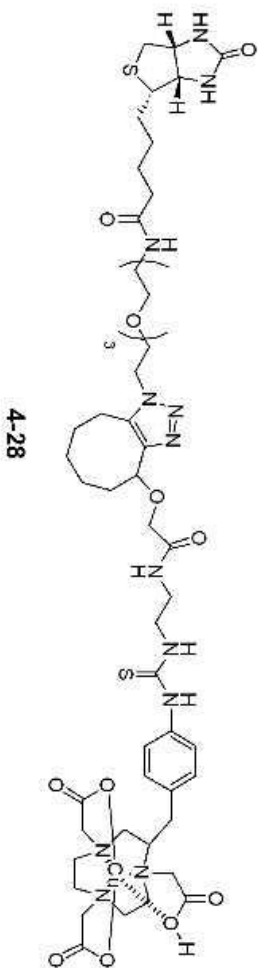


4-28



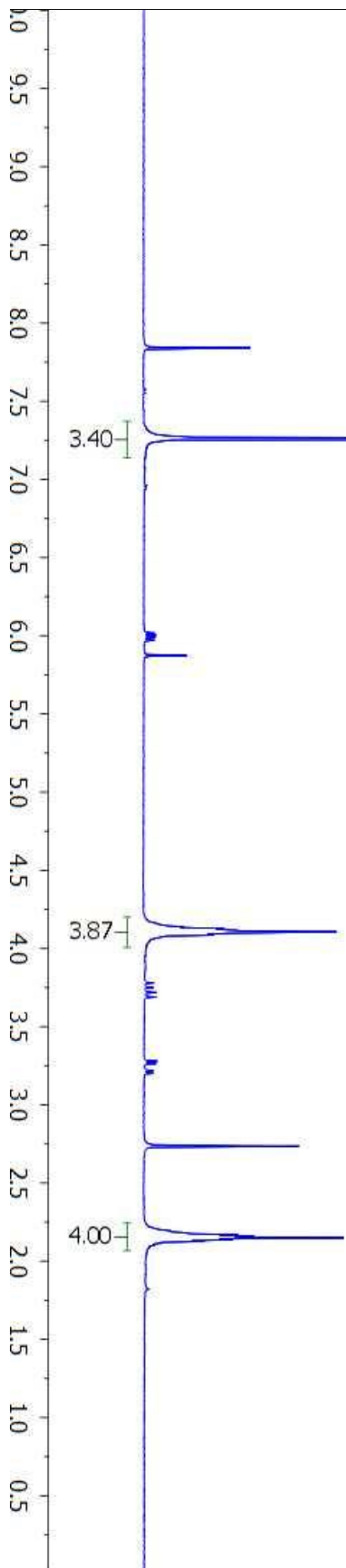
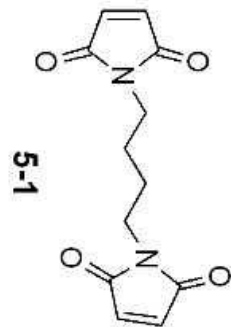


Compound Name TW-B07-P28-700MHz-D2O  
Processed by twang  
Solvent D2O  
Temperature 298.1  
Number of Scans 2279  
Pulse Sequence zgpg30  
Relaxation Delay 2.0000  
Spectral Width 41666.7  
Spectrometer Frequency 176.07

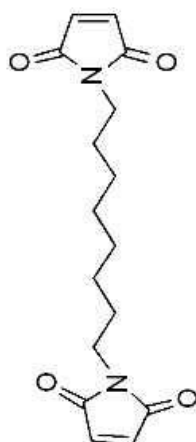


## Appendix Chapter 5 NMR Spectra

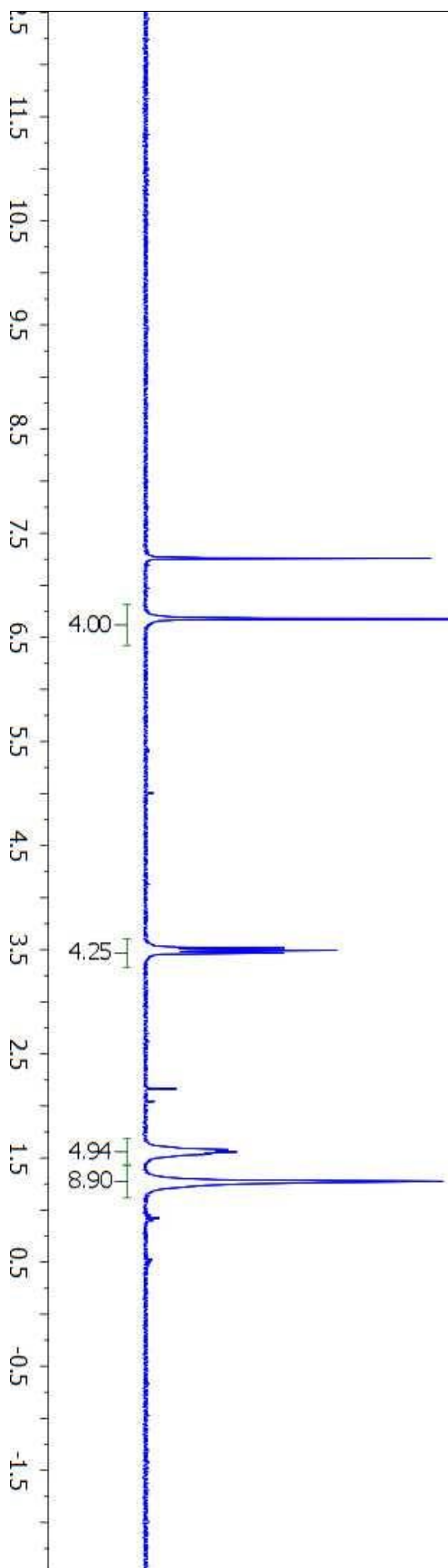
Compound Name TW-B02-P3-N4CN  
Processed by  
Solvent CDCl3  
Temperature 25.0  
Number of Scans 32  
Pulse Sequence s2pul  
Relaxation Delay 1.0000  
Spectral Width 4500.5  
Spectrometer Frequency 300.07  
Spectral Size 32768



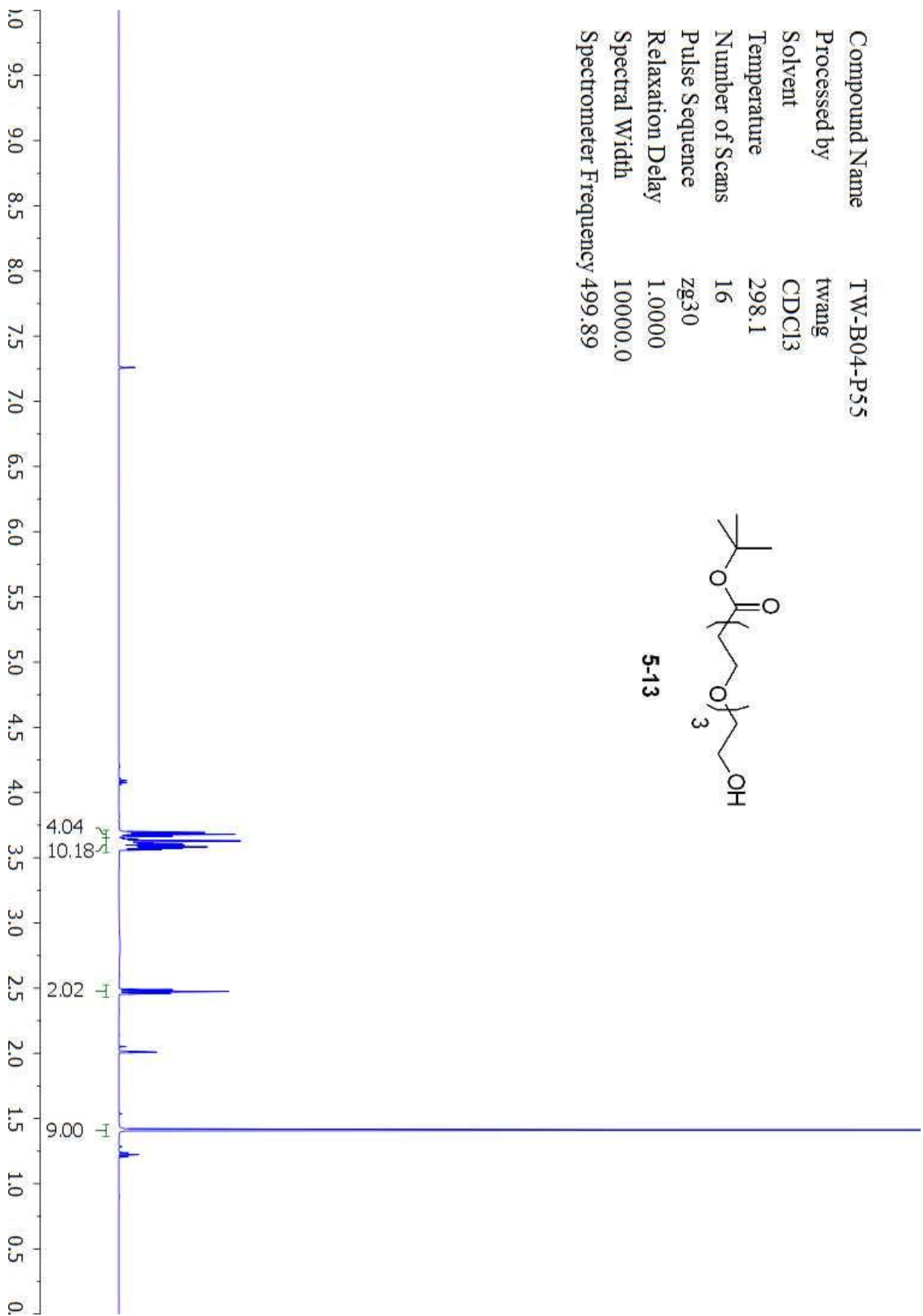
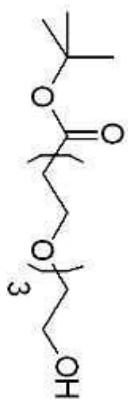
Compound Name TW-B02-P7-N8CNpurified  
Processed by  
Solvent CDCl3  
Temperature 25.0  
Number of Scans 32  
Pulse Sequence s2pul  
Relaxation Delay 1.0000  
Spectral Width 4500.5  
Spectrometer Frequency 300.07  
Spectral Size 32768



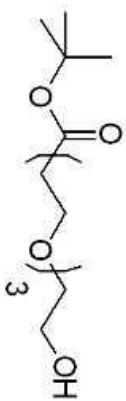
5-2



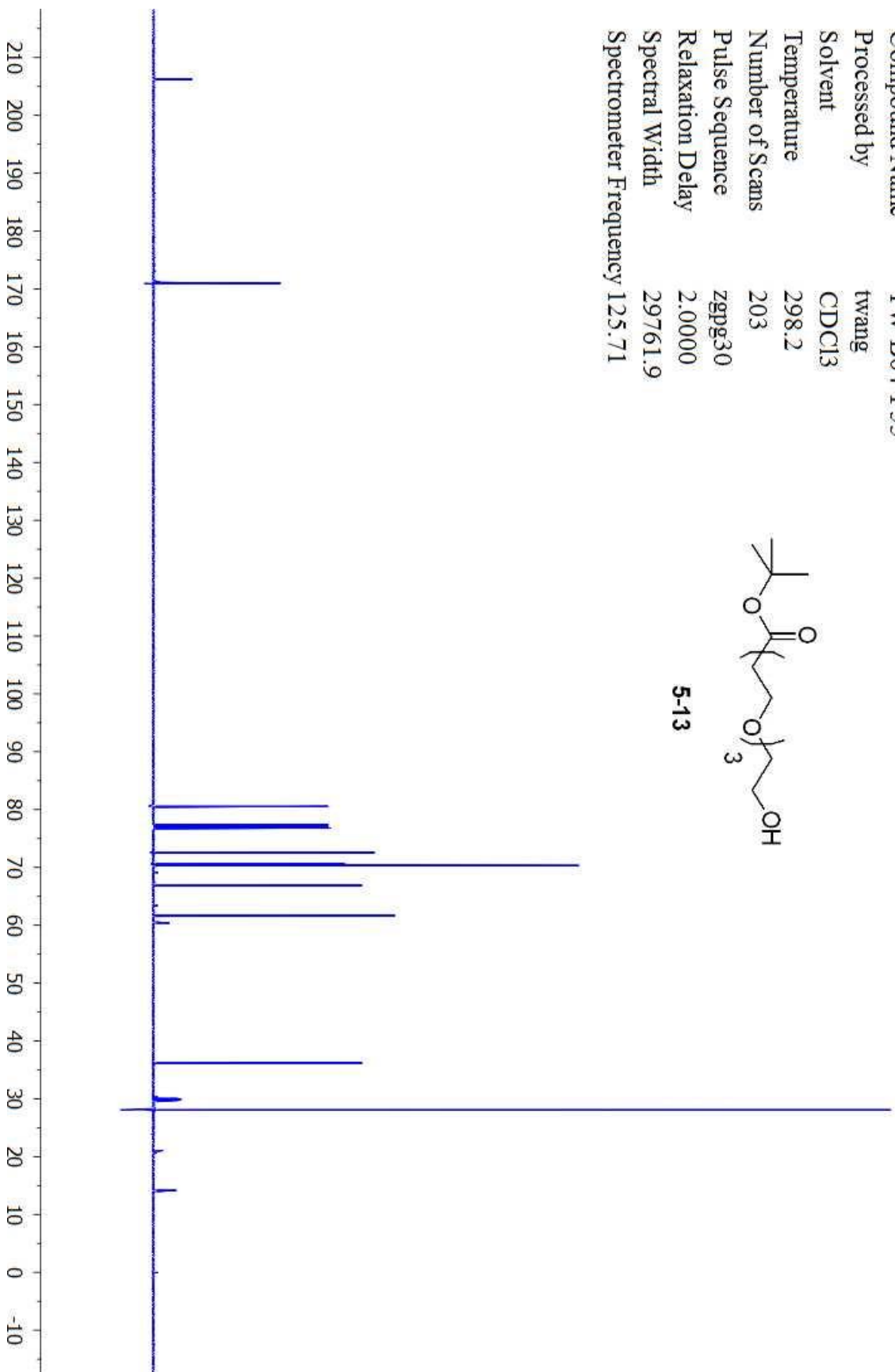
Compound Name TW-B04-P55  
Processed by twang  
Solvent CDCl3  
Temperature 298.1  
Number of Scans 16  
Pulse Sequence zg30  
Relaxation Delay 1.0000  
Spectral Width 10000.0  
Spectrometer Frequency 499.89



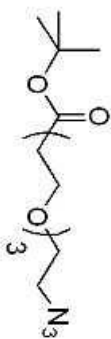
Compound Name TW-B04-P55  
Processed by twang  
Solvent CDCl3  
Temperature 298.2  
Number of Scans 203  
Pulse Sequence zgpg30  
Relaxation Delay 2.0000  
Spectral Width 29761.9  
Spectrometer Frequency 125.71



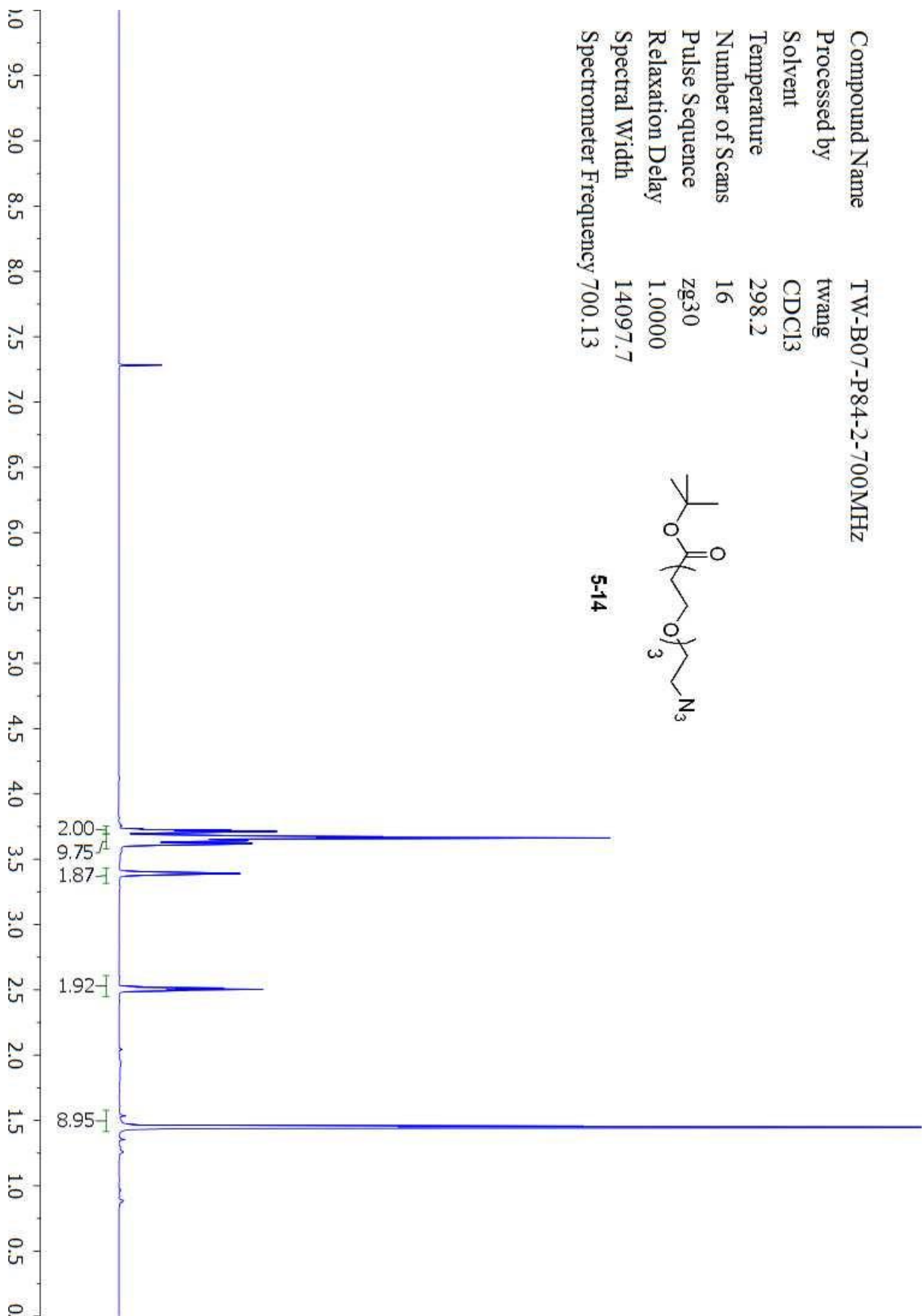
5-13



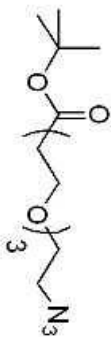
Compound Name TW-B07-P84-2-700MHZ  
Processed by twang  
Solvent CDCl3  
Temperature 298.2  
Number of Scans 16  
Pulse Sequence zg30  
Relaxation Delay 1.0000  
Spectral Width 14097.7  
Spectrometer Frequency 700.13



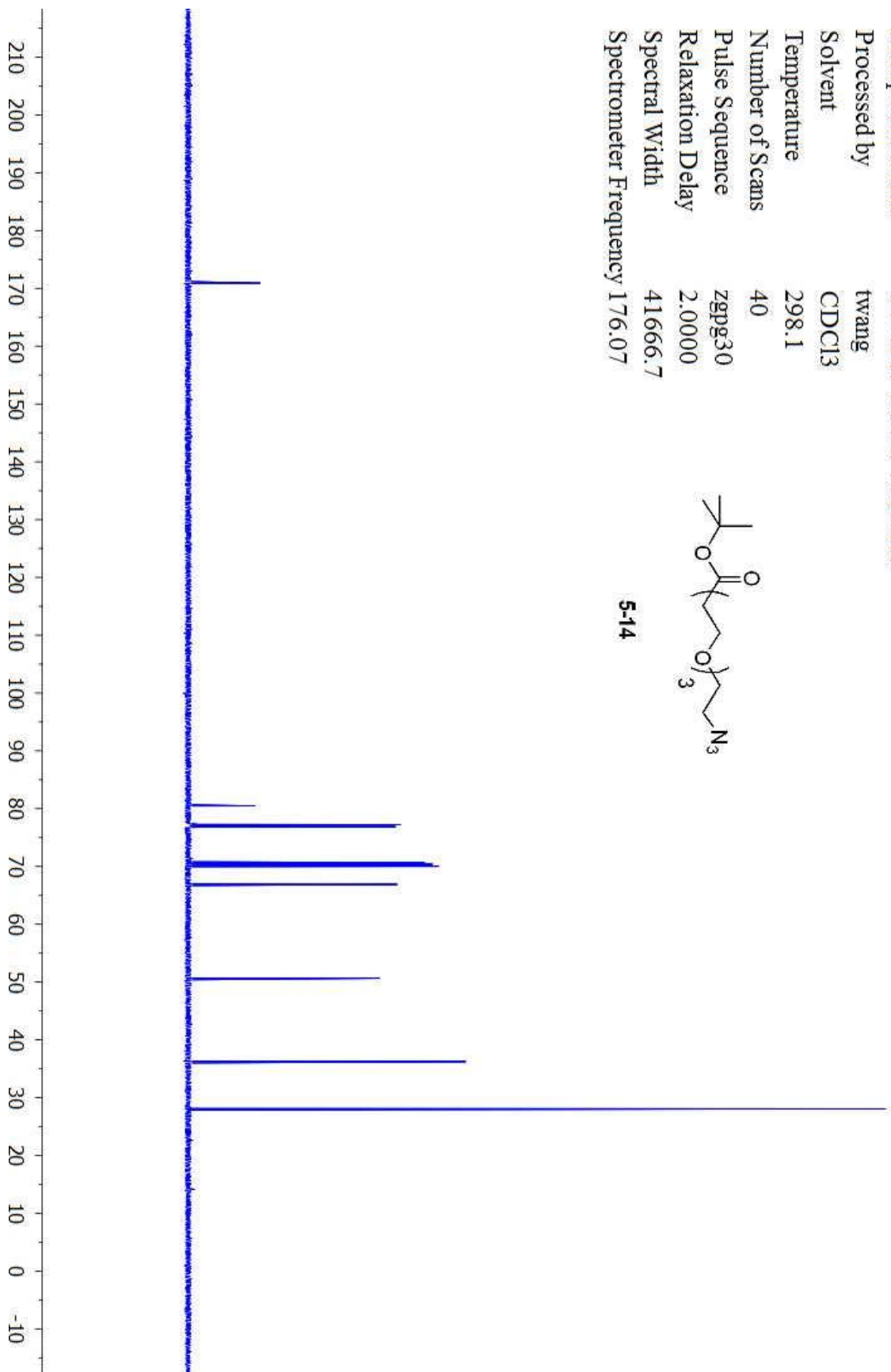
5-14



Compound Name TW-B07-P84-2-700MHz  
Processed by twang  
Solvent CDCl3  
Temperature 298.1  
Number of Scans 40  
Pulse Sequence zgpg30  
Relaxation Delay 2.0000  
Spectral Width 41666.7  
Spectrometer Frequency 176.07

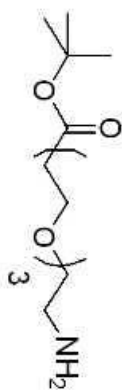


5-14

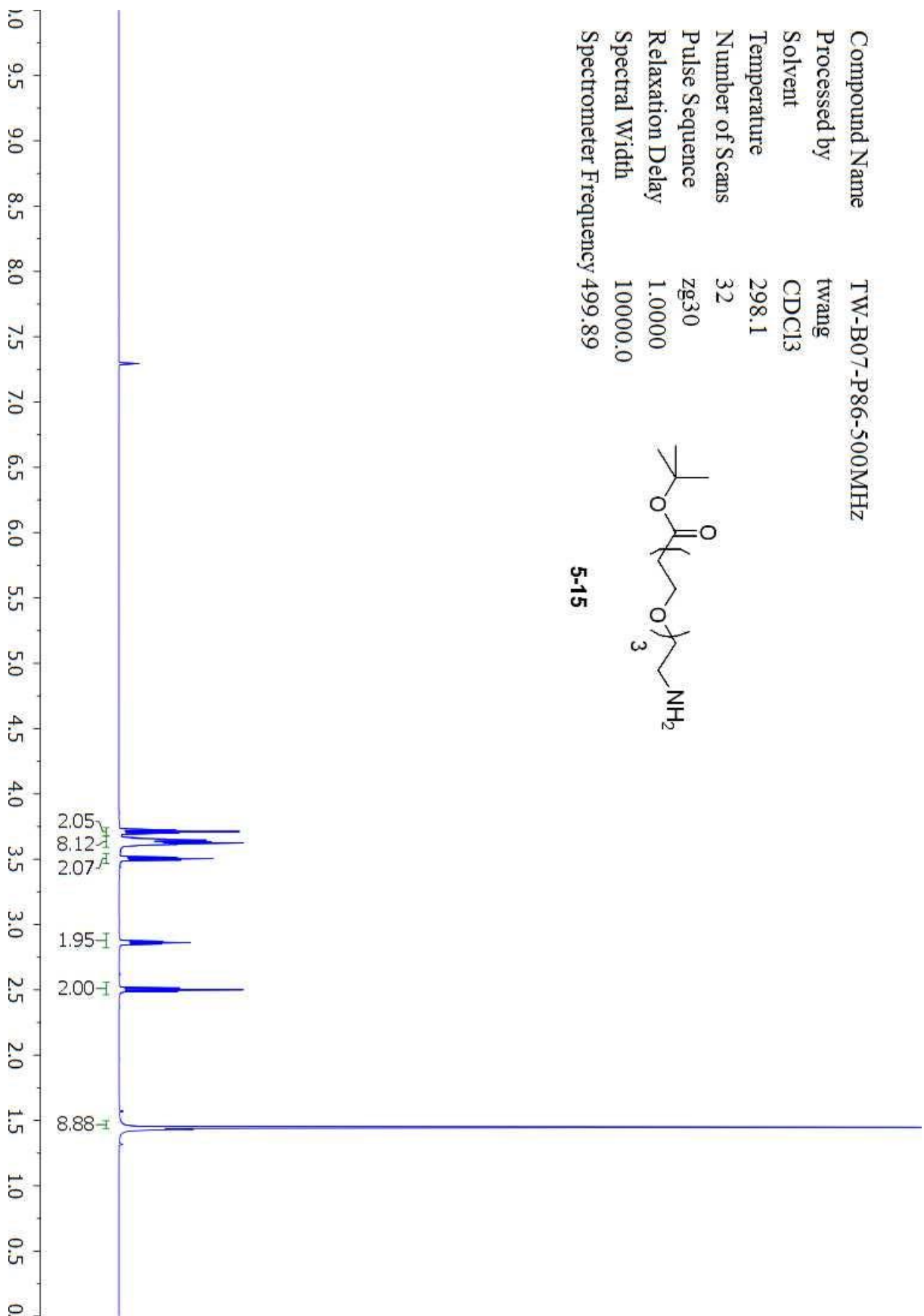




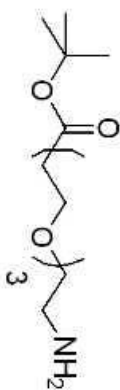
Compound Name TW-B07-P86-500MHZ  
Processed by twang  
Solvent CDCl3  
Temperature 298.1  
Number of Scans 32  
Pulse Sequence zg30  
Relaxation Delay 1.0000  
Spectral Width 10000.0  
Spectrometer Frequency 499.89



5-15



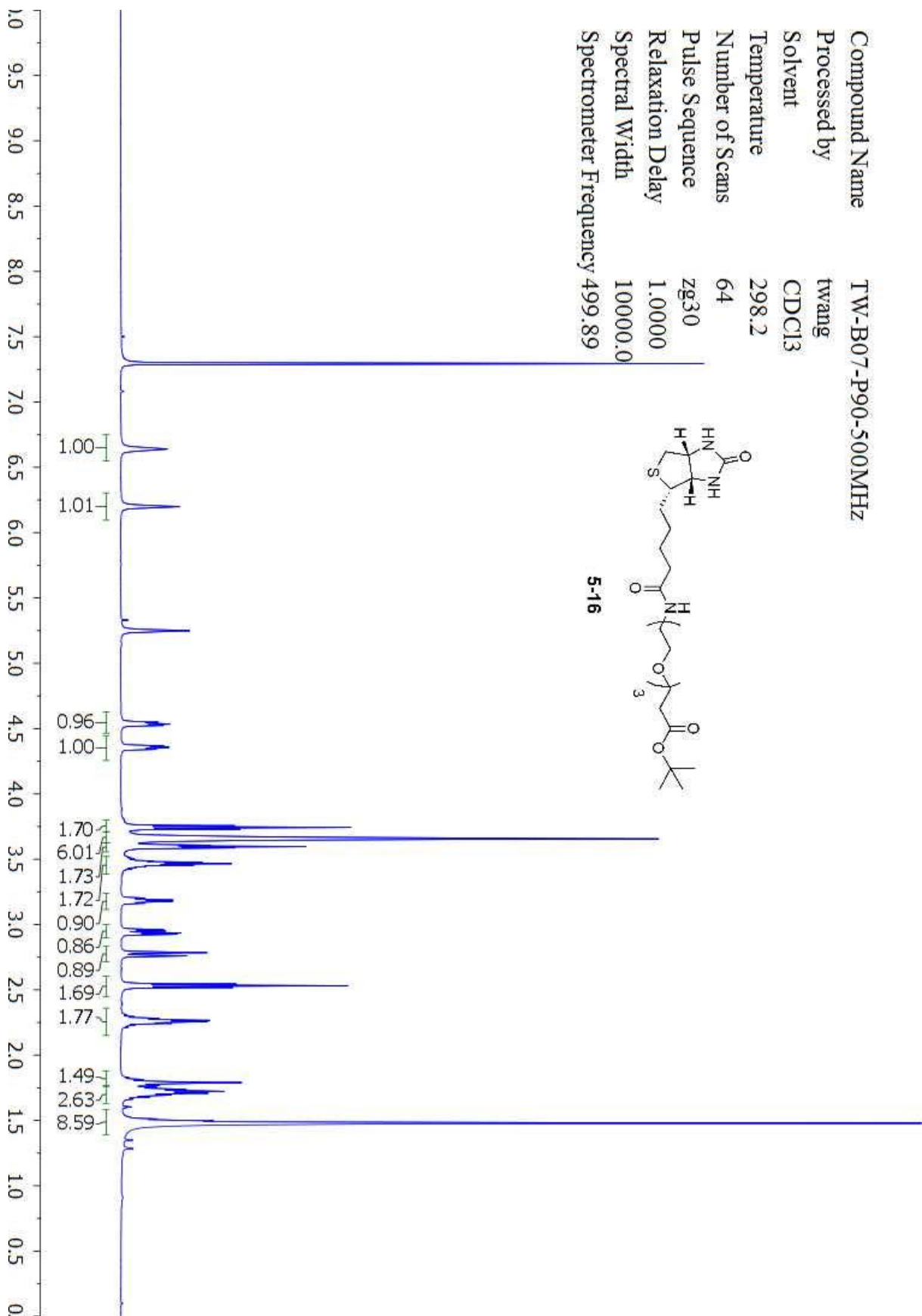
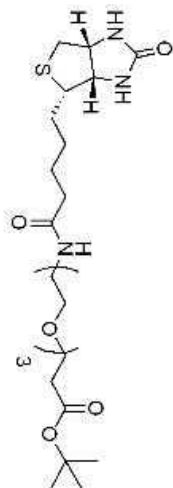
Compound Name TW-B07-P86-500MHz  
Processed by twang  
Solvent CDCl3  
Temperature 298.2  
Number of Scans 34  
Pulse Sequence zgpg30  
Relaxation Delay 2.0000  
Spectral Width 29761.9  
Spectrometer Frequency 125.71



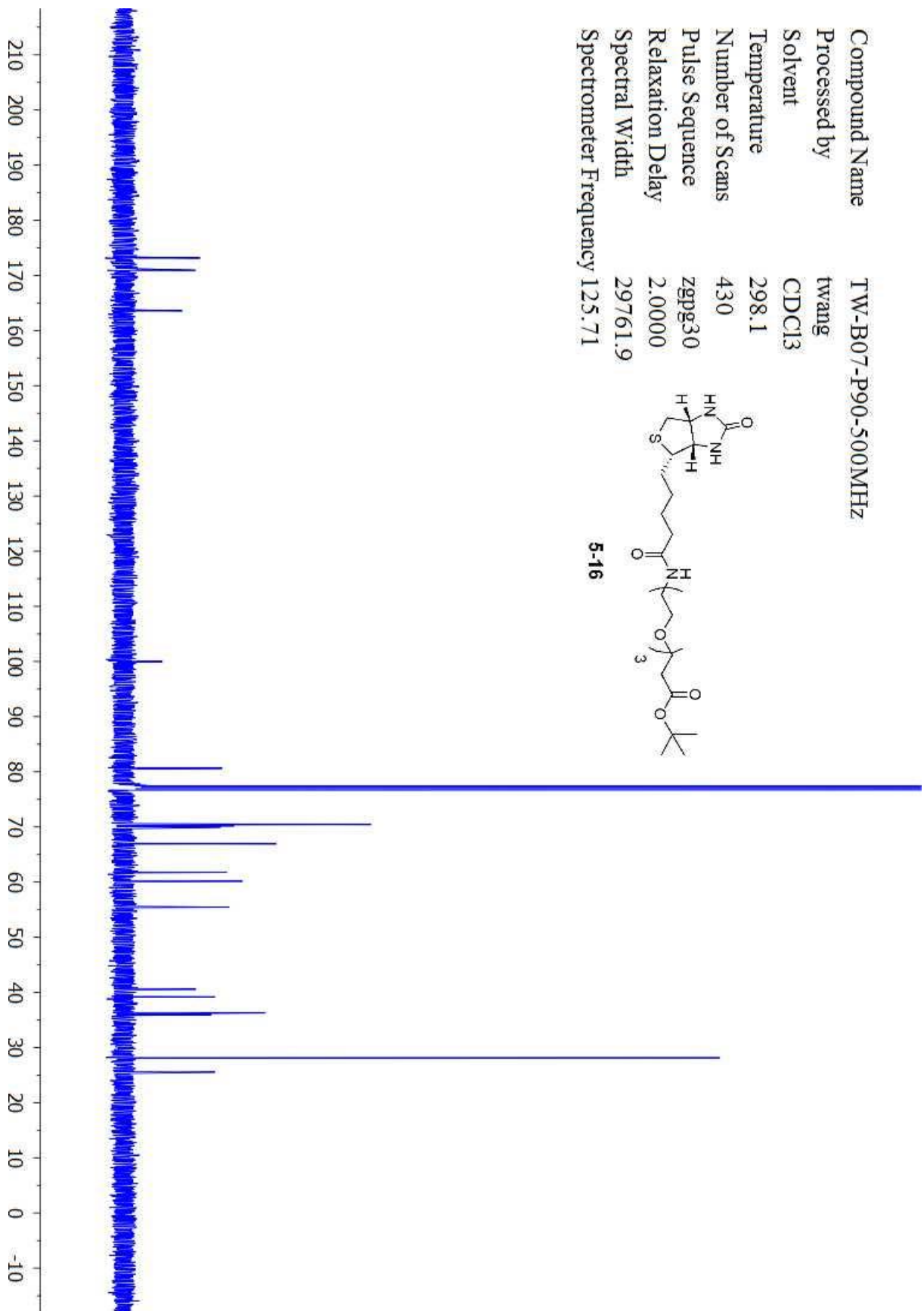
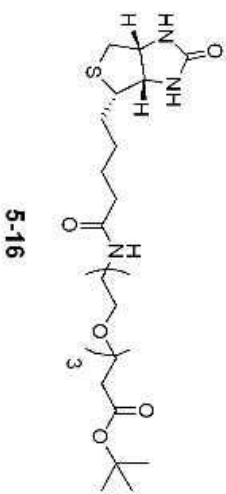
5-15



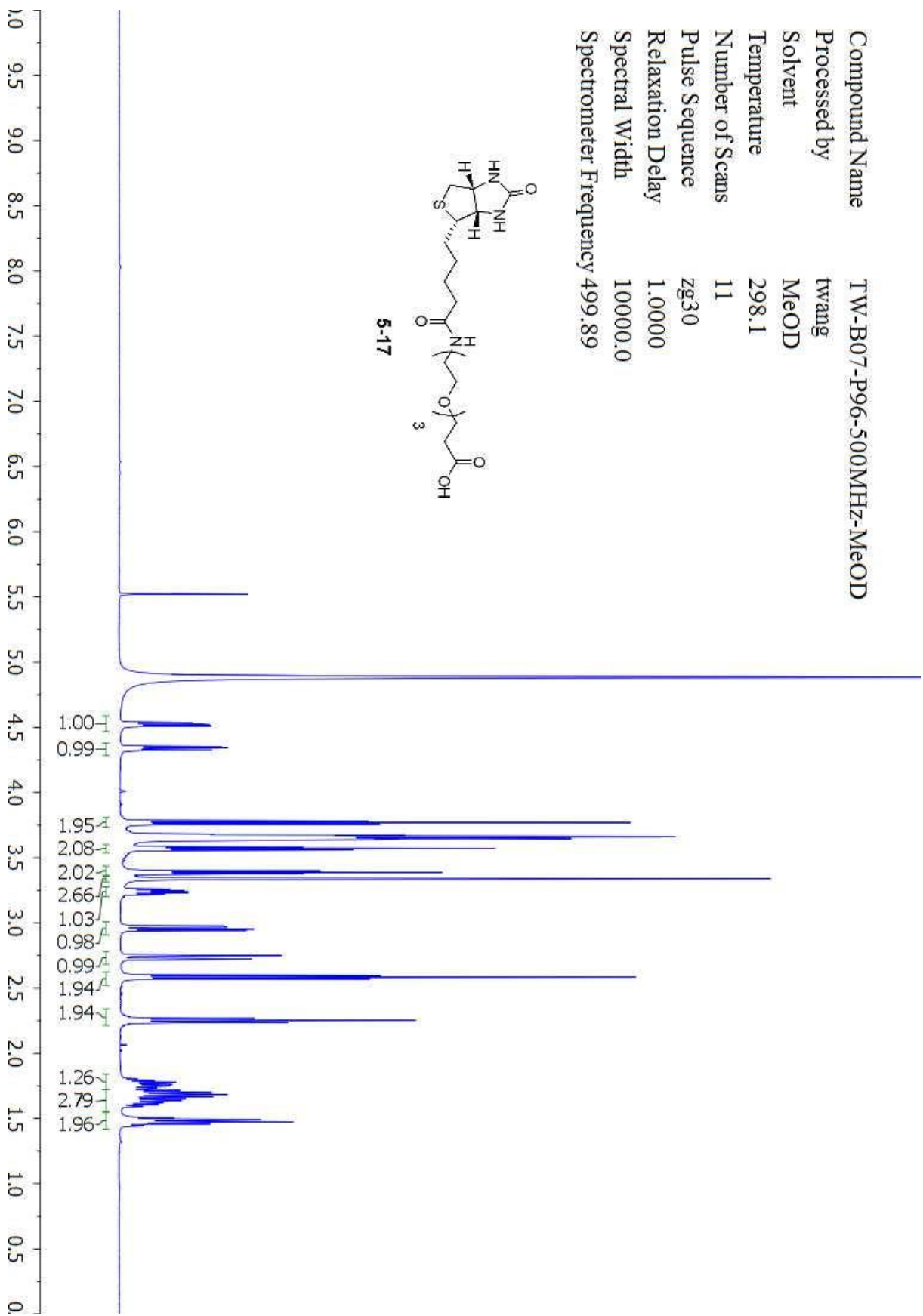
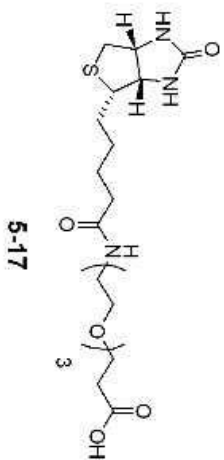
Compound Name TW-B07-P90-500MHZ  
 Processed by twang  
 Solvent CDCl3  
 Temperature 298.2  
 Number of Scans 64  
 Pulse Sequence zg30  
 Relaxation Delay 1.0000  
 Spectral Width 10000.0  
 Spectrometer Frequency 499.89



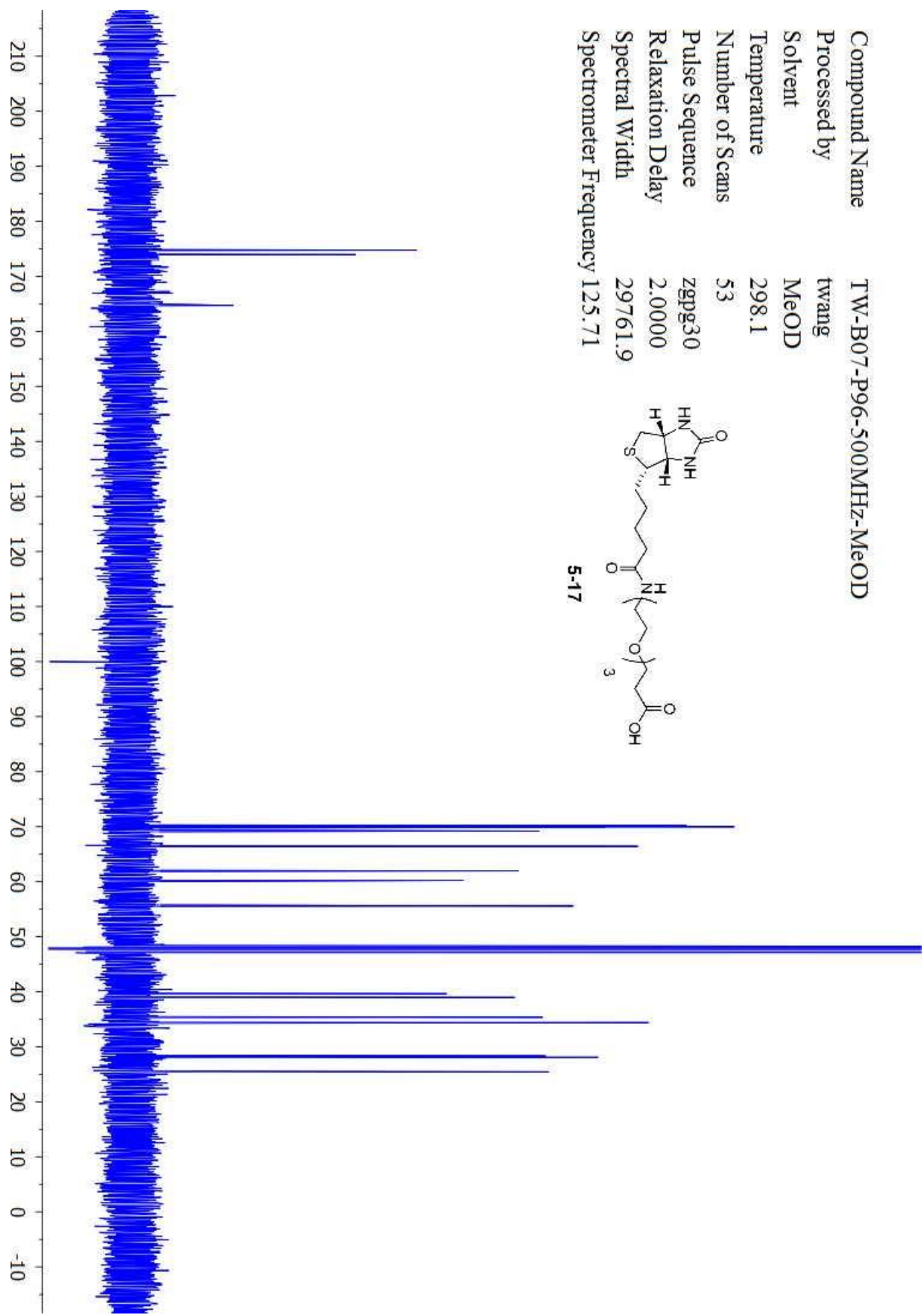
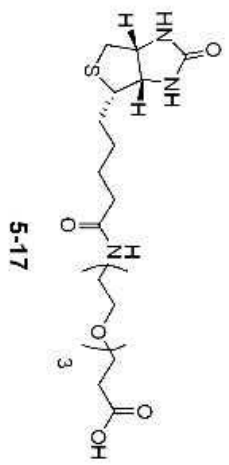
Compound Name TW-B07-P90-500MHZ  
Processed by twang  
Solvent CDCl3  
Temperature 298.1  
Number of Scans 430  
Pulse Sequence zgpg30  
Relaxation Delay 2.0000  
Spectral Width 29761.9  
Spectrometer Frequency 125.71



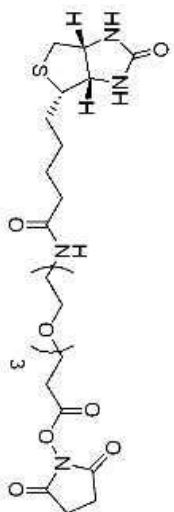
Compound Name TW-B07-P96-500MHz-MeOD  
 Processed by twang  
 Solvent MeOD  
 Temperature 298.1  
 Number of Scans 11  
 Pulse Sequence zg30  
 Relaxation Delay 1.0000  
 Spectral Width 10000.0  
 Spectrometer Frequency 499.89



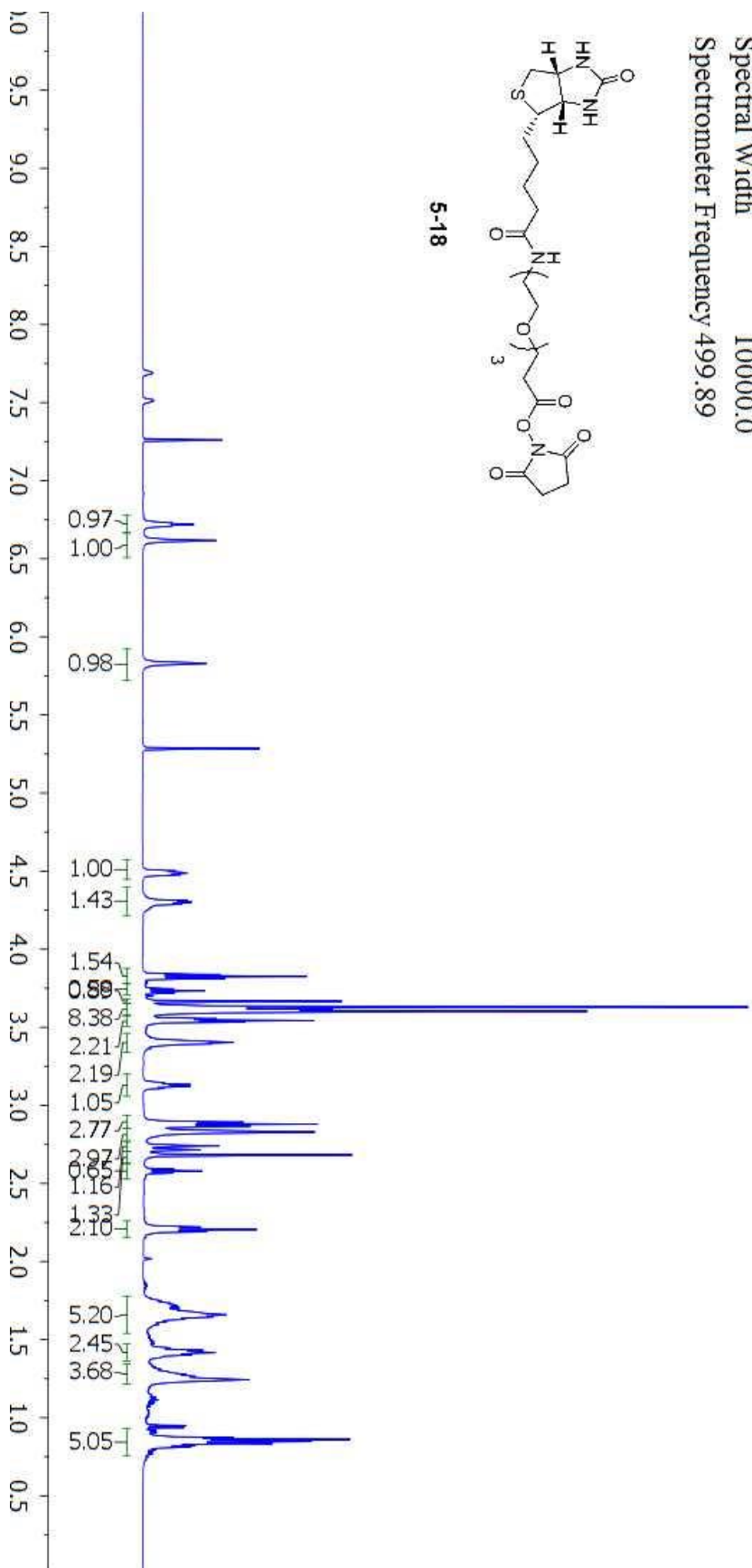
Compound Name TW-B07-P96-500MHz-MeOD  
Processed by twang  
Solvent MeOD  
Temperature 298.1  
Number of Scans 53  
Pulse Sequence zgpg30  
Relaxation Delay 2.0000  
Spectral Width 29761.9  
Spectrometer Frequency 125.71



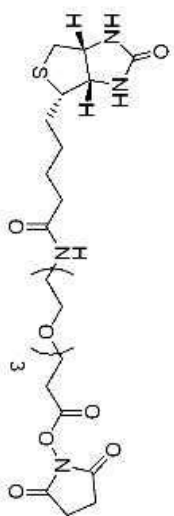
Compound Name TW-B05-P25  
 Processed by twang  
 Solvent CDCl3  
 Temperature 298.2  
 Number of Scans 16  
 Pulse Sequence zg30  
 Relaxation Delay 1.0000  
 Spectral Width 10000.0  
 Spectrometer Frequency 499.89



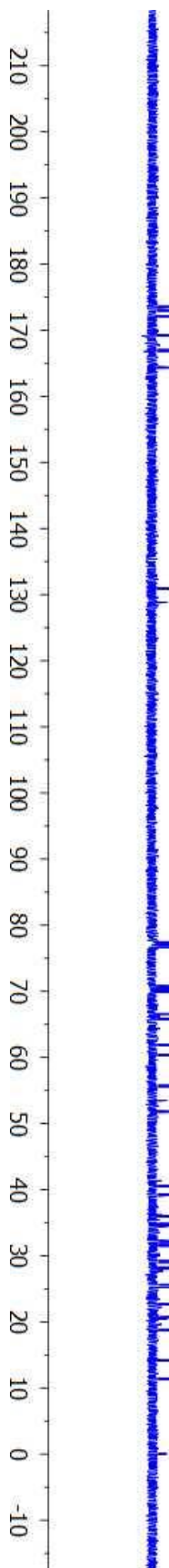
5-18



Compound Name TW-B05-P25  
Processed by twang  
Solvent CDCl3  
Temperature 298.2  
Number of Scans 203  
Pulse Sequence zgpg30  
Relaxation Delay 2.0000  
Spectral Width 29761.9  
Spectrometer Frequency 125.71

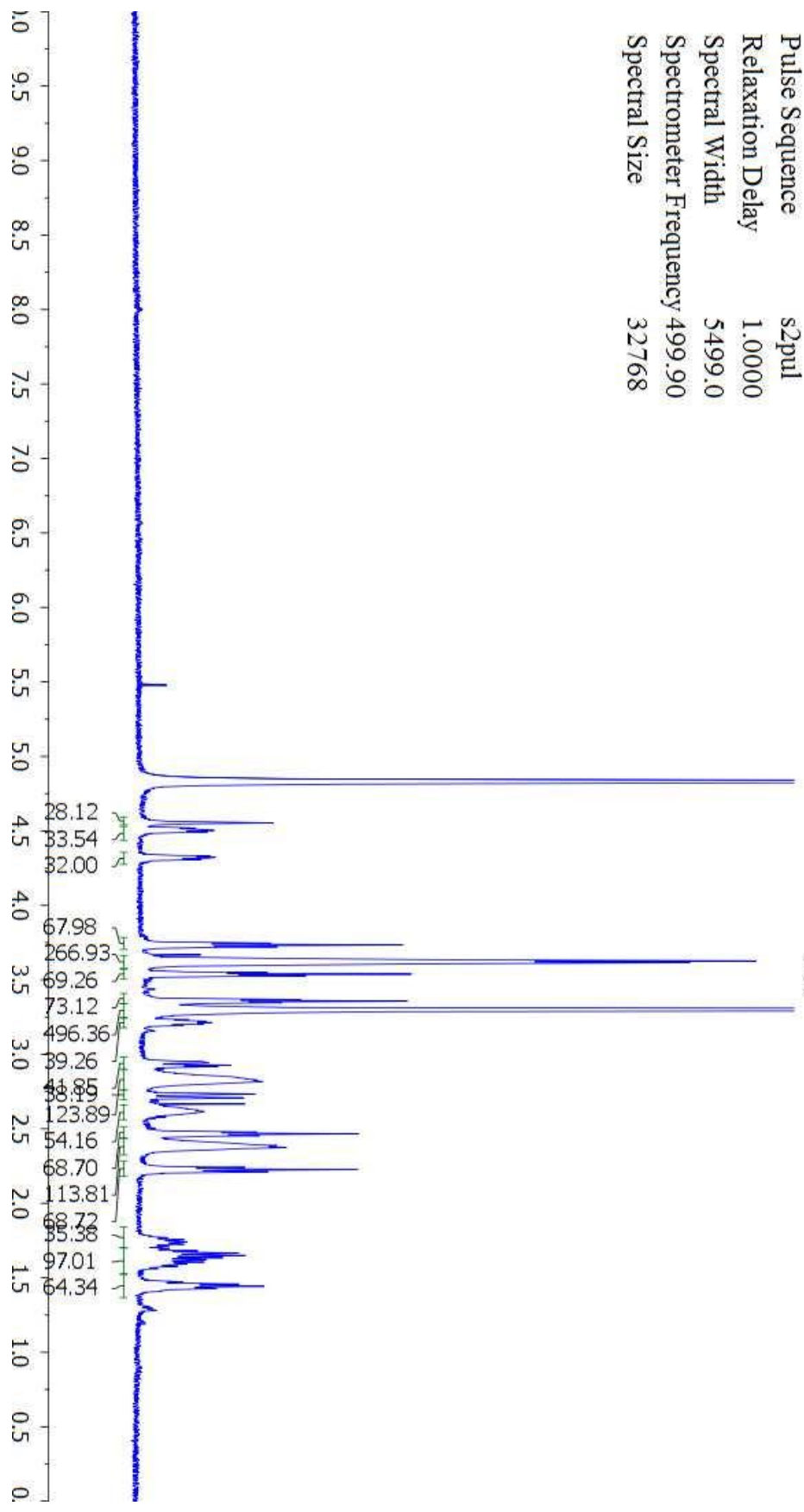
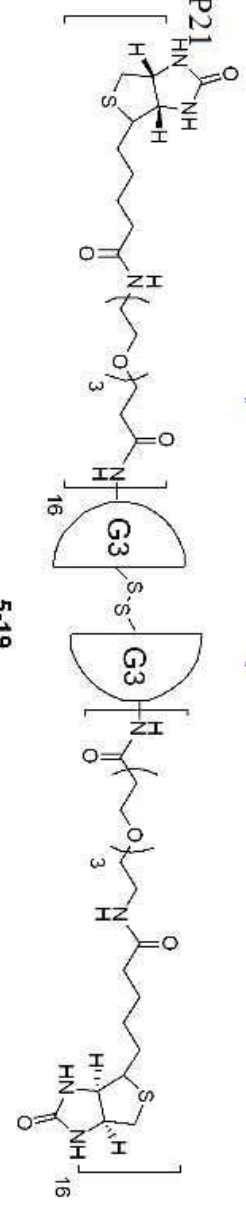


5-18

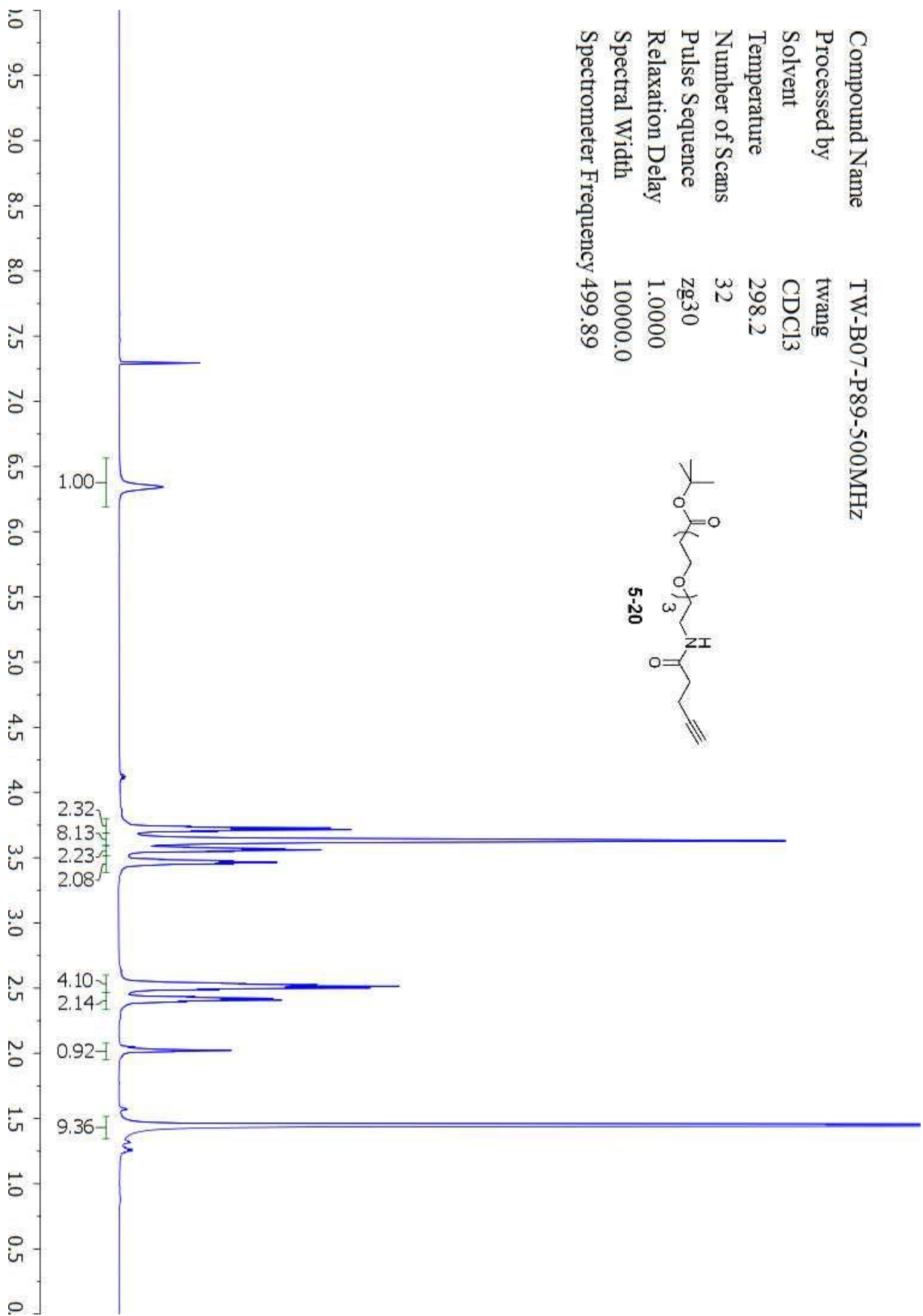
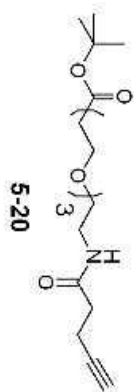




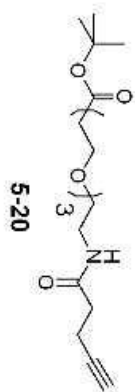
Compound Name TW-B03-P21  
 Processed by CD3OD  
 Solvent 25.0  
 Temperature 117  
 Number of Scans s2pul  
 Pulse Sequence 1.0000  
 Relaxation Delay 5499.0  
 Spectral Width 499.90  
 Spectrometer Frequency 32768  
 Spectral Size



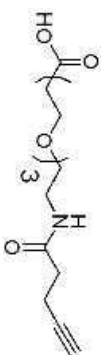
Compound Name TW-B07-P89-500MHZ  
Processed by twang  
Solvent CDCl3  
Temperature 298.2  
Number of Scans 32  
Pulse Sequence zg30  
Relaxation Delay 1.0000  
Spectral Width 10000.0  
Spectrometer Frequency 499.89



Compound Name TW-B07-P89-500MHZ  
Processed by twang  
Solvent CDCl3  
Temperature 298.2  
Number of Scans 117  
Pulse Sequence zgpg30  
Relaxation Delay 2.0000  
Spectral Width 29761.9  
Spectrometer Frequency 125.71



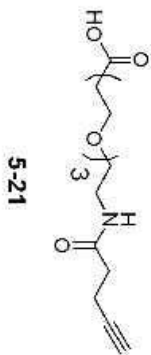
Compound Name TW-B07-P92-500MHZ  
 Processed by twang  
 Solvent CDCl3  
 Temperature 298.2  
 Number of Scans 32  
 Pulse Sequence zg30  
 Relaxation Delay 1.0000  
 Spectral Width 10000.0  
 Spectrometer Frequency 499.89



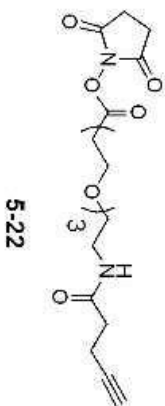
5-21



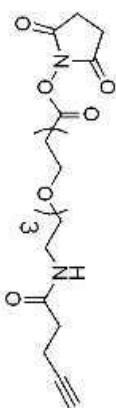
Compound Name TW-B07-P92-500MHZ  
Processed by twang  
Solvent CDCl3  
Temperature 298.2  
Number of Scans 97  
Pulse Sequence zgpg30  
Relaxation Delay 2.0000  
Spectral Width 29761.9  
Spectrometer Frequency 125.71



Compound Name TW-B07-P93-500MHZ  
Processed by twang  
Solvent CDCl3  
Temperature 298.2  
Number of Scans 16  
Pulse Sequence zg30  
Relaxation Delay 1.0000  
Spectral Width 10000.0  
Spectrometer Frequency 499.89



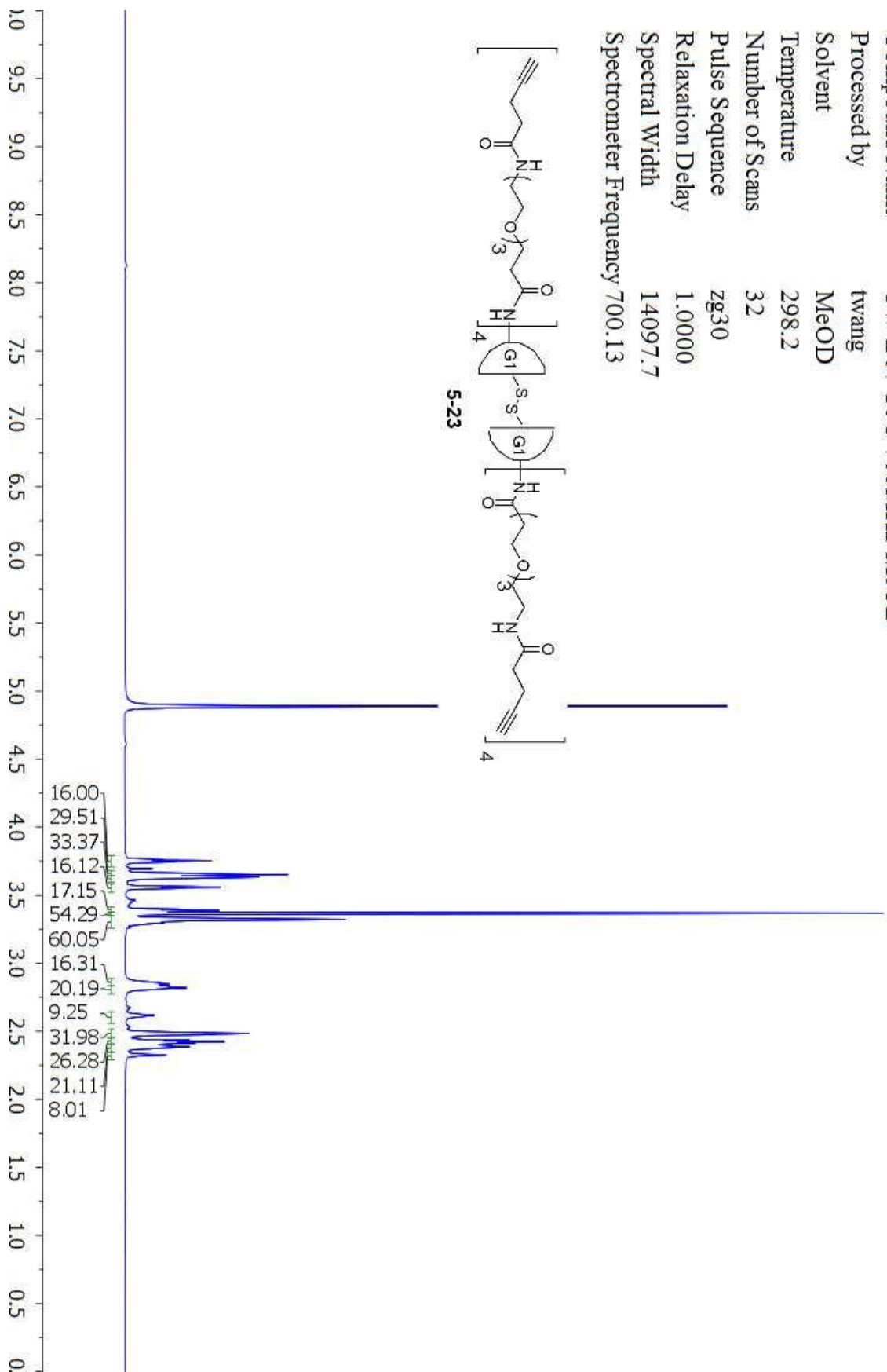
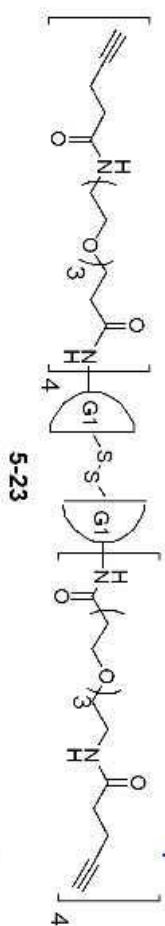
Compound Name TW-B07-P93-500MHZ  
Processed by twang  
Solvent CDCl3  
Temperature 298.1  
Number of Scans 69  
Pulse Sequence zgpg30  
Relaxation Delay 2.0000  
Spectral Width 29761.9  
Spectrometer Frequency 125.71



5-22

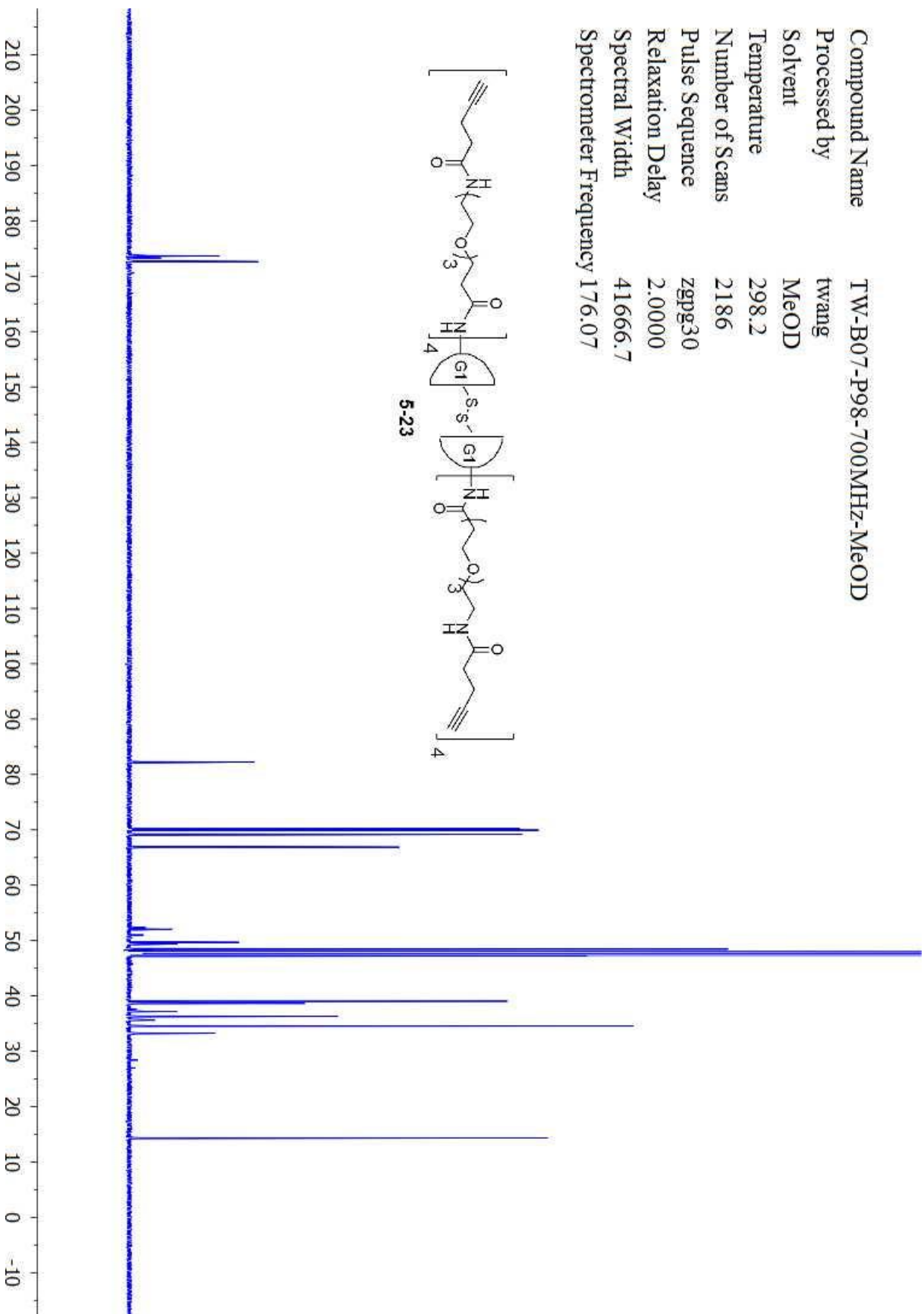
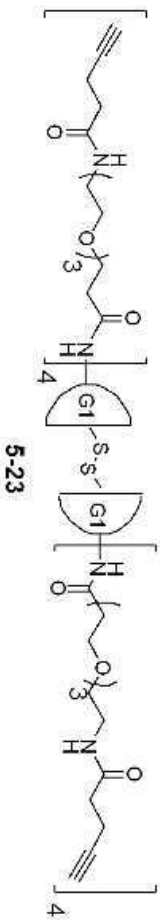


Compound Name TW-B07-P98-700MHz-MeOD  
 Processed by twang  
 Solvent MeOD  
 Temperature 298.2  
 Number of Scans 32  
 Pulse Sequence zg30  
 Relaxation Delay 1.0000  
 Spectral Width 14097.7  
 Spectrometer Frequency 700.13

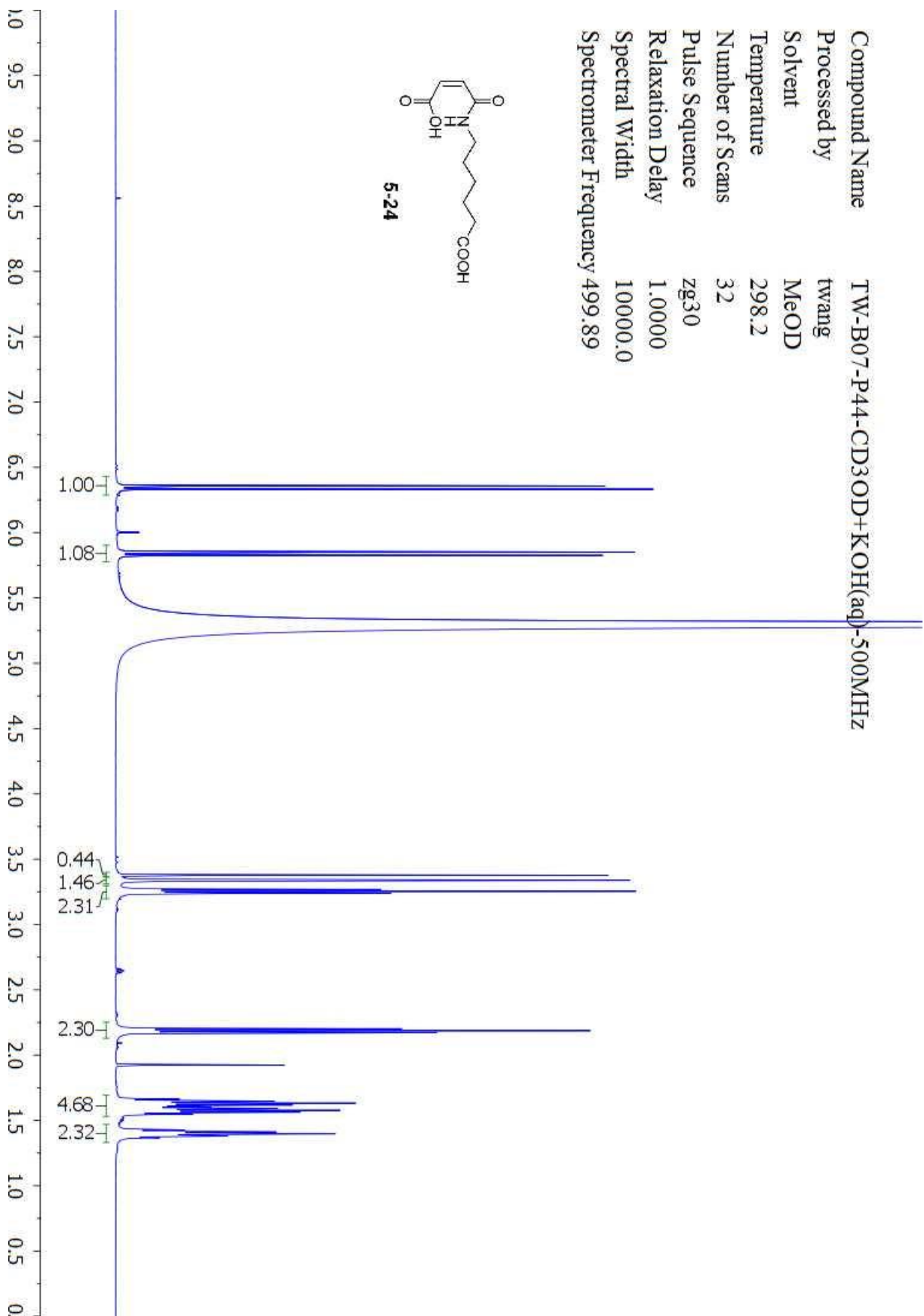
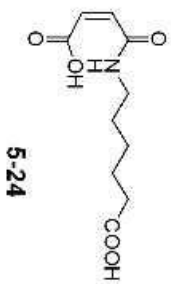




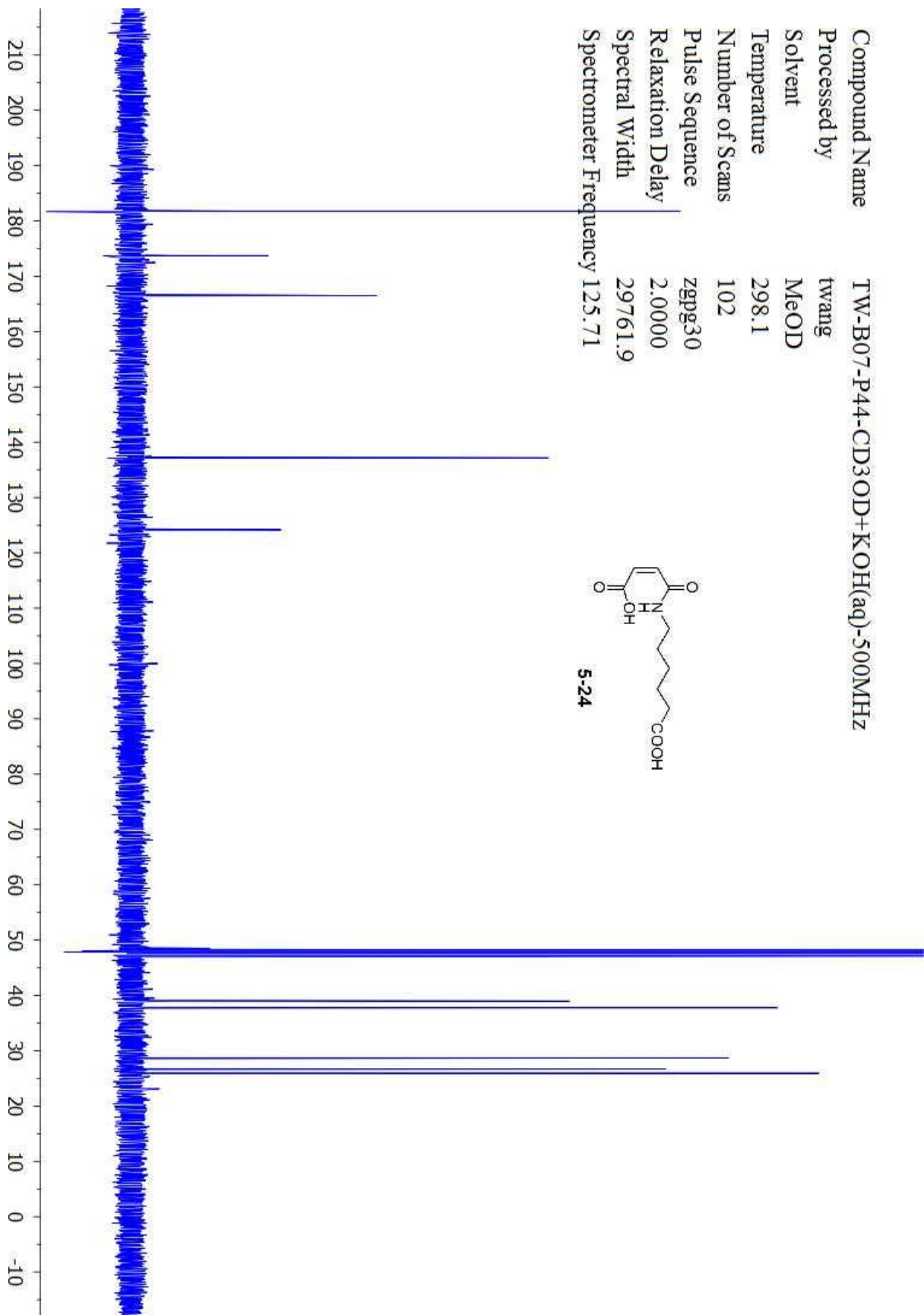
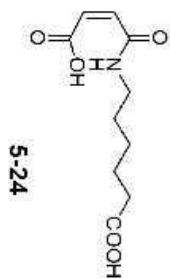
Compound Name TW-B07-P98-700MHz-MeOD  
 Processed by twang  
 Solvent MeOD  
 Temperature 298.2  
 Number of Scans 2186  
 Pulse Sequence zgpg30  
 Relaxation Delay 2.0000  
 Spectral Width 41666.7  
 Spectrometer Frequency 176.07



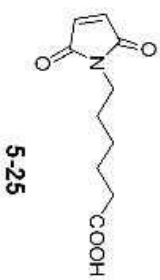
Compound Name TW-B07-P44-CD3OD+KOH(aq)-500MHz  
 Processed by twang  
 Solvent MeOD  
 Temperature 298.2  
 Number of Scans 32  
 Pulse Sequence zg30  
 Relaxation Delay 1.0000  
 Spectral Width 10000.0  
 Spectrometer Frequency 499.89



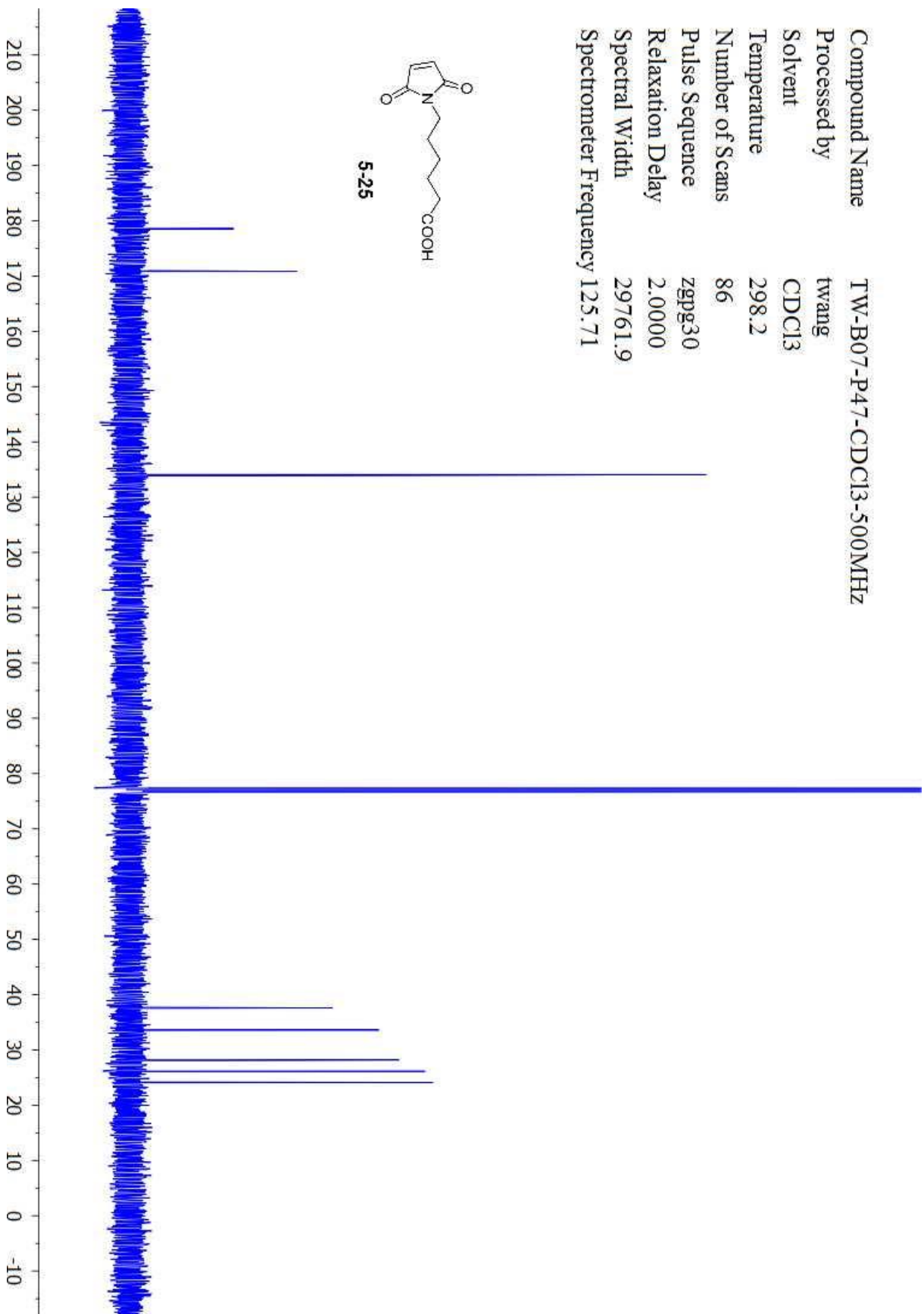
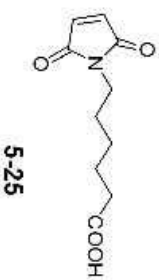
Compound Name TW-B07-P44-CD3OD+KOH(aq)-500MHZ  
 Processed by twang  
 Solvent MeOD  
 Temperature 298.1  
 Number of Scans 102  
 Pulse Sequence zgpg30  
 Relaxation Delay 2.0000  
 Spectral Width 29761.9  
 Spectrometer Frequency 125.71



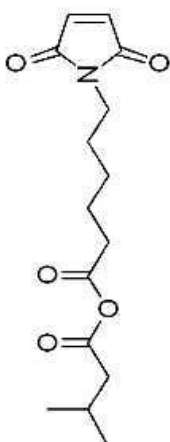
Compound Name TW-B07-P47-CDCl3-500MHZ  
Processed by twang  
Solvent CDCl3  
Temperature 298.1  
Number of Scans 17  
Pulse Sequence zg30  
Relaxation Delay 1.0000  
Spectral Width 10000.0  
Spectrometer Frequency 499.89



Compound Name TW-B07-P47-CDCl3-500MHZ  
Processed by twang  
Solvent CDCl3  
Temperature 298.2  
Number of Scans 86  
Pulse Sequence zgpg30  
Relaxation Delay 2.0000  
Spectral Width 29761.9  
Spectrometer Frequency 125.71



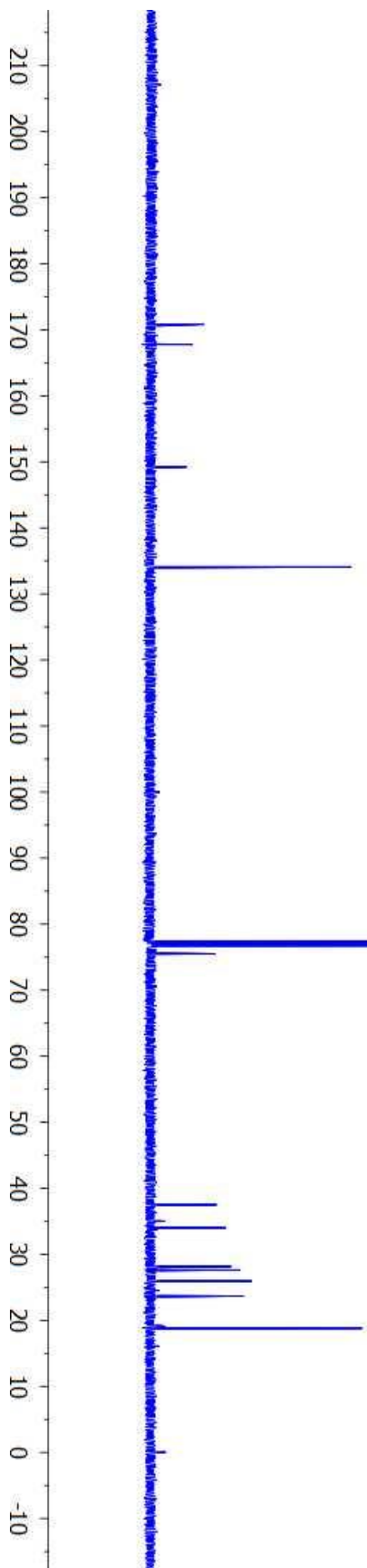
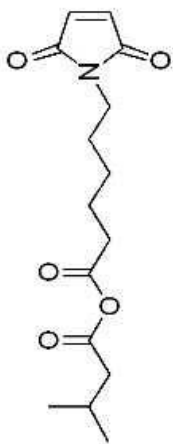
Compound Name TW-B05-P66  
Processed by twang  
Solvent CDCl3  
Temperature 298.2  
Number of Scans 16  
Pulse Sequence zg30  
Relaxation Delay 1.0000  
Spectral Width 10000.0  
Spectrometer Frequency 499.89



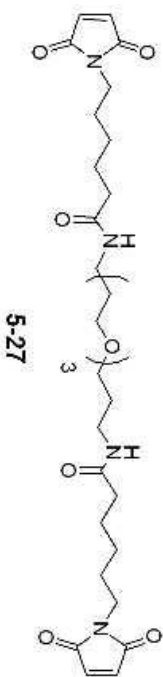
5-26



Compound Name TW-B05-P66  
Processed by twang  
Solvent CDCl3  
Temperature 298.2  
Number of Scans 202  
Pulse Sequence zgpg30  
Relaxation Delay 2.0000  
Spectral Width 29761.9  
Spectrometer Frequency 125.71

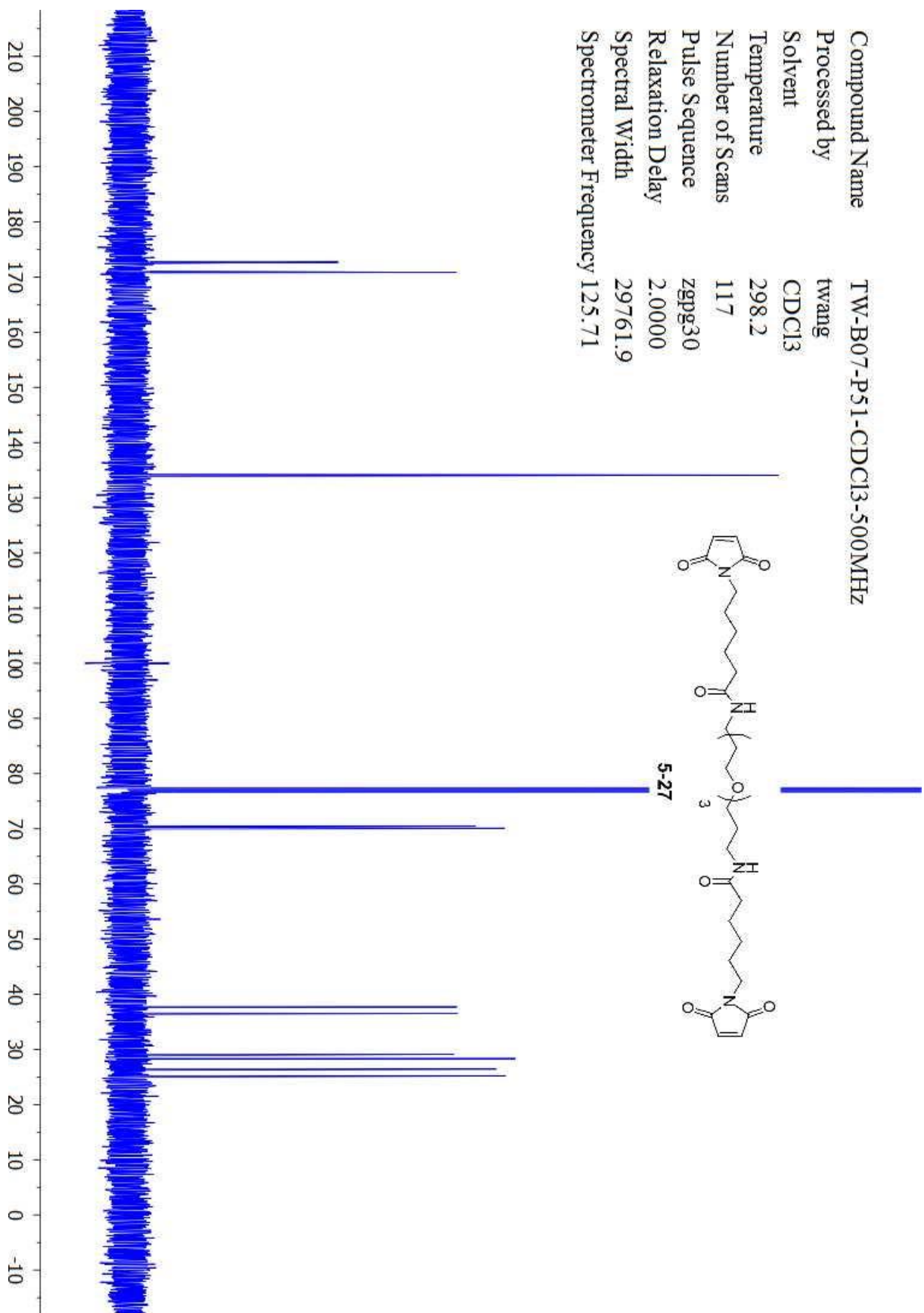
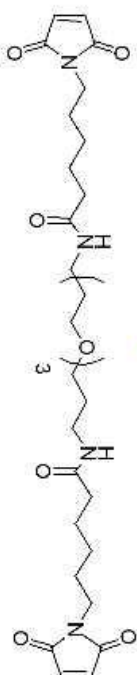


Compound Name TW-B07-P51-CDCl3-500MHZ  
 Processed by twang  
 Solvent CDCl3  
 Temperature 298.1  
 Number of Scans 32  
 Pulse Sequence zg30  
 Relaxation Delay 1.0000  
 Spectral Width 10000.0  
 Spectrometer Frequency 499.89



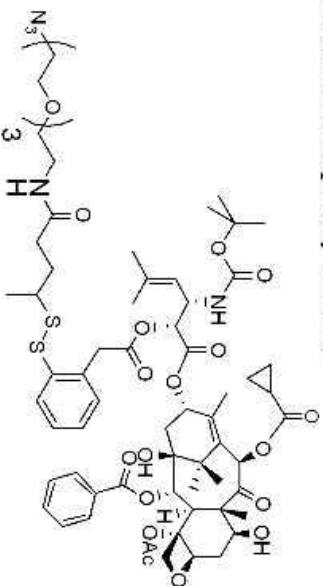


Compound Name TW-B07-P51-CDCl3-500MHZ  
Processed by twang  
Solvent CDCl3  
Temperature 298.2  
Number of Scans 117  
Pulse Sequence zgpg30  
Relaxation Delay 2.0000  
Spectral Width 29761.9  
Spectrometer Frequency 125.71



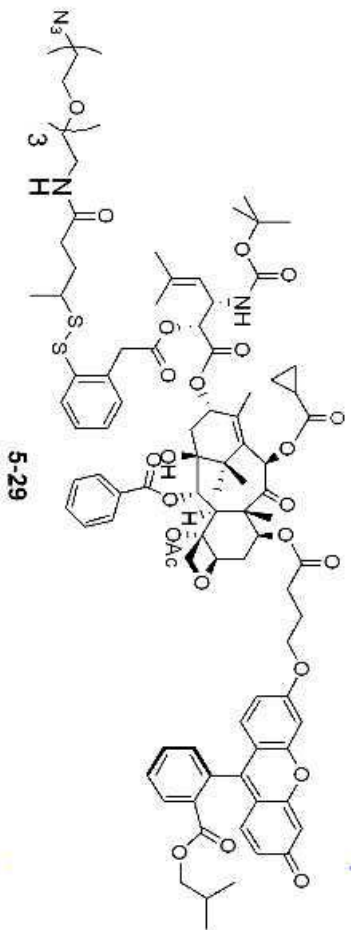


Compound Name TW-B05-P63-prep-500MHz-CD3OD  
Processed by twang  
Solvent MeOD  
Temperature 298.1  
Number of Scans 401  
Pulse Sequence zgpg30  
Relaxation Delay 2.0000  
Spectral Width 29761.9  
Spectrometer Frequency 125.71

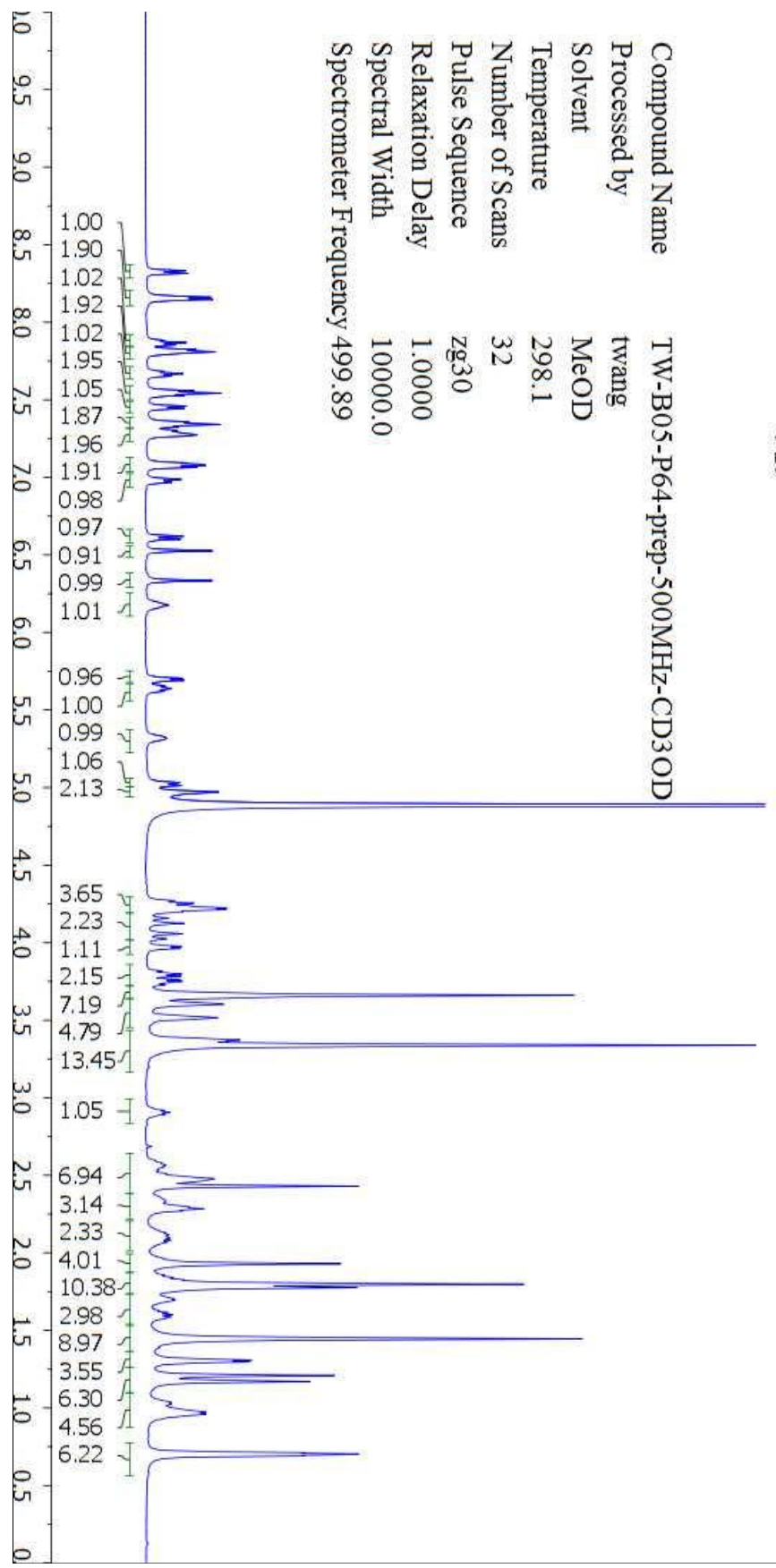


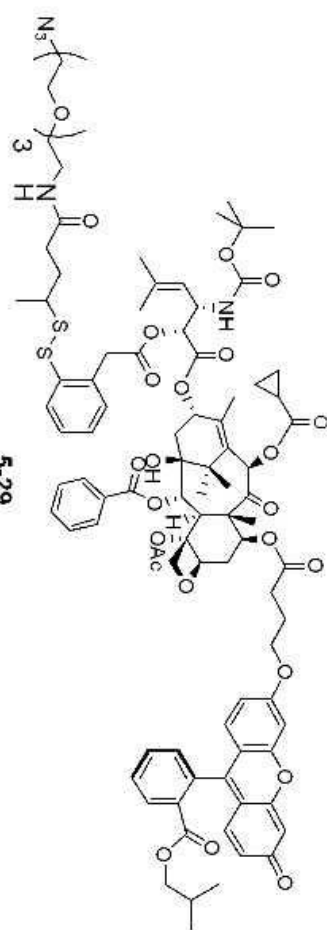
5-28



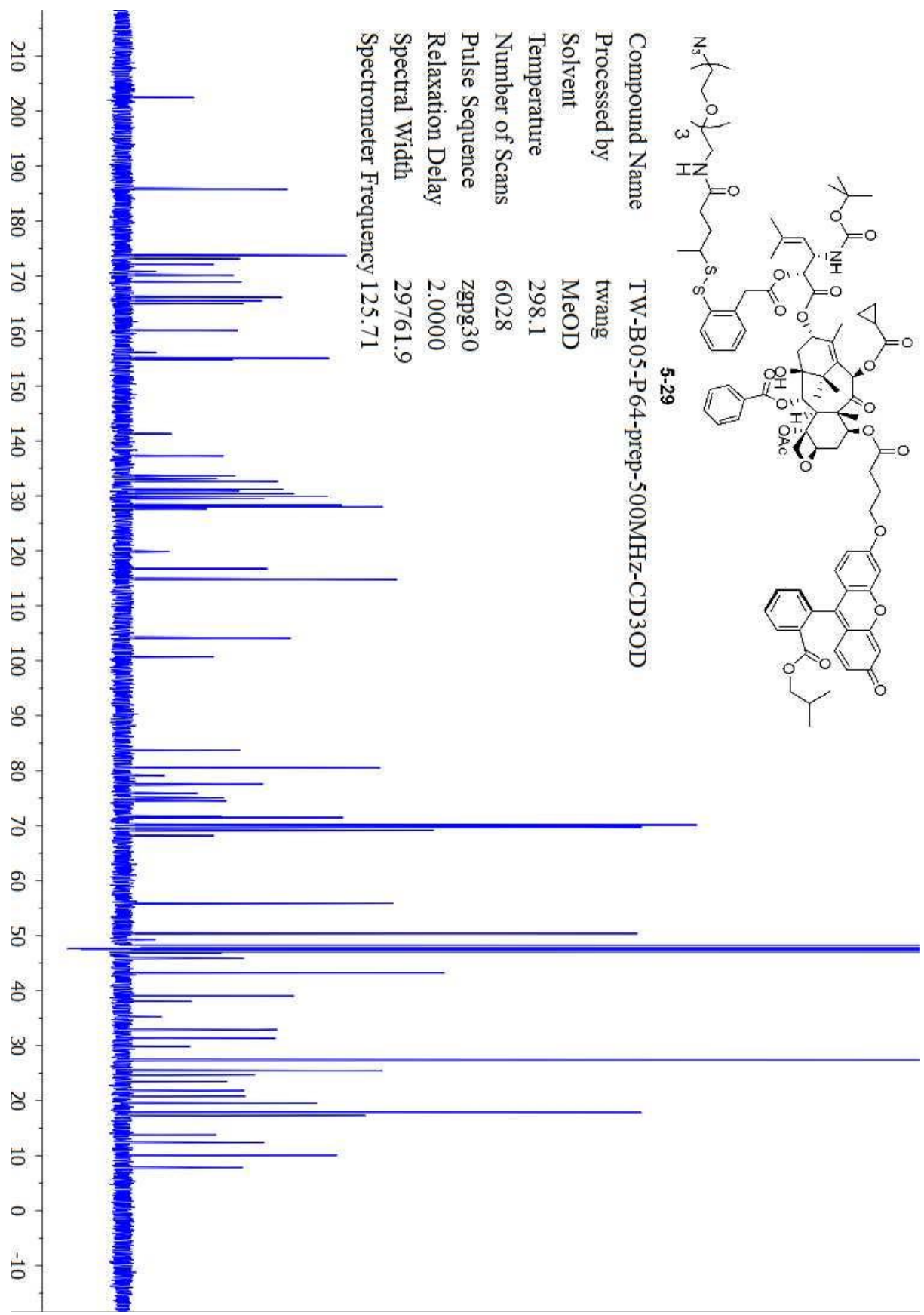


Compound Name TW-B05-P64-prep-500MHz-CD3OD  
 Processed by twang  
 Solvent MeOD  
 Temperature 298.1  
 Number of Scans 32  
 Pulse Sequence zg30  
 Relaxation Delay 1.0000  
 Spectral Width 10000.0  
 Spectrometer Frequency 499.89

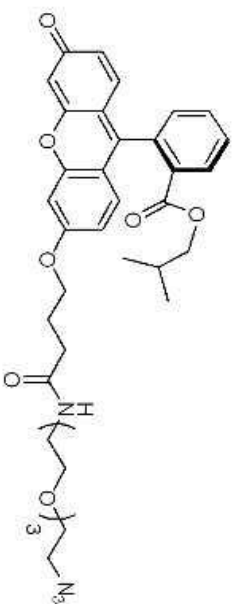




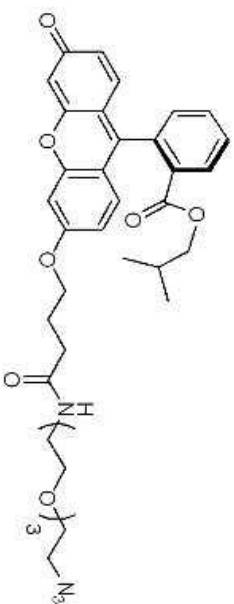
Compound Name TW-B05-P64-prep-500MHz-CD3OD  
 Processed by twang  
 Solvent MeOD  
 Temperature 298.1  
 Number of Scans 6028  
 Pulse Sequence zgpg30  
 Relaxation Delay 2.0000  
 Spectral Width 29761.9  
 Spectrometer Frequency 125.71



Compound Name TW-B05-P09-prep-500MHz-CD3OD  
 Processed by twang  
 Solvent MeOD  
 Temperature 298.2  
 Number of Scans 32  
 Pulse Sequence zg30  
 Relaxation Delay 1.0000  
 Spectral Width 10000.0  
 Spectrometer Frequency 499.89



Compound Name TW-B05-P09-prep-500MHz-CD3OD  
Processed by twang  
Solvent MeOD  
Temperature 298.1  
Number of Scans 214  
Pulse Sequence zgpg30  
Relaxation Delay 2.0000  
Spectral Width 29761.9  
Spectrometer Frequency 125.70

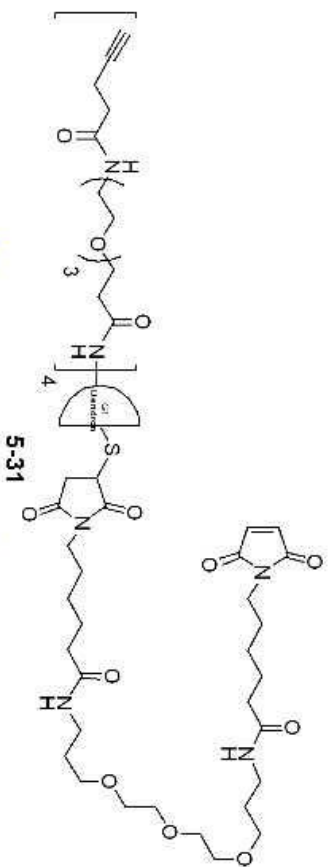






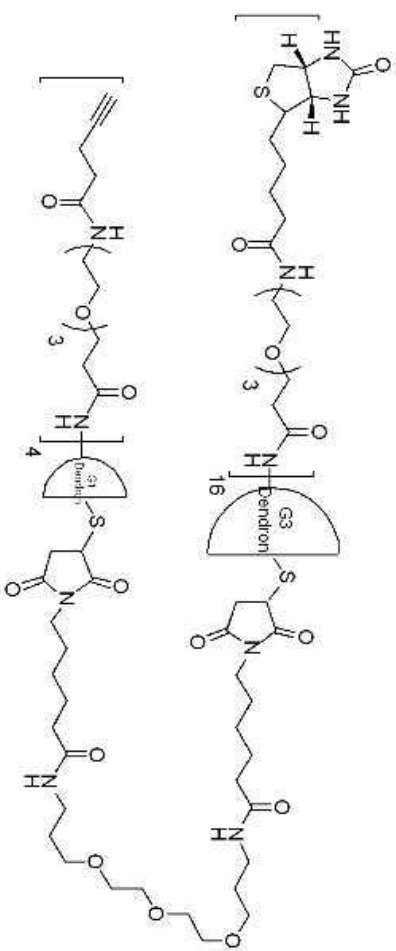


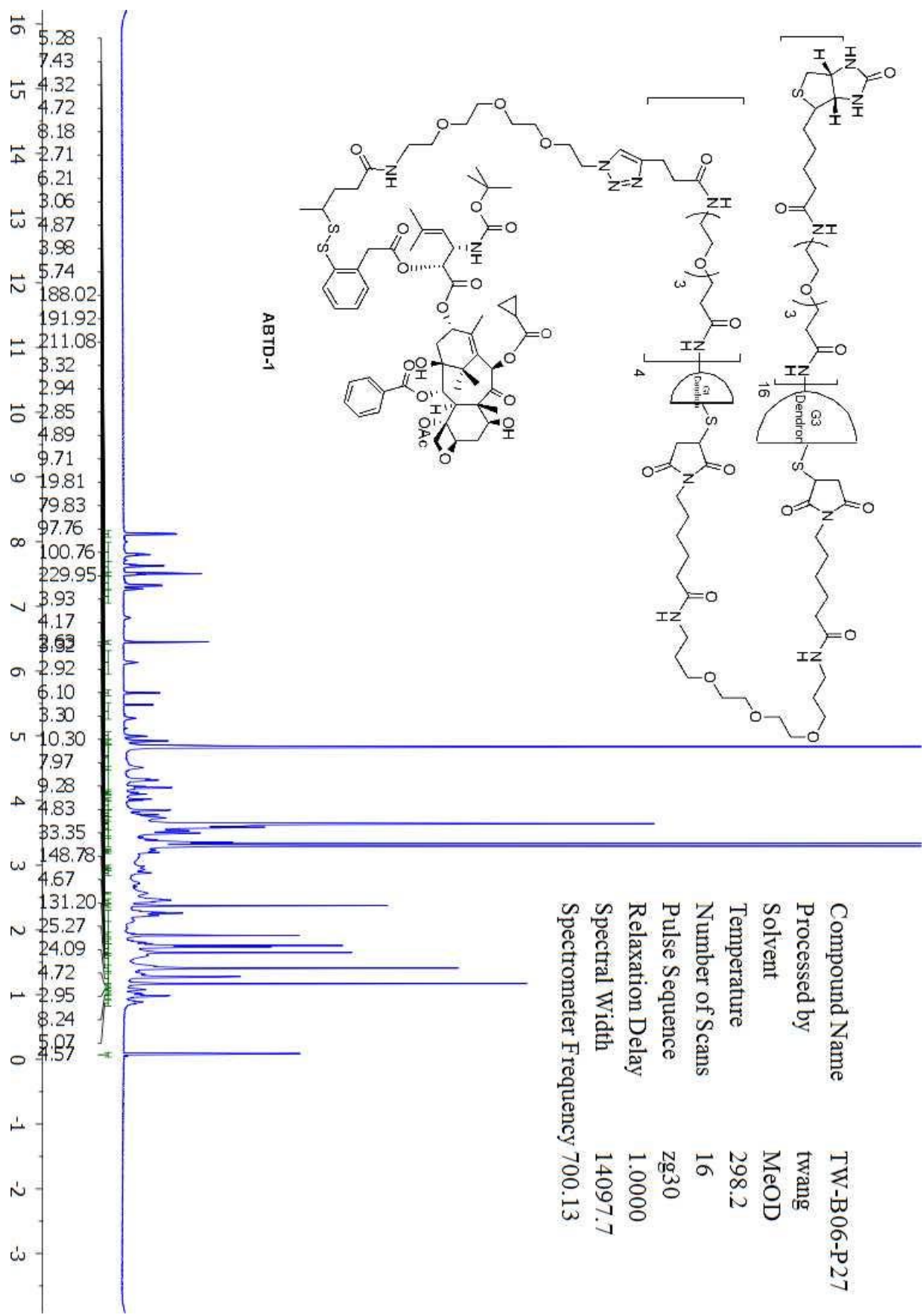
Compound Name TW-B06-P70-500MHZ  
 Processed by twang  
 Solvent D2O  
 Temperature 298.1  
 Number of Scans 18196  
 Pulse Sequence zgpg30  
 Relaxation Delay 2.0000  
 Spectral Width 29761.9  
 Spectrometer Frequency 125.71





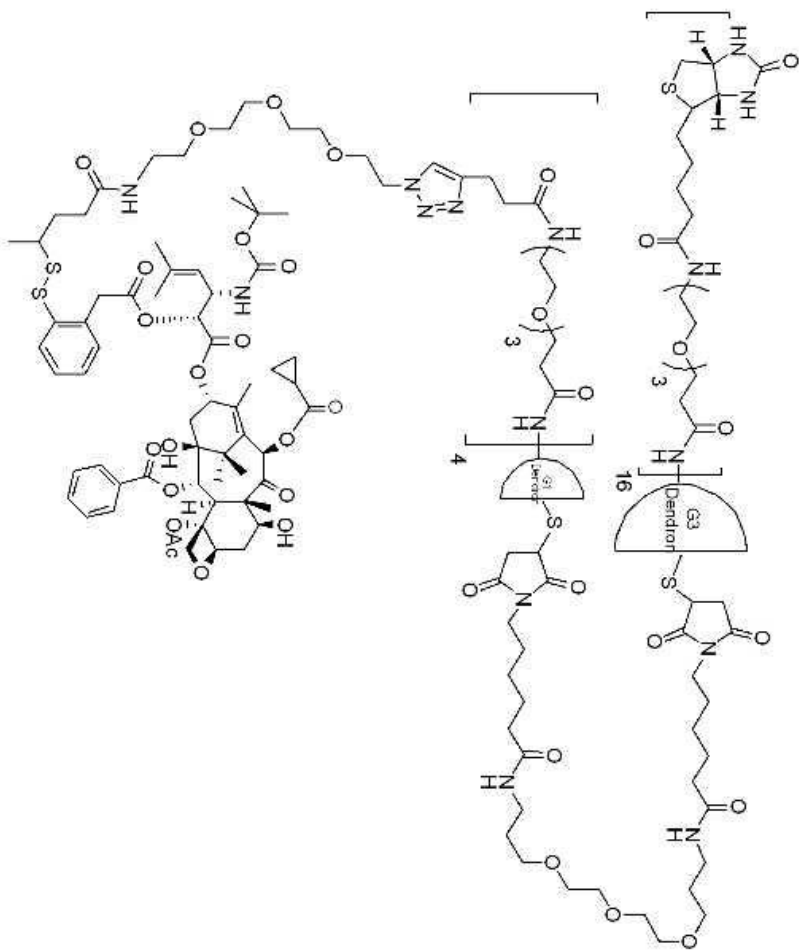
Compound Name TW-B06-P14  
 Processed by twang  
 Solvent MeOD  
 Temperature 298.1  
 Number of Scans 10240  
 Pulse Sequence zgpg30  
 Relaxation Delay 2.0000  
 Spectral Width 41666.7  
 Spectrometer Frequency 176.07



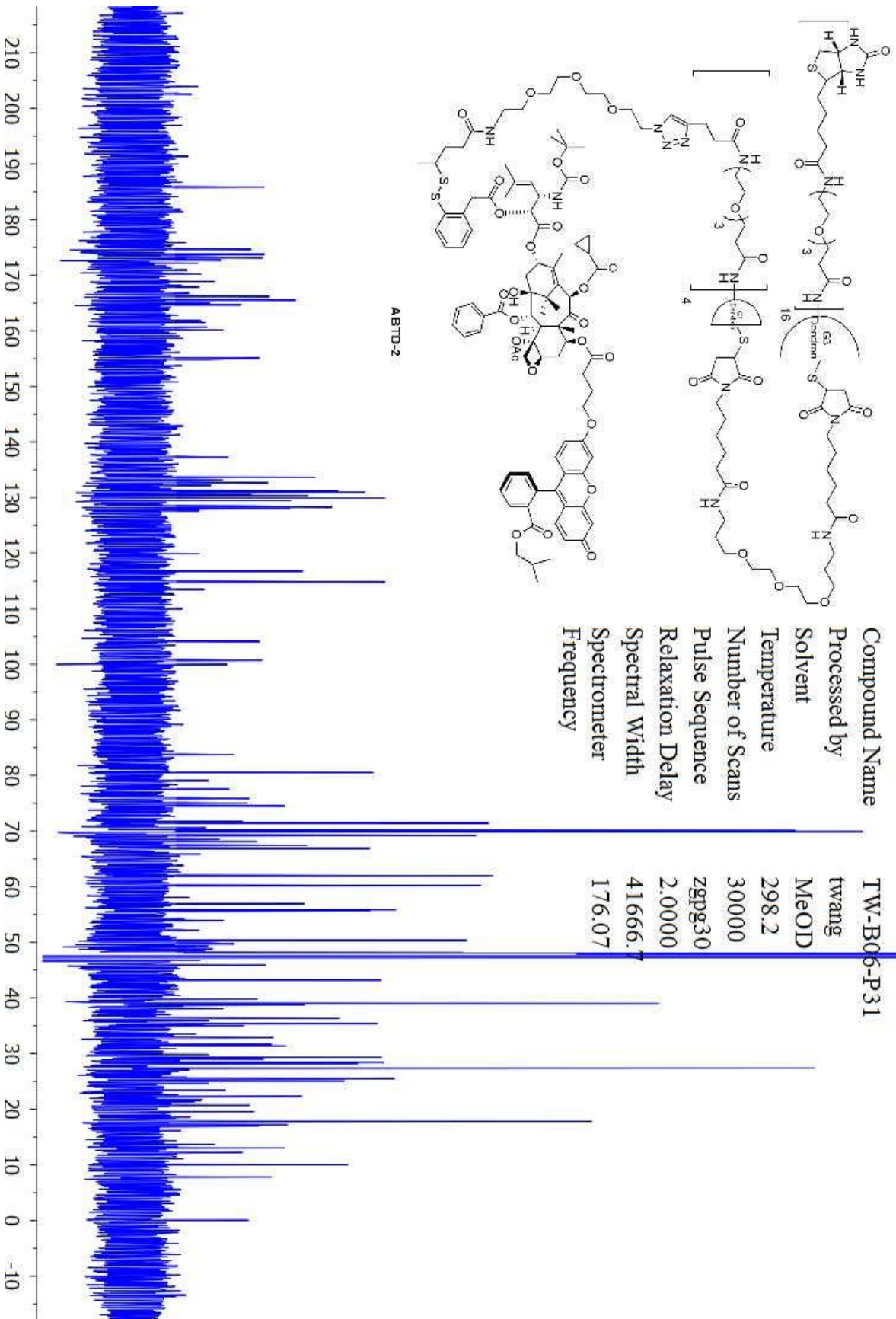


Compound Name TW-B06-P27  
 Processed by twang  
 Solvent MeOD  
 Temperature 298.2  
 Number of Scans 16  
 Pulse Sequence zg30  
 Relaxation Delay 1.0000  
 Spectral Width 14097.7  
 Spectrometer Frequency 700.13

Compound Name TW-B06-P27  
 Processed by twang  
 Solvent MeOD  
 Temperature 298.1  
 Number of Scans 22956  
 Pulse Sequence zgpg30  
 Relaxation Delay 2.0000  
 Spectral Width 41666.7  
 Spectrometer Frequency 176.07







Compound Name

TW-B06-P31

Processed by

twang

Solvent

MeOD

Temperature

298.2

Number of Scans

30000

Pulse Sequence

zgp30

Relaxation Delay

2.0000

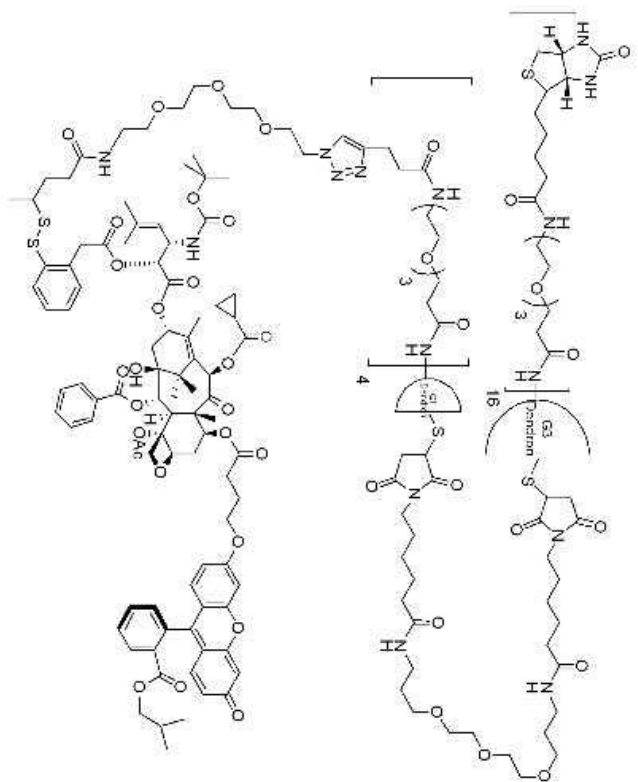
Spectral Width

41666.

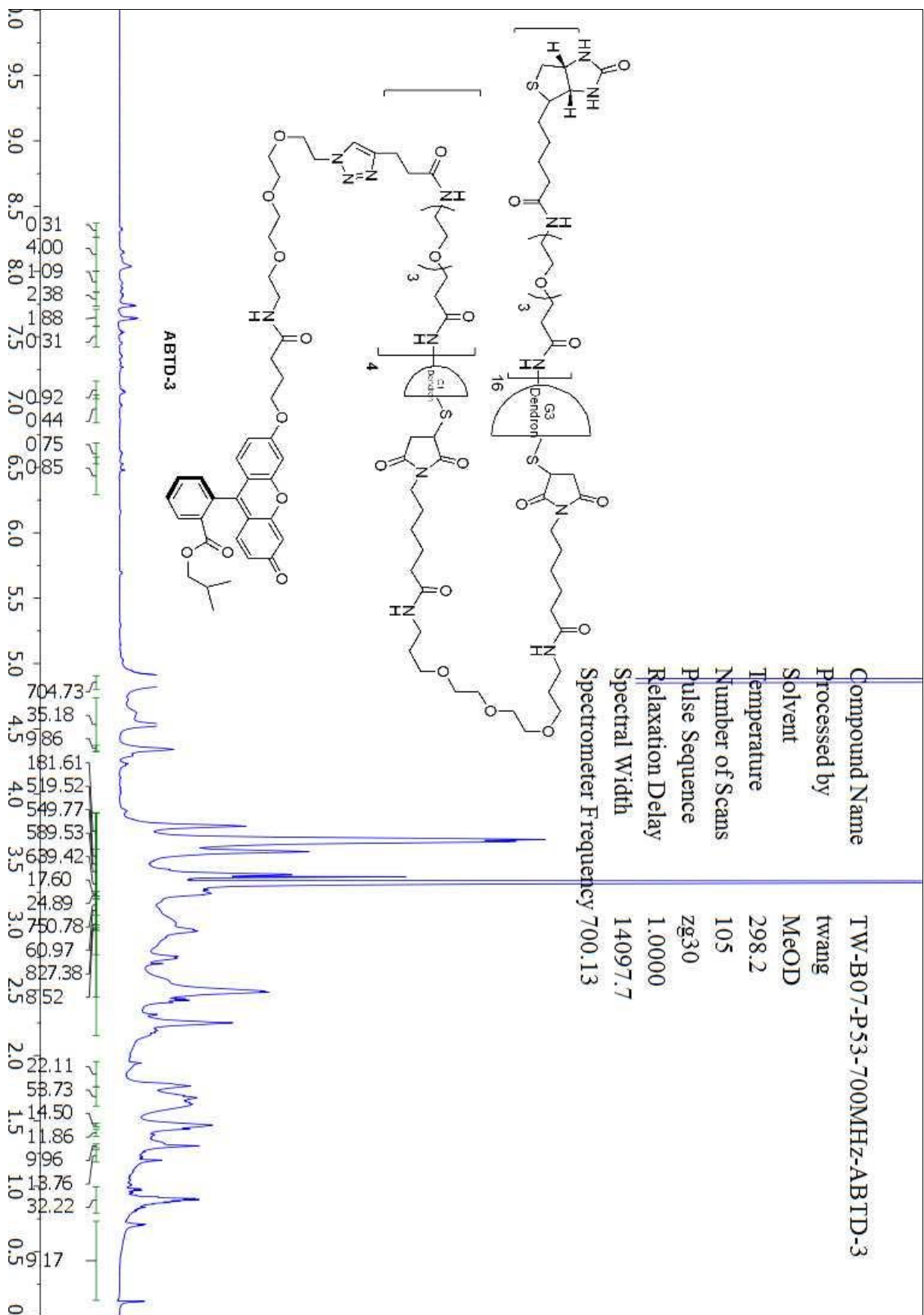
Spectrometer

176.07

Frequency

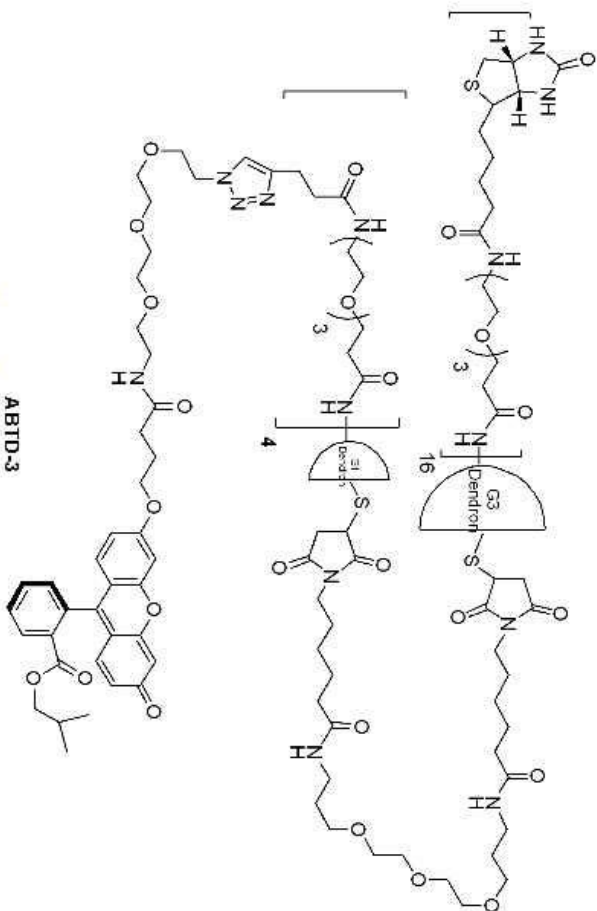






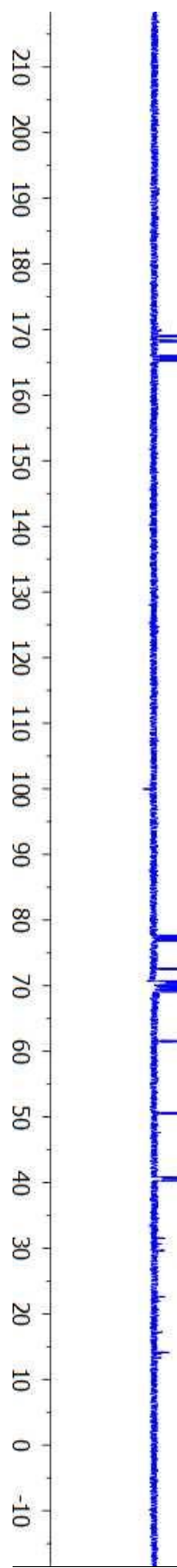
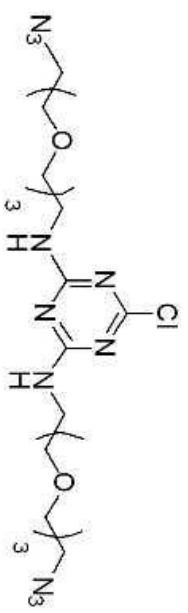
Compound Name  
 Processed by  
 Solvent  
 Temperature  
 Number of Scans  
 Pulse Sequence  
 Relaxation Delay  
 Spectral Width  
 Spectrometer Frequency

TW-B07-P53-700MHz-ABTD-3  
 twang  
 MeOD  
 298.2  
 30000  
 zgpg30  
 2.0000  
 41666.7  
 176.07

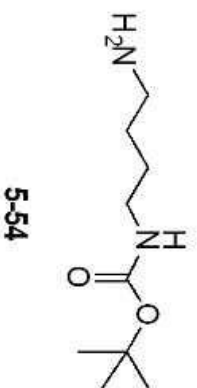




Compound Name TW-B05-P88  
Processed by twang  
Solvent CDCl3  
Temperature 298.2  
Number of Scans 101  
Pulse Sequence zgpg30  
Relaxation Delay 2.0000  
Spectral Width 29761.9  
Spectrometer Frequency 125.71



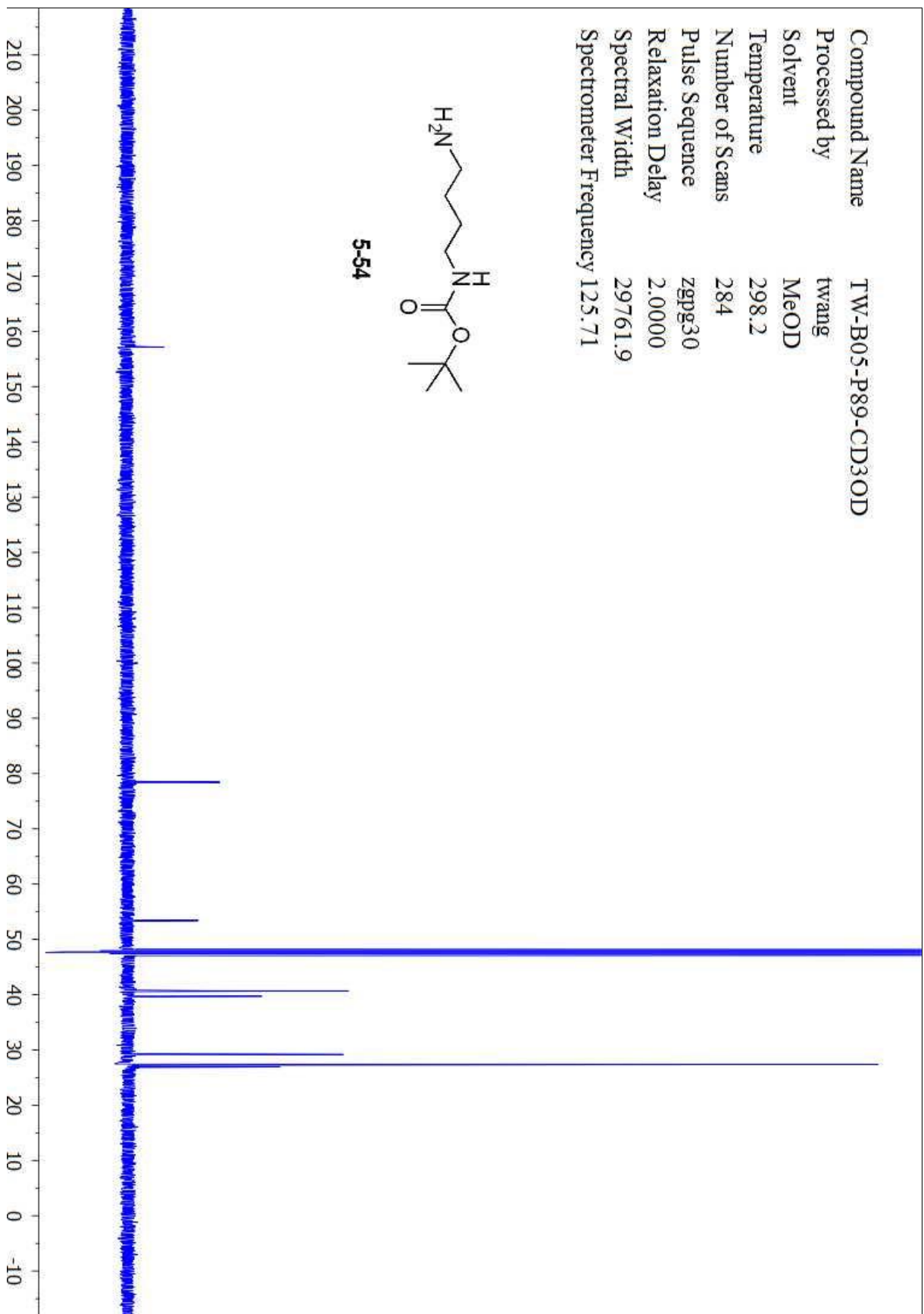
Compound Name TW-B05-P89-CD3OD  
Processed by twang  
Solvent MeOD  
Temperature 298.2  
Number of Scans 32  
Pulse Sequence zg30  
Relaxation Delay 1.0000  
Spectral Width 10000.0  
Spectrometer Frequency 499.89



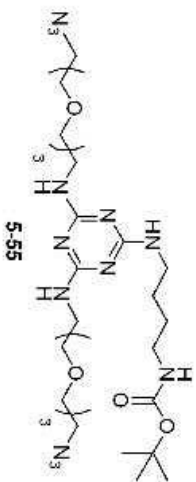
Compound Name TW-B05-P89-CD3OD  
Processed by twang  
Solvent MeOD  
Temperature 298.2  
Number of Scans 284  
Pulse Sequence zgpg30  
Relaxation Delay 2.0000  
Spectral Width 29761.9  
Spectrometer Frequency 125.71



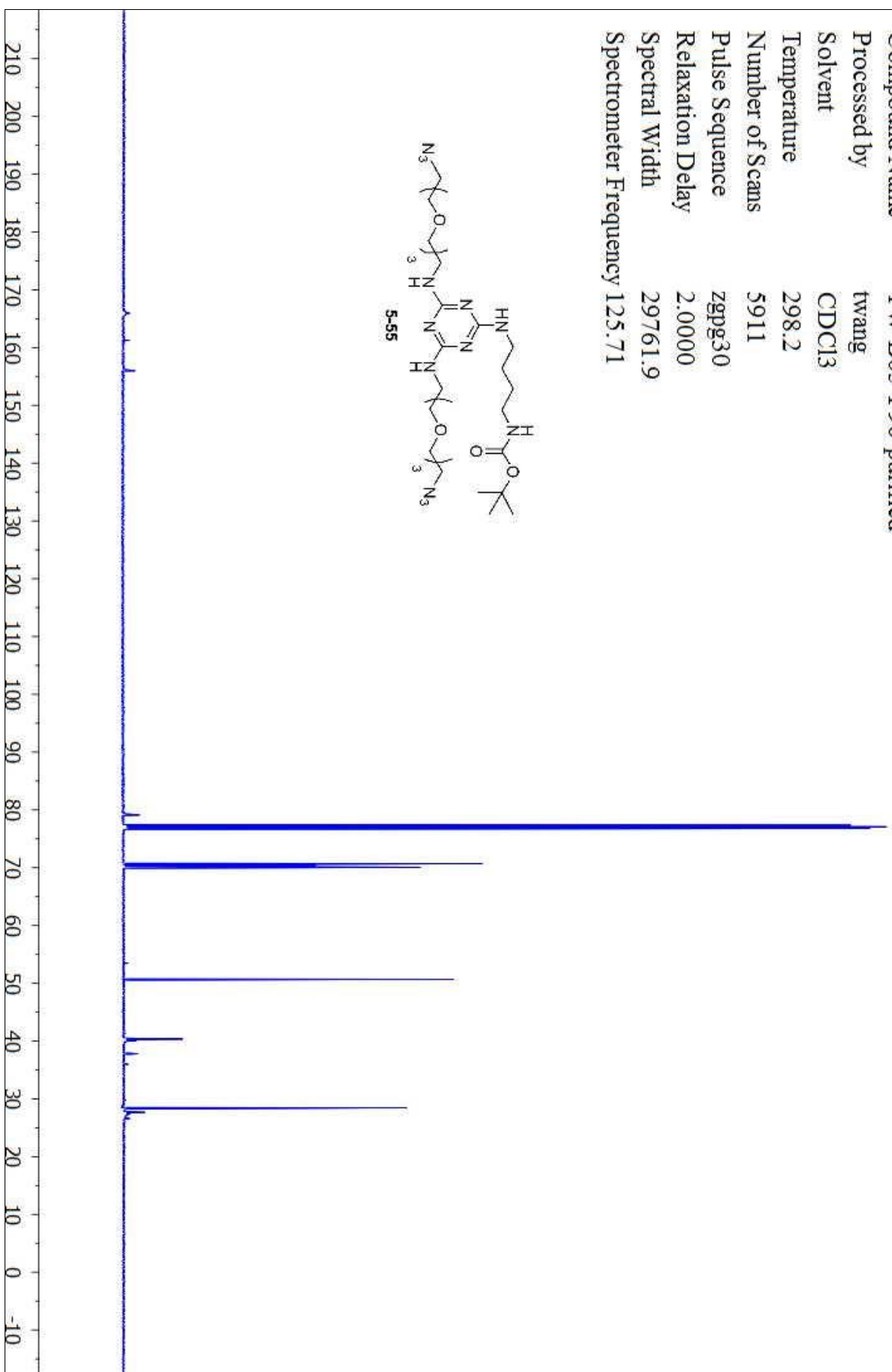
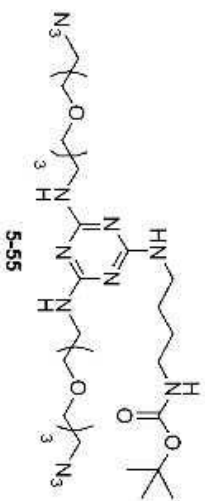
5-54



Compound Name TW-B05-P90-purified  
 Processed by twang  
 Solvent CDCl3  
 Temperature 298.1  
 Number of Scans 64  
 Pulse Sequence zg30  
 Relaxation Delay 1.0000  
 Spectral Width 10000.0  
 Spectrometer Frequency 499.89

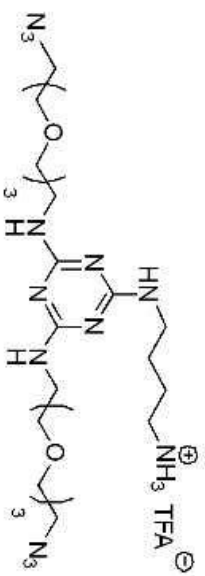


Compound Name TW-B05-P90-purified  
Processed by twang  
Solvent CDCl3  
Temperature 298.2  
Number of Scans 5911  
Pulse Sequence zgpg30  
Relaxation Delay 2.0000  
Spectral Width 29761.9  
Spectrometer Frequency 125.71





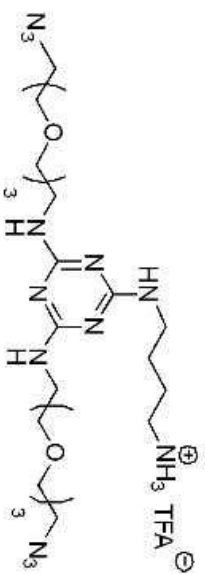
Compound Name TW-B05-P98-2  
 Processed by twang  
 Solvent MeOD  
 Temperature 298.1  
 Number of Scans 16  
 Pulse Sequence zg30  
 Relaxation Delay 1.0000  
 Spectral Width 10000.0  
 Spectrometer Frequency 499.89



5-56



Compound Name TW-B05-P98-2  
Processed by twang  
Solvent MeOD  
Temperature 298.2  
Number of Scans 304  
Pulse Sequence zgpg30  
Relaxation Delay 2.0000  
Spectral Width 29761.9  
Spectrometer Frequency 125.71

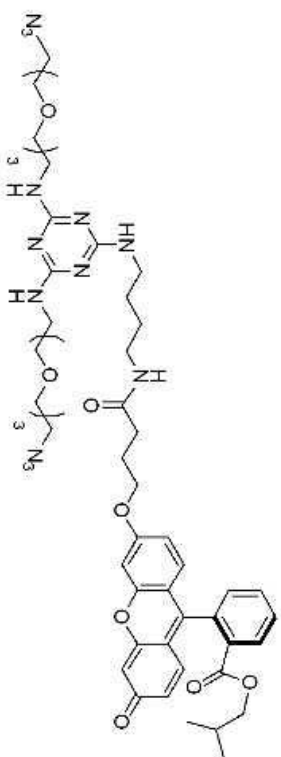


5-56

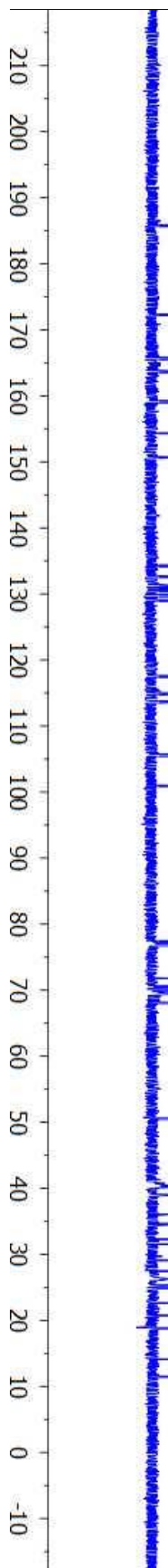




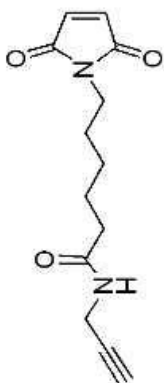
Compound Name TW-B05-P101  
Processed by twang  
Solvent CDCl3  
Temperature 298.2  
Number of Scans 304  
Pulse Sequence zgpg30  
Relaxation Delay 2.0000  
Spectral Width 29761.9  
Spectrometer Frequency 125.71



S-57



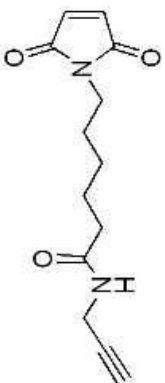
Compound Name TW-B05-P92  
Processed by twang  
Solvent CDCl3  
Temperature 298.1  
Number of Scans 16  
Pulse Sequence zg30  
Relaxation Delay 1.0000  
Spectral Width 10000.0  
Spectrometer Frequency 499.89



5-58



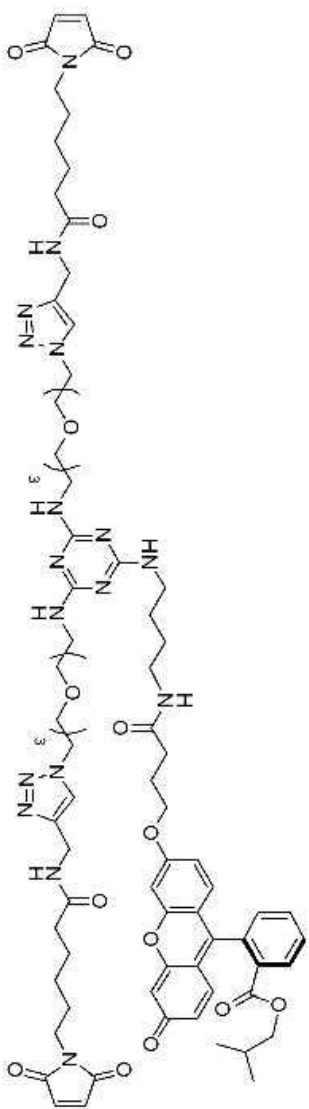
Compound Name TW-B05-P92  
Processed by twang  
Solvent CDCl3  
Temperature 298.2  
Number of Scans 225  
Pulse Sequence zgpg30  
Relaxation Delay 2.0000  
Spectral Width 29761.9  
Spectrometer Frequency 125.71



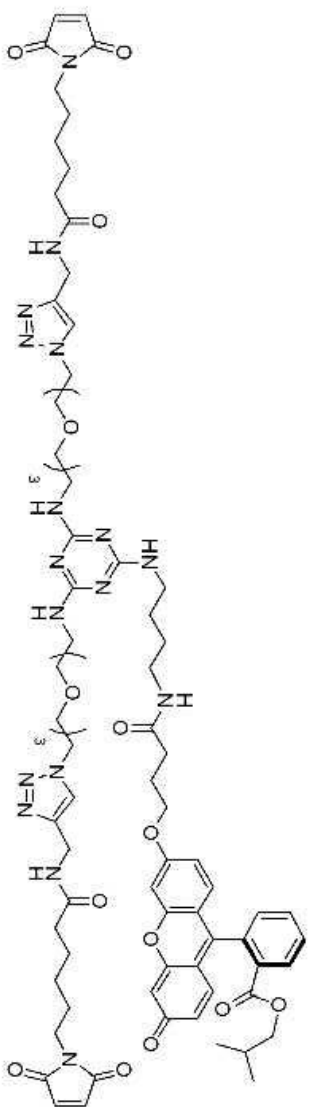
5-58



Compound Name TW-B05-P109  
 Processed by twang  
 Solvent CDCl3  
 Temperature 298.1  
 Number of Scans 32  
 Pulse Sequence zg30  
 Relaxation Delay 1.0000  
 Spectral Width 10000.0  
 Spectrometer Frequency 499.89

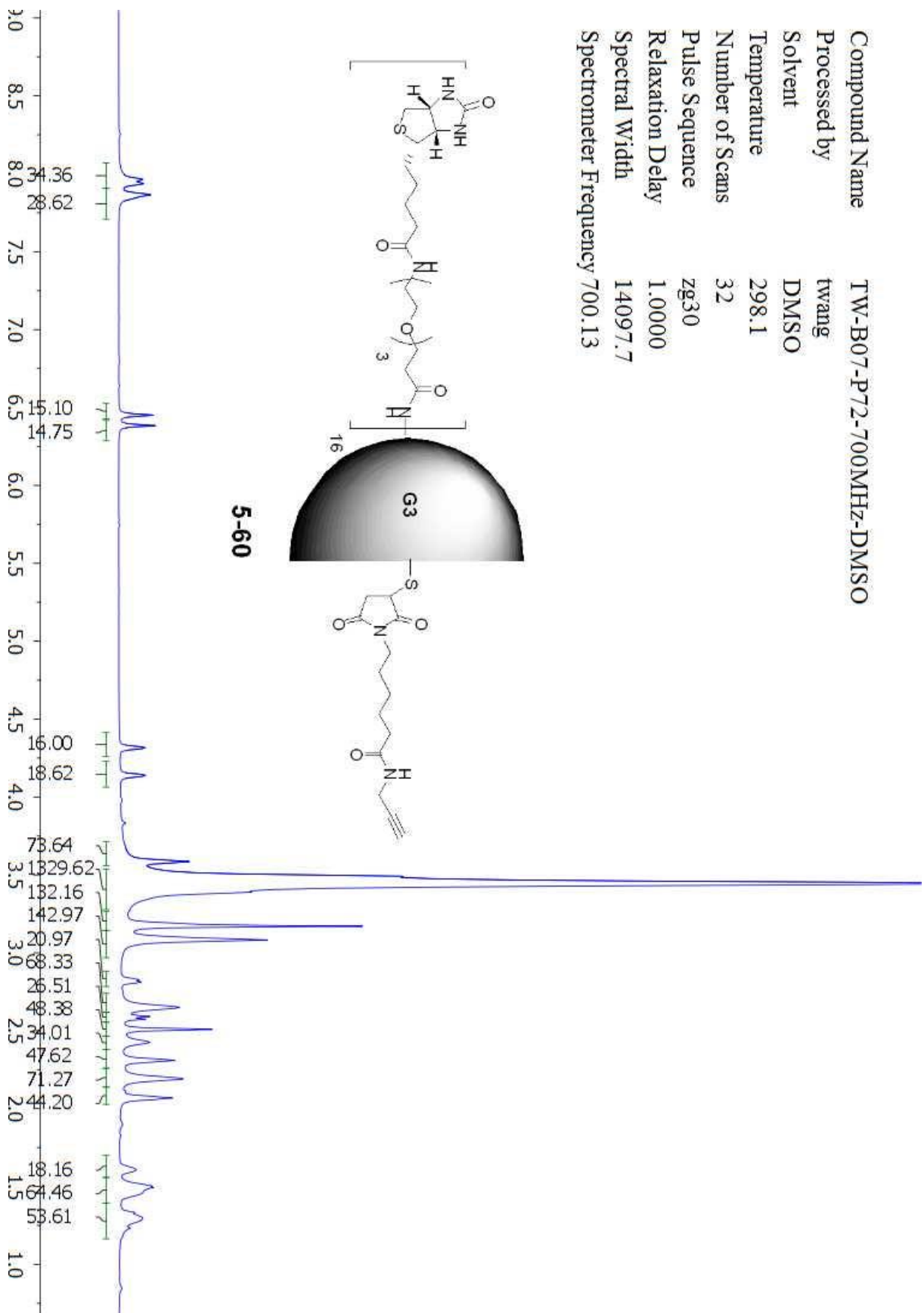


Compound Name TW-B05-P109  
 Processed by twang  
 Solvent CDCl3  
 Temperature 298.1  
 Number of Scans 802  
 Pulse Sequence zgpg30  
 Relaxation Delay 2.0000  
 Spectral Width 29761.9  
 Spectrometer Frequency 125.71

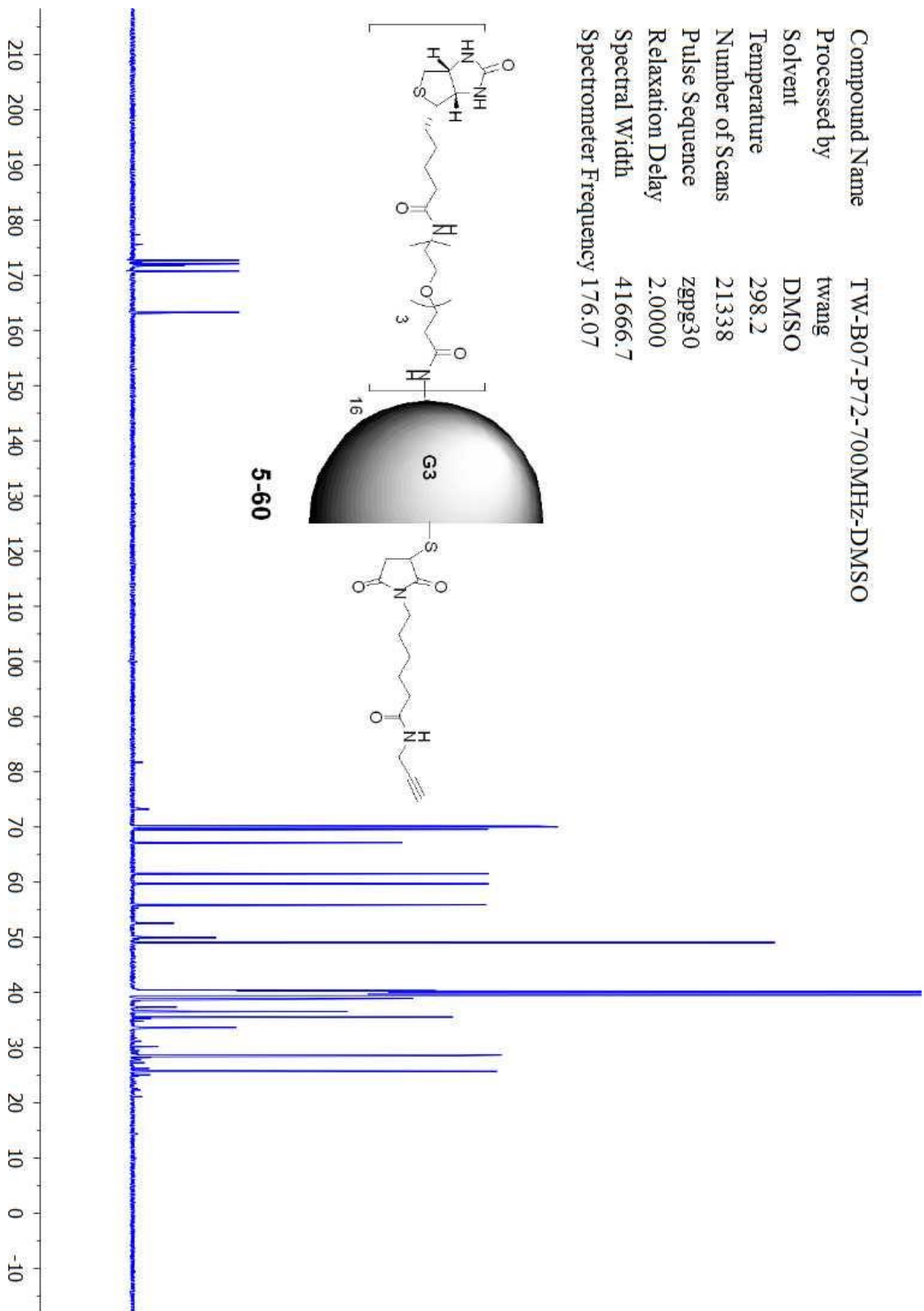




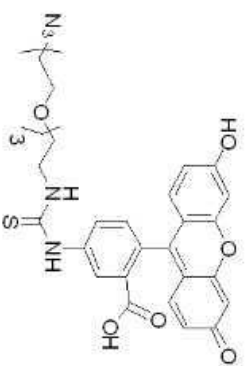
Compound Name TW-B07-P72-700MHz-DMSO  
 Processed by twang  
 Solvent DMSO  
 Temperature 298.1  
 Number of Scans 32  
 Pulse Sequence zg30  
 Relaxation Delay 1.0000  
 Spectral Width 14097.7  
 Spectrometer Frequency 700.13



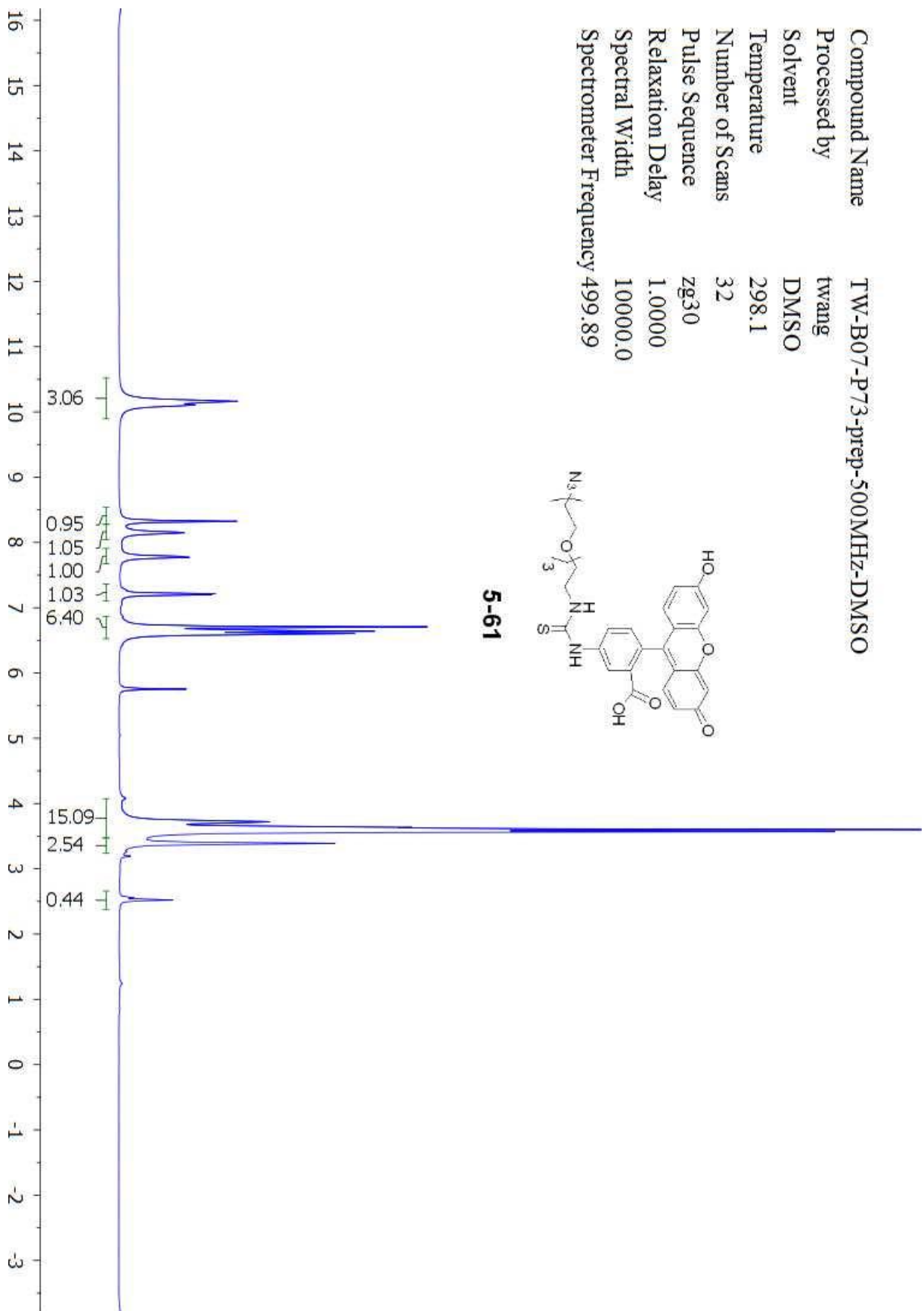
Compound Name TW-B07-P72-700MHz-DMSO  
 Processed by twang  
 Solvent DMSO  
 Temperature 298.2  
 Number of Scans 21338  
 Pulse Sequence zgpg30  
 Relaxation Delay 2.0000  
 Spectral Width 41666.7  
 Spectrometer Frequency 176.07



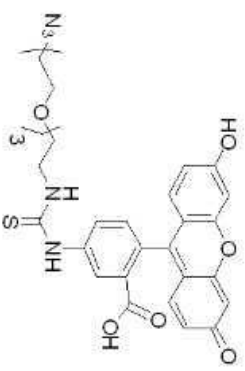
Compound Name TW-B07-P73-prep-500MHz-DMSO  
 Processed by twang  
 Solvent DMSO  
 Temperature 298.1  
 Number of Scans 32  
 Pulse Sequence zg30  
 Relaxation Delay 1.0000  
 Spectral Width 10000.0  
 Spectrometer Frequency 499.89



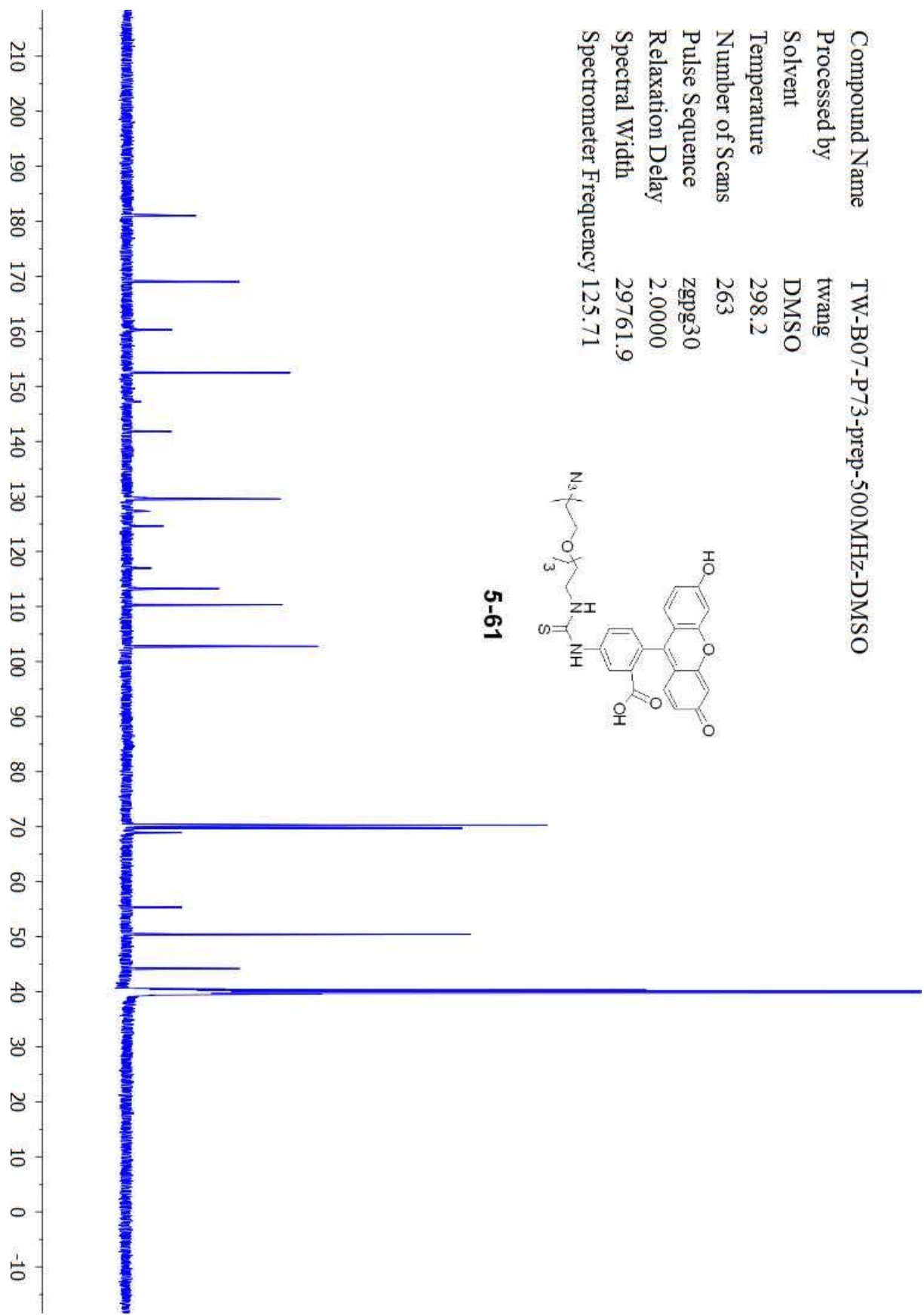
**5-61**



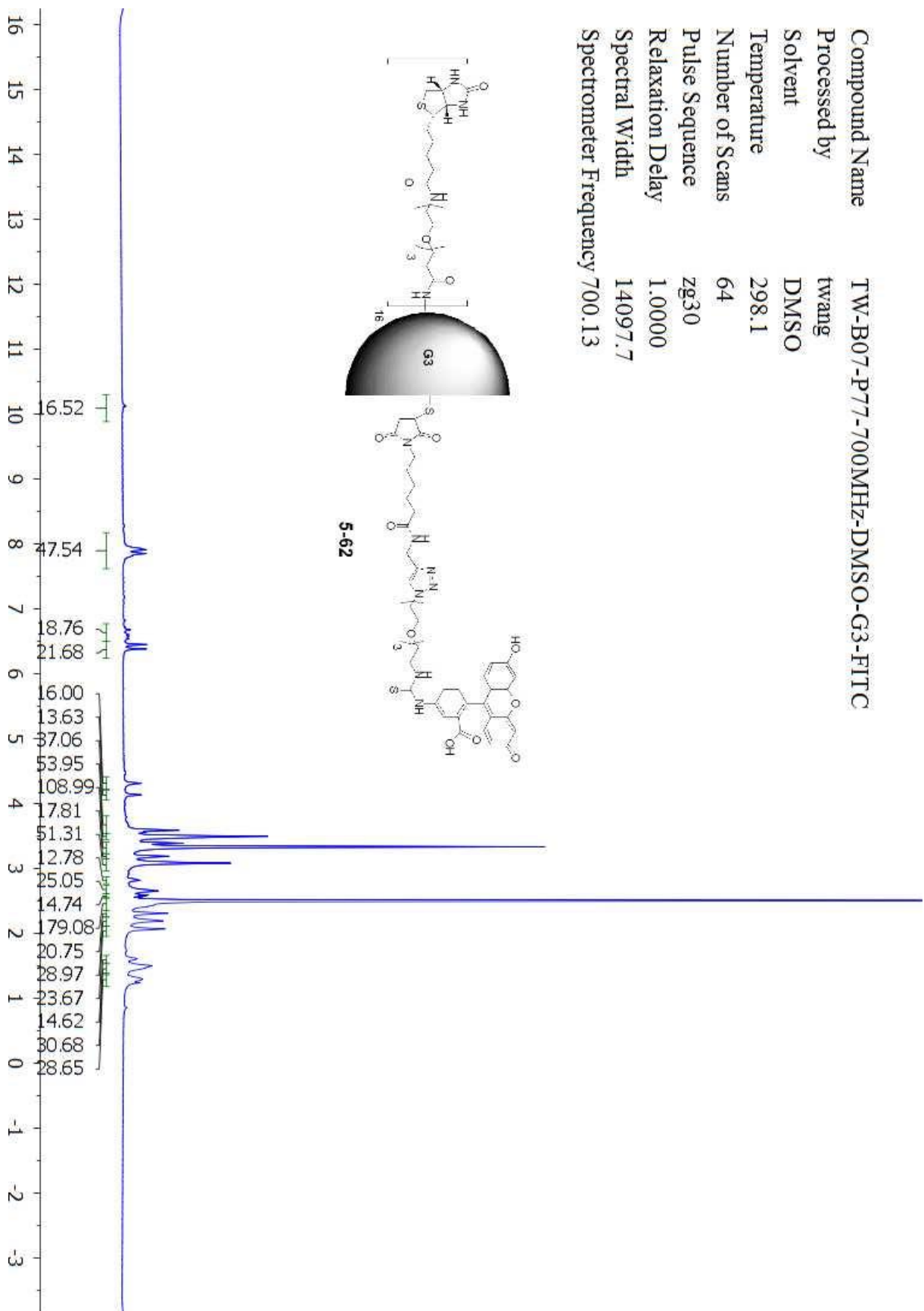
Compound Name TW-B07-P73-prep-500MHz-DMSO  
 Processed by twang  
 Solvent DMSO  
 Temperature 298.2  
 Number of Scans 263  
 Pulse Sequence zgpg30  
 Relaxation Delay 2.0000  
 Spectral Width 29761.9  
 Spectrometer Frequency 125.71



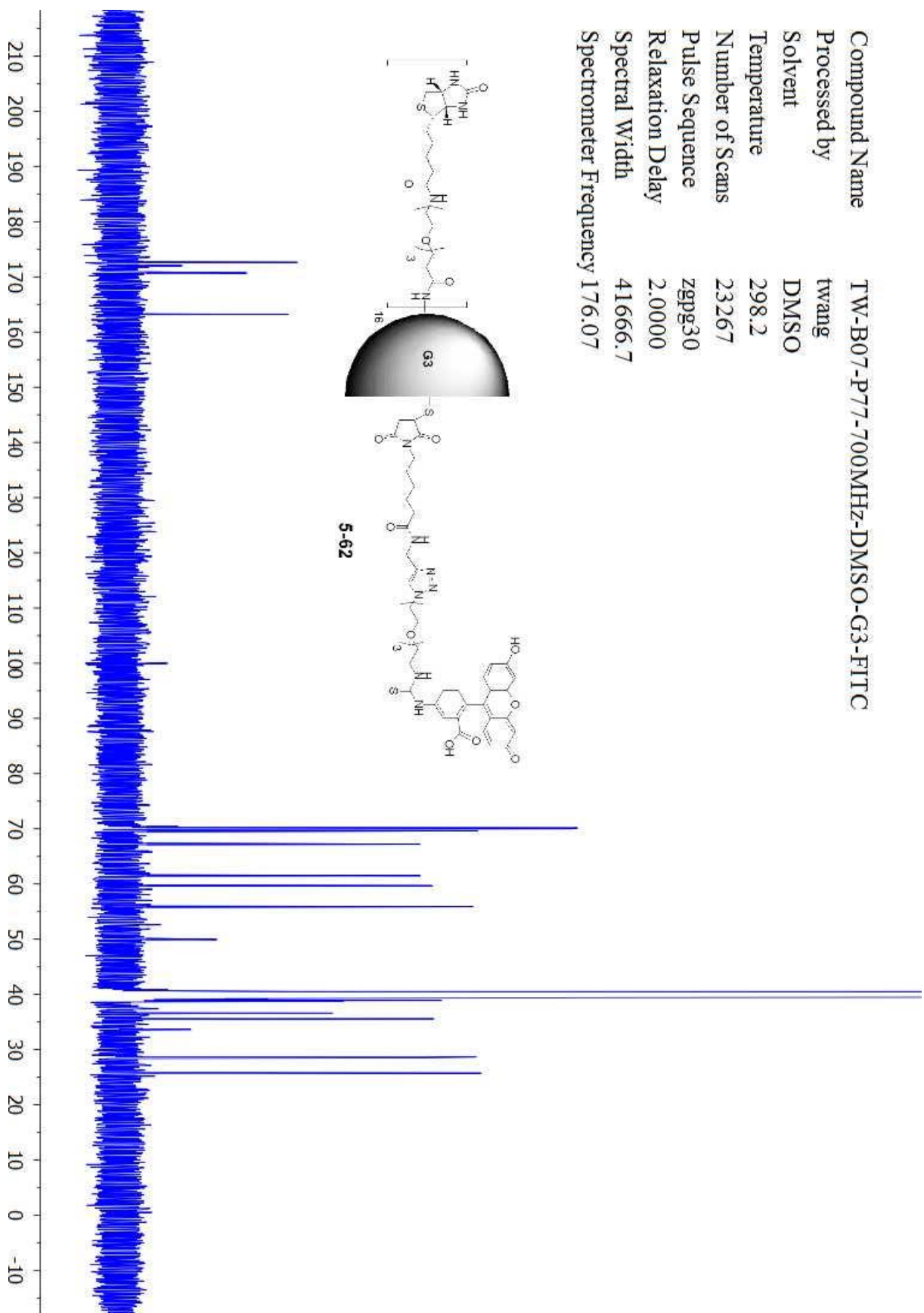
5-61



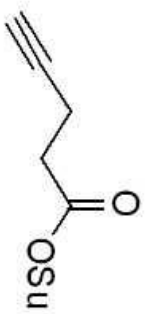
Compound Name TW-B07-P77-700MHz-DMSO-G3-FITC  
 Processed by twang  
 Solvent DMSO  
 Temperature 298.1  
 Number of Scans 64  
 Pulse Sequence zg30  
 Relaxation Delay 1.0000  
 Spectral Width 14097.7  
 Spectrometer Frequency 700.13



Compound Name TW-B07-P77-700MHz-DMSO-G3-FITC  
 Processed by twang  
 Solvent DMSO  
 Temperature 298.2  
 Number of Scans 23267  
 Pulse Sequence zgpg30  
 Relaxation Delay 2.0000  
 Spectral Width 41666.7  
 Spectrometer Frequency 176.07



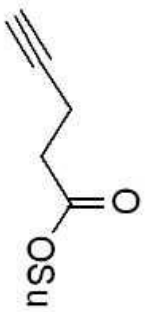
Compound Name TW-B07-P48-CDCl3-500MHZ  
Processed by twang  
Solvent CDCl3  
Temperature 298.1  
Number of Scans 37  
Pulse Sequence zg30  
Relaxation Delay 1.0000  
Spectral Width 10000.0  
Spectrometer Frequency 499.89



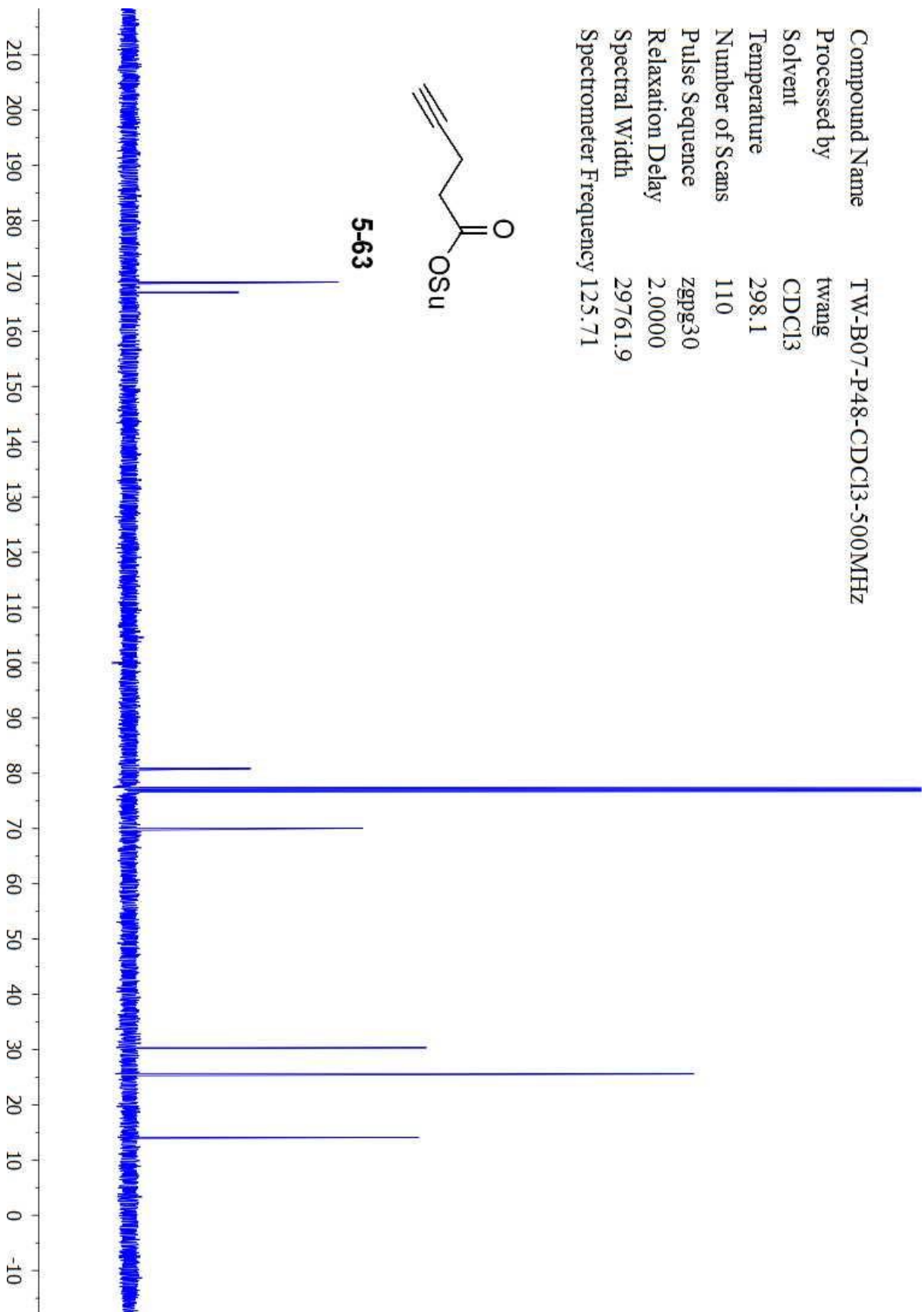
5-63



Compound Name TW-B07-P48-CDCl3-500MHZ  
Processed by twang  
Solvent CDCl3  
Temperature 298.1  
Number of Scans 110  
Pulse Sequence zgpg30  
Relaxation Delay 2.0000  
Spectral Width 29761.9  
Spectrometer Frequency 125.71



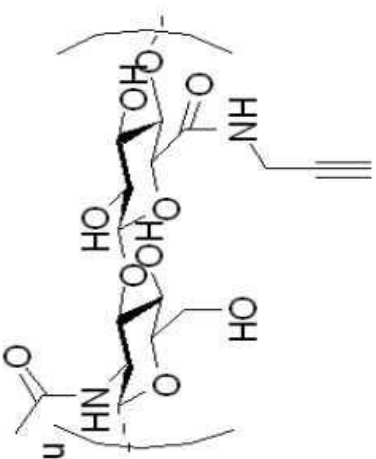
5-63



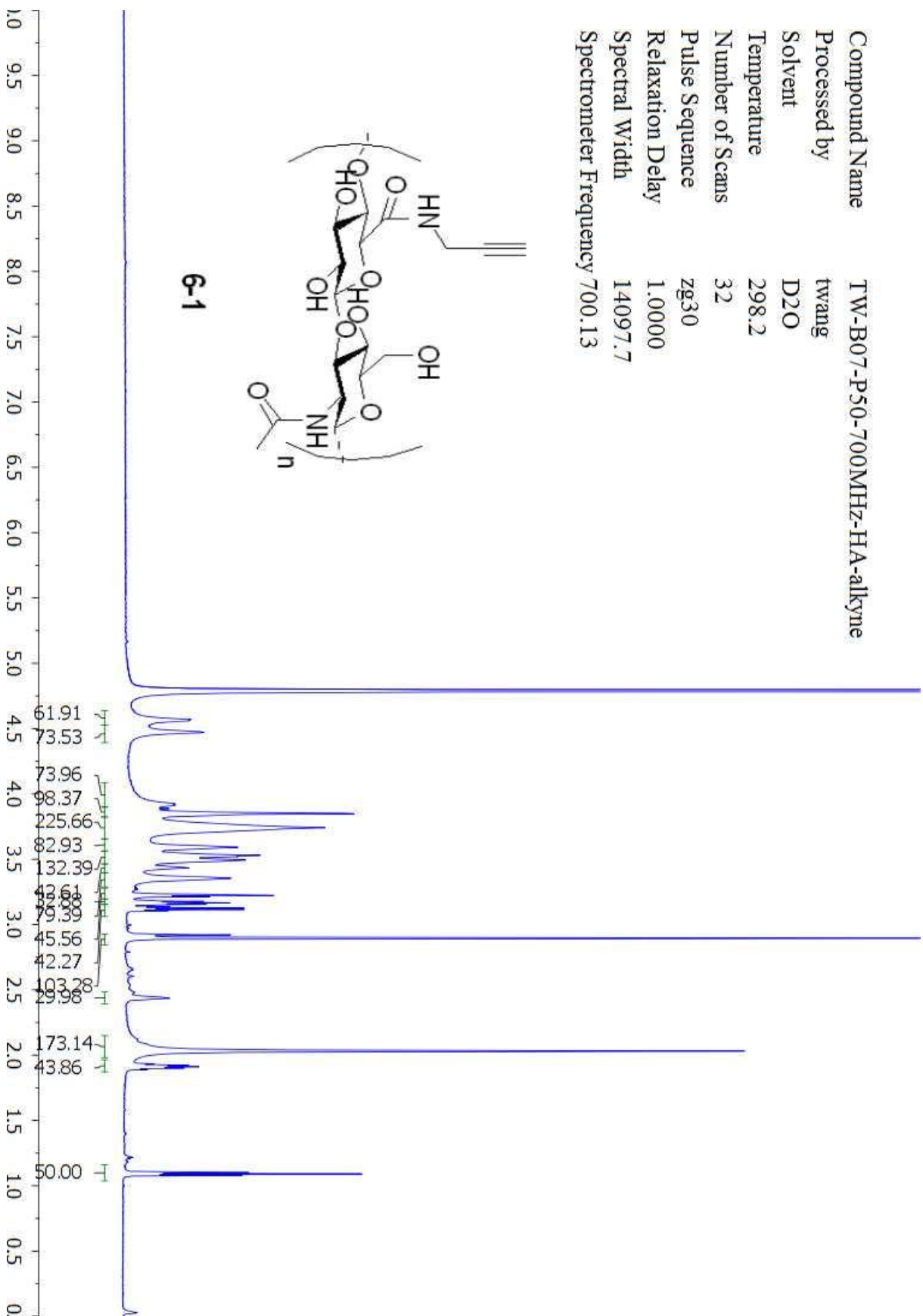


## Appendix Chapter 6 NMR Spectra

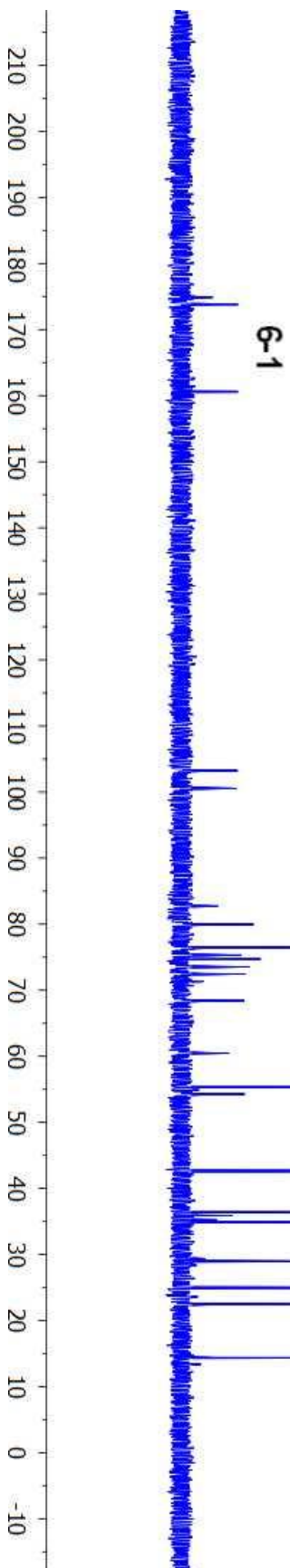
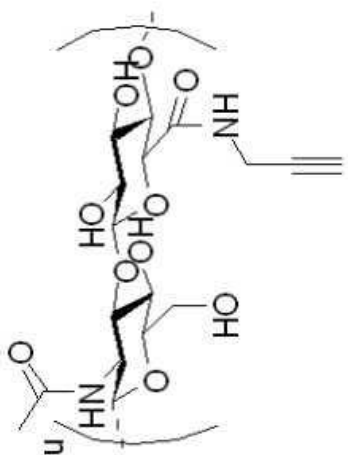
Compound Name TW-B07-P50-700MHz-HA-alkyne  
 Processed by twang  
 Solvent D2O  
 Temperature 298.2  
 Number of Scans 32  
 Pulse Sequence zg30  
 Relaxation Delay 1.0000  
 Spectral Width 14097.7  
 Spectrometer Frequency 700.13



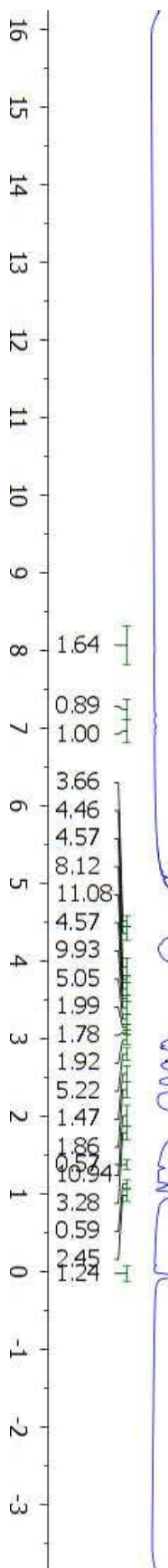
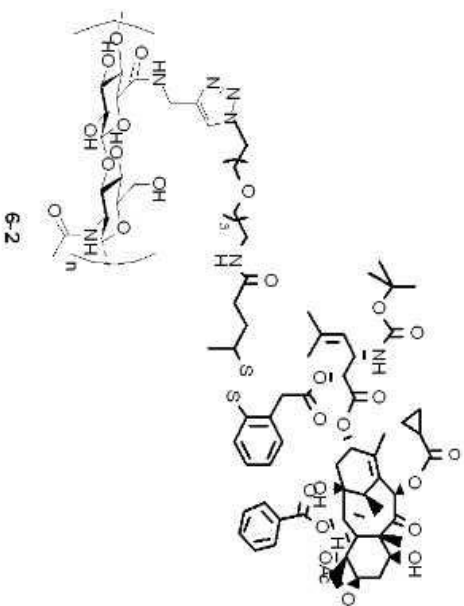
6-1



Compound Name TW-B07-P50-700MHz-HA-alkyne  
Processed by twang  
Solvent D2O  
Temperature 298.2  
Number of Scans 27567  
Pulse Sequence zgpg30  
Relaxation Delay 2.0000  
Spectral Width 41666.7  
Spectrometer Frequency 176.07



Compound Name TW-B07-P57-700MHz-D2O-10%drugloading  
 Processed by twang  
 Solvent D2O  
 Temperature 298.2  
 Number of Scans 309  
 Pulse Sequence zg30  
 Relaxation Delay 1.0000  
 Spectral Width 14097.7  
 Spectrometer Frequency 700.13



Compound Name TW-B07-P57-700MHz-D2O-10%drugloading  
 Processed by twang  
 Solvent D2O  
 Temperature 298.1  
 Number of Scans 27659  
 Pulse Sequence zgpg30  
 Relaxation Delay 2.0000  
 Spectral Width 41666.7  
 Spectrometer Frequency 176.07

